Department of Chemical
and Biochemical Engineering
Technical University of Denmark

Graduate Schools Yearbook 2010

Editors:
Kim Dam-Johansen
Rui Xue
Krist V. Gernaey

Address: Department of Chemical and Biochemical Engineering
Søltofts Plads, Building 229
Technical University of Denmark
DK-2800 Kgs. Lyngby
Denmark

Telephone: +45 4525 2800
Fax: +45 4588 2258
Email: kt@kt.dtu.dk
Internet: http://www.kt.dtu.dk

Print: J&R Frydenberg A/S
København
March 2011

Cover: Suzanne Fog

Cover Photo: Klaus Holsting

ISBN-13: 978-87-92481-36-8

Contents

Enzymatic Production of Cross-linked Plant Cell Wall Polymers
Dayang Norulfairuz Abang Zaidel ····· 1

An Overview of ICAS-IPDC - A Software for Integrated Process Design and Controller Design of Chemical Processes
Mohd. Kamaruddin bin Abd. Hamid ····· 3

Systematic Procedure for Generating Operational Policies to Achieve Target Crystal Size Distribution (CSD) in Batch Cooling Crystallization
Noor Asma Fazli Bin Abdul Samad ····· 7

pH Catalysed Pretreatment of Corn Bran for Enhanced Enzymatic Arabinoxylan Degradation
Jane Agger ····· 11

Extraction and Production of Prebiotic and Hydrocolloids Oligosaccharides from Waste Streams from the Agricultural and Ingredient Industries
Hassan Ahmadi Gavlighi ····· 15

Modelling of Controlled Supply of Substrate Using Solid Resins in Biocatalysis
Naweed Al-Haque ····· 17

Investigation of the Efficiency of Alternative Enzyme Production Technologies
Mads Orla Albæk ····· 19

Assessment of Algae Productivity Responses and Biomass Potentials
Marcel Tutor Ale ····· 21

Multi-enzyme in-pot Processes in the Application of Synthetic Cascade Reactions
Paloma Andrade Santacoloma ····· 23

Characterization and Quantification of Deposits Build up and Removal in Straw Suspension-Fired Boilers
Muhammad Shafique Bashir ····· 25

Experimental Determination, Modeling and Utilization of the Phase Behavior in the Selective Oxidation of Alcohols in Pressurized CO_2
Matthias Josef Beier ····· 29

Monitoring Continuous Fermentation Processes in Microbioreactor Systems
Andrijana Bolic ····· 31

Oxy-Fuel Combustion of Coal
Jacob Brix ····· 33

Moving from Batch towards Continuous Organic-Chemical Pharmaceutical Production
Albert E. Cervera Padrell ····· 37

Novel Reactor Design for Organic-Chemical Crystallization of Active Pharmaceutical Ingredients
Joussef H. Chaaban ····· 41

Enzymatic Production of Prebiotic Polysaccharides with Hydrophobic Decoration
Inês Rodrigues da Silva ····· 43

CO_2 Capture using Aqueous Ammonia
Victor Darde ····· 45

Lipid Processing Technology: Building a Multilevel Modeling Network
Carlos Axel Diaz-Tovar ····· 49

Thermodynamic Properties from Fluctuation Solution Theory
Martin D. Ellegaard ····· 53

A Biomimetic Material based on Cinnamic Acid Derivatised Poly(Ethylene Glycol)
Sarah Maria Grundahl Frankær ····· 55

Process Design of Chemo-enzymatic Synthetic Cascades
Wenjing Fu ····· 59

Computer-Aided Modelling for Efficient and Innovative Product-Process Engineering
Martina Heitzig ····· 63

Thermodynamic and Process Modelling of Gas Hydrate Systems in CO_2 Capture Processes
Peter Jørgensen Herslund ····· 67

Enzymatic Production of Prebiotics from Sugar Beet Pectin
Jesper Holck ····· 69

Elongational Dynamics of Low Density Polyethylene
Qian Huang ····· 73

Model Based Integrated Product-Process Design
Amol Shivajirao Hukkerikar ····· 75

Nanoparticle Design using Flame Spray Pyrolysis for Catalysis
Martin Høj ····· 77

Effect of Biomass Mineral Matter on the Pyrolysis Product Yields
Norazana binti Ibrahim ····· 79

Compositional Simulation of In-Situ Combustion EOR
Priyanka Jain ····· 83

Population Balance Models and Computational Fluid Dynamics: an Integrated Model Framework to Describe Heterogeneity in Fermentors
Rita Lencastre Fernandes ····· 85

CO_2 Capture from Flue Gas using Amino Acid Salt Solutions
Benedicte Mai Lerche ····· 89

Nanoporous Membranes with Tunable Surface Morphology
Li Li ····· 91

Development of An Integrated Downstream Processing for Biocatalytic Reactions
Watson Neto ····· 95

Guiding Biocatalytic Processes Improvements Using Engineering Evaluation Tools
Joana de Lima Ramos ····· 97

Development of a Systematic Synthesis/ Design Methodology to Achieve Process Intensification
Philip Lutze ····· 99

Mercury Chemistry in Flue Gas
Karin Madsen ····· 103

Development of an Electrolyte CPA Equation of State for Applications in the Petroleum and Chemical Industries
Bjørn Maribo-Mogensen ····· 105

Production and Purification of Prebiotic Oligosaccharides by Chromatography and Membrane Systems
Malwina Michalak ····· 107

A Methodology for Systematic Design and Selection of Green Solvents for Increased Yield in Organic Reactions
Igor Mitrofanov ····· 109

Mathematical Modeling of Solid Oxide Fuel Cells
David Mogensen ····· 111

Catalytic Upgrading of Bio-oil
Peter Mølgaard Mortensen ····· 115

Heterogeneously Catalysed Aldol Reactions in Supercritical Carbon Dioxide
Nikolai E. Musko ····· 117

Analysis of Group Contribution^{Plus} Models for Property Prediction of Organic Chemical Systems
Azizul Azri Bin Mustaffa ····· 119

Self-Healing Anticorrosive Coatings
Tatyana Nesterova ····· 123

Fuel Flexible Rotary Kilns for Cement Production
Anders Rooma Nielsen ····· 125

Fuel Flexible Burners for Cement and Mineral Industry
Linda Nørskov ····· 127

Processes for Low CO_2 Emissions
Sharat Kumar Pathi ····· 129

High-Temperature Entrained Flow Gasification of Biomass
Ke Qin ····· 131

Incremental Refinement of Process Design
Alberto Quaglia ····· 135

Preheater Design for High Energy Efficiency and Low Emissions
Claus Maarup Rasmussen ····· 137

Size Exclusion Chromatography for the Quantitative Profiling of the Enzyme Catalyzed Hydrolysis of Xylo-oligosaccharides
Louise E. Rasmussen ····· 139

Reduction of SO_2 Emission from Modern Cement Plants
Martin Hagsted Rasmussen ····· 143

Distribution of Complex Chemicals in Oil-Water Systems
Muhammad Riaz ····· 145

A Model-Based Generic Framework for Design and Development of Integrated Enzymatic Processes
Alicia Román-Martínez ····· 149

Thermodynamic Modeling of Water-Acid gases-Alkanolamine Systems
Negar Sadegh ····· 153

Pretreatment of Biomass for the Use of 100% Renewable Fuels on Suspension Fired Boiler
Suriyati binti Saleh ····· 155

Enhanced Oil Recovery with Single Component Surfactant Flooding
Sara Bülow Sandersen ····· 157

Investigation of the Reaction Mechanism and Kinetics During the Clinkerization of Cement Raw Meal at High Temperatures and Improvement of the Burning Technology
Samira Telschow ····· 161

Maximal Release of Highly Bifidogenic Soluble Dietary Fibers from Industrial Potato Pulp by Minimal Enzymatic Treatment
Lise Vestergaard Thomassen ····· 165

Oxy-Fuel Combustion of Coal and Biomass
Maja Bøg Toftegaard ····· 167

Catalytic Steam Reforming of Bio-Oil to a Hydrogen Rich Gas
Rasmus Trane ····· 171

Validation of Structured Model for Autotrophic Nitrogen Removal in High Strength Wastewater
Anna Katrine Vangsgaard ····· 173

Sustainability and Catalytic Conversion of Bio-Ethanol on a Cu Catalyst
Bodil Voss ····· 175

Co-combustion of Fossil Fuels and Waste
Hao Wu ····· 177

Supported Cu-Ni Catalysts for CO Hydrogenation
Qiongxiao Wu ····· 181

Process Technology for Lipase-catalyzed Reactions
Yuan Xu ····· 183

Modeling Reservoir Formation Damage due to Water Injection for Oil Recovery
Hao Yuan ····· 185

Membrane Assisted Enzyme Fractionation-using amino acids as a model
Linfeng Yuan ····· 189

Tailor-made Design of Chemical Products: Bio-fuels and Other Blended Products
Nor Alafiza Yunus ····· 193

Advanced Waterflooding in Low Permeable Carbonate Reservoirs
Adeel Zahid ····· 195

Activity and Stability of Feruloyl Esterase A from Aspergillus niger in Ionic Liquid Systems
Birgitte Zeuner ····· 199

Multiphase Flow in Porous Media
Xuan Zhang ····· 201

Mercury Removal from Cement Plants by Sorbent Injection upstream of a Pulse Jet Fabric Filter
Yuanjing Zheng ····· 205

Preface

In the Graduate Schools Yearbook 2010 our PhD students present their individual projects. Some of the students have just initiated their research and therefore provide a short description of their research in the Yearbook, whereas others are close to concluding their work and present the most significant project results. We hope that the readers will find the Yearbook interesting and we invite you to contact us in case you would like to receive more details.

The PhD projects cover activities in the traditional core disciplines of Chemical Engineering combined with applications in polymer chemistry and technology, chemical product design, high temperature processes, combustion and gasification of renewable resources, biorefineries and biocatalysis, enhanced oil recovery, pharmaceutical engineering, process analytical technology, environmental technology and of course process technology, to name some examples. Many of the projects are carried out in close cooperation with industrial enterprises, and we have succeeded to increase the number of PhD students at the department substantially during the past years. This way we soon expect to reach a population of 100 PhD students. We expect to maintain this high activity level for the years to come and to secure high quality students by recruiting from all over the world.

We wish you a pleasant reading.

Yours Sincerely

Kim Dam-Johansen
Professor, Head of Department

Krist V. Gernaey
Associate Professor, Editor

Dayang Norulfairuz Abang Zaidel
Phone: +45 4525 2861
E-mail: daz@kt.dtu.dk
Discipline: Enzyme Technology

Supervisors: Anne S. Meyer

PhD Study
Started: August 2008
To be completed: July 2011

Enzymatic Production of Cross-linked Plant Cell Wall Polymers

Abstract
This PhD project is based on the premise that improved emulsification and prebiotic effects in sugar beet pulp (SBP) and barley spent grain (BSG) can be achieved by cross-linking of feruloylated polysaccharide structures. The aims of the project are to establish the kinetic basis of the cross-linking reactions and characterize the macromolecular function of the resulting cross-linked polysaccharides in terms of their rheological properties and emulsion stabilizing effects.

Introduction
Recently, it has been recognized that polysaccharides, categorized as dietary fibres and prebiotic oligosaccharides, may exert potential physiological benefits beyond their classical effects. For instance, their ability to bind bile acids, cholesterol, and toxic compounds present in the digestive tract suggest that a number of oligosaccharides and polysaccharides may have an important preventative role against various chronic diseases such as coronary heart disease [1].

It is well established that many plant cell walls contain phenolic acids that are ester-linked to polysaccharides. They are mainly ester-linked to *0*-2 of the α-(1→5)-linked arabinan chains and to *0*-6 of β-(1→4)-linked type I of galactan chains [2]. It was reported that ferulic acid esters in plant cell walls could undergo oxidative coupling reactions to form dehydromers (diFAs) [2-4]. This oxidative reaction can be catalyzed by various systems such as peroxidases (with hydrogen peroxide), polyphenol oxidases, including laccases, as well as some purely chemical systems [4]. From these reactions various diFAs are formed: 5-5′, 8-O-4′, 8-5′ and 8-8′ (Figure 1). Formation of diFA enables covalent cross-linking of the polysaccharides they esterify. The previous studies indicated that the feruloylated polymers have an effect on the mechanical properties of plant cell wall *i.e.* a tightening effect on the plant cell wall (contributing to wall assembly, promotion of tissue cohesion and resistance against fungal penetration). This project is built on the premise that the cross-linked polysaccharides are able to enhance the emulsification stability of the polysaccharides [5].

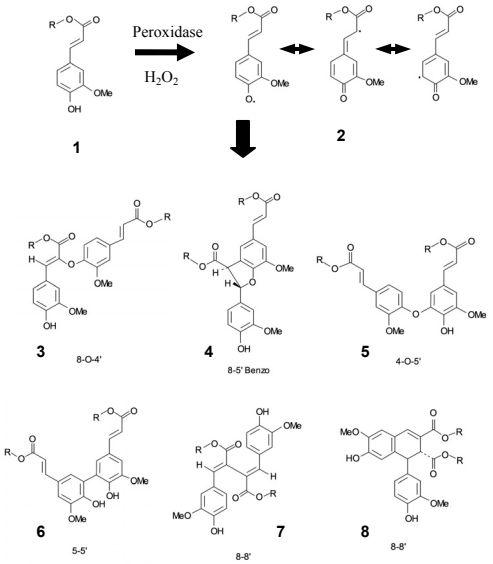

Figure 1: Dimerization of ferulate esters **1** via phenoxy radical **2** which react to form dehydrodiferulate esters **3-8** [4,6].

Objectives
The first objective of this project is to establish and describe the kinetic reactions of the enzymes involved in the *in vitro* cross-linking of the polysaccharides with the various substrates. It is expected that the concentration of ferulic acid substrate and the size of the substrate affect the kinetics of the enzymatic reaction. The second objective is to characterize the macromolecular properties of the cross-linked

polysaccharides in terms of rheological measurements and then establish the correlation between the macromolecular function of the cross-linked polysaccharides and the reaction kinetics. Finally, it is aimed to investigate the effect of emulsification stability of the cross-linked polysaccharide.

Current Work

In this work, cross linking of ferulic acid (FA) in arabinan sample was done by the addition of horseradish peroxidase (HRP) and hydrogen peroxide H_2O_2. The cross-linking was monitored by the disappearance of FA absorbance at 316 nm for 10 minutes. The absorbance decreased steeply at the beginning of the reaction and then decreased more gradually until it reached a stationary state (Figure 2).

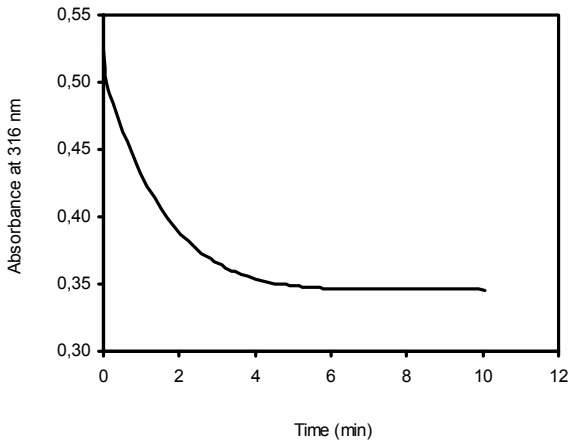

Figure 2: Influence of HRP/H_2O_2 addition on the absorbance of 0.50 g/L arabinan from SBP at 316 nm

From HPLC analysis, total FA content in the untreated arabinan residues extracted by saponification was about 1.5 mg/g dry matter. Naturally occurring diFAs was detected before the cross-linking. It was found that the amount of FA in the arabinan decreases about 90% and diFAs increases after the cross-linking. This indicates that the ferulic acid was cross-linked to produce ferulate dimers by addition of HRP and H_2O_2 as shown by the decreasing in absorbance.

Conclusion and Future Work

From this project, it is expected that a new enzymatic biocatalytis process will be developed, with a better understanding of the kinetics in order to improve the cross-linking of polysaccharides. This study will provide a distinctive contribution in the application of biological processes for the knowledge-based production of food ingredients, notably health promoting products. The knowledge gained will improve fundamental understanding of the molecular and kinetic basis of specific enzyme catalyzed processes.

Future work will be directed towards the establishment of enzyme kinetics of the cross-linked polysaccharides and their correlations with the macromolecular properties and emulsification stability.

Acknowledgement

The author would like to acknowledge Universiti Teknologi Malaysia, Skudai and the Ministry of Higher Education, Malaysia for their financial support.

References

1. T. Jalili, R.E.C. Wildman, Journal of Nutraceuticals, Functional & Medical Foods 2(4) (2000) 19-34.
2. M.C. Ralet, G. Andre-Leroux, B. Quemener, J.F. Thibault, Phytochemistry 66 (2005) 2800-2814.
3. K. Nishitani, D.J. Nevins, Plant Physiol. 93 (1990) 396-402.
4. L. Saulnier, J–F. Thibault, J. Sci. Food Agr. 79 (1999) 396-402.
5. F. Littoz, D.J. McClements, Food Hydrocolloid 22(7) (2008) 1203-1211.
6. J. Ralph, S. Quideau, J.H. Grabber, R.D. Hatfield, Journal of Chemical Society Perkin Transactions 1. The Royal Society of Chemistry. (1994). 3485-3498.

Mohd. Kamaruddin bin Abd. Hamid
Phone: +45 4525 2912
E-mail: mka@kt.dtu.dk
Discipline: Systems Engineering

Supervisors: Rafiqul Gani
Gürkan Sin

PhD Study
Started: July 2007
To be completed: January 2011

An Overview of *ICAS-IPDC* - A Software for Integrated Process Design and Controller Design of Chemical Processes

Abstract
The objective of this contribution is to introduce software that has been developed based on a new systematic model-based methodology for performing integrated process design and controller design (*IPDC*) [1] of chemical processes. The software called *ICAS-IPDC* has been implemented into a systematic computer-aided framework within which the *VBA* (visual basic for applications) programming language with Microsoft Excel interface is used. The *ICAS-IPDC* framework is overviewed together with the main features of the software. *ICAS-IPDC* allows simple, accurate and faster analysis of the *IPDC* problem of chemical processes, which helps in obtaining the optimal solution of the complex *IPDC* problem easily.

Introduction
A new model-based methodology for performing integrated process design and controller design (*IPDC*) has been proposed [1]. The developed methodology is capable of identifying and obtaining an optimal solution for *IPDC* problem for chemical processes in an easy, simple and efficient way. The methodology is based on decomposition of the complex *IPDC* problem into four sequential hierarchical sub-problems: (i) pre-analysis; (ii) design analysis; (iii) controller design analysis; and (iv) final selection and verification. In the pre-analysis sub-problem, the concepts of attainable region (*AR*) and driving force (*DF*) are used to locate the optimal process-controller design solution in terms of optimal condition of operation from design and control viewpoints. While other optimization methods may or may not be able to find the optimal solution, depending on the performance of their search space algorithms and computational demand, the use of *AR* and *DF* concepts is simple and able to find at least near-optimal designs (if not optimal) to *IPDC* problems. Please refer to [1] for more details of this methodology.

Specific Objective
The objective of this contribution is to overview software that has been developed based on a new systematic model-based methodology for *IPDC* [1]. The contribution will highlight the software framework together with its main features.

An Overview of *ICAS-IPDC*
The developed methodology [1] has been implemented into a systematic computer-aided framework to develop software which is called *ICAS-IPDC* for solving *IPDC* problems for chemical processes. The *VBA* (visual basic for applications) programming language with Microsoft Excel interface is used to develop the *ICAS-IPDC*.

A *Start Menu* (see Fig. 1) has been created to be the starting interface of the software. It can be seen in Fig. 1 that the starting point for the software is to select one of the three different systems; i) a single reactor (*R*) system, ii) a single separator (*S*) system, and iii) a reactor-separator-recycle (*RSR*) system by clicking on the system button. There are also three info buttons located at the left side of the *Start Menu* interface, which are “Software Overview”, “User’s Manual”, and “Tutorials”. A “Software Overview” button will show the software framework as shown in Fig. 2. This framework, which is based on the developed methodology [1], illustrates the step-by-step algorithm that has been implemented into this software. The “User’s Manual” button will describe the details of each implemented step, whereas the “Tutorials” button will guide the user to understand/how to apply the software through solved case studies.

***ICAS-IPDC* Framework**
Fig. 2 shows the framework overview of the *ICAS-IPDC* software. It can be seen that once the option either to open/create a case study has been selected the

user will be guided to the step-by-step algorithm (from step 1 until step 6.2) sequentially. At the left side of the framework, the equations used at every steps of this software are presented. These equations are basically the constraints of the optimization problem (see problem formulation equation at the top-right of the framework) that has been decomposed into several stages. For example, the identification of the design-control solution in step 3.3 will require Eq. (3) which is the constitutive constraints. It should also be noticed that at the right side of the framework, the results buttons are located which is once clicked, the results for that specific step will be shown. This will help users to review the results easily without going into the details of each step. In addition, the supporting tools used with this software are also shown in the right side of the framework. The supporting tool such as *ICAS-MoT* [2] is used for the process model simulation, and *MoT-Excel* interface is used to communicate between *ICAS-MoT* and *Excel*.

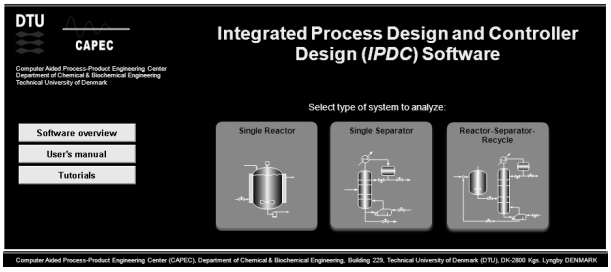

Fig. 1: A Start Menu interface of *ICAS-IPDC* software.

A "Main Menu" (see Fig. 3) has been created to be the general main menu interface of the software. The "Main Menu" performs all steps that have been outlined in Fig. 2. It can be clearly seen from Fig. 3 that the "Main Menu" is divided into five sequential parts: Part I – Problem definition, Part II – Pre-analysis stage, Part III – Design analysis stage, Part IV – Controller design analysis stage and Part V – Final selection and verification. In order to solve an *IPDC* problem, the user needs to perform all parts sequentially. The built-in color code system together with the conditional logic (if-then rule) guides the user through the different steps.

As shown in Fig. 3, the *ICAS-IPDC* framework needs to be performed sequentially. The user needs to complete Part I first, where the user will ask to supply some information about the system to be analyzed. This can be done by clicking button "1.1 Problem Definition", and "Problem Definition" interface for a single reactor system will appear as shown in Fig. 4. It can be seen from Fig. 4, there are two frames in the "Problem Definition" interface, which are "Problem Definition" and "Process Flow Diagram". The "Problem Definition" frame is where the user will perform selection of components, reactants and products (for a single reactor system) or selection of components, top products and bottom products (for a single separator system). It can clearly be seen that for a single reactor system, only three buttons which related to a reactor are active.

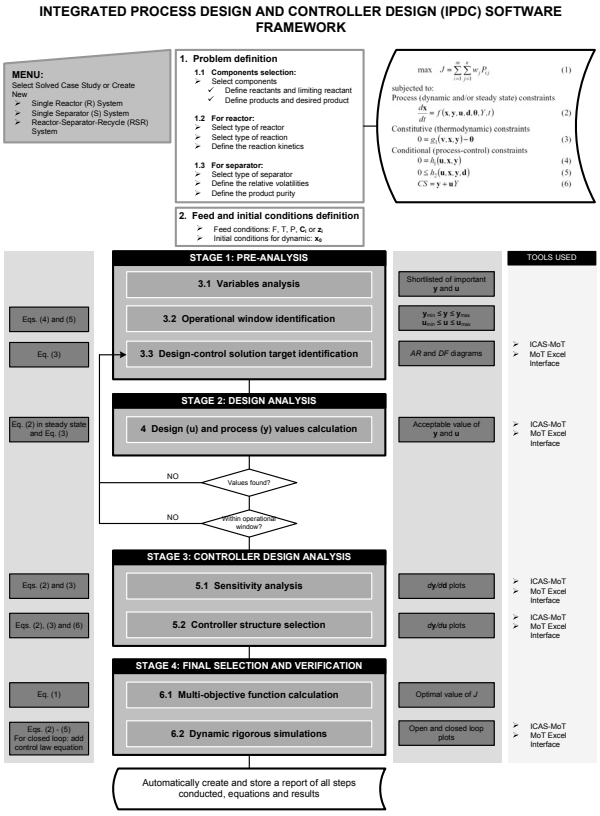

Fig. 2: *IPDC* framework implementation to the *ICAS-IPDC* software.

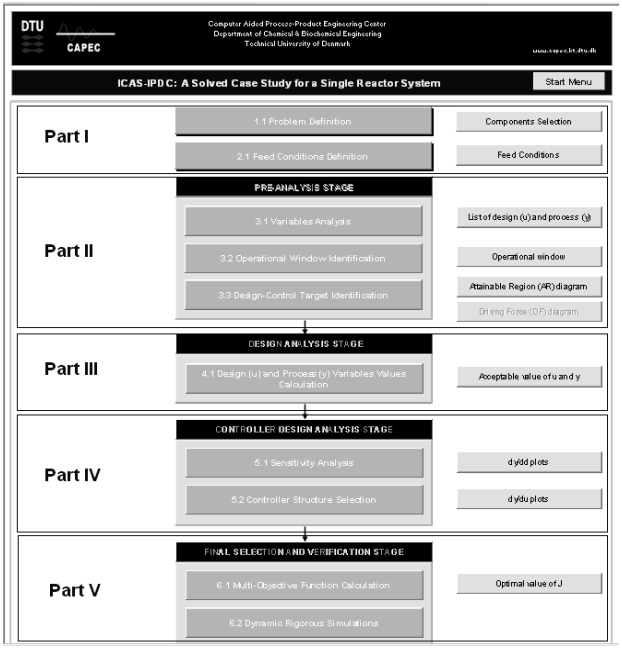

Fig. 3: A Main Menu interface of the *ICAS-IPDC* software.

The second frame is called "Process Flow Diagram" in where the process flow diagram of the analyzed system is shown. In this example, the process flow diagram of a reactor system is shown (see Fig. 4).

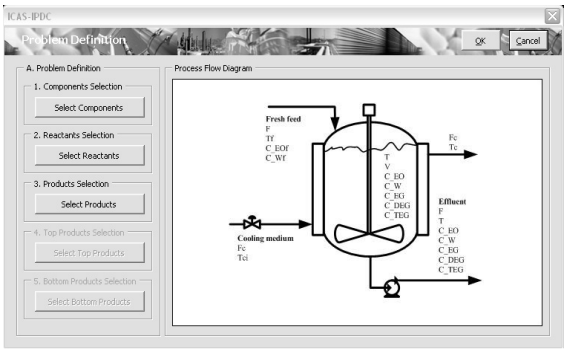

Fig. 4: Problem definition interface for a single reaction system.

Once all information required has been supplied, the user can click the "OK" button at the right-top corner of the interface. This will save all the information in the corresponding worksheet (sheet 1.1 for this example) and then change the button "1.1 Problem Definition" color into dark blue, indicates that step 1.1 has been completed as shown in Fig. 5. Then, users are required to perform step 2.1 in order to complete Part 1. Once Part I is completed, users need to perform all the remaining steps until all parts are completed. Users will know either all steps have been completed or not by make sure that all buttons colors are changed into a dark blue (see Fig. 5).

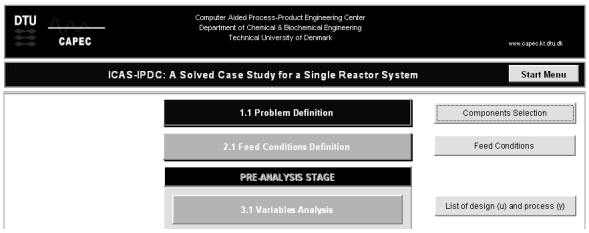

Fig. 5: Updated Main Menu with completed step 1.1.

ICAS-IPDC Main Features

The main features of the *ICAS-IPDC* are overviewed in this section.

User Guide Alerts

As mentioned previously, all steps shown in Fig. 3 should be performed sequentially. This software capable to give the user an alert (warning) if they are not followed the sequences or accidently clicked the wrong button as shown in Fig. 6. The main idea is to make sure that the user follows exactly the software framework in the right way. As can be seen in Fig. 6, the software gives an alert when the user clicked the button "3.1 Variables Analysis" which is not in the sequence. Once completed step 1.1, the user needs to perform step 2.1 to complete Part I. If the user clicks other buttons that are not in the sequence, the alert will be given. The alert also provides suggestion for the user which step he/she needs to perform.

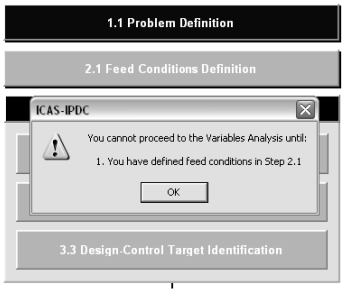

Fig. 6: User guide alert feature in *ICAS-IPDC*.

Results Review

Another feature that available in this software is the option for the user to review the results for the corresponding completed step. This can be accomplished by clicking on the button at the right side of the completed step (see Fig. 5). In Fig. 5, step 1.1 (Problem Definition) has been completed (which indicated by the dark blue color). By clicking the "Components Selection" button, results that have been saved are presented as shown in Fig. 7. The advantage of this feature is that it helps the user to review the results easily without go into the details of each steps. This will enable the user to verify the results before going further to the next steps.

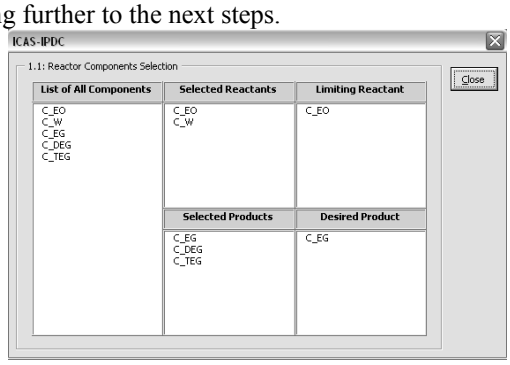

Fig. 7: Results review of the completed step.

Charts User Interface

One of the important features available within the *ICAS-IPDC* software is called Charts User Interface. This interface provides the user to analyze and manipulate charts as illustrated in Fig. 8. It can be seen from Fig. 8 that there is frame in which the user can format the axis of the chart. In addition, the user also can perform some analysis from the chart such as calculation of the first-order-plus-time-delay (*FOPTD*) model parameters and calculation of the controller tuning parameters as shown in Fig 8.

Calculation Progress Monitor

ICAS-IPDC software deals with lots with calculations in which some may require a big number of iterations. Because of this reason, some calculation can take a longer time to perform than others. Therefore, it is important to monitor the progress of this calculation such that the user will have information about the duration or time required to perform such calculation. In

this software, all calculation that required *MoT* model will be monitored as the one shown in Fig. 9.

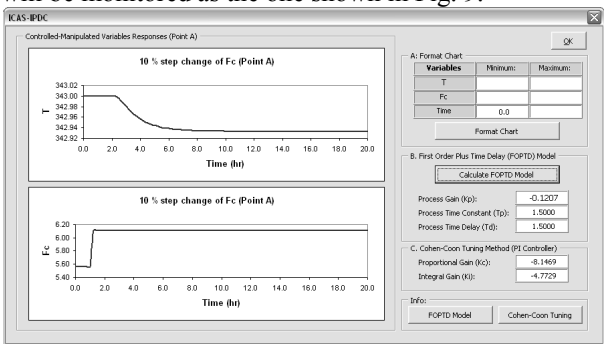

Fig. 8: Charts user interface within the *ICAS-IPDC* software.

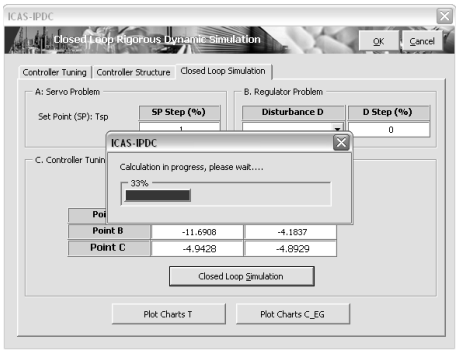

Fig. 9: Calculation progress monitor during closed loop simulation.

ICAS-MoT Model Interface

In this software, models used within the developed *IPDC* methodology which are simulated using *ICAS-MoT* can be integrated into the *ICAS-IPDC* interface using *MoT Model Interface* as illustrated in Fig. 10. *MoT Model Interface* is an Excel-based interface which is integrated with the *MoT* solver as well as connected with the *MoT* model.

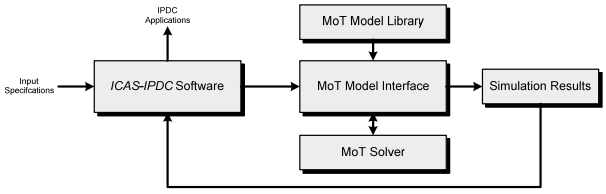

Fig. 10: Workflow of the integration of *ICAS-IPDC* interface with *MoT* models through *MoT* Model interface.

Conclusion

In this contribution, software called *ICAS-IPDC* has been overviewed. *ICAS-IPDC* is based on the developed *IPDC* methodology [1], which guides the user through each methodology steps. Developed within VBA-Excel based environment offers the user of *ICAS-IPDC* a customized graphical user interface-spreadsheets looks software that fully used of spreadsheets features such as graphing tools. Integrated to a set of supporting tools such as *ICAS-MoT* and Excel-based *MoT Model Interface*, makes this software such a complete package for solving *IPDC* problem for chemical processes. By using *ICAS-IPDC,* the optimal solution of the complex *IPDC* problem can easily and accurately be obtained. *ICAS-IPDC* allows simple, accurate and faster analysis of the *IPDC* problem for chemical processes. The software is generic and its applicability can be extended to any chemical (biochemical) processes.

References

1. M.K.A. Hamid, G. Sin, R. Gani, Comput. Chem. Eng. 34 (5) (2010) 683-699.
2. A.M. Salez-Cruz, Development of a computer aided modeling system for bio and chemical process and product design. Ph.D. Dissertation Thesis, 2006, Technical University of Denmark.

List of Publications

1. M. Alvarado-Morales, M.K.A. Hamid, G. Sin, K.V. Gernaey, J.M. Woodley, R. Gani, Comput. Chem. Eng. 34 (12) (2010) 2043-2061.
2. M.K.A. Hamid, G. Sin, R. Gani, Comput. Chem. Eng. 34 (5) (2010) 683-699.
3. M.K.A. Hamid, G. Sin, R. Gani, in: M. Kothare, M. Tade, A. Van de Wouwer, I. Smets (Eds.), Proceedings of the 9th. International Symposium on Dynamics and Control of Process Systems (DYCOPS 2010), 2010, p. 449.
4. M.K.A. Hamid, G. Sin, R. Gani, in: Proceedings of Dansk Kemiingeniørkonference (DK2-2010), 2010, p. 148.
5. M. Alvarado-Morales, M.K.A. Hamid, G. Sin, K.V. Gernaey, J.M. Woodley, R. Gani, in: R.M. de Brito Alves, C.A. Oller do Nascimento, E.C. Biscia Jr. (Eds.), Computer-Aided Chemical Engineering, 27 (Part A), Elsevier B. V., Amsterdam, 2009, p. 237.
6. M.K.A. Hamid, G. Sin, R. Gani, in: J. Jezowski, J. Thullie (Eds.), Computer-Aided Chemical Engineering, 26, Elsevier B. V., Amsterdam, 2009, p. 839.
7. M.K.A. Hamid, G. Sin, R. Gani, in: M.M. El-Halwagi, A.A. Linninger (Eds.), Design for Energy and the Environment, CRC Press, 2009, p. 593.
8. M.K. Hamid, R. Gani, in: M. Ierapetritou, M. Bassett, E. N. Pistilopoulos (Eds.), Proceedings of the Fifth. International Conference on Foundations of Computer-Aided Process Operations (FOCAPO 2008), 2008, p. 205.

Noor Asma Fazli Bin Abdul Samad
Phone: +45 4525 2912
E-mail: nas@kt.dtu.dk
Discipline: Systems Engineering

Supervisors: Rafiqul Gani
Krist V. Gernaey
Gürkan Sin

PhD Study
Started: January 2009
To be completed: December 2011

Systematic Procedure for Generating Operational Policies to Achieve Target Crystal Size Distribution (CSD) in Batch Cooling Crystallization

Abstract
A systematic model-based procedure to achieve a target crystal size distribution (CSD) under generated operational policies in batch cooling crystallization is presented. An analytical CSD estimator has been employed in the procedure to generate the necessary operational policies to achieve the target CSD. Furthermore, this systematic procedure has been integrated with a generic multi-dimensional model-based framework. The generic nature of the model-based framework allows the study of a wide range of chemical systems under different operational scenarios, enabling thereby, the analysis of various crystallization operations and conditions. Therefore this generic multi-dimensional model-based framework can be used to generate "specific" models for crystallization processes and further verify the operational policies generated by the analytical CSD estimator for achieving the targeted CSD consistently. The application of the systematic procedure is illustrated for a potassium dichromate case study.

Introduction
Batch cooling crystallization is one of the important unit operations involving separation of solid-liquid phases. Usually the most common crystal product qualities are directly related to the crystal size distribution (CSD) [1]. However the main difficulty in batch cooling crystallization is to obtain a uniform and reproducible CSD [2]. Therefore supersaturation control can be applied to drive the process within the metastable zone and thereby enhance the control of the CSD. Although this approach has been shown to produce high quality crystals, the set point operating profiles for the supersaturation controller are usually chosen arbitrarily or by trial-and-error [3]. Therefore there is a need for a systematic procedure to generate operational policies that guarantee that the target CSD can be achieved consistently. Furthermore, to predict the desired crystal morphology by means of model-based approaches, appropriate models covering the effects of the various operational parameters on the behavior of the crystals are necessary. That is, a generic multi-dimensional model-based framework that covers a wide range of crystallization models and operational scenarios is needed.

The objectives of this work are to develop a systematic procedure for generating operational policies to achieve the target CSD for batch cooling crystallization processes. In this procedure, an analytical CSD estimator will be employed to generate an operational policy. The estimator is based on the assumptions of constant supersaturation and an operation that is dominated by size dependent growth [2]. The generated operational policy provides the supersaturation set point and by maintaining the operation at this point, a target CSD is achieved. However the main weakness in the analytical CSD estimator is the estimator's capability to generate any operational policy achieving the target CSD without the ability to identify the best operational policies. To overcome this limitation, different operational policies that yield the same target CSD are also generated using this analytical CSD estimator and validated with closed-loop control. The validation requires a "specific" model to represent the operation. For this purpose, the generic multi-dimensional model-based framework for batch cooling crystallization processes has been developed [4] and integrated with the systematic procedure. Through this generic multi-dimensional model-based framework, a "specific" model can be generated and used for closed loop control to verify the operational policies. Finally the performance of simulation models and the analytical estimator will be compared and analyzed in terms of the CSD obtained. Additional information regarding the total crystal mass is also targeted here, which is a novelty compared to earlier works [2]. Therefore the best operational policies will be selected in term of CSD

obtained compared to the target and total crystal mass. The integration of generic multi-dimensional models with systematic procedure to achieve target CSD based on analytical estimators is highlighted using potassium dichromate as a case study.

Systematic Procedure for Generating Operational Policies to Achieve Target Crystal Size Distribution

An overview of the systematic procedure to generate and employ operational policies is shown in Fig. 1 where the generic multi-dimensional model has been integrated to the systematic procedure.

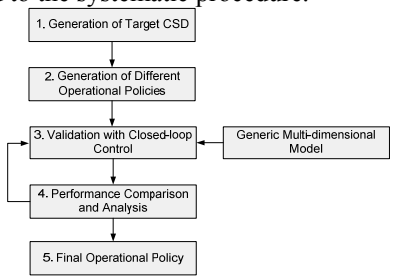

Fig. 1: Systematic procedure for generating operational policies

The starting point of this systematic procedure is the generation of the target CSD. The operational policy to obtain a target CSD can be generated by employing an analytical CSD estimator [2]. This analytical CSD estimator consists of 2 main equations as follows:

$$f_n = f_{n0}\left(1+\frac{\gamma(1-p)k_g S^g t}{(1+\gamma L_0)^{1-p}}\right)^{\frac{p}{p-1}} \quad (1)$$

$$L = \frac{\left(\gamma(1-p)k_g S^g t+(1+\gamma L_0)^{1-p}\right)^{\frac{1}{1-p}}-1}{\gamma} \quad (2)$$

Where f_n is the target CSD, f_{n0} is the CSD of the initial seed, k_g is the growth rate constant, γ and p are the growth constants, g is the growth order constant, t is total crystallization time, S is the supersaturation, L_0 is the initial characteristic length, and L represents the final characteristic length.

The target CSD is obtained by specifying the initial characteristic length and initial seed of the CSD as well as kinetic growth parameters. Meanwhile the kinetic growth parameters are obtained from the chemical system that needs to be investigated. In this way, the supersaturation set point and total crystallization time needed to achieve the target CSD can be obtained. This supersaturation set point represents the operational policy that needs to be maintained during the crystallization operation in order to achieve the target CSD. Then a different operational policy that also yields the same target CSD needs to be generated from the analytical CSD estimator. The idea behind the generation of different operational policies is to identify the best policies to achieve the target CSD during closed loop simulation. Usually, the generation of different operational policies is done by choosing either (a) the operation close to the saturation line, or (b) close to the metastable limit, else (c) in the middle between the saturation line and the metastable limit. All of the operational policies will then be simulated in closed-loop simulation in order to validate the target CSD given by the analytical CSD estimator. Furthermore the information on total crystal mass can be obtained during closed-loop simulation which overcomes the limitation of the analytical CSD estimator to provide this information. In order to perform closed-loop simulation, a full mathematical model representing the specific system to be studied is needed.

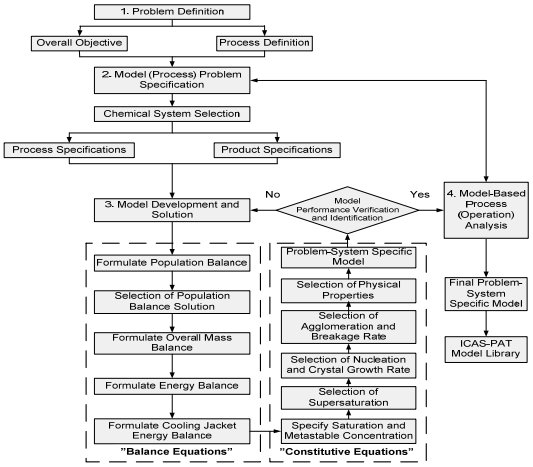

Fig. 2: Generic multi-dimensional model-based framework [4]

For this purpose, a generic multi-dimensional model-based framework (Fig. 2) has been developed to create the specific models which are needed to describe various crystallization processes based on the generic batch cooling crystallization model [4]. There are 4 main steps through which the problem-system specific model is created on the basis of the generic multi-dimensional model-based framework. The first step is the problem definition for the crystallization process under study: the overall objective of the study is defined, and process definition of the specific crystallization process being investigated is provided. The step 2, problem specification, involves the selection of the chemical system that needs to be studied and the collection of the relevant information about the process and the product. The third step is concerned with the listing of the necessary balance and constitutive equations needed to model the crystallization process. The balance equations consist of population, overall mass and energy balances for the defined crystallization volume supplemented with energy balance equations for the cooling jacket. The constitutive equations contain a set of models describing nucleation, crystal growth rate, supersaturation, saturation and metastable concentration as well as physical properties corresponding to different types of chemical systems found in the crystallization processes. More detailed about the generic balance and constitutive equations can be found in [4]. Subsequently a problem-system specific model is created which is verified through process (operation) analysis (step 4). If the specific model is satisfactory with respect to the desired performance, then it is included in the model library. In this way, the generic model is adapted to reflect a specific case study and thereby allows the

analysis of various crystallization operations and conditions.

The complete set of mathematical models for a specific model is then solved under closed loop simulation to verify the generated operational policies. Finally the CSD obtained from the verified simulated operation will then be compared with the target CSD and the total crystal mass obtained is analyzed. Subsequently the final operational policy will then be selected based on the best performance obtained during the performance comparison and analysis.

Case study: Potassium Dichromate Crystallization

The application of the systematic procedure to obtain the target CSD is highlighted using a potassium dichromate case study. The potassium dichromate crystallization process is adopted from the literature [2].

Step 1: Generation of target CSD

The initial seed of the CSD has been generated as a normal distribution by using a mean of 156.89 µm and a standard deviation of 43.75 µm. The target CSD and final characteristic length are then calculated by using the potassium dichromate growth parameters as well as the supersaturation set point of 0.029 g solute/g water and assuming a total crystallization time of 110 minutes. The initial seed and target CSD obtained from the analytical CSD estimator are shown in Fig. 3.

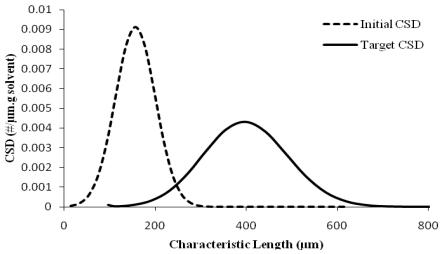

Fig. 3: Initial seed and target of the CSD

Step 2: Generation of different operational policies

By fixing the growth parameters and target CSD in the analytical CSD estimator, a new data set comprising of different values for the operation time and the supersaturation set point can be obtained as shown in Table 1. Each data set has been generated by choosing the operation close to the saturation line (data set 1), in the middle between the saturation line and the metastable limit (data set 2) and close to the metastable limit (data set 3).

Table 1: Data set for different operational policies

Data set	Supersaturation set point	Time (min)
1	0.0145	192
2	0.029	110
3	0.0435	80

Step 3: Validation with closed-loop control

In order to validate the operational policies generated by the analytical CSD estimator, a complete mathematical model for potassium dichromate will be generated using the generic multi-dimensional model-based framework. PI controller has been employed for all data sets in order to maintain the concentration of potassium dichromate at the generated set point. The potassium dichromate concentration initially started at 0.26 g solute/g water and the PI controller successfully maintained the concentration at the set point once the concentration set point was reached. In Fig. 4-6, approximately 0.07 g solute/g water (data set 1), 0.09 g solute/g water (data set 2) and 0.1 g solute/g water (data set 3) remains by the end of operation.

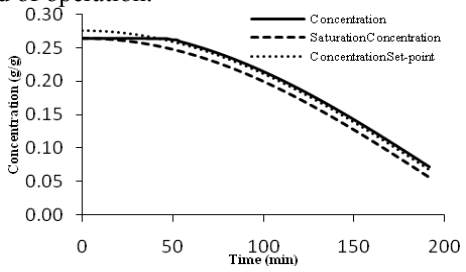

Fig. 4: Closed loop control for data set 1

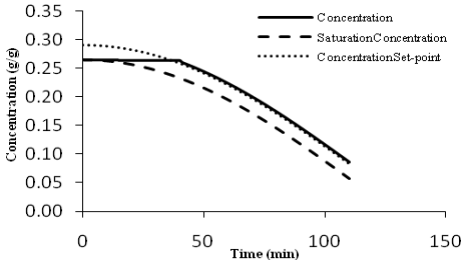

Fig. 5: Closed loop control for data set 2

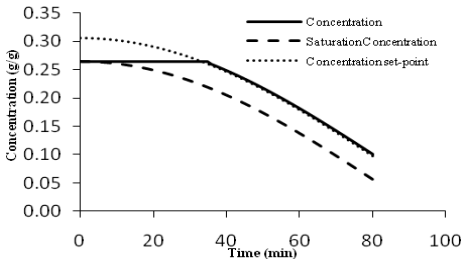

Fig. 6: Closed loop control for data set 3

Step 4: Performance comparison and analysis

In the step 3, all concentrations were maintained at the set point indicating that all operational policies were feasible. In order to determine the best operational policy to achieve the target CSD, the performance of the simulated operation is compared with the generated policy as highlighted in Fig. 7-9. A good agreement between both models was achieved in data set 1, i.e. the detailed simulation model predicted almost identical target CSD compared to the analytical estimator. In data set 2, only a slight difference can be observed (Fig. 8) between the simulated model and the analytical estimator. Nevertheless, the final CSD obtained from this simulated model is still in a reasonable range compared to the target CSD. However there are obvious differences between the simulated model and the analytical estimator for data set 3, as illustrated in Fig. 9. The final CSD obtained is rather far from the target

CSD obtained from the analytical estimator. Furthermore a secondary peak has been observed in the lowest part of the final characteristic length curve, indicating that a secondary nucleation has occurred in the operation. This is because the crystallizer has been operated close to the metastable limit, and thus secondary nucleation is expected. These phenomena however cannot be captured by the analytical estimator, which explains the mismatch between both CSD profiles in Fig. 9.

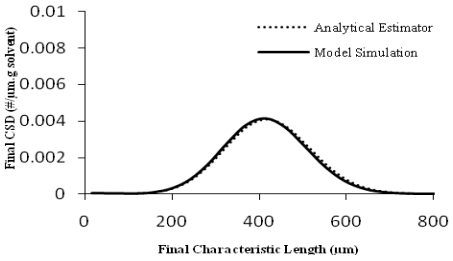

Fig. 7: Final seed of CSD for data set 1

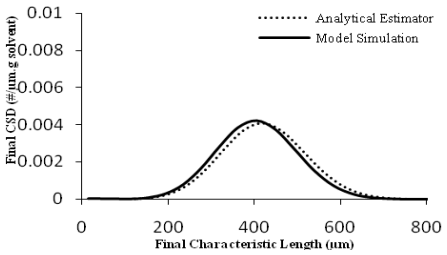

Fig. 8: Final seed of CSD for data set 2

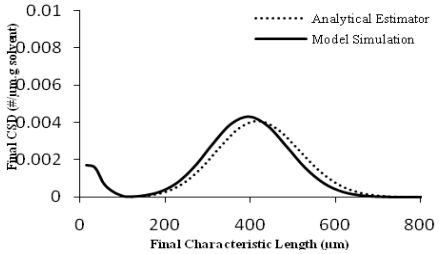

Fig.9: Final seed of CSD for data set 3

Table 2: Performance comparison

Data set	Final crystal mass (g)	Final average characteristic length (µm)
Analytical estimator	-	420.2629 (target)
1	20.08	412.8693
2	18.63	405.246
3	17.18	397.7542

The performance comparison of all data sets has been provided in Table 2. The data set 1 with lower supersaturation yields the highest total crystal mass approximately 20.08 g starting from an initial seed mass of 1.2 g. The data sets 2 and 3 produced about 18.63 g and 17.18 g of crystals respectively. In term of CSD, data set 1 produces the closest CSD compared to the target based on final average characteristic length followed by data set 2. Although data set 1 produces the best CSD compared to the target, and also has the highest total crystal mass obtained, the total crystallization time for this operation is too long (more than 3 hours). This is mainly because to the crystallizer has been operated close to the saturation line, and under such conditions it will take a long time to achieve the target CSD. If the total crystallization time is taken into consideration then the data set 1 will not be very practical since the operating costs typically increase the longer the batch runs. As an alternative data set 2 can be selected due to its reasonable operation time while the performance is still acceptable, producing a CSD that is close to the target CSD generated by the analytical CSD estimator. Meanwhile data set 3 is not considered here since it produced the lowest crystal mass and the CSD obtained far from the given target.

Conclusion

A systematic procedure to achieve a target CSD under generated operational policies has been developed for batch cooling crystallization processes. This systematic procedure has been integrated with generic multi-dimensional model-based framework to generate specific crystallization process operational models. The generation of operational policies involving an analytical CSD estimator has been illustrated using a potassium dichromate case study and the generic multi-dimensional model-based framework has been applied to generate a model for potassium dichromate crystallization. The generated operational policies have then been validated using closed-loop simulation, and the best operational policies were found to be capable of achieving the target CSD quite accurately as well as producing an acceptable total crystal mass.

Acknowledgements

The PhD project of Noor Asma FazliAbdul Samad is financed by a PhD scholarship from the Ministry of Higher Education of Malaysia and Universiti Malaysia Pahang (UMP).

List of Publications

1. N.A.F.A. Samad, R. Singh, G. Sin, K.V. Gernaey, R. Gani, Comput. Chem. Eng. 28 (2010), 613-618.
2. N.A.F.A. Samad, R. Singh, G. Sin, K.V. Gernaey, R. Gani, Special Issue of Comput. Chem. Eng. (2010) (Submitted).
3. N.A.F.A. Samad, R. Singh, G. Sin, K.V. Gernaey, R. Gani, ESCAPE-21 (2011) (Submitted).
4. N.A.F.A. Samad, R. Singh, G. Sin, K.V. Gernaey, R. Gani, ICMSAO (2011) (Submitted).

References

1. M.J. Hounslow, G.K. Reynolds, AIChE. J. 52 (7) (2006) 2507-2517.
2. E. Aamir, Z.K. Nagy, C.D. Rielly, T. Kleinert, B. Judat, Ind. Eng. Chem. Res. 48 (2009) 8575-8584.
3. E. Aamir, Z.K. Nagy, C.D. Rielly, Comput. Chem. Eng. 28 (2010), 763-768.
4. N.A.F.A. Samad, R. Singh, G. Sin, K.V. Gernaey, R. Gani, Special Issue of Comput. Chem. Eng. (2010) (Submitted).

Jane Agger
Phone: +45 4525 2943
E-mail: jag@kt.dtu.dk
Discipline: Enzyme Technology

Supervisors: Anne Meyer
Katja Salomon Johansen, Novozymes A/S

PhD Study
Started: March 2007
To be completed: March 2011

pH Catalysed Pretreatment of Corn Bran for Enhanced Enzymatic Arabinoxylan Degradation

Abstract
Corn bran is mainly made up of the pericarp of corn kernels and is a byproduct stream resulting from the wet milling step in corn starch processing. This study examined the optimization of pretreatment of corn bran for enzymatic hydrolysis through statistic modeling. A low pH pretreatment (pH 2, 150 ºC, 65 min) boosted the enzymatic release of xylose and glucose. With more acidic pretreatment the total xylose release was maximized (at pH 1.3) reaching ~50% by weight, but the enzyme catalyzed xylose release was maximal at approx. pH 2. The total glucose release peaked at pretreatment of approx. pH 1.5 with an enzymatic release of approx. 68% by weight of the original amounts present in destarched corn bran. For arabinose the enzymatic release was negatively affected by the acidic pretreatment as labile arabinosyl-linkages were presumably hydrolysed directly during the pretreatment. The work presented here is based on [1].

Introduction
Corn bran consists of the pericarp tissue, testa and pedicel tip of corn kernels [2] and is a by-product resulting from the wet milling step in corn starch processing. Corn bran is mainly made up of polysaccharides and is particularly rich in pentoses, i.e. arabinose and xylose. These C5 monosaccharides have the potential of being a resource for production of bioethanol, xylitol, and value added platform chemicals like furans, formic acid, and levulinic acid [3,4]. The arabinoxylan may even be upgraded to functional nano particle structures or bioactive food ingredients [5,6]. Arabinoxylan comprises up to 56% of the corn bran biomass dry matter [7] - with the rest of the dry matter being mainly made up of starch, cellulose and protein [8], in addition to 10% by weight of lignin [7]. Arabinoxylan from corn bran has proven recalcitrant to enzymatic degradation [9,10,11], a trait that has been attributed to its structural complexity, i.e. notably the various substitutions on the xylan backbone.

A form of hydrothermal pretreatment of corn bran before enzymatic hydrolysis seems indispensable at present and may be justified as long as the energy, chemicals, and process expenses do not exceed the final value of the corn bran products. However, the majority of studies reported on corn bran pretreatment have employed harsh pretreatment conditions with respect to temperature and chemical use leading to special process and equipment requirements. However, an overview of the exact influence of different pretreatment parameters (pH, temperature, and pretreatment time), and notably a quantitative understanding of their interactions to allow the design of mild, but efficient pretreatment of corn bran is lacking.

Specific objectives
In the present work, we hypothesized that an optimal pretreatment method could be developed by investigating the influence of pH, temperature and pretreatment time on the enzymatic accessibility of arabinoxylan, in particular evaluated through the assessment of the enzymatic release of xylose. The objective of the present study therefore was to test this hypothesis and at the same time assess the influence of the pretreatment parameters for subsequently achieving maximal enzymatic arabinoxylan hydrolysis.

Results and discussion
Monosaccharide release
The pretreatment conditions and the corresponding release of arabinose, xylose and glucose both from the pretreatments and from the subsequent enzymatic hydrolysis showed that the most drastic effects seemingly occurred in the pretreatment when pH was low. Thus the largest release of all three monosaccharides occurred at pH 2, where enzymatic

Table 1: Monosaccharide release from acidic and alkaline pH pretreatments and enzymatic hydrolysis. n.d.: not detected. Releases are given as % of that originally found in the material. pH measured after pretreatment.

Pretreatment conditions			Effects of pretreatment			Effects of enzymatic hydrolysis after pretreatment		
Temp. (ºC)	pH	Time (min)	Arabinose (%)	Xylose (%)	Glucose (%)	Arabinose (%)	Xylose (%)	Glucose (%)
100	6.7	10	n.d.	n.d.	n.d.	15.24	4.16	11.60
150	5.9	10	n.d.	n.d.	n.d.	18.74	5.23	16.70
100	7.0	120	n.d.	n.d.	n.d.	19.55	5.64	10.94
150	4.9	120	n.d.	n.d.	n.d.	20.62	5.63	18.33
100	1.9	65	11.1	0.40	n.d.	10.82	5.48	10.37
150	2.3	65	43.94	17.80	n.d.	9.35	25.25	64.50
100	9.8	65	n.d.	n.d.	n.d.	19.95	7.33	22.29
150	7.9	65	n.d.	n.d.	n.d.	22.17	9.75	30.42
125	1.8	10	12.72	0.48	n.d.	11.63	6.06	17.24
125	1.7	120	54.44	11.33	n.d.	1.39	23.87	63.71
125	9.8	10	n.d.	n.d.	n.d.	21.37	8.46	25.15
125	8.7	120	n.d.	n.d.	n.d.	26.27	10.25	13.62
125	6.4	65	n.d.	n.d.	n.d.	20.46	5.94	16.56

release of xylose was significantly enhanced to reach 25% (~94 g/kg DM, Table 1). The corresponding arabinose and glucose releases were 53% (142 g/kg DM) and 64% (151 g glucose/kg DM) respectively; in comparison, enzymatic release from unpretreated DCB resulted in liberation of only approx. 3% xylose and 12% of both arabinose and glucose (data not shown).

Significant amounts of arabinose were released during the acidic pretreatments (Table 1) and this resulted in low release by the subsequent enzymatic hydrolysis presumably because the pretreatments had scavenged the available substrate for the α-L-arabinofuranosidases. After alkaline pH pretreatment, release of monosaccharides was only obtained after enzymatic hydrolysis and not as a result of the pretreatments alone. The effects of alkaline pretreatment were not as prominent as for the acidic pH pretreatments. The highest enzymatic release of arabinose resulted in liberation of ~26% of that originally present in DCB, and was obtained after 2 hours of alkaline pretreatment.

An acid hydrolysis (HCl hydrolysis) of the solid fraction after pretreatment at low pH showed that 70-120 g/kg DM of xylose and only 10-25 g/kg DM arabinose remained in the insoluble fraction after these low pH pretreatments. A similar acid hydrolysis of the solid fraction after alkaline pretreatment showed that approx. 220 g/kg DM of xylose and 125 g/kg DM of arabinose remained in the solid fraction. Considering the released monosaccharides after pretreatment this indicated that low pH pretreatments apparently induced a loss of approx. 60% xylose and 40-50% arabinose as compared to the amounts in the starting material, whereas the alkaline pretreatment caused a loss of approx. 40% xylose and 55% arabinose. If the enzymatic release was related to the content actually remaining in the solid fractions, the enzymatic release after acidic pretreatments actually caused a full release of the remaining xylose and arabinose. Correspondingly, approx. 17% of xylose and 55% of arabinose was released from the alkaline pretreatment. Indeed this implied that the acidic pretreatments were more effective in rendering the material more susceptible to enzymatic hydrolysis as compared to the alkaline, but the loss ought to be considered substantial from both pretreatment forms. Interestingly, even though no free monosaccharides were observed after the alkaline pretreatments the loss was almost as significant as that of the acidic pretreatments. However, only minor amounts of 2-furfuralaldehyde after pretreatments were detected and could not explain the gap and it was therefore concluded that the pentoses degraded to other components.

Modeling the release of monosaccharides

The significance parameters and regression coefficients for fitting a linear regression model to the release of monosaccharides showed that the best model fit within a 95% confidence interval was obtained by that illustrated in Figure 1 giving model fits (R^2) in the range 0.839-0.889. Despite good model fits, model predictability (Q2) and model validity showed poor fitting, indicating that the models would not be adequate for predicting the

outcome of experiments with factor limits beyond the ones employed in the present experiment. This is completely in accord with the finding that none of the monomer releases reached a maximum under the applied circumstances – as also visualized in the 3D response surface plot exemplified by enzymatic xylose release (Figure 1). Despite the lack of predictability, the model did reveal the significance of all three pretreatment factors pH, temperature, and time; the pretreatment pH was in all cases the most prominent factor, whereas time generally seemed to have the least effect on monomer release.

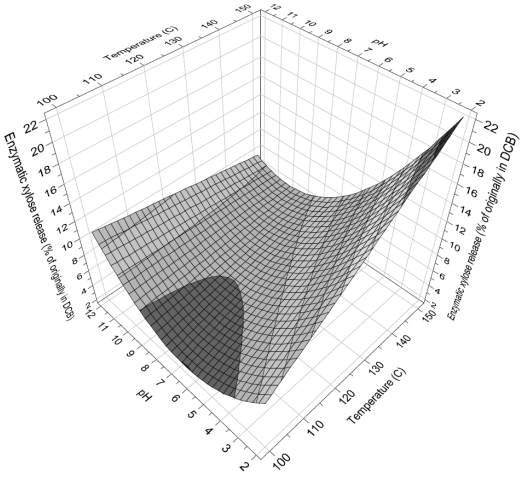

Figure 1: 3D response surface plot of model fitting for enzymatic xylose release after acidic and alkaline pretreatments.

Intensive low pH pretreatments

Since the data obtained in the initial pretreatments did not reach a maximum for release of monosaccharides, a second set of intensive low pH pretreatments were investigated. Because pH was generally the most significant factor the interval investigated was set to pH 1-2. Temperature was the second most significant factor but due to equipment limitations higher process temperature was not an option and temperature was maintained at 150 ºC for all experiments. Finally, as pretreatment time was the least significant factor we hypothesized that it would be possible to scale down the time frame to 10-65 min.

The models describing parameters for total release of arabinose and xylose these were all significantly better than the previous models. This is related to the fact that a maximum in total release was reached within the given parameter ranges which is also realized from Figure 2A and B. Hence, according to these models, a maximum release of both arabinose and xylose can be obtained at 150 ºC, pH 1.3, 50-55 min. Here, approx. 61% (~163 g/kg DM) of arabinose and 50% (~187 g/kg DM) of xylose will be released. Modeling enzymatic xylose and glucose release showed good model fitting parameters as well (Figure 3A and B). No enzymatic release of arabinose was observed. pH was still the most significant single factor but quite the contrary to previous results, increase in pH now had an increasing effect on the enzymatic xylose release.

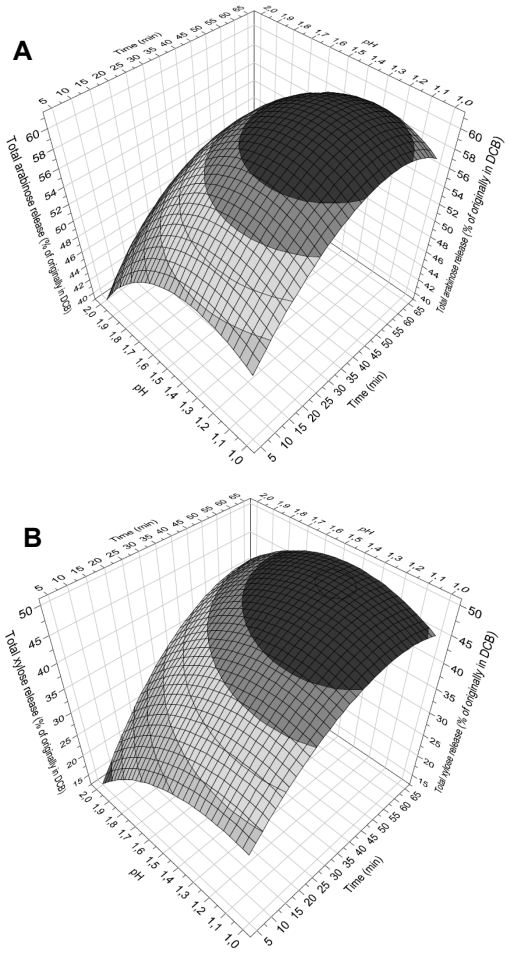

Figure 2: 3D response surface plot of total arabinose (A) and total xylose (B) release after intensive low pH pretreatments.

Lowering pH too much simply had a negative effect on the enzymatic xylose release (Figure 3A). A comparison of the total xylose release and the enzymatic xylose release (Figure 2B and 3A) point to the fact that acidic pretreatment at these specific severities will alter the native structure of the substrate to a degree that renders enzymatic hydrolysis a secondary process and not the main route to xylan hydrolysis.

Modeling of the enzymatic release of glucose showed enhancement by the acidic pretreatment, however pH as a single factor was not significant. Instead the interactive effect of time and pH was highly significant. This was the complete opposite situation compared to the initial modeling of enzymatic glucose release and showed that it can be intricate to formulate interpretations based on inadequate model fitting. The optimal enzymatic release of glucose is illustrated in Figure 3B and will occur after pretreatment at 150 ºC, pH 1.5 and 45 min and result in approx. 68% release of glucose.

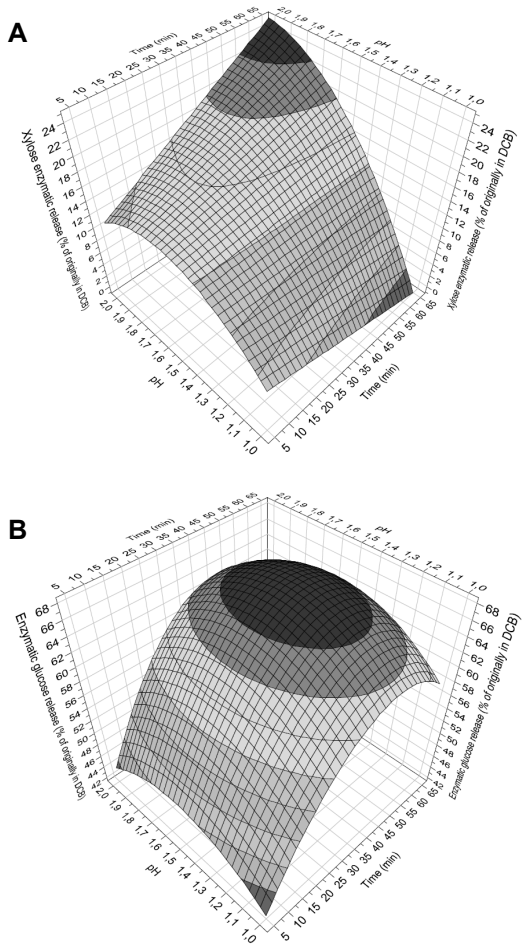

Figure 3: 3D response surface plot of enzymatic xylose (A) and enzymatic glucose (B) release after intensive low pH pretreatments.

In these experiments temperature was maintained at the highest possible level causing time to become a significant factor. Therefore future experiments might pursue even higher pretreatment temperatures if shortening of pretreatment time is to be achieved.

Conclusion

The results inform that increased enzymatic accessibility of corn bran arabinoxylan was achieved after pretreatments; acidic pretreatment was the most effective route to follow. The low pH pretreatment generated an unspecific acidic prehydrolysis thus leaving the substrate open for enzymatic attack. However, the results also showed that large amounts of valuable monosaccharides were lost during the pretreatments and that increasingly severe acidic and alkaline pretreatments significantly altered and disrupted the native structure of the substrate. A maximum of 60% by weight of the available arabinose and 50% by weight of the available xylose was released. However, the substantial loss of xylose and arabinose in the range of 40-60% by extreme pH pretreatments would be unacceptable in commercial utilization of corn bran arabinoxylan.

Within the methods tested here, the results indicated that the optimal pretreatment method for maximal enzymatic release of xylose would be close to operating at 150 ºC, pH 2 for 65 min., whereas lower pH during pretreatment, i.e. pH 1.3, resulted in higher total xylose release because of increased xylose liberation during the pretreatment. Hydrolysis of arabinoxylan from corn bran continues to be a demanding task and obtaining better hydrolysis stresses the importance of understanding the polysaccharide composition and molecular interactions. Comprehension of the biomass complexity is achieved better through enzymatic reactions than through physiochemical pretreatments that will randomly attack and destroy the material. Besides obtaining scientific valuable knowledge, replacement of physiochemical processes by enzymatic ones may well be the future strategy within a “lean and green” process philosophy.

Acknowledgement

The work presented here has been co-financed by Novozymes A/S and the Food Graduate School Denmark to whom we are very thankful.

References

1. J. Agger, K.S. Johanson, A.S. Meyer. DOI: 10.1016/j.nbt.2010.09.012
2. L. Saulnier, C. Marot, E. Chanliaud, J-F. Thibault, Carbohydr. Polym. 26 (1995) 279-287.
3. R. Branco, T. Santos, J. Santos, S. Silva, New Biotechnol. 25 (suppl. 1) (2009) 158.
4. D.J. Hayes, J.R.H. Ross, M.H.B. Hayes, S.W. Fitzpatrick, in: B. Kamm, V.R. Gruber, M. Kamm, (Eds.), Biorefineries – Industrial processes and products: Status quo and future directions, Volume 1, Wiley-VCH., Weinheim, 2006, p. 139-164.
5. H. Pastell, P. Westermann, A.S. Meyer, P. Toumainen, M. Tenkanen, J. Agric. Food Chem. 57 (2009) 8598-8606.
6. M-M. Titirici, M. Antonietti, N. Baccile. Green Chem. 10 (2008) 1204-1212.
7. J. Agger, A. Viksø-Nielsen, A.S. Meyer, J. Agric. Food Chem. 58 (2010) 6141-6148.
8. K. Grohmann, R.J. Bothast, Process Biochem. 32 (1997) 405-415.
9. C.B. Faulds, P.A. Kroon, L. Saulnier, J-F. Thibault, G. Williamson, Carbohydr. Polym. 27 (1995) 187-190.
10. B.C. Saha, B.S. Dien, R.J. Bothast, Appl. Biochem. Biotechnol. 70-72 (1998) 115-125.
11. L. Saulnier, J.-F. Thibault, J. Sci. Food Agric. 79 (1999) 396-402.

List of Publications

1. J. Agger, A. Viksø-Nielsen, A.S. Meyer, J. Agric. Food Chem. 58 (2010) 6141-6148.
2. J. Agger, K.S. Johanson, A.S. Meyer, DOI: 10.1016/j.nbt.2010.09.012.

Hassan Ahmadi Gavlighi
Phone: +45 4525 2947
E-mail: hag@kt.dtu.dk
Discipline: Enzyme Technology

Supervisors: Jørn Dalgaard Mikkelsen
Anne Meyer

PhD Study
Started: June 2009
To be completed: May 2012

Extraction and Production of Prebiotic and Hydrocolloids Oligosaccharides from Waste Streams from the Agricultural and Ingredient Industries

Abstract
A prebiotic oligosaccharide is a functional food component that confers a health benefit on the host which is associated with growth modulation of the gut microbiota. The interest in the use of nondigestible oligosaccharides (NDO) as functional food components targeted at gut health has increased during recent years. NDO are selectively fermented in the human colon and can be described as prebiotics. The waste streams from agricultural industry are a large source of oligosaccharides with potential prebiotic effects. The possibilities to manufacture new prebiotic oligosaccharides from large agricultural side-streams are therefore an attractive avenue and especially when it can be carried out using mono-component enzymes.

Introduction
It is now well established that the colonic microflora has a profound influence on health .Consequently, there is currently a great deal of interest in the use of prebiotic as functional food ingredients to manipulate the composition of colonic microflora in order to improve health. Prebiotics show both important technological characteristics and interesting nutritional properties. Several are found in vegetables and fruits and can be industrially processed from renewable materials. In food formulations, they can significantly improve organoleptic characteristics, upgrading both taste and mouthfeel. For prebiotics to serve as functional food ingredients, they must be chemically stable to food processing treatments, such as heat, low pH, and Maillard reaction conditions. That is, a prebiotic would no longer provide selective stimulation of beneficial microorganisms if the prebiotic was degraded to its component mono- and disaccharides or chemically altered so that it was unavailable for bacterial metabolism determined the effect of processing conditions on the prebiotic activity of commercial prebiotics using a prebiotic activity assay. The results showed that only heating at low pH caused a significant reduction in prebiotic activity, with one of the fructooligosaccharides (FOS) products being the least stable. The other conditions caused little change in activity. Stability of prebiotics to processing conditions has been considered. These results provide the basis for selecting prebiotics for use as functional food ingredients and for predicting the extent to which processing affects prebiotic activity. Most prebiotics and prebiotic candidates identified today are nondigestible oligosaccharides. They are obtained either by extraction from plants (e.g., chicory inulin), possibly followed by an enzymatic hydrolysis (e.g., oligofructose from inulin) or by synthesis (by trans-glycosylation reactions) from mono- or disaccharides such as sucrose (fructooligosaccharides) or lactose (trans-galactosylated oligosaccharides or galactooligosaccharides). Among these prebiotics, inulin and oligosaccharides are the most studied prebiotics and have been recognized as dietary fibers in most countries.

Specific objectives
The main idea of the proposed project is to employ selective enzymatic catalysis to extract and design beneficial hydrocolloids and prebiotic oligosaccharides from agricultural industry.

Pectin is an abundant ubiquitous and multifunctional component of the cell wall of all land plants [1]. Pectic polysaccharides consist mostly of polymers rich in galacturonic acid (GalA), containing significant amounts of rhamnose (Rha), arabinose (Ara) and galactose (Gal) as well as other 13 different monosaccharides [2,3,4]. The three major pectic polysaccharides currently defined are homogalacturonan (HG), rhamnogalacturonan I (RG-I) and rhamnogalacturonan II (RG-II) [5]. The industrial process for extraction of pectin is generally based on a

chemical treatment at low pH. It generates large amounts of effluents (such as chemical waste) that need further treatment. It may also give rise to undesired degradation of pectin during extraction. There are a growing demand for sustainable processes with mild extraction and modification conditions to produce hydrocolloids and prebiotic oligosaccharides without the use and generation of hazardous substances. The present idea in this PhD study is to evaluate the use of new mono-component enzymes as an environmentally friendly method for pectin extraction and modification.

Current Work

Optimization of enzyme activity is very important to minimize enzyme dosage and get high yield.

In this experimental plan we found optimum condition for one of enzymes that could be degrades xyloglucan-oligomers.The optimum condition is done with RSM technique and Standard substrate.

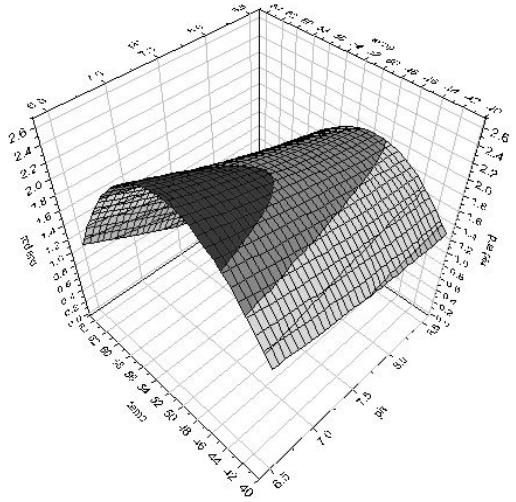

Figure 1: A three Dimensional RSM showing the optimum pH and Temperature for Endo-Xyloglucanse

Conclusion and Future work

In this project, we will extract hydrocolloids with mono or multi enzyme and then evaluate the prebiotic effect.
In this case based on structural of the cell wall, we will use enzyme directly to get oligosaccharides or use different enzyme to extract intact hydrocolloids and the use enzyme for production oligosaccharide.

References

1. W.G.T. Willats, P. Knox, J.D. Mikkelsen, Trends Food Sci. Tech. 17 (3) (2006) 97-104.
2. D. Mohnen, Curr. Opin. Plant Biol. 11 (3) (2008) 266-277.
3. J.P. Vincken, H.A. Schols, R. Oomen, M.C. McCann, P. Ulvskov, A.G.J. Voragen, R.G.F. Visser, Plant Physiol. 132 (4) (2003) 1781-1789.
4. J. Vincken, H. Schols, R. JFJ, A. Voragen, Advances in Pectin and Pectinase Research, 47 (2003).
5. K. Waldron, M. Parker, A. Smith, Compr. Rev. Food Sci. F. 2 (4) (2003) 128-146.

Naweed Al-Haque

Phone: +45 4525 2990
E-mail: nah@kt.dtu.dk
Discipline: Process Technology and Unit Operations
Systems Engineering
Supervisors: John M Woodley
Rafiqul Gani
Pär Tufvesson

PhD Study
Started: November 2009
To be completed: November 2012

Modelling of Controlled Supply of Substrate Using Solid Resins in Biocatalysis

Abstract
Biocatalysts (either as isolated enzyme and whole-cell systems) are increasingly being used to assist in synthetic routes to complex molecules of industrial interest. In many cases, the attractive features of higher selectivity and benign reactive operations make it an interesting option. There are some limitations (enzyme inhibition, toxicity) to biocatalysis which can in some cases be overcome with methods such as controlled release of substrates combined with *in-situ* product removal (ISPR) using solid resins. In this project, controlled substrate supply biocatalysis will be studied using a mechanistic model to predict the reactor performance as a basis for process implementation.

Introduction
Biocataltytic reactions benefit from benign operating condition, high stereo, regio and chemo selectivity, and more importantly has the potential to enable difficult syntheses to be circumvented [1]. One of the major challenges associated with biocatalytic reactions is that the substrate and product may inhibit or damage the biological catalyst or interfere with other components in the reaction medium above a critical concentration [2]. In this project, a novel approach is applied where the substrate is supplied to the reaction in a controlled manner by means of solid resins. This substrate release technology will aid in increasing the productivity and yield of the product. A mechanistic model will be used for predicting the performance of the process technology and as well to guide the systematic selection of the necessary resin and the appropriate reactor.

Fundamentals of slow release mechanism
This technology will behave such that the resin will act as a 'reservoir' for the substrate and the product. The substrate will slowly diffuse into the solution maintaining an aqueous concentration beneath the inhibitory level [3]. The biocatalyst converts the substrate(s) into the required product(s) which can subsequently be recovered by means of *in-situ* product removal (ISPR). At the end of the reaction, the product is eluted from the resin to give a high concentration solution. This therefore represents an innovative way of intensifying bioprocesses, via the combination of controlled substrate supply, reaction and product removal in an integrated unit operation. Figure 1 displays a schematic of the methodology.

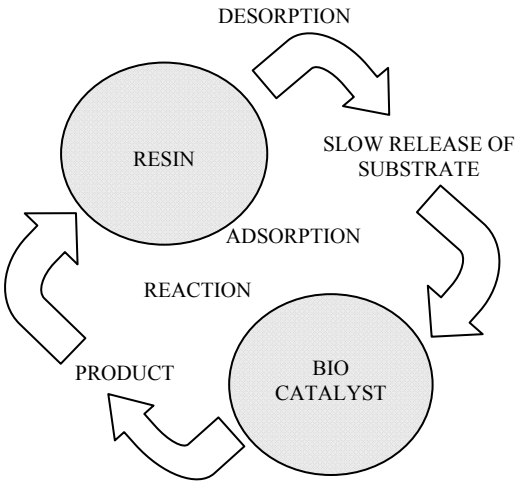

Figure 1: Principle of a resin based ISPR using the slow release mechanism

Systematic Methodology for Design/Analysis
To approach this project, a methodology has to be constructed to develop this scheme in an optimized manner. The main stages in the proposed methodology are briefly described below.

1. Data collection of the process to establish a base case design

2. Modelling and simulation of the base case design to generate data for analysis
3. Perform experiments to quantify kinetic and equilibrium data to fit into the model
4. Optimal reactor design generated based on the mechanistic model
5. A database and a model can then be devised for the systematic selection of an adsorbent

Case Study: Kinetic Modelling of ω-Transamination of Acetophenone

To illustrate the methodology, the reaction kinetics of the transamination (TAm) of Acetophenone (APH) and co-substrate 2-Propylamine (IPA) to produce α-Methylbenzylamine (MBA) and co-product Acetone (ACE) is used. Figure 2 below illustrates the reaction scheme.

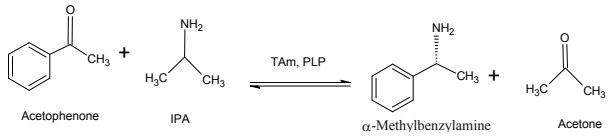

Figure 2: Transamination catalysed by ω-transaminase

Kinetic Model

The reaction mechanism follows the ping pong bi bi mechanism where there is an exchange of amines in which the first product is formed from the first substrate and conversely the final product is formed from the second substrate. However, in this reaction, both substrate and product inhibit the catalytic activity. The simplified form of the model derived from first principles to depict the initial rates can be expressed in Equation 1 as follows:

$$v_o = \frac{V_f\left([APH]\cdot[IPA]\right)}{K_{APH}\cdot[IPA] + K_{IPA}\cdot[APH]\cdot\left(1+\frac{[APH]}{K_{SAPH}}\right)+[IPA]\cdot[APH]}$$

List of abbreviations

V_f: Maximum rate of reaction [mM/min]
K: Michaelis constants [mM]
K_{SAPH}: Inhibition constant [mM]

Systematic Methodology for Parameter Estimation

To identify the kinetic parameters of the model, the following methodology as described in Figure 3 is used.

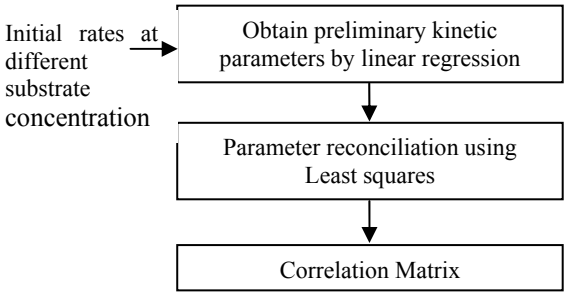

Figure 3: Methodology for Parameter Estimation

Results of Parameter Estimation

The initial guesses to be used for the parameter reconciliation are the values calculated from the linear plotting method. The optimization tool used is non linear least square function, which is in-built to the program Matlab program. The optimized parameter values are shown in Table 1:

Table 1: Estimated parameters

Parameters	values	95 % Confidence interval
V_f	0.0042 mM/min	± 0
K_{APH}	0.67 mM	± 0.0024
K_{IPA}	157.23 mM	± 0.2027
K_{SAPH}	2.68 mM	± 0.0071

The extremely small confidence intervals denote that the estimation of the parameters is quite satisfactory. The data lies within the confidence interval and thus it can be predicted that the uncertainties of the parameter are quite small.

Table 2: Correlation matrix

	V_f	K_{APH}	K_{IPA}	K_{SAPH}
V_f	1			
K_{APH}	0.9955	1		
K_{IPA}	-0.7023	-0.7196	1	
K_{SAPH}	-0.8397	-0.8477	0.9756	1

From the correlation matrix in Table 2, it can be seen that the parameters are considerably correlated. Therefore, a unique value of the parameter is perhaps not possible to be identified.

Conclusions

With the current research, a mechanistic model will be developed which will incorporate the novel technique of controlled release of substrate. With the creation of this robust model, the optimal recovery method can be selected. Using this as a basis, a resin selection guide can be created to assist in predicting the appropriate sorbent for the desired system.

Acknowledgement

The author kindly acknowledges Technical University of Denmark and the project AMBIOCAS financed through the European Union Seventh Framework Programme (Grant Agreement no. 245144) for the financial support.

References

1. D.J. Pollard, J.M. Woodley, Trends Biotechnol. 25 (2006) 66 – 73.
2. P. Tufvesson, W. Fu, J.S. Jensen, J.M. Woodley, Food Bioprod. Process. 88 (2010) 3-11.
3. P-Y Kim, D.J. Pollard, J.M. Woodley, Biotechnol. Prog. 23 (2007) 74 – 82.

Mads Orla Albæk
Phone: +45 6126 4748
E-mail: maoa@novozymes.com
Discipline Process Technology and Unit Operations

Supervisors: Krist V. Gernaey
Morten S. Hansen, Novozymes A/S
Stuart M. Stocks, Novozymes A/S

Industrial PhD Study
Started: April 2009
To be completed: March 2012

Investigation of the Efficiency of Alternative Enzyme Production Technologies

Abstract
The aim of this industrial Ph.D project is to investigate the efficiency of alternative technologies for enzyme production and evaluate these objectively in a comparison with the existing production platform. The fed batch stirred tank reactor is the standard technology for many biotech processes; however this may not always be the most economical production technology. In this project the reference process is a submerged fed batch fermentation of the filamentous fungus *Trichoderma reesei.* A model of the reference process is used to compare literature data from promising alternative technologies, which have typically been tested in laboratory scale. The overall goal of the project is to verify alternative technologies with the model predictions at an industrial relevant scale.

Introduction
Industrial enzymes are currently mainly produced in fed batch stirred tank reactors using what might be termed traditional technology. This technology platform is well known since it has been the most popular technology for about 50 years. There have been many attempts to improve the current technology by changing dosing strategy, optimizing impeller design, implementing more advanced control strategies etc. A number of alternative technologies which might replace the current one exist and have been reported in the open literature.

The underlying hypothesis for this research project is that alternative technologies exist that profitably could be used in industrial enzyme production so that the energy- and or resource consumption would be lowered. In order to objectively evaluate alternative technologies it is necessary to use similar scale. Research in bioreactors is often based on geometric similarity, which is why the Novozymes Fermentation Pilot Plant provides an obvious setting for this work.

Specific objectives
The purpose of this contribution is to describe the progress of the project. The main activities of this project are: I) Determination of the key parameters for the reference process. II) Modeling of the reference process. III) Identification of alternative production technologies. IV) Characterization of a least 1 alternative technology. V) Conclusion on performance of at least 1 alternative technology.

Results and discussion
The key parameters of the enzyme production were identified as:

- Final protein concentration (g/kg)
- Energy yield (g protein/kWh consumed)
- Productivity (g protein/m^3/h)

Preliminary (and scaled) data for two different industrial scales (80 m^3 and 160 m^3 fermentors) were presented in last year's edition of the Yearbook.

The next activity of the project was modeling of the reference process. In order to characterize and attempt to model the fed batch fermentation process 9 fermentations have been carried out in 550 L pilot plant vessels at Novozymes, Bagsvaerd. The fermentation process is an aseptic cultivation of the filamentous fungus *T. reesei*. The main difficulty – and limiting rate – of the process is oxygen transfer from the gas to the liquid phase. The process is run with a variable substrate feed flow rate according to the level of dissolved oxygen tension (DOT). This strategy ensures that the batch is not over- or underfed situations that would both lead to suboptimal conditions with low yield or increased viscosity as a consequence.

The modeling approach is schematically illustrated in Figure (1). The model basically consists of two parts: a reactor model and a biological model. The reactor model includes the estimation of the available oxygen

mass transfer in the fermenter. The mass transfer can be estimated by the mass transfer coefficient, k_La, and the driving force, which is the difference between the actual oxygen concentration in the liquid and the oxygen concentration in the liquid at equilibrium with the gas phase. k_La of stirred tank reactors is usually estimated by the specific power input, the superficial gas velocity and – for non-Newtonian fluids – the viscosity of the medium.

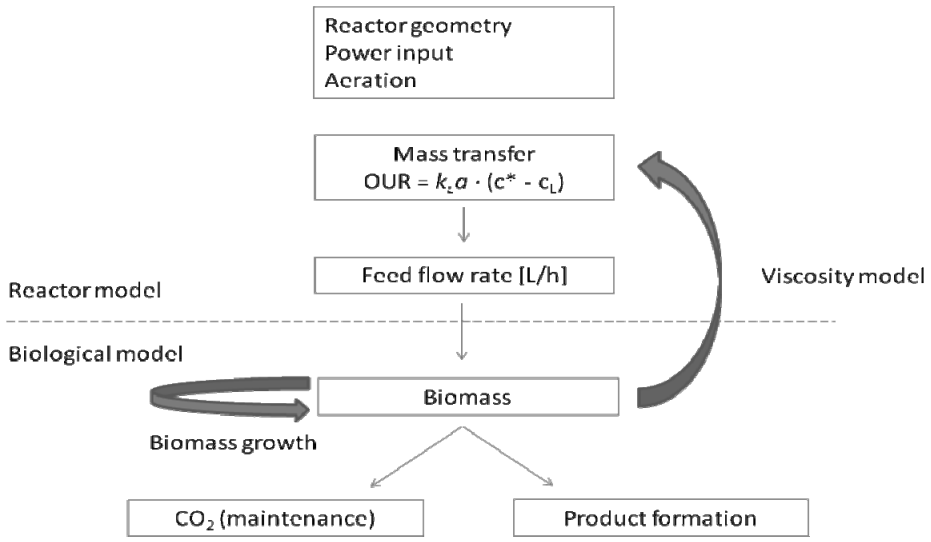

Figure 1: Schematic overview of the mechanistic model used to simulate the fed batch fermentation process. The reactor model determines the oxygen mass transfer of the system and the substrate feed flow rate. The biological model describes the formation of biomass and product as well as the substrate uptake used for maintenance. A viscosity model links the reactor and the biological model as the mass transfer is highly affected by the fermentation broth viscosity.

To estimate the k_La of the system, 3 process parameters were changed in a design of experiments aimed at using the model at different scales and operating conditions: Head space pressure, agitation rate and aeration rate. By changing these 3 parameters a wide span of oxygen uptake rates and k_La values were obtained. This allowed for a satisfactory estimation of the parameters for a typical mass transfer correlation. Now that the mass transfer of the system could be estimated the biological model could be applied.

A simple maintenance model describing the uptake of substrate and oxygen for non-growth related processes in the fungus was applied [1]. The model assumes quasi-steady-state for substrate concentration which is a reasonable assumption since this is a fed batch. Thereby the growth rate can be estimated from the substrate feed flow rate [2,3].

The link between the biological model and the reactor model is the estimated viscosity of the fermentation broth. The mass transfer is known to decrease in viscous fluids. Nienow [4] showed that k_La decreases approximately with the square root of the apparent viscosity. In this model the viscosity is estimated by the biomass concentration of the fermentation broth.

The process model has shown to simulate the progress of the pilot scale fermentations well and will be applied to relevant industrial scale. The model will then be used to evaluate alternative technologies.

Conclusions and outlook

A process model has been built that simulates the fed batch process well. The model has furthermore been applied to screen for alternative technologies. Low energy input systems promise a high energy efficiency even at the desired productivity, but require a larger broth volume. Further investigations in pilot scale are needed to validate the model for other fermentation technologies.

References/List of Publications

1. J. Nielsen, J. Villadsen, G. Lidén, Biorection engineering principles, 2nd. ed. 2003, Kluwer Academic/Plenum Publishers, New York
2. M.O. Albaek, K.V. Gernaey, S.M. Stocks, Modelling of industrial enzyme fermentation by mass transfer estimation. Presented at 8th World Congress of Chemical Engineering, August 2009, Montreal, Canada
3. M.O. Albaek, S.M. Stocks, A.W. Nienow, Comparison of Traditional Rushton Disc Turbines with Up-pumping Hydrofoil B2 Impellers in 550 L Pilot Scale Aerobic Submerged Fermentations. Presented at AIChE Annual Meeting, November 2009, Nashville, Tennessee
4. A. Nienow, Mixing studies on high viscosity fermentation processes - Xanthan gum, in: The World Biotechnology Report, Vol I, Europe, Online, London, 1984 pp. 293-304

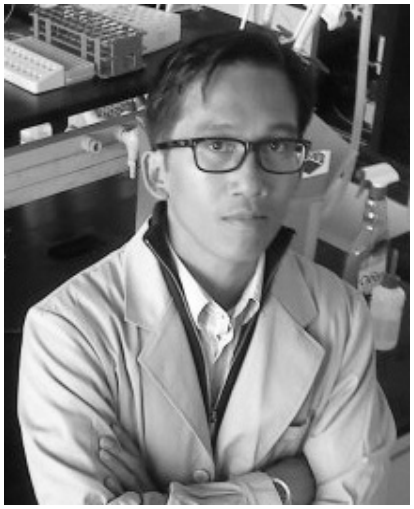

Marcel Tutor Ale
Phone: +45 4525 2861
E-mail: mta@kt.dtu.dk
Discipline Enzyme Technology

Supervisors: Anne S. Meyer
Jørn Dalgaard Mikkelsen

PhD Study
Started: March 2008
To be completed: June 2011

Assessment of Algae Productivity Responses and Biomass Potentials

Abstract
Seaweed can efficiently assimilate nutrients such as N or C and effectively capture light energy for biomass accumulation. Successful exploitation of seaweed requires our understanding of seaweed growth kinetics. The different nutrient flux has affected seaweed growth and nutrient uptake mechanism. This may have profound influence on the yield and properties of the seaweed products. The aim of this study is to assess growth responses to different nutrient source; and to evaluate the influences of this nutrients supply on the potential product of seaweed biomass.

Introduction
Algae are simple unicellular organisms, either found as single or in groups as colonies, or they can be present as macroscopic multicellular organisms sometimes collaborating together as simple tissues (i.e. seaweed). Seaweed or algae are like land plants, they can efficiently capture solar energy by photosynthetic processes and assimilate nutrients e.g. C and N for growth. Exponential growth can be achieved only in short period thus they can accumulate biomass faster than terrestrial plants. Seaweeds are classified according to their physiology, morphology and taxonomic characteristics into three groups: Chlorophyta (green), Rhodophyta (red) and Phaeophyta (brown). Each species have their own distinct characteristics and differ generally on chemical composition, structure and properties. The diversity of the seaweeds and their products are an unused potential for new products and applications. Most common seaweed products are agar, alginate and carrageenans.

The utilization of seaweed for food; feed stuff and alternative medicine have existed for many centuries ago. Recently, algae have gained more attention from commercial as well as scientific interests. Micro and macro algae sales account approximately for 22% of the 39.4 million metric tons of aquaculture products sold worldwide [1]. The production of alternative fuels from non-starch biomass has directed attention to utilization of the micro and macroalgae or seaweed as sources of biomass for biofuels production. The utilization of seaweed has increased popularity in cosmetics and has also been proposed for functional foods and functional food ingredients; as well as pharmaceutical applications.

Seaweed farming and collection is an integral part for commercial exploitation and mass production. Most of commercially exploited seaweed species such as *K. alvarezii* and *E. denticulatum* for hydrocolloid production are farmed offshore while other important species such as *Laminaria* and *Macrocystis* are often harvested or collected naturally. For this reason monitoring of productivity responses and growth kinetics is a challenge. However, there are few who have successfully cultivated seaweed in culture tanks. This paves the way for scientific investigation on seaweed growth responses to different nutrient under controlled condition [2]. Major prerequisite for successful exploitation of cultivated seaweed for commercial application is that the growth rate and yields are optimized. This in turn requires both an understanding of the influence of different nutrients response and a precise methodology to measure the growth.

Working Objectives
During the course of this study, the objectives are: to develop a simple technique to quantitatively monitor algae growth; to assess growth responses to different nutrient source; and to evaluate the influences of this nutrients supply on the potential product of seaweed biomass.

Experimental work

A photo-scanning evaluation of Ulva lactuca growth response to different nitrogen sources

Ulva lactuca a.k.a. "sea lettuce" is an important macroalga in marine ecology. *Ulva* species are particularly rich in dietary fiber, mainly soluble fiber [3] and have been proposed as being a good source of Vitamin A, B2, B12 and C and is rich in γ-tocopherol and *U. lactuca* extracts exhibit antioxidant, anti-microbial, and anti-viral activities [4].

It has been shown previously, that *U. lactuca* is suitable for propagation under controlled conditions [5]. Precise monitoring of the growth for obtaining maximal yields is a crucial prerequisite for achieving these goals. Current methods for growth monitoring of macroalgae rely on gravimetric assessment of samples of the fronds. This approach requires removal of surface moisture from the fronds and is therefore inherently prone to inaccuracy. The objective of this work was to assess the applicability of photo-scanning technology for monitoring of the growth kinetics of *U. lactuca*.

Results

A simple and non-destructive growth monitoring technique based on assessment of area expansion of prepared *U. lactuca* discs was developed [6]. Growth was evaluated quantitatively by use of photo-scanning for taking digital images and image processing software for measuring disc area. The images revealed differential increases of the surface area of *U. lactuca* discs with time in response to different N-nutrient enrichments (Figure 1).

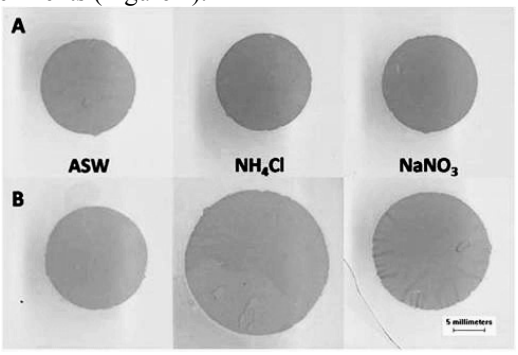

Figure 1: The growth difference of the surface area in the images (A) Day-1 and, (B) Day-10 culture in artificial sea water (ASW) enriched with different N-nutrients. Images were generated after photo-scanning using Canon Scan 5600F scanner at 300 dpi resolution.

The NH_4Cl and $NaNO_3$ rich media accelerated *U. lactuca* growth to a maximum specific growth rate of 16.4 ± 0.18% d^{-1} and 9.4 ± 0.72% d^{-1}. The highest biomass production rate obtained was 22.6 ± 0.24 mg-DW·m^{-2}·d^{-1} (Figure 2).

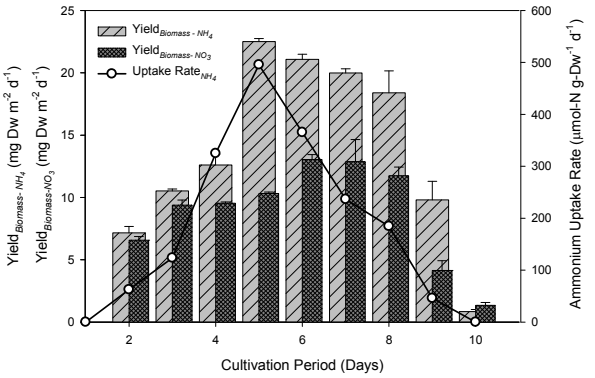

Figure 2: The ammonium uptake rate of *U. lactuca* as function of time and the influence of ammonium-N and nitrate-N source on the biomass yield. The maximum specific uptake rate was 495.59 ± 0.22 µmol-N·g-DW^{-1} d^{-1} and maximum biomass yield were 22.50 ± 0.24 mg m^{-2} d^{-1} by ammonium and 13.03 ± 0.40 mg m^{-2} d^{-1} by nitrate enrichment.

Conclusion

We have introduced a novel method to monitor the growth development including nutrient uptake of *U. lactuca* [6]. The method was able to assess distinct and subtle differences in growth response to two different nitrogen sources. The images provided information that enabled us to determine the biomass productivity, and provided a better understanding of the importance of N-nutrients on the growth kinetics of this important benthic macrophyte.

References

1. R.A. Andersen, Algal Culturing Techniques, Elsevier Academic Press, London, UK, 2005, p. IX.
2. J. del Rio et. al., Hydrobiologia 326/327, p 61-66, 1996
3. M. Lahaye, J. Sci. Food Agric. 54, p587-594, 1991
4. H.H. Abd El-Baky et. al., EJEAFChe. 7(11), p3353-3367, 2008.
5. H.F. Christensen, K. Sand-Jensen, Mar. Biol. 104, p497-501,1990
6. M.T. Ale et. al. A photo-scanning methodology for evaluation of Ulva lactuca growth response to different nitrogen sources. [submitted manuscript]

Paloma Andrade Santacoloma
Phone: +45 4525 2974
E-mail: psa@kt.dtu.dk
Discipline: Process Technology and Unit Operations

Supervisors: John Woodley
Krist V. Gernaey
Gürkan Sin

PhD Study
Started: November 2008
To be completed: October 2011

Multi-enzyme in-pot Processes in the Application of Synthetic Cascade Reactions

Abstract
This paper presents a methodological approach for modeling multi-enzyme in-pot processes. The methodology is exemplified stepwise through the bi-enzymatic production of N-acetyl-D-neuraminic acid (Neu5Ac) from N-acetyl-D-glucosamine (GlcNAc). In this case study, sensitivity analysis is also used to evaluate the reliability of all parameters of the model suggested in literature [5]. Results, from the sensitivity analysis, are used as criteria for a systematic simplification of the model structure. Consequently, model complexity was reduced without compromising the general predictive performance. A deviation of less than 5% from the original model was found.

Introduction

Multi-enzyme processes are particularly interesting from a scientific perspective when operated as a mixture of enzymes (catalyzing several reactions) in a single pot [1], so called multi-enzyme 'in-pot' processes. In addition, these processes can be considered as an application of process intensification, since separation and purification steps of intermediate products may be eliminated [2]. Consequently, this potentially leads to considerable process improvements (e.g. reduction in downstream processing and operating costs).

Mathematical modeling plays an important role in developing this multi-enzyme in-pot approach, integrated with a computer-aided framework [3]. In order to build reliable models in an efficient manner, it is necessary to apply a systematic framework [4].

The objective of this contribution is to apply the methodological approach suggested by Santacoloma *et al* [4], exemplified through the bi-enzyme synthesis of N–acetyl-D-neuraminic acid (Neu5Ac) from N-acetyl-D-glucosamine (GlcNAc), as a case study.

Case Study (N-acetyl-D-neuraminic acid)

The pharmaceutical intermediate N-acetyl-D-neuraminic acid (Neu5Ac) is needed as a result of its use in the synthesis of relenza, an anti-viral, anti-cancer and anti-inflammatory drug [5]. One innovative option for producing this compound is by combining two enzymes in a single reactor [3], and then considering this as a multi-enzyme in-pot process. This bi-enzymatic process consists of two cascade reactions, as shown in Figure 1, where the first enzyme (epimerase, E.C. 5.1.3.8) uses N-acetyl-D-glucosamine (GlcNAc) as a substrate to be transformed into N-acetyl-D-manosamine (ManNAc) which is, at the same time, used as a substrate for a second enzyme (aldolase, E.C. 4.1.3.3) in combination with pyruvic acid to yield the desired product (Neu5Ac).

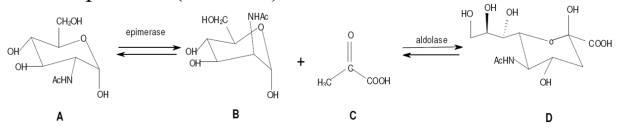

Figure 1: Synthesis of Neu5Ac from GlcNAc in two cascade reactions; A: N-acetyl-D-glucosamine (GlcNAc); B: N-acetyl-D-manosamine (ManNAc); C: pyruvic acid (Pyr); D: N-acetyl-D-neuraminic acid (Neu5Ac); Enzymes: N-acylglucosamine-2-epimerase, N-acetylneuraminic acid aldolase.

The model for this case is analyzed following the methodological framework [4], step-by-step thus,

Step 1. Modeling objective: the objective here is to study the effects in the outputs (compound concentrations) of the process due to model simplifications based on sensitivity analysis.

Step 2. Information: the mathematical model for this process was taken from literature [5]. The suggested

model includes parameter values with confidence intervals, (see Table1).

Table 1: Kinetic parameter values and operating conditions for the process

Parameter	Value
Av^{GlcNAc}	(5.31±0.74)x10^{-7} U/l
K_m^{GlcNAc}	(1.76±0.26)x10^{-2} M
Av^{ManNAc}	(1.16±0.33)x10^{-5} U/l
$K_m^{ManNAc,e}$	(9.93±1.14)x10^{-2} M
$K_i^{Pyr,e}$	0.146±0.019 M
$K_i^{Neu5Ac,e}$	0.719±0.158 M
Av^{f}	(7.51±1.11)x10^{-8} U/l
K_i^{Pyr}	(8.49±1.06)x10^{-3} M
K_m^{ManNAc}	(1.31±0.15)x10^{-2} M
Av^{r}	(1.05±0.05)x10^{-7} U/l
K_m^{Neu5Ac}	(4.26±0.8)x10^{-2} M
K_m^{Pyr}	(9.41±0.91) x10^{-2} M
K_i^{ManNAc}	(1.19±0.91)x10^{-2} M

The operating conditions for the process are given as: initial concentrations of *GlcNAc*: 0.3M and *PyrAc*: 0.38M. Initial volume 0.1 L. Feed concentrations of *GlcNAc*: 1M and *PyrAc*: 0.9M. Flow rate 2e-5 L/min. Epimerase and aldolase activity 150U and 2400U, respectively.

Step 3. Formulation: according to the information compiled in the step 2. The generic mass balance model is described for fed-batch, feed started after 990 min.

$$\frac{d(GlcNAc)}{dt} = \frac{(GlcNAc_f - GlcNAc)\cdot F}{V} - r_1 \quad 1$$

$$\frac{d(ManNAc)}{dt} = r_1 - r_2 \quad 2$$

$$\frac{d(Pyr)}{dt} = \frac{(Pyr_f - Pyr)\cdot F}{V} - r_2 \quad 3$$

$$\frac{d(Neu5Ac)}{dt} = r_2 \quad 4$$

$$\frac{dV}{dt} = F \quad 5$$

The reaction rates for enzymatic reactions r_1 and r_2 are:

$$r_1 = \frac{E_{epi}\left(\frac{A_V^{GlcNAc} GlcNAc}{K_M^{GlcNAc}} - \frac{A_V^{ManNAc} ManNAc}{K_M^{ManNAc,e}}\right) GlcNAc}{1 + \frac{GlcNAc}{K_M^{GlcNAc}} + \frac{ManNAc}{K_M^{ManNAc,e}} + \frac{Pyr}{K_i^{Pyr,e}} + \frac{Neu5Ac}{K_i^{Neu5Ac,e}}} \quad 6$$

$$r_2 = \frac{E_{ald}\left(\frac{A_V^{f}\cdot ManNAc\cdot Pyr}{K_i^{Pyr} K_M^{ManNAc}} - \frac{A_V^{r}\cdot Neu5Ac}{K_M^{Neu5Ac}}\right)}{1 + \frac{Pyr}{K_i^{Pyr}} + \frac{K_M^{Pyr}\cdot ManNAc}{K_i^{Pyr}\cdot K_M^{ManNAc}} + \frac{ManNAc\cdot Pyr}{K_i^{Pyr}\cdot K_M^{ManNAc}} + \cdots} \quad 7$$

$$\cdots \frac{}{+ \frac{Neu5Ac}{K_M^{Neu5Ac}} + \frac{Neu5Ac\cdot ManNAc}{K_i^{ManNAc}\cdot K_M^{Neu5Ac}}}$$

Step 4. Calculation: parameter estimation is not carried out since no experimental data was available. Consequently, sensitivity analysis is performed in order to evaluate parameter reliability in the model structure. The described model contains 13 parameters which are analyzed by applying the Morris Screening method [6]. The analysis indicates that 4 parameters have no high effect on the model output at the evaluated conditions. Hence, simplifications in the model structure were considered.

Step 3. (Re) Formulation: according to the results obtained in step 4, the model structure was modified simplifying the parameters in turn. A comparison between the original model and simplified models was performed in order to quantify the deviation from the original model. Results are shown in Table 2.

Step 5. Experimentation: for the purpose of the paper, this step is not developed. However, results obtained from uncertainty and sensitivity analyses can be used as a basis to formulate an optimal experimental design in order to validate the model.

Table 2: Output model comparison between original model and the simplified models

Model	Eliminated parameters	Deviation (%)
Model 1	$K_i^{Neu5Ac,e}$	0.799
Model 2	$K_i^{Neu5Ac,e}$, $K_i^{Pyr,e}$	3.470
Model 3	$K_i^{Neu5Ac,e}$, $K_i^{Pyr,e}$, K_i^{ManNAc}	3.557
Model 4	$K_i^{Neu5Ac,e}$, $K_i^{Pyr,e}$, K_i^{ManNAc}, K_m^{Pyr}	4.283

Conclusions

A description for model formulation in the application of multi-enzymatic processes was shown. Since complex models are expected due to the interaction of compounds and enzymes, this methodology could be used to simplify the structure of the models in a systematic manner based on sensitivity analysis, as exemplified with the Neu5Ac case study. It was also found that the simplified models (see Table 2) still showed a good performance with a deviation of less than 5% from the original model. For a validation of the model, optimal experimental design can be formulated for defined environmental and operating conditions using the simplified model. In that case, fewer parameters must be experimentally analyzed, thus decreasing further the cost and time in the laboratory.

References

1. R. Bruggink, T. Schoevaart and Kieboom, Org. Proc. Res. Dev. 4 (2003) 622
2. P. Lutze, A. Román-Martinez, J.M. Woodley, R. Gani, European Symposium on Computer Aided Process Engineering – proceeding, 2010, 20th, 241
3. R. Morales-Rodriguez, R. Gani, Comput. Chem. Eng. 24 (2007) 207
4. P.A. Santacoloma, in: K.D. Johansen, V. Darde, K.V. Gernaey (Eds), Graduate Schools Yerabook 2009, Copenhagen, 2010, p. 169
5. V. Zimmermann, H. Hennemann, T. Daußmann, U. Kragl, Appl. Microbiol. Biot. 76 (2007) 597
6. F. Campolongo, A. Saltelli, Relian Engng Syst. Saf. 57 (1997) 49

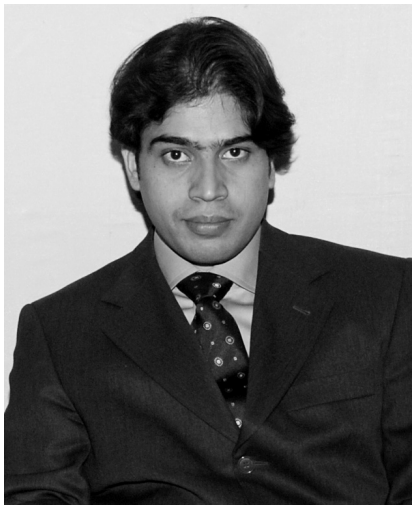

Muhammad Shafique Bashir
Phone: +45 4525 2853
E-mail: msb@kt.dtu.dk
Discipline: Reaction and Transport Engineering

Supervisors: Kim Dam-Johansen
Peter Arendt Jensen
Flemming Frandsen
Stig Wedel

PhD Study
Started: September 2008
To be completed: December 2011

Characterization and Quantification of Deposits Build up and Removal in Straw Suspension-Fired Boilers

Abstract
An increased use of straw on large suspension-fired power plants will be a relatively economic and potentially also efficient way to utilize straw for heat and power production. However, large deposit formation problems limit the electrical efficiency by limiting the maximum applicable superheater temperature, and the deposits also cause many boiler stops where different parts of the boiler have to be cleaned. Most studies have been based on measurements in grate boilers, while only limited data is available from biomass suspension-firing, where improved knowledge on the transient deposit formation process, the influence of fuel characteristics and the mechanisms of ash deposits removal are wanted. The aim of this project is to investigate ash deposition and shedding in suspension-fired straw boilers and to provide recommendations for the optimal operation strategy of boilers with respect to minimization of deposit related problems. The experiments were conducted during last year (2010) in a biomass suspension-fired boiler and the results indicate that the rate of deposit build up increased with an increased probe surface temperature from 500 to 600 ^{o}C. It was also observed that deposit shedding was primarily through debonding. At a probe surface temperature of 500 ^{o}C, the deposits of less than 91 h exposure time were easy to remove and PIP (Peak Impact Pressure) needed was less than 55 kPa. With an increase in probe surface temperature from 500 to 600 ^{o}C, the PIP needed to remove the deposits increased.

Introduction
One of the main sources for sustainable energy now and in the near future is biomass. In Denmark, straw and wood chips are the most abundant biomass sources used for power production. A fairly large surplus of wheat straw exists in certain parts of Denmark, and it can be a better substitute for coal [1]. However, compared to coal ashes, the biomass-derived ashes contain significant amounts of potassium and chlorine, and the use of biomass, primarily straw, in power plant boilers is a serious technical challenge [1, 4]. The potassium ash components play a significant role in the deposit formation because they act as glue bonding the individual fly ash particles together [4]. The deposit formation is a dynamic process, and consists of both deposit growth [5, 6] and removal processes [5, 6, 7]. The major contributing process for deposit build up is inertial impaction where large particles (> 5 μm) with a large inertial momentum impact on the boiler surfaces. The capture efficiency of the particles depends on the size and density of the particle, the viscosity of the outer layer of the particle plus the deposit surface layer morphology and viscosity. When pure straw fuel is utilized in large suspension-fired boilers, the heat transfer surfaces may be covered by severe ash deposits, impeding the plant operation. The deposit formation and removal (shedding) in biomass-fired boilers has been the objectives of some previous studies [6]; however some biomass deposit related processes are still not well described. Most studies have been based on measurements in grate boilers, while only limited data is available from biomass suspension-firing where improved knowledge on the transient deposit formation process, the influence of fuel characteristics and mechanisms of ash deposits removal are wanted. From a scientific point of view, the quantification of ash deposit build up and removal naturally and/or by sootblowing in suspension-fired boilers is an area where relatively limited accurate knowledge is available [6, 12].

Project Description and Specific Objectives
The objective of this project is to provide recommendations for the optimal operation strategy of straw suspension-fired boilers with respect to

minimization of deposit related problems. The specific objectives of the project are:

- Understanding removal behavior of deposits in the boiler chamber and superheater region (convective pass) of biomass-fired boilers.
- Investigating the influence of load, operation conditions and fuel changes (straw, wood or coal firing) on boiler deposits.
- To develop a model accounting for deposit formation and removal with changed temperature, ash composition and flow conditions. The model is intended to describe the deposit related processes as a function of the local parameters as gas velocity, ash particle size distribution, ash particle composition and gas and surface temperature.

The practical probe measurements will form the basis for the transient mathematical model for ash deposition and shedding. The results of this project will help to provide tools to minimize the deposit formation and increase the efficiency of deposit removal processes.

Methodology

- Full scale measurements in biomass suspension-fired boilers to characterize and quantify deposit build up and removal for different shares of straw in wood, using air and water cooled horizontal and vertical deposition/shedding probes.
- Development of sub-models for ash deposition and shedding in the boiler furnace region.
- Comparison of simulation results against observations from real furnaces.

Full Scale Experimental Measurements

The experiments were conducted at the Amagerværket suspension-fired boiler (AMV1) shown in Figure 1.

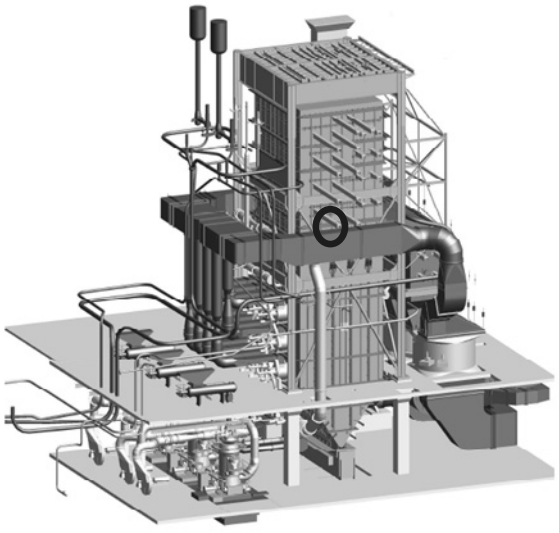

Figure 1: AMV1 suspension-fired boiler (350 MW_{th}) with identified probe position.

A series of 2-18 days deposit probe experiments were conducted utilizing 0% to 80 % straw with wood on mass basis at different boiler loads. An experimental resume is shown in Table 1. A double annular water and air probe made of stainless steel, with a total length of 3 m and an outer diameter of 40.5 mm was used during the experiments. The probe hung on a hinge which was connected to a flange. A balance at the rear was used to fix the probe horizontally. A load cell was used to detect variations of the force caused by the mass of the ash deposit on the probe inside the boiler. In total, 12 thermocouples were placed inside the outer probe metal tube with four thermo-elements (North, East, South and West) at three different positions. A charged-couple device (CCD) camera registered the deposit formation and removal process on the probe.

Table 1: Experimental resume

Test No	1	2	3	5	4	7	6	8
Straw (%)	80	65	50	45	40	10	5	0
Ash (%)	5.1	4.1	3.5	3.3	3.4	1.0	0.8	0.7
Probe Temp (°C)	500	600	500	500 (600)	500	550	550	550
Exposure Time (h)	56	45	185	168	73	335	434	212

The flue gas temperature near the probe was continuously measured, using a simple thermocouple in a protective shell. A suction pyrometer (IFRF [11]) was used during different intervals in almost each experiment in order to confirm the accuracy of the flue gas temperature measurements. An artificial sootblowing probe with an external diameter of 42.2 mm and 3 m length was used for in-situ removal of deposits. The sootblower nozzle was fixed at the end of the probe. Peak Impact Pressure (PIP) through the nozzle was measured along the axial centerline as a function of the supplying air pressure, using a pitot tube.

Ash Deposit Build up

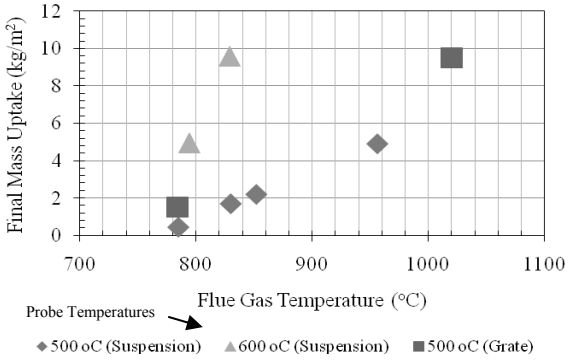

Figure 2: Influence of flue gas temperature on final deposit mass uptake (final 2 hours average) for biomass grate and suspension-firing conditions with more than 40% straw fuel on mass basis [6]. Results are shown for two different probe metal temperatures (500 and 600 °C) and 46 h exposure time.

In Figure 2 is shown the impact of flue gas temperature on 46 hours deposit mass uptake during grate and suspension-firing conditions at 500 and 600 °C probe metal temperature. It is evident that the deposit mass uptake during biomass suspension-firing and grate-firing

increases with increase in flue gas temperature. It is also clear that when the straw fuel share was greater than 40 % on mass basis, the flue gas temperature was a key factor controlling the deposit mass uptake. This trend is possibly due to partial melting of fly ash particles and deposit surface and resultantly the capture efficiency of the fly ash particles is enhanced. It is also evident that increasing the probe metal temperature from 500 to 600 ^{o}C lead to a significantly increased deposit formation rate. Figure 2 also indicates that the final deposit mass uptake during biomass suspension-firing is not higher compared to biomass grate-firing at almost similar conditions.

Important finding related to deposit formation process were:

- It was identified that an increase in flue gas temperature increased the deposit weight uptake during suspension-firing of wood and straw. The deposit weight uptake increased significantly when flue gas temperature exceeded 940 ^{o}C. Potassium components play a significant role in the deposit formation because they act as glue whereby particle capture efficiency is increased.
- The fouling and slagging propensity during co-combustion of straw and wood was reduced to that for maximum share of straw due to ash dilution effects and change in the elemental composition. When the straw share was greater than 40 % on mass basis in the fuel, the flue gas temperature was the key factor controlling the deposition rate.
- With increase in probe surface temperature from 500 ^{o}C to 600 ^{o}C, the deposit mass uptake increased due to partial melting of the condensed salt layer.
- Deposits were more sintered in the windward direction during maximum straw-firing.
- It was also observed that the final deposit weight uptake was not higher compared to biomass grate-firing at almost similar conditions. This is surprising since the fly ash fraction is higher in the suspension-fired boiler (typically 80% in a suspension-fired boiler, while only 20-30% of the fuel ash is transformed to fly ash in a grate boiler).

Deposit Shedding

The video recordings of all deposit probe experiments reveal that deposit shedding was primarily through debonding in the superheater region as shown in Figure 3.

The needed peak impact pressure (PIP) of the sootblower jet to remove the probe deposits at different conditions was investigated and the results are summarized in Figure 4. An increase in exposure time and probe metal temperature increased the PIP needed to remove the deposits. As shown in Figure 4, the deposits of less than 91 h probe exposure time were easy to remove and PIP needed was less than 55 kPa at 500 ^{o}C probe metal temperature.

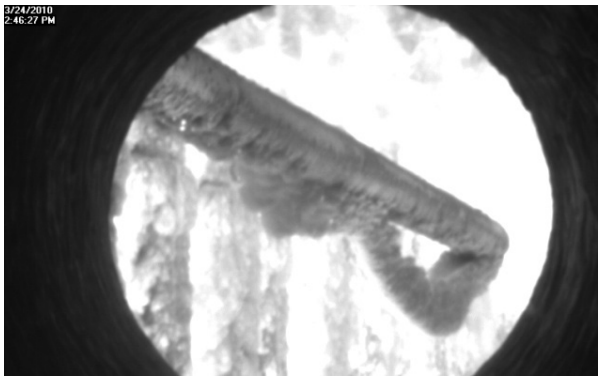

Figure 3: Image showing deposit removal through debonding.

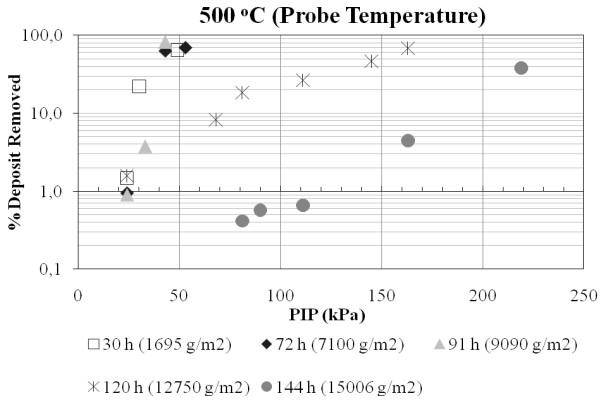

a)

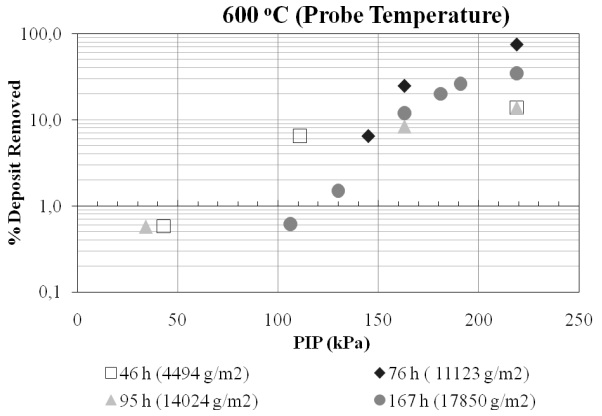

b)

Figure 4: Influence of probe exposure time and probe metal temperature on deposit removal for different weight uptake signals a) 500 ^{o}C probe metal temperature; b) 600 ^{o}C probe metal temperature.

With increase in probe surface temperature from 500 ^{o}C to 600 ^{o}C, the PIP needed to remove the deposits increased. Higher probe surface temperature caused melting of the inner most deposit layer and the adhesion strength between the deposit and the tube was enhanced. At higher probe surface temperatures (> 550 ^{o}C) and longer probe exposure times, a 2-10 mm thick layer was formed on the downstream surface and was being attached to the thick front layer, making it difficult to remove the windward side deposit layer. At lower temperatures (500 ^{o}C), the layer formed on the

downstream side was thin and the distinct front layer was easy to remove using the artificial sootblower.

Characterization of Residual Ash and Deposits

Elemental analysis of fly ashes and deposit samples was made in order to determine concentrations of the major elements such as Al, Ca, Fe, K, Mg, Na, P, Si, S and Cl using both SEM/EDX and ICP-OES. It was identified that the straw suspension-firing fly ashes contained high contents of Si and Ca, while grate-firing fly ashes contained higher contents of volatile elements such as K, Cl and S. The detailed elemental analysis of fuel ash, fly ash, and bottom ash and deposit samples is being carried out by Vattenfall Laboratory and at CEN DTU. Detailed elemental analysis of fuel ash, deposits, and residual ash will be presented in future for short and long run experiments at different straw shares and probe metal temperatures. The influence of fuel type, probe exposure time, probe surface temperature, flue gas temperature, and boiler load on deposit characteristics based on visual analysis and SEM/EDX analysis will be investigated in future.

Conclusions

It was found that with an increased probe surface temperature from 500 to 600 ^{o}C, the rate of deposit build up increased. It was also observed that when the straw fuel share was greater than 40 % on mass basis, the flue gas temperature was the key factor controlling the deposit formation rate. It was observed that deposit shedding was primarily through debonding and deposits of less than 91 h exposure time were easy to remove and the PIP needed was less than 55 kPa at a 500 ^{o}C probe surface temperature. With an increase in probe surface temperature from 500 to 600 ^{o}C, the PIP needed to remove the deposits increased.

Based on the current findings, recommendations for the optimal operation strategy of straw and wood suspension-fired boilers with respect to minimization of deposit related problems can be provided. From a research point of view, new methods has been applied for the quantification of ash deposit build up and removal naturally and/or by sootblowing in suspension-fired boilers and will be useful for future research in this field.

Acknowledgement

The financial support under the Energinet.DK PSO project 7217 and financial support by Vattenfall A/S is gratefully acknowledged. The author wants to thank the operational people at Amagerværket Power Plant, owned by Vattenfall A/S for their technical support and participation in the project.

References

1. M.S. Bashir, P.A. Jensen, F. Frandsen, S. Wedel, K. Dam-Johansen, T. Wolfe, S.T. Pedersen, J. Wadenbäck, OA5.1, (2010), 18th European Biomass Conference, 03-07 May, Lyon, France.
2. M.S. Bashir, P.A. Jensen, F. Frandsen, S. Wedel, K. Dam-Johansen, S.T. Pedersen, J. Wadenbäck, (2010), Impact of Fuel Quality on Power Production and the Environment, 29 Aug-03 Sep, Lapland, Finland.
3. M.S. Bashir, P.A. Jensen, F. Frandsen, S. Wedel, K. Dam-Johansen, S.T. Pedersen, J. Wadenbäck, (2010) Dansk Kemiingeniør Konference, June, Lyngby, Denmark, pp 176-177.
4. H.P. Nielsen, Deposition and High Temperature Corrosion in Biomass-Fired Boilers, PhD Thesis, Technical University of Denmark, (1998), ISBN 87-90142-47-0.
5. A. Zabogar, F.J. Frandsen, P.A. Jensen, P. Glaborg, Prog. Energ. Combust. 31 (2009) 371-421.
6. H. Zhou, F.J. Frandsen, P.A. Jensen, P. Glarborg, (2006), PSO Project 4106, CHEC Research Centre, Technical University of Denmark.
7. A. Zabogar, F.J. Frandsen, P.A. Jensen, P. Glaborg, P. Hansen, Energ. Fuel. 20 (2) (2006) 512-519.
8. M. Theis, B.J. Skrifvars, M. Hupa, H. Trans, Fuel 85 (2006) 1125-1130.
9. F.J. Frandsen, Fuel 84 (2005) 1277-1294.
10. L. Tobiasen, R. Skytte, L.S. Pedersen, S.T. Pedersen, M.A. Lindberg, Fuel Process. Technol. 88 (2007) 1108-1117.
11. IFRF Suction Pyrometer, User Information Document, International Flame Research Foundation.
12. B.-Skrifvars et al., Fuel 83 (2004) 1371-1379.

List of Publications

1. M.S. Bashir, P.A. Jensen, F. Frandsen, S. Wedel, K. Dam-Johansen, T. Wolfe, S.T. Pedersen, J. Wadenbäck, OA5.1, (2010), 18th European Biomass Conference, 03-07 May, Lyon, France.
2. M.S. Bashir, P.A. Jensen, F. Frandsen, S. Wedel, K. Dam-Johansen, S.T. Pedersen, J. Wadenbäck, (2010) Dansk Kemiingeniør Konference, June, Lyngby, Denmark, pp 176-177.
3. M.S. Bashir, P.A. Jensen, F. Frandsen, S. Wedel, K. Dam-Johansen, S.T. Pedersen, J. Wadenbäck, (2010), Impact of Fuel Quality on Power Production and the Environment, 29 Aug-03 Sep, Lapland, Finland.

Matthias Josef Beier

Phone: +45 4525 2936
E-mail: mjb@kt.dtu.dk
Discipline: Reaction and Transport Engineering

Supervisors: Anker D. Jensen
Jan-Dierk Grunwaldt, KIT
Georgios Kontogeorgis

PhD Study
Started: February 2008
To be completed: February 2011

Experimental Determination, Modeling and Utilization of the Phase Behavior in the Selective Oxidation of Alcohols in Pressurized CO_2

Abstract
The catalytic oxidation of benzyl alcohol to benzaldehyde with molecular oxygen in "supercritical" CO_2 is significantly influenced by the phase behavior. Depending on pressure and temperature all substrates are either present in a single phase or in two phases for a given composition. The Cubic plus Association Equation of State was used in order to predict the phase behavior of ternary mixtures relevant to the catalytic oxidation of benzyl alcohol and validated experimentally. The model was successfully exploited to predict optimal reaction conditions for the continuous catalytic oxidation of benzyl alcohol to benzaldehyde. Operating the reactor in the biphasic pressure region close to the dew point gave the best results.

Introduction
The selective oxidation of alcohols to aldehydes or ketones by molecular oxygen in the liquid phase has been intensively investigated in the recent years [1]. A problem associated with the aerobic alcohol oxidation is the low oxygen solubility in organic solvents frequently used for these reactions. Using pressurized CO_2 as a solvent, the oxygen availability can be markedly improved which led to higher reaction rates compared to standard organic solvents [2]. The solvent power of CO_2 can be tuned by the pressure. Hence, at high pressures the reaction mixture exists as a single phase. At low pressures the dissolution of substrate is incomplete and thus two phases are present. Phase behavior has an important influence on the reaction rate in reaction with pressurized CO_2 as a solvent [3]. Therefore, modeling of the phase behavior in order to predict dew points can significantly simplify the experimental effort for determining optimal reaction conditions. The description of the phase behavior of ternary systems consisting of benzyl alcohol, O_2 and CO_2 requires a model accounting for the strong association between the molecules. The Cubic plus Association (CPA) Equation of State takes these contributions into account and has been used successfully for systems with pressurized CO_2 in the past [4].

Specific Objectives
At first a short overview over the results on the model predictions for the ternary system benzyl alcohol – O_2 – CO_2 are presented. Next, the usefulness of the model for the catalytic oxidation of benzyl alcohol in "supercritical" CO_2 with molecular oxygen as the oxidant will be evaluated over a commercial Pd/Al_2O_3 catalyst (Scheme 1).

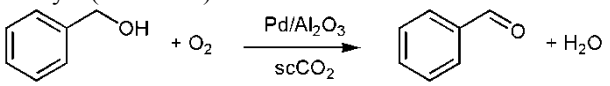

Scheme 1: Oxidation of benzyl alcohol to benzaldehyde over 0.5 % Pd/Al_2O_3.

Experimental
Phase behavior predictions were made with the Cubic plus Association Equation of State using pure compound and fitted binary interaction parameters. Experimental phase behavior measurements for ternary mixtures for the substrate mixture (benzyl alcohol – O_2 – CO_2) and the product mixture (benzaldehyde – H_2O – CO_2) under conditions relevant for the catalytic process were done in a custom-made view cell [5]. Catalytic measurements were performed in a continuous high pressure fixed bed reactor operated at 80 °C and pressures between 100 – 200 bar with a shell-impregnated 0.5% Pd/Al_2O_3 catalyst [2].

Results and Discussion
Phase transitions for systems with a high CO2 fraction were obtained by CPA modeling and agreed well with experimental data (Figure 1), especially at low benzyl

alcohol concentrations [6]. Dew points at higher substrate concentrations are only slightly over-predicted. Similar observations were made for the

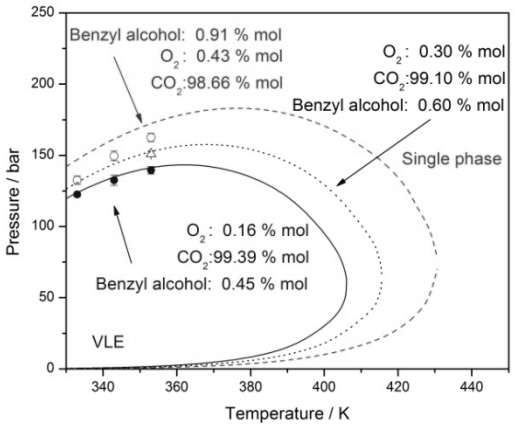

Figure 1: CPA prediction (lines) and experi-mental dew points for the ternary substrate mixture.

product mixture referring to full conversion and 100% selectivity (*not shown*). Dew points occurred in general at lower pressures which mean that the maximum pressure necessary for forming a single phase system is dictated by the substrate mixture for a given composition.

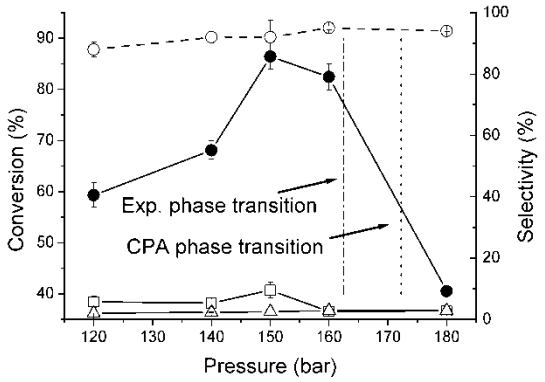

Figure 2: Oxidation of benzyl alcohol over Pd/Al_2O_3 depending on the pressure. Feed composition: 0.9 mol-% benzyl alcohol, 0.45 mol-% O_2, rest CO_2. (●) conversion, (○) benzaldehyde selectivity (□) toluene selectivity (Δ) selectivity to overoxidation products.

In order to evaluate the applicability of phase behavior modeling in catalytic studies, the benzyl alcohol conversion was measured over 0.5% Pd/Al_2O_3 in a continuous reactor as a function of pressure (Figure 2). Indeed, model predictions and experimental data for the dew points coincided with substantial changes in the reaction rate. At low pressures, higher reaction rates were observed and the major side-product was toluene. Under single phase conditions (above about 160 bar), the conversion dropped significantly. Overoxidation products became the main side products. The increase between 140 and 150 bar was not due to a phase transition. In contrast to previous studies [7], optimal reaction conditions were found close to the experimental phase transition but still in the biphasic pressure region. This was supported by batch reactions with simultaneous phase behavior monitoring. The worse performance of the catalyst in the single phase regime at high pressures could be connected to deactivation of palladium by oxidation or blocking of surface sites by strongly adsorbing side-products.

Conclusions

The phase behavior of ternary system relevant for the selective oxidation of benzyl alcohol in "supercritical" CO_2 could be modeled with the Cubic plus Association Equation of State and showed reasonable agreement with experimental data. A strong dependence on the system pressure was found in the dew point region for the catalytic oxidation reaction. Biphasic conditions at a pressure close to the dew point were found to result in the highest reaction rates. The model's capability of predicting the phase behavior is therefore useful to optimize the catalytic reaction without elaborate experimental phase behavior investigations. In the future, estimation of the oxygen concentration at the catalyst surface would be interesting in order to correlate catalytic activities.

References

1. T. Mallat, A. Baiker, Chem. Rev. 104 (2004) 3037.
2. M. Caravati, J.-D. Grunwaldt, A. Baiker, Catal. Today 91-2 (2004) 1.
3. M. Caravati, D.M. Meier, J. Grunwaldt, A. Baiker, J. Catal. 240 (2006) 126.
4. G.M. Kontogeorgis, M.L. Michelsen, G.K. Folas, S. Derawi, N. von Solms, E.H. Stenby, Ind. Eng. Chem. Res. 45 (2006) 4869.
5. R. Wandeler, N. Kunzle, M.S. Schneider, T. Mallat, A. Baiker, J. Catal. 200 (2001) 377.
6. I. Tsivintzelis, M.J. Beier, J. Grunwaldt, A. Baiker, G.M. Kontogeorgis, Fluid Phase Equilibr. In Press, Corrected Proof. doi:10.1016/j.fluid.2010.10.001
7. M. Caravati, J.-D. Grunwaldt, A. Baiker, Phys. Chem. Chem. Phys. 7 (2005) 278.

List of Publications

1. I. Tsivintzelis, M.J. Beier, J.-D. Grunwaldt, A. Baiker, G.M. Kontogeorgis, Fluid Phase Equilibr. In Press, Corrected Proof, doi:10.1016/ j.fluid.2010.10.001
2. M. Hoj, M.J. Beier, J.-D. Grunwaldt, S. Dahl, Appl. Catal. B 93 (2009) 166.
3. M.J. Beier, T.W. Hansen, J.-D. Grunwaldt, J. Catal. 266 (2009) 320.
4. M.J. Beier, B. Schimmoeller, T.W. Hansen, J.E.T. Andersen, S.E. Pratsinis, J.-D. Grunwaldt, J. Molec. Catal. A 331 (2010) 40.

Andrijana Bolic
Phone: +45 4525 2958
E-mail: anb@kt.dtu.dk
Discipline: Process Technology and Unit Operations

Supervisors: Krist V. Gernaey
Anna Eliasson Lantz, DTU Systembiologi
Karsten Rottwitt, DTU Fotonik
Nicolas Szita, UCL

PhD Study
Started: March 2010
To be completed: February 2013

Monitoring Continuous Fermentation Processes in Microbioreactor Systems

Abstract
At present, research in bioprocess science and engineering requires fast and accurate analytical data (rapid testing) that can be used for investigation of the interaction between bioprocess operation conditions and the performance of the bioprocess. Miniaturization could provide an attractive tool necessary for obtaining vast amounts of experimental data. The objectives of this project are to perform continuous cultivations with *Saccharomyces cerevisiae* in a microbioreactor, and to implement NIR and Raman spectroscopy for rapid on-line measurement of process variables like substrate and biomass concentration.

Introduction
Conventional microbial cell cultivation techniques are not sufficient anymore considering the fast development of tools for genetic manipulation of biological systems resulting in large numbers of strains and conditions that need to be screened. Usually bench-scale reactors, flasks and tubes are used for obtaining relevant experimental data of microbial cultivations. Although bench-scale reactors have efficient control of process variables and yield valuable data, they are expensive, labor intensive and they provide a relatively small amount of data.

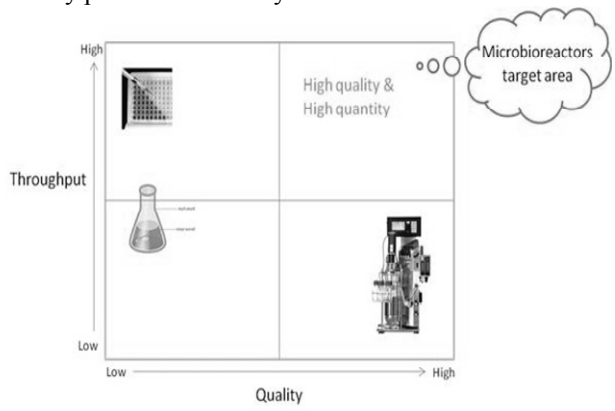

Figure 1: Different vessels (microtiter plates, flasks and bench-scale bioreactor) and their positioning according to throughput and data quality

Regarding microbial cultivations in flasks and tubes, there is a general lack of control and the amount of data collected per experiment is usually not sufficient. Beside the above-mentioned vessels, today, microtiter plates are becoming dominant for screening experiments considering that they provide easy handling, low cost and high throughput. Nevertheless, the process control in microtiter plates is often not reliable enough to provide realistic figures for scale up which is affecting the overall value of data. Different reactor configurations and their positioning according to throughput and data quality are presented in Figure 1.

There is a big driving force and interest in the last decade for development of new techniques which could provide both high quality data and also a high quantity of experimental data. In recent years microbioreactors have been researched intensely due to their clear advantages like small volume, little or no need for cleaning (one time usage), high throughput (multiple microbioreactors in parallel), high information content and control capabilities.[1] Microbioreactors together with analytical methods are providing the opportunity for a potentially automated and well defined experimental system, which can deliver results that are more comparable to bench-scale reactors in comparison to e.g. a shake flask. For bioprocess development, it is interesting to follow different substrates and metabolites during microbial cultivation, besides measuring basic process variables like temperature, pH, optical density and dissolved oxygen. Raman and NIR spectroscopy have the potential to provide non-invasive, on-line monitoring of different metabolites during microbial cultivations in microbioreactors, which makes this combination promising for obtaining a high quantity of high quality data.

Project objectives

Considering the points mentioned above, the main objective of this research project is to obtain continuous microbial cultivations in a microbioreactor – MBR (100µl-1ml) using *S. cerevisiae* as a model strain and to establish good on-line process monitoring which could provide vast amounts of experimental data which are important for achieving a better understanding of microbial cultivations and facilitating scale-up. Schematic overview of project structure is presented in Figure 2.

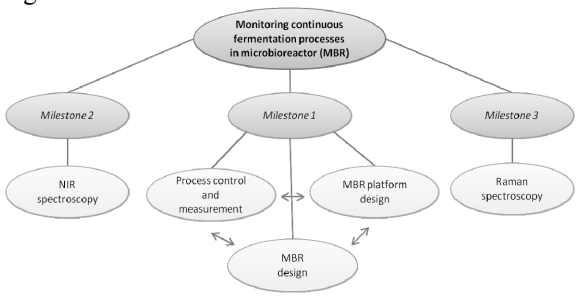

Figure 2: Schematic overview of project structure and overall objectives

Results and Discussion

Current set up

The volume of the current microbioreactor design is 100 µl; it is made from polydimethylsiloxane (PDMS), which is biocompatible, gas permeable and has good optical properties. The microbioreactor consists of two layers with a PDMS membrane placed in between. The main role of the membrane is to provide bubbleless aeration as well as removal of CO_2. [2] Stirring is obtained by a magnetic spinning bar. The microbioreactor geometry and appearance are presented in Figure 3.

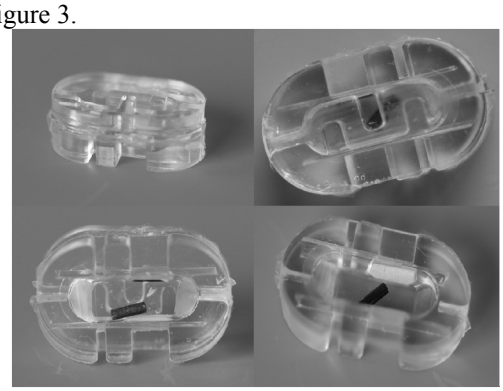

Figure 3: Microbioreactor (100µl)

Process variables measured in the microbioreactor are dissolved oxygen, pH, temperature and optical density. Dissolved oxygen and pH are measured with fluorescent sensor spots where phase shift is correlated with the measured variable. Optical density is recorded during the cultivation by transmission of light throughout the broth. Temperature is measured by a Pt-100 element. In addition to the measurement of the mentioned process variables, control of pH and temperature are established. A heating element consisting of a resistance wire embedded in polymer is placed underneath the reactor and is used for temperature control. [3] pH control is established by addition of CO_2 and NH_3 gases to the aeration gas which diffuses through the PDMS membrane. Batch cultivation of *S. cerevisiae* has been performed in the microbioreactor, while reproducible continuous cultivation still has to be realized.

Conclusion

Even though microbioreactors have many advantages and they represent a promising tool for bioprocess development, it is important to bear in mind that they also have some issues related to their size and handling. Evaporation, proper and reliable mixing, interconnections between micro and macro world are just some of the burning problems that need to be addressed.

In addition, signal collection of different process variables in microbioreactors is not straightforward. It relies on analytical methods which are not sufficient at the moment. Optodes for pH measurement have a limited range (5.5-8.5) and signal collection is not cheap and not straightforward.

Another important question is which microbioreactor volume is optimal while keeping in mind the final objective –application. Do we need a sample or not? Do we talk about cells in suspension or adhered on some substrate? The final microbioreactor design should thus strongly depend on the final goal and application.

Next Step

Considering the above, the next step in this project is the development of a microbioreactor with increased volume (1ml) which will be made of PMMA. It will have well-defined mixing which could mimic a process environment from lab scale reactors. A supporting platform will be developed which is expected to contribute significantly to the reliability and reproducibility of the cultivation. Connections will be established with chromatographic fittings which will prevent leakages in the system.

Acknowledgements

This project is supported by the Danish Council for Strategic Research in the frame of the project "Towards robust fermentation processes by targeting population heterogeneity at microscale" (project number 09-065160).

References

1. D. Schäpper, M.N.H.Z. Alam, N. Szita, A.E. Lantz, K.V. Gernaey, Anal. Bioanal. Chem. 395 (2009) 679–695
2. D. Schäpper, S.M. Stocks, N. Szita, A.E. Lantz, K.V. Gernaey, Chem. Eng. J. 160 (3) (2010) 891-898
3. M.N.H.Z. Alam, D. Schäpper, K.V. Gernaey, J. Micromech. Microen. 20 (2010) 055014

Jacob Brix

Phone: +45 4525 2922
E-mail: jac@kt.dtu.dk
Discipline: Reaction and Transport Engineering

Supervisors: Anker Degn Jensen
Peter Arendt Jensen

PhD Study
Started: October 2007
To be completed: January 2011

Oxy-Fuel Combustion of Coal

Abstract
Increasing awareness of the alleged global temperature increase, caused by an increasing level of anthropogenic CO_2 in the atmosphere, has increased the interest for a CO_2-friendly use of coal for heat and power generation. A promising method to achieve this goal is oxy-fuel combustion, a process where coal is burned in a mixture of O_2 and recycled flue gas (RFG). This gives a process exit gas consisting mostly of H_2O and CO_2 along with impurities such as NO_x and SO_x. After condensation of H_2O and flue gas cleaning for impurities a near pure CO_2 stream is obtained, which is ready for underground sequestration. The purpose of this project is to investigate the impact of a changed gaseous environment on coal conversion and NO_x emissions.

Introduction
In recent years there has been an increased focus on the environmental role of CO_2 and this focus has initiated stricter environmental legislations both globally and within the EU [1]. To overcome these legislations and to solve the problems related to CO_2 emission, the energy industry relaying on coal will need to find technological alternatives to the present combustion processes that will utilize coal in a more environmentally friendly way. This technological development is necessary since the dependence on coal as an energy source can be expected to be present for many years to come [1,2].

One solution that seems to be promising in the nearby to midterm future is oxy-fuel combustion [2]. Oxy-Fuel combustion is a combustion technique, which has been shown considerable research attention in recent years [3-9]. There are several reasons for this continuously increasing interest, among which the following should be emphasized:

- Existing plants can be retrofitted to function under oxy-fuel conditions relatively easy using O_2 concentrations of ~ 30 vol. % in the inlet gas [2].
- Oxy-Fuel combustion produces an exit stream with a very high CO_2 content (~90-95 %) [2,8,10], which is ready for sequestration. The CO_2 purity of the exit gas on industrial scale mainly depends on the efficiency of the Air Separation Unit (ASU) and the degree of leakage into the furnace.
- Combustion in an oxy-fuel environment has the potential to reduce NO_x emissions, when compared to traditional air-blown plants [2-4].

As a further benefit all of the oxy-fuel combustion unit operations, except the boiler, are in some sense relaying on existing and known equipment [11]. A scheme of the oxy-fuel combustion process can be seen in Figure 1.

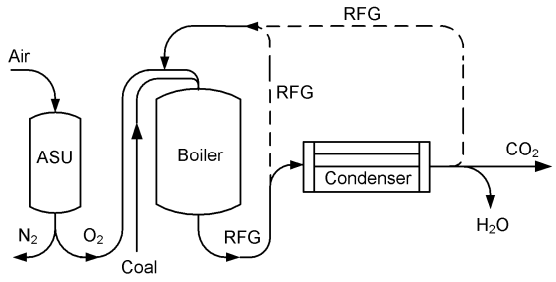

Figure 1: The overall idea behind the oxy-fuel combustion process is shown. Units such as flue gas cleaning units and compressors are omitted. The need for desulphurization will depend on the feedstock and if recycle is wet or dry.

Specific Objectives
This project is devoted to the investigation of coal conversion and NO emission in O_2/CO_2 and O_2/N_2 atmospheres.

Combustion of char in O_2 enriched CO_2 atmospheres, such as those prevailing in oxy-fuel combustion, is not fully understood, and the influence of gasification at higher temperatures has been observed [12] though the conditions under which it occurs are not

well documented. The possible differences in combustion behavior between conventional air-blown furnaces and oxy-fuel furnaces make a detailed study of the fuel combustion kinetics necessary. Such an investigation can focus on both effects arising from increased levels of CO_2 but also on kinetic effects of elevated O_2 concentrations [13]. Along with experiments accurate models predicting and interpreting test results are necessary before large scale plant construction can be initiated.

The NO_x evolution changes between air-blown combustion and oxy-fuel combustion [1]. This is mostly due to the recirculation of the flue gas into the flame and the reduction of NO over char. These effects are functions of O_2 concentration, temperature and fuel feed rate [14]. It is also possible that increased levels of CO facilitate an increased reduction of especially NO over the char surface [3]. These dependences on NO_x evolution are important to understand in detail in order to benefit fully from the possibilities of oxy-fuel combustion to reduce the NO_x emission [15].

Experimental

Experiments relating to fuel conversion are carried out using an entrained flow reactor (EFR). A schematic representation of the reactor is shown in Figure 2.

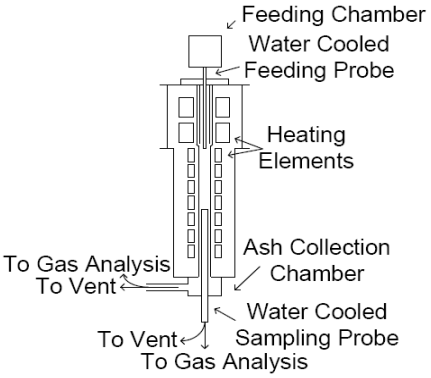

Figure 2: The electrically heated isothermal EFR used to investigate char conversion rate in O_2/N_2 and O_2/CO_2 atmospheres.

Using the EFR, experiments have been carried out in both O_2/CO_2 and O_2/N_2 mixtures in order to compare trends in char conversion profiles. Experiments have been carried out using bituminous coal particles sieved to the size interval 90 -106 µm. Reactor temperatures have been between 1073 K - 1673 K and inlet O_2 concentrations were between 5 - 28 vol. %. Char has been sampled at different reactor positions through an adjustable water cooled probe. At the sampling positions gas analysis for O_2, CO and CO_2 has also been carried out. In order to evaluate the fuel consumption due to char conversion devolatilization experiments have been carried out at each of the experimental temperatures using an O_2 concentration of 5 – 6 vol. % to avoid problems with tar.

A thermogravimetric analyzer (TGA) has been used to obtain reactivity profiles of chars sampled in the EFR in order to obtain intrinsic kinetic parameters. Combustion reactivity is measured at 5 vol. % O_2 at a heating rate of 5 K/min to a peak temperature of 1273 K. CO_2 gasification reactivity is measured at 80 vol. % CO_2 at the same heating rate to a peak temperature of 1373 K.

Experiments carried out to investigate NO formation are conducted using a laboratory scale fixed bed reactor (FBR). The reactor is equipped with a 16 bit Charged-Coupled Device (CCD) camera that measures the radiation of the burning particles. These emission signals are subsequently used to calculate particle surface temperatures. A schematic representation of the reactor is shown in Figure 3.

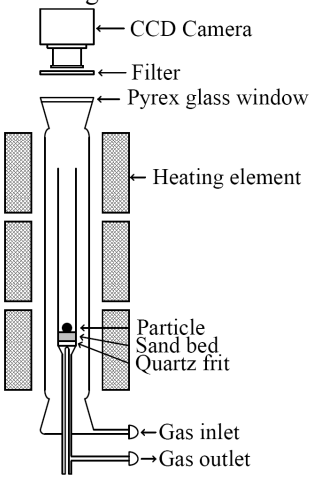

Figure 3: The laboratory scale FBR used to measure NO emissions in N_2/O_2 and CO_2/O_2 atmospheres.

The FBR was operated isothermally at 1073 K in O_2/N_2 and O_2/CO_2 mixtures with O_2 concentrations in the range 5 – 80 vol. % and millimeter sized lignite- and bituminous char particles as fuels. Chars are prepared from pyrolysis at 1173 K in N_2 and are in the size range 0.71 – 12.1 mm. Most of the experiments have been conducted at single particle conditions but a series with 5, 10, 15 and 20 particles were carried out to investigate the effect of particle concentration.

Results

Devolatilization experiments did not show differences in volatile yield between N_2 and CO_2 atmospheres, as shown in Figure 4.

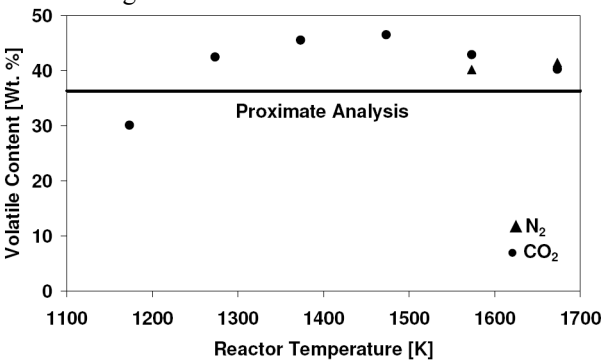

Figure 4: Volatile content as a function of reactor temperature.

Scanning Electron Microscopy (SEM) imaging and N_2-BET surface area measurements on chars sampled during devolatilization at 1673 K in N_2 and CO_2 did not reveal differences between the two atmospheres. TGA reactivity profiles, shown in Figure 5, did not reveal differences either. That there are no differences in combustion reactivity between EFR chars formed and partly consumed in O_2/N_2 or O_2/CO_2 was a consistent conclusion from all the TGA experiments.

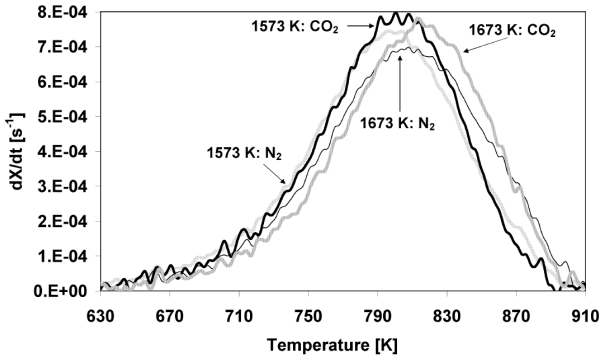

Figure 5: Combustion reactivity of EFR char obtained from devolatilization at 1573 K and 1673 K in N_2 and CO_2.

From TGA reactivity profiles of EFR chars sampled during devolatilization kinetic parameters were obtained for both combustion and CO_2 gasification. The Arrhenius expressions are shown in equation (1) and (2) [kg m^{-2} s^{-1} (mol m^{-3})$^{-0.5}$].

$$k_{O_2} = 1.4359 \cdot \exp\left(\frac{20500}{R \cdot T^*}\right) \cdot \exp\left(\frac{-137500}{R \cdot T}\right) \quad \textbf{(1)}$$

$$k_{CO_2} = 7.3282 \cdot \exp\left(\frac{-230800}{R \cdot T}\right) \quad \textbf{(2)}$$

Equation (1) and (2) have been implemented in a detailed COal COmbustion MOdel (COCOMO) encompassing the three char morphologies; cenospheres, network- and dense chars. Physical and chemical properties in the model are calculated as temperature and composition dependent. Figure 6 compares experimental EFR conversion profiles with model simulations and witness of a high degree of model accuracy, which is in general found when simulated profiles are compared to the EFR experiments. Significant deviation between COCOMO and experiments are seen only in two cases as shown in Figure 7. The first case is combustion at low temperature and O_2 concentration. Here an experimental delay in ignition causes a large absolute error in predicted char conversion though the conversion rate is described well by the model.

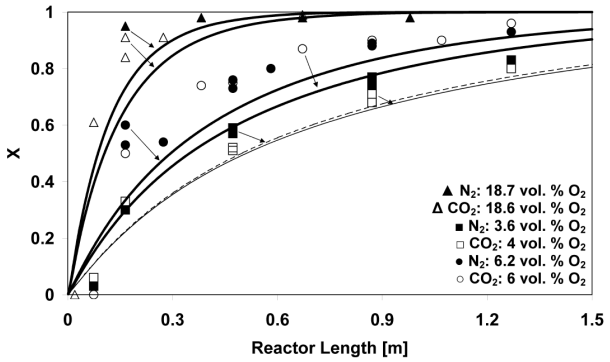

Figure 6: COCOMO profiles and experimental profiles obtained at 1373 K in N_2 and CO_2. $\lambda \sim 2.3 - 9.8$.

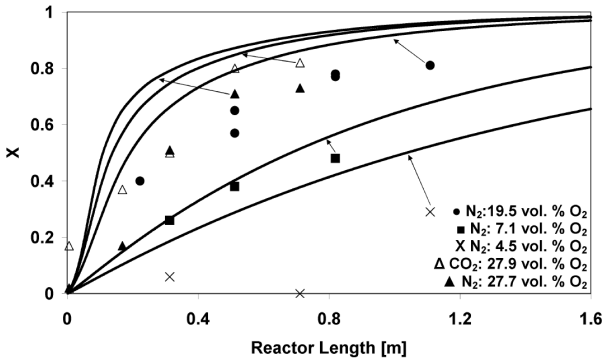

Figure 7: COCOMO profiles and experimental profiles obtained at 1173 K in N_2 and CO_2. $\lambda \sim 2.7 - 15.2$.

The second case is combustion at low temperature and high O_2 concentration. At these conditions two char phases, a moderately reactive and a non-reactive, are formed due to a fierce heating upon ignition at the high O_2 concentrations. COCOMO assumes that deactivation is taking place homogeneously and does therefore not capture the transient conversion profile precisely. COCOMO does however capture that a significant and abrupt deactivation takes place. An effect of CO_2 gasification was not found to play a significant role in the EFR experiments.

Figure 8 shows that the NO emission from combustion of bituminous char drops significantly as N_2 is replaced with CO_2 whereas emissions from lignite char combustion are not affected by gaseous atmosphere. This is a general conclusion from the FBR experiments. Also the NO emissions from lignite char are lower than that from bituminous char, which is in general found in the FBR experiments and in the literature. This is believed to be caused by a lignite char that is more reactive towards heterogeneous NO reduction.

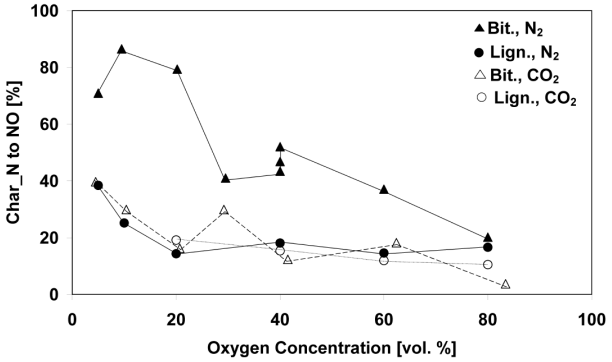

Figure 8: NO emissions from single particle combustion as a function of O_2 concentration. d_p = 2 – 4 mm. $T_{reactor}$ = 1073 K.

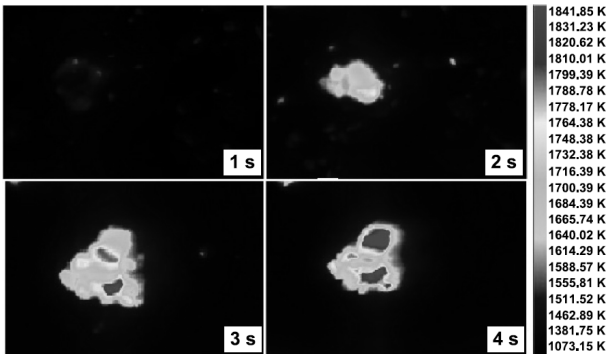

Figure 9: Still images of a single bituminous particle burning at 80 vol. % O_2 in N_2. d_p = 3.5 mm. $T_{reactor}$ = 1073 K. Time zero is ignition.

Using the CCD camera film recordings of particle surface temperature and therefore structural development can be made. Figure 9 shows still images from a film recording of combustion at 80 vol. %. It can be seen in the figure that the particle explodes initially due to a rapid heat release, thereby leaving fragments glowing on the bed. The CCD camera in general proved a valuable tool for accurate in situ measurements of particle temperature.

Conclusions

From EFR experiments no differences in volatile weight loss or char conversion rate have been found between O_2/N_2 and O_2/CO_2 atmospheres. TGA reactivity profiles have likewise shown that char sampled in the EFR in the two different atmospheres have similar reactivities. The use of intrinsic kinetic parameters, obtained from TGA combustion of chars collected during EFR devolatilization, in a detailed char conversion model has proven to describe char combustion rate accurately. Measurement of NO emissions during combustion of lignite- and bituminous char has shown a significant decrease of NO emission in O_2/CO_2 compared to O_2/N_2 for bituminous char. Emissions from lignite char are not affected significantly by the gaseous atmosphere.

Acknowledgements

The research leading to these results has received funding from the European Community's Research Fund for Coal and Steel (RFCS) under contract nRFCR-CT-2006-00007, project FRIENDLY COAL, and is also sponsored by the Danish Agency for Science, Technology and Innovation, Energinet.dk, Vattenfall Research and Development AB and ALSTOM Power Systems Gmbh. The support and funding from these entities are greatly valued.

Reference

1. R. Tan, G. Corragio, S. Santos, Oxy-Coal Combustion with Flue Gas Recycle for the Power Generation Industri, Report No. G 23/y/1, International Flame Research Foundation, 2005.
2. B.J.P. Buhre, L.K. Elliott, C.D. Sheng, R.P. Gupta, T.F. Wall, Prog. Energ. Combust. (31) (2005) 283-307.
3. K. Okazaki, T. Ando, Energy (22) (1997) 207-215.
4. H. Liu, R. Zailani, B.M. Gibbs, Fuel (84) (2005) 2109-2115
5. Y.Q. Hu, N. Kobayashi, M. Hasatani, Fuel (80) (2001) 1851-1855
6. Y. Hu, S. Naito, N. Kobayashi, M. Hasatani, Fuel (79) (2000) 1925-1932
7. K. Andersson, F. Normann, F. Johnsson, B. Leckner, Ind. Eng. Chem. Res. (47) (2008) 1835-1845
8. H. Liu, R. Zailani, B.M. Gibbs, Fuel (84) (2005)
9. P.A. Bejarano, Y.A. Levendis, Combust. Flame (153) (2008) 270-287
10. C.S. Wang, G.F. Berry, K.C. Chang, A.M. Wolsky, Combust. Flame (72) (1988) 301-310
11. L. Strömberg, Combustion in a CO_2/O_2 Mixture for a CO_2 Emission Free Process, Second Nordic Minisymposium on Carbon Dioxide Capture and Storage, 2001, 58-63.
12. T.F. Wall, Proc. Combust. Inst. (31) (2007) 31-47.
13. J.J. Murphy, C.R. Shaddix, Combust. Flame (144) (2006) 710-729.
14. Y.Q. Hu, N. Kobayashi, M. Hasatani, Energ. Convers. Manage. (44) (2003) 2331-2340.
15. Y. Tan, E. Croiset, M.A. Douglas, K.V. Thambimuthu, Fuel (85) (2006) 507-512.

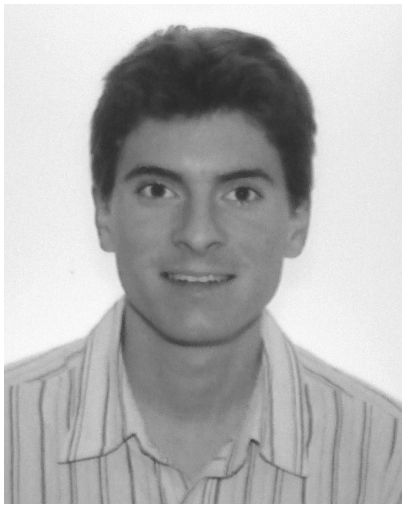

Albert E. Cervera Padrell

Phone: +45 4525 2949
E-mail: acp@kt.dtu.dk
Discipline: Process Technology and Unit Operations
Systems Engineering
Supervisors: Krist V. Gernaey
Rafiqul Gani
Søren Kiil
Tommy Skovby, Lundbeck A/S

PhD Study
Started: August 2008
To be completed: July 2011

Moving from Batch towards Continuous Organic-Chemical Pharmaceutical Production

Abstract
Continuous pharmaceutical manufacturing (CPM) offers the possibility to achieve higher reaction yields and improved separation efficiencies compared to batch-wise production, potentially leading to simplified process flowsheets, reduced total costs, lower environmental impacts, and safer and more flexible production. However, the change from batch-wise production towards continuous operation requires a high degree of process knowledge. The aim of this PhD project is to develop a toolbox of continuous unit operations which cover the spectrum of typical operations employed for organic-synthesis based active pharmaceutical ingredient (API) production, and to develop a methodology that systematically identifies PSE methods and tools which can assist in the design of CPM processes.

Introduction
The pharmaceutical industry is nowadays investing a large amount of resources in the development of optimized production technologies in order to decrease the manufacturing costs [1]. Continuous pharmaceutical production has emerged as a relatively unexplored field within this industry, with the potential to improve quality and efficiency, and decrease risk, waste and production costs as compared to traditional batch manufacturing [2]. However, the change from batch to continuous-based production is not straightforward and requires a multi-scale approach.

Many already existing APIs produced in batch mode consist of two or more separate production stages, with isolation and storage of intermediates. In order to exploit the full benefits of continuous production, the different stages should be connected in a feasible manner while preserving an acceptable degree of quality. Secondly, each of these stages may involve several solvent exchange steps and as a consequence a large solvent use. Changing the production to continuous mode offers a good opportunity to remove unnecessary solvent exchange steps and minimize solvent use. Thirdly, each unit operation in the process may be redesigned to obtain more efficient heat and mass transfer or to fit better to the particular physics or chemistry of the process. For example, the classical continuous reactor designs such as plug flow reactor or continuously stirred tank reactor (CSTR) may be modified to adapt to the kinetics of the reaction or to allow multiple phases. Operations which are relatively simple to carry out in batch mode such as those involving solids or requiring long residence times pose severe challenges in a continuous production environment. In fact, not every operation in a process should be run in continuous mode and hybrid operation (continuous unit operations combined with batch operations) should be enabled. Last but not least, each unit should be flexible enough to allow different operating conditions, in order to reach optimal conditions or to respond to disturbances in the process. A large amount of knowledge about the process is required in this step, and different modeling tasks will be involved.

In this PhD project a methodology for the design of continuous processes for organic-synthesis based production of APIs is proposed. This methodology systematically explores the opportunities that continuous production offers at different levels of detail, from the process flowsheet to the basic process modeling through the unit operation design. Executing each step in this method requires gathering some data and employing several methods. The methods applied have been used before in many different fields and are selected from the literature when needed. The application of the methodology will be exemplified with a case study - the production of an API developed by Lundbeck A/S.

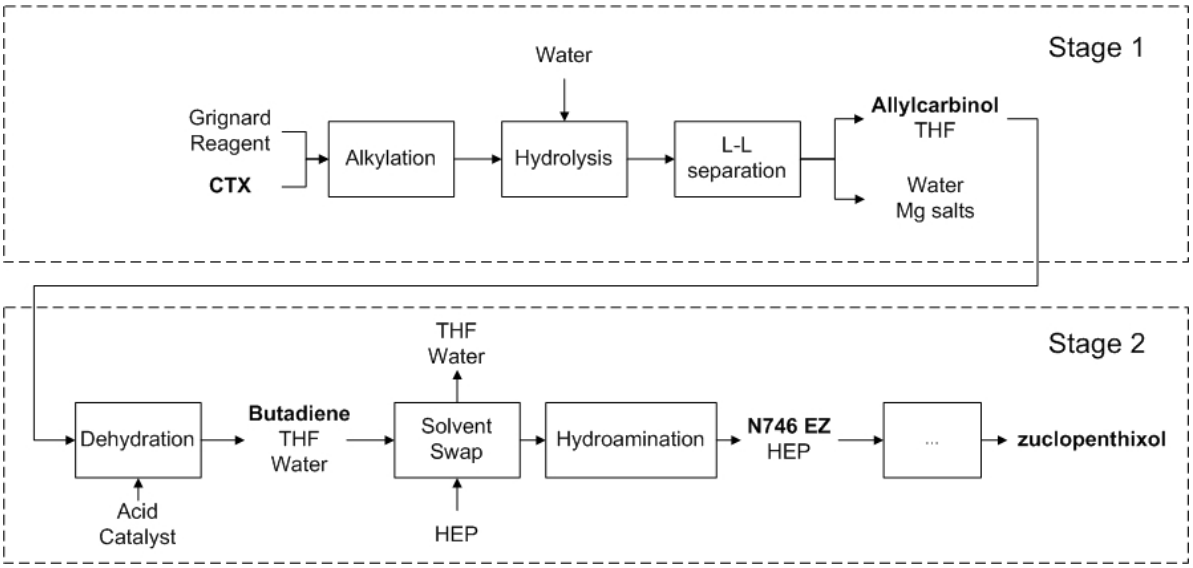

Figure 1: Simplified process flowsheet for the production of zuclopenthixol.

Specific Objectives

The case study of this project is the production of an active pharmaceutical ingredient (API) developed by Lundbeck A/S: zuclopenthixol. The first objective is to eliminate intermediate production steps in order to obtain a less time-consuming and less complex production process. The original batch-wise process is divided into two stages. The first stage consists of the alkylation of chlorothioxanthone (CTX) with a Grignard reagent in THF, and the isolation of the first intermediate in the synthetic route: allylcarbinol. This product is separated by a crystallization step, dried and stored. In the second stage, allylcarbinol is dissolved in toluene, dehydrated and hydroaminated to obtain the API after several separation and purification steps.

A simplified process flowsheet has been proposed (Figure 1). The intermediate crystallization step and subsequent storage of allylcarbinol have been removed, thereby connecting the two stages in the process. Besides, the use of toluene for the dehydration of allylcarbinol is avoided by performing this reaction directly in THF.

Once the process flowsheet has been modified to a continuous production system, each unit operation needs to be analyzed in detail individually, but also in combination with the rest of the operations. Therefore, the main objectives are:

- Propose continuous unit operations for reaction, L-L separation, distillation, etc.
- Operate the individual operations so that the full potential of the physical and chemical properties is exploited. Continuous operation may enable operation at very low temperatures, superheating under high pressure or microwave radiation, etc.
- Study the effect of impurities which are carried on in the process and their effect on process performance.
- Seek for opportunities for process intensification. For example, obtain synergy by combining reaction and separation.
- Apply a solvent selection methodology so that not only reaction conditions are improved but also down-stream processing.

The experience gained throughout the redesign process will serve as a basis for developing a methodology to convert pharmaceutical production processes from batch to continuous operation. The individual unit operations will be included in a library of pharmaceutical continuous manufacturing operations, which should be easily adaptable to other production processes. Therefore, an effort will be done to obtain standardized units which can be connected as modules in a short development time [1].

One of the additional demands of the pharmaceutical industry is the fast development of a new product and launching it to the market in the shortest time [1]. This implies that a large amount of knowledge must be gained from the API production process in a short time, and this knowledge should not be lost when scaling-up the process. Therefore, one of the objectives of this project is developing fast experimentation methods, involve modeling in the design of new processes, and when applicable follow a scaling out approach to facilitate moving the production from lab scale to industrial scale.

Last but not least, quality should be built in the process and not analyzed in the product obtained [3]. A set of process analytical technologies (PAT) need to be implemented in order to monitor the process in real time, ensuring that the process status remains within the design space through appropriate control loops [3].

Methodology

The structure of the proposed methodology is shown in Figure 2 and consists of 6 main steps [4]. In *step 1*, the design problem is defined. In *step 2*, the design specifications are gathered. These data will form the basis for the definition of the critical quality attributes (CQA) [3] to be met by the process, and will thus form the basis for the definition of the design space. In step 3,

one or more near-optimal flowsheets will be generated. Different methods may be employed for flowsheet generation [5,6], solvent selection [7], solvent integration [8] and definition of monitoring and control tools [9]. This step requires a large amount of data in addition to property prediction tools. The data may be missing and will have to be obtained in the next steps. In step 4, for each unit operation obtained from step 3, a rigorous analysis must be performed and a detailed design must be proposed. A model-based systems approach [10] should be followed, with optimal use of experimental data. In step 5, experiments are optimally combined with simulation in order to evaluate the feasibility of the proposed unit operations. In step 6, feasible flowsheets may be evaluated under multiple criteria, including a combined economic evaluation and environmental footprint assessment [5], risk assessment, and flexibility analysis. If the evaluation is satisfactory, a continuous process is obtained as well as a defined design space with the required CQA-inputs-process parameters relationships.

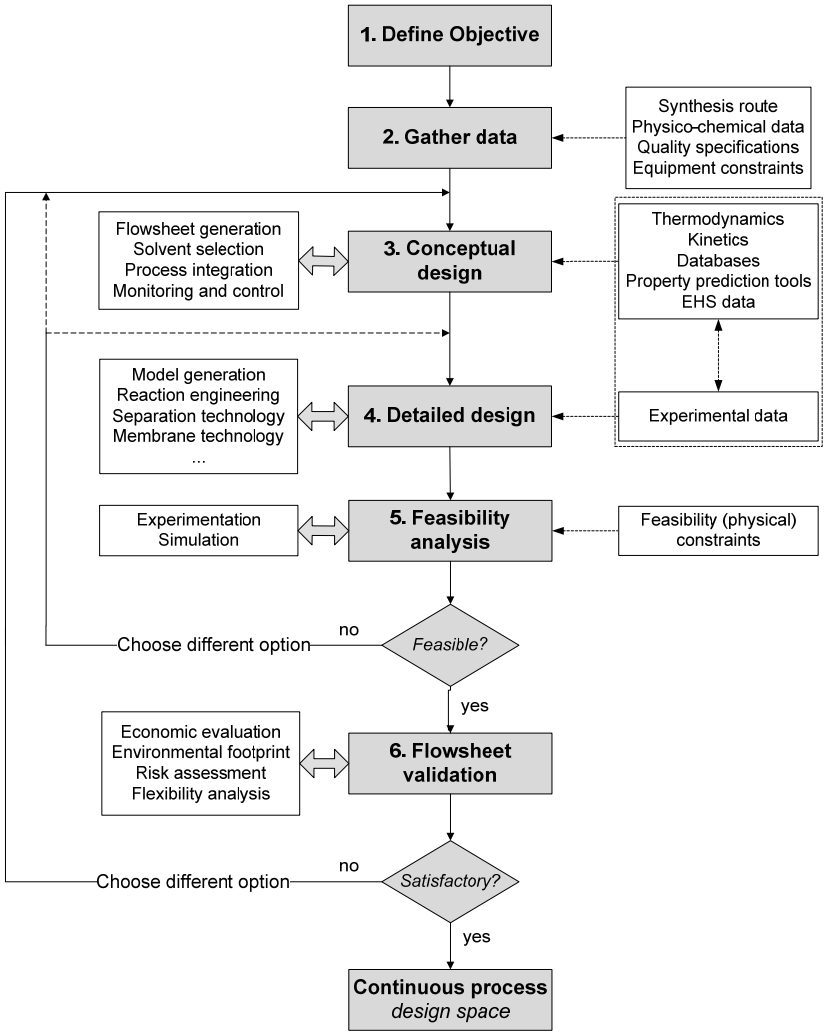

Figure 2: Structure of the methodology for the design of continuous pharmaceutical manufacturing processes, indicating the methods used (left column), work flow (central column) and the data flow (right column) [4].

Results and Discussion

The process flowsheet shown in Figure 1 was selected as the simplest process option. This decision was based on a study of thermodynamic properties using databases and a simulation package (ICAS), and performing laboratory experiments to check the feasibility of the dehydration of allylcarbinol in THF as solvent.

The alkylation reaction (Figure 1) to obtain allylcarbinol (Grignard reaction) poses interesting challenges. It is a highly exothermic reaction, with very fast kinetics with a reaction mechanism that is not well understood. Furthermore, the substrate of this reaction (CTX) has a very low solubility in many solvents. A design for a continuous reactor has been proposed and validated. The product obtained in continuous mode has the same or better purity compared to the product obtained in traditional batch mode without the need of a crystallization step to purify the product (data not published). However, the reaction yield is very sensitive to deviations from the stoichiometric ratio. In order to control this reaction in real time, an on-line monitoring strategy based on near-infrared (NIR) spectroscopy measurements has been proposed and is currently under development.

A first suggestion to carry out L-L separation (Figure 1) in continuous mode is to employ a small scale plate coalescer [11]. Experiments have been initiated with a first prototype.

The dehydration reaction (Figure 1) was tested at different temperatures and acid catalyst concentrations using a simple design of experiments. From these results a simple kinetic model was obtained. Sensitivity analysis of the process parameters was performed and the confidence intervals for model predictions were obtained. The model has been used to design a continuous reactor. Plug-flow, CSTR and several CSTR in series were compared, concluding that two CSTR in series or a CSTR followed by a plug-flow reactor will be optimal to approach plug-flow conditions under reduced flow rate. Future experiments will involve a pressurized plug flow reactor enabling the use of temperatures above the normal THF boiling point, potentially achieving a drastic decrease of the reaction time.

After the dehydration reaction, THF will be flashed out after depressurization, which should result in a simple means of solvent exchange to hydroxyethylpiperazine (HEP) (Figure 1).

The last reaction step (Figure 1) –the hydroamination reaction – may be catalyzed by certain Pd catalysts [12]. Future experiments will involve the use of Pd-based catalysts in homogeneous and heterogeneous form in order to increase the rate and/or yield of this slow reaction. Standard heating methods will also be compared to microwave-based heating.

Conclusions

The pharmaceutical industry is making efforts in different directions to reduce manufacturing costs. A key strategy is to move certain batch processes to continuous operation. A methodology for the design of CPM processes -in particular for the production of organic synthesis based APIs- has been introduced [4]. The methodology identifies already existing PSE methods and tools which can assist in the design of CPM processes. The application of the methodology has been exemplified with an API production process developed by H. Lundbeck A/S, showing a reduction in flowsheet size and complexity as well as a potential reduction in total costs, environmental footprint and production-associated risks. Future work will focus on the extension of the proposed methodology as well as a fully detailed demonstration of its use.

A toolbox of standardized continuous operating units typically employed in organic-synthesis based API production (fast reactions such as Grignard reaction, L-L separation, medium/slow rate reactions and solvent exchange operations) is currently under development at the Department of Chemical and Biochemical Engineering (KT) at DTU.

Acknowledgements

The authors would like to acknowledge the Technical University of Denmark and H. Lundbeck A/S for financial support and fruitful discussions.

References

1. A. Behr, V.A. Brehme, C.L.J. Ewers, H. Grön, T. Kimmel, S. Küppers, I. Symietz, Eng. Life Sci. 4 (1) (2004) 15-24.
2. T.L. LaPorte, C. Wang, 2007, Curr. Opin. Drug Disc. Dev. 10 (6) (2007) 738-745.
3. Q8(R2) ICH Quality Guideline (2009).
4. A.E. Cervera, R. Gani, S. Kiil, T. Skovby, K.V. Gernaey, 21st European Symposium on Computer Aided Process Engineering – ESCAPE 21, 2011 (*submitted*).
5. A. Chakraborty, A.A. Linninger, Ind. Eng. Chem. Res. 41 (2002) 4591-4604.
6. C.A. Jaksland, R. Gani, K.M. Lien, Chem. Eng. Sci. 50 (3) (1995) 211-530.
7. R. Gani, P. Arenas Gómez, M. Folić, C. Jiménez-González, D.J.C. Constable, Comput. Chem. Eng. 32 (2008) 2420-2444.
8. B.S. Ahmad, P.I. Barton, Comput. Chem. Eng. 23 (1999) 1365-1380.
9. R. Singh, K.V. Gernaey, R. Gani, Comput. Chem. Eng. 34 (2010) 1108-1136.
10. K.V. Gernaey, R. Gani, Chem. Eng. Sci. 65 (2010) 5757-5769.
11. E. Kolehmainen, I. Turunen, Chem. Eng. Process. 46 (2007) 834-839.
12. O. Löber, M. Kawatsura, J.F. Hartwig, J. Am. Chem. Soc. 123 (2001) 4366-4367.

List of publications

1. A.E. Cervera, N. Petersen, A. Eliasson Lantz, A. Larsen and K.V. Gernaey. Biotechnol. Progr. 25 (6) (2009) 1561-1581.
2. N. Petersen, P. Ödman, A.E. Cervera Padrell, S. Stocks, A. Eliasson Lantz, K.V. Gernaey, Biotechnol. Progr. 26 (1) (2010) 263-271.
3. A.E. Cervera, R. Gani, S. Kiil, T. Skovby, K.V. Gernaey, 21st European Symposium on Computer Aided Process Engineering – ESCAPE 21, 2011 (*submitted*).
4. K.V. Gernaey, A.E. Cervera, J.M. Woodley, 21st European Symposium on Computer Aided Process Engineering – ESCAPE 21, 2011 (*submitted*).

Joussef H. Chaaban
Phone: +45 4525 2846
E-mail: joc@kt.dtu.dk
Discipline: Reaction and Transport Engineering

Supervisors: Kim Dam-Johansen
Søren Kiil
Tommy Skovby, H. Lundbeck A/S

PhD Study
Started: January 2010
To be completed: December 2012

Novel Reactor Design for Organic-Chemical Crystallization of Active Pharmaceutical Ingredients

Abstract
The present PhD project concerns the design and optimization of continuous crystallization operations as part of pharmaceutical production using reaction engineering principles. Increasing public demand and strict regulatory requirements have sparked the search for more cost-effective and reliable selective API crystallization processes. Currently, preferential API crystallization processes are operated in Batch mode and there is an increasing interest in converting to the attractive continuous operation due to valuable advantages connected to continuous operation. The continuous operation should improve the control of particle size distribution (PSD) and polymorphism of the API's in order to meet regulatory requirements and to ease the further downstream processing and formulation.

Introduction
Throughout its history, crystallization of Active Pharmaceutical Ingredients (API's) has been the most important separation and purification process in the pharmaceutical industry. In this context, the importance of stereochemistry, herein chirality, has been widely recognized since more than 50% of known API's are chiral and 9 out of the top 10 drugs have chiral active ingredients. The chirality of API's and their intermediates is expressed in terms of optical isomerism as enantiomers that are chemically identical and mirror-images of each other. The physical properties of enantiomers such as heats of reaction, melting points, boiling points etc. are identical, but the difference between them lies within the stereochemical configuration, which has an influence on the biological activity of the API [1-4]. In this context, the development of more cost-effective and environment-friendly continuous enantioselective (or preferential) crystallization processes of API's or their intermediates is of outmost importance to the pharmaceutical industry due to increasing public demand and strict regulatory requirements. Continuous operation of crystallization will provide savings in chemicals and energy, improved process control, ease of scale-up, improved safety and flexible and reliable process.

Thermodynamics of racemic mixtures
As a separation and purification process, the enantioselective or preferential crystallization of pure enantiomers from racemic mixtures can be applied to different systems of chiral mixtures according to their solid-liquid phase behavior [1-4]. It is well-known that active ingredients in drugs are able to form three different types of solid-liquid phase equilibria systems [1-4]: 1) Conglomerate forming systems, 2) Racemic compound forming systems and 3) Pseudoracemate (Solid solution) forming systems.

Solid-liquid phase behavior of *conglomerate forming systems* includes the formation of a conglomerate, which is a mechanical eutectic mixture of pure crystals of the two enantiomers, i.e. each enantiomer forms a solid. The fraction of organic racemic mixtures that exist as conglomerate forming systems is estimated to 5-10%. *Racemic compound forming systems* are the most common type of racemate corresponding to about 90-95% [2-4]. The formed racemic compound, also referred to as true racemate, corresponds to a crystalline racemate in which the two enantiomers are present in a 1:1-ratio in a well-defined arrangement within the same crystal lattice. A third type of solid-liquid equilibria systems for chiral mixtures is the *pseudoracemate forming system*. Pseudoracemate refers to the formation of a solid solution between the two enantiomers coexisting in a completely random distribution in the crystal lattice. This type of solid solution systems is relatively rare and three classical cases of such systems occur depending on the melting point of the racemate compared to that of pure enantiomers [2]. Figure 1 illustrates the solid-liquid

equilibria systems for conglomerate forming system and racemic compound forming system.

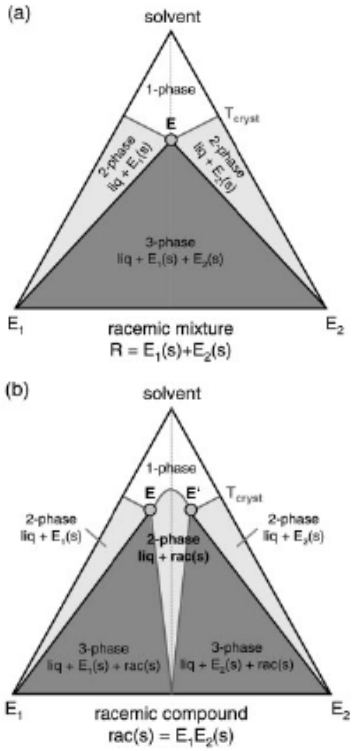

Figure 1: Solid-liquid phase behavior of (a) Conglomerate forming system and (b) Racemic compound forming system [3].

Current Developments

The development of effective enantioselective or preferential crystallization processes for separation and purification of API's or their intermediates has attracted great attention due to increasing public demand and strict regulatory requirements for purity and quality of API's. A variety of developments have been demonstrated for preferential crystallization of chiral API's and their intermediates [3,5]. For instance, Elsner et al. [3] developed a separative crystallization process for the simultaneous crystallization of pure D- and L-Threonine from conglomerate forming DL-Threonine racemate in water by employing two coupled vessels operating batch-wise. Figure 2 illustrated this concept.

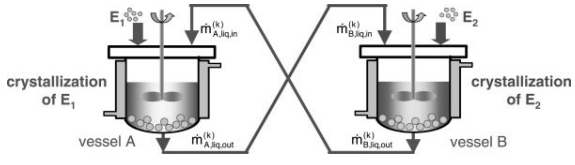

Figure 2: Concept of two coupled vessel batch preferential crystallization [3].

This concept could also be utilized for the simultaneous separation of racemic compound and one of the pure enantiomers in case the solid-liquid behaviour of the solute-solvent system is a racemic compound forming system depicted in Figure 1 *(b)*. The challenge in this context is to adopt the continuous concept in cost-effective processes for component systems possessing racemic properties, especially enantiomers, in order to obtain pure enantiomers of API or intermediate.

Conclusion

Due to increasing public demand and strict regulatory requirements the development of cost-effective and environment-friendly crystallization processes for chiral and non-chiral API's and their intermediates (as part of continuous production) is inevitable. In this context, an enantioselective separation process by crystallization is strongly dependent on solid-liquid phase behavior of the racemic system considered. Several continuous crystallization processes are developed for chiral and non-chiral API's and their intermediates. However, the main concern is the cost of these processes. Therefore, future work should focus on *cost-effective* options and alternative designs of continuous crystallizer system capable of performing preferential crystallization.

Acknowledgments

The author acknowledges the financial and professional support of H. Lundbeck A/S and CHEC Research Center at the Department of Chemical and Biochemical Engineering at DTU.

References

1. A.S. Myerson, Handbook of Industrial Crystallization, Butterworth-Heinemann, USA, 2002.
2. Y. Wang, A.M. Chen, Org. Process Res. Dev. 12 (2008) 282-290.
3. M.P. Elsner, G. Ziomek, A. Seidel-Morgenstern, AIChE. J. 55 (2009) 640-649.
4. H. Lorenz, A. Perlberg, D. Sapoundjiev, M.P. Elsner, A. Seidel-Morgenstern, Chem. Eng. Process. 45 (2006) 863-873.
5. D. Polenske, H. Lorenz, A. Seidel-Morgenstern, Chirality, 21 (2009) 728-737.

Inês Rodrigues da Silva
Phone: +45 4525 2610
E-mail: ins@kt.dtu.dk
Discipline: Enzyme Technology

Supervisors: Jørn Dalgaard Mikkelsen
Anne S. Meyer

PhD Study
Started: February 2009
To be completed: January 2013

Enzymatic Production of Prebiotic Polysaccharides with Hydrophobic Decoration

Abstract
Prebiotics are non-digestible carbohydrates that beneficially affect the host by selectively stimulating the growth of a limited number of bacteria in the colon. Known examples of prebiotic food ingredients are oligosaccharides, e.g. fructans and fructooligosaccharides from Jerusalem artischokes, galactooligosaccharides from lactose and maltooligosaccharides from starch. The waste streams from agricultural industry are a large source of oligosaccharides with potential prebiotic effects. These streams comprise barley bran, sugar beet pulp and potato pulp from the brewing, sugar and starch industries. Modification of oligomers to achieve the desired prebiotic effect requires a number of specific enzymes which can be acquired by cloning and expression in the yeast *Pichia pastoris*. The oligosaccharides produced by the enzymatic catalyses may be purified and further modified by hydrophobic decoration.

Introduction
Functional food ingredients possessing potential health benefits have recently attracted strong attention. Some of the functional food ingredients are prebiotic oligosaccharides. Dietary fibers and prebiotics are non-digestible carbohydrates that beneficially affect the host by selectively stimulating the growth and/or activity of one or a limited number of bacteria in the colon. Oligosaccharides could be obtained as products of hydrolysis of plant derived polysaccharides, or directly from plant cell walls. Rational enzyme catalysed reactions are going to be develop to modify heterogeneous samples of substrates to create 'designer' oligosaccharides with defined structures and high prebiotic potential.

Specific objectives
The idea of the project is to use selective enzyme catalysts to convert polysaccharides into oligomers and furthermore decorate the oligomers by hydrophobic residues. Only few commercial enzymes are available for this task. Most of the commercial enzymes in addition contain other enzyme activities which degrade the desired oligosaccharides. Mono-component enzymes can, however, be produced by cloning and expression of suitable enzymes in the yeast, *P. pastoris.* This process can be performed in the laboratory at our department. Furthermore, the optimal conditions of enzymatically catalyzed reactions have to be worked out as well. This include up-scaling of the enzymatic reaction in order to deliver sufficient amount of oligosaccharides with potential prebiotic activity.

As an example we have expressed the enzyme of interests, Enzyme A, with a MW of 83 kDa in *P. pastoris*. *P. pastoris* has been used for production of GRAS (General Regarded As Safe) protein and enzyme products to food, feed and pharmaceutical applications. The methylotrophic yeast, *P. pastoris*, has been shown to be an outstanding host for high-level heterologous gene expression for both basic research and industrial use **[1**]. The recombinant proteins we want to produce are isolated by diversity screening or identified in genomic databases. The genes are inserted into *P. pastoris* under the control of the AOX1 (Alcohol Oxidase 1) promotor, in order to induce the gene of interest in the presence of methanol **[2, 3]**.

Results
The genetic engineered strain was grown in a 5L Sartorius Biostat Aplus fermentor using glycerol as the C-source and ammonia as the N-source. The production of the heterologous protein was followed by measuring the optical density (OD), determining the enzyme activity, and monitoring the MW by SDS-PAGE. The OD (cell density) and the total level of enzyme are shown in Figure 1. The protein was also purified by Gel

Filtration (PD-10 desalting columns) and by Immobilized Metal Affinity Chromatography (IMAC).

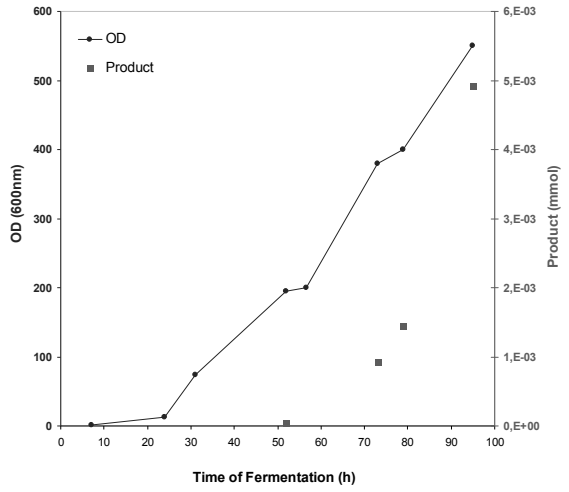

Figure 1: Cell density was followed at OD_{600} whereas the induction of Enzyme A was measured by the release of hydrolysed products.

The fermentation of Enzyme A was also followed by SDS–PAGE to verify the presence and yield of the enzyme. Except for the strong protein band of Enzyme A, only very few minor bands were present in the SDS-PAGE gel in Figure 2. The MW of Enzyme A was approx. 83kDa, which correspond to the theoretically molecular mass of the recombinant protein.

Figure 2: Protein samples from the methanol Fed Batch phase after analysis by SDS-PAGE. Wells were: 1. Standard - dual color; 2. Standard – unstained; 3.4. Enzyme A (52h) - 25µl ; 5. Enzyme A (73h) - 25µl ; 6 Enzyme A (95h) - 25 µl ; 10. Enzyme A (52h) - 5µl ; 11. Enzyme A (73h) - 5µl ; 12. Enzyme A (95) - 5µl ; 16 Standard - dual color; 17. Standard - unstained

The total activity of Enzyme A was also calculated and the fermentation results are sumarixed in Table 1.

Table 1: Activity of the enzyme of interests, Enzyme A, after induction with methanol

Time of Fermentation (h)	Average (U/mL)
52	0,2
73	4,2
79	9,5
95	42,3

Conclusions

It was possible to produce high level of the desired recombinant, Enzyme A, in a high density cell culture. The protein was expressed and identified positively by a specific enzyme assay. The expected MW was furthermore confirmed by SDS-PAGE. The activity of Enzyme A increased as expected in response to time and methanol induction. The Highest activity was detected after 95h of fermentation and the final amount was 42,3U/mL.

References

1. J.L. Cereghino, J.M. Cregg, FEMS Microbiol. Rev. 24 (1) (2000) 45-66.
2. G.P.L. Cereghino, J.L. Cereghino, C. Ilgen, J.M. Cregg, Curr. Opin. Biotech. 13 (4) (2002) 329-332.
3. J. Stratton, V. Chiruvolu, M. Meagher, High Cell Density Fermentation. Pichia Protocols. D. Higgins and J. Cregg. New Jersey, Humana Press. 103 (1998) 107-120.

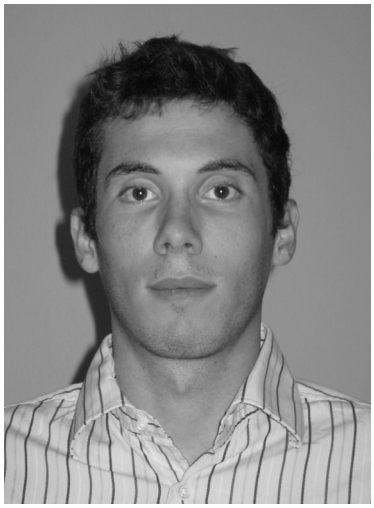

Victor Darde
Phone: +45 9955 4667
E-mail: vid@kt.dtu.dk
Discipline: Engineering Thermodynamics

Supervisors: Kaj Thomsen
Erling H. Stenby
Willy JM van Well, DONG Energy

Industrial PhD Study
Started: February 2008
To be completed: July 2011

CO_2 Capture using Aqueous Ammonia

Abstract
The CO_2 capture process using aqueous ammonia shows good perspectives for decreasing the energy requirement thanks to the low enthalpy of absorption of CO_2 by NH_3. However, a scientific understanding of the process is required. The properties of the NH_3-CO_2-H_2O system were described using an upgraded version of the Extended UNIQUAC electrolyte model developed by Thomsen and Rasmussen in a temperature range from 0 to 150°C [1]. In addition, the rate of absorption of carbon dioxide by ammonia solvent has been experimentally measured using a wetted wall column apparatus. The overall mass transfer coefficients measured when MEA and aqueous ammonia solutions have been compared and the rate of absorption using aqueous ammonia has been successfully modeled. The thermodynamic model has been implemented on the commercial simulator Aspen Plus in order to simulate the process using equilibrium-based calculations. Several main cases have been considered in order to evaluate the different variants of the process. The heat and electricity requirements have been evaluated and the influence of several parameters has been analyzed. The results show the potential of the different variants of the capture process.

Introduction
The amount of carbon dioxide emissions from power production is very significant in industrialized countries. Carbon dioxide capture implies separating the CO_2 from the flue gases from a power plant or other industry instead of releasing the CO_2 in the atmosphere. Post-combustion techniques separate the carbon dioxide from the flue gas after a traditional combustion process. Amine solutions have been commonly used for the commercial production of CO_2. However, this technology requires a large amount of energy, especially in the desorption part of the process. Therefore, new alternatives for post-combustion capture are searched for. Processes using aqueous ammonia as solvent are some of the promising alternatives. They can be found in two variants. The first variant absorbs the CO_2 at low temperature (2-10°C) and is called chilled ammonia process. It is a patented process [2]. This process allows precipitation of several ammonium carbonate compounds in the absorber. The second process absorbs CO_2 at ambient temperature (25-40°C) and does not allow precipitation.

Specific objective
The purpose of this study is to get a scientific understanding of the CO_2 capture process using aqueous ammonia. It is based on the extended UNIQUAC thermodynamic model developed for the CO_2-NH_3-H_2O system by Thomsen and Rasmussen [1]. An updated version of the model has been developed with an enlarged range of temperature by using additional experimental data. The rate of absorption has also been investigated by designing and using a wetted wall column apparatus and modeling the rate of absorption of CO_2 by ammonia and comparing the one observed with MEA-based solvents. The thermodynamic model has been implemented on the commercial simulator Aspen Plus in order to simulate the process using equilibrium based calculations. The integration of the capture process with the power plant will be investigated.

Results and discussion
Description of the thermodynamic model
The study of this process requires the use of a thermodynamic model that can take into account the speciation, the vapor liquid equilibrium (VLE), the solid liquid equilibrium (SLE) and the enthalpy change entailed by the mix of ammonia, carbon dioxide and water.

The model allows for calculating the activity coefficient for the liquid phase using the extended UNIQUAC model, and the gas phase fugacity using the Soave-Redlich-Kwong (SRK) equation for the volatile compounds. The original version of the model has

shown to be capable of describing accurately the vapor-liquid-solid equilibria and thermal properties for the CO_2-NH_3-H_2O system for a wide range of concentration (up to 80 molal NH3), for a temperature in the range of 0-110°C and for a pressure up to 100 bars [1]. In this new version of the model, additional experimental data were used in order to extend the valid temperature range up to 150°C. More than 3800 experimental data from various publications were used to fit the parameters. In addition, some new features have been added in order to improve the accuracy of the model. The analysis of the CO_2-NH_3-H_2O system implies the study of several equilibrium processes. The following reactions are considered in the model:

- Speciation equilibria

$$NH_3(aq)+H_2O \longleftrightarrow NH_4^+ + OH^-$$

$$CO_2(aq)+H_2O(l) \longleftrightarrow HCO_3^- + H^+$$

$$HCO_3^- \longleftrightarrow CO_3^{2-} + H^+$$

$$H_2O(l) \longleftrightarrow OH^- + H^+$$

$$NH_3(aq)+HCO_3^- \longleftrightarrow NH_2COO^- + H_2O(l)$$

- Vapor-liquid equilibria

$$CO_2(g) \longleftrightarrow CO_2(aq)$$

$$NH_3(g) \longleftrightarrow NH_3(aq)$$

$$H_2O(g) \longleftrightarrow H_2O(l)$$

- Liquid-solid equilibria

$$NH_4^+ + HCO_3^- \longleftrightarrow NH_4HCO_3(s)$$

$$NH_4^+ + NH_2COO^- \longleftrightarrow NH_2COONH_4(s)$$

$$2NH_4^+ + CO_3^{2-} + H_2O \longleftrightarrow (NH_4)_2CO_3.H_2O(s)$$

$$4NH_4^+ + CO_3^{2-} + 2HCO_3^- \longleftrightarrow (NH_4)_2CO_3.2NH_4HCO_3(s)$$

$$H_2O(l) \longleftrightarrow H_2O(s)$$

To extend the valid temperature range of the model, additional VLE data have been included for the parameter estimation. Figure 1 plots the pressure calculated with the extended UNIQUAC model for NH_3-CO_2-H_2O mixtures at 120°C and various molality of ammonia as a function of the molality of carbon dioxide. The corresponding experimental data from two publications have also been included [3, 4]. The model is able to predict the formation of solid phases.

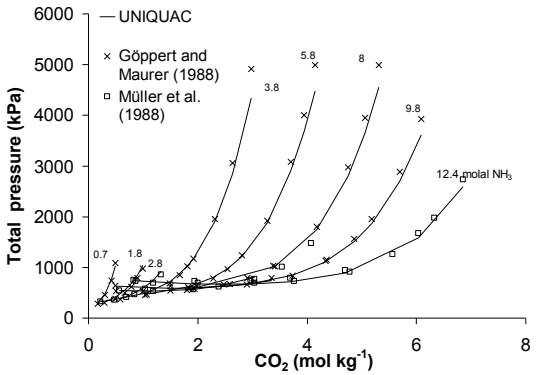

Figure 1: Total pressure in NH_3-CO_2-H_2O mixtures at 120°C

Compared to the previous version of the model, new types of experimental data were used for parameter estimation.

First, IR spectrometry data from Lichtfers [5] were used. These are speciation data for the NH_3-CO_2-H_2O system that were measured at a temperature from 40 to 120°C at various concentrations of ammonia and carbon dioxide. The ratio between the amount of ammonium carbamate ion and the total amount of ammonia was used in the object function during the determination of the parameters.

Enthalpy data from partial evaporation of CO_2-NH_3-H_2O mixtures published by Rumpf et al. in 1998 [6] were also used during the parameter estimation. The object function that was used consists of minimizing the difference of the calculated and the experimental enthalpy, based on a flash calculation simulating the experiment.

Hence, this model is capable of describing accurately the vapor-liquid-solid equilibria and thermal properties for this system for a wide range of concentrations (up to 80 molal), for a temperature in the range of 0-150°C and for a pressure up to 100 bars. This work has been published (Darde *et al.*, 2010a)

Experimental measurement of the rate of absorption

The study of the kinetic rate of absorption of carbon dioxide by aqueous ammonia solvent is regarding the evaluation of the process. This study is crucial to size accurately absorber columns and to assess the capital cost of the capture process. To be able to perform this task, an experimental apparatus has been designed and built. It is called a wetted wall column. It allows for contacting counter currently an aqueous amine solution with a defined gaseous mixture of carbon dioxide and nitrogen on the surface of a stainless steel tube with a known contact area. The apparatus can be operated from atmospheric to a pressure up to 8 bars and at a temperature from 5 to 80°C. Figure 2 shows a schematic flow sheet of the apparatus.

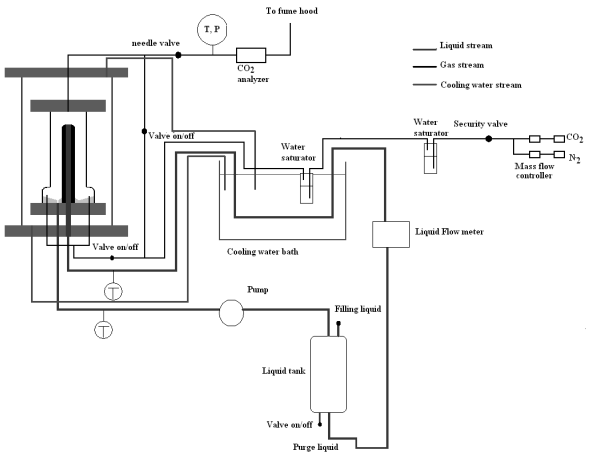

Figure 2: Schematic flow sheet of the apparatus

The apparatus allows for measuring the carbon dioxide absorption flux at a given temperature and partial pressure of carbon dioxide. By measuring the

flux of carbon dioxide at several partial pressures of carbon dioxide for given solvent and temperature, it is possible to obtain the overall mass transfer coefficient (K_G) as the slope of the linear curve between the flux and the partial pressure of carbon dioxide. $1/K_G$ represents the global resistance to the absorption trough the gas film, interface, and liquid film. It can be expressed as the sum of the resistance from the gas side and from the liquid side:

$$\frac{1}{K_G} = \frac{1}{k_G} + \frac{1}{k'_G}$$

k_G is the gas side mass transfer coefficient. k'_G is the liquid side mass transfer coefficient that accounts for the transport of carbon dioxide from the gas-liquid interface to the bulk liquid and for the chemical reaction that occurs at the interface. The influence of the hydrodynamic conditions on k_G has been modeled. Hence, by measuring the overall mass transfer coefficient, it is possible to determine k'_G. Figure 3 shows the liquid side mass transfer coefficient for 1, 5 and 10 wt.% ammonia solutions at a temperature between 11 and 21°C as a function of the loading. The measurements for 30 wt.% MEA at 21 and 41°C have also been included. It can be observed that k'_G decreases with the loading and with the concentration. The measurement also show that the mass transfer decreases when the temperature decreases but that the decrease is much faster from 31 to 21°C than from 21 to 11°C. It shows that lowering the temperature of absorption from 21 to 11°C in order to limit the vaporization of ammonia would not affect significantly the kinetics. The results for 10 wt.% NH_3 solutions at 21°C are in the same range as the ones observed using 30 wt.% MEA at 41°C. However, the absorption rate using aqueous ammonia solutions at lower temperature is significantly slower than the one obtained with MEA. This shows that a larger contact area would be required in the case of the chilled ammonia process that in the MEA process.

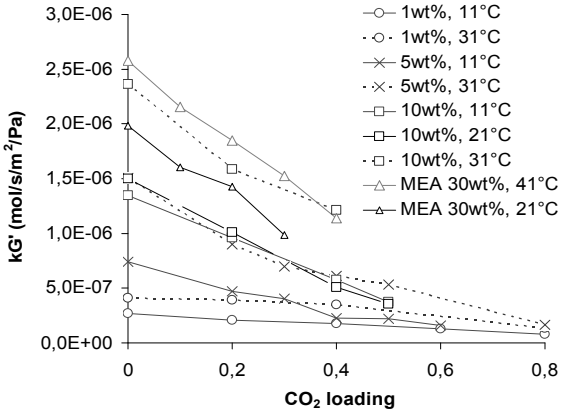

Figure 3: Liquid side mass transfer coefficient as a function of the CO_2 loading for 1, 5 and 10 wt.% ammonia solutions at various temperatures and for 30 wt.% MEA solutions at 21 and 41°C.

The modeling of the rate of absorption of carbon dioxide by ammonia solutions has also been done using the zwitter-ion mechanism and the measurements of overall mass transfer coefficient with unloaded ammonia solutions. The model has shown satisfactory results regarding the prediction of the rate of absorption of carbon dioxide in loaded aqueous ammonia solutions for a temperature in the range 6-31°C and an ammonia concentration up to 10wt%.

Simulation of the process

A thermodynamic study with this model has shown the potential for low heat consumption (Darde *et al.*, 2010b). In order to make a process optimization study, flow sheet calculations are required. Therefore the extended UNIQUAC thermodynamic model has been implemented on the commercial simulator ASPEN Plus by applying a user model interface [7]. This allows for using the functionalities of ASPEN Plus coupled with the calculations abilities from the thermodynamic model. The carbon dioxide process using aqueous ammonia is more complex than conventional MEA based processes. The absorption at low temperature requires chilling duty that depends on the temperature of the cooling water available. The high volatility of ammonia requires extensive washing of the gas stream exiting the absorber and the use of an ammonia stripper to regenerate the washing water. The low temperature of absorption may allow for the formation of precipitate in the absorber. In addition, desorption of carbon dioxide can be made at high pressure thereby saving power during compression. Hence, more parameters can be adjusted and the optimization of the process is therefore not trivial. In this study, three main cases have been analyzed:

- Absorption at low temperature (chilling 10°C) with solid formation
- Absorption at low temperature (chilling 10°C) without solid formation
- Absorption at higher temperature (cooling at 20°C and above)

For each of the cases, two process configurations have been tested: absorption with a single absorber column with recycling and cooling of a fraction of the bottom stream back in to the absorber and absorption with two absorber columns with inter-cooling and without recycling. As shown by our previous experiments are the kinetics of absorption of CO_2 by ammonia solvent rather slow. A Murphee efficiency of 0.1 has therefore been assumed for the absorber. By using the modeling of the rate of absorption of carbon dioxide by aqueous ammonia, it was possible to estimate the height of the required packing.

It has been shown that the heat requirement and the cooling duty are very dependant on the concentration of ammonia, the lean loading, the chilling temperature and the desorption pressure. The temperature of the cooling water available also has a strong impact on the electricity consumption. An estimate of the

consequences for integration with the power plant has been made.

Figure 4 shows as an example the influence of the lean loading on the heat requirements in the CO_2 desorber and the NH_3 stripper and on the chilling duty for absorption at low temperature without precipitation (ammonia concentration 4.8wt%, chilling temperature 10°C, cooling water temperature 8°C, desorption pressure 10bar, capture rate 90%). Increasing the lean loading reduces the volatility of ammonia in the absorber and therefore the heat consumption in the NH_3 stripper, but increases the flow rate of solvent and therefore the chilling duty. A minimum can be observed for the heat consumption in the CO_2 desorber. The sum of the heat duties in the CO_2 desorber and NH_3 stripper is below 3000 kJ/kg CO_2 captured in this case without solid formation.

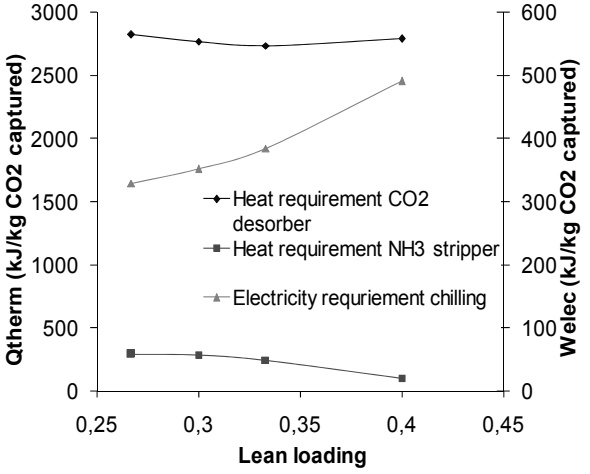

Figure 4: Heat and electricity requirements as a function of the lean loading for absorption at low temperature without solid formation.

The following main conclusions can be drawn from the simulation calculations:

- Lowest heat duties are achieved for low temperature absorption with solid formation thanks to the possibility of high ammonia concentrations. However, additional low quality heat is needed to dissolve the solids in the CO_2-rich stream from the absorber.
- When no precipitation is allowed, limited ammonia concentration has to be used. However, the heat requirement is still competitive with amine processes.
- When absorption at ambient temperatures is applied, the concentration of ammonia has to be limited to control vaporization. The heat consumption CO_2 desorber comparable is to the low temperature absorption case, but the heat consumption in the NH_3 stripper is higher. However, no chilling duty is required.
- This work has shown the potential of applying ammonia for post combustion capture, both with or without precipitation and with or without extensive cooling duty.

Conclusions

In this study, a thermodynamic model that can accurately describe the vapor-liquid-solid equilibrium and the thermal properties of the NH_3-CO_2-H_2O system for a temperature up to 150°C has been developed.

An experimental set up has been designed and built in order to measure the kinetic rate of absorption of carbon dioxide by aqueous ammonia solvent. This rate has been modeled for a temperature in the range 6-31°C and for an ammonia concentration up to 10wt%

By implementing the thermodynamic model in the commercial simulator Aspen Plus applying a user model interface developed at DTU Chemical Engineering, the capture process has been simulated. Different cases and scenarios have been considered in order to study the influence of the different process parameters on the heat and electricity consumption. The simulations showed the high potential of the different variants of the process. The study of the integration of the capture process with the power plant will be analyzed in the next phase of the project.

Acknowledgements

We want to thank the Danish Ministry of Science Technology and Innovation and DONG Energy for co-funding this industrial PhD project.

References

1. K. Thomsen, P. Rasmussen**,** Chem. Eng. Sci. 54 (1999) 1787-1802.
2. E. Gal, Ultra cleaning combustion gas including the removal of CO_2, World Intellectual Property, Patent WO 2006022885 (2006).
3. U. Göppert, G. Maurer, Fluid Phase Equilibr. 41 (1988) 153.
4. G. Müller, E. Bender, G. Maurer, Ber. Bunsenges. Phys. Chem. 92 (1988) 92 148.
5. Lichtfers U, (2001) Aachen, Shaker Verlag
6. B. Rumpf, F. Weyrich, G. Maurer, Ind. Eng. Chem. Res. 37 (1998) 2983-2995.
7. B. Maribo-Mogensen, K. Thomsen, Modelling Separation Processes of Mixed Solvent-Electrolyte Systems Using an Extended UNIQUAC User Model Implemented in Aspen Plus. 24th ESAT 2009;91 (PA-5).

List of Publications

1. V. Darde, W.J.M. van Well, E.H.S. Stenby, K. Thomsen, Ind. Eng. Chem. Res. 49 (2010a) 12663-12674.
2. V. Darde, K. Thomsen, W.J.M. van Well, E.H.S. Stenby, Int. J. Greenh. Gas Con. 4 (2010b) 131–136.

Carlos Axel Diaz-Tovar
Phone: +45 4525 2808
E-mail: adi@kt.dtu.dk
Discipline: Systems Engineering

Supervisors: Rafiqul Gani
Bent Sarup, Alfa Laval

PhD Study
Started: April 2008
To be completed: July 2011

Lipid Processing Technology: Building a Multilevel Modeling Network

Abstract
The aim of this work is to present the development of a computer aided multilevel modeling network for the systematic design and analysis of processes employing lipid technologies. This is achieved by decomposing the problem into four levels of modeling: i) pure component property modeling; ii) modeling of phase behavior of relevant lipid mixtures; ii) development of a model library consisting of process models of relevant unit operations; and iv) development of methods and tools for computer-aided synthesis and design of process flowsheets. The applicability of this methodology is highlighted in each level of modeling through the analysis of the physical refining process of oils and fats.

Introduction
Over the past few decades, the world's fats and edible oils production has been growing rapidly, far beyond the need for human nutrition [1]. This overproduction combined with the growing consumer preferences for healthier food products and the interest in bio-fuels, has led the oleo chemical industry to face major challenges in terms of design and development of better products and more sustainable processes. However, although the oleo chemical industry is mature and based on well established processes, the complex systems that lipid compounds form, the lack of accurate predictive models for their physical properties and unit operation models for their processing have limited a wide application of computer-aided methods and tools for process synthesis, modeling and simulation within this industry.

In consequence, the aim of this work is to present the development of a computer aided multilevel modeling network consisting a collection of new and adopted models (properties and processes), methods and tools for the systematic design and analysis of processes employing lipid technologies. This is achieved by decomposing the problem into four levels of modeling (see Figure 1): 1.) Pure component properties; 2.) Mixtures and phase behavior; 3.) Unit operations; and 4.) Process synthesis, design, and retrofit. The applicability of the proposed methodology is highlighted in each level of modeling through a case study involving a physical refining (deodorization) process of oils and fats [2]. This lipid process has significance in the edible oil and biodiesel industries since it determines the quality of the final oil [3]. Hence, optimization of process parameters is critical for the production of any acceptable oil product.

The Multilevel Modeling Network
First Level: Pure Component Modeling
The development of the first modeling level of the multilevel network framework for the analysis/design of any process involving lipid technology is achieved by: a) identifying the most significant and widely produced edible oils/fats, as well as their corresponding representative families of chemical species; b) molecular description of the identified chemical species in terms of the property model (e.g. the Marrero and Gani [4] method); c) creating a list of the physical-chemical properties needed for model-based design and analysis of edible oil and biodiesel processes; d) collecting the available experimental data from different sources for the identified lipid compounds and their corresponding properties; and, e) selecting and adopting the appropriate models to predict the necessary properties, to fill-out the gaps in the lipid-database (CAPEC_Lipids_Database) and to make it suitable for applications with other computer-aided tools.

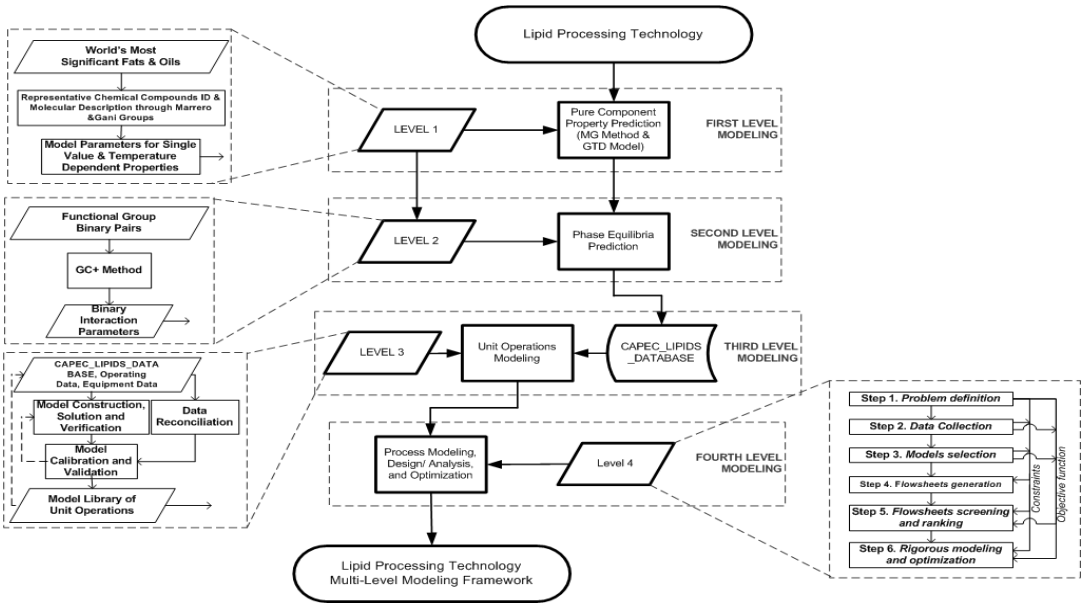

Figure 1: Overview of the proposed multilevel modeling network

The natural fats and oils are complex chemical mixtures composed of different families of chemicals. Fatty acids (from C4-C24) esterified to glycerol (mono-, di-, and tri- acylglycerides), are the main constituents of these mixtures; while tocopherols, sterols, carotenes, and phospholipids are minor compounds that are considered as high-value by-products of the refining processes. The CAPEC_Lipids_Dabase [1] contains a total of 235 compounds divided into three major families: acylglycerides (65 triacylglycerides [TAGs], 41 diacylglycerides [DAGs], and 15 monoacylglycerides [MAGs]), fatty acids [FFA] (29) and esters (29 methyl and 29 ethyl), and minor compounds (4 tocopherols, 4 tocotrienols, 2 phospholipids, 9 terpenes, 4 sterols, 2 sterol esters, and 2 sterol glycosides). For these compounds a total of 15 physical-chemical properties have been identified: 10 single value (critical, basic, and heats of formation) and 5 temperature dependent (vapor pressure, liquid heat capacity, liquid density, liquid viscosity, and surface tension). And a total of 2560 experimental data points for 12 pure component properties have been collected and included within the database.

For the deodorization case study, the composition of the crude oil represents a typical palm oil [2]. The models used to predict the property behavior of the selected compounds were taken from Diaz-Tovar et al. [1].

Second Level: Mixtures and Phase Behavior Modeling

Understanding the phase behavior is essential in edible oil/lipid processing, which involves separation processes such physical refining and deodorization of edible oils. The information obtained from the equilibrium calculations helps to design unit operations and to dimension the equipments. In this paper, the use of the UNIFAC-CI model [5] to predict the activity coefficients of the multicomponent chemical systems under study involved in the deodorization process of palm oil is highlighted. As the deodorization process occurs at high temperature and low pressure, the vapor phase is set as ideal and only the non-ideality of the liquid phase is considered through the UNIFAC-CI model [6].

The identified compounds are represented according to their corresponding UNIFAC functional groups. Triacylglycerides, like most of the lipid compounds, are described by a small set of functional groups: CH3, CH2, CH (UNIFAC main group 1), CH2COO (UNIFAC main group 11), and CH=CH (UNIFAC main group 2). Di- and mono- acylglycerides and free fatty acids are also described by these groups plus the groups OH and COOH (UNIFAC main groups 5 and 20), respectively.

For those mixtures or compounds where the needed group interaction parameters (GIPs) are missing, the UNIFAC-CI is used. The advantage of the UNIFAC-CI model is that phase equilibria for any lipid system can be predicted especially when the GIPs for the reference UNIFAC model are not available. For the deodorization case study being highlighted in this paper, all GIPs for the reference UNIFAC model are available and therefore the parameters are fine-tuned using the UNIFAC-CI method to validate the applicability of this model.

Activity coefficients of each compound at 250°C and 3.5 mmHg, often used operation conditions of the deodorization process, were calculated using the UNIFAC-CI method. The results showed that the calculated activity coefficients for TAGs are almost equal to unity, indicating that they do not have a non-ideal effect. However, this is not the case for the FFAs were the calculated activity coefficients are far from unity.

Table 1: CAFD problem definition for the deodorization process.

Step	Task/Action
1	Synthesis/design problem definition - Retrofit of the deodorization process and selection of the Net Present Value (NPV) as the objective function.
2	Establishment of the appropriate link to Levels 1-3 of the multilevel modeling network - Generate the superstructure to represent different flowsheet alternatives for the selected process. - List of logical constraints (e.g. Food safety, EHS regulations, etc.). - Collect performance metrics of existing and competing oil deodorization processes for benchmark purposes. - Reconciliation and consistency of data as well as systematization into an efficient database structure, accessible from different project phases.
3	Generate the correspondent superstructure - Collect the needed submodels for the multiscale model formulation. - Complement the models contained with the CAPEC_Lipids_Database (physical properties and unit operations) with all cost/value and sustainability models needed to calculate the objective function from the design variables. - Apply systematic model development framework ensuring consistency among different scales.
4	Generate feasible flow sheet alternatives - Fix sets of binary variables in the superstructure. - Perform a fast screening to eliminate unfeasible alternatives as well as redundant options
5	Reduce the search space - Screen out options that violate operational constraints (shortcut models are used). - Select the most promising alternative based on the value of the maximized objective function.
6	Define the optimal process design - Perform a detailed/rigorous modeling and optimization of the previously selected alternative - Calculate from the model output, indicators used as benchmarks and as inputs for project and portfolio management decisions (e.g. sustainability metrics, financial indicators, and portfolio management indicators). - Perform sensitivity analysis and design of experiments to reduce the uncertainty by estimating the contribution of each parameters and models to output uncertainty.

Third Level: Unit Operations Modeling

The production (from crude oil production to the final product) of edible oils/fats involves a variety of processing steps and unit operations. For example, fluid handling, heat transfer, separation processes such as adsorption, two-phase separation (liquid-solid, liquid-liquid, and liquid-gas), crystallisation, filtering, chemical reactions (interesterification, hydrogenation), and steam stripping under vacuum. In this level of the modeling network, a model library consisting of new and adopted models of the involved unit operations is developed.

In the first step, the unit operations involved in deodorization process is listed, as given by Ceriani et al [2], and the availability of built-in models in commercial simulators is verified. In the second step, the required physical property data of the chemical species involved, equipment specifications, and operating data of existing process plants are retrieved. In the third step, a detailed computer aided modeling of selected unit operations is carried out based on the type of the model (e.g. steady state/dynamic, meso scale/micro scale) and intended goals (design / optimization / retrofit). In the fourth step, the operating data is reconciled with respect to quality of the data and measurement errors. The developed models are validated using reconciled operating data of the existing process plant. The validated models are incorporated in the model library as new and/or adapted models for use in process simulation tools such as PRO/II®. Once validated, the developed model library is made available for use in CAFD studies involving lipids. For the case study a new steam stripping model has been developed

Fourth Level: Process Synthesis and Design

In this level, computer-aided synthesis and design of process flowsheets (CAFD) is carried out. The proposed methodology is divided into two main stages [7], each composed of three steps (see Figure 1): i) the CAFD problem is defined and identified (steps 1-3) and solved sequentially using simplified models to screen out unfeasible alternatives and reduce the search space; ii) rigorous models (steps 4-6) are used to perform the final selection of the best alternative. For the case study analyzed in this paper, the CAFD problem definition is given Table 1.

Simulation results showed on one hand that the amount of stripping stream and the operation conditions in the deodorizer (temperature and pressure), are the main design variables that affect the quality of the final product (acidity, tocopherol retention, and neutral oil loss); while on the other hand, the proposed double scrubber system is a novel addition to the process to add a higher commercial value to the by-product stream.

Conclusions and Future Work

In this work the development of a multilevel modeling network for the design/analysis of processes involved in the edible oil and biodiesel industries has been presented. A comprehensive database containing the most representative chemical species, physical properties predictive models, and binary interaction for phase behavior description (liquid-liquid and vapor-liquid) has been created (Levels 1 and 2). In the third level of the modeling network, the created database was further improved by adding new and adopted models of typical unit operation present in the lipid industry and an external version of it has been made available as a user-added database for the commercial simulator PRO/II®. In the last level, alternatives to the original configuration of the process have been proposed and analyzed in terms of cost and energy efficiency. The applicability of the proposed network has been highlighted through the analysis of a lipid process involving the physical refining (deodorization) of palm oil. Results showed that, even though the process is fulfilling its aim, process variables and the configuration of the unit operations can be modified to improve the oil yield, the retention of tocopherol, and acidity removal. Current and future work is heading towards a better understanding of the phenomena that takes place in the stripping column (e.g. hydrolysis, degradation, etc.) and the design/analysis of the deodorization distillate treatment process, as this was identified as a critical unit operation of the process, by means of a double scrubber system.

Acknowledgements

The author wishes to thank the Technical University of Denmark for founding the PhD project; Prof. Rqfiqul Gani and Dr. Bent Sarup for their support and guidance as supervisor of the project; and the PhD colleagues involved in the development of this work.

List of Publications

1. Y.C. Su, Y.A. Liu, C.A. Diaz-Tovar, R. Gani, Ind. Eng. Chem. Res. (submitted on December 6th 2010).
2. C.A. Diaz-Tovar, R. Gani, B. Sarup, Fluid Phase Equilibr. 2010, doi:10.1016/j.fluid.2010.09.011.
3. C.A. Diaz-Tovar, R. Ceriani, R. Gani, B. Sarup, Braz. J. Chem. Eng. 27 (2010) 401-412.

References

1. C.A. Diaz-Tovar, R. Gani, B. Sarup, Fluid Phase Equilibr. 2010, doi:10.1016/j.fluid.2010.09.011.
2. R. Ceriani, A.J. Meirelles, R. Gani, J. Food Process Eng. 33 (2010) 208-225.
3. A. Maza, R.A. Ormsbee, L.R. Strecker, JAOCS 69 (10) (1992) 1003-1008.
4. J. Marrero, R. Gani, Fluid Phase Equilibr. 183 (2001) 183-208.
5. H.E. González, J. Abildskov, R. Gani, P. Rosseaux, B. Le Bert, AIChE J. 53 (6) (2007) 1393–1634.
6. A.A. Mustaffa, G.M. Kontogeorgis, R. Gani, Fluid Phase Equilibr. (2010) doi: 10.1016 / j. fluid. 2010. 09. 033.
7. P. Lutze, R. Gani, J.M. Woodley, Chem. Eng. Process. 49 (2010) 547–558.

Martin D. Ellegaard
Phone: +45 4525 2808
E-mail: mec@kt.dtu.dk
Discipline: Engineering Thermodynamics

Supervisor: Jens Abildskov

PhD Study
Started: February 2008
To be completed: March 2011

Thermodynamic Properties from Fluctuation Solution Theory

Abstract
A simple, yet rigorously based, method has been deployed for estimating solubilities in mixed solvents. The method accurately predicts the mixed solvent behavior for a large group of solutes using a minium of input data.

Introduction

The solubilities of solids in mixtures of liquid solvents play an important role in the design of chemical and pharmaceutial processing. The solubility of a solid often varies strongly with solvent composition; ranging from strongly nonideal deviation from ideal mixing to nearly ideal. These phenomena (and others) mean that modeling of mixed solvent solubility is a research discipline, which remains to be fully understood.

This Ph.D. project brings about an application of the solution theory of Kirkwood and Buff [1] for the solubilities of solids in mixtures of solvents. While much work within the area has progressed the molecular and modeling aspects of describing the mixed solvent solubility, all models capable of describing complex solids require extensive amouts of experimental data for parameter evaluation. Here, we present a method that is based on rigorous statistical mechanical theory, but in practive is simple to use and gives excellent descriptions of the mixed solvent solubility with a minimum of input.

Thermodynamic framework

We define an *excess* solubility of a single solute i as the solubility in the mixed solvent relative to ideal mixing

$$\ln x_i^{\mathrm{E}} \equiv \ln x_i - \sum_{j\neq ?} x'_j \ln x_{i,j}. \qquad (1)$$

Here, x_i is the mole fraction solubility of i in the mixture, while $x_{i,j}$ is the solubility in pure solvent j. The notation x'_j indicates composition on a solute-free basis. The right-hand side of Equation (1) can be related to the activity coefficients of the solute in pure and mixed solvents. These can, in turn, be related to theoretical developments on liquid-phase theories, which connect these to integrals of molecular pair correlation functions. An example is for a binary mixture

$$\left[\frac{\partial \ln \gamma_1}{\partial x_1}\right]_{T,P,n_2} = -\frac{x_2 f_{12}}{1 + x_1 x_2 f_{12}}, \qquad (2)$$

where f_{ji} relates to the spatial integrals of the total correlation functions of j and i. The formal definitions are given elsewhere [1–3], and will not be repeated here. The composition dependence of f_{ji} is generally not known, so integrating Equation (2) to obtain the species activity coefficient is not possible. Instead, useful results can be obtained by expanding ln γ_i about infinite dilution. The derivation is not lengthy, but is omitted from this communication. Instead, the reader is referred to the relevant literature [2,3]. To terms consistent to the second order in mole fraction, the following equation can be derived for the excess solubility of a solid solute (1) in a two-component solvent mixture (2,3)

$$\ln x_1^{\mathrm{E}} = -\frac{x_3}{2}\left[\frac{\partial \ln \gamma_3}{\partial x_3}\right]^{+}_{T,P,n_2} \left[1 + x_2 f_{12}^0 + x_3 f_{13}^0\right]. \qquad (3)$$

In this equation, + denotes infinite dilution of the solute in the mixed solvent; thus $\partial \ln \gamma_3 / \partial x_3$ is a property of the solvent mixture solely, and may be found from binary vapor-liquid equilibrium data forming the basis of an excess Gibbs energy model. The set $\{f_{12}^0, f_{13}^0\}$ are solute-solvent characteristics, formally defined above, but evaluated in pure solvent, thus the two are completely independent of each other. Among other things, Equation (3) separates the contributions arising from nonideality of the solvent-solvent pair and that from the solute-solvent pairs.

While the parameters of the model (f_{1j}^0) can be determined from regression of mixture data, they can also be predicted from theory, using Equation(2). This requires the melting point of the pure solute, its heat of

fusion at the melting point, and the solubility in pure solvent.

In the following, we will highlight examples, which illustrate the ability of the model to describe the solubility behavior of a set of solids in a variety of solvent mixtures.

Results

Figure 1 shows excess solubility estimates for sulfamethazine in water with dioxane. Solubilities and excess solubilities are displayed on the vertical axis.

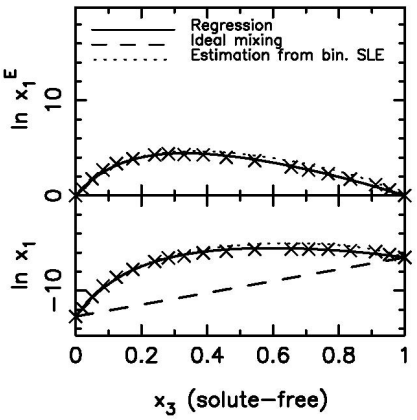

Figure 1: Solubility and excess solubility of sulfamethazine (1) in water (2) –dioxane(3) mixtures at 298 K.

The symbols denote experimental measurements. The solid curve gives the results with the regressed parameters; the dashes give the ideal mixture solubility, while the dot-dot lines show predicted excess solubilities obtained with f_{1i}^{0} estimates from pure solv-

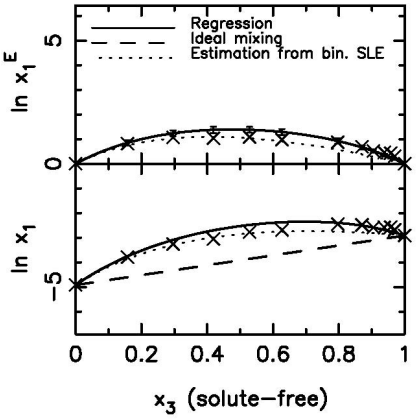

Figure 2: Paracetamol(1) in ethyl acetate(2) – ethanol(3) mixtures at 298 K.

ent solubilities. The solubilities are calculated by adding the excess solubility term to the ideal mixture term from Equation(1). The predicted value of f_{12}^{0} for sulfamethazine (1) and water (2) is quite close to the value obtained from ternary data, and much greater than f_{13}^{0} for the other solvent. The regressed values are estimated from multiple data sets where those solute-solvent combinations are found. Both estimates give excellent agreement with experimental solubility measurements and the asymmetry of the excess solubility is fully captured. Figure 2 shows the results for the system paracetamol(1)–ethyl acetate(2)–ethanol(3). Interestingly, both binary parameter values are less than those ternary values from regression of the entire set of solubilities. However, since in the midrange the ternary parameters overestimate the solubility, the binary-based predictions give better overall agreement with the measured data.

In a recent publication [3], the excess solubilities of nearly 70 pharmaceutical solutes was examined in the context of the above mentioned modeling framework. It was found, that overall the model was able to correlate and predict the excess solubility in a large variety of solvent mixtures, ranging from nearly ideal to strongly nonideal. Figure 3 shows the distrubution of the average absolute deviation, defined by

$$\mathrm{AAD} = \frac{1}{n}\sum_{j}^{n}\left|\frac{\delta x_1}{x_1}\right|, \qquad (4)$$

where δx_1 is the difference in estimated and experimental solubility, x_1. The majority of the errors

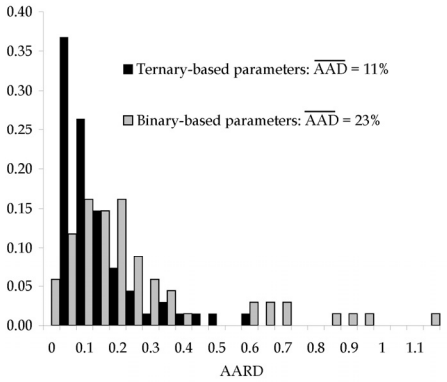

Figure 3: Distribution of average error AAD with parameters based on regression of ternary data and those found from binary solute-solvent data.

lie within 0.1–0.2. This is comparable with most competing methods, but the method presented here requries less data for evaluation of parameters. Furthermore, the method given separates the influence of solvent–solvent and solute–solvent nonidealities, which helps analyze defencies in the modeling approach.

Acknowledgements

The author is indebted to J.P. O'Connell at the University of Virginia, VA, USA, for a fruitful collaboration.

References

1. J.G. Kirkwood, F.P. Buff, J. Chem. Phys. 19 (1951) 774–777.
2. M.D. Ellegaard, J. Abildskov, J.P. O'Connell, AIChE J. 55 (2009) 1256–1264.
3. M.D. Ellegaard, J. Abildskov, J.P. O'Connell, Ind. Eng. Chem. Res. 49 (2010) 11621–11632.

Sarah Maria Grundahl Frankær
Phone: +45 4525 6885
E-mail: saf@kt.dtu.dk
Discipline: Polymer Technology

Supervisors: Anne Ladegaard Skov
Søren Kiil

PhD Study
Started: May 2009
To be completed: April 2012

A Biomimetic Material based on Cinnamic Acid Derivatised Poly(Ethylene Glycol)

Abstract
We wish to make a material that has the ability to change from a soft to a rigid state on short timescale. Our approach is to make a system consisting of a permanent polymer matrix with specific properties and a switching segment that controls the properties of the material when it is "switched on". We made a simple system to start investigating how this material could be made. We wish to use cinnamate chemistry for this material. A PEG/isocyanate network with a cinnamate switching segment was made and elasticity and relaxation processes within were investigated by means of rheology. The results show a change in the material when the switching segment is "on".

Introduction
Smart materials are materials that show a significant and controlled response when exposed to external stimuli such as stress, temperature, moisture, pH, electric or magnetic fields. Smart materials are also referred to as stimuli-adaptable or stimuli-responsive materials. This field of research spans wide and has a potential to give many new and innovative products and solutions.

For polymers, which are the focus of the project, the list is shorter since only smart polymers that respond to temperature, pH, electromagnetic radiation and electrical fields have been reported.[1]

A growing area where especially smart polymer materials are likely to find a great amount of applications is the development of materials that mimic the properties of natural systems; so-called biomimetic materials. This project was originally inspired by the sea cucumber, which can change from a relaxed to a protective stiffened phase in a few seconds if the animal is threatened, see Figure 1.[2] Another type of biomimetic systems is reversible adhesives inspired by mussels and geckos. These systems are interesting because the mussel is capable of adhere well to rough surfaces in the harsh marine environment and the gecko is able to adhere to many types of surfaces because of the nanostructures on its feet.[3]

Specific Objectives
The overall idea for the project is to make a material that can go from having one set of properties to another on short timescales (preferably seconds). Our approach is to make a material consisting of two parts – first a

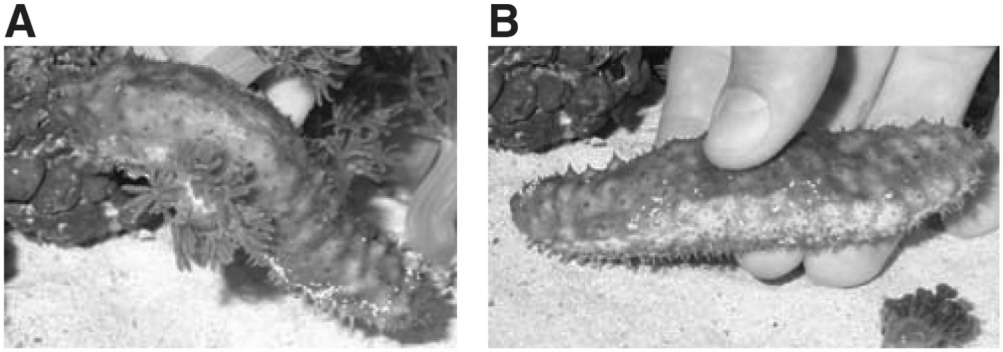

Figure 1: The sea cucumber in its relaxed (A) and stiffened (B) state.[2]

permanent polymer matrix with well-defined properties defining the first state of the material, and second a part which can be switched on and off and thus control the properties in the second state. The switching segment of the system will change the properties of the material when it is switched on and recover the original properties when it is switched off. Figure 2 shows a schematic representation of the material.

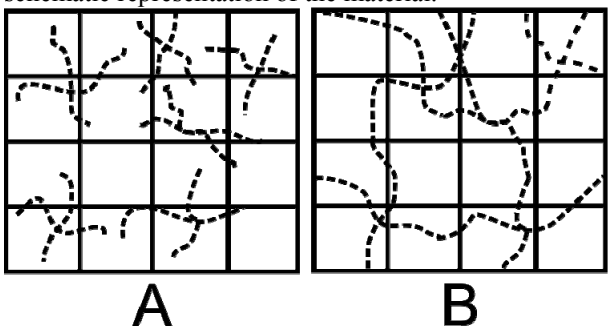

Figure 2: A: The initial material consisting of a permanent network (─) and a switching segment (─ ─) which is not crosslinked. B: The switching segment has now reacted and an inter-penetrating network is formed. This will change the material properties and may possibly also make the material shrink.

It would be attractive to have a permanent network of polydimethylsiloxane (PDMS) and a switching segment of this polymer type as well. However there are clear indications that doing chemistry on silicones could be difficult so an alternative system consisting of a permanent PDMS-network and a switching segment of an alternative polymer was proposed. The alternative polymer can be a poly(methyl methacrylate) with hydroxy end groups or α,ω-dihydroxy terminated polyisoprene.
To obtain the switch on/off ability of the properties we decided to use cinnamate chemistry. This chemistry is based on the formation of cyclobutane rings from derivatives of cinnamic acid (CA). The reaction is seen in Figure 3.

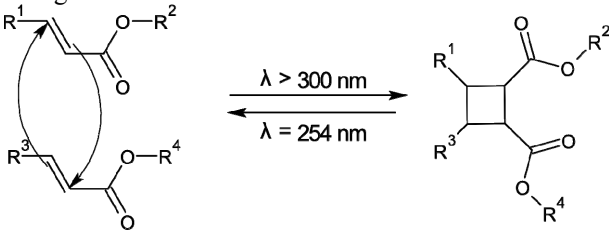

Figure 3: A schematic presentation of the reaction occuring when materials containing cinnamic acid (CA) derivatives are irradiated with UV-light with the mentioned wavelengths (λ). When irradiated with λ above 300nm the double bonds in the CA-groups react to form cyclobutane. Irradation with λ = 254nm cleaves the cyclobutane bonds and returns the material to its original state.[4]

The reaction is controlled by UV-light and it is reversible. There are a number of reactions that can be controlled this way, but the advantage of using CA is, among others, that the chemistry is relatively simple and accessible and that a high versatility of the reaction have been demonstrated. Yamaoka et al. have applied the chemistry group to phenoxy resins [5], Andreopoulos et al. applied the functional group to different PEG-polymers to make hydrogels [6, 7], Coqueret have applied the chemistry to siloxanes [8], Lendlein et al. have applied the functional group to butyl acrylates and PEGs [9] while Gattás-Asfura et al. made functional gelatines.[10]

Initial experiments with PDMS showed a number of complications and it was therefore decided to try a simpler system. For this system poly(ethylene glycol) (PEG) derivatised with cinnamic acid (PEG-CA) was synthesized and incorporated into a network consisting of PEG-chains linked with hexamethylene diisocyanate (HDI). In Figure 4 the general reaction between the OH-end groups and the isocyanate groups in HDI can be seen. The reaction forms a urethane bond.

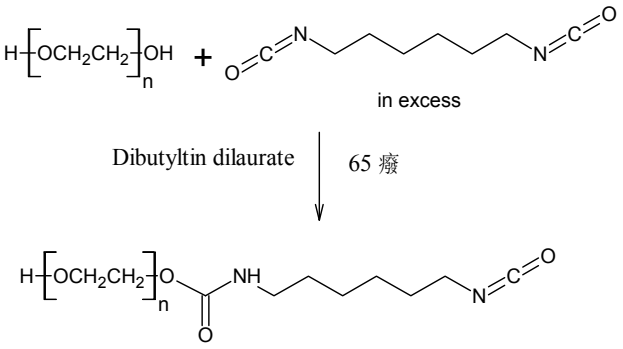

Figure 4: The reaction between the OH-groups in the PEG-polymer and the isocyanate group in hexamethylene diisocyanate yields an amide linkage. This reaction can be used to make polymer networks.

Experimental

PEG-CA: 7.526 (0.051 mole) g CA acid was dried and dissolved in 20 mL dry toluene and purged with N_2 for 10 minutes. 19 mL (0.26 mole) $SOCl_2$ added dropwise. Refluxed for three hours at app. 90°C. Concentrated in vacuo and the product was dissolved in dry tetrahydrofurane (THF). 1.052 g ($5.26 \cdot 10^{-4}$ mole) PEG (4-armed star, M_n=2000 g/mol) was dried and dissolved in 10 mL dry THF and 5 mL dry toluene and purged with N_2 for 10 minutes. The product from above was added dropwise and 1 mL triethylamine was added. Refluxed at app. 80 °C overnight. The product was recovered by pouring the reaction mixture into cold diethyl ether. The modified PEG, a viscous orange liquid, was isolated. Linear PEG (Mn=1000) as well as linear (M_n=15000) and 4-armed PEG (M_n=2000) derivatised with cinnamylidene acetic acid (CAA) was derivatised in a similar way.

PEG-HDI network: 0.213 g ($0.11 \cdot 10^{-3}$ mole) dry PEG (4-armed star, M_n=2000 g/mole) is dissolved in 15 mL toluene and mixed with 0.5 mL ($3.1 \cdot 10^{-3}$ mole) hexamethylene diisocyanate (HDI) and 1 drop of dibutyltin dilaurate was added. After three hours at 90°C the reaction mixture is poured into cold heptane. The product precipitates as a viscous clear liquid. The

heptane is removed by decantation and the product is dissolved in toluene and concentrated in vacuo. 0.8365 g PEG (linear, M_n=10000 g/mole) and 0.246 g PEG-CA (M_n=1000) were dried and dissolved in 2 mL $CHCl_3$. 2 drops dibutyltin dilaurate is added. The mixture is cured in teflon mold at 90°C overnight.

Irradiation procedure: The samples were irradiated with a SolData Ultra Violet Lamp UVA 315-400 nm. Irradiation time and distance between the sample and the light source were varied. The specific data can be found in the Results-section.

ATR-FTIR analysis was conducted on Perkin-Elmer Spectrum One apparatus. The spectra were recorded in the range of 4000-525 cm^{-1} with 4 cm^{-1} resolution and 16 scans. UV-visible spectrum has been recorded on Perkin-Elmer Lambda 5 spectrometer.

The samples were investigated with linear rheology. The measurements were made with a TA 2000 Rheometer from TA Instruments set to a controlled strain mode. The measurements were done with parallel plate geometry of 20 mm in the frequency range from 0.01 Hz to 100 Hz and at temperatures between 50 and 120°C. The data was shifted using the time-temperature superposition principle (TTS).

Results and Discussion

It was crucial for the project to find chemistry which is orthogonal – basically meaning two types of reactions which can appear in presence of each other, but which do not interfere. In Figure 5 IR-spectra showing the development of the PEG-isocyanate network with PEG-CAA chains in the network can be seen. The isocyante band (2245 cm^{-1}) is present in the modified PEG (— — in the figure) but disappears in the final network. The urethane band (1720 cm^{-1}) appears in the modified PEG-star and is still present in the final network. This shows that the urethane bond between the PEG-chains and the HDI is formed, and can be controlled so now isocyanate bonds are present after the reaction. It is difficult to see the presence of the PEG-CAA chain in the spectrum of the final network (— in the figure). This is most probably due to a relatively low concentration (37 w/w% PEG-CAA, but the concentration of the active end groups is much lower approx. 1 w/w%) but also to the fact that other bands in the spectrum lie on top of the CAA-bands. However the PEG-CAA-polymer has a clear orange colour which was visible in the sample, and furthermore the presence of the polymer was verified by UV-spectroscopy.

A PEG-network, with 37 w/w% PEG-CAA, was tested with rheology, the obtained data was shifted to 50°C using TTS, see Figure 6. In Figure 6 it is observed that the data before and after irradiation is very similar. We think that the lack of change is due to the fact that the used PEG has a molecular weight (M_n) far above the molecular entanglement weight (M_e). The value for G' increases with increasing molecular weight, at M_e the polymer chains start to entangle and for molecular weights around 2-3M_e and larger the value for G' is constant. M_n for the used PEG-chains is 15000 (for the PEG-CAA-chains which make up the switching segment) and 10000 (for the PEG-chains that make up the PEG-network) are far above the M_e for PEG (M_e(PEG)=1624[11]). This explains why no change is seen.

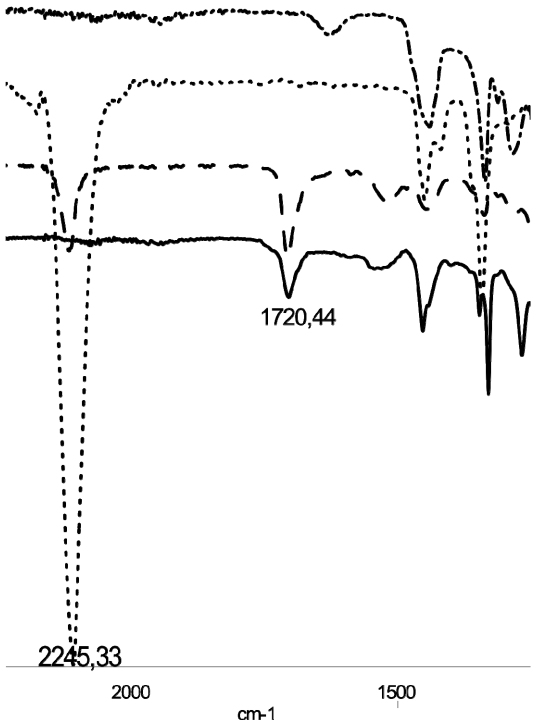

Figure 5: The formation of the PEG/isocyanate network. — · — ·: The PEG-star; ···: HDI; — —: The HDI-modified PEG-star; —: The final network. The isocyante band (2245 cm^{-1}) is present in the modified PEG but disappears in the final network. The urethane band (1720 cm^{-1}) appears in the modified PEG-star and is still present in the final network.

When the problems with M_n and M_e were observed it was decided to try to overcome these by changing the molecular weights of the chains in the network and in the switching segment. A network with chains with a M_n of app. 5000 and a switching segment consisting of CA-derivatised PEG (M_n=1000) (the concentration of PEG-CA in the network was 20 w/w%) was made and in Figure 7 the rheological data for this material can be seen. The data in Figure 7 shows a difference from before radiation to after. However, the results do not show what would be expected. It was expected that the value for the plateau seen at low frequencies (observe the flattening in the curves marked with black markers at low frequencies) would go up after irradiation with UV. However it is actually observed that this value goes down (from app. 300 Pa before irradiation with UV to app 80 Pa after).

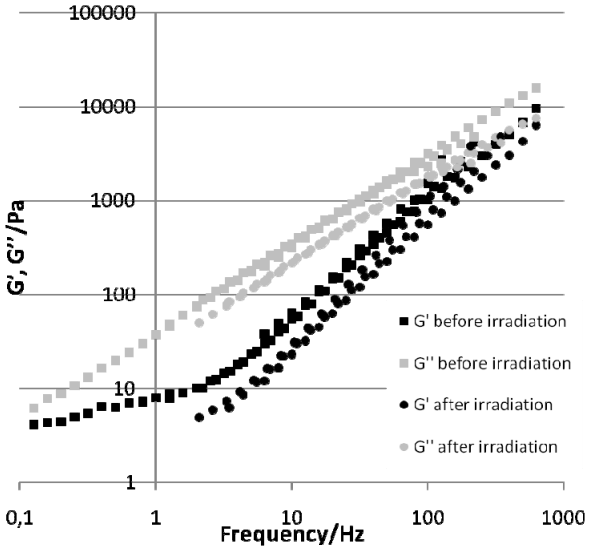

Figure 6: Rheology data for the network before and after irradiation. Only small change is seen in the material. (UV irradiation was carried out in a distance of 17 mm from the light source and for 30 minutes. The intensity of the UV-light was 3 mW/cm^2).

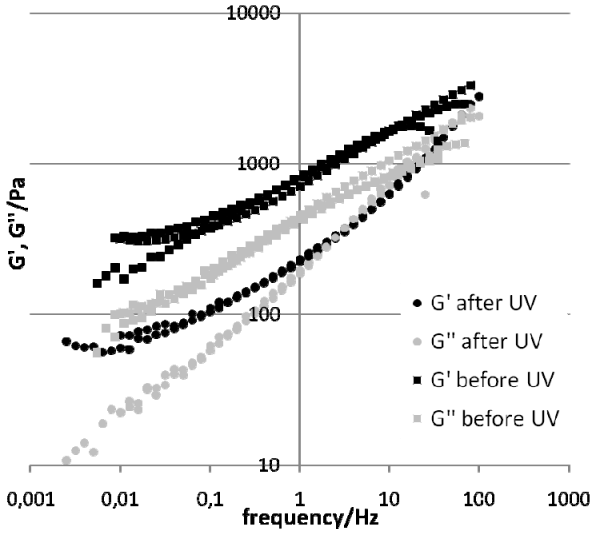

Figure 7: Rheology data for the network before and after irradiation. A difference between before and after is clearly seen, but the results do not correlate with what was expected. (UV irradiation was carried out in a distance of 23 mm from the light source and for 60 minutes. The intensity of the UV-light was 7.9 mW/cm^2).

The result is puzzling but we think that maybe the reason is that this system acts differently than what was initially expected simply because of the way it is made up. The low molecular weight of the switching segment actually means that before the switching segment is "switched on" it acts as a solvent trapped in the network. A network that contains solvent will have fast dynamics. When the switching segment is "on" then the solvent effect is gone and the dynamics are much slower. If this is the case then there is a possibility that what is observed before irradiation is in fact relaxation in the chains and not a true plateau because the dynamics are simply too fast. But to verify this, a further study is needed.

Conclusion

We managed to make a PEG/HDI-network with PEG-CA or PEG-CAA inside. We observed changes in the rheological properties of this material when the molecular weights are kept significantly below M_e. It is still unclear exactly what is going on with the material and a systematic study of the material will be carried out.

References

1. F. Liu, M.W. Urban, Prog. Polym. Sci. 35 (2010) 3–23
2. J.R. Capadona, K. Shanmuganathan, D.J. Tyler, S.J. Rowan, C. Weder, Science 319 (5868) (2008) 1370
3. H. Lee, B.P. Lee, P.B. Messersmith, Nature 448 (7151) (2007) 338–341
4. H. Tanaka, K. Honda, J. Polym. Sci., Polym. Chem. Ed., 15 (1977) 2985–2689
5. T. Yamaoka, K. Ueno, T. Tsunoda, Polymer 18 (1977) 81–86
6. F.M. Andreopoulos, C.R. Deible, M.T. Stauffer, S.G. Weber, W.R. Wagner, E.J. Beckman, A.J. Russell, J. Am. Chem. Soc. 118 (1996) 6235–6240
7. F.M. Andreopoulos, E.J. Beckman, A.J. Russell, Biomaterials 19 (1998) 1343–1352
8. X. Coqueret, Macromol. Chem. Phys. 200 (1999) 1567–1579
9. A. Lendlein, H. Jiang, O. Jünger, R. Langer, Nature 434 (7035) (2005) 879–882
10. K.M. Gattás-Asfura, E. Weisman, F.M. Andreopoulos, M. Micic, B. Muller, S. Sirpal, S.M. Pham, R.M. Leblanc, Biomacromolecules 6 (2005) 1503–1509
11. L.J. Fetters, D.J. Lohse, D. Richter, T.A. Witten, A. Zirkel, Macromolecules, 27 (17) (1994) 4639–4647

Wenjing Fu
Phone: +45 4525 2804
E-mail: wfu@kt.dtu.dk
Discipline: Process Technology and Unit Operations

Supervisors: John M Woodley
Rafiqul Gani
Anders Riisager, DTU Chemistry

PhD Study
Started: March 2008
To be completed: May 2011

Process Design of Chemo-enzymatic Synthetic Cascades

Abstract
Limited fossil resources and the unstable oil price are likely to make it increasingly important to create new chemical processes based on renewable resources. For many of these new processes a combination of enzymatic as well as heterogeneous and homogeneous catalysis will be required to direct the reaction toward the desired products. Hence there is a need to create a suitable process model to manage a range of technologies and products in the optimal way starting from renewable resources, such as glucose or fructose for example. Specifically, this project focuses on the design of a chemo-enzymatic synthetic cascade from glucose.

Introduction
Chemo-enzymatic synthesis is a method to achieve selective catalysis, with potential application to many classes of reaction where conventional approaches are very difficult. A combination of enzymatic as well as heterogeneous and homogeneous catalysis will direct the reaction toward the desired products. It has found success in a number of pharmaceutical processes to produce high value and specialty chemicals. The challenge now is how to apply this approach in synthesis of bulk chemicals. For example, in biorefineries, how can this approach be used create platform chemicals for the chemical industry of tomorrow from renewable resources.

Characteristic of many chemo-enzymatic syntheses, even for small reaction pathways, there are many alternative technologies. Some can be integrated together, but many are difficult to implement and remain untested at scale [1]. Thus, this makes it difficult to justify effort and resource on process design, especially in the early stages of process development, where information is limited [2]. A particularly valuable tool would therefore be a methodology capable of fast evaluation of different processes with limited information to reduce the number of potential process flowsheets and identify bottlenecks [2, 3].

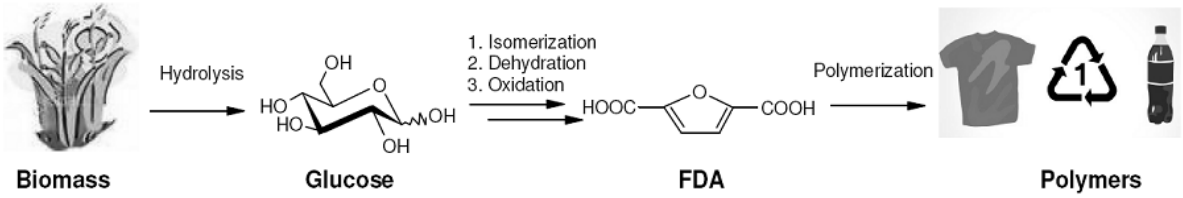

Figure 1: Main pathway of synthesis FDA from glucose

This PhD project examines the use of renewable resources as new, versatile feed-stocks for the chemical industry and the associated tools for evaluation of alternative routes. For example, one case study aims to understand the production of a new building block for the polymer industry, 2,5- furandicarboxylic acid (FDA), from glucose via the intermediate 5-hydroxymethyl furfural (HMF) and employs a combination of chemical and enzymatic catalysis. The new polymer building block (FDA) has applications and properties similar to terephthalic acid which is derived from fossil resources and is currently the main building block for polyester resins and fibers.

Glucose could be a suitable feedstock since it can be readily obtained from starch. The production of FDA from glucose involves isomerization, dehydration and

oxidation. Figure 1 shows the pathway of the process to produce FDA from glucose. The reaction conditions for the three main reactions are listed in Table 1. One of the biggest challenges in the proposed pathway is to match all three sets of reaction conditions, including reaction media, temperature, pH and concentration. In addition, there are many alternative technologies in the route from glucose to FDA, making the complete process design particularly complicated and challenging.

Table 1: Typical reaction conditions for the three main reactions involved in the synthesis of FDA.

Reaction	Temperature (°C)	pH	Catalyst
Isomerization	50 - 60	7 - 8	Glucose isomerase
Dehydration	80 - 200	acidic	Heterogeneous Homogeneous
Oxidation	room	basic	Inorganic

Background

One of the objectives in this work has been to develop a systematic model framework to addresses the necessary definition and design of an optimal process to produce FDA from glucose within specification and economic constraints as an example of the process design for chemo-enzymatic syntheses. The documented methodology and the developed tools should be suitable to be applied to a range of similar chemo-enzymatic process design problems. Some specific objectives have also included:

- Identify different possible flowsheets in routes from glucose to FDA, which including both process options with and without integration.
- Develop a systematic method using computer-aided process modeling and cost analysis tools to compare alternative technologies and routes from glucose to FDA within economic constraints.
- Analyze the potential process options to form the basis of process and cost models for detailed sensitivity analysis, in order to set targets for catalyst and process improvement.
- Identify and document the necessary types of property and thermodynamic data according to different types of modeling and analysis. This is necessary since collecting the correct and suitable property and thermodynamic data is essential for process modelling. However, for many chemicals involved in biorefineries, such data are frequently scarce.
- Examine and document the feasibility of using different types of modelling software which were developed for the conventional chemical processes for the bioprocess design.

Methodology

The methodology used in this study is shown in Figure 2.

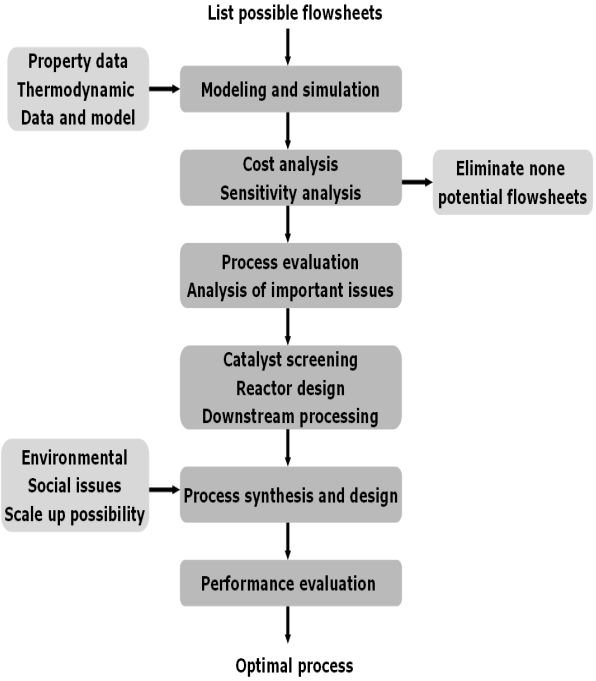

Figure 2: Plot of methodology of the study.

Case study: Process design for synthesis HMF from fructose

In order to illustrate some of the findings form this project, we discuss here the selection of either an aqueous or organic solvent-based dehydration step for the conversion of fructose into HMF (the central reaction). Any decision made here has a direct influence on the technology chosen for the preceding isomerisation step as well as the following oxidation step. Indeed, it affects directly how much up-stream and down-stream processing is required in order to run the whole process from glucose to FDA. For example, if the organic solvent-based route is used for the second step, it then requires a solvent removal, or switch back to water, to match the reaction media used to oxidize HMF to FDA. Here we compare two processes to produce HMF from fructose. One process was patented by Bazoa and co-workers for the preparation of high purity HMF through an organic solvent-based route [4]. They also produces high purity HMF but through an aqueous-based route, patented by Rapp and co-workers [5].

Organic solvent-based synthetic route for producing HMF from fructose

The process flowsheet for the organic solvent-based synthetic route is outlined in Figure 3. The feed to the dehydration reaction for this process is fructose and the organic solvent is DMSO. In this case no catalyst is added. The mixture is stirred mechanically at 160 °C for 8 hours. The yield for the dehydration of fructose in DMSO is 0.8 mol HMF/mol fructose (0.56 g HMF/g fructose), with a 100 % conversion and 80 % selectivity. Afterwards, the reaction mixture is cooled down to room temperature and neutralized with 50 g / L KOH solution. Water is added in the same amount as DMSO

prior to filtration to remove any precipitates. The mixture is then extracted with dichloromethane (DCM) (same amount as the mixture) at 8 °C in a column extractor unit (with 6 theoretical extraction stages). 97 % HMF in the mixture can be extracted by DCM into the organic layer. The organic layer is concentrated at 20 °C in a vacuum evaporator (50 mm Hg) to separate HMF from DCM. The concentrated syrup containing mainly HMF is passed to the crystallization reactor (with slow mechanical stirring). The solution is cooled to -5 °C to produce crystals of HMF.After filtration of the crystalline HMF, the mother liquor is sent to vacuum distillation to concentrate it further before sending it for a second crystallization. The final crystallization yield is 90%. The required organic solvent after stripping off water is recycled in the system. Process water is also recycled.

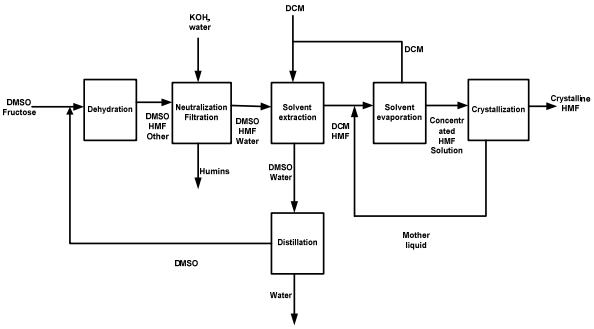

Figure 3: Process flowsheet of dehydration fructose in DMSO, modified from [4].

Aqueous-based synthetic route for producing HMF from fructose

The process flowsheet for the aqueous-based synthetic route is outlined in Figure 4. The feed to the dehydration reaction for this process is fructose and water. The feed concentration is around 25 wt% fructose (on a wet weight basis). Oxalic acid is added as a catalyst. The mixture is stirred mechanically and maintained at around 135 °C to 142 °C for 2.1 hours. The yield for the dehydration of fructose in water is 0.34 mol HMF / mol fructose (0.24 g HMF/g fructose), with a 61 % conversion (mol HMF/mol fructose) and 55% selectivity (mol HMF/mol fructose). Afterwards, the reaction mixture was cooled down to 40 °C and the solids (poly-HMF) were filtered by pressure filtration. The filtrate was then neutralized with calcium carbonate. After filtration and neutralization, the mixture is then sent to chromatography to separate HMF and unconverted fructose from the mixed fractions. 78 % of HMF can be recovered in this way. The separated HMF solution is then sent to evaporators for concentration, prior to crystallization. The concentrated syrup containing mainly HMF in water is slowly stirred and cooled to 4 °C to produce crystals of HMF. After filtration of the crystalline HMF, the mother liquor is sent to evaporators to concentrate further prior to a second crystallization. The total crystallization yield is 66 % and the purity of obtained HMF crystals is 97%. The process water is recycled as shown in the flowsheet. And the excess water produced in dehydration reaction is stripped-off.

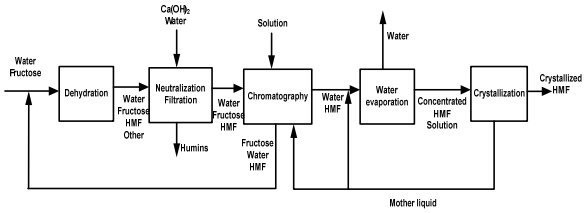

Figure 4: Process flowsheet of dehydration fructose in water, modified from [5].

Results

A mass balance was done on the basis of producing 1 kg HMF using both routes described above. The required raw materials and process reagents, together with required process energy to produce 1 kg HMF for both routes is shown in Figure 5. Compared with the feed sugar, for the organic solvent-based synthetic route, almost 2 kgs of fructose is required to make 1 kg HMF (overall yield is 0.49 g HMF /g fructose) and more than 3 kgs of fructose is required to make 1 kg HMF by the aqueous based route (overall yield is 0.32 g HMF /g fructose). Although, avoiding organic solvent may be a significant advantage, the poor use of fructose makes the aqueous based route unfavorable. On the other hand, using organic solvent for the dehydration assures an acceptable yield. In addition, the aqueous based synthetic route is an energy intensive process. For each unit operation, the required energy in the aqueous based route is much higher than that for the organic solvent based route. Due to the lower concentration in the aqueous route and lower yield, a large amount of fructose and water are required in the feed. Consequently, a particularly high energy for preheating and dehydration is required. Due to the high volume of water required, the required energy for heating and cooling is also much higher than the organic solvent-based route. For the aqueous synthetic route, the most energy intensive step is the evaporation (62.5 %). The reason for this is that using chromatography for the separation leads to significant dilution. In the ino-exchange separation, washing 1 g HMF out of the reaction mixture requires 115 g of water. The large dilution therefore requires a lot of energy to evaporate the water to concentrate the solution before crystallization. The overall energy required for the water route (2.6 GJ/kg HMF) is around 28 times more than the energy required for the organic solvent route (0.09 GJ/kg HMF). The effective use of the energy in the water route is also much lower than that for the organic solvent route.

Based on the raw material and energy price listed in Table 2, the production cost (raw material and energy cost only) for producing 1 kg HMF by the organic solvent-based synthetic route is 1.6 USD/kg and 11.5 USD/kg using the aqueous based route. The cost distribution for both routes is shown in Figure 6. For the

organic solvent based synthetic route, the major cost arises from the reactant cost (63 %), followed by the energy cost (21 %). On the contrary, for the aqueous based synthetic route, the energy cost covers 86 % of the total cost. This is due to the large amount energy required to evaporate the water which is used to wash the HMF in downstream processing. The cost analysis further confirms that the aqueous based synthetic route is not a cost-effective route for synthetic HMF from fructose.

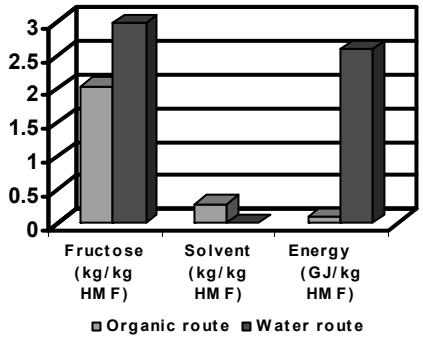

Figure 5: Comparison of required mass and energy for producing 1 kg HMF for two routes.

Table 2: Raw material and energy cost.

Raw material	Price(USD/kg)
Fructose	1
DMSO	2
DCM	0.5
$Ca(OH)_2$, KOH	0.2
Energy	**Price (USD/GJ)**
Heating stream	0.6
Cooling water	1.6

Conclusions

For the dehydration of fructose to HMF, the organic solvent-based synthetic route is superior to the aqueous based synthetic route. The organic solvent-based route has a much better use of both raw material and energy. Besides, less waste is produced in organic route. The emphasis and challenge in process design should then be placed on choosing the right solvent (more environmental friendly and easier to recover) and reduce the solvent loss in the whole synthetic process. For the aqueous based synthetic route, maintaining a high yield and keeping a high concentration are very crucial. Although the use of ion-exchange is common in the sugar industry, the generally high dilution of the resulting solutions is a disadvantage for the type product we discuss here and probably require further improvement.

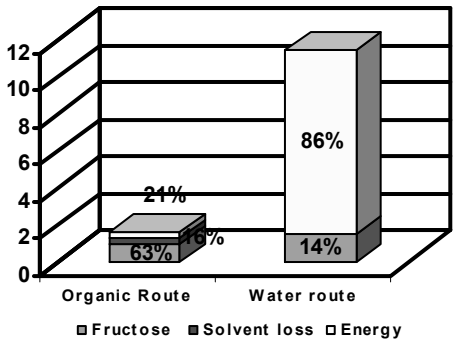

Figure 6: HMF production cost distribution by organic solvent based route and aqueous based route.

Acknowledgement

The author wants to thank Technical University of Denmark, Novozymes A/S, and the Danish National Advanced Technology Foundation (DNATF) for financial support.

References

1. A. Boisen, T.B. Christiansen, W. Fu, Y.Y. Gorbanev, T.S. Hansen, J.S. Jensen, S.K. Klitgaard, S. Pedersen, A. Riisager, T. Ståhlberg, J.M. Woodley, Chem. Eng. Res. Des. 87 (2008) 1318
2. J. Shaeri, R. Wohlgemuth, J.M. Woodley, 2006, Org. Process Res. Dev. 10 (2006) 605-610
3. N. Sammons, M. Eden, H. Cullinan, L. Perine, E. Connor, Environ. Prog. 26 (2007) 349–354
4. C. Bazoa, F. Raymond, L.G.A. Rigal, "Produce de fabrication 5-hydroxymethylfurfural (HMF) de purete elevee", 1990, FR 2669635-A1 (in French).
5. M.K. Rapp, "Process for the preparation of 5-hydroxymethylfurfural, including a crystalline product, using exclusively water as solvent", 1987, DE Patent 3601281 A1.

Martina Heitzig
Phone: +45 4525 2986
E-mail: mat@kt.dtu.dk
Discipline: Systems Engineering

Supervisors: Rafiqul Gani
Gürkan Sin
Peter Glarborg

PhD Study
Started: December 2008
To be completed: November 2011

Computer-Aided Modelling for Efficient and Innovative Product-Process Engineering

Abstract
Model-based computer aided product-process engineering requires models of different types, forms and application purposes. In this project a computer-aided modelling framework capable of handling the multi-scale modelling needs for product-process design and analysis is being developed. The framework supports the systematic and efficient development of multi-scale models, their interconnections, numerical analysis, parameter regression and solution. A case study related to design and evaluation of fragrance aerosol products is briefly presented to validate the methodology. The developed modelling scenario spans four length scales and describes how droplets of different sizes are formed when a liquid fragrance product is sprayed from a pressurized can and how these droplets evaporate while they settle down due to sedimentation and convective mixing.

Introduction
Models are playing roles of increasing importance in design and analysis of chemicals/bio-chemicals based products and the processes that manufacture them because of the increasing use of computer-aided methods and tools. The advantage of using these model-based methods and tools is that they have the potential to reduce the number of experiments, which can be expensive and time consuming, while at the same time, lead to truly innovative solutions. As the required models may be complex and require multiple time and/or lengths scales, their development and application for product-process design is not trivial. Therefore, the developed modelling framework can contribute by reducing the time and resources needed for model development and application, thereby reducing the overall time and cost for product-process development. This is achieved by designing the structure of the framework such that it can handle the work-flows and data-flows associated with different modelling tasks, combining state-of-the-art modelling techniques for the different work-flow steps as well as supporting model-documentation and model reuse.

Specific Objectives
The project is targeted to derive the work- and data-flows for the different modelling tasks in chemical and bio-chemical engineering (single-scale and multi-scale model development, model identification, model application for simulation and optimization). These work-flows are then implemented into user-friendly software combining for each work-flow step the required expertise, tools, database and library connections. The computer-aided modelling framework is developed and validated by case studies from different areas in chemical engineering.

Results and Discussion
The structure of the computer-aided modelling framework with the different modelling tasks is shown in Figure 1. The framework incorporates work-flows for model development (single-scale and multi-scale) as well as for model identification and model application for simulation and optimization.

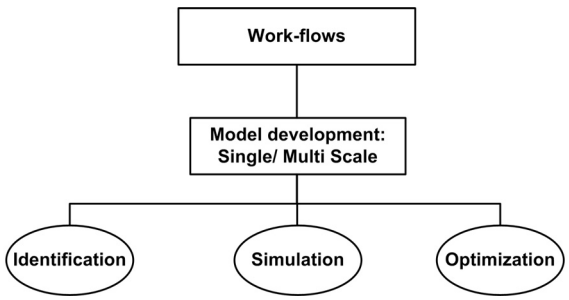

Figure 1: Structure of computer-aided modelling framework [1]

In this contribution the focus is on the work-flow for multi-scale model development which can be summarized as: step 1) Modelling objective and system description; step 2) Identification of required models and model types; step 3) Development, analysis, identification and validation of models; step 4) Linking of models involved and solution strategy; step 5) Application and evaluation of results. In step 1 the modelling objective is defined and available information on the system is collected. In step 2 the different elements of the system are identified and for each element it is investigated how it can be modelled. The work-flow identifies the need for multiple time and/or length scales for models based on the model assumptions, considered phenomena and desired model outputs. Once the models have been developed (step 3) they are evaluated on how they should be linked and whether to be solved sequentially or simultaneously (step 4). Step 5 represents the application of the developed model which requires the use of a separate work-flow. Like shown in Figure 1 the framework incorporates application work-flows for model identification, simulation and optimization. The model development process is iterative and whenever the model performance at the end is not satisfactory or new information becomes available/is required the modeller needs to go back to the previous steps.

Case Study

The modelling scenario describes the spraying of a liquid fragrance product and the fate of the formed droplets [2]. In the following, the case study is applied to highlight the steps of the multi-scale model development work-flow. The developed models have been implemented in the model library of the framework so that they are available for application by other modelling projects.

Step 1) Modelling objective and system description

The modelling objective is to describe the spraying process of a fragrance product (for example fine fragrance, air freshener) so that the product qualities can be evaluated. The system under investigation is depicted in Figure 2. A pressurized liquid mixture of active ingredients, solvents, additives and propellants is released from a can to the surrounding atmosphere. The compounds are limonene (fragrance) and ethanol (carrier). During the release process a part of the liquid evaporates while the remaining liquid forms droplets of different sizes which account for the fragrance delivery. The generated droplets move downwards due to sedimentation and convective mixing as fragrance chemicals evaporate. Consequently, the modelling objectives of the system can be divided into two parts (see Figure 2):

Part I: Describe the spraying of the compressed liquid from a can to the atmosphere and predict the ratio of released vapour to liquid as well as the size distribution of the formed droplets and their temperature.

Part II: Model the fate of the droplets as they settle down and evaporate.

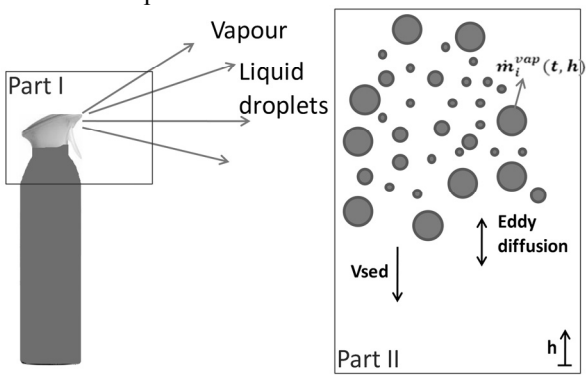

Figure 2: Spraying process (Vsed - sedimentation velocity; $\dot{m}_i^{vap}(t,h)$ - evaporation mass flow of compound i) [2]

Step 2) Identification of required models and model types

Part I: The ratio of liquid to vapour released as well as the initial temperature and composition of the droplets is predicted by an adiabatic flash model. Based on these results the droplet size distribution is determined by an experimentally regressed correlation (alternatively, a normal distribution may also be assumed).

Part II: In order to describe the fate of the droplets, models are needed to describe the transport process as well as the evaporation together with appropriate constitutive models for different properties.

Step 3) Development, analysis, identification and validation of models

Because of page limits, only the modelling of Part II is presented in this contribution.

3.1) Transport of droplets: The transport model of the droplets in the atmosphere (W. Koch, SprayExpo Program Description, Toxikologie und Experimentelle Medizin, Frauenhofer Institut, Hannover, Germany) has been adopted here. It considers the transport due to sedimentation as well as eddy diffusion. The sedimentation is modelled based on Stoke's friction law. Coalescence between droplets and transport in horizontal directions is neglected. The droplets are assumed to be spherical. The corresponding model equations are given below:

$$A = \frac{\rho_{mix} \cdot g}{18 \cdot \eta_{air}} \tag{1}$$

$$\frac{\partial C_{droplet}}{\partial t} = K_{eddy} \cdot \frac{\partial^2 C_{droplet}}{\partial h^2} - A \cdot D_{dr}{}^2 \cdot \frac{\partial C_{droplet}}{\partial h} \tag{2}$$

3.2) Droplet evaporation: For the droplet evaporation the model from [3] has been modified by adding a dynamic energy balance. Important model assumptions are: the droplet is spherical, ideally mixed and consists only of ethanol and limonene; VLE is

established at the droplet surface; convection and thermal diffusion are neglected; the gas phase is ideal; the temperature profile around the droplet is given by zeroth order approximation; the temperature of the surrounding gas phase T_{am} is constant; and the concentration of the droplet compounds $y_{am,i}$ far away from the droplet is zero. The corresponding model equations are:

$$T_s = \frac{\left(mcp^{mix} T_s\right)}{\sum_{i=1}^{Ncomp} m_i \cdot cp_i} \tag{3}$$

$$n_i = \frac{m_i}{MW_i}, x_i = \frac{n_i}{\sum n_i}, i = 1,..., Ncomp \tag{4),(5}$$

$$V_{dr} = \sum_{i=1}^{Ncomp} \frac{m_i}{\rho_i}, D_{dr} = \left(\frac{6V_{dr}}{\pi}\right)^{1/3} \tag{6),(7}$$

$$m = \sum_{i=1}^{Ncomp} m_i, w_i = \frac{m_i}{m}, i = 1,..., Ncomp \tag{8),(9}$$

$$\rho_{mix} = \sum_{i=1}^{Ncomp} w_i \cdot \rho_i \tag{10}$$

$$R_{Kelvin,i} = \exp\left\{\frac{-4 \cdot MW_i \cdot \sigma_i}{\rho_i \cdot R_m \cdot T_s \cdot D_{dr}}\right\} \tag{11}$$

$$P_i^s = P_i^{s,plane} \cdot R_{Kelvin,i} \tag{12}$$

$$\frac{dm_i}{dt} = \frac{2\pi D_{dr} \cdot MW_i \cdot D_i \cdot P}{R_m \cdot T_{am}} \ln\left\{\frac{1 - P_i^s \cdot x_i \cdot \gamma_i / P}{1 - y_{am,i}}\right\} \tag{13}$$

$$\frac{d(mcp^{mix} T_s)}{dt} = 2\pi D_{dr} K_{air} (T_{am} - T_s) + \pi D_{dr}^2 \Gamma (T_{am}^4 - T_s^4) + \sum_{i=1}^{Ncomp} L_i \frac{dm_i}{dt} \tag{14}$$

Here, T_s is the droplet temperature, D_{dr} the droplet diameter and m_i is the mass of compound i inside the droplet. The model has been successfully validated using data by [4] for evaporating water droplets.

3.3) Constitutive models: Correlations for the pure component properties with respect to changing temperature are taken from the ICAS database which is linked to the modelling framework. The required properties are: liquid heat capacity cp_i, liquid density ρ_i, vapor diffusion coefficient in air D_i, surface tension σ_i, heat of vapourization L_i and vapour pressure P_i^s for all system compounds. For these properties mixing effects are neglected in the model. Furthermore, the thermal conductivity of air K_{air} at ambient temperature is required. For the liquid phase activity coefficients γ_i the UNIQUAC model has been applied with parameters for limonene and water regressed by [5].

Step 4) Linking of models and solution strategy

The developed models for the spraying process span four different length scales. The models of Part I, that is the adiabatic flash model and the droplet size distribution model, are at the macro scale. In order to describe the fate of the droplets (Part II), three size scales have been employed. On the meso scale (Eqs. 1-2) the transport of the droplet size fraction is considered, while the micro scale (Eqs. 3-14) describes the evaporation of a single droplet and the required properties are calculated on the nano scale with respect to temperature and composition. Figure 3 shows the linking scheme of the different models together with the data-flow and sketches of the modelled system on the different scales. The macro scale model is solved sequentially. Due to the data-flow requirements between the size scales, the remaining lower scale models must be solved simultaneously (for solution sequence, see numbers in Figure 3). The lower scale models need to be solved for each discrete droplet diameter j in the macro scale (N_{dis} times). The droplet temperature T_s, the compound masses in the droplet $m_i^{(j)}$ and the number of droplets $ND_r^{(j)}$ need to be communicated from the macro scale to the lower scale models for each discrete diameter j where they are used as initial values. In order to solve the meso scale model, the partial differential equation (Eq. 2) is discretized (in vertical direction h). This is done automatically by the modelling framework based on user specifications (method of lines, h_{min}=0.4 m, h_{max}=2.7 m, 184 discretization points). The height where the droplets are generated is 1.6 m. Results communicated back to the macro scale for each discrete droplet diameter j are the number of droplets in each discrete height h $ND_r^{(j)}(h,t)$, the mass of the compounds i inside the droplet $m_i^{(j)}(t)$ and the mass flow evaporating from the droplet $m_i^{evaporating}(t)$, all with respect to time. After solving the lower scale models for each discrete diameter, the macro scale combines the results for the different size fractions j to overall results. Figure 3 also shows the output variables of each model in the linking scheme.

Step 5) Application and evaluation of results

Simulations have been conducted for a total number of 1.02×10^{10} droplets having a droplet size distribution of 22 discrete diameters between 1.3 and 34 µm. Initially, all droplets had a composition of 5 vol% limonene and 95 vol% ethanol. The micro scale results are highlighted in Figure 4. Figures 5 and 6 show the results of the meso and macro scales, respectively.

Conclusions

A generic methodology (work-flow and data-flow) to develop multi-scale models as well as for model identification and application has been developed. Based on that the required features of a modelling tool have been identified and a conceptual computer-aided modelling framework has been constructed. The framework has been validated applying case studies from different areas in chemical engineering. Current and future work is the implementation of the modelling framework into the existing modelling toolbox ICAS-MoT [6] as well as the extension and validation of the Aerosol case study models.

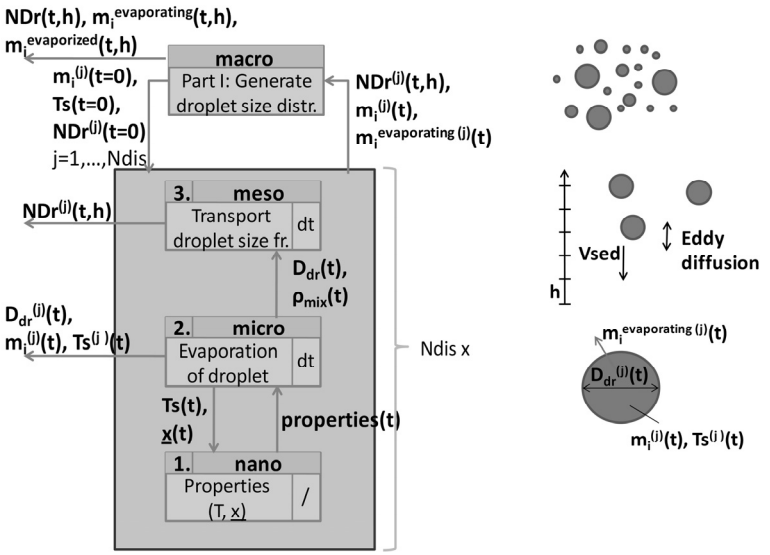

Figure 3: Linking scheme for spraying and fate of aerosol [2].

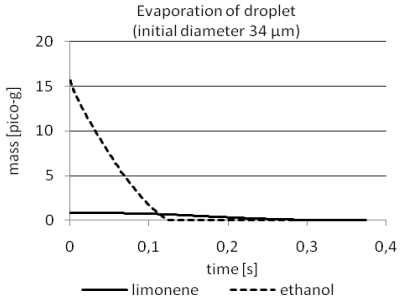

Figure 4: Micro scale results: droplet composition during evaporation (34 µm droplet) [2].

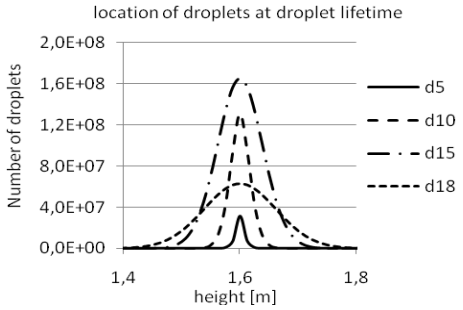

Figure 5: Meso scale results: location of droplets at droplet lifetime for different discrete diameters [2].

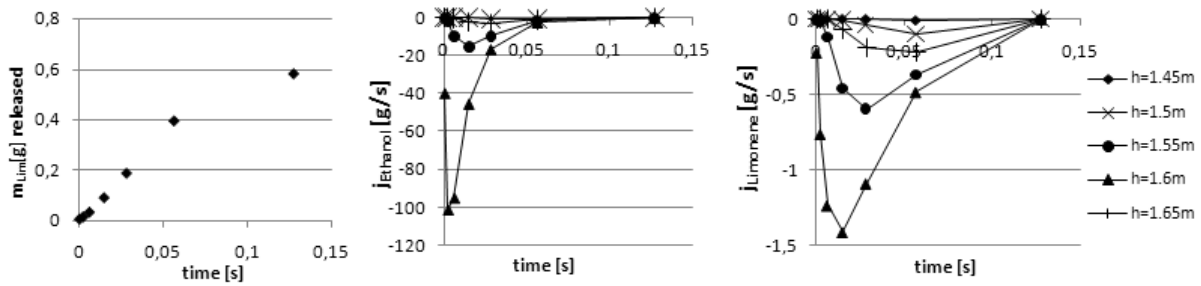

Figure 6: Macro scale results. Left: Total mass of limonene released (all droplets) vs. time, Right: Total mass flow of ethanol and limonene at different heights vs. time [2].

Acknowledgements
This PhD project is funded by a scholarship from the Technical University of Denmark.

References

1. M. Heitzig, G. Sin, M. Sales-Cruz, P. Glarborg, R. Gani, Ind. Eng. Chem. Res. Puigjaner Special Issue (2010).
2. M. Heitzig, C. Gregson, G. Sin, R. Gani, submitted to ESCAPE 21 (2011).
3. J. Kukkonen, T. Vesala, M. Kulmala, J. Aerosol. Sci. 20 (7) (1989) 749-763.
4. W.E. Ranz, W.R. Marshall Jr., Chem. Eng. Prog. 48 (4) (1952) 173-180.
5. A. Cháfer, R. Muñoz, M.C. Burguet, A. Berna, Fluid Phase Equilibr. 224 (2004) 251-256.
6. A.M. Sales-Cruz, Development of a Computer Aided Modelling System for Bio and Chemical Process and Product Design, PhD Thesis, Technical University of Denmark, 2006.

List of Publications

1. M. Heitzig, G. Sin, M. Sales-Cruz, P. Glarborg, R. Gani, Ind. Eng. Chem. Res. Puigjaner Special Issue (2010).

Peter Jørgensen Herslund
Phone: +45 4525 2863
E-mail: pjh@kt.dtu.dk
Discipline: Engineering Thermodynamics

Supervisors: Nicolas von Solms
Kaj Thomsen
Jens Abildskov

PhD Study
Started: February 2010
To be completed: February 2013

Thermodynamic and Process Modelling of Gas Hydrate Systems in CO_2 Capture Processes

Abstract
This work presents a state of the art thermodynamic model for the phase behavior of gas hydrates. The model is to be applied in a recently proposed CO_2 capture technology, where CO_2 is removed from power station flue gasses in the form of solid gas hydrates. The model combines the van der Waals-Platteeuw hydrate model for the solid hydrate phase with the Cubic Plus Association (CPA) equation of state (EOS) for the co-existing equilibrium phases.

Introduction
In post-combustion CO_2 capture from power station flue-gases, chemical absorption has been considered the most mature of the carbon capture technologies. There are however problems associated with it, the main ones being large and expensive plants and energy demanding solvents. Nevertheless this is still an active field of research.

As part of a recently funded EU project – iCap (Innovative CO_2 Capture) - three novel separation concepts have been proposed, one of which is precipitated systems where CO_2 is removed by gas clathrate hydrate (gas hydrate) formation enhanced by thermodynamic promoters. In order to evaluate the efficacy of CO_2 removal in this process, accurate thermodynamic models are required over a wide range of temperatures and pressures and including complex components (such as water, hydrates and hydrate promoters).

Gas Hydrates
Gas hydrates are ice-like, solid inclusion bodies of water and guest molecules. Hydrogen bonded water clusters form cavities, where small guest molecules may be encapsulated.

The three most common occurring hydrate structures are; Structure I (sI), Structure II (sII) and Structure H (sH), all with different crystal structures.

These three structures are formed by five different water cavities, the 5^{12}, $5^{12}6^2$, $5^{12}6^4$, $5^{12}6^8$ and the $4^35^66^3$ [1]. The unit cell of the sI hydrate contains two 5^{12} and six $5^{12}6^2$ cavities while a unit cell of the sII hydrate contains sixteen 5^{12} and eight $5^{12}6^4$ cavities. Both of these unit cell structures belong to the cubic type. The sH hydrate structure is more complex and contains three 5^{12}, two $4^35^66^3$ and one $5^{12}6^8$ cavities [1]. This structure forms a hexagonal unit cell.

A given hydrate structure is typically determined by the size and shape of the guest molecule. Each cavity may encapsulate one or in rare cases more guest molecules of proper sizes. It is the presence of the guest molecule that stabilizes the water cavity.

Hydrate Formation from Flue Gas Mixtures
Figure 1 illustrates dissociation (equilibrium) pressures for mixed CO_2/N_2 hydrates using tetra-hydrofuran (THF) as promoter, measured by Kang et al. [2].

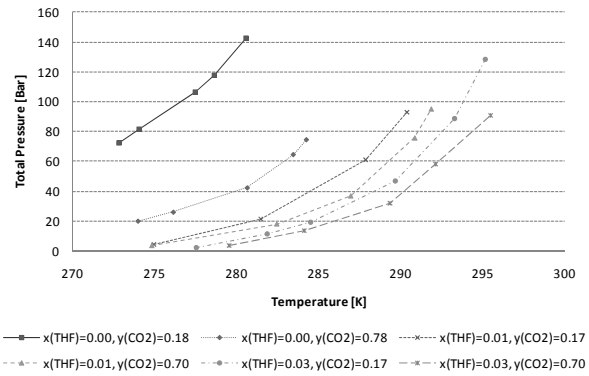

Figure 1: Hydrate dissociation pressures. Kang et al [2].

In Figure 1, x(THF) denotes the initial mole fraction of THF in the water phase. y(CO_2) denotes the initial mole fraction of CO_2 in the (synthetic) flue gas phase.

As can be seen from Figure 1, the presence of THF lowers the necessary total pressure of the flue gas for hydrates to form, resulting in a more efficient capture process. Note also that a low initial CO_2 concentration necessitates a high total flue gas pressure, before hydrates will form.

Van der Waals-Platteeuw Hydrate Model

This model was first presented by J. H. van der Waals and J. C. Platteeuw in 1958 [3]. Part of it is based on classical statistical mechanics. The model is typically combined with an equation of state (EOS) or an activity coefficient model for the gas/liquid phase. This work will utilize the van der Waals-Platteeuw model (algorithm) as presented by Parrish and Prausnitz in 1972 [4].

The basic idea behind the Van der Waals-Platteeuw model is that at equilibrium, the chemical potential of water must be identical for all phases

$$\mu_{water}^{HydratePhase} = \mu_{water}^{Co-exist.Phase} \tag{1}$$

For a CO_2 capture plant, the co-existing phases in the hydrate reactor will be liquid water, flue gas and solid hydrate. Hence the difference in water chemical potential between a theoretical empty hydrate water lattice (empty cavities) and the actual hydrate may be described by

$$\begin{aligned}\Delta\mu_{water}^{HydratePhase}(T,P) &= \mu_{water}^{Empty\,hydrate(\beta)} - \mu_{water}^{LiquidPhase} \\ &= R\cdot T\cdot\sum_m\left[\nu_m\cdot\ln(1+\sum_j(C_{m,j}\cdot\varphi_j\cdot y_j\cdot P))\right] + R\cdot T\cdot\ln(\alpha_{water})\end{aligned} \tag{2}$$

Where R is the gas constant, T is temperature; ν_m is the number of cavities type m per water molecule in the hydrate structure. $C_{m,j}$ is the Langmuir constant for gas component j in cavity type m. φ_j is the fugacity coefficient of component j in the flue gas phase. y_j is the mole fraction of component j in the gas phase. α_{water} is the activity of water in the liquid phase. This accounts for the highly non-ideal behaviour of water at the presence of hydrogen bonding promoters in the liquid phase. The Langmuir constants may be estimated by the use of the Lennard-Jones-Devonshire cell theory with e.q. Lennard-Jones or Kihara cell potentials.

By use of an experimental reference hydrate, the above difference in chemical potential may be estimated as follows [4]

$$\begin{aligned}\frac{\Delta\mu_{water}^{ref.hydrate}(T,P_R)}{R\cdot T} &= \frac{\Delta\mu_{water}^{ref.hydrate}(T_0,P_0)}{R\cdot T_0} \\ -\int_{T_0}^{T}\frac{\Delta h_{water}^{hydrate/ice}+\Delta h_{water}^{ice/liq.}}{R\cdot T^2}dt &+ \int_{T_0}^{T}\frac{\Delta v_{water}^{hydrate/ice}+\Delta v_{water}^{ice/liq.}}{R\cdot T}\cdot\frac{dP}{dt}dt\end{aligned} \tag{3}$$

where P_R is the dissociation pressure of the reference hydrate at temperature T. $\Delta\mu_{water}^{ref.hydrate}(T_0,P_0)$ is the chemical potential difference of water measured for the reference hydrate at reference temperature T_0 and reference pressure P_0. $\Delta h_{water}^{hydrate/ice}$ and $\Delta h_{water}^{ice/liq.}$ are the differences in molar enthal-py between the reference hydrate and ice and ice and liquid water at temperature, T.

$\Delta v_{water}^{hydrate/ice}$ and $\Delta v_{water}^{ice/liq.}$ are the differences in molar volume between the reference hydrate and ice and ice and liquid water at temperature, T.

dP/dT is the slope of the dissociation pressure-temperature curve for the reference hydrate at temperature, T. Reference values for the above constants may be found in the literature.

Finally the chemical potential difference for the reference hydrate is correlated to the actual pressure, P

$$\begin{aligned}\Delta\mu_{water}^{ref.hydrate}(T,P) &= \Delta\mu_{water}^{ref.hydrate}(T,P_R) \\ &+\left(\Delta v_{water}^{hydrate/ice}+\Delta v_{water}^{ice/liq.}\right)\cdot\left(P-P_R\right)\end{aligned} \tag{4}$$

Assuming the difference in chemical potential of water in the hydrate structure is independent of the guest molecule, the right hand side of Eq. 4 must equal that of Eq. 2. Note however that the reference hydrate must have a similar crystal structure to the hydrate of interest.

Specific Objectives

It is the purpose of this work to develop a thermodynamic model for the phase behaviour of gas hydrates and to validate it against experimental measurements of pure CO_2 hydrate dissociation pressures as well as mixed hydrate (including CO_2 and thermodynamic promoters) dissociation pressures.

A proven model for the hydrate phase will be combined with a state of the art equation of state – the Cubic Plus Association (CPA) EOS [5]. CPA accurately accounts for the presence of water as well as promoters, which may be hydrogen bonding, in the liquid phase.

Future Work

A software module incorporating the model is to be written in FORTRAN95. Component specific parameters both for the CPA EOS and the hydrate model must be estimated from experimental data, which are sparse for the promoted hydrate systems of interest.

Acknowledgements

The financial contributions from the iCap project (EU FP7) and the Department of Chemical and Biochemical Engineering (MP_2T) at The Technical University of Denmark, are greatly acknowledged.

References

1. A.K. Sum, C.A. Koh, E.D. Sloan, Ind. Eng. Chem. Res., 48 (2009) 7457-7465.
2. S.P. Kang, H. Lee, C.-S. Lee, W.-M. Sung, Fluid Phase Equilibr. 185 (2001) 101-109.
3. J.C. Platteeuw, J.H. van der Waals, Mol. Phys. 1 (1) (1958) 91-95.
4. W.R. Parrish, J.M. Prausnitz, Ind. Eng. Chem. Process Des. Develop. 11 (1) (1972) 26-35.
5. G.M. Kontogeorgis, E.C. Voutsas, I.V. Yakoumis, D.P. Tassios, Ind. Eng. Chem. Res. 35 (1996) 4310-4318.

Jesper Holck
Phone: +45 4525 2979
E-mail: jeh@kt.dtu.dk
Discipline: Enzyme Technology

Supervisors: Anne S. Meyer
Jørn Dalgaard Mikkelsen

PhD Study
Started: November 2007
To be completed: February 2011

Enzymatic Production of Prebiotics from Sugar Beet Pectin

Abstract
The potential importance of dietary fibres and oligosaccharides in modulating the microbial ecology of the human colon to exert beneficial health effects is currently receiving significant attention. By targeting dietary fibre structures and prebiotics by selective enzymatic hydrolysis of complex plant substrates, such as pectin, defined poly- and oligomers can be derived. This study reveals an integrated biorefining method that provides an option for advanced upgrading of sugar beet pectin into HG and RGI oligosaccharides of defined size and structure. In vitro microbial fermentation by human faecal samples showed a different response to the DP4 and DP5 HG structures on the ratio between *Bacteroidetes* and *Firmicutes*. This indicates that pectic oligosaccharides with only slightly different structures have significantly different biological effects.

Introduction
Dietary fibres and prebiotics are non-digestible dietary carbohydrate structures that can be health promoting by supporting the growth of beneficial bacteria in the human colon, such as *Bifidobacterium sp*. [1] and induce apoptosis in cancer cells in colon [2] and prostate [3]. This PhD project builds on that a significant potential exists for targeting dietary fibre and prebiotics structures by selective enzymatic hydrolysis of pectinaceous plant cell wall structures present in sugar beet pulp – the byproduct stream left over from industrial production of sugar.

Project outline
A common theme in numerous papers regarding health promoting effects of pectin is the dependency of size of the applied poly- and oligosaccharides. Nevertheless, the studies assessing the putative bioactivity of pectin have been performed using mixtures of heterogeneous pectin derived fractions with a relatively broad size distribution. Therefore the focus of the project is on enzyme assisted modification of sugar beet pectin in order to manufacture target oligomer products which can have a potential beneficial effect. The production is made via an intelligent reaction optimisation and combination of monoactive experimental enzymes available in the Prebiotics Center.

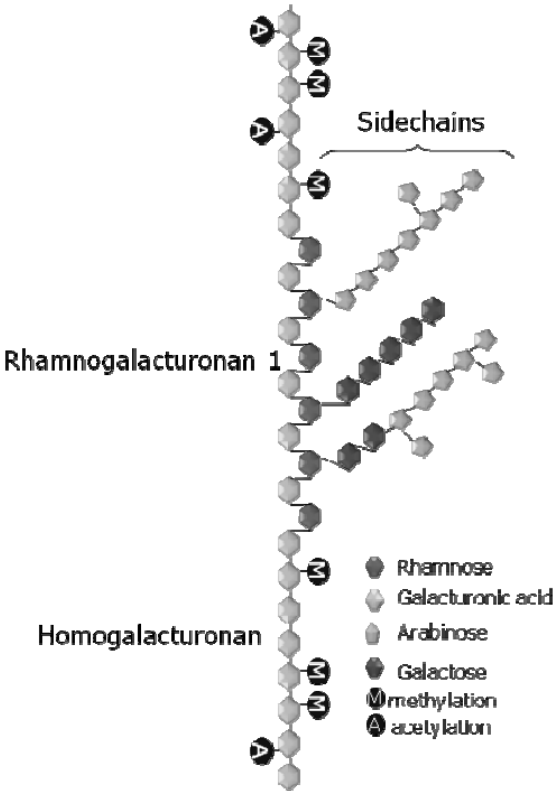

Figure 1: Schematic illustration of sugar beet pectin structural elements.

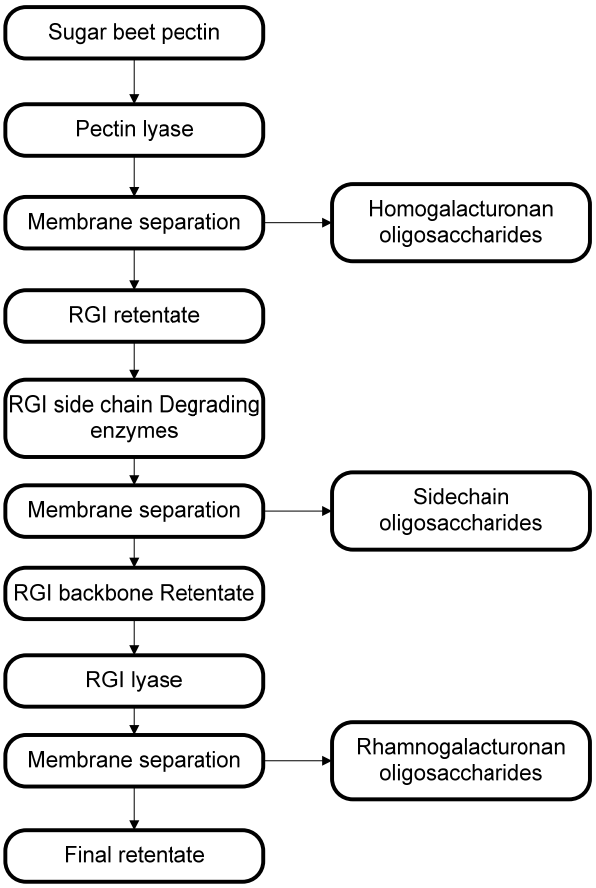

Figure 2: Schematic flow sheet for biorefining strategy indicating the enzymatic treatments and membrane separation steps.

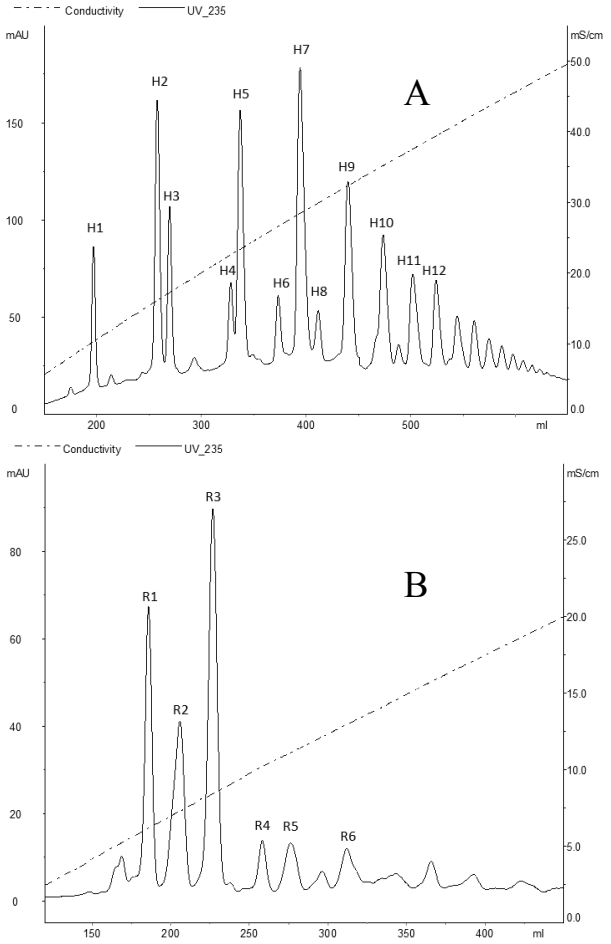

Figure 3: Elution profile of HG (A) and RGI (B) oligosaccharides during ionic exchange chromatography.

Specific objectives

A method was introduced for integrated production of homogalacturonan and rhamnogalacturonan oligosaccharides with a defined degree of polymerization from sugar beet pectin (Figure 1). The method builds on sequential dissection of sugar beet pectin using monocomponent enzymes, membrane separations (Figure 2), and ion exchange chromatography to obtain the structural elements and avoids the use of organic solvents.

To assess the possible effect of different chain length, the study includes evaluation of the biological activity of homogalacturonan oligosaccharides DP4 and DP5 based on their capacity to alter the ratio between *Bacteroidetes* and *Firmicutes,* which represent the dominant bacterial phyla in the human intestine. The balance between the *Bacteroidetes* and *Firmicutes* phyla is believed to play a role in risk of obesity development [4]. This is assessed by *in vitro* bacterial fermentation using human faecal samples.

Results and Discussion

Homogalacturonan (HG) (Figure 3A) and rhamnogalacturonan (RGI) (Figure 3B) oligosaccharides were separated using ion exchange chromatography and the exact structure of each was compound was verified by MALDI-TOF and TOF/TOF.

HG purification

Pure and defined HG oligosaccharides with DP from 2 to 8 (Table 1 HG) were successfully separated and purified with an isolation efficiency of 0.6-4.2 mg/peak·h.

Table 1: Peak identity and identified compounds for HG and RGI oligosaccharides.

HG		RGI	
H1	$galA_2$	R1	$galA_2rha_2gal_2$
H2	$galA_2$	R2	$galA_2rha_2gal$
H5	$galA_3$	R3	$galA_2rha_2$
H7	$galA_4$	R4	$galA_3rha_3gal_3$
H9	$galA_5$	R5	$galA_3rha_3gal_2$
H10	$galA_6$	R6	$galA_3rha_3$
H11	$galA_7$		$galA_3rha_2gal_2$
H12	$galA_8$		

RGI purification

Similar, RGI oligosaccharides with 2 or 3 alternating galacturonic acid - rhamnose disaccharide moieties with differential galactose substitutions (Table 1 RGI) were successfully separated and purified with an isolation efficiency of 0.1-0.4 mg/peak·h. These results proved that this method enabled separation of a molecule consistent of a galA-rha-galA-rha backbone with galactose substitution on both rhamnoses (Figure 4) from a molecule consistent of a galA-rha-galA-rha backbone with a single galactose substitution.

The use of MALDI-TOF/TOF was especially useful for the structure characterization of RGI oligosaccharides. The fractionation pattern in Figure 4 clearly indicates an even distribution of galactose substitution on rhamnose.

Fermentation study

To assess the fermentability of selected oligosaccharides on human faecal samples, a small scale *in vitro* fermentation method was developed.

Data from *in vitro* fermentations showed differences in the relative ratio of *Bacteroidetes* (Figure 5A) and *Firmicutes* (Figure 5B) dependent on the type of substrate. The density of *Bacteroidetes* was significantly lower in both fermentations compared to the inocula (DP4 and DP5 compared to inocula; $P < 0.001$ and $P < 0.01$, respectively). The density of *Firmicutes* was significantly higher in the faecal samples fermented on DP4 compared to the inoculum ($P < 0.001$).

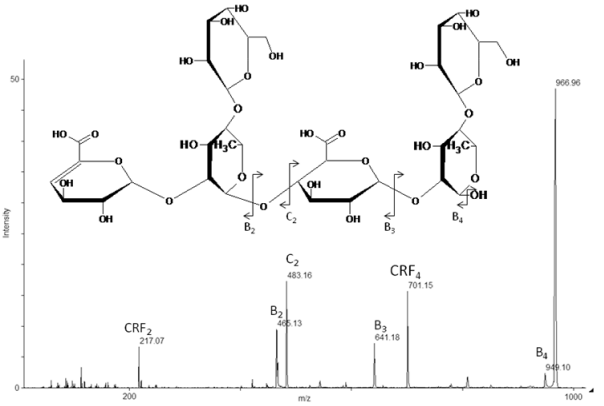

Figure 4: MS/MS High energy CID spectrum of $galA_2rha_2gal_2$ illustrating the fragmentation pattern and nomenclature, and the proposed structure.

Surprisingly, fermentation of homogalacturonan oligosaccharides with DP5 yielded a density of *Bacteroidetes* which was significantly higher than obtained by fermentation of DP4 ($P<0.05$), while conversely, fermentation of the DP4 substrate resulted in densities of *Firmicutes* significantly higher than obtained after fermentation of DP5 ($P<0.01$).

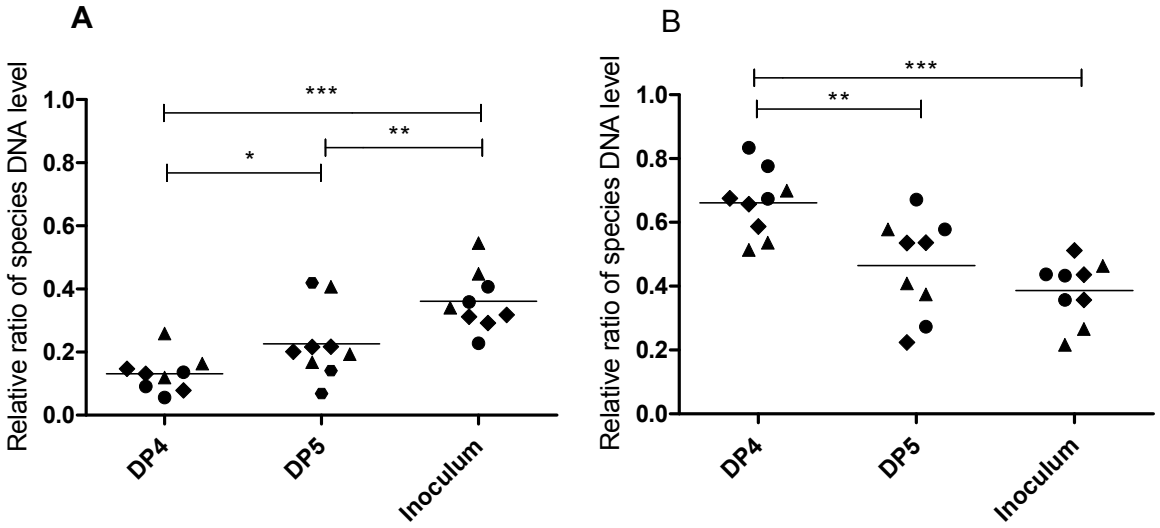

Figure 5: Relative amounts of target genes in samples from original bacterial communities, and after fermentation of DP4 and DP5 by these microbial communities. Target genes encoded 16S rRNA from *Bacteroidetes* (A) and *Firmicutes* (B). The horizontal lines show the mean of the nine observations. Asterisks indicate a significant difference among groups $P < 0.05$ (*); $P < 0.01$ (**); $P < 0.001$ (***).

Conclusion

The present work provided a new lean method for biorefining of pectin involving the sequential targeted enzyme catalyzed dissection to produce homogalacturonides and rhamnogalacturonides of defined molecular size. The results showed that it was possible to separate individual HG oligomers, as well as short RGI oligomers by one integrated procedure. *In vitro* assessment of the influence of DP4 and DP5 homogalacturonides on the relative abundance of two different bacterial phyla in faecal microbial communities revealed a significantly different effect of the two slightly different structures, which opens a range of possibilities for further research addressing the effect of oligosaccharide length on the metabolic syndrome associated with obesity, inflammatory bowel disease and prebiotic potential

Acknowledgements

All MALDI-TOF analysis was performed at Southern Danish University. The *in vitro* fermentation studies on human faecal samples were performed at DTU Food.

The project is anchored in the Center for Biological Production of Dietary Fibres and Prebiotics at DTU ("Prebiotics Center"), granted by DSF. The project has significant involvement from Danisco A/S which provides the sugar beet pectin.

List of references

1. K. Manderson, M. Pinart, K.M. Tuohy, W.E. Grace, A.T. Hotchkiss, W. Widmer, M.P. Yadhav, G.R. Gibson, R.A. Rastall, Appl. Environ. Microbiol. 71 (2005) 8383-8389
2. E. Olano-Martin, G.H. Rimbach, G.R. Gibson, R.A. Rastall, Anticancer Res. 23 (2003) 341-346
3. C.L. Jackson, T.M. Dreaden, L.K. Theobald, N.M. Tran, T.L. Beal, M. Eid, M.Y. Gao, R.B. Shirley, M.T. Stoffel, M.V. Kumar, D. Mohnen, Glycobiology 17 (2007) 805-819
4. P.J. Turnbaugh, R.E. Ley, M.A. Mahowald, V. Magrini, E.R. Mardis, J.I. Gordon, Nature 444 (2006) 1027-1131

Publication

1. J. Holck, K. Hjernø, A. Lorentzen, L.K. Vigsnæs, L. Hemmingsen, T.R. Licht, J.D. Mikkelsen, A.S. Meyer, Process Biochem. 2011, in press.

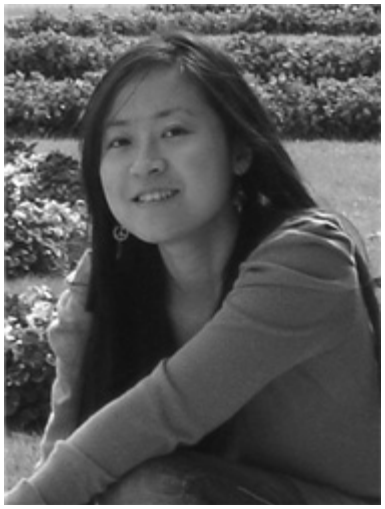

Qian Huang

Phone: +45 4525 6809
E-mail: qh@kt.dtu.dk
Discipline: Polymer Technology

Supervisors: Ole Hassager
Anne L. Skov
Henrik K. Rasmussen, DTU Mekanik

PhD Study
Started: February 2010
To be completed: February 2013

Elongational Dynamics of Low Density Polyethylene

Abstract
The startup of uni-axial elongational flow followed by stress relaxation and reversed bi-axial flow has been measured for two branched Low Density Polyethylene (LDPE) melts using the Filament Stretching Rheometer (FSR). The measured LDPE samples were made of the commercial LDPEs including Lupolen 3020D and Lupolen 1840D. The experimental results of these LDPEs were compared with those of polystyrene which has been published before. Predictions by Doi-Edwards model were also performed to compare with the experimental results.

Introduction
In many polymer processing operations the polymer molecules experience a significant amount of chain orientation and stretching. The shear rheology measured by the conventional shear rheometer is good at describing chain orientation but is not usable for probing stretching, whereas the extensional rheology gives a good way of inducing chain stretching. Furthermore, it is known that the rheology of polymers and macromolecules is highly sensitive to branching, but the precise connection between branching architecture and non-linear rheology is still not fully understood.

Commercial LDPEs are normally highly branched polymers. A maximum in the transient extentional viscosity has been reported for LDPE in 1985 [1]. However, a steady stress after the maximum was not observed at that time. The first observation of a steady stress following a stress maximum was reported for two commercial LDPE melts Lupolen 3020D and Lupolen 1840D [2]. Here we continue investigating the behavior of these two LDPE melts in stress relaxation and reversed bi-axial flow.

Filament Stretching Rheometry
Our elongational experiments are performed with a Filament Stretching Rheometer (FSR) equipped with an oven to allow measurements up to about 200˚C [3]. Besides uni-axial elongation, this rheometer can also make measurements of stress relaxation and bi-axial reversed flow [4], both following uni-axial extensional flow.

During the experiments the Hencky strain and the mean value of the stress difference over the mid-filament plane [5] are calculated from observations of the radius of the filament $R(t)$ and the force on the bottom plate $F(t)$ as

$$\epsilon(t) = -2\ln\left(R(t)/R_0\right) \tag{1}$$

$$\langle \sigma_{zz} - \sigma_{rr} \rangle = \frac{F(t) - m_f g/2}{\pi R(t)^2} \tag{2}$$

where R_0 is the radius of the sample at the start of the extension, g the gravitational acceleration and m_f the weight of the polymer filament. At small strains part of the stress difference comes from a radial pressure variation in the cross-section due to the shear flow that is unavoidable at small aspect ratios. To compensate for this effect we define the corrected mean value of the stress difference by [6]

$$\langle \sigma_{zz} - \sigma_{rr} \rangle_{corr} = \langle \sigma_{zz} - \sigma_{rr} \rangle \left(1 + \frac{\exp\left(-5\epsilon/3 - \Lambda_0^3\right)}{3\Lambda_0^2} \right)^{-1} \tag{3}$$

where $\Lambda_0 = L_0/R_0$ is the initial aspect ratio.

Sample Preparation
The LDPEs Lupolen 3020D and Lupolen 1840D were supplied in pellets and were pressed into cylindrical test specimens by a Carver hydraulic press, with radius R_0=4.5mm and length L_0=2.5mm, giving an aspect ratio $\Lambda_0 = L_0/R_0$=0.556.

Results of Stress Relaxation
The experiments of stress relaxation on LDPE Lupolen 3020D and Lupolen 1840D were both performed at 130˚C. The startup of the flow was uni-axial elongation;

the flow was stopped at a given Hencky strain and then followed by the stress relaxation.

In Figure 1 we show the experimental results for Lupolen 3020D. The flow was started up by a uni-axial elongation with constant strain rate $0.03s^{-1}$ and then stopped at several given Hencky strain before and after the maximum respectively. Significantly different flow behavior in stress relaxation before and after the maximum has been observed. It can be seen from the figure that the relaxation curve after the maximum goes down across the two before the maximum, which indicates that after the maximum it relaxes much faster.

We also show the predictions by Doi-Edwards model with independent alignment approximation in Figure 1 to compare with the experimental results. For those before the maximum, the experimental relaxation curves are almost parallel with the predicted ones, whereas for the one after the maximum, the experimental relaxation curve tends to meet the predicted curve at the end. As for linear polystyrene melt, it has been shown that in stress relaxation all the experimental curves meet the Doi–Edwards predictions at the end [7]. It indicates that before the maximum the branched LDPE melts are more difficult to relax compared with the linear polymers; but after the maximum they intend to behave as the linear ones. The experimental results for Lupolen 1840D show the similar behavior as Lupolen 3020D in stress relaxation.

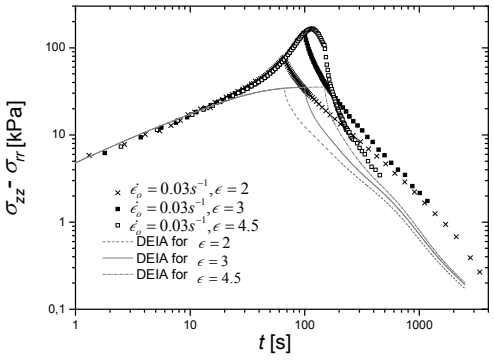

Figure 1: The corrected extensional stress of Lupolen 3020D as a function of the time at 130˚C. The startup of the flow was uni-axial elongation with constant strain rate $0.03s^{-1}$; The flow was stopped at an extension of ε = 2, 3 and 4.5 respectively. The lines are the Doi–Edwards predictions with independent alignment approximation.

Results of Reversed Bi-axial Flow

The experiments of reversed bi-axial flow on LDPE Lupolen 3020D and Lupolen 1840D were both performed at 130˚C as well. The startup of the flow was uni-axial elongation; the flow was reversed at a given Hencky strain with the identical strain rate in the startup.

In Figure 2 we show the experimental results for Lupolen 1840D. The flow was started up by a uni-axial elongation with constant strain rate $0.01s^{-1}$ and then reversed at several given Hencky strain before and after the maximum respectively with the identical strain rate. The strain recovery is defined as $\varepsilon_R = \varepsilon_0 - \varepsilon(t_R)$. ε_0 is the Hencky strain where the flow starts to reverse, t_R is the time where $\sigma_{zz}-\sigma_{rr}=0$. It can be seen from the figure that before the maximum the strain recovery tends to increase when the flow is reversed at higher Hencky strain, while after the maximum the strain recovery tends to the opposite way. The experimental results for Lupolen 3020D show the similar behavior as Lupolen 1840D in reversed bi-axial flow.

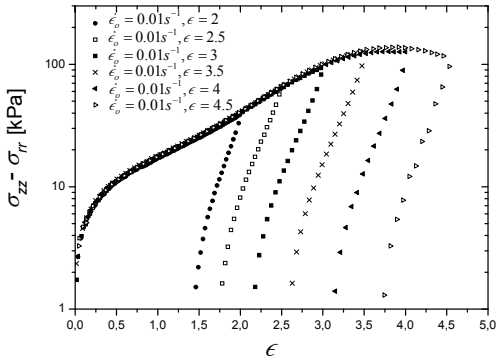

Figure 2: The corrected startup and reverse stress of Lupolen 1840D at 130˚C as a function of Hencky strain. The startup of the flow was uni-axial elongation with constant strain rate $0.01s^{-1}$; The flow was reversed at Hencky strain ε= 2, 2.5, 3, 3.5, 4 and 4.5 respectively with the identical strain rate.

Conclusion

The startup of uni-axial elongational flow followed by stress relaxation and reversed bi-axial flow has been measured for two branched LDPE Lupolen 3020D and Lupolen 1840D. Significantly different flow behaviors before and after the maximum in both stress relaxation and reversed bi-axial flow have been observed.

Acknowledgement

This project is part of Dynacop which is funded under the Initial Training Network in the Seventh Framework Marie Curie Programme.

References

1. J. Meissner, Chem. Engr. Commun. 33 (1985) 159–180.
2. H.K. Rasmussen, J.K. Nielsen, A. Bach, O. Hassager, J. Rheol. 49(2) (2005) 369–381.
3. A. Bach, H. Rasmussen, O. Hassager, J. Rheol. 47 (2003) 429–441.
4. J.K. Nielsen, H.K. Rasmussen, J. Non-Newtonian Fluid Mech. 155 (2008) 15–19.
5. P. Szabo, Rheologica Acta. 36 (1997) 277–284.
6. H.K. Rasmussen, A.G. Bejenariu, O. Hassager, D. Auhl, J. Rheol. 54 (2010) 1325–1336.
7. J.K. Nielsen, H.K. Rasmussen, O. Hassager, J. Rheol. 52(4) (2008) 885–899.

Amol Shivajirao Hukkerikar
Phone: +45 4525 2812
E-mail: amh@kt.dtu.dk
Discipline: Systems Engineering

Supervisors: Rafiqul Gani
Gürkan Sin
Bent Sarup, Alfa Laval

PhD Study
Started: July 2010
To be completed: June 2013

Model Based Integrated Product-Process Design

Abstract
One of the common ways to match the desired product-process characteristics is through trial and error based experiments which can be expensive and time consuming. An alternative approach is the use of a systematic model-based framework in product-process design, replacing some of the time consuming experimental steps. The main objective of the project is to develop a systematic framework for model based design and optimizations of the principal unit operations involved in edible oil/bio-fuel industry and apply the developed methodology for improvement in the operations of existing installations for edible oil/bio-fuel processes.

Introduction
Over the past few decades, the world's fats and edible oils production has been growing rapidly, far beyond the need for human nutrition. This overproduction combined with the growing consumer preferences for healthier food products and the interest in bio-fuels, has led the oleo chemical industry to face major challenges in terms of design and development of better products and more sustainable processes. However, although the oleo chemical industry is mature and based on well established processes, the complex systems that lipid compounds form, and the lack of accurate unit operation models have limited a wide application of computer-aided methods and tools for process synthesis, modeling and simulation within this industry [1]. In consequence, the first part of this project will be the development of unit operations model library consisting a collection of new and adopted models that are not available in existing process simulation tools. Typical unit operations include fluid handling, heat transfer process, chemical synthesis (interesterification, hydrogenation, transesterification etc.) separation processes (liquid-solid, liquid-liquid, and liquid-gas), crystallization, filtration, steam stripping under vacuum and many more. The second part of the work will focus on optimization of existing process plants with respect to performance indicators such as minimum operational cost, product yield improvement and sustainability index. The project specific tasks that need to be carried out to achieve above said objectives is illustrated in Figure 1.

Specific Tasks
In the first step, the unit operations involved in edible oil / bio-fuel process will be listed and the availability of built-in models in commercial simulators will be verified. In the second step, the required physical property data of the chemical species involved, equipment specifications, and operating data of existing process plants will be retrieved. In the third step, a detailed computer aided modeling of selected unit operations will be carried out based on the type of the model (e.g. steady state/dynamic, meso scale/micro scale) and intended goals (design / optimization / retrofit). In the fourth step, the operating data will be reconciled with respect to quality of the data and measurement errors. The developed models will be then validated using reconciled operating data of the existing process plant. The validated models will be incorporated in the model library as new and/or adapted models for use in process simulation tools such as PRO/II®. Once validated, the developed model library will be made available for use in computer aided flowsheet design (CAFD) studies involving lipids on which CAPEC co-worker [2] is working.

Results and Discussion
To consider the effect of uncertainty of property prediction models on product/process design, we have developed a methodology to carry out uncertainty analysis [3] of group contribution based [4] and atom connectivity index [5] based pure component property prediction models. The developed methodology will be

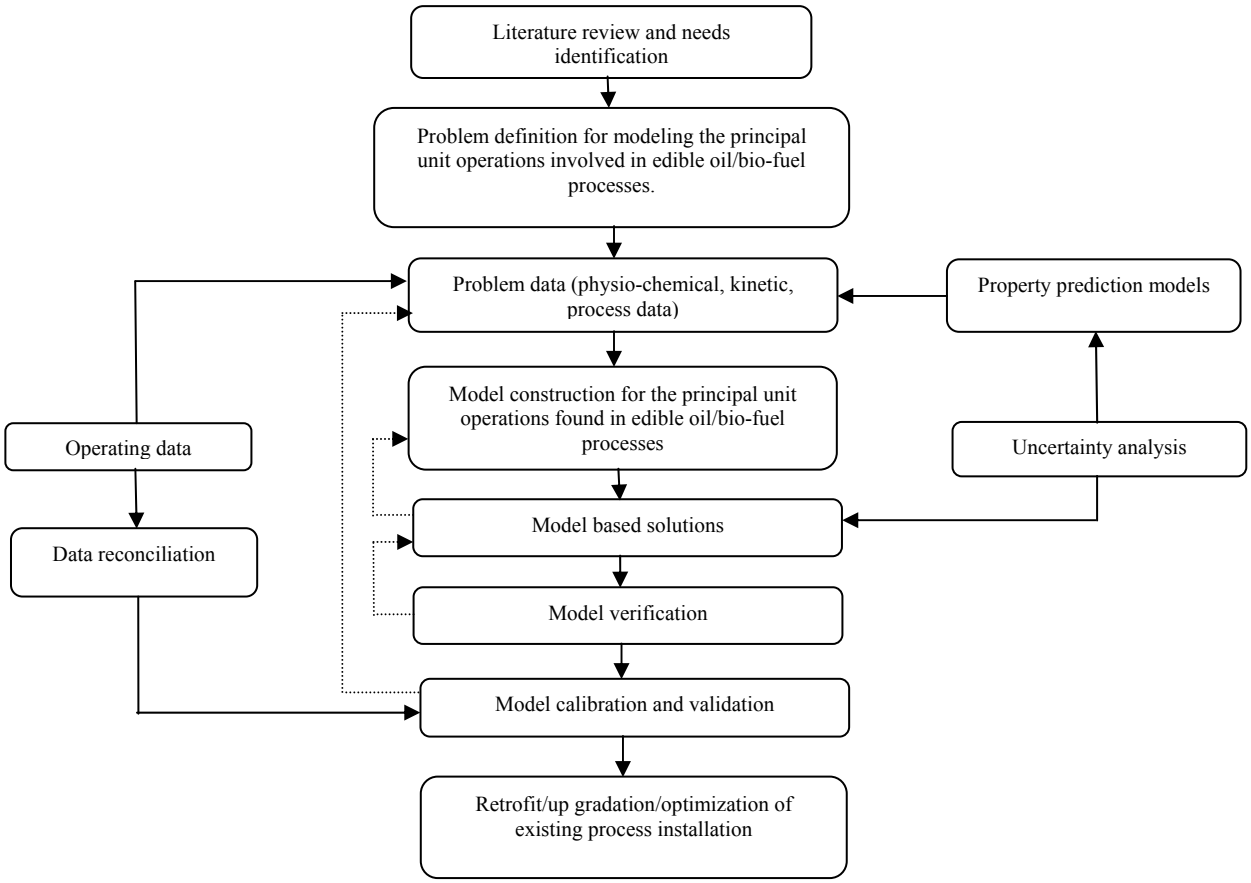

Figure 1: Systematic framework for model based design and optimization of unit operations involved in edible oil / bio-fuel industry

used to assist uncertainty and sensitivity analysis of unit operation models of edible oil/bio-fuel process to obtain rationally the risk/ safety factors and to provide confidence in the product/process design calculations. So far, we have completed uncertainty analysis of 12 (of 25) pure component properties such as critical constants, normal boiling point, normal melting point among others.

Conclusions

A systematic model based framework for integrated product-process design of unit operations is being proposed. As a first step, we have developed the methodology for uncertainty analysis of property prediction models. The developed methodology was used to obtain improved model parameters of property prediction models and to quantify prediction error in the estimated property values. As a next step, we will develop a library of new and/or adapted models for unit operations involved in edible oil/bio-fuel industry. The validated models will be used for improvement in the operations of existing installations for edible oil/bio-fuel processes. The model library will be made available for use in computer aided flowsheet design (CAFD) to solve interesting product/process design studies involving lipids.

Acknowledgements

This PhD project is funded by the European Commission under the 7th Framework Programme under the grant agreement no. 238013.

References

1. C.Tovar, R. Gani, B. Sarup, in press. Fluid Phase Equilibr. (2010), doi:10.1016/j.fluid.2010.09.011
2. A. Quaglia, 2010, Incremental Refinement of Process Design, Graduate Schools Yearbook 2010, Dept. of Chemical and Biochemical Engineering.
3. G. Sin, A.S. Meyer, K.V. Gernaey, Comput. Chem. Eng. 34 (2010) 1385-1392.
4. J. Marrero, R. Gani, Fluid Phase Equilibr. (2001), 183-208.
5. R. Gani, P. Harper, M. Hostrup, Ind. Eng. Chem. Res. 44 (2005) 7262-7269.

Martin Høj
Phone: +45 4525 2842
E-mail: mh@kt.dtu.dk
Discipline: Reaction and Transport Engineering

Supervisors: Anker Degn Jensen
Jan-Dierk Grunwaldt, KIT
Tobias Dokkedal Elmøe

PhD Study
Started: September 2009
To be completed: September 2012

Nanoparticle Design using Flame Spray Pyrolysis for Catalysis

Abstract
The unifying topic of my PhD project is flame spray pyrolysis (FSP), a novel method for synthesizing nanoparticle sized metal oxides. Nanoparticulate materials have very high surface area, which is advantageous for heterogeneous catalysis. The work mainly focuses on two systems for applying FSP made materials: Selective oxidation of propane to propene and hydrotreating of diesel, two very different areas of heterogeneous catalysis employing oxide and sulfide catalyst, respectively.

Introduction
Liquid fed flame spray pyrolysis (FSP) is a novel one-step synthesis method for preparation of nano-sized particles [1]. Typically, organo metallic compounds are dissolved in an organic solvent and the precursor solution is sprayed as micrometer sized droplets with high velocity oxygen and ignited with a small premixed methane-oxygen flame [2].

The solvent and metal compounds evaporate and combust to form atomically dispersed vapors, which nucleate to form clusters when reaching cooler parts of the flame. The formed clusters grow by surface growth and coalescence, accompanied by sintering [3].

This result in non-porous nanoparticles which coagulate and sinter to form agglomerates and aggregates with high inter particle porosity [1]. The flame process gives high maximum temperature and a short residence time with thermally stable homogeneous nanoparticles as the product.

Hydrotreating
Hydrotreating is performed at oil refineries in order to remove sulfur and nitrogen from the heterocyclic compounds in which these elements typically occur in crude oil [5].

Industrial hydrotreating catalysts contain cobalt or nickel promoted molybdenum (IV) sulfide as active phase, on an alumina support [5]. The transition metal sulfide phase is obtained after sulfiding an oxide precursor. An oxide precursor containing molybdenum and cobalt on alumina can be prepared by FSP.

Oxidative dehydrogenation of propane
Demands for short chain olefins like ethylene and propylene are expected to increase in the near future [4]. Current production methods include steam cracking, fluid catalytic cracking and catalytic dehydrogenation.

Oxidative dehydrogenation of propane to propylene is another option. This is an exothermic reaction which could be operated autothermally. However, a catalyst with sufficient activity and selectivity for industrial production of propylene by this method has not been discovered yet [4].

The most promising catalyst candidates are supported vanadium and molybdenum oxide [4], which can be prepared by FSP. Supports like Al_2O_3, SiO_2, TiO_2, ZrO_2, MgO and ZrO_2 or mixtures thereof have been used. Mixed oxide phases are easily prepared by FSP in one step, in particular.

Specific objectives
The objectives of my project are to prepare catalytically active nanomaterials using the FSP method. The catalysts will be tested for their catalytic activity and the physical and chemical structure will be investigated using spectroscopy, X-ray diffraction and electron microscopy.

Results and discussion
Hydrotreating
Seven $CoMo/Al_2O_3$ samples were synthesized by FSP where all three metallic elements were sprayed in one flame. Four samples contained 8, 16, 24 and 32 wt.% Mo with a Mo:Co atomic ratio of 3:1 (alumina balance), and two samples 16 wt.% Mo with Mo:Co atomic ratio

3:2 and 3:3 and finally one unsupported reference samples with Mo:Co atomic ratio 3:1.

The catalysts had specific surface areas between 221 and 90 m^2/g, decreasing surface area with increasing transition metal content. This corresponds to average primary particle sizes of 7 to 13 nm, showing that nanoparticles were the product of the flame synthesis.

The activities of the catalysts for removal of heterocyclic sulfur and nitrogen were measured after sulfidation. The best catalysts contained 16 wt.% Mo with atomic ratio Mo:Co = 3:1, which activity was marginally lower than a sample where Mo and Co are impregnated on pre-shaped alumina extrudates. Increasing the Co content in the FSP material caused a small drop in activity, while increasing or decreasing the Mo content resulted in significantly lower activity.

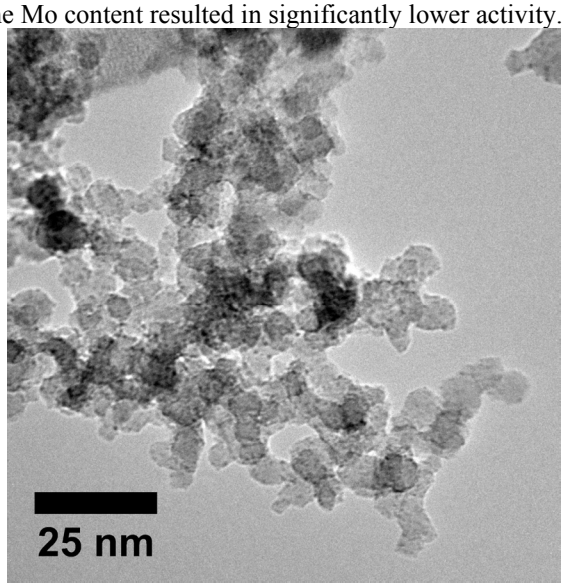

Figure 1: TEM image of 16 wt.% Mo oxide sample.

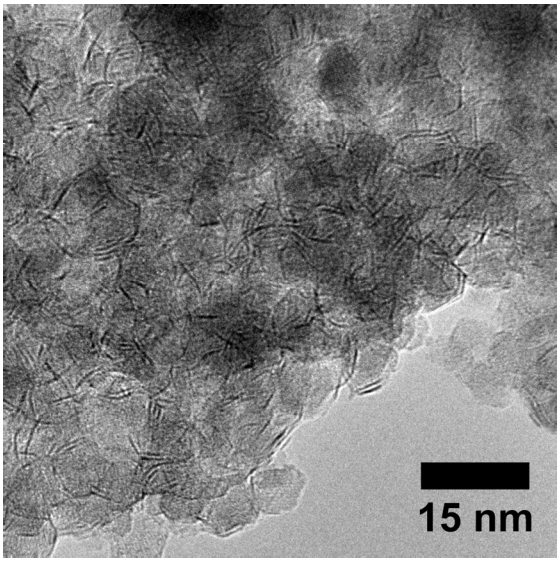

Figure 2: TEM image of 16 wt.% Mo sulfide sample.

TEM images of the flame made oxides confirmed that the primary particles were nano-sized and images of the sulfided catalysts showed a significant increase in MoS_2 particles size with increasing Mo content, explaining the lower activity of the 24 and 32 wt.% Mo catalysts and the unsupported reference catalyst (see Figure 1 and 2).

X-ray diffraction (XRD) and UV-vis reflectance spectroscopy showed that the oxide precursor contained γ-Al_2O_3 with some $CoAl_2O_4$ spinel, while MoO_3 was XRD amorphous. The $CoAl_2O_4$ spinel is unwanted since the cobalt does not promote the MoS_2 active phase. Experiments of suppressing this phase are under way.

Oxidative dehydrogenation of propane

A new activity test setup with three sequential reactors in series/by-pass configuration has been constructed. The analysis is performed by a dual channel GC-MS, also fitted with FID and TCD detectors.

Several alumina supported vanadia catalysts with varying amounts of vanadia and using different starting materials have been synthesized by FSP. The catalysts had surface areas between 200 and 250 m^2/g, showing that the products are nanoparticles. The vanadia was XRD amorphous while the support was γ-Al_2O_3.

Titania and silica supported vanadia have also been synthesized, resulting in anatase, with traces of rutile, and surface area 130 m^2/g and amorphous silica with surface area 385 m^2/g.

Activity testing of these materials has just started. Initial results show high conversion of propane, but only moderate propylene selectivity.

Conclusion

FSP is a promising new method for preparation of catalytically active nanoparticles in various fields of heterogeneous catalysis. The prepared hydrotreating catalysts show high activity for initial experiments with a new synthesis method.

Acknowledgements

DSF grant nr. 2106-08-0039. M. Brorson from Haldor Topsøe A/S for hydrotreating activity tests. J. B. Wagner and T. W. Hansen from DTU CEN for TEM.

References

1. R. Strobel, S.E. Pratsinis, J. Mater. Chem. 17 (2007) 4743-4756.
2. L. Mädler, H.K. Kammler, R. Mueller, S.E. Pratsinis, J. Aerosol. Sci. 33 (2002) 369-389.
3. H.K. Kammler, L. Mädler, S.E. Pratsinis, Chem. Eng. Technol. 24 (2001) 583-596.
4. F. Cavani, N. Ballerini, A. Cericola, Catal. Today 127 (2007) 113-131
5. H. Topsøe, B.S. Clausen, F.E. Massoth, in: J.R. Anderson, M. Boudart (Eds.), Catalysis: Science and Technology, vol. 11, Springer-Verlag, Berlin, 1996.

Publications

1. M. Høj, K. Linde, T.K. Hansen, M. Brorson, J.-D.Grunwaldt, A.D. Jensen, Flame spray synthesis of $CoMo/Al_2O_3$ hydrotreating catalysts. In preparation.

Norazana binti Ibrahim
Phone: +45 4525 2922
E-mail: nbi@kt.dtu.dk
Discipline: Reaction and Transport Engineering

Supervisors: Kim Dam-Johansen
Peter Arendt Jensen

PhD Study
Started: July 2007
To be completed: April 2011

Effect of Biomass Mineral Matter on the Pyrolysis Product Yields

Abstract
Experiments on flash pyrolysis of wheat straw, rice husk and pine wood were carried out in a pyrolysis centrifuge reactor (PCR) at different reactor temperatures, ranging from 475 to 575 ° C. The aim was to study the influence of biomass types, particularly the contents of mineral matter in biomass, on the pyrolysis product yield. The ash content in wheat straw, rice husk and pine wood were 6.02, 13.6 and 0.5 % db, respectively. Wheat straw ash contains a high fraction of potassium, rice husk is rich in silica and pine wood is characterized by high calcium content. The experimental results showed that the maximum liquid organics yield temperature was around 525 °C for wheat straw and around 550 °C for both rice husk and pine wood. At their optimum temperatures, the liquid organics yield of 49, 52 and 58 wt % (daf) respectively were obtained for wheat straw, rice husk and pine wood. Compared to straw and wood, the char yield obtained from rice husk was the highest. The obtained results indicate that alkali metals in biomass ash significantly affect the pyrolysis products yield and pyrolysis behavior by shifting the optimum degradation temperature and by catalyzing the conversion of tar to gases.

Introduction
Any biomass on the earth can be transformed into energy carriers such as liquid oil and gases by many thermodynamic routes such as gasification, liquefaction, combustion and pyrolysis. The latter received much demand attention since 1980s because of high quality of liquid oil produce with nearly ash-free. The high heating rate of heat transfer, moderate temperatures (400-600 °C), and a short gas residence time (< 1 s) are amongst the common features of flash pyrolysis process [1]. With these reaction conditions, flash pyrolysis processes are able to produce about 50-75 wt % of liquid bio-oil (including water), 15-25 wt % of solid char and 10-20 wt.% of noncondensable gases. However, the conversions of these three products are greatly depending on the types of biomass used and operating conditions [2-3].

Biomass consists of cellulose, hemicellulose, lignin and a small amount of extractives and inorganic compounds. Inorganic compounds contain more than 19 metals, which including alkali metal such as sodium, magnesium, silicate and potassium [4]. These alkali metals can act as a catalyst that can alter the rate of biomass degradation during pyrolysis. Because of this alteration, the yield of the pyrolysis products also varies. The variation of mineral matter in biomass fuels ash is vary, for example wood usually contains < 1 % wt whereas husks and straw contain up to 25 % wt [5]. Generally biomass ash consists of K, Na, Mg, Ca, Si and a small amount of P, S, Fe, Al and Mn and these elements can form as silicates, oxides, carbonates, sulfates, chlorides and phosphates during combustion.

The effect of alkali metals and other inorganic mineral matters that naturally present in biomass on the pyrolysis process and products distribution has been investigated by many researchers [4-7]. The addition of artificial alkali metal on biomass also was carried out in order to get a detailed understanding of the complexity of pyrolysis process. For example the addition of 0.1 % NaCl to cellulose increased the char yield by 235 % [8] and by mixing of calcium oxide with wood increased the liquid product yield [9].

Most of the work has concentrated on woody biomass and only a little on non-woody material such as grass, sunflower stem and almond shells. Therefore, in the present work, the effect of biomass types, particularly the alkali and minerals content in Danish wheat straw, rice husk and pine wood on the pyrolysis products was investigated. The aim was to get a better understanding how the variation of chemical compositions and mineral matters that naturally present in non woody and woody biomass that can direct or indirectly influence the pyrolysis product yields as well as the change of pyrolysis behavior.

Specific Objectives

The main objective of the current study is to investigate the influence of biomass types on the flash pyrolysis products yield in the reactor temperature domain of 475-575 °C.

Experimental Section

Pyrolysis of wheat straw, pine wood and rice husk were carried out in a bench scale of Pyrolysis Centirfuge Reactor (PCR) developed at CHEC DTU, by employing flash pyrolysis principle as shown in Figure 1. The principle of the process is by tangentially feeding solid biomass particles into the horizontally oriented Ø 82 x 200 mm tubular reactor. The centrifugal force created by the rotation of three blade rotors keeps the particles sliding on the heated wall while passing through the reactor. The solid particles transform to vapors by the high efficiency of heat transfer and while undergoing reaction, particles move down the reactor pipe before leaving suspended in the gas through the tangential outlet. Larger char particles were removed by a change-in-flow separator whereas fines were collected by the cyclone. Vapors were condensed in a direct water cooled condenser (bubble chamber) filled with previously produced bio-oil. Aerosols that were not retained by the condenser were collected in a coalescer filled with ROCKWOOL (fibers). The gas was pumped to the preheater and heated to 400 °C before it is recirculated to the reactor in order to maintain a desired gas residence time and avoid condensation of liquid products within the reactor. The amount of produced gas was measured by a temperature compensated gas meter and a sample was collected in a gas bag.

In this work, the biomass feedstock was fed to the reactor of approximately 20-23 g/min and with an approximately gas residence time of 0.3 s, and initial heating rate of approximately 250-1000 °K/s. The performed measurements made it possible to determine the yield of char, gas, water and oil of the single measurements.

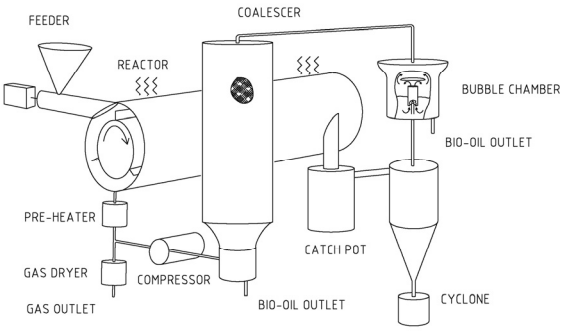

Figure 1: Schematic diagram of the developed ablative pyrolysis bench reactor system.

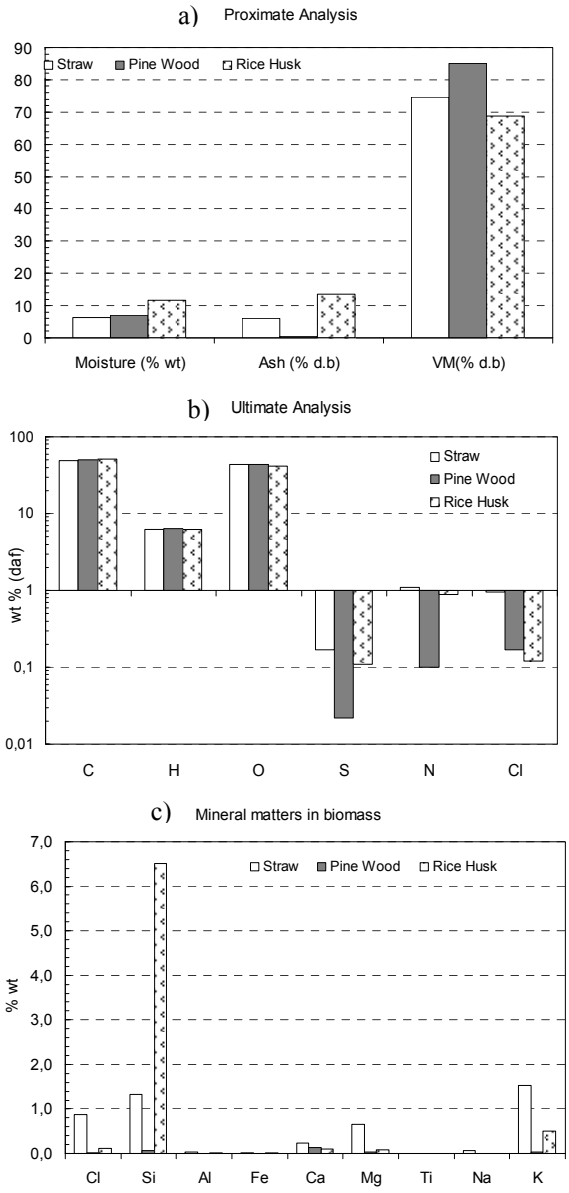

Figure 2 Chemical analysis of biomass a) Proximate analysis b) Ultimate analysis c) Concentration of the ash forming elements in the biomass feedstoks used.

Results and Discussion

The chemical composition of a feedstock has a major influence on the flash pyrolysis products distribution. Figure 2 lists the chemical properties of wheat straw, rice husk, and pine wood to highlight the particular differences in feedstock. Rice husk is characterized by low volatile matter and high ash content compared to the wheat straw. Pine wood has the highest volatile matter and the lowest ash content.

The biomass ash mainly comprises of K, Ca, Mg, Si, Al, Fe, Ti, Na, and P. The ash content in straw, rice husk and pine wood were 6.02, 13.6 and 0.50 % wt db respectively. The straw ash is dominated by K, Mg and Na while rice husk ash is dominated by Si and pine wood ash has a high Ca content. Especially, alkali

metals are known to catalyze the pyrolysis process such that a relatively high gas and char yield are obtained and a relatively low liquid organics yield [8].

Liquid Organics

Figure 3 shows the yields of liquid organics, char and gas + water generated from straw, wood and rice husk. In general, a maximum organics yield is obtained at an intermediate temperature. At high temperatures, a part of the tar decomposes and larger amounts of gas are formed.

The liquid organics yield from straw attained a maximum level at a reactor temperature of 525 °C (see Figure 3a). The maximum liquid organics yield from pine wood and rice husk was observed at 550 °C. The lower maximum yield temperature of straw is probably caused by the high potassium straw content that shifted the cellulose and hemicellulose decomposition to a lower temperature. Previous study showed that the addition of KCl to the washed straw moved the cellulose decomposition to lower temperature by about 8 % [8].

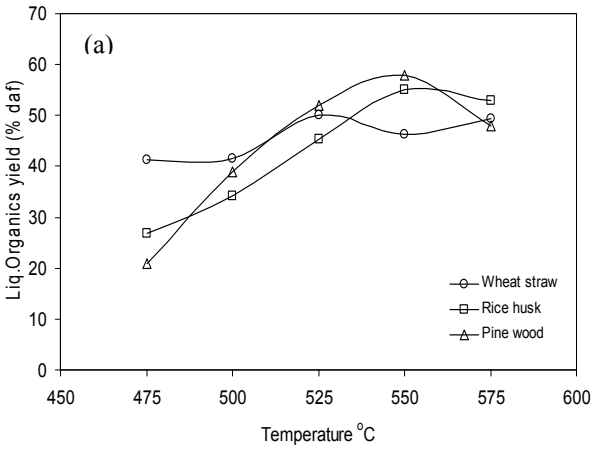

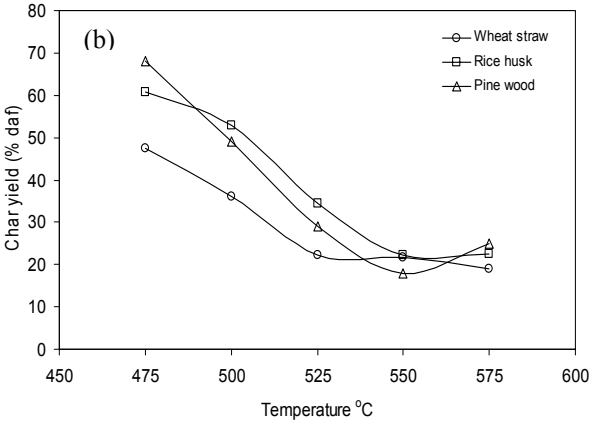

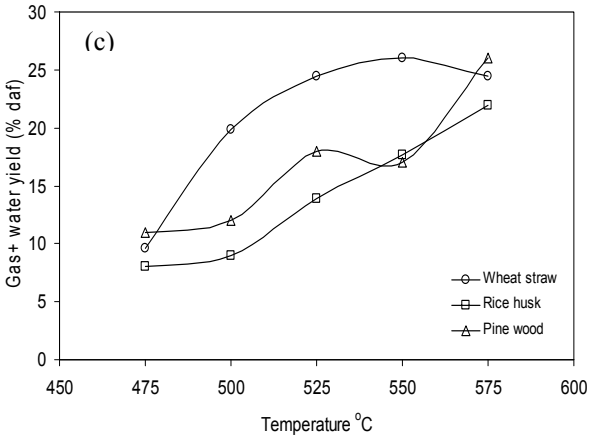

Figure 3: Flash pyrolysis product yields as a function of pyrolysis temperature

At the optimum temperature, pine wood has the highest liquid organics yield followed by rice husk and finally straw. The maximum liquid organics yields for pine wood, rice husk and straw were 58, 55 and 50 % wt daf, respectively. The lower organics maximum yields of rice husk and straw compared to wood at temperature above 500 °C are probably caused by the alkali metals that catalyze a conversion of tar and fed to gas.

Char

The char yields for all biomasses types show a declining trend with increasing temperatures (see Figure 3b). Overall, the highest char yield is obtained from rice husk followed by pine wood and finally wheat straw. This can be explained by the high ash content in rice husk. The lowest char yield for straw is due to the high potassium content that catalyzed the pyrolysis process, to form more gasses and thus reducing char yield.

Gas + Water

The formation of gas and water during pyrolysis is shown in Figure 3c. The yield of gas + water kept increasing with pyrolysis temperatures. The high yield at high temperatures is causes by the pyrolysis oil vapor being converted into gases and water through secondary cracking of tar. It can be seen that straw produces high yield of gas+ water compared to others and this result is in good agreement with other findings [9]. The higher gas + water yield for wheat straw is mainly due to high potassium content in straw and thereby decreasing the char yield and it is simultaneously explain why straw char is the lowest compared to others.

Conclusion

The pyrolysis of wheat straw, rice husk and pine wood was investigated by means of a pyrolysis centrifuge reactor. Potassium and sodium are the major alkali metals in biomass ash that can significantly affect the pyrolysis products yield and pyrolysis behavior. The maximum organics yield for straw occurred at 525 °C and at 550 °C for both rice husk and pine wood. At these optimum temperatures the yield of liquid organics

were 49, 52 and 58 % daf for straw, rice husk and pine wood, respectively. The optimum yield temperature of straw is slightly lower than that of wood and rice husk. However the gas + water formation for straw was higher compared to the others and the amount kept increasing with temperatures due to the secondary reaction take places at higher temperatures.

The presence of alkali matters in biomass ash especially potassium and sodium reduce the yield of liquid organics by catalytic decomposition of tar and also lowering the optimum yield temperature.

Acknowledgement
CHEC is financially supported by the Technical University of Denmark, DONG Energy A/S, Vattenfall A/S, FLSmidth A/S, Hempel A/S, Energinet.dk, the Danish Research Council for Technology Sciences, the Danish Energy Research Program, the Nordic Energy Research Program, and EU. The author acknowledges the financial support of the Ministry of Higher Education (MOHE) of Malaysia, Universiti Teknologi Malaysia (UTM), the Nordic Energy Research Program and the DTU-BIOCHAR project.

References

1. J.L. Gaunt, J. Lehmann, Environ. Sci. Technol. 42 (2008) 4152.
2. J.A. Mathews, Energ. Policy 26 (2008) 940.
3. A.V. Bridgwater, G.V.C. Peacocke, Renew. Sust. Energ. Rev. 41 (2000)
4. N. Bech, M.B. Larsen, P.A. Jensen, K. Dam-Johansen, Biomass Bioenerg. 33 (2009) 999.
5. M.J. Antal, Ind. Eng. Prod. Res. Dev. 22 (1983) 66.
6. M.J. Antal, Fundamentals of biomass thermochemical conversion, Elsevier, London, U.K., 1985, p.511.
7. A.V. Bridgwater, Appl. Catal. 5 (1994).
8. A. Jensen, K. Dam-Johansen, Energ. Fuel. 12 (1998) 929.
9. L. Fagbemi, L. Khezami, R. Capart, Appl. Energ. 69 (2001) 293-306.

Priyanka Jain
Phone: +45 4525 2891
E-mail: pja@kt.dtu.dk
Discipline: Engineering Thermodynamics

Supervisors: Alexander A.Shapiro
Erling H.Stenby
Nicolas von Solms

PhD Study
Started: January 2009
To be completed: December 2011

Compositional Simulation of In-Situ Combustion EOR

Abstract
In-Situ Combustion (ISC) is a widely acknowledged oil recovery technology for thermal recovery of heavy oils. Modeling of a thermal process as complex as In-situ combustion requires in-depth understanding of detailed reaction kinetics and multidisciplinary process data. Preceding work primarily focused on the kinetic model to study the impact of oxidation reactions and combustion reactions of crude oils. Recent and ongoing studies extend the understanding of initial work done in this research project by investigating fluid displacement characteristics and the effect of residual saturations in an ISC process. The intention is to combine the results with a blend of analytical and numerical methods to define and implement an optimal simulation strategy for reactive transport processes, leading towards developing enhanced oil recovery methodologies.

Introduction
In-situ combustion (ISC), also known as fire-flooding, is receiving strong renewed interest in the petroleum industry because of the depleting oil reserves. ISC is the process of injecting air (or air enriched with oxygen) into oil reservoirs to oxidize a portion of crude oil and enhance recovery through heat and pressure produced. ISC is generally applied for heavy oils due to the dramatic reduction in the oil viscosity with temperature.

This research work, in order to facilitate the study of ISC, relies on laboratory scale combustion simulation. The equation-of-state based compositional one-dimensional model of Virtual Combustion Tube (VCT) is used for recent studies. The VCT is a thermal, reactive, and compositional model; consisting of the series of the cells, each of which is considered as a virtual reactor. The excesses of substance after reaction are transferred to the next cell, which models the transport process. The model also accounts for the simultaneous flow, transport of heat and mass, chemical reactions, and phase equilibrium. Two reaction models - Minimal model (6 components, 4 reactions) and SARA model (14 components, 14 reactions) - are engaged for the study.

Specific Objectives
The preliminary objective of the thesis work is to verify and further enhance the approach of In-Situ Combustion Modeling tools such as the Virtual Kinetic Cell (VKC) and Virtual Combustion Tube (VCT). These two models combine a blend of analytical and numerical methods to define and implement an optimal simulation strategy for reactive transport processes by considering various factors that account for oil recovery. The aim is to study in-depth the process characteristics by integrating the kinetics of the different reactive transport processes into efficient and accurate simulation results. The basic scope of this research work is to develop enhanced understanding of the "reactive cell" model and the subsequent integration of this knowledge in the overall solution procedure. Without efficient solution procedures at the grid block (cell) level, where millions of individual calculations are required, the overall simulation becomes infeasible. The scope of the research work is extended further by introducing the study of the presence of residuals on the efficiency of ISC process for enhanced oil recovery. This is studied to specific to the VCT model.

Approach
To achieve the desired objectives, the approach that this research work maintained is to first study the influence of reservoir process characteristics on In-Situ combustion by designing different simulation scenarios. The approach has been to determine optimal experimental conditions by performing sensitivity analysis using the VKC and the VCT; where simulation data is generated using the Minimal model and SARA model. While first phase of the studies concentrated around the compositional effects [1], the recent studies

paid special attention to residual saturations and possibility for immobile phases. The influence of operational and functional factors, like oxygen concentration in injection gas or temperature, on the distribution of saturations and recovery, is studied. Baker's prediction of three-phase relative permeability, using the interpolation between the two -phase relative permeability, is modeled herewith for the study of residuals. The associated calculations are as below [2]:

$$k_{ro} = \frac{(S_w - S_{wr})k_{row} + (S_g - S_{gr})k_{rog}}{(S_w - S_{wr}) + (S_g - S_{gr})}$$

The two-phase relative permeability here is estimated using two phase models as:

$$k_{row} = k_{row}{}^0 \left(\frac{S_o - S_{orw}}{1 - S_{wr} - S_{orw}} \right)^{e_{ow}}$$

$$k_{rog} = k_{rog}{}^0 \left(\frac{1 - S_g - S_{Lrg}}{1 - S_{Lrg} - S_{gr}} \right)^{e_{og}}$$

where, k_{row} and k_{rog} are oil relative permeability in oil-water system and oil relative permeability in oil-gas system; e_{ow} and e_{og} are the exponents of relative permeability curve in oil-water system and in oil-gas system; and $k_{row}{}^0$, $k_{rog}{}^0$ are the end point oil relative permeability in the oil-water system and end point oil relative permeability in oil-gas system, respectively. The saturations used in the aforesaid permeability calculations are formulated as below:

$S_g = 1 - S_o - min(S_w - S_{wr})$ and, $S_{Lrg} = S_{wr} - S_{org}$

where, S_{Lrg} is the total residual liquid saturation to gas phase during two-phase flow of gas and oil. Furthermore, S_{orw} is the oil residual saturation in oil-water system; whereas, S_o, S_g, S_w are the saturations of oil, water and gas respectively. S_{wr} and S_{gr} are residual saturation of water and gas phase respectively.

Results and Discussions

The research work, involving the VKC model for ISC simulations, analyzed the influence of changing oxygen-feed concentration and activation energy on Light and Heavy Oils during thermal recovery process of ISC. The Peng-Robinson equation of state was then compared with the Wilson K-Value correlation. Since no appreciable difference between the two was observed, the Peng-Robinson equation of state was then used to further study the influence of- characterization (critical pressure, critical temperature and acentric factor) of Light and Heavy Oils on different VKC simulation output parameters. The results within this context of comparing the Light Oil to Heavy Oil shows that it is the heavy oil critical properties which significantly influence the simulation of the minimal model. Operating parameters like air injection rate, oxygen feed concentration and activation energy was indicative of having significant influence on oil recovery. Increase in air injection rate was found to be indicative of decrease in oil recovery, by supplementing the cooling of combustion front; whereas, increase in oxygen feed assisted combustion thus leading towards improved oil recovery. The VKC model is then extended further to study the oxidation kinetics of the SARA fractions of crude oil during in-situ combustion. The study of SARA model made an important observation that composition plays a key role in ISC simulation; due to asphaltenes being most resistant toward oxidation and saturates being the easiest oxidizable ones. As regards studies of the residuals, the results obtained indicate that increasing the air injection rate contributes to a corresponding decrease, with time, in higher oil saturation - thus improving oil mobility. It is also observed that at the start of simulation correlating to combustion zone of the ISC process, with increase in system pressure, the oil saturation increases. It is also seen that in the steam zone, identified by decrease in temperature, an increase in the system pressure decreases the oil saturation. Furthermore, at temperatures above that in steam plateau, the oil saturation is independent of the initial oil and water saturations.

Conclusion

A general framework for simulation of in-situ combustion induced enhanced oil recovery process is considered. The work done under the thesis work till date has some interesting conclusions to share with both the research and the industrial community. Adapting the minimal model for a VKC it was found that increasing the critical pressure of heavy oil increases the concentration of heavy oil in the recovery flow which then cracks to result in increase of light oil concentration. In contrast, increase in critical temperature of heavy oil results in decrease of both heavy and light oil concentrations. Adapting the SARA model, where the critical properties of the pseudo components are not determined experimentally, and fluid characterization holds certain significance. Referring to the results and observations of the residual studies, it can be concluded that to maintain the mobility of residual oil for enhanced recovery; increase air injection rates are required.

Future Work

To compare and validate both the compositional models, the VKC and the VCT, using experimental data for their feasibility in field trials.

References

1. P. Jain, E. Stenby, N. Solms, Compositional Simulation of In-Situ Combustion EOR: A Study of Process Characteristics, SPE Improved Oil Recovery Symposium, Tulsa, USA, 2010.
2. F. Ahmadloo, K. Asghari, B. Yadali Jamaloei, Experimental and Theoretical Studies of Three-Phase Relative Permeability, SPE Annual Technical Conference and Exhibition, New Orleans, USA, 2009

List of Publications

1. P. Jain, E. Stenby, N. Solms, Compositional Simulation of In-Situ Combustion EOR: A Study of Process Characteristics, presented at the 2010 SPE Improved Oil Recovery Symposium, Tulsa, Oklahoma, USA, 24–28 April 2010

Rita Lencastre Fernandes

Phone: +45 4525 2903
E-mail: rlf@kt.dtu.dk
Discipline: Process Technology and Unit Operations
Systems Engineering
Supervisors: Krist V. Gernaey
Anker D. Jensen
Ingmar Nopens, University of Ghent

PhD Study
Started: November 2009
To be completed: October 2012

Population Balance Models and Computational Fluid Dynamics: an Integrated Model Framework to Describe Heterogeneity in Fermentors

Abstract
Traditionally, a microbial population has been considered homogeneous in optimization studies of fermentation processes. However, research has shown that a typical microbial population in a fermentor is heterogeneous. The aim of this Ph.D. project is to establish a model framework where Population Balance Models (PBM) and Computational Fluid Dynamics (CFD) are integrated in order to describe heterogeneous microbial populations in stirred-tank reactors. This contribution will reflect the work developed in the project's first year, and it focuses on the formulation of a PBM with total protein content as the model variable. Besides describing the development of the microbial population structure under varying substrate availability, the model additionally accounts for cell-to-cell variability due to cell cycle and cell ageing.

Introduction
Although microbial populations are typically described by averaged properties, individual cells present a certain degree of variability. Indeed, initially clonal microbial populations develop into heterogeneous populations even when growing in a homogeneous environment.

A heterogeneous microbial population consists of cells in different states, and it implies a heterogeneous distribution of activities (e.g. respiration, product efficiency). Furthermore, cell-to-cell variability implies different responses to extracellular stimuli. This will result in the development of a heterogeneous population with a possibly different structure when the microbial population is subjected to changes in the surrounding environment, relatively to when growing under a constant extracellular environment. In fact, this difference in the population structure may explain the lower productivities, and higher viability obtained for cultivations in large-scale reactors where substrate and oxygen gradients are observed, relatively to cultivations in well-mixed bench scale reactors [1].

From a process robustness perspective, a certain degree of heterogeneity in the microbial populations may be advantageous. This PhD project aims at understanding and modeling the development of heterogeneous microbial populations subjected to varying environmental conditions.

Heterogeneity in microbial populations can be classified as genetic or phenotypic; in the case cell-to-cell variability is due to possession of different genes, or the case of differential expression of basal genes, respectively [2]. Given the short time frame of a typical cultivation (i.e. days, weeks), the contribution of genetic drift to the development of heterogeneity within a population was assumed negligible, and the focus of this project is set on understanding and modeling phenotypic heterogeneity.

Models able to account for distributed properties are classified as *segregated and structured*, and commonly take the shape of Population Balance Models (PBMs) [3]. Generally, a PBM for microbial populations aims at predicting the temporal change of the cell number distribution, which is characterized by a descriptor variable x (e.g. cell age, mass, protein content, intracellular metabolites). Different model formulations have been proposed for the cell descriptor variables.

Specific Objectives
The first main goal of this PhD project is to formulate and validate a PBM, which is able to simulate a dynamic microbial population under varying substrate availability conditions. In order to achieve this goal, it was defined that the model would predict the development of a heterogeneous population of *Saccharomyces cerevisiae*. The following specific objectives were defined:

- Identify, based on a literature search, the main factors responsible for cell-to-cell variability within

microbial populations (with special focus on *S. cerevisiae*), for a non-changing extracellular environment.
- Identify a population model structure, (i.e. model variable(s), nr. of stages) which can account for the heterogeneity drivers, as well as include the effect of changing extracellular conditions as a potential enhancer of the population heterogeneity driving forces.
- Establish correlations between substrate availability and the PBM kernel functions, based on experimental observations.
- Formulate and solve the PBM using a finite difference scheme; validate the model predictions with experimental observations.

Results and Discussion

Phenotypic heterogeneity arises as a result of the variability inherent to the metabolic mechanisms of single cells. Two dominant cell variables responsible for differential gene expression are cell cycle and cell ageing [2]. Cells at different phases in the cell cycle, or with different ages, have been observed to respond differently to stress conditions [4]. It is therefore of interest that the dynamic population model accounts for these two heterogeneity drivers.

In the specific case of *S. cerevisiae*, the budding division process leads to a variability of cell sizes. It has been shown that the distribution of cell sizes in a population is characteristic of the growth condition Indeed, protein content distributions (a measure of cell size) are stable for populations in balanced exponential growth [5] and are adjusted, during a transient period, when the population is subjected to a change in the environment [6].

Multistage mass structured PBM

It was thus found desirable to use a PBM based on protein content as model variable, which is applied to different stages (i.e. subpopulations) corresponding to budding and unbudding (cell cycle) phases within successive generations (cell ages), as suggested by Hatzis and Porro [7]. The model is schematically represented in Figure 1. For example, if only one parent generation is considered, four stages (subpopulations) are modeled: Daughter Unbudding (DU), Daughter Budding (DB), Parent Unbudding (PU) and Parent Budding (PB). For each stage, a population balance equation (such as Equation 1, the last term on the right-hand side is only considered in the case of continuous cultivations) based on protein content as equation variable is defined. Upon a budding transition, cells in unbudding stages are transferred to the following budding stages. Upon division, mother cells transfer to the following unbudding stage, while all newborn daughter cells are considered in the daughter unbudding stage.

The budding and division transitions are governed by probability density functions, which have maxima at the critical budding and division protein contents (P_s and P_m, respectively). These critical transition protein contents reflect the cell control mechanisms that coordinate cell growth and prevent cells from becoming too small or too large.

$$\frac{\partial N(m,t)}{\partial t} = -\frac{\partial}{\partial m}\left[r_m(m,S)N(m,t)\right] - \Gamma(m,S)N(m,t) + 2\int_m^\infty \Gamma(m',S)P(m,m',S)N(m',t)dm' - DN(m,t) \quad \text{Eq. 1}$$

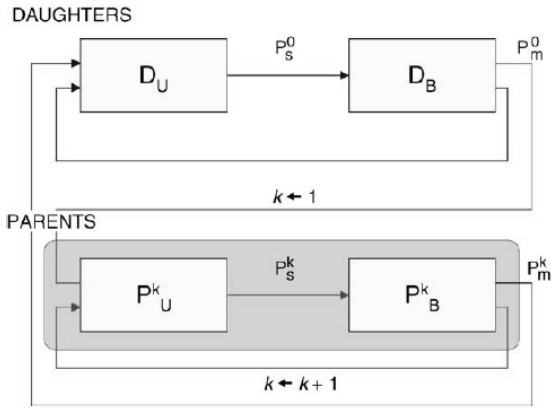

Figure 1: Schematic representation of the multi-stage representation of a microbial population consisting of a daughter unbudding stage (D_U), a daughter budding (D_B) stage, k (i.e. number of generations) stages of parent unbudding (P_U) and budding (P_B) cells. The critical sizes (protein content) that condition the transition between unbudding stages are represented by P_s, while the critical cell sizes necessary to division are designated by P_m. [7]

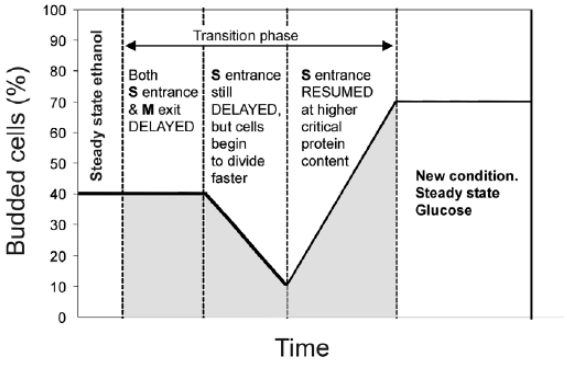

Figure 2: A schematic view of the effects of a nutritional ethanol/glucose shift-up on the budding cells fraction in a yeast population. A similar drop and later recovery has been observed for the down shift (glucose/ethanol), although in this case, the initial steady state presents a higher budding cells fraction than the new condition. [8]

The link to the extracellular environment is accounted for by including substrate dependency in the growth function (increase of cell protein content) as well as transition functions (budding and division) for each of the stages: (1) growth: a Monod type expression can be coupled to the first linear kinetics describing the

increase of the cell protein content; (2a) budding transition: the critical cell protein content for the transition to budding stage P_s, is a function of the type and availability of the carbon source; (2b) division transition: also the critical protein content at division P_m, is a function of the available substrate.

When a microbial population is subject to a change in the substrate availability, both budding and division transitions are delayed. The division transition is however resumed earlier than the budding transition. This explains the experimentally observed abrupt drop in the fraction of budding cells in the population, followed by a recovery of the budding fraction, when a population is subject to a nutritional up or down shift [8] (see Figure 2).

Transition functions for changing substrate availability

The formulation of the budding and division transition functions, for a dynamic model, relies on understanding the effect of the changing substrate availability on the critical transition sizes, as well on the relative weight (% of total cells) and structure of the cell subpopulations undertaking these transitions. In order to establish realistic transition functions, the experimental data was collected in triplicate for a batch cultivation of a haploid *S. cerevisiae* strain on glucose (in 2L bioreactors with controlled pH). Samples were taken along the cultivation, with a higher frequency during non-balanced growth periods (i.e. diauxic shift, and entrance to stationary state). Besides the traditional monitoring of optical density, glucose and ethanol concentrations, samples were analyzed by flow cytometry. Distributions of forward scattering (typically proportional to cell size), side scattering (a measure of intracellular granularity) DNA and protein content distributions were obtained by fluorescence staining for each sample.

Flow cytometry: data analysis

Flow cytometry is a robust technique that relies on the properties of light scattering, excitation and emission to measure a variety of properties at single cell level. The ability of FCM to measure the properties of single cells allows the study of phenotypic diversity of individual microorganisms [9]. Measurements are collected for each analyzed cell (i.e. event) and data is typically present in the form of histograms (measured property vs. cell count) or 2D dot plots (one cell property vs. a second cell property, where each event is presented as a dot).

The DNA distribution is commonly used for classifying cells according to cell cycle phase. The histogram contains two peaks separated by an intermediate flatter area. The first peak corresponds to cells in G_1 cell cycle phases (i.e. possess one DNA copy, Figure 3). The second peak corresponds to cells in phases G_2/M which have two copies of DNA (Figure 3), and should be at double fluorescence intensity of the first. Cells scoring an intermediate fluorescence are in phase S, during which the DNA replication takes place.

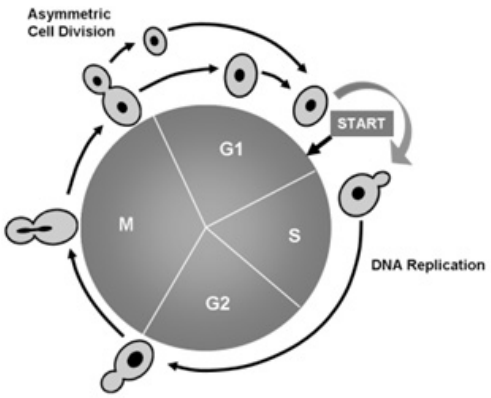

Figure 3: Schematic representation of the cell cycle for microorganisms that divide by budding. The phase G_1 corresponds to the PBM unbudding stages, while the budding stages include the phases S, G_2 and M. The cell size control point which regulates the initiation of the bud formation and DNA replication is marked with START.

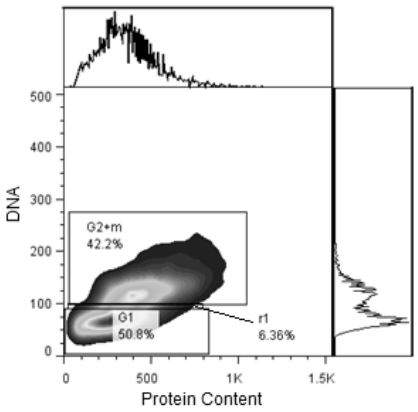

Figure 4: 2D dot plot corresponding to the distributions of DNA and protein content (fluorescence intensity) of a population of *S. cerevisiae* during diauxic shift. The protein content histogram is presented on the top, and the DNA histogram on the right side.

In a two dimensional representation of the distributions of DNA and protein content (Figure 4), it is possible to distinguish two subpopulations: one with lower DNA and protein content, and another with higher DNA and protein content. The first corresponds to the cells in phase G_1, and the latter to the G_2+M subpopulations. The cells in intermediate region (R1, Figure 4) are in phase S, and the corresponding protein content distribution is used for estimation of the critical budding transition cell protein content.

Isolating the cells in mitosis (i.e. which are releasing the newborn daughter cell), at a given time instant, from the G_2+M region presents further challenges. Indeed, the clearer distinguishing feature which may allow for differentiating M cells from G_2 based on data collected by flow cytometry, is the existence of two individual nuclei. Further literature search is required to identify methods for distinguishing the two subpopulations, and being able to evaluate the behavior of the subpopulation

undertaking division under changing substrate availability.

Conclusions

Individual microorganisms, even if part of a 'clonal' or isogenetic population, may differ greatly in terms of physiology, biochemistry, or behavior [9]. This heterogeneity results from differences in the microenvironment surrounding each individual cell, as well as the physiological stage of an individual cell when subjected to a given change in the extracellular medium.

A PBM describing the protein content distribution of the microbial population, and with stages reflecting the unbudding and budding phases of the cell cycle, as well as different generations, is used for predicting the dynamic behavior of heterogeneous populations of *S. cerevisiae*. The interaction of the cells with the extracellular environment (i.e. changing substrate availability) is accounted by including substrate depending terms in the model kernel functions.

Aiming at building a model able to predict the development of heterogeneous yeast populations under changing substrate availability conditions, special focus was set in formulating the substrate dependent transition functions which describe the initiation of the budding process, and the cell division (i.e. release of the bud). In an experimental study, three batch cultivations of *S. cerevisiae*, using glucose rich media, were performed. DNA and protein content distributions were measured by flow cytometry for samples taken along the cultivations. Also the forward and side scatter signals obtained for each cell during the flow cytometry analysis were collected.

The analysis of this data will allow for establishing correlations between the critical transition protein content for both budding and division, and the substrate availability. Once these correlations are established, it will be possible to formulate the transition kernels in the PBM. The predictions of the development of the protein content distributions will be validated against the experimentally observed protein distributions.

Acknowledgements

The Danish Council for Strategic Research is gratefully acknowledged for financial support in the frame of the project "Towards robust fermentation processes by targeting population heterogeneity at microscale" (project number 09-065160).

References

1. S.-O. Enfors, M. Jahic, A. Rozkov, B. Xu, M. Hecker, B. Jürgen, J. Biotechnol. 85 (2) (2001) 175-185.
2. E.R. Sumner, S.V. Avery, Microbiology 148 (2) (2002) 345-351.
3. K.V. Gernaey, A.E. Lantz, P. Tufvesson, J.M. Woodley, G. Sin, Trends Biotechnol. 28 (7) (2010) 346-354
4. S. Avery, Nature Rev. Microbiol. 4 (8) (2006) 577-587
5. L. Alberghina, D. Porro, Yeast 9 (8) (1993) 815-823
6. L. Alberghina, C. Smeraldi, B.M. Ranzi, D. Porro, J. Bacteriol. 180 (15) (1998) 3864-3872.
7. C. Hatzis, D. Porro, J. Biotechnol. 124 (2) (2006) 420-438.
8. L. Alberghina, R.L. Rossi, D. Porro, M.A. Vanoni, in: L. Alberghina, H.V. Westerhoff (Eds.): Systems Biology, Topics in Current Genetics Vol. 13 Springer-Verlag Berlin Heidelberg, 2005, p. 325
9. B.F. Brehm-Stecher, E.A. Johnson, Microbiol. Mol. Biol. Rev. 68 (3) (2004) 538-559.

List of Publications

1. D. Schäpper, R.L. Fernandes, A.E. Lantz, F. Okkels, H. Bruus, K.V. Gernaey, Biotechnol. Bioeng. n/a. doi: 10.1002/bit.23001

Benedicte Mai Lerche
Phone: +45 4525 2821
E-mail: bml@kt.dtu.dk
Discipline: Engineering Thermodynamics

Supervisors: Kaj Thomsen
Erling H. Stenby

PhD Study
Started: December 2008
To be completed: February 2012

CO_2 Capture from Flue Gas using Amino Acid Salt Solutions

Abstract
The reversible absorption of CO_2 into a chemical solvent is currently the leading CO_2 capture technology. Available solvents are almost exclusively based on aqueous alkanolamine solutions, which entail both economic and environmental complications. A new type of solvents based on the salts of amino acids has emerged as an alternative to the alkanolamine solutions. A number of advantages make amino acid salt solutions attractive solvents for CO_2 capture. The goal of this project is to find the optimal amino acid salt solution for CO_2 capture from flue gas.

Introduction
The leading technology for CO_2 capture is chemical absorption, which is a technique where a chemical solvent reacts reversibly with the CO_2 in flue gas. During contact with the flue gas, the solvent chemically absorbs the CO_2. Heating of the CO_2 rich solvent leads to release of the CO_2 from the solvent, which is hereby regenerated and ready for another round of absorption. The captured CO_2 can now be compressed and transported to a storage location. [1] Available solvents for the chemical absorption process are almost exclusively based on aqueous alkanolamine solutions. Unfortunately CO_2 capture using alkanolamine solutions entails economic drawbacks as well as environmental complications, making the large scale implementation of the technology difficult. [2]

Disadvantages of alkanolamine solutions
CO_2 capture using alkanolamine solutions is very energy intensive, mostly due to the large amount of heat/energy needed to release the CO_2 form the solution, but also due to loss of solvent caused by its degradation and evaporation. It has been widely reported that alkanolamines undergo degradation in oxygen-rich atmospheres, such as those typically encountered in the treatment of flue gases, resulting in very toxic degradation products. [2] Besides the economical problem this creates with loss of solvent, there is an increasing environmental concern, due to the possible emission of small amounts of these toxic degradation products to the air. [3] Because the desire to capture CO_2 is gaining momentum, there is an urgent need for the development of new solvents that have the ability to capture CO_2 in both a cost efficient and environmental safe manner. [4]

Amino acids salt solutions as CO_2 absorbents
In comparison to alkanolamines amino acid salt solutions have several desirable properties for CO_2 capture from flue gas. Their ionic nature makes them more stable to oxidative degradation and also gives them certain other desirable physical properties such as low volatility. [2,4] A further advantage can be achieved by the interesting feature of several amino acid salts solutions to form solid precipitates when absorbing CO_2. [5] It has been found that the driving force for absorption can be maintained at a high level even at high CO_2 loadings as a result of precipitation, significantly improving the absorber performance. [2] In addition some amino acid salt solutions have been shown to react with CO_2 with fast reaction kinetics. [4,6] Despite the rising interest, few studies have been performed so far on amino acids as CO_2 absorbents. When a pure amino acid, with the overall formula $HOOC\text{-}R\text{-}NH_2$, is dissolved in water, the following equilibriums are established. [6]

$$\underset{\text{I}}{HOOC\text{-}R\text{-}NH_3^+} \overset{-H^+}{\rightleftharpoons} \underset{\text{II}}{^-OOC\text{-}R\text{-}NH_3^+} \overset{-H^+}{\rightleftharpoons} \underset{\text{III}}{^-OOC\text{-}R\text{-}NH_2}$$

The amino acid is predominantly on its zwitterionic form (II), where the carboxylic acid group has lost a proton while the amine group is protonated, and the pH of the solution is equivalent to the isoelectric point of the given amino acid. As CO_2 reacts only with deprotonated amines, the zwitterionic form of the amino

acid is incapable of reaction with CO_2. Hence it is necessary to add an equivalent amount of strong base to deprotonate the amine group and produce the negatively charged form of the amino acid (III). The base which is used for this purpose is usually potassium hydroxide, with the potassium salt of the amino acid becoming the active component, which reacts with CO_2. [6] It is generally agreed that alkaline salt solutions of amino acids react with CO_2 similar to alkanolamines having primary or secondary amine functionalities. The reactions that occur in the liquid phase are thus as follows (with the amino acid salt represented as AmA). [4]

$$CO_2 + 2AmA \rightarrow AmACOO^- + AmAH^+ \quad (1)$$

$$CO_2 + OH^- \rightarrow HCO_3^- \quad (2)$$

$$H_2O \rightarrow H^+ + OH^- \quad (3)$$

As seen CO_2 absorption can either take place by carbamate formation (Eq. 1) or bicarbonate formation (Eq. 2). There have been conflicting chemical mechanisms proposed to describe the absorption process. However, it is clear from the reaction rates that the initial absorption reaction is the formation of the carbamate. [4]

Specific objective of the project

The objective of the project is to evaluate the potential of amino acid salt solutions as solvents for CO_2 capture from flue gas. The goal is to provide general conclusions and recommendations on which amino acids will be most appropriate for the process.

Experimental work

We have developed a screening procedure, in which amino acid salts are tested in regard to important solvent properties including: Water solubility, heat stability, CO_2 loading capacity, as well as the ability to form precipitation upon the absorption of CO_2. Amino acids showing good water solubility and heat stability were tested in regard to their CO_2 loading capacity. In order to study the CO_2 loading capacity of the amino acid salt solutions an experimental set-up was built (Figure 1). Our aim has been to mimic, the actual conditions for CO_2 absorption from a coal fired power plant, as closely as possible. The set-up, which is entirely made of glass, is operated in a dynamic analytical mode, with analysis of the effluent gas. Synthetic flue gas (meaning 10% CO_2 and 90% N_2) is bubbled into the amino acid salt solution situated in the cell (reactor), with the total pressure of the system being 100 kPa. The cell is placed in a water bath, to keep a constant temperature throughout the experiment. The CO_2 absorption is followed by measuring the percentage of CO_2 in the outlet gas, using a CO_2 analyzer. Also the temperature and pH in the solution is measured during the experiment. All data are collected as a function of time.

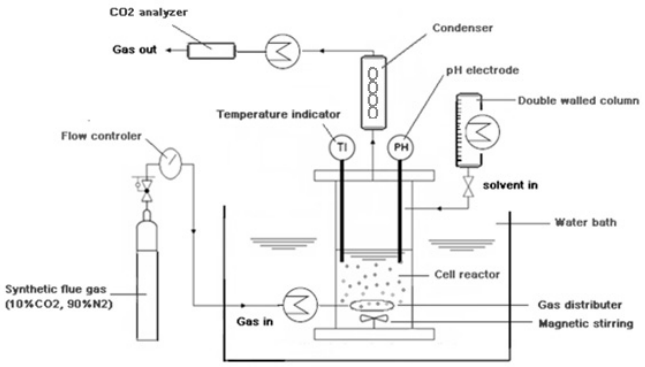

Figure 1: Representation of experimental set-up

The CO_2 loading capacity of the solution is obtained by integrating the CO_2 signal (CO_2 in the inlet gas minus the CO_2 in the outlet gas) over time. X-ray diffraction (XRD) and inferred (IR) spectroscopy have been applied to study the precipitates, which forms as a result of the CO_2 absorption. Knowing the chemical nature of the solids formed helps to understand the interplay between CO_2 loading capacity and precipitation ability of amino acid salt solutions.

Future work

Future work includes vapour liquid-equilibrium (VLE) experiments to evaluate the ability of the amino acid salt solutions to release the captured CO_2. Also the kinetics of the reaction between CO_2 and selected amino acid salt solutions will be addressed in the future.

Acknowledgements

This project is sponsored by DONG Energy and Vattenfall A/S Heat Nordic.

References

1. IPCC Special Report on Carbon Dioxide Capture and storage. (2005)
2. P.S. Kumar et al. Ind. Eng. Chem. Res. 42 (2003) 2832-2840.
3. J. Gabrielsen, Ph.D. Thesis, IVC-SEP, DTU. (2007)
4. J. van Holst et al. GHGT8 Trondheim. CATO publications(2006)
5. M. Majchrowicz et al. GHGT8 Trondheim. CATO publications(2006)
6. A.F. Portugal et al. Chem. Eng. Sci. 62 (2007) 6534–6547.

Publications

1. B.M. Lerche, E.H. Stenby, K. Thomsen, CO_2 Capture from Flue Gas using Amino Acid Salt Solutions, Proceedings from Risoe International Energy Conference 2009.
2. B.M. Lerche, Fang CO_2 med aminosyrer, Aktuel Naturvidenskab nr. 6, december 2010.

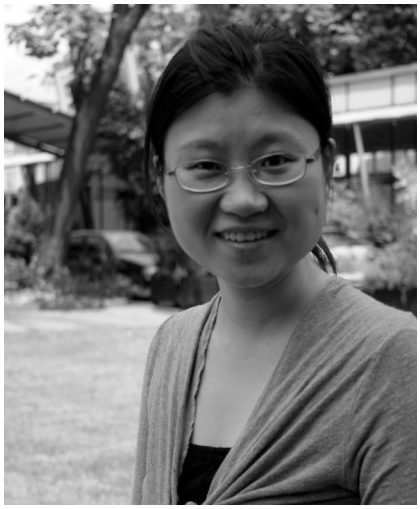

Li Li

Phone: +45 4525 6813
E-mail: li@kt.dtu.dk
Discipline: Polymer Technology

Supervisors: Gunnar Eigil Jonsson
Sokol Ndoni, DTU Nanotech
Lydia D. Clausen, Radiometer Medical
Kristian M. Hansen, Radiometer Medical

PhD Study
Started: Feb 2008
To be completed: May 2011

Nanoporous Membranes with Tunable Surface Morphology

Abstract
Nanoporous 1,2-polybutadiene (1,2-PB) membranes of gyroid morphology with nanopores of 10 nm in diameter were fabricated from 1,2-polybutadiene-b-polydimethylsiloxane block copolymer. The morphology of the membranes' outer surface was investigated by scanning electron microscopy and contact angle measurement. An 'opened' or 'closed' surface can be simply manipulated by using different substrates in the process of membrane fabrication. A glass substrate resulted in a porous surface with a randomly-distributed nanoporosity, having a pore size of ~ 10 nm and a surface porosity 45%. The entire skin layer might consist of multi sublayers instead of a single uniform layer; the lamellae layer is present at the outmost surface followed by the hexagonally perforated layer layer.

Introduction
Nanoporous materials are of great interest for use in a variety of membrane applications for health, food, sustainable water and energy conversion. [1-4] Block copolymer-templated nanoporous materials are being extensively developed. Due to the incompatibility of the constituent blocks, the block copolymers self assemble into arrays of various well-defined structures, such as spheres, cylinders, lamellae or more complex morphologies, with a microdomain dimension of molecular scale. [5] Nanoporous matrices can be derived from self-assembling block copolymers by partially or totally removing one block with UV, oxygen plasma, ozone, base, or acid. [6] We also successfully generated a series of nanoporous polystyrene by selectively and quantitatively etching polydimethylsiloxane (PDMS) with anhydrous hydrogen fluoride. [7] Unique features like controllable pore size and orientation, high porosity, narrow pore size distribution, and functionalized surface make this type of nanoporous material to be advanced membranes for many applications.

More interestingly, while the bulk morphology for a given block polymer is well controlled by temperature; the outer surface morphology can be manipulated by controlling interfacial energy. [5] This can in turn affect the properties and performance of the resultant nanoporous membrane, such as permeation rate, selectivity and biocompatibility. We fabricated nanoporous membranes from the self-assembled 1,2-polybutadiene-*b*-polydimethylsiloxane (1,2-PB-*b*-PDMS) via quantitative and selective cleavage of the PDMS block, as illustrated in Figure 1. A gyroid nanostructure was designed from the polymer synthesis stage in order to ensure isotropic percolation with no need for structure alignement. Such a membrane has narrowly dispersed pore size and high porosity so high throughput and selectivity are expected. We selected two different substrates to interface-direct two distinct morphologies at the outer surface of the nanoporous membranes. The surface morphology of membrane was comprehensively investigated by scanning electron microscopy (SEM) and contact angle (CA).

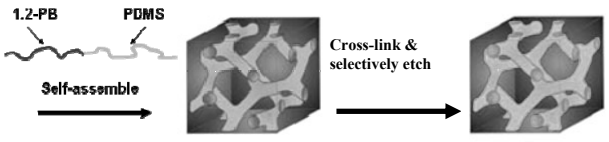

Figure 1: Schematic illustration of the fabrication of cross-linked nanoporous 1,2-PB polymer from 1,2-PB-*b*-PDMS block copolymer. The precursor 1,2-PB-*b*-PDMS (left) self-assembles into gyroid morphology at the cross-linking temperature (middle). PDMS is selectively cleaved from the sample and a nanoporous polymer matrix is obtained (right).

Methods

Membrane preparation

The 1,2-PB-*b*-PDMS copolymer was synthesized by living anionic polymerization as described in ref. 8. The overall molecular weight (14100 g/mol), polydispersity index (1.04) and mass fraction of PDMS (0.41) were determined by a combination of ^{1}H-NMR and size exclusion chromatography.

The general procedure to prepare a nanoporous 1,2-PB membrane is as follows. Two different substrates were used for fabricating the flat sheet membrane. One is a glass plate; the other is a FDTS-coated glass plate via molecular vapor deposition. FDTS stands for $Cl_3Si(CH_2)_2(CF_2)_7CF_3$. The 1,2-PB-*b*-PDMS precursor was dissolved in Tetrahydrofuran (THF, Sigma-Aldrich) containing 0.01 moles of dicumyl peroxide cross-linker (DCP, Sigma-Aldrich) per mole of 1,2-PB repeating units. For each membrane sheet to be prepared, the solution was cast onto a clean substrate (glass or FDTS coated glass), followed by drying under nitrogen flow first and then in a vacuum at room temperature. The dried sample was then covered with a second plate (glass or FDTS coated glass). The two plates were squeezed together under 4 bars in a pneumatic-drive compressing set-up under vacuum for 2 h at room temperature. The thickness of the sample was controlled with a few pieces of 0.5 cm wide aluminum spacers. The sandwiched block copolymer samples were cross-linked at 140 °C for 2 hours under nitrogen atmosphere. After cross-linking, the circular flat sheets were removed from the plates and immersed in tetra-n-butylammonium fluoride solution (TBAF, Sigma-Aldrich) in THF to selectively and quantitatively remove the PDMS at room temperature. The etched samples were rinsed by a mixture of THF and methanol and further dried under nitrogen flow at room temperature. Membrane disks 1 cm in diameter was cut out of the flat membrane sheet for the diffusion tests.

Characterization

Atomic force microscopy (AFM) was performed at ambient conditions using NanoMan AFM in tapping mode, with NANOSENSORS™ SSS-NCH AFM probe. The scan area was 1 μm x 1 μm, and 512 x 512 pixels. The sample to be measured was cut with a blade. The cutting surface was trimmed flat and further microtomed on a Leica ultramicrotome with a cryo 35º diamond knife (DIATOME) at room temperature. The microtomed sample was glued on a silicon plate for AFM measurement.

Transmission electron microscopy (TEM) was performed on a FEI TECNAI T20 at acceleration voltage of 200 kV. 90 nm slices of nanoporous 1,2-PB were sectioned on the Leica ultramicrotome with the cryo 35º diamond knife at room temperature. The slices were deposited onto a holly carbon coated copper grid for TEM measurements.

Scanning electron microscopy (SEM) was done on a HELIOS instrument using an acceleration voltage of 5 kV and spot size 3. The samples were sputter-coated with 2 nm thick Pt/Pd prior to SEM imaging.

Contact angle measurements (CA) were conducted on a Contact Angle System OCA 20.

Results and Discussion

Figure 2 shows a typical nanoporous 1,2-PB membrane prepared in this study. It is colorless, transparent and flexible. The bulk morphology of the membranes was confirmed by AFM and TEM as shown in Figures 2b and 2c. Two typical projections of gyroid morphology, so-called, knitting view (211) (Fig. 2b) and wagon-wheel view (111) (Fig. 2c) were observed in the bulk of the membrane. The AFM micrograph reveals a characteristic feature of the regularly spaced nanochannels with a diameter of ~ 10 nm, related to the PDMS microdomain size. The TEM image shows a regular pattern with uniform pore size of ~ 10 nm, similar to the dimension of the feature seen in the AFM image. The membranes used in the present work are identical in the bulk morphology, porosity, pore size and size distribution.

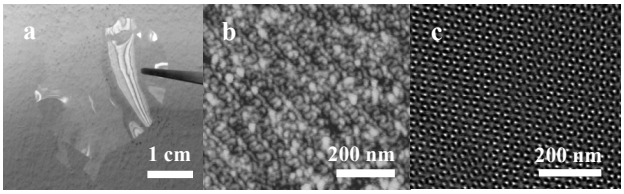

Figure 2 a: A photograph of a nanoporous membrane; **b:** An AFM image of cross section of a nanoporous membrane showing a 'knitting' projection (211) of gyroid morphology; **c:** A TEM micrograph of ultrathin section of a nanoprous membrane showing a 'wagon-wheel' projection (111) of gyroid morphology.

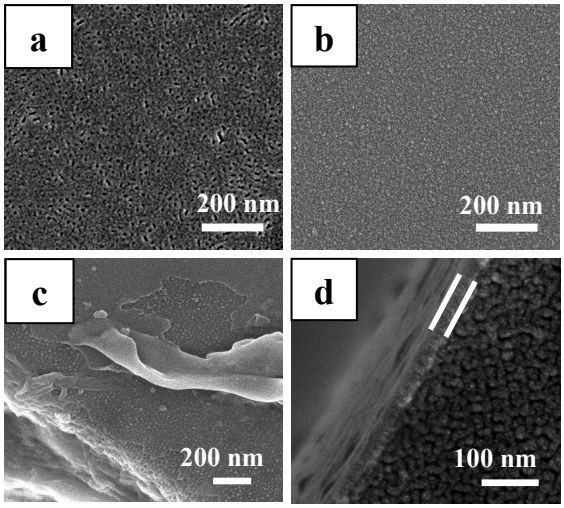

Figure 3: SEM images of the nanoporous membranes (a) Surface in contact with the glass; (b) Surface in contact with the fluorinated-glass; (c) A top view of the edge of a nanoporous membrane prepared between the fluorinated-glass plates; (d) Cross-section near the free surface of a 500 μm nanoporous casted film in a glass petri-dish.

We used two different substrates, a glass and a fluorinated glass, to solvent cast 1,2-PB-*b*-PDMS polymer solutions, thus creating a distinct interfacial environment for the block copolymer films as-casted. During cross-linking, as the temperature increases from 20 ℃ to 140 ℃ the microphase in the film bulk (far away from the surface) are expected to transform from lamellar (LAM) to gyroid (GYR) passing through the metastable hexagonally perforated layer (HPL). LAM is the stable structure at room temperature and GYR at 140 ℃. Therefore a gyroid structure is captured in the film bulk after cross-linking as shown in Fig. 2. However, outer surface morphology of the block copolymer film is directed by the substrate selected.

Accordingly, we investigated the outer surface of the resultant nanoporous membranes by SEM. Figures 3a and 3b show SEM images of the surface of nanoporous membranes prepared between a pair of glass plates (Fig.3a) and a pair of fluorinated glass plates (Fig.3b). Apparently, neither of the two surfaces is similar to the bulk morphology of the membrane (Fig.2b). The surface in contact with the glass shows a surface with a randomly-distributed nanoporosity, having a pore size of ~ 10 nm and a surface porosity 45% as estimated by image analysis. In contrast, the fluorinated substrate resulted in a flat dense surface with no discriminable in the SEM image. Figure 3c shows a top view of the edge of a nanoporous membrane prepared between the fluorinated substrates. A piece of 'skin' is partially peeled off from the surface showing the same surface feature as seen in Figure 3b. The surface beneath presents a characteristic topological feature of HPL morphology which is the transient morphology between LAM and GYR. A dense skin layer is present on the near surface of the nanoporous membrane prepared with the fluorinated substrates. The entire skin layer might consist of multi sublayers instead of a single uniform layer; the LAM layer is present at the outmost surface followed by the HPL layer. Figure 3d shows cross section near the free surface of a 500 μm nanoporous film solvent-casted in a glass petri-dish, showing a dense skin layer on the near surface in contact with air. The thickness of the skin layer is roughly 30 nm, which gives a thickness estimation of the skin layer in the present work. The periods of both LAM and HPL for the precursor 1,2-PB-*b*-PDMS are ~ 21 nm as determined by SAXS. Therefore the observed average skin layer is equal to 1.5 periods of the precursor HPL (32 nm), or to one PB lamella and one period of HPL (34 nm). For the sake of convenience, the membranes prepared between the glasses are referred to hereafter as non-skin membranes while the membranes prepared between fluorinated glasses are referred to as double-skin membranes. Single-skin membranes are prepared between one fluorinated glass and one glass.

To clarify the observations from SEM, advancing contact angle (CA) measurements were carried out on the surfaces of skin and non-skin membranes before and after PDMS removal. The experimental data are summarized in the first row of Table 1.

Table 1: Experimental and predicted values of advancing contact angle of water on the surface of double-skin and non-skin samples before and after PDMS removal.

	Non-skin		Double-skin	
	X-NS[c]	E-NS[c]	X-S[c]	E-S[c]
θ_{exp}[a] (º)	91.1	107.1	105.6	93.3
θ_{cal}[b] (º)	91.0 / 96.9	114.2	106	91.0

a. The experimental values of advanced contact angle of water on the sample measured;
b. The calculated values of water contact angle based on the observations from SEM, using equation 1;
c. X-NS: cross-linked non-skin samples; E-NS: etched non-skin samples; X-S: cross-linked skin samples; E-S: etched skin samples.

For the double-skin membranes, the CA value of the cross-linked sample (X-S) is similar to the reported value [Ref.9] 106º for pure PDMS; while the CA value from the etched sample (E-S) is close to that of the cross-linked 1,2-PB homopolymer, 91º. It is most likely that only PDMS block segregated on the outmost surface of the X-S sample; accordingly a 1,2-PB layer fully covered the outmost surface of the E-S sample after PDMS removal. For the non-skin membranes, the water contact angle increased from the cross linked sample (X-NS) to the etched sample (E-NS). This might be due to the porous surface (Fig 3a) of the etched sample where air-filled nanopores lowered thesurface energy. In addition, we found that the experimental CA value for the X-NS sample is similar to that of 1,2-PB homopolymer, which may hint to a pure 1,2-PB layer on the outer surface of the X-NS sample. However, due to the experimental uncertainty, we cannot exclude the possibility of PDMS on the outer surface.

The observed surface behavior can be well explained by Cassie's equation, using the information of surface structure from SEM images.

$$\cos\theta_p = f_A \cos\theta_A + f_B \cos\theta_B \qquad (1)$$

where θ_p is the water contact angle of the surface made of A and B. f_A or f_B is the surface fraction of component A or B. In our case, A is 1,2-PB and B is PDMS for the cross-linked samples or air for the etched samples.

The calculated values are given in the second row of Table 1 for an easy comparison with the experimental values. For the X-NS sample, there are two possibilities. (1) The outmost surface is covered by a layer of pure 1,2-PB, then the calculated CA value is 91.0 º; or (2) a calculated CA value of 96.9 º can be derived if we assume coexistence of 1,2-PB and PDMS on the outmost surface with the same ratio as the volume ratio (60% 1,2-PB and 40% PDMS). After PDMS removal, the E-NS sample shows a porous surface with surface porosity of 45% (see fig. 3a). The surface composition of the skin and non-skin samples was further assessed with XPS in Ref. 10. A discussion of the XPS results, their consistency with the results from the other

techniques and the role of the surface energy to the surface morphology are also presented.

We evaluated the outer surface of nanoporous membranes in terms of morphology and composition. It was verified that the glass substrate can generate a porous surface while the fluorinated substrate can produce a dense skin layer on the near surface of the nanoporous membrane. As previously reported [11-12], if one component of any binary fluid mixture has a lower surface energy than the other then the system as a whole may save free energy by having a surface enriched by the lower surface energy component which is higher than the bulk composition. On the other hand, there is a free energy cost associated with creating a surface layer with a different composition to the bulk; meantime an additional unfavorable free energy is also associated with the interface between the surface layer and the bulk material. The equilibrium surface composition and morphology are given by the minimization of the overall system free energy. In our case, the glass substrate showed relative preference toward the 1,2-PB block whereas the fluorinated glass exhibited the higher selectivity to the PDMS block, as confirmed by surface energy measurements [10]. For the cross-linked block copolymer film prepared between the fluorinated substrates, lamellae morphology is stabilized at this interface driven by PDMS coverage of the top surface to minimize the interfacial energy between polymer and fluorinated surface. In the meantime, a HPL layer formed beneath the outmost LAM layer and linked down to GYR bulk. After selectively etching PDMS, the skin layer on the nanoporous membrane is a layer of the cross-linked 1,2-PB with coexistence of the LAM and HPL morphologes in series from the outmost surface. In other words, we can selectively pattern the self-assembled architecture using different substrates. This in turn significantly affects the membrane permeation and separation as demonstrated elsewhere [10].

Conclusions

Nanoporous 1,2-PB membranes with a nanopore of 10 nm was prepared from block copolymer 1,2-b-PDMS, having gyroid nanochannels percolating the overall membrane. We undertook systematic work evaluating the surface of nanoporous membranes in terms of morphology and composition. Two distinct surface morphologies resulted from the substrates selected. A nanoporosity surface can be generated using a glass substrate, while a dense skin layer can be created using a fluorinated substrate.

References

1. D.F. Stamatialis, B.J. Papenburg, M. Girones, S. Saiful, S.N.M. Bettahalli, S. Schmitmeier, M.J. Wessling, Mem. Sci. (3) (2008) 1–34.
2. L. Bazinet, F. Lamarchey, D. Ippersiel, Trends Food Sci. Tech. (9) (1998) 107–113.
3. C. Visvanathan, R.B. Aim, K. Parameshwaran, Crit. Rev. Env. Sci. Tec. (30) (2000) 1–48.
4. K.V. Peinemann, S.P. Nunes, Membrane Technology, Volume 1: Membranes for Energy Conversion. WILEY-VCH Verlag GmbH & Co. KGaA,Weinheim, 2008.
5. F.S. Bates, Annu. Rev. Phys. Chem. (41) (1990) 525–557.
6. M.A. Hillmyer, Adv. Polym. Sci. (190) (2005) 137–181.
7. S. Ndoni, M.E. Vigild, R.H. Berg, J. Am. Chem. Soc. (125) (2003) 13366–13367.
8. M.S. Hansen, M.E. Vigild, R.H. Berg, S. Ndoni, Polym. Bull. (56) (2004) 403–409.
9. J.E. Mark, Polymer Data Handbook, Oxford University Press, 1999.
10. Manuscript in preparation
11. R.A.L. Jones, E.J. Kramer, Polymer 34 (1993) 115-118.
12. C.L. Feng, G.J. Vancso, H. Schnherr, Langmuir 21 (2005) 2356-2363.

Watson Neto
Phone: +45 4525 52958
E-mail: wan@kt.dtu.dk
Discipline: Process Technology and Unit Operations

Supervisors: John M. Woodley
Pär Tufvesson

PhD Study
Started: June 2010
To be completed: May 2013

Development of An Integrated Downstream Processing for Biocatalytic Reactions

Abstract
Chiral amines are important building blocks for pharmaceutical and chemical industries and they can be produced enzymatically with high enatioselectivity using ω-transaminase (EC 2.6.1.18) (ω-TAm). However, the use of this enzyme has some drawbacks such as substrates and products inhibition and unfavorable equilibrium which together limit the process productivity. In order to make its industrial utilization more attractive and efficient, these drawbacks need to be addressed. The aim of this project is to develop process technology for an efficient integrated downstream process for chiral amines, alleviating these drawbacks, hence increasing the process attractiveness.

Introduction
In the past decades the amount of research and publications related to the use of transaminase (ω-TAm) has greatly increased. The potential of this enzyme to synthesize a broad list of products such as amino acids, chiral amines, chiral alcohols, sugars and others with high enatioselectivity and reasonably high reaction rate and stability [1-2], gives it an advantage over the traditional chemical synthesis to produce chemical and pharmaceutical intermediates containing amines and makes this enzyme attractive for industry.

However, despite all the advantages, limiting factors have been reported in reactions using ω-TAm, making its application only possible if such issues are solved. The list includes high product and substrate inhibition, unfavorable equilibrium and low substrates solubility [3].

For instance, in the asymmetric synthesis of (*S*)-(-)-α- methylbenzylamine (MBA) using isopropylamine (IPA) as amine donor and the acetophenone (APH) as amine acceptor (Fig. 1), both APH and MBA cause severe inhibition to the enzyme, negatively affecting the reaction rate. Furthermore, this reaction is also more favorable in the reverse direction which limits the production of MBA. A common strategy normally used to alleviate this issue is to use an excess of one of the substrates [4], for instance, using 200-1000 excess of IPA.

Another strategy to improve the productivity in this process is to solve the substrate and product inhibition and this can be achieved applying controlled supply of the inhibitory substrate, ensuring that it is present in non toxic concentrations and remove the inhibitory product as soon as it is formed in the reactor, respectively.

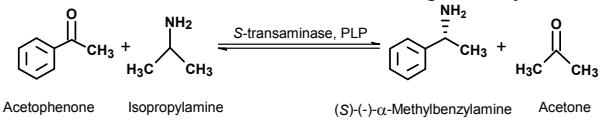

Figure 1: Transamination catalyzed by ω-transaminase.

The last strategy has the advantage of both alleviating the inhibition caused by the product and at the same time shifting the equilibrium towards the products formation.

In situ product removal (ISPR) can play an important role in increasing the productivity in transaminase catalyzed reactions.

Specific objectives
The aim of this project is to develop process and technology for production and efficient integrated separation and purification of chiral amines, alleviating the unfavorable equilibrium, substrate and product inhibition present. The project is divided in three main topics.

Integrated downstream processing:
Development of tools to recover the product while the reaction takes place (using *e.g* resins, solvents or membranes), working as strategy to increase the

productivity by both shifting the equilibrium towards the desired direction and controlling product inhibition;

Design of the reactor set up:
Applying ISPR will visually imply design of the reactor set up. Conditions have to be made to make possible the application of the recovery method. Decisions have to be made concerning to the location of the recovery method (e.g inside the reactor or outside), the location and formulation of the biocatalyst (e.g free or immobilized cells, inside or outside the tank) etc. Figure 2 A and B compare two possible alternatives set up that will be tested in the lab. In A, immobilized cells are used in a column and the reaction media is pumped from the reservoir to the cells column and the resulting product is later recovered in a resin column or solvent reservoir. In B, a fed batch reaction is applied with the biocatalyst located inside the tank. Continuously the reaction mixture is pumped towards the recovery column after a biocatalyst separation step.

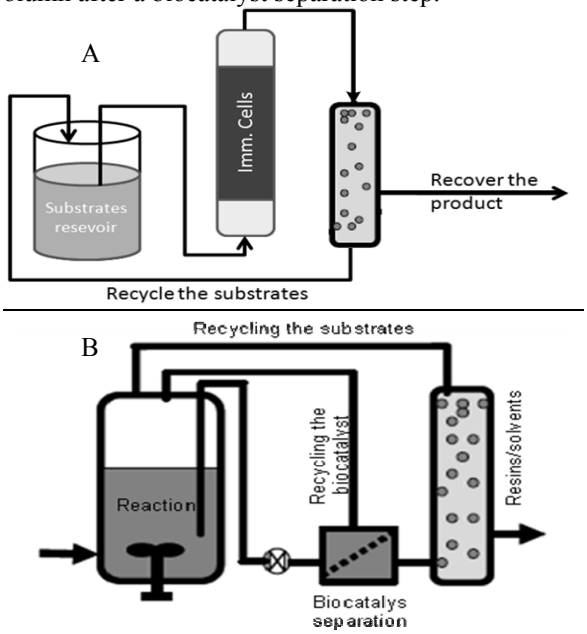

Figure 2: Strategies for ISPR (A and B)

Process scale up:
The most promising set up obtained in the lab will be scaled up to 1L in order to test the operability of the developed method at a larger scale.

Results and Discussion
In order to quantify the level of inhibition present in the process presented in Figure 1, the effect of increasing concentrations of the substrate and products were analyzed and Figure 3 A and B summarize these results.
It was found that increasing concentrations of IPA plotted against initial rate gives a typical Michaelis-Menten curve (*not shown*), while increasing concentrations of APH reveals an inhibitory profile, with the rate dropping after achieving a maximum value (Fig 3.A).

Increasing concentrations of the product MBA reveals also an inhibitory pattern with the reaction rate continuously dropping (Fig. 3B). These results strengthen the importance of applying ISPR as well as controlled supply of substrate in this process.

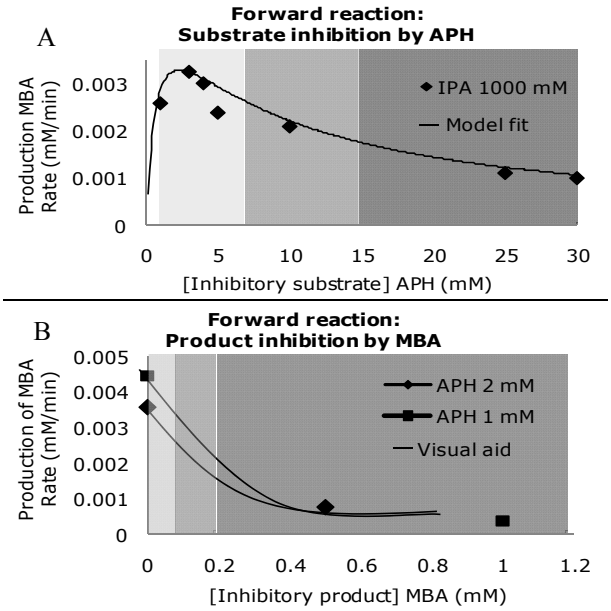

Figure 3: Substrate (A) and Product (B),
≤ 20% inhibition 20% to 50% inhibition ≥50% inhibition

Conclusions
The current research shows the important role that ISPR can play in the transaminase catalyzed processes. The process productivity can be improved by removing the inhibitory product, which will also be reflected in process economics, since fewer steps will be required in the downstream processing. Different alternatives (discussed in the "Specific objectives") will be tested to achieve the desired effect.

Acknowledgements
The student acknowledges the support from BIOTRAINS Marie Curie ITN, financed by the European Union through the Seventh Framework People Programme (Grant Agreement no. 238531).

References
1. J.S. Shin, B.G. Kim, A. Liese, C. Wandrey, Biotechnol. Bioeng. 73 (3), (2001) 179-87.
2. B.Y. Hwang, B.K. Cho, H. Yun, K. Koteshwar, B.G. Kim, J. Mol. Catal. (37) (2005) 47-55
3. J.S. Shin, B.G. Kim, Biotechnol. Bioeng. 60 (5) (1998) 534-540.
4. D. Koszelewski, D. Clay, K. Faber, W. Kroutil, J. Mol. Catal. B-Enzym. 60 (2009) 191–194.

Joana de Lima Ramos
Phone: +45 4525 2990
E-mail: jlr@kt.dtu.dk
Discipline: Process Technology and Unit Operations

Supervisors: John M. Woodley
Pär Tufvesson

PhD Study
Started: March 2010
To be completed: March 2013

Guiding Biocatalytic Processes Improvements Using Engineering Evaluation Tools

Abstract
Biocatalysis is an emerging area of technology and to date few reports have documented the economics or environmental input of such processes. As a relatively new technology many processes do not immediately fulfill the economic and environmental requirements for commercial operation. Hence early stage economic and environmental assessment could be powerful tools to guide research and development activities in order to achieve commercial potential.

Introduction
During the development of a biocatalytic process (such as biocatalytic synthesis of chiral amines by transaminases) and in particular during its scale-up, there are some required considerations. Two of the most important are the economic and environmental profile. The present project will be focused on the development of engineering tools in order to assist a fast and accurate economic and environmental analysis. When applied to a given process these have a decisive role in helping to identify bottlenecks in the process development, and to justify where to put effort and resources.

The outcome of the proposed research will establish new tools and knowledge useful in biocatalysis and (bio-)process development. The research will be divided in two different sections: process evaluation (both economic and environmental) and experimental assessment.

The process evaluation (including tool development and validation) will be performed on the ω-transaminase case-study (TAm) for synthesis of chiral amine, as a case study.

Transaminases have received much attention as suitable biocatalysts for producing these amines by either direct asymmetric synthesis from pro-chiral ketones or by kinetic resolution of racemic amines. Chiral amines are key building blocks for many new pharmaceuticals. Despite the great effort that has been put into developing effictive means for its chemical synthesis, the efficient synthesis of chiral amines still remains a challenge. Transaminases have emerged recently as alternative candidate to the chemical synthesis, since these enzymes catalyze the transfer of an amino ($-NH_2$) group from an amine donor, usually an amino acid or a simple amine such as isopropylamine, to a prochiral acceptor ketone, yielding a chiral amine as well as a co-product ketone or alpha-keto acid.

In spite of the many attractive features of transaminase catalyzed reactions, there are still a number of challenges that need to be dealt with in order make transaminase processes competitive for a wider range of amines. Guidelines for a successful biocatalytic production of chiral amines will be identified through process economic and environmental assessment.

Specific objectives
The project objectives are:

- Develop a fast and accurate tool that allows process evaluation, integrating process modeling and process evaluation (economic and environmental analysis).
- Application of the proposed tool using a specific model process: synthesis of phenyl amines using the biocatalyst TAm.
- Revision and application of the developed tool using case studies provided by industrial partners.
- Bottleneck identification of the model process, followed by solutions suggestions.

Evaluation tools, which are built on top of the developed model, have as an output on economic and environmental evaluation of a given process. The economic and environmental analysis obtained will allow the identification of process bottlenecks leading to several solution suggestions (Figure 1).

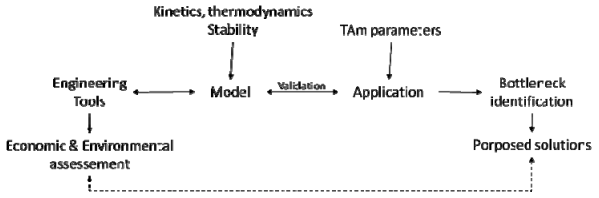

Figure 1: Methodology for the engineering tool use for process evaluation.

Methodology for cost estimation

Cost estimation can be divided into two categories: capital investment (CapEx) and operation cost (OpEx), see Figure 2.

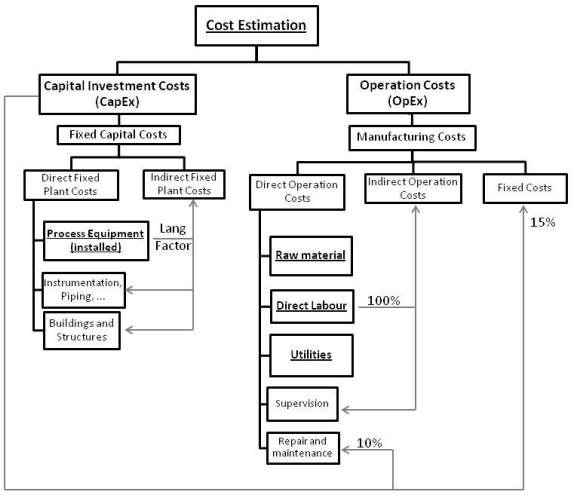

Figure 2: Cost estimation categories and sub-categories that are important for cost analysis. Underlined costs are calculated separately, while the other costs are estimated through the first ones, represented here with grey lines [1].

Fixed capital represents the capital necessary for the installed process equipment with all the accessories needed for the process start-up and operation [2,3].

The operating (or manufacturing) cost consists of direct, indirect and fixed OpEx. Direct operating costs includes the cost of raw materials, utilities, waste management and operating labor. Other direct operating costs (i.e. indirect and fixed operating costs) can be calculated from direct labor cost and/or annual capital investment cost [2,3].

Production cost for biocatalytic processes

To determine the productivities required in a biocatalytic process that match a reasonable cost contribution of the biocatalyst, the manufacturing cost of the catalyst needs to be calculated. Here, these calculations have been divided into three main sections: fermentation, purification and immobilization (see Figure 3). The influence of the costs on scale, accounting and process parameters will be also analyzed.

The study will show and rank the factors that work together determining the cost of the biocatalytic product. In the first step of the production (fermentation), the enzyme titer is crucial; a product yield in the gram per liter range is required to avoid excessive costs. Furthermore, any purification steps might also increase the production costs within an order of magnitude. While in the reaction step, parameters as the biocatalytic productivity (g product/e enzyme) might affect greatly the cost [1].

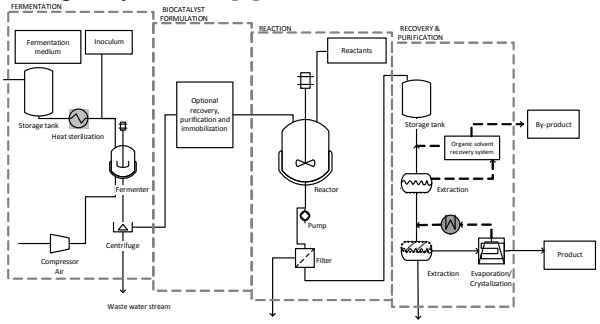

Figure 3: Example of a biocatalytic process, including biocatalyst production (fermentation and biocatalyst formulation), biocatalysis (reaction) and down-stream processing (recovery and purification)

As with any new technology, a cost-benefit analysis has to be performed to weigh the added cost of the biocatalyst and associated with the value of the process improvements [1]. In a biocatalytic process, direct development of the catalyst specifically for the reaction of interest is frequently required. However, some industries (such as the pharmaceutical industry) cannot always afford time-consuming research on protein development, and the possibility for process development is limited. This PhD-project aims the development a fast method to assess costs, environmental constrains, set guidelines for biocatalytic process, and in a later stage to quantify the development efforts needed.

Acknowledgements

The author would like to acknowledge the support from BIOTRAINS Marie Curie ITN, financed by the European Union through the 7th Framework people Programme (Grant agreement no.: 238531).

References

1. P. Tufvesson, J. Lima-Ramos, M. Nordblad, J.M. Woodley, Org. Process Res. Dev. DOI 10.1021/op 1002165
2. M.C. Flickinger, S.W. Drew, Encyclopedia of Bioprocess Technology-Fermentation, Biocatalysis, and Bioseparation, Wiley, New York, 1999
3. M.S. Peters, K.D. Timmerhaus, Plant Design and Economics for Chemical Engineers, McGraw-Hill, New York, 1990

Philip Lutze
Phone: +45 4525 2960
E-mail: pil@kt.dtu.dk
Discipline: Process Technology and Unit Operations
Systems Engineering
Supervisors: John M Woodley
Rafiqul Gani

PhD Study
Started: December 2008
To be completed: November 2011

Development of a Systematic Synthesis/ Design Methodology to Achieve Process Intensification

Abstract
In order to improve processes incorporating process intensification (PI), a systematic synthesis/ design methodology has been developed and successfully applied to several examples [1, 2] using existing PI technology. In order to make improvements going beyond pre-defined unit operations, the process has to be viewed at a lower scale of aggregation, namely the phenomena scale. Hence, current research is to develop a systematic approach for aggregating processes through phenomena building blocks. First, all potential phenomena are identified, and then synthesized to phenomena-based flowsheets which are then screened against pre-defined constraints before the most promising options are identified, optimized and verified at the unit operation level.

Introduction

PI has attracted considerable interest as a potential means of process improvement and to meet the increasing demands for sustainable production. PI aims to improve processes without sacrificing product quality by increasing efficiency, reducing energy consumption, costs, volume, and waste as well as improving safety.

PI can be defined as the improvement of a process by adding/enhancing phenomena in a process through the integration of operations, integration of functions, integration of phenomena and/or through the target enhancement of phenomena in a given operation [1].

Examples of already developed PI equipment are given in the following Table 1.

Table 1: Examples for PI equipment with respect to the definition of PI.

Principle	Examples of PI Equipment
Integration of operation	Reactive distillation, distillation-pervaporation.
Integration of functions	Heat-exchange reactor, static mixer reactor.
Integration of phenomena	Spinning disc reactor, static mixer.
Target enhancement of phenomena	Micro mixer, micro reactor

One of the most prominent is the reactive distillation in which the reaction and the distillation are integrated internally. Reported case-based improvements have been economical and environmental, mostly reported for equilibrium limited exothermic reactions and close boiling point mixtures [3].

In previous work [1,2], we reported the development of a general computer-aided systematic synthesis and design methodology incorporating PI. Even though, process improvements were achieved, this methodology is limited to pre-defined PI unit operations which are retrieved from a knowledge base tool.

In the next step now, in order to invent new unit operations, going beyond those currently in existence, to achieve potentially even higher improvements, the process should be viewed at a lower level of aggregation [4, 5]. The similarity of the structure of flowsheets and molecules has been reported before [6] comparing molecules to processes and groups in molecules to unit operations respectively. This analogy can be extended through phenomena since they can be compared to atoms. That is, different combinations of phenomena lead to different characteristics/ performances and therefore to different physical unit operations/ flowsheets, just as different combinations of atoms lead to different molecules with different characteristics/performances. Hence, to extend the search space for process improvement, process synthesis and design incorporating PI needs to be investigated at the phenomenological level.

Table 2: Examples of direct connectivity between phenomena building block (EQ: Equilibrium, Hom: Homogeneous, V: Vapor, L: Liquid).

		Second (following) phenomena block			
		Mixing	Reaction	Phase enabling-contact	
First phenomena block		Ideal	Hom. $A \leftrightarrow B$	V-L (EQ)	L-L (EQ)
Mixing	Ideal	Yes	Yes	Yes	Yes
Reaction	Hom. $A \leftrightarrow B$	Yes	Yes	Yes depending on the system	
Phase enabling - contact	V-L (EQ)	Yes	Yes	No	No
	L-L (EQ)	Yes	No	Yes	No

Specific Objectives

The specific objectives of this project are:

- Development of a general systematic synthesis/ design methodology to achieve PI
- Development of a systematic synthesis/ design approach to go beyond predefined PI unit operations by looking at the phenomena level
- Test/ validate methodology through several case studies
- Development/ Implementation of the computer-aided methodology into a software environment

General Phenomena- based Synthesis Framework

The developed phenomena-based synthesis and design approach is based on two contributions: a) the use of phenomena building blocks together with connection equations to represent a process; b) the use of a methodology for identification, generation and screening of phenomena-based flowsheets that systematically reduces the search space for the optimal solution.

Phenomena building blocks consist of mass, component, energy and momentum balances as well as constraint equations describing the phenomenon and the inlet and outlet stream conditions. In general, phenomena building blocks can be classified by the number of distinct phenomena involved which are further sub-classified into mixing, stream dividing, phase enabling and phase contact, reaction and energy transfer phenomena. One-phase mixing phenomena have minimum one inlet stream and one outlet stream while dividing phenomena have one inlet and minimum two outlet streams. Reaction blocks are defined to have one inlet and one outlet stream. Phase enabling blocks have one inlet and the number of outlets is given by the number of phases enabled in this block. All outlets of the phase enabling block have to become an inlet of a phase contact phenomena building block in which the number of outlet streams depends on the number of moving phases. Between phase enabling and phase contact building blocks, phenomena describing the behavior of the phases such as mixing are needed. Energy transfer phenomena are defined to have either one inlet and one outlet, for example in conductive heat phenomena, or two inlet and two outlet streams, for example in convective heat transfer phenomena in which the streams are not in contact.

Phenomena blocks can be connected through the use of suitable connection rules. For example, an ideal mixing block can be connected to any building block while a connected vapor-liquid equilibrium phase enabling-contact block cannot because it requires an inlet stream with a two-phase mixture (see Table. 2). Another example of a connection rule is that a liquid-liquid equilibrium phase enabling-contact phenomenon should come before an equilibrium vapor-liquid phase enabling-creation block since the vapor is in equilibrium with each of the two liquid phases and not with the total liquid mixture.

In order to use this developed phenomena-based concept to synthesize new processing units and to manage the potentially high number of options in which the optimal has to be identified, a systematic synthesis and design methodology is proposed.

This methodology follows a stepwise hierarchical decomposition in which the lower level steps employ simple and easy calculations, while the higher level steps employ more and more rigorous and detailed calculations (see Figure 1).

First, the scenario, the goal and the constraints of the synthesis/ design problem and a performance metrics are defined. Second, the system is analyzed with respect to pure component, mixture and reaction properties to identify a set of phenomena building blocks that may be used in the processing steps of a flowsheet. These are retrieved from a phenomena building block library.

Third, the identified phenomena building blocks are connected using the general connectivity rules (see Table 2) resulting in a superstructure. The superstructure may represent a large number of alternatives from which redundant options are removed through structural constraints. Fourth, the remaining alternatives are screened out through pre-defined operational constraints and benchmarked through performance metrics. Fifth, for each of the remaining phenomena-based flowsheet alternatives, currently available or novel unit operations are identified, assisted by algorithms or a library of pre-defined units. Linking the phenomena to the actual physical unit is important since additional constraints related to physical units

such as wall boundary conditions need to be introduced. The performance criteria may be revised in this step for subsequent optimization of the most promising alternatives and verification by rigorous simulation and experimentation in the last step.

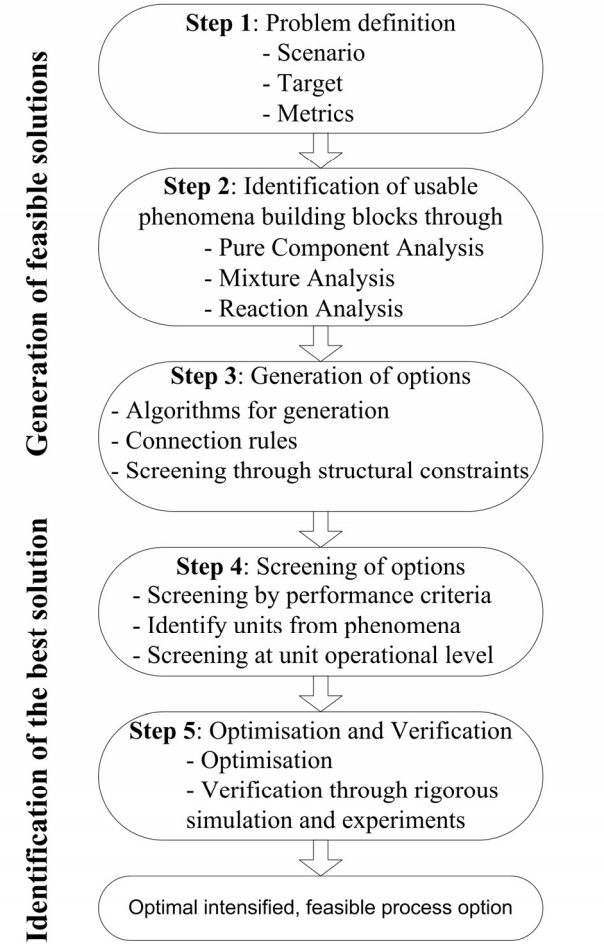

Figure 1: Workflow for the phenomena-based synthesis and design to achieve PI.

Results and Discussion

The key steps of the phenomena-based synthesis and design methodology are highlighted through a case study involving the production of isopropyl-acetate from isopropanol and acetic-acid. The liquid-phase reaction is catalyzed by Amberlyst 15 and follows the stoichiometry:

$$CH_3COOH + C_3H_7OH \leftrightarrow C_5H_{10}O_2 + H_2O \qquad (1)$$

In step 1, the scenario is restricted to the reaction step of the continuous production of isopropyl-acetate. Downstream-processing of the product is not part of the case study here. As objective function, the total annualized costs including operational costs (energy and raw material (RM)) and annualized capital costs (CC) are set as the target (Equation 2). Additionally, a simple performance metrics, such as the yield and the number of units is selected for comparison and evaluation of alternatives.

$$F_{Obj} = TAC = \sum \left(C_{RM} + C_{Energy} \right) + C_{CC} \,/\, years_{Payback} \qquad (2)$$

In step 2, pure component and mixture analysis is performed using ICAS [7]. The operational window of the liquid phase reaction, lies between the lowest boiling point, that is the temperature (347.34 K) of the ternary azeotrope of isopropanol, isopropyl-acetate and water at P=1atm and the highest melting point, that is the melting point temperature (289.8 K) of acetic acid at P=1atm. A phase split was not determined. The reaction analysis based on kinetics from Sanz and Gmehling (2006) [8] confirmed the exothermic irreversibility and the equilibrium limitation of the reaction (K>1). Since, Amberlyst 15 was used as a catalyst the maximum allowable temperature to avoid catalyst degradation was set at 403K.

With this accumulated information, the following phenomena were identified: mixing (ideal), dividing phenomena, heating/ cooling (countercurrent, co-current, conductive), heterogeneous reaction and phase contact. Additionally, from the analysis of ratios of pure component properties, phase enabling phenomena for separation of products from reactants are identified (Table 3) such as VL separation through evaporation (boiling points) or pervaporation (radius of gyration).

For purposes of illustration, only phase enabling through pervaporation, ideal mixing, heating/cooling (countercurrent), phase contact until equilibrium between ideally mixed phase is reached, dividing and pseudo-homogeneous reaction in which the transport to the catalyst is not taken into account, are considered in the search space of phenomena. The pervaporation phenomenon is described by a flux equation [8] and the heat of vaporization necessary for the phase creation is introduced into the energy balance. Also, an additional constraint equation is necessary to assure that the liquid outlet stream is not freezing.

Table 3: Normal property ratios between products and reactants

Binary mixture	Boiling point	Melting point	Dipole moment	Radius of gyration	Molar volume
Water/ Acetic Acid	1.05	1.06	1.06	4.24	3.21
Water/ Isopropanol	1.05	1.47	1.11	4.56	3.94
Acetic Acid/ Isoproyl acetate	1.08	1.45	1.01	1.41	1.87
Isopropanol/ Isopropyl acetate	1.02	1.08	1.05	1.31	1.53

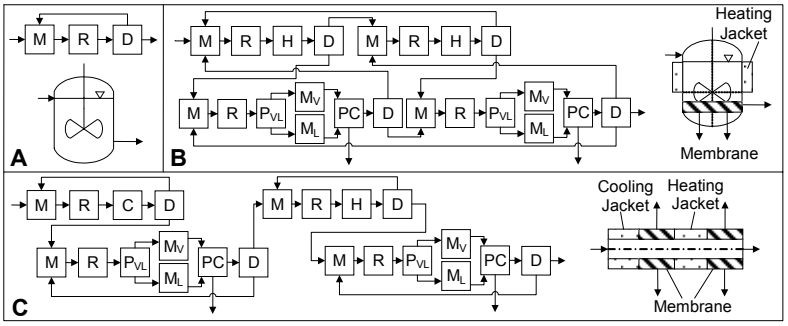

Figure 2: Examples of identified units from generated phenomena-based flowsheets: A: single phase CSTR, B: CSTR with integrated heating jacket and membrane, and C: integrated membrane, thermal controlled tubular reactor. Phenomena: Ideal mixing M, Reaction R, Phase enabling by pervaporation P, Phase contact PC, Heating H, Cooling C and Dividing D. Phases: Vapor V, Liquid L. Utility streams are not shown.

In step 3, the phenomena were connected to form phenomena-based flowsheets using connectivity rules. For example, outlet streams of a dividing phenomenon have to leave the system as a product or have to be connected to a mixing phenomena block. More examples for connectivity rules are presented in the previous section and in Table 1. Additional, structural constraints were added for the phenomena-based flowsheet generation (such as, the presence of at least one reaction phenomenon and a maximum of four reaction phenomena in one flowsheet). Examples of four generated phenomena-based flowsheets from step 3 and the corresponding identified physical units in step 4 are illustrated in Figure 2. A uniform single phase CSTR was identified through a series of a mixing, reaction and a dividing phenomenon while a single phase CSTR divided into four compartments was identified in which neighboring compartments are linked (outlet stream of a dividing phenomenon becomes the inlet stream of a mixing phenomenon). A tubular reactor was identified as consisting of at least three ideal mixing and reaction phenomena in series. A heating jacket around a reactor part is characterized by a heating phenomenon following a reactor in a recycle. Since the no connections to other compartments in parallel are made, the simultaneous heating and reaction module is isothermal.

In step 4, the performance of the phenomena-based flowsheet options was compared against product yield (Equation 3) and the number of unit operations (see Table 4). Ideally, assuming indefinite volumes and equimolar feed, alternatives B and C were found to be equally good (see Table 3) since both options potentially achieve a yield of 0.99 in one single unit.

$$\eta = \dot{n}_{product} / \dot{n}_{isopropanol} \qquad (3)$$

Table 4: Benchmarking results of three examples (Assumption: equimolar feed)

Option	Yield	Number of units
A	0.74	1
B	0.99	1
C	0.99	1

In step 5, the most promising alternatives were optimized with respect to the objective function (Equation 2) and verified through simulation.

Conclusions

A phenomena-based methodology for synthesis and design to achieve process intensification in (bio)chemical processes has been developed and tested through a conceptual case study. It is necessary to achieve PI without pre-defined unit operations in order to achieve even higher benefits in the performance of a process through process intensification. The advantage of this approach is that it generates potentially novel process options (truly predictive models lead to reliable predictive solutions) as well as the simultaneous development of the necessary process models. The obtained results are promising and further development of this approach together with the necessary algorithms and tools needed for each step of the methodology is current and future work.

Acknowledgements

The author wishes to thank the Technical University of Denmark for financial support.

List of publications

1. P. Lutze, R. Gani, J.M. Woodley, Chem. Eng. Process. 49 (6) (2010) 547-558.
2. P. Lutze, A. Roman-Martinez, J.M. Woodley, R. Gani, Comput. Chem. Eng. Submitted (2010).
3. P.Lutze, E.A. Dada, R. Gani, J.M. Woodley, Rec. Pat. Chem. Eng. 3 (3) (2010) 208-229.

References

1. K.P. Papalexandri, E.N. Pistikopoulos, AIChE J. 42 (4) (1996) 1010-1032.
2. H. Freund, K. Sundmacher, Chem. Eng. Process. 47 (12) (2008) 2051-2060.
3. L. d'Anterroches, R. Gani, Fluid Phase Equilibr. 228-9 (2005) 141-146.
4. R. Gani, G. Hytoft, C. Jaksland, A.K. Jensen, Chem. Eng. 21 (10) (1997) 2822-2841.
5. M.T. Sanz, J. Gmehling, Chem. Eng. J. 123 (2006) 9-14.

Karin Madsen
Phone: +45 4525 2826
E-mail: kam@kt.dtu.dk/kama@topsoe.dk
Discipline: Reaction and Transport Engineering

Supervisors: Anker Degn Jensen
Flemming Frandsen
Joakim Reimer Thøgersen, Haldor Topsøe

Industrial PhD Study
Started: May 2008
To be completed: May 2011

Mercury Chemistry in Flue Gas

Abstract
The speciation of mercury in flue gases from combustion processes is important to understand in order to optimize the mercury removal in the flue gas cleaning equipment. Mercury in oxidized form favors a high degree of removal, because $HgCl_2$ is soluble in water and is effectively removed in a wet scrubber. The vanadium-based selective catalytic reduction (SCR) catalyst has been shown to have catalytic activity on mercury oxidation. This project is devoted to examining the catalytic oxidation of mercury across the SCR catalyst.

Introduction
Mercury emissions from coal-fired utility plants range from 1-20 $\mu g/Nm^3$ depending on the type of coal applied, the flue gas composition, operating conditions and the air pollution control devices (APCDs) [1].

Three mercury species are normally considered: elemental Hg^0, oxidized Hg^{2+} and particle bound Hg^p. It is important to understand the speciation of mercury in flue gases in order to optimize the mercury removal in the flue gas cleaning equipment. Oxidized mercury is soluble in water and is effectively removed in a wet scrubber or by adsorption on fly ash in fabric filters. Elemental mercury is in contrast difficult to capture in existing APCDs due to its high volatility and low solubility.

Coal mercury is converted to gaseous Hg^0 in the combustion flame and is subsequently partially oxidized as the combustion gas cool. According to thermodynamic calculations all mercury should exist in the oxidized form for temperatures lower than 400°C [2]. Various full-scale and laboratory measurements show that the fraction of oxidized mercury ranges from 35-95% in flue gases, which indicates that the conversion is kinetically controlled [1].

Mercury chlorination ($HgCl_2$) is generally considered to be the most dominating mercury transformation mechanism. The degree of mercury oxidation is also strongly correlated with the chlorine content in the coal, but many other parameters have been demonstrated to influence the mercury speciation. A fundamental understanding of the reactions taking place in the flue gas is needed in order to predict the mercury speciation.

International research of this type is under way and can generally be broken down into the study of homogeneous gas-phase reaction during quenching of the flue gas and heterogeneous gas/solid reactions with the fly ash. Furthermore, the vanadium-based selective catalytic reduction catalyst (SCR) has been shown to have catalytic activity on the mercury oxidation [3,4].

Specific Objectives
The current PhD-project is devoted to examining the mercury oxidation across SCR catalyst.

The mechanism for the catalytic oxidation across the SCR is not fully understood. In both lab- and full-scale experiments, a positive effect of chlorine and an inhibitory effect from ammonia has been reported [3,4]. However, the influence of other flue gas constituents and also of operating conditions is not as unambiguously reported in literature. A better understanding of this complex interplay is needed in order to optimize the oxidation.

Methodology
The catalytic reaction is being studied in a laboratory setup at Haldor Topsøe A/S. Here a simulated flue gas containing Hg^0 is passed through a SCR-reactor. The influence of flue gas constituents (such as HCl, SO_2, NO, NH_3, O_2 and H_2O) and also operating conditions (such as temperature, space velocity and catalyst age) are being examined.

Full-scale experiments have been carried out at Plant Crist in Pensacola, Fl, where the mercury conversion across an SCR catalyst was measured in a slipstream facility.

Kinetic and thermodynamic modeling is being performed based on this data in order to get a better understanding of the mechanism for mercury oxidation on the catalyst.

Results and discussion

In the given laboratory set-up the positive effect of chlorine and an inhibitory effect from ammonia on mercury oxidation as previously discussed have been confirmed.

The first round of laboratory experiment has been run for a simple flue gas containing 7 µg/Nm3 Hg^0, 2%O_2, 2 %H_2O and balance N_2. The SCR catalyst in these laboratory experiments has the effect of rendering the mercury speciation at the outlet close to equilibrium. Yet in the pilot-scale scale experiments, mercury in the flue gas does not appear to come as close to equilibrium. This is in line with data seen from other laboratory experiments [5].

Figure 1 shows the conversion of elemental mercury across SCR catalysts for increasing HCl-concentration for laboratory experiments at Haldor Topsoe A/S and for pilot-scale experiments at Plant Crist.

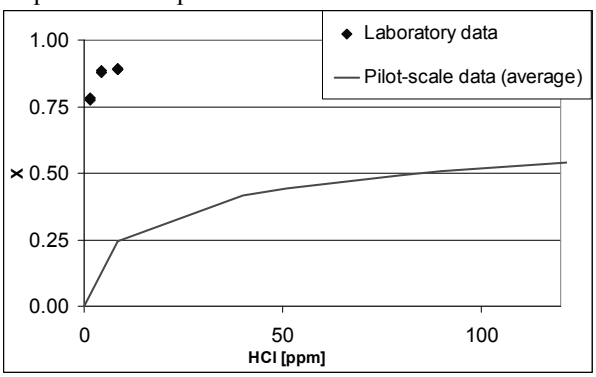

Figure 1: Oxidation of elemental mercury across commercial SCR catalysts for T=350-370ºC.

The pilot-scale experiments are carried out in a real flue gas from subbituminous coal combustion. The difference in catalyst activity is expected to be due to components in the real flue gas that are influencing the mercury chemistry, which are not present in the simple simulated flue gas, such as fly ash.

The gap between laboratory and pilot-scale data was further examined. Figure 2 shows the catalyst activity for increasing water concentration with/without a concomitant NOx-reduction with NH_3 (DeNOx) Data show that the mercury oxidation is greatly inhibited by the combination of an elevated water concentration (H_2O=10%) and the DeNOx-reaction at 250 ppm NO and NH_3. However, a factor 5 difference in catalyst activity remains between laboratory and pilot scale.

The effect of SO_2 and CO was also tested at concentrations up to 500 ppm. These components only had minor effect on the mercury oxidation in the presence of HCl. The effect of fly ash on mercury oxidation across SCR catalyst is indeed relevant and is at present the most likely source for the remaining gap between scales. Unfortunately, the current laboratory setup is not applicable for testing with fly ash and so the matter has not been explored further in this study.

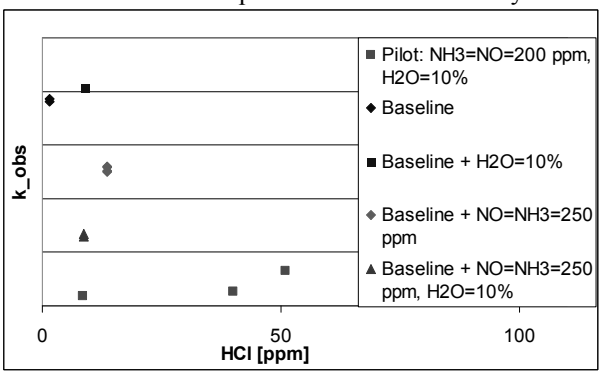

Figure 2: Comparison of catalyst activity (Nm/h) in pilot scale and laboratory experiments with the baseline flue gas Hg^0=7µg/m^3, O_2=2%, H_2O=2% and balance N_2.

Conclusion

An increased understanding of the mercury oxidation across the SCR catalyst can potentially be a means of optimizing the mercury removal from flue gasses in existing air pollution control devices.

The current study identifies a synergistic inhibition of H_2O and the DeNOx reaction on the catalytic mercury oxidation. Future work will further decouple the effect of various components on the mercury oxidation across SCR catalyst.

The quantitative use of laboratory data for predicting mercury oxidation across full-scale installations of SCR reactors remains limited, since experiments based on a simulated flue gas does not reproduce the degree of mercury oxidation found in real flue gases. Future studies should aim at identifying the source to the gap between lab- and full-scale mercury oxidation degrees.

Acknowledgments

The project is financially support by Haldor Topsoe A/S and the Danish Agency for Science, Technology and Innovation. The author acknowledges her supervisors for their help and patience: Joakim Reimer Thøgersen, Anker Degn Jensen and Flemming Frandsen.

References

1. J.H. Pavlish, E.A. Sondreal, M.D. Mann, E.S. Olson, K.C. Galbreath, D.L. Laudal, S.A. Benson, Fuel Process. Technol. 82 (2003) 89-165.
2. F. Frandsen, K. Dam-Johansen, P. Rasmussen, Prog. Energ. Combust. 20 (1994), 115-138.
3. R. Meij, L.H.J. Vredenbregt, H. te Winkel, Air & Waste Management Association 52 (2002), 912-917.
4. Pilot-scale screening evaluation of the impact of selective catalytic reduction for NOx on mercury speciation, EPRI, Palo Alto, U.S. Department of Energy, Morgantown, Wv, and U.S. Environmental Protection Agency, Raleigh, NC: 2000. 1000755.
5. Communication with C. Senior (2004), Reaction Engineering International, Salt Lake City, UT.

Bjørn Maribo-Mogensen
Phone: +45 4525 2869
E-mail: bmm@kt.dtu.dk
Discipline: Engineering Thermodynamics

Supervisors: Georgios Kontogeorgis
Kaj Thomsen

PhD Study
Started: August 2010
To be completed: August 2013

Development of an Electrolyte CPA Equation of State for Applications in the Petroleum and Chemical Industries

Abstract
Complex mixtures of associating/polar components and electrolytes are often encountered in the oil- and gas and chemical industry. It is important to be able to adequately describe the phase behaviour of these mixtures e.g. in order to reduce the environmental impact of natural gas processing, to optimize the performance of CO_2 capture and sequestration, and to improve purification of complex chemicals in the pharmaceutical and biochemical industries. This PhD project works on developing a new equation of state for modelling phase behaviour of complex mixtures containing electrolytes.

Introduction
Complex mixtures of associating/polar components and electrolytes are often encountered in the oil- and gas and chemical industry. It is well-known in the oil- and gas industry that electrolytes have a substantial effect (typically decreasing) on e.g. solubilities of gases in water-hydrocarbon mixtures (salting-out effect), and furthermore, the presence of electrolytes may enhance the inhibitory effect of methanol and glycol on the formation of gas hydrates in natural gas pipelines, thus allowing for problem-free flow. In the pharmaceutical and biochemical industry, electrolytes, associating and polar compounds are present during downstream processing. Electrolytes are also very important to the energy industry e.g. with regards to wet flue gas desulphurization or CO_2 capture from power plants using aqueous solutions of alkanolamines.

Despite their great importance, thermodynamic models have been *separately* developed over the last years for hydrogen bonding mixtures e.g. water-alcohol-hydrocarbons and for salt-solutions e.g. NaCl-water, but *few* systematic approaches have been proposed for mixtures which contain both polar compounds and salts or other electrolytes. Many of the proposed models have an overwhelming number of parameters and they have not been tested with practical multi-phase mixed solvent systems that are of interest to the oil- and gas industry.

Theoretical Background
The most widely used thermodynamic models are the cubic equations of state (EoS) such as Soave-Redlich-Kwong (SRK), where the liquid-vapor equilibrium is modeled using Eq. (1) [1, p. 42]:

$$P = \frac{RT}{V_m - b} - \frac{a(T)}{V_m(V_m + b)} \quad (1)$$

Where P is the pressure, T is the temperature, V_m is the molar volume and the parameters a and b are calculated from pure component parameters using e.g. the van der Waals mixing rules shown in Eqs. (2)-(3):

$$a = \sum_i \sum_j x_i x_j \left[a_i(T) a_j(T)\right]^{0.5} \left(1 - k_{ij}\right) \quad (2)$$

$$b = \sum_i \sum_j x_i x_j \left(\frac{b_i + b_j}{2}\right) \quad (3)$$

While the cubic EoS performs well for predicting vapor-liquid equilibrium at both high and low pressures for simple compounds such as hydrocarbons, it is usually not applicable to mixtures containing polar or associating compounds, especially for multicomponent mixtures. Despite the shortcomings, cubic EoS are the most widely used due to e.g. their relatively simple implementation and large parameter databases. Additionally, advanced mixing rules for the equation parameters can yield much better agreement with experimental data.

The cubic EoS gives a macroscopic description of repulsive and attractive intermolecular forces. Through the Helmholtz energy it is possible to extent the EoS to incorporate new terms that describe other intermolecular forces, such as association (hydrogen bonding) and electrostatic interactions as illustrated by Eq. (4):

$$A^r = A^r_{SRK} + A^r_{Association} + A^r_{Electrostatic} \quad (4)$$

Other physical properties can be determined from derivatives of the Helmholtz energy – e.g. is it possible to calculate the pressure using Eq. (5):

$$P = \frac{RT}{V_m} - \left(\frac{\partial A^r}{\partial V}\right)_{T,\underline{n}} \quad (5)$$

The association term is calculated using a model for the hydrogen bonding. A popular model originates from the perturbation theory of SAFT (Statistical Associating Fluid Theory) where the association energy is expressed as Eq. (6) [1, p. 202]:

$$\frac{A^r_{Association}}{RT} = \sum_i^{comp.} x_i \left[\sum_{A_i}^{assoc.\ sites} \left(\ln X^{A_i} - \frac{X^{A_i}}{2} \right) + \frac{1}{2} M_i \right] \quad (6)$$

In which M_i is the number of association sites on a molecule and X^{A_i} is the fraction of component i not bonded at site A, which can be calculated from Eq. (7):

$$X^{A_i} = \left(1 + \sum_j^{components} \rho_j X^{B_j} \Delta^{A_i B_j} \right)^{-1} \quad (7)$$

Where $\Delta^{A_i B_j}$ is the association strength between site A on molecule i and site B on molecule j.

The long-range electrostatic interactions can e.g. be modeled using the Debye-Hückel expression given by Eq. (8) [1, p. 470]:

$$\frac{A^E}{kT} = -\frac{1}{4\pi\varepsilon kT} \sum_i \frac{x_i q_i^2}{3} \kappa \chi_i \quad (8)$$

Where ε is the permittivity, q_i is the charge of molecule i, κ is the Debye Hückel screening length, and χ_i a function of κ and the distance of closest approach (effective ion diameter).

The CPA EoS [1, p. 261] consists of the SRK term plus the association term from SAFT. The electrolyte-CPA (e-CPA) being developed in this PhD project will consist of the CPA equation of state plus a model for the electrostatic interactions. Various models for the electrostatic interactions will be evaluated during the course of the project.

Industrial Applications

The CPA EoS is becoming gradually more used in the oil- and gas industries, but industry adoption has been slow e.g. due to limited availability in process simulators. The PhD project also continues the work at the Center for Energy Resources Engineering (CERE) to make complex EoS available in process simulators such as Aspen HYSYS and Aspen Plus through the use of CAPE-OPEN and Aspen Plus User Models.

One of the possible applications of the CPA equation of state is for calculation of gas hydrate formation curves in multi-component mixtures containing hydrocarbons, water and hydrate inhibitor (such as methanol or ethylene glycol) as shown in Figure 1.

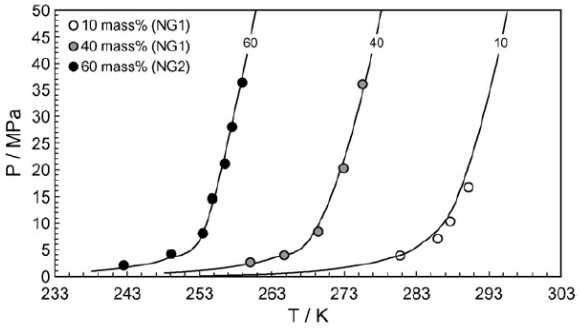

Figure 1: CPA predictions of hydrate dissociation temperatures for a natural gas mixture with different amounts of hydrate inhibitor [2].

When there sea water is present in natural gas pipelines, the gas hydrate dissociation temperatures are shifted to the left, as shown in Figure 2.

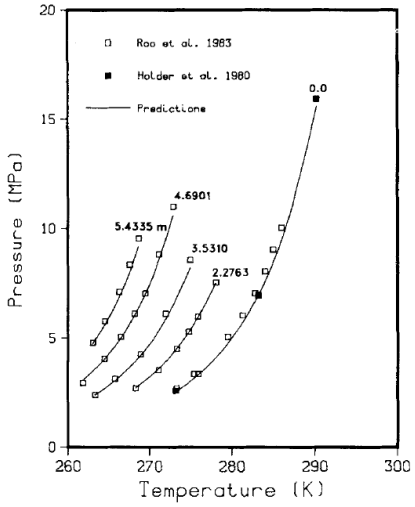

Figure 2: Experimental and predicted pressures for gas hydrate formation from methane in aqueous sodium chloride solutions. [3]

The model developed in this work should be able to predict the gas hydrate formation curves, but also be generally applicable to other challenges related to engineering thermodynamics.

Acknowledgement:

This work is a partly funded by the Department of Chemical and Biochemical Engineering and the CHIGP member companies (Mærsk Oil, DONG Energy, Statoil, GASSCO, BP).

References

1. G.M. Kontogeorgis, G.K. Folas, Thermodynamic Models for Industrial Applications-From Classical and Advanced Mixing Rules to Association Theories, Wiley, 2010
2. H. Haghighi, A. Chapoy, R. Burgess, S. Mazloum, B. Tohidi, Fluid Phase Equilibr. 278 (2009), 109-116
3. P. Englezos, P.R. Bishnoi, AIChE. J. 34 (2004), 1718-1721

Malwina Michalak
Phone: +45 4525 2979
E-mail: mmi@kt.dtu.dk
Discipline: Enzyme Technology

Supervisors: Jørn Dalgaard Mikkelsen
Gunnar Jonson
Manuel Pinelo

PhD Study
Started: November 2008
To be completed: September 2012

Production and Purification of Prebiotic Oligosaccharides by Chromatography and Membrane Systems

Abstract
Prebiotics are non-digestable food ingredients that have beneficial effect on the host microbiota. Known examples of prebiotic food ingredients are oligosaccharides, e.g. maltooligosaccharides from starch or dietary fibers, like pectins and β-glucans. A large number of dietary fibers and oligosaccharides with potential prebiotic effects can be obtained by degradation of side streams form the agricultural industry. This requires a number of specific enzymes which can be obtained by cloning and expression, e.g. in the yeast *Pichia pastoris*. The oligosaccharides produced by the enzymatic catalysis may be potentially purified by membrane separation and chromatography. The prebiotic potential of the products can be determined by functionality tests.

Introduction
Functional food ingredients possessing potential health benefits have become popular nowadays. Some of compounds displaying capability to improve the food are prebiotics. Prebiotics are non-digestable substances, which provide a beneficial effect on the host by selective stimulation of growth of a limited number of indigenous bacteria. The growth of such bacteria can be promoted by, for example, provision of dietary fibers or oligosaccharides. Oligosaccharides, as well as, fibers could be obtained as products of hydrolysis of polysaccharides, like food hydrocolloids. Performing the hydrolysis by means of enzymes would make this process selective and sustainable.

Specific objectives
The idea of the project is to use selective enzyme catalysts to convert polysaccharides into prebiotics. Only few of the commercial enzymes are available for this task. Most of the commercial enzymes in addition contain other enzyme activities which degrade the desired oligosaccharides. Mono-component enzymes can, however, be produced by cloning and expression of suitable enzymes in the yeast, *Pichia pastoris.* This process is performed in the laboratory of Genetically Modified Orgamisms (GMO) located at our department.

Furthermore, the optimal conditions of enzymatically catalyzed reactions have to be worked out. This includes up-scaling of the enzymatic reaction in order to deliver sufficient amount of oligosaccharides with potential prebiotic activity for evaluation. Moreover, the separation and purification process comprising chromatography and membrane systems, has to be established and optimized.

Production of enzymes by fermentation of *Pichia pastoris*
In order to produce a desired enzyme, the gene is cloned and inserted into the genome of the host cell of *Pichia pastoris*. Subsequently, the recombinant product is expressed in the yeast. The genetically engineered strain of yeast is grown in a fermentor. During this process such parameters as pH, temperature, rate of aeration are maintained at optimal level. Glycerol is used as a carbon source both in the batch and fed-batch mode to generate high cell density. Methanol is used for induction of the enzyme expression. The enzymes are excreted into the media. Thus, in order to recover the enzymes, the yeast cells are collected by centrifugation. The supernatant is subjected to sterile – and ultrafiltration.

The harvested enzyme is subjected to a number of analysis and purification processes. This comprises determination of protein concentration, SDS-PAGE, measurements of enzyme activity, thermostability, influence of metal ions and determination of kinetic parameters.

Enzyme purification requires further methods, such as affinity chromatography (His-Tag), gel filtration and/or ion exchange chromatography (IEX). Our genetically engineered proteins contain a His-Tag tail,

which comprise 6 histidines. This enables separation of the desired protein from other contaminating proteins. His-Tag protein is captured in a metal affinity column where Cu^{2+} or Ni^{2+} are used as the ligand. Contaminating proteins without the His-Tag are present in the run-off fraction of the column. His-Tag protein is eluted with solution of imidazole.

The activity of enzymes is assessed by different assays depending on the enzyme produced. But there is also a method universal for all enzymes hydrolyzing polymers, e.g. the reducing sugars assay. When the polymer is degraded the sugars with reducing ends are created.

Enzymatic hydrolysis and separation of products

The purified mono-component enzymes with the desired activity are used to catalyse the hydrolysis of polymeric substrates. The progress of the reaction can be monitored by reducing sugar analysis, size exclusion chromatography (SEC), high performance anion exchange chromatography (HPAEC) or by thin layer chromatography (TLC). Reducing sugars analysis gives information about number of reducing ends created during the hydrolysis. It doesn't say anything about the composition of products. It is, however, simple and qualitative method. Size exclusion chromatography gives mainly information about substrate molecular weight change during the reaction, as shown in Figure 1. The first bottom line in the chromatogram is a polymeric substrate, which then is gradually converted by the enzyme to smaller polymers and oligomers. The conversion of the substrate in time is depicted by the other lines in this chromatogram. HPAEC can determine the smaller reaction products, i.e. oligomers, as depicted in Figure 2. It can be also a qualitative method. TLC, on the other hand, is hard to use to get a qualitative data, but it is the fastest, the cheapest technology. TLC enables separation of oligosaccharides of different degree of polymerization.

The reaction conditions need to be optimized to perform the reaction in the most efficient way. The influence of an enzyme to substrate ratio, temperature and time of the reaction has to be investigated. Then the reaction can be up-scaled and the products separation can be performed. E.g., oligosaccharides can be separated from the polymeric substrate by membrane filtration.

The composition of obtained products can be analyzed by means of acid treatment and subsequent monomer analysis with HPLC.

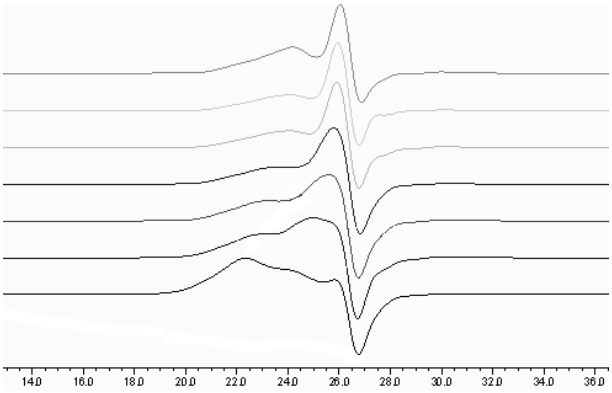

Figure 1: SEC Chromatogram of polysaccharide conversion; counting from the bottom line: first line, substrate; reaction mixtures: second line, after 2 minutes; third line, after 5 minutes; fourth line, after 15 minutes; fifth line, after 1 hour; sixth line, after 2 hours; seventh line, after 4,5 hour

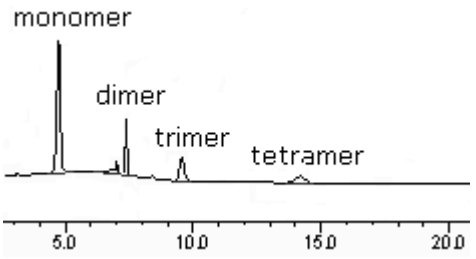

Figure 2: HPAEC chromatogram of monomer and low molecular weight oligosaccharides obtained by hydrolysis of polysaccharide

Acknowledgements

The project is carried out within the Center for Biological Production of Dietary Fibers and Prebiotics at DTU ("Prebiotics Center").

Igor Mitrofanov
Phone: +45 4525 2812
E-mail: igm@kt.dtu.dk
Discipline: Systems Engineering

Supervisors: Rafiqul Gani
Gürkan Sin
Bent Sarup, Alfa Laval

PhD Study
Started: November 2010
To be completed: October 2013

A Methodology for Systematic Design and Selection of Green Solvents for Increased Yield in Organic Reactions

Abstract
Methodology for selection and design of single organic reactions has previously been developed at CAPEC (Gani et al, Computers and Chemical Engineering, 2005, 2008). This methodology is based on a rule-based algorithm. However, the methodology is applicable only to organic chemicals that are inert within the reaction system. The next step is extending the application range of current methodology to multi-stage reactions (because, for example, pharmaceutical reactions are normally multi-step), more complex reaction systems, known solvent substitution problems as well as reaction promotion.

Introduction
Organic solvents (this is primarily petroleum solvents, alcohols, ethers, esters, ketones, nitro compounds) have of great importance. Organic solvents are widely used in plastics, varnishes and paints, synthetic fibers, resins, adhesives, printing, the extraction of vegetable fats, etc. Solvents are widely used in fine chemicals and pharmaceutical industry where they serve to facilitate reaction-based processes by, for example, dissolving reactants and/or bringing them together in suitable concentrations. But there is a problem that, because of the excessive consumption, millions of tons solvents have to be disposed off every year. So, it becomes very important to minimize and optimize the use of organic solvents as much as possible, as stated in the Green Chemistry Principles [1].

Background
Solvents are the substances able to dissolve or solvate other substances. Solvents may be used as a reaction medium to bring reactants together, as a reactant to react with a solute when it cannot be dissolved, and as carrier, to deliver chemical compounds in solutions to their point of use in the required amounts. A good solvent should meet the following criteria:

- It should be inert at reaction conditions
- It should dissolve reactants and reagents
- It should have an appropriate boiling point and melting point
- It should be easily removed at the end of reaction
- It should have nice environment, health and safety (EHS) properties

A method to select greener solvent for the promotion of organic reactions has been already developed [2,3]. This method based on thermodynamic properties with knowledge of reaction and solvent properties. Current methodology is a combination of knowledge from industrial practice and computer-aided tools for property prediction and molecular generation and etc.

The solvent design and selection will be based on the technique called Computer Aided Molecular Design (CAMD - Gani et al, Computers and Chemical Engineering, 2005, 2008), where building blocks for organic chemicals are combined together to form chemically feasible molecules and then evaluated (tested) for their solvent properties. This idea will now be extended to multi-stage reactions, more complex reaction systems, known solvent substitution problems as well as reaction promotion.

Specific Objectives
The aim of the project is to design and select solvents that, when used as a reaction media for liquid phase organic reactions, including multi-stage reactions, lead to an increase in reaction rate and simultaneously minimize the environmental impact of underlying reactions. Solving this problem requires to use the most modern techniques such as molecular design, property prediction, reactor operation modeling, and process-assisting product (solvent) optimization.

Solvent Selection

Generally, solvent selection occurs in two stages. In the first stage, a list of common using solvents is used to identify those solvents that match a sub-set of user-specified constraints, and based on this, a score allocated to each solvent. Simultaneously, a computer-aided molecular design (CAMD) technique is used to generate a list of solvents candidates which are ranked with respect to their allocated scores.

In the second stage, the candidate solvents are further evaluated through detailed calculations to identify most promising solvents for further experiments or other verification tests. [4]

Solvent Selection Methodology

The solvent selection methodology developed earlier by Gani et al. [2,3] has been extended to handle multi-step chemical syntheses as well as solvent substitution for specific reaction steps in existing processes. The latter option has been receiving increased attention as more and more solvents in current use are being identified as having a series of environmental, health and safety challenges and therefore, "greener" substitutes are required.

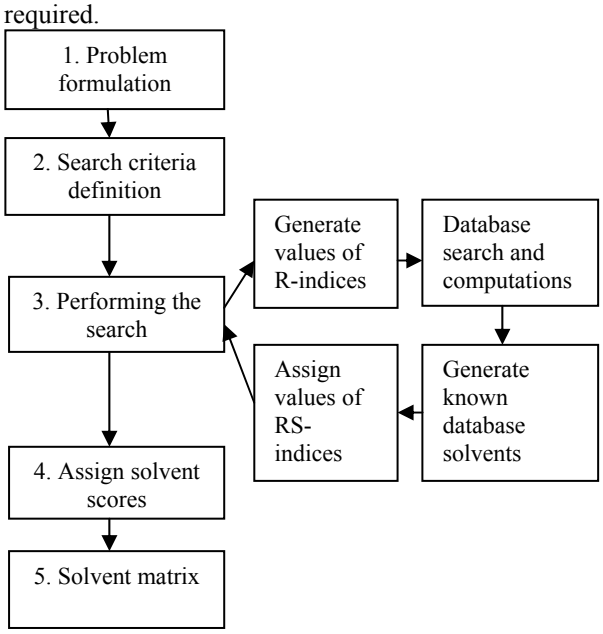

Figure 1: Step-by-step algorithm which is a systematic rule-based methodology to identify a suitable solvent for a specified reacting system.

The solvent selection methodology for organic synthesis involves five steps for each reaction, as illustrated in Fig.1:

1. Problem identification. Finding an objective for given system, identifying actual functions of the solvent.
2. Search criteria definition. The solvent functions that satisfy the operational needs of the process are defined in terms of a set of search criteria (R-indices), defined in terms of: physical and chemical properties (solvent-pure properties); EHS characteristic (solvent-EHS properties); operational properties (solvent–solute properties).
3. Performing the search. The search step consists of two stages. The first is a generation of solvent candidates. The second consists of assigning the RS-indices following the reaction–solvent and then consulting the known solvent database and identifying the set of solvents that satisfy search criteria.
4. Score table assignment. A list of feasible solvents needs to be created. The scores are assigned from the calculated values of RS indices. The scores give a weight to each of the calculated RS indices.
5. Matrix of solvents. After the scores table has been generated, a short list of feasible solvents is obtained for each reaction step.

Conclusions

The project will involve aspects of molecular design, property prediction, reactor operation modeling, and process-assisting product solven optimization. It will require an integration of ideas, methods and tools into a systematic model-based framework through which the solvent design and/or selection problems can be solved.

References

1. P.T. Anastas, J.C. Warner, Green Chemistry: theory and practice, Oxford, Oxford University Press, U.K., 1998
2. R. Gani, C .Jimenez-Gonzalez, D.J.C. Constable, Comput. Chem. Eng. 29 (2005) 1661-1676.
3. M. Folic, R. Gani, C. Jiménez-González, D.J.C. Constable, Chinese J. Chem. Eng. 16 (3) (2008) 376-383.
4. M. Folic, R. Gani, C. Jiménez-González, D.J.C. Constable, P. Arenas Gomez, Comput. Chem. Eng. 32 (2008) 2420-2444.

David Mogensen

Phone: +45 4525 2922
E-mail: dmog@kt.dtu.dk
Discipline: Reaction and Transport Engineering

Supervisors: Kim Dam-Johansen
Jan-Dierk Grunwaldt
Peter Vang-Hendriksen, Risø-DTU
Jens Ulrik Nielsen, Topsoe Fuel Cell A/S

PhD Study
Started: November 2007
To be completed: January 2011

Mathematical Modeling of Solid Oxide Fuel Cells

Abstract
Solid Oxide Fuel Cells (SOFC) is a technology that potentially allows an increase of the efficiency of electricity production. Furthermore it has the advantage that even small units can be operated at high efficiency, which allows a decentralized power supply and thereby an increased utilization of local energy sources. To achieve an optimal design and operation of an SOFC fueled by natural gas, kinetic expressions are required which are able to accurately describe the steam reforming rate. There are significant differences in the reported kinetic expressions over the anode material Ni-YSZ. The primary goal of this project is to determine both the intrinsic kinetics and global kinetic expression in an SOFC anode environment.

Introduction
The fossil fuel reserves are limited and because of this, it is necessary to investigate technologies that can be used to make our society independent of fossil fuels [1]. SOFC technology is highly versatile since it can use a large number of different fuels either from fossil or renewable sources/carriers, such as H_2, CH_4 and NH_3, methanol, dimethylether and diesel [2].

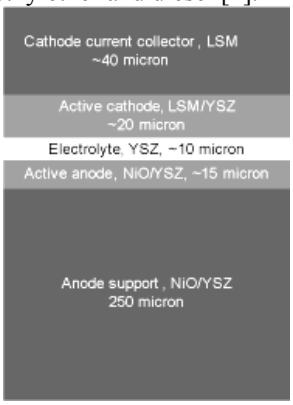

Figure 1: A schematic illustration of an SOFC as produced by Topsøe Fuel Cell A/S [4].

An SOFC is an electrochemical cell, which is continuously supplied with separated streams of gaseous fuel and air/oxygen. The species that is transported through the solid electrolyte is O^{2-}.

Both electrolyte and electrodes in the cell are made of ceramic materials and in order to obtain a sufficient rate of oxygen ion transport through the electrolyte a temperature in the range 600 K to 800 K is needed. The configuration and materials of an SOFC are shown schematically in Figure 1. In this case the cathode is composed of strontium doped $LaMnO_3$ (LSM) and LSM on yttria-stabilized zicronia (YSZ), the electrolyte of YSZ, and the anode of NiO/YSZ [3,4].

The main electrode reactions taking place in the cell are:

Anode:

$$H_2 + O^{2-} \rightarrow H_2O + 2e^-$$

Cathode:

$$1/2O_2 + 2e^- \rightarrow O^{2-}$$

If methane is used directly as the fuel, it is catalytically converted into hydrogen by the Ni present in the anode material [6]. The overall steam reforming reaction is:

$$CH_4 + 2H_2O \rightleftarrows 4H_2 + CO_2$$

At the high temperatures that have typically been used in SOFCs the steam reforming reaction is very rapid (> 750 ºC), which means that little interest has been paid to the exact kinetics. Recent research has been focused on lowering operating temperature of an SOFC. Hence, it is now possible to tune the degree of internal reforming by carefully controlling the rate.

However, there are big differences in the kinetic expressions that have been reported for steam reforming over Ni-YSZ [5-10]. Therefore a more thorough examination of the kinetics is necessary before optimization with corresponding simulation studies is possible.

Experimental

The steam reforming rate has been measured over Ni-YSZ, both in a packed bed setup and in a stack setup. Experiments on both setups where performed in the Temperature range 600-800°C and all reactants and product partial pressures were varied.

The quartz reactor used to perform the packed bed is shown in Figure 2.

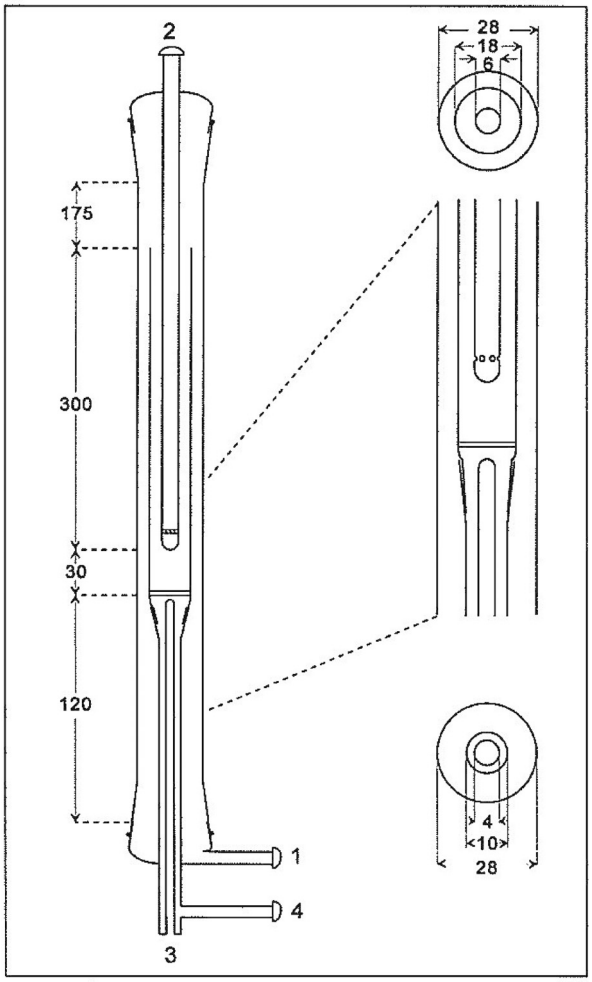

Figure 2: Quartz reactor for the packed bed setup.

In the stack setup, it was first attempted to measure the reforming rate on a 12x12cm 5 cell stack From Topsoe Fuel Cell A/S. This resulted in complete conversion of methane, even at flow rates approximately 5 times larger than for normal SOFC operation.

In order to reduce the amount of catalyst in the setup, a number of special stacks were made, also by Topsoe Fuel Cell A/S. These stacks had only a single cell, and had either half or three quarters of the cell cut away, so that a number of cathode flow channels were removed and the length of the anode flow channels were shortened. This is illustrated in Figure 3, for a quarter cell stack.

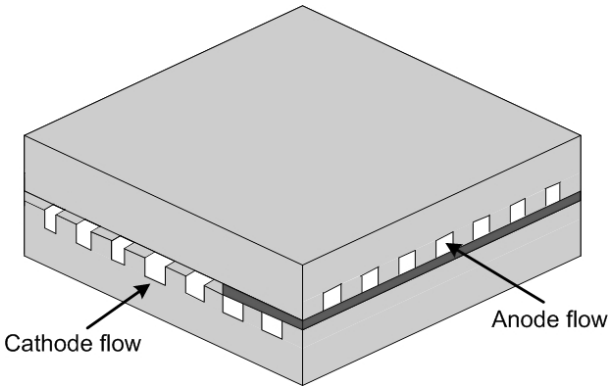

Figure 3: Illustration of a single 12x12cm cell stack with three quarters of the cell removed.

The activity was found by measuring the CO and CO_2 concentration in the outlet with an IR analyzer of the (type NGA 2000 MLT). From this the concentrations of the other gasses were calculated by the mass balance. This method was verified by GC measurements of all gas components for selected samples.

Dynamic Behavior

During the rate measurements a previously unreported long-term dynamic behavior of the catalyst was observed. The observed behavior was the same in the two setups, but with a bit slower approach to steady state for the stack setup.

First of all it was found that after startup a deactivation occurred over a time period ranging from a couple of days up to two weeks, depending on operating temperature. An example of this is shown in Figure 4, for a startup at 640°C in the packed bed setup on the model anode material.

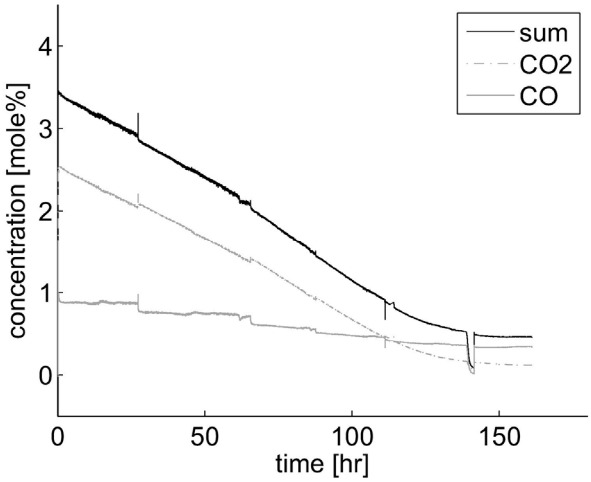

Figure 4: Approach to steady state after startup in a packed bed reactor at 640°C.

A similar slow approach to steady state was also observed after changes in temperature or hydrogen partial pressure. Changes in gas species other than hydrogen did not have a similar effect.

Furthermore it was found that a prolonged exposure (24 hours) to a H_2/H_2O gas mixture without methane

resulted in a complete re-activation of the catalytic activity.

These observations are highly useful for achieving optimal operation in an SOFC with internal steam reforming. For example it is possible to increase the degree of internal reforming after a few weeks of operation, but it is necessary to be aware of the possibility of reactivation of the catalytic activity.

Results

In the packed bed setup, two different samples was tested an industrial anode from Topsoe Fuel Cell A/S and a model anode material. The production procedure for the model anode is described by M. Pihlatie et al.[11]. The Sample used for this work is designated as sample E in the article.

The two samples showed near identical catalytic activity and behavior. The measured kinetic data was found to be described best by assuming methane dissociation as the rate determining step and with CO as the most abundant species on the surface. The expression obtained on the model anode is shown below.

$$r = \frac{110\frac{mole}{gsPa}\exp\left(\frac{-198kJ/mole}{RT}\right)P_{CH_4}\left(1-\frac{Q_{sr}}{K_{sr}}\right)}{\left(1+1.7\cdot10^{-6}Pa^{-1}\exp\left(\frac{26kJ/mole}{RT}\right)P_{CO}\right)}$$

$(1-Q_{sr}/K_{sr})$ describes the approach to equilibrium, K_{sr} is the equilibrium constant and Q is described as follows:

$$Q_{sr} = \frac{P_{H_2}^3 P_{CO}}{P_{CH_4} P_{H_2O}}$$

The stack measurements were designed to investigate the observed rate under realistic SOFC conditions. This means that the measurements are subject to both mass transport limitations and temperature gradients. Because of this the rate is described by a power law expression, which is shown below.

$$r = 2\cdot10^4\frac{mole}{m^2sPa}\exp\left(\frac{-166kJ/mole}{RT}\right)P_{CH_4}^{0.7}$$

There is a large variation in the activation energies reported in literature for methane steam reforming over Ni-YSZ, i.e. 58-229 kJ/mole [7]. Because of this it was tested how the observed activation energy would be affected by using very short waiting time instead of waiting for steady state. These measurements were made in the packed bed setup on the model anode material and the obtained Arrhenius expression is shown in Figure 5.

The observed activation energy, 76 kJ/mole, is less than half of that obtained when waiting for steady state. It is suspected that this is actually the activation energy of the reaction. The slow approach to steady state, and the resulting increase in activation energy is then caused by changes in the catalyst structure or possibly a reversible poisoning of the catalyst surface.

It should be noted that these measurements were performed after the initial deactivation had taken place. If similar measurements were made without being aware of this behavior the observed activation energy will depend on both the time between each temperature change and whether the changes are made in decreasing or increasing order.

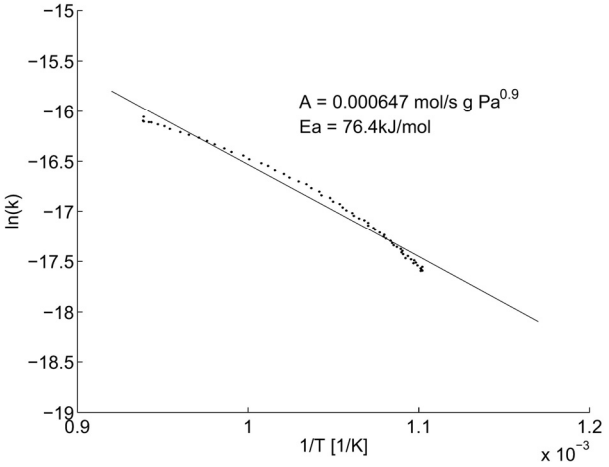

Figure 5: Arrhenius plot for the measurements made without waiting to obtain steady state after each temperature change.

Rate Prediction in Stack

The kinetic measurements made in a stack configuration is, as mentioned earlier, influenced by both mass transport limitations and temperature gradients. This means that such measurements cannot necessarily be used to describe activity in a stack with different configuration.

Hence, in order to get a more generally useful description of the methane reforming activity in an SOFC stack, we have attempted to predict the stack rate from the intrinsic rate expression obtained in the packed bed experiments. The method is kept as simple as possible so that it can be used in flow sheeting models.

The thought is to describe the cell via the design equation for a fixed bed reactor, as shown below.

$$\frac{dX_{CH_4}}{dW_{cat}} = \frac{r_{eff}}{N_{CH_{4,in}}}$$

X_{CH4} is the conversion of methane, W_{cat} is the catalyst weight, $N_{CH4,in}$ is the molar inlet flow of methane and r_{eff} is the effective reaction rate described by the following equation.

$$r_{eff} = \eta\cdot r_{\text{int}}$$

r_{int} is the rate calculated from the kinetic expression determined over the industrial anode and η is the efficiency factor, which described how big a fraction of the available catalyst is being fully used i.e. an efficiency factor = 1 corresponds to full usage of the catalyst [12]. η is calculated from the equation below

$$\eta = \frac{Tanh(\phi)}{\phi}$$

Φ is the Thiele modulus: $\phi = L\sqrt{\frac{k}{D}}$

L is the anode thickness, k is the first order rate constant (s^{-1}) and D is the effective diffusion coefficient (m^2s^{-1}) of methane which is set to 10^{-5}.

Figure 6 shows a comparison of the conversion predicted using this method, with the methane conversions measured in the quarter cell stack.

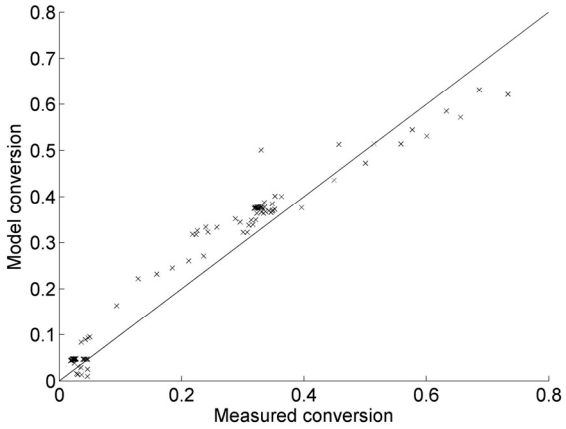

Figure 6: Deviation between measured conversion and predicted conversion in a stack configuration.

Taking into account the simplicity of the method used for predicting the activity it has a surprisingly good agreement with the experimental data.

Conclusion

The catalytic activity of methane steam reforming over Ni-YSZ was measured in both a packed bed setup and a stack configuration.

During the experiments a previously unreported long-term dynamic behavior was observed. This behavior was examined closely and was found to have a significant impact on optimal operation of SOFC systems with internal reforming. It was further seen that lack of awareness of this behavior could be origin of the large range of activation energies reported in the literature.

Finally a method for predicting methane conversion in a stack from an intrinsic rate expression was suggested and validated against quarter cell stack measurements. The combined simplicity and good accuracy of this method makes it ideal for flow sheeting SOFC models.

Acknowledgments

The work was carried out in collaboration between the Combustion and Harmful Emission Control (CHEC) Research Centre at the Technical University of Denmark, Topsøe Fuel Cell A/S, and the Graduate School in Chemical Engineering: MP_2T. Furthermore, several persons at Risø-DTU are strongly involved in the work and have given valuable help. The CHEC research Centre is co-founded by the Technical University of Denmark, Dong Energy, FLSmidth, Hempel's Fond, Vattenfall, Haldor Topsøe, Energinet.dk, The Danish Technical Research Council, The Danish Energy Research Programme, Nordic Energy Research, the European Union and several other industrial partners.

References

1. M. Asif, T. Muneer, Renew. Sust. Energ. Rev. 11 (2007) 1388-1413.
2. N.Christiansen, J.B. Hansen, H. Holm-Larsen, S. Linderoth, P.H. Larsen, P.V. Hendriksen, M. Mogensen, Fuel Cells Bulletin 8 (2006) 12-15.
3. http://www.topsoefuelcell.com/, 27/11-2007.
4. W. Vielstich, A. Lamm, H.A. Gasteiger, Handbook of Fuel Cells, John Wiley & Sons Ltd, 2003 ISBN: 0-471-49926-9.
5. J. Wei, E. Iglesia, J. Catal. 224 (2004) 370-383
6. S.H. Clarke, A.L. Dicks, K. Pointon, T.A. Smith, A. Swann., Catal. Today 38 (1997) 411-423
7. D. Mogensen J.-D. Grunwaldt, P.V. Hendriksen, K. Dam-Johansen, J.U. Nielsen, J. Power Sources 196 (2011) 25-38
8. S. Bebelis, A. Zeritis, C. Tiropani, S.G. Neophytides, Eng. Chem. Res. 39 (2000) 4920-4927.
9. M. Boder, R. Dittmeyer, J. Power Sources 155 (2006) 13-22
10. D.L. King, J.J. Strohm, X. Wang, H.-S. Roh, C. Wang, Y.-H. Chin, Y. Wang, Y. Lin, R. Rozmiarek, P. Singh, J. Catal. 258 (2008) 356-365
11. M. Pihlatie, T. Ramos, A. Kaiser., J. Power Sources, 193 (2009) 322-330
12. I. Chorkendorff, J.W. Niemantsverdriet, Concepts of Modern Catalysis and Kinetics, 2nd edition, Wiley-VCH Verlag GmbH, 2007

Peter Mølgaard Mortensen
Phone: +45 4525 2809
E-mail: pmm@kt.dtu.dk
Discipline: Reaction and Transport Engineering

Supervisors: Anker Degn Jensen
Jan-Dierk Grunwaldt
Peter Arendt Jensen

PhD Study
Started: August 2010
To be completed: August 2013

Catalytic Upgrading of Bio-oil

Abstract
Catalytic bio-oil upgrading constitutes a prospective path for biofuels in the future as it has been proven as a cost competitive process relative to crude oil derived fuels. However, many aspects within the process still need to be elucidated, where specifically limited catalytic lifetimes constitute a problem. This could be associated with both choice of catalyst, but also transport problems. This project focuses on the development and elucidation of the process, with the main goals within catalyst formulation and description of the process from a chemical engineering perspective.

Introduction
It has become generally accepted that the oil reserves are depleting due to an increased utilisation of fossil fuels throughout the last 100 years. This has lead to an increased concentration of CO_2 in the atmosphere, being correlated to a greenhouse effect on the Earth. These aspects raise concerns and gives incitement for investigation of alternative ways for production of fuels, as well as bulk chemicals. A prospective path to these could be biomass based, as this constitutes a carbon based resource which can be reproduced within a relatively short lifecycle. So far first generation biofuels have already been implemented in different parts of the world, but these are produced from crops as corn and plant-oils, which also are needed in the food industry. Thus, in order not to compete with the food demand on the Earth, it is a request that biofuel production in the future can be more versatile and utilise any type of biomass, as wood, wastes, etc.

A problem with the biomass is that it has a relative low energy- and mass-density. This makes transport expensive and gives a constraint in the utilisation. Thus, it has been proposed that biomass can be converted into bio-oil through flash pyrolysis, which can coop with practically any type of biomass. In the process biomass is treated at high temperatures with high heating rates over short residence times, producing oil (so called bio-oil) with an energy density about 8 times higher than the biomass [1]. This bio-oil has a high oxygen content (up to 40wt%) due to a high content of water and oxygenates as alcohols, ketones, carboxylic acids, phenols, etc., rendering it acidic, immiscible with crude oil, and unstable during prolonged storage. This means that the bio-oil is a prospective platform chemical, but not a suitable engine fuel or chemical [2].

Hydrodeoxygenation (HDO) constitutes a very prospective upgrading route for bio-oil. This is a high pressure catalytic upgrading process where hydrogen is used for exclusion of oxygen. In table 1 a comparison between the bio-oil, the upgraded bio-oil (HDO oil), and crude oil is seen. Through the upgrading process it is seen that the oxygen content drops from 28-40wt% in the bio-oil to <5wt% in the HDO oil, being one of the main reasons for that the higher heating value (HHV) and the pH increases to levels equivalent of the crude oil. Overall this shows that pyrolysis of biomass followed by HDO could constitute a path to a renewable crude oil like product.

The combined process of pyrolysis and HDO has been shown to have the potential for production of engine fuels at a price competitive with the current crude oil derived fuels, due to increased feasibility when basing the production on bio-oil as platform chemical and furthermore a relative high efficiency of the process [4].

The present study treats HDO, where aspects of transport mechanism, catalyst formulation, kinetics, and ideal operating conditions still has to be elucidated before the process can be implemented in industrial scale. Currently one of the central tasks within the technology is formulation of catalysts with sufficient lifetimes, as it has been found that operation over extended periods result in blockage of the active sites

and plugging of the system due to carbon depositions [5].

Table 1: Properties of bio-oil, upgraded bio-oil (HDO oil), and crude oil (as benchmark). Information obtained from [2,3].

	Bio-oil	HDO oil	Crude oil
Water [wt%]	15-30	1.5	0.1
pH	2.8-3.8	5.8	-
rho [kg/l]	1.1-1.3	1.2	0.9
$\mu_{50°C}$ [cP]	40-100	1-5	180
HHV [MJ/kg]	16-19	42-45	44
C [wt%]	55-65	85-89	83-86
O [wt%]	28-40	<5	<1
H [wt%]	5-7	10-14	11-14
S [wt%]	<0.05	<0.005	<4
H/C	0.9-1.5	1.3-2.0	1.5-2.0
O/C	0.3-0.5	<0.1	0

$CoMoS_2$ has been one of the most frequently tested catalysts for HDO, as this is associated with conventional hydrotreating processes. However, this catalyst might not be optimal in the current context, as the sulphur in the structure has been reported to deposit in the oil product [6]. Noble metal catalysts have been shown to work for the system as well, but are unfavourable due to the high price. New research therefore focuses on base metal type catalysts, where a recent study has shown Ni/ZrO_2 as a potential catalyst [7].

Specific Objectives

It is the scope of this project to investigate suitable catalysts for HDO. This involves two tasks, finding an active material, but also finding a system which is not substantially deactivated during operation. The later aspect is associated with carbon deposition and can involve several fields which also should be elucidated. First of all the mechanism of the coke forming reactions would be of interest to clarify as this potentially could indicate how to prevent the coke to form. However, the coke deposition could also be related to transport mechanisms in the system, where specifically the availability of hydrogen in the vicinity of the catalyst could constitute a problem. This has not yet been clarified [8].

The above aspects will be investigated in both a batch reactor and a continuous flow setup. The batch reactor will be used in the screening process for catalysts and constitutes a relative quick method for measurement of the apparent activity of a given catalyst. Results from these experiments will be elaborated in the continuous flow system, where catalytic lifetime, transport phenomena, and kinetics can be investigated.

The work in the laboratory will be assisted by investigation of the catalysts through different characterization methods as BET, XRD, XAS, and TEM. These analyses could help indicate where and why the coke depositions occur.

Conclusion

Conversion of biomass to bio-oil and upgrading of this into engine fuels through respectively flash pyrolysis and HDO has been found as a prospective route for biofuels production, as the process has been found cost competitive with current crude oil derived fuels. However, the process is still far from industrial application due to insufficient catalyst lifetime. Therefore it is the scope of this project to elucidate potential catalysts for the system and investigate the coke forming mechanism.

Acknowledgment

This work is part of the CHEC (Combustion and Harmful Emission Control) research center and is financed by the CASE (Catalysis for Sustainable Energy) project at DTU.

References

1. T. Bridgwater, J. Sci. Food Agr. 86 (12) (2006) 1755-1768.
2. Q. Zhang, J. Chang, T. Wang, Y. Xu, Energ. Convers. Manage. 48 (1) (2007) 87-92.
3. G.W. Huber, S. Iborra, A. Corma, Chem. Rev. 106 (9) (2006) 4044-4098.
4. S.B. Jones, C. Valkenburg, C.W. Walton, D.C. Elliott, J.E. Holladay, D.J. Stevens, C. Kinchin, S. Czernik, Production of Gasoline and Diesel from Biomass via Fast Pyrolysis, Hydrotreating and Hydrocracking: a Design Case, U. S. Department of Energy, 2009. PNNL-18284.
5. D.C. Elliott, T.R. Hart, G.G. Neuenschwander, L.J. Rotness, A.H. Zacher, Environ. Prog. 28 (3) (2009) 441-449.
6. A. Gutierrez, R.K. Kaila, M.L. Honkela, R. Slioor, A.O.I. Krause, Catal. Today 147 (3-4) (2009) 239-246.
7. V.A. Yakovlev, S.A. Krhromova, O.V. Sherstyuk, V.O. Dundich, D.Y. Ermakov, V.M. Novopashina, M.Y. Lebedev, O. Bulavchenko, V.N. Parmon, Catal. Today 144 (3-4) (2009) 362-366.
8. R.H. Venderbosch, A.R. Ardiyanti, J. Wildschut, A. Oasmaa, H.J. Heeres, J. Chem. Technol. Biot. 85 (5) (2010) 674-686.

Nikolai E. Musko

Phone: +45 4525 2923
E-mail: nm@kt.dtu.dk
Discipline: Reaction and Transport Engineering
Engineering Thermodynamics
Supervisors: Georgios M. Kontogeorgis
Anker Degn Jensen
Jan-Dierk Grunwaldt, KIT

PhD Study
Started: October 2009
To be completed: October 2012

Heterogeneously Catalysed Aldol Reactions in Supercritical Carbon Dioxide

Abstract
The aldol reaction is one of the most important reactions in chemical syntheses as it leads to C-C bond formation. Heterogeneous catalysis together with the use of dense carbon dioxide as reaction medium provides a number of opportunities to intensify chemical reactions. In the present PhD-study aldol reactions of a number of aldehydes have been investigated over acidic and basic catalysts in supercritical carbon dioxide at 180 bar and 100°C in a high-pressure batch reactor. Catalyst characterisation techniques, such as NH_3-TPD, TEM, XAS, etc. have been used to get an insight into the catalyst structure. Since the phase behaviour plays an important role in the process, thermodynamic calculations have been performed in order to find optimal conditions for the reactions.

Introduction
Aldol reactions are industrially very important as they yield products that can be used as solvents, flavours, additives, etc. [1]. Traditionally, they are carried out in liquid phase with stoichiometric amounts of the aqueous solution of inorganic bases (NaOH, $Ca(OH)_2$, etc.) or acids [2]. Therefore, a huge amount of waste is produced, whereas conversion and selectivity are usually quite low. The use of a heterogeneous catalyst and liquid or supercritical carbon dioxide instead of conventional solvents is one of the possible ways to make the technology "greener" and more effective [3]. This is due to the fact that dense CO_2 combines both gas-like and liquid-like properties. Gas-like properties significantly decrease heat and mass transfer limitations, and the relatively high density, which is determined by liquid-like properties, leads to increased solubility and allows the use of CO_2 as a "green" and recyclable alternative to conventional solvents. The properties of $scCO_2$ are strongly dependent on temperature and pressure in the system, especially near the critical point, which makes both chemical and separation processes quite tunable.

An interesting idea of performing aldol reactions using unsaturated aldehydes as starting materials via preceded selective hydrogenation of the latter was proposed by Seki *et al*. [4] (Fig.1). 1%Pd/Amberlyst-15 catalyst was proposed as an active catalyst for this "one-pot" synthesis. The catalytic studies were performed in a continuous-flow system. It also was found that palladium is the best metal for the hydrogenation step and Amberlyst-15 shows the best results in aldol condensation [4,5].

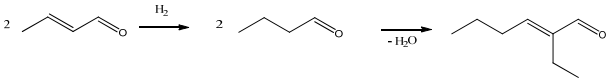

Figure 1: The "one-pot" synthesis of 2-ethylhexenal-2.

However, as a number of questions remain open, there is still a lot of space for improvement and further extension to other substrates and reactions. The main aims of this PhD-project comprise (1) catalyst screening for aldol reaction step, (2) investigation of bifunctional catalysts for the "one-pot" synthesis and (3) thermodynamic calculations of the phase behaviour during the reaction in order to optimise the reaction conditions.

Experimental
Different types of acidic and basic carriers were obtained both commercially and by synthesis from literature. In particular, carriers as hydrotalcite, $H_4SiW_{12}O_{40}$/MCM-41 (TSA/MCM-41), and TSA/SiO_2 were recently synthesised.

The catalyst samples were characterised using the following techniques: X-ray diffraction (XRD), X-ray absorption spectroscopy (XAS), transmission electron spectroscopy (TEM), temperature-programmed desorption of ammonia (NH_3-TPD), nitrogen adsorption-desorption (BET). The samples were tested in aldol reactions with the following saturated aldehydes: propanal, butanal, pentanal, hexanal, and 3-methylbutanal.

All the reactions were carried out in a high-pressure batch reactor with a sapphire window; therefore, phase behaviour was monitored during the reactions.

Results

All the catalyst samples were tested in the aldol reaction with butanal (Table 1). Amberlyst-15 turned out to be the most active catalyst, however, when the catalytic activity is expressed using turnover frequency the TSA/SiO_2 sample showed more than 2 times higher activity.

Table 1: Aldol reaction of butanal over different catalysts in $scCO_2$. Conditions: substrate 0.02 mol, m_{cat} = 0.1 g, temp. 100°C, m_{CO2} =10 g, total pressure 180 bar, reaction time 120 min.

Catalyst	Conv., %	Reaction rate, mol/(g_{cat}·h)	TOF, h^{-1}
Amberlyst-15	51	5.1	1087
Hydrotalcite[a]	14	1.4	-
HZSM-5 (15)	13	1.3	311
γ-Al_2O_3	11	1.1	585
10% TSA/SiO_2	9	0.9	2432
MCM-41	9	0.9	1154

[a] basic catalyst

Since Amberlyst-15 was the most active in the reaction with butanal, it was used in aldol reaction of the other aldehydes (Table 2). Small and linear aldehydes, such as propanal, butanal, pentanal and hexanal, react more efficiently than the branched 3-methylbutanal, which is converted much slower.

Table 2: Aldol reaction of different saturated aldehydes over Amberlyst-15 in $scCO_2$. Conditions: substrate 0.02 mol, m_{cat} = 0.1 g, temp. 100°C, m_{CO2} =10 g, total pressure 180 bar, reaction time 120 min.

Catalyst	Conv., %	Select., %	Reaction rate, mol/(g_{cat}·h)
Propanal	84	100	8.4
Butanal	51	100	5.1
Pentanal	31	99	3.1
Hexanal	21	98	2.1
3-Me-butanal	11	99	1.1

Tungstosilicic acid (TSA) catalysts on silica or MCM-41 basis showed very interesting properties. They are quite active in the aldol reaction of butanal. Additionally, the samples showed good hydrogenation activity in the reaction with unsaturated 2-butenal. Therefore, they potentially could be used as bifunctional catalysts for the "one-pot" synthesis.

The catalyst characterisation techniques used in the present study allowed getting further insight into the catalyst structure. The TSA particles are finely dispersed on the carrier; however, the full structure of the TSA deposited on the surface remains to be uncovered. Therefore, some further and deeper investigations are necessary to understand the reaction mechanism and improve the catalyst properties and performance.

All the reactions regardless of the starting material were carried out in the single phase region as it was uncovered by the view cell during the catalytic investigations. The phase equilibrium in the system is mostly determined by temperature and pressure, and a small change in a parameter can cause significant changes in the process, for example, the system can become two phase instead of one phase. Therefore, phase modeling and theoretical calculations were performed for better understanding of the process. An advanced thermodynamic model, the Cubic plus Association Equation of State (CPA), which can describe $scCO_2$ and polar hydrogen bonding compounds, is used for that purpose [6]. The pure fluid CPA parameters were estimated based on the vapour pressures and liquid densities and some interaction parameters k_{ij} for binary systems were obtained using experimental vapour-liquid equilibria data.

Conclusions

Amberlyst-15 turned out to be the most active and effective catalyst for the aldol reaction. However, TSA-based catalysts have been found to be equally interesting and intrinsically more active. Further investigations will be devoted to screening other acidic support materials in different modes (batch reactor, continuous-flow, etc.), investigating the TSA catalyst structure, and synthesising bifunctional catalysts. It is moreover important to elucidate the reaction mechanism.

The reaction conditions will be optimised based on the phase behaviour of the system using advanced thermodynamic models. Extensive literature search and some phase behaviour measurements will be necessary for that purpose.

Acknowledgments

The authors are grateful to The Danish Research Council (FTP-proposal) for financial support of the project. ANKA at KIT and HASYLAB at DESY, Hamburg, are acknowledged for beamtime and DANSCAT and the EU (Contract RII13-CT-2004-506008) for financial support of the synchrotron radiation experiments.

References

1. M.M. Green, H.A. Wittcoff, Organic Chemical Principles and Industrial Practice, Wiley-VCH, Weinheim, 2003.
2. R. Mestres, Green Chem. 6 (2004) 583.
3. J.-D. Grunwaldt, R. Wandeler, A. Baiker, Catal. Rev. – Sci. Eng. 45 (2003) 1.
4. T. Seki, J.-D. Grunwaldt, A. Baiker, Adv. Synth. Catal. 350 (2008) 691.
5. J.G. Stevens, R.A. Bourne, M. Poliakoff, Green Chem. 11 (2009) 409.
6. G.M. Kontogeorgis, G.K. Folas, Thermodynamic Models for Industrial Applications, from Classical and Advanced Mixing Rules to Association Theories; John Wiley & Sons, 2010.

Azizul Azri Bin Mustaffa
Phone: +45 4525 2811
E-mail: azm@kt.dtu.dk
Discipline: Systems Engineering

Supervisors: Rafiqul Gani
Georgios Kontogeorgis

PhD Study
Started: April 2009
To be completed: March 2012

Analysis of Group Contribution^{Plus} Models for Property Prediction of Organic Chemical Systems

Abstract
In this paper, a detailed analysis of the performance and trends of predictions of vapour–liquid phase equilibrium with the UNIFAC-CI model, employing a method to predict missing group interaction parameters (GIPs) through the use of connectivity indices, are presented. The cases where the model using the predicted GIPs perform well and cases where the performance is unreliable are investigated. The causes for the unreliable performance of the UNIFAC-CI model are explained and results from one of the remedies that gave very good results are presented.

Introduction
The GC^{Plus} approach was developed by Gani et al. [1] through the establishment of a methodology for predicting missing group contributions for the Marrero and Gani [2] group contribution method for pure component property estimation with the aid of valence connectivity indices. Recently, a GC^{Plus} approach for predicting mixture properties by combining the UNIFAC group contribution based activity coefficient model with valence connectivity indices (CIs) developed by Kier and Hall [3] to be called UNIFAC-CI have been developed [4]. Note that the group interaction parameters (GIPs) for any UNIFAC model are regressed from experimental data separately for vapour–liquid equilibrium (VLE) data and liquid–liquid equilibrium (LLE) data. Other data, such as activity coefficients at infinite dilution data and heat of mixing data, may also be added to the VLE and/or LLE data. There are, however, many gaps in the UNIFAC parameter tables due to lack of the necessary experimental data, some of which may not be possible to measure. The objective therefore is to predict the missing GIPs of the reference UNIFAC model through the GC^{Plus} approach. In this way, the application range of the reference UNIFAC model can be significantly increased by providing a reliable predictive option for obtaining the necessary GIPs in a fast, cheap and efficient manner. In the developed UNIFAC-CI method, an expression was established for relating the GIPs to the number of atoms involved in the UNIFAC groups, the connectivity indices and a set of atom interaction parameters (AIPs). The atom stoichiometry and the values of the CIs can be obtained directly from the group definition while the AIPs were regressed using available experimental data [4]. González et al. [4,5] published the AIPs and the corresponding GIPs for the original UNIFAC [9] model for groups formed by C, H, O, N, Cl and S atoms and for the modified UNIFAC (Dortmund) model for groups formed by C, H, O, and N atoms. Just like the reference-UNIFAC model, the UNIFAC-CI model has also been found to not work for some systems [6,7] and therefore further analysis of the UNIFAC-CI model in terms of their performance and accuracy is done to increase the irreliability and flexibility. The objective of this paper is to revisit the UNIFAC-CI model and the method for the prediction of the GIPs in order to identify the reasons for why the method does not perform as well as the reference UNIFAC model for some systems while performing surprisingly better than the reference for other systems. Although the UNIFAC-CI model should not be expected to perform better than the reference with a smaller set of parameters, the aim here is to identify through a thorough investigation, where the reference and the UNIFAC-CI models are going wrong for some of the systems. Then, having identified some of the causes, perform a new regression of the AIPs, evaluate the performance of the UNIFAC-CI model and the reference UNIFAC model with its filled GIPs.

Identification of the problem systems
We have restricted our analysis in this work to the systems that include the atoms C, H and O since nearly 58% of the VLE data used for the reference UNIFAC GIPs concern only these three atoms. Therefore,

analyzing the causes first through these systems and implanting the solution on the others is a good starting point. The AIPs, which involve the groups formed by C, H and O atoms, were regressed using 228 datasets [4].

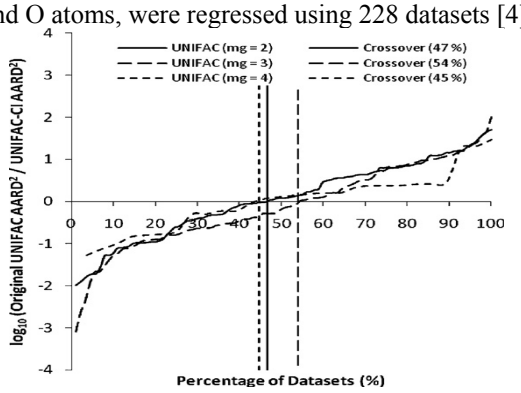

Figure 1: Ratio of AARD of reference UNIFAC and the UNIFAC-CI models against fraction of the datasets for systems containing the C, O, H atoms. The crossover indicates the percentage of the datasets which are better correlated by the reference model.

In Figure 1, the ratio of the average absolute relative deviation (AARD) values of reference UNIFAC and the UNIFAC-CI models obtained for the 228 datasets are plotted against the fraction of datasets. It can be observed that for the systems with two main groups (mg), UNIFAC-CI performs better for 53% of the datasets while 54% of the data sets with three main groups were better predicted by the reference UNIFAC model. Meanwhile, for the systems with four main groups, UNIFAC-CI performs better compared to the reference model for 55% of the datasets. The error is expressed as the average absolute relative deviation (AARD) for both reference UNIFAC and UNIFAC-CI models:

$$AARD(\%) = \frac{1}{N}\sum_{i=1}^{N}\left|\frac{P_{\exp} - P_{calc}}{P_{\exp}}\right| \times 100 \qquad (1)$$

where N is the number of data points in the whole set of data, P_{exp} is the experimental pressure and P_{calc} is the calculated pressure. The values of AARD for each dataset are calculated in terms of molecular types and are shown in Figure 2. This analysis clearly identifies the types of systems that are well correlated and those that are not. This figure also shows that all systems which involve the C-C interactions, such as the alkane/cyclic alkane–cyclic alkane, alkane–alkene, alkane/cyclic alkane–aromatic, and alkene–aromatic are well correlated. Some systems are in fact far better correlated than the reference model, such as, alkane/cyclic alkane–ethoxy, alcohol–carboxylic acid, ether–ethoxy alcohol and ethanediol–ether. However, the correlation results of several systems for the UNIFAC-CI model are not good, such as, the alkane–aldehyde, hydroxyl aromatic–aromatic and ester–aromatic systems. Note that only one data set was used in the regression for the last two systems. This is the current state of the performance of the UNIFAC-CI model developed by González et al. [4] for systems involving C, O, H atoms. Please note that, for the systems which involve carboxylic acids, the association constants based on the method of Hayden and O'Connell [8] were employed in the calculations of the vapour phase fugacities. For further analysis, a limit of 5% AARD was assumed to be an acceptable value and the datasets which have higher AARD values with respect to UNIFAC-CI method were further extracted and are also highlighted in Fig. 2 (note the systems that have AARD greater than 5%). The systems showing AARD values greater than 10% was then selected for further analysis. From Fig. 2, the alkane–aldehyde systems (1-butanal-n-heptane at 343 K, 1-butanal-n-heptane at 318 K, 1-pentanal-n-heptane at 348 K, 2-methylpropanal-n-heptane at 335 K and 2-methylpropanal-n-heptane at 318 K) and the phenol–styrene system were found to have AARD greater than 10% (with the largest AARD being 13%).

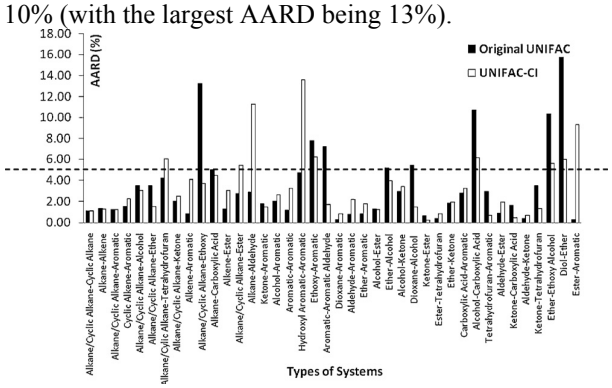

Figure 2: Average AARD (%) for each types of systems used in the regression for systems containing atoms C, O, H between reference UNIFAC and UNIFAC-CI.

Identification of the problems in the model expression and/or parameters

The AIPs employed by the five alkane–aldehyde systems are listed in Table 1.

Table 1: AIPs used by several systems

Systems	AIPs used
Alkane-Aldehyde	$b_{C\text{-}C}$, $b_{C\text{-}O}$, $c_{C\text{-}C}$, $c_{C\text{-}O}$, $bh_{C\text{-}C}$, $bh_{O\text{-}C}$
Alkane-Alcohol	$b_{C\text{-}C}$, $b_{C\text{-}O}$, $bh_{C\text{-}C}$, $bh_{O\text{-}C}$
Alkane-Ether	$b_{C\text{-}C}$, $b_{C\text{-}O}$, $c_{C\text{-}C}$, $c_{C\text{-}O}$, $bh_{C\text{-}C}$, $bh_{O\text{-}C}$

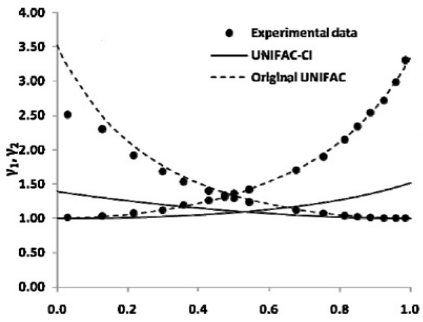

Figure 3: Comparison of the activity coefficients calculated using the original UNIFAC and UNIFAC-CI methods with experimental data for (a) 1-butanal-n-heptane at 318 K

For each of the binary systems, activity coefficients were next calculated and analyzed for the reference and the UNIFAC-CI models and compared with experimental data in Figure 3 (shown for system 1-butanal-n-heptane at 318 K). Figure 3 shows that the predicted activity coefficients by the reference UNIFAC model agree well with the experimental values but not so for UNIFAC-CI model. The problem appears to be at both infinite dilution regions for the binary system. It also looks like the activity coefficient values are under-predicted in all cases. At the next step, it was decided to check the relationship between the different terms of the residual activity coefficient contribution and the corresponding GIP values. A new term, F, was defined for this purpose:

$$F = \sum_k \left(\theta_k \frac{\beta_{ik}}{s_k} - e_{ki} \ln \frac{\beta_{ik}}{s_k} \right) \quad (2)$$

F is obtained from the residual contribution of the activity coefficient of the reference UNIFAC model,

$$\ln \gamma_i^R = q_i \left[1 - \sum_k \left(\theta_k \frac{\beta_{ik}}{s_k} - e_{ki} \ln \frac{\beta_{ik}}{s_k} \right) \right] \quad (3)$$

By analyzing Eqs. (2) and (3), we can see that the higher the value of F for a certain group (subscript k), the less is the contribution from that specific group. Also, the larger the value of F, the smaller is the residual contribution to the activity coefficient. The F-values of Eq. (2) are shown in Figure 4 for system 1-butanal-n-hexane at 318 K as a function of composition. Figure 4 show that the contributions of the CHO group are higher compared to the CH_3 group for both reference UNIFAC and UNIFAC-CI models. Contributions from group CH_3 are almost the same for the reference UNIFAC and UNIFAC-CI models but different for group CHO (at the infinite dilution range of both compound of the binary system) suggesting that the difference between the two models is caused by the AIPs related to the CHO group. The figure also reveals problems of the UNIFAC-CI model at low concentrations, i.e., in the near infinite dilution region both compounds of the binary systems. From this analysis, several alternatives were identified in order to improve the performance of the UNIFAC-CI model.

- Use more weights on the objective function (for parameter regression) for those problematic systems at lower concentrations.
- Introduce a higher order CI for group CHO or introduce a new unique CI parameter only for the alkane–aldehyde systems for the interaction which involves C–O atom interaction.
- Add infinite dilution activity coefficient data for regression of the interaction parameters. However, this alternative will not be applied yet in order to get a fair comparison with the reference UNIFAC model where their GIPs were not regressed from infinite dilution activity coefficient data. The performance of the UNIFAC-CI model involving hydrocarbons (alkane–cyclic alkane, alkane–alkene, cyclic alkane/alkane– aromatic, cyclic alkene/alkene–aromatic) which only involves C–C interaction are quite good and does not need further improvement. Therefore, for further analysis only systems which involve C, O, and H atoms were investigated. This means that only C–O, O–C and O–O related AIPs are refitted (involving 171 datasets).

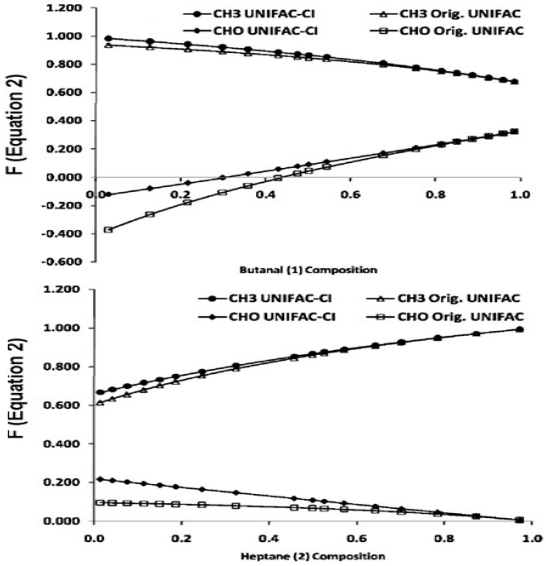

Figure 4: Values of F with respect to composition for 1-butanal-n-heptane at 318K.

Assigning higher order CI parameters

The second alternative was found to improve the model performance. A second order CI ($^{\upsilon}\chi^2 = 0.1179$) was introduced for the CHO group specifically for the alkane–aldehyde systems which are represented by group interaction CH_3–CHO. Therefore, a new AIP which is e_{C-O} is introduced to the original set of AIPs as presented in Table 1. All 171 datasets were regressed sequentially according to the AIPs that they employ. The scheme for this sequential regression is as follows, step-1 (regress the parameters for the systems alkane/cyclic alkane–alcohol); step-2 (keeping all parameters regressed in step-1 fixed, regress only the new parameters introduced by the systems alkane/cyclic alkane–ethoxy, alkane/cyclic alkane–ether, alkane/cyclic alkane–tetrahydrofuran); step-3 (keeping all parameters regressed in step-2, regress only the new parameters introduced by the systems alkane–aldehyde, alkane/cyclic alkane–ester, alkane–carboxylic acid, alkane/cyclic alkane–ketone); the procedure is repeated where the alkane–aldehyde system appears, the new higher order CI and its parameter is introduced. The reader can obtain the complete regression-order list and until step-8 (keeping all parameters fixed at step-7, regress only the parameters introduced by the system aldehyde–ester, ether–ketone, tetrahydrofuran–ester, tetrahydrofuran–ketone, aldehyde–ketone, carboxylic acid–ketone, ketone–ester, diol–ether). Only in step-3 their corresponding binary systems and the involved AIPs from the author: (http://www.capec.kt.dtu.dk /documents/research/reg_order.pdf). It was found that when the second order CI is introduced for the CHO

group for interactions with all other groups, the correlation results of all other systems which contain aldehyde, such as, aldehyde–aromatic, aromatic–aromatic aldehyde, aldehyde–ester and aldehyde–ketone became worse.

Table 2: Correlation results for alkane–aldehyde systems compared between different representations of the CHO group.

Systems	AARD (%)	
	CHO group represented by 0^{th} and 1^{st} order CI	CHO group represented by 0^{th}, 1^{st} and 2^{nd} order CI
1-Butanal-n-heptane (318K)	12.18	1.27
2-Methylpropanal-n-heptane (318K)	11.51	1.06
2-Methylpropanal-n-heptane (335K)	11.43	1.01
1-Butanal-n-heptane (343K)	10.35	2.02
1-Pentanal-n-heptane (348K)	10.75	0.45

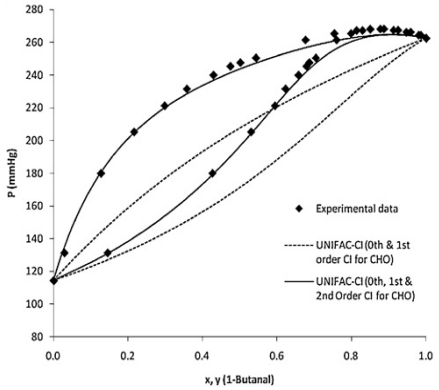

Figure 5: UNIFAC-CI VLE prediction for the system of 1-butanal-n-heptane at 318 K

Therefore, the second order CI interaction was introduced only in the step-3 to account specifically for the CH_3–CHO group interaction. Very good correlation results were obtained for the alkane–aldehyde systems although some systems involving alkane–ketone and cyclic alkane–ester show a slight (but negligible) increase in the AARD. The correlation results for the alkane–aldehyde systems are given in Table 2 and compared against the AARD corresponding to only using the zeroth and first order CI for the CHO group. Figure 5 shows the VLE phase diagram for the 1-butanal-n-heptane (318 K) systems for UNIFAC-CI when the zeroth and first order CI were assigned for the CHO group and when second order CI was added. Figure 5 shows that when the second order CI was introduced for the CHO group, the prediction by the UNIFAC-CI model conforms very closely to the experimental data compared to when only zeroth and first order CI were used for describing the CHO group. This shows that by revising the group representation through CI might improve the correlation for certain problematic systems. That is, providing more structural information to the model. The new sets of AIPs for systems that have been refitted represented in Table 3. This procedure now will be repeated for systems with other atoms (N, S, etc.) – not being covered in this paper.

Table 3: New set of AIPs regressed after the introduction of a second order CI for CHO group.

AIPs	Value	AIPs	Value
$b_{C\text{-}C}$	977.7980	$c_{C\text{-}O}$	-65.5433
$c_{C\text{-}C}$	-108.1096	$e_{C\text{-}O}$	67.5523
$e_{C\text{-}C}$	-109.4275	$bh_{C\text{-}C}$	-145.1011
$b_{C\text{-}O}$	-1149.5886	$bh_{O\text{-}C}$	71.5612

Conclusions

The UNIFAC-CI models developed by González et al. [4] are powerful predictive tools which can be used in cases where reference UNIFAC model parameters are missing. However, UNIFAC-CI model does not always perform well and deviations are seen also against the reference model, for certain systems. An analysis was therefore initiated, at first in order to study molecules containing C, H and O with special focus at low concentrations. Furthermore, by revising the CI description of group CHO, which appeared to be the cause for unreliable predictions, the performance of UNIFAC-CI model improved, especially for alkane–aldehyde systems.

Acknowledgement

The author gratefully acknowledges the financial support from the Ministry of Higher Education of Malaysia and Universiti Teknologi Malaysia.

References

1. R. Gani, P. Harper, M. Hostrup, Ind. Eng. Chem. Res. 44 (2005) 7262–7269.
2. J. Marrero, R. Gani, Fluid Phase Equilibr. 183–184 (2001) 183–208.
3. L.B. Kier, L.H. Hall, J. Pharm. Sci. 70 (1981) 583–589.
4. H.E. González, J. Abildskov, R. Gani, P. Rosseaux, B. Le Bert, AIChE. J. 53 (6) (2007) 1393–1634.
5. H.E. González, J. Abildskov, R. Gani, Fluid Phase Equilibr. 261 (2007) 199–204.
6. A. Mohs, A. Jakob, J. Gmehling, AIChE. J. 55 (6) (2009) 1614–1625.
7. R. Gani, H.E. González, AIChE. J. 55 (6) (2009) 1626–1627.
8. J.G. Hayden, J.P. O'Connell, Ind. Eng. Chem. Process Des. Dev. 14 (1975) 209–216.
9. H. Hansen, P. Rasmussen, Aa. Fredenslund, M. Schiller, J. Gmehling, Ind. Eng. Chem. Res. 30 (1991) 2352–2355.

List of Publication

1. A.A. Mustaffa, G.M. Kontogeorgis, R. Gani, Fluid Phase Equilibr. (2010), doi:10.1016/j.fluid.2010.09.033

Tatyana Nesterova
Phone: +45 4525 2848
E-mail: tan@kt.dtu.dk
Discipline: Reaction and Transport Engineering

Supervisors: Søren Kiil
Kim Dam-Johansen

PhD Study
Started: January 2009
To be completed: December 2011

Self-Healing Anticorrosive Coatings

Abstract
Self-healing coatings have received increased attention during the last decade as a new approach to corrosion protection. In this project, microcapsule-based approach is investigated. Four microcapsule synthetic procedures have been analysed, microcapsules with six different core materials have been prepared, and issues relevant to formulation of an epoxy-based self-healing anticorrosive coating are investigated.

Introduction
Self-healing materials have become a very intense field of research in the last decade [1,2]. These materials have a built in capability to retain functionalities and restore structural integrity autonomically after material damage. Different triggering mechanisms, that can impose self-healing processes in thermoset polymeric systems, have been proposed. Among them, judging from the number of publications [1] self-healing systems utilizing a mechanical stimulus, seem to be the most realistic approach to truly autonomous self-healing polymeric coatings. The approach is based on incorporation of microcapsules, filled with reactive chemicals, into the polymer matrix. The microcapsules, one of which is shown schematically in Fig. 1, are spherical particles with a typical diameter of 10 – 200 μm, consisting of a solid polymeric shell and a liquid core material.

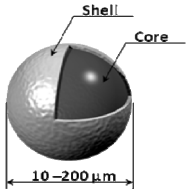

Fig. 1: Schematic picture of a microcapsule

When a microcrack, originating from internal stress or a physical damage, propagates through the coating, the microcapsules rupture and release healing agents, which flow to the fracture plane due to capillary forces. The healing agents then start to react, form a polymer network, and 'glue' the crack.

Specific Objectives
This PhD project aims to develop self-healing coating for above water heavy-duty anticorrosion protection. To reach the aim, first of all, a model coating system has to be chosen. Secondly, microcapsules suitable for introducing them to the coating system need to be prepared. This requires choice of shell materials and healing agents, optimization of methods for their encapsulation, and syntheses with subsequent product analysis. The obtained microcapsules have to comply with the following requirements: remain intact during storage, coating formulation and application; contain sufficient amount of chemicals with fast reaction kinetics, rupture readily when a coating is damaged; exhibit good adhesion with the polymer matrix; not compromise mechanical properties of the matrix.

Once the microcapsules are prepared, investigation of the mutual influence of capsules and binder system needs to be carried out. It includes assessment of solvent resistance of the capsules; investigation of microcapsule dispersion in a chosen binder; determination of a critical microcapsule volume concentration; formulation and application of a microcapsule-containing anticorrosive coating; study of coating performance and comparison to a coating with pigment/filler in place of microcapsules. On this stage modeling is also desired to estimate theoretical healing efficiency and its dependence on concentration of capsules, their diameter and crack volume.

The last part of the project is investigation of self-healing ability of the coating and its verification.

Results and Discussion

Polyepoxide barrier coating has been chosen as a model system for modification and further investigation. For the maximum materials compatibility with the matrix and cross-linking at the application temperature interval an epoxy-amine pair was considered as self-healing system. The materials of interest were bisphenol A and F epoxidized resins, alkylglycidyl ether (C12-C14) and triglycidyl ether of polyoxypropyleneglycol. Encapsulation of dicyclopentadiene and linseed oil was also performed. Poly(urea-forlmaldehyde) and poly(melamine-urea-formaldehyde), known for cross-linked and insoluble polymer formation, were used as the shell materials to ensure mechanical strength and stability of the capsules.

Four out of several microencapsulation methods, proposed in the literature, have been investigated. Each method has been evaluated and compared to the alternatives. The important parameters considered were stability of the microcapsules and ease and time of their preparation. The results of the performed study are described in [3].

Due to good repeatability of results of the synthesis, linseed oil-filled microcapsules have been introduced to the coating system for further investigation. The same was performed with alkylglycidylether-filled microcapsules, Fig. 2, due to expected high mechanical strength.

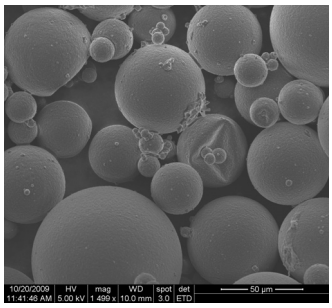

Fig. 2: SEM micrograph of poly(melamine-urea-formaldehyde) microcapsules

Initial studies have shown that the both kinds of microcapsules remain intact in xylene for more than a week. This time is sufficient for coating formulation and curing. Investigation of dispersion of microcapsules in bisphenol A epoxidized resin included stirring 5, 15 and 30 minutes at 550 and 1100 rpm stirring rates with and without addition of solvent. The most drastic decrease in a number of intact linseed oil-filled capsules was observed at the first 5 minutes of stirring in undiluted epoxy resin. This indicates that viscosity of the medium and not the mechanical stress originating from stirrer is the main factor affecting stability of microcapsule on the dispersion stage. It has been also found that capsules with poly(melamine-urea-formaldehyde) possess superior strength compared to poly(urea-formaldehyde) capsules and can be dispersed in undiluted binder. Oil absorption measurement could not be performed successfully for determination of critical capsule volume concentration because capsules were destroyed by mixing with a spatula.

The preliminary model, based on representative volume element filled with spherical microcapsules, which are randomly distributed and do not touch each other, has been developed. The model allows estimation of different parameters, for example, number of intersected capsules, volume released, healing efficiency, which is a ratio of volume released to volume of crack, in dependence of variable capsule volume concentration, their diameter and shell wall thickness. Fig. 3 shows that 15 vol % of microcapsules with 30 μm diameter will be sufficient for complete (theoretical) healing of a crack with dimensions 100x50x26 μm.

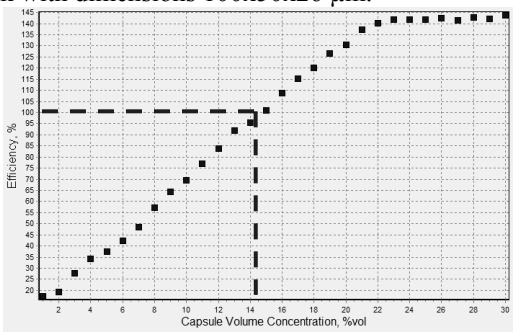

Fig. 3: Dependence of healing efficiency on capsule volume concentration

Conclusions

Self-healing anticorrosive coatings are the new and intelligent approach to long-lasting corrosion protection. In this project the microcapsule-based system is studied. Four methods for capsule preparation have been investigated. Two kinds of capsules – poly(urea-formaldehyde), filled with linseed oil, and poly(melamine-urea-formaldehyde), filled with alkylglycidylether, were introduced to the coating system for further studies. It has been already found that the latter capsules possess higher mechanical strength due to the shell wall chemistry.

Acknowledgements

Financial support by J.C. Hempel's Foundation and The Technical University of Denmark is gratefully acknowledged.

List of Publications

1. T. Nesterova, L.T. Pedersen, K. Dam-Johansen, S. Kiil, Dansk KemiingeniørKonference 2010, 46-47. Presented 16-17 June 2010
2. T. Nesterova, K. Dam-Johansen, S. Kiil, Coatings Science International 2010, 240-243. Poster 29 June 2010
3. T. Nesterova, K. Dam-Johansen, S. Kiil. Prog. Org. Coat. 2010, doi:10.1016/j.porgcoat.2010.09.

References

1. E.B. Murphy, F. Wudl, Prog. Polym. Sci. 35 (2010) 223-251
2. D.Y. Wu, S. Meure, D. Solomon, Prog. Polym. Sci., 33 (2008) 479-522
3. T. Nesterova, K. Dam-Johansen, S. Kiil, Prog. Org. Coat. 2010, doi:10.1016/j.porgcoat.2010.09

Anders Rooma Nielsen
Phone: +45 4525 2831
E-mail: arn@kt.dtu.dk
Discipline: Reaction and Transport Engineering

Supervisors: Kim Dam-Johansen
Peter Glarborg
Morten Boberg Larsen, FLSmidth A/S

Industrial PhD Study
Started: April 2008
To be completed: June 2011

Fuel Flexible Rotary Kilns for Cement Production

Abstract
The aim of this PhD project is to develop scientific based knowledge for precise prediction of the use of different alternative fuels in the material inlet end of cement rotary kilns. An important goal is to identify optimal rotary kiln design(s) and operation parameters for combustion of coarse, solid alternative fuels and at the same time maintain optimal conditions for cement clinker burning. This requires a solid understanding of how solid fuel combustion may affect the process stability in the rotary kiln system.

Introduction
Cement production is highly energy intensive. The global energy consumption by the cement industry is about 11 times the total energy consumption of Denmark [1, 2]. Coal and pet coke have traditionally been the primary fuels in the industry, but increasing fossil fuel prices and environmental concerns make other fuels attractive. Since energy costs accounts for 30-40% of the total costs of cement production, a great potential to reduce the overall production costs by replacing fossil fuels with alternative fuels exists. In this context "alternative fuels" refers to all non-fossil fuels and waste from other industries. Alternative fuels are typically cheaper than fossil fuels and in some cases the cement producer may even be paid to receive the alternative fuels. It is expected that the share of alternative fuels will continue to increase in the coming years, which will create a need for new technology to handle, treat and combust these fuel types.

Many types of alternative fuels are applied in the cement industry. The majority of the alternative fuels are on solid form, while liquids and gasses are less common. Some of the most common alternative fuels are refuse derived fuels (RDF, a mixture of house hold waste and industrial waste), tyre derived fuels (TDF), meat and bone meal (MBM) and waste wood. Technical feasibility, public acceptance, price and availability are typically the determining parameters for the type of alternative fuel that will be utilised at a specific cement plant.

It may be attractive to utilize coarse, solid alternative fuels into the material inlet end of cement rotary kilns in order to save expenses for shredding of the fuels to smaller particles and to increase flexibility. High temperatures in the rotary kiln and material retention times of 15-25 minutes provide good conditions for fuel burnout.

The main challenge is, however, that the solid fuel particles may be fully or partly covered by cement raw materials, which can lead to incomplete oxidation of the fuel char, forming reducing agents such as CO.

Local reducing conditions in the raw material bed are known to affect the product quality and process stability of the kiln system. The product quality can be influenced by raw material components such as Fe(III) being reduced to Fe(II). Fe(II) affects the formation of belite ($2CaO{\cdot}SiO_2$) and alite ($3CaO{\cdot}SiO_2$), the two strength-giving components in cement. The process stability is affected by increased release of sulphur from the raw materials, mainly by decomposition of $CaSO_4$:

$$CaSO_4\,(s) + CO\,(g) \rightarrow CaO\,(s) + CO_2\,(g) + SO_2\,(g) \quad (1)$$

SO_2 may react with alkali salts, forming eutectic salt mixtures which stick to the walls. Dust can adhere to this sticky layer and lead to deposit build-ups. These deposit build-ups accumulates typically in the material inlet end of the rotary kiln, or in the riser duct between the calciner and rotary kiln, where they lead to blockages that requires temporarily plant shut-down to remove.

Specific Objectives
The specific objective of this PhD project is to investigate how cement raw materials are affected by combustion of different alternative fuels under process

conditions similar to those in the material inlet end of rotary kilns. The project should also clarify how fuel-air mixing may be optimized in order to minimize the risk of local reducing conditions in the kiln system.

The investigations are based on a combination of theoretical studies, mixing experiments in a rotary drum at FLSmidth and sulphur release from cement raw materials in a fixed bed reactor at CHEC. Finally, a new high temperature rotary drum has been constructed in order to study fuel/raw material interactions during fuel combustion. A sketch of the high temperature rotary drum is shown on Figure 1.

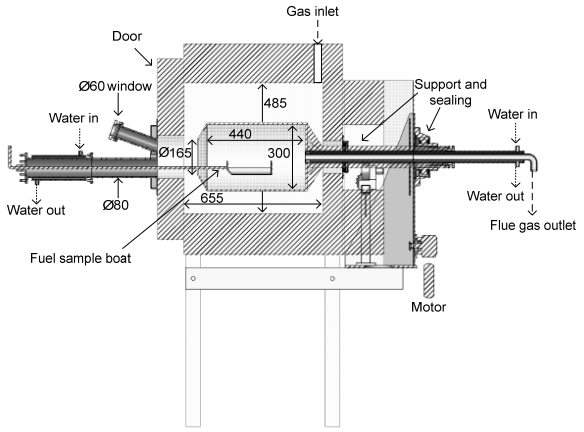

Figure 1: Sketch of high temperature rotary drum reactor for alternative fuel/cement raw material experiments.

Results and discussion

A parameter study has been conducted in the high temperature rotary drum in order to obtain quantitative information about the effect of temperature, oxygen concentration, drum rotational speed, volumetric fill degree of raw materials, fuel and raw material characteristics on the devolatilization and char oxidation of relevant alternative fuels. The main focus has been on tyre rubber and pine wood, but experiments have also been made with sewage sludge, pet coke and poly propylene.

The experimental results will be used to validate models for tyre rubber and pine wood devolatilization and char combustion. The devolatilization times of both tyre rubber and pine wood has successfully been predicted by the analytical solution to the heat transport model:

$$\frac{\partial T_p}{\partial t} = \frac{1}{r^2}\frac{\partial}{\partial r}\left(r^2 \alpha \frac{\partial T_p}{\partial r}\right) \tag{2}$$

with boundary conditions:

$$k_p \frac{\partial T_p}{\partial r} = h_{eff}\left(T_\infty - T_p\right) \quad \text{for r = R} \tag{3}$$

$$\frac{\partial T_p}{\partial r} = 0 \quad \text{for r = 0} \tag{4}$$

Figure 2 shows a comparison between experimentally found devolatilization times for tyre rubber and those predicted by the model. The deviations are generally within ± 20% - this was also the case for pine wood.

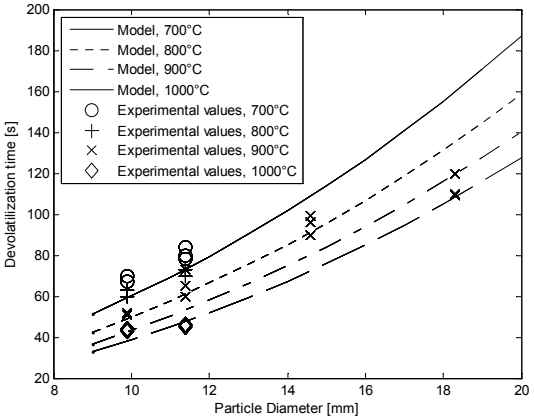

Figure 2: Comparison of tyre rubber devolatilization time predicted by model and by experimentally found values. 10% O_2. 5% volumetric fill degree in rotary drum. $\alpha = 1.25 \cdot 10^{-7}$ m^2/s.

Char combustion models are currently being developed. Sulphur release from the cement raw materials as a function of fuel type and fuel particle size has also been studied. It can be concluded that the fuel chemical and physical properties has a significant effect on the sulphur release. It is currently considered to submit a patent application for a method to reduce sulphur release from cement raw materials.

Conclusion

This industrial PhD project deals with combustion of solid, alternative fuels, fired into the material inlet of cement rotary kilns. The goal is to clarify how the combustion at this location may be optimized without negative impact on product quality or process stability.

Acknowledgements

This project is part of a research platform on future cement technology financed by The Danish National Advanced Technology Foundation, DTU and FLSmidth A/S.

References

1. Cembureau, Activity Report 2009, http://www.cembureau.be/.
2. Energistyrelsen, energistatistik 2009, http://www.ens.dk.

Linda Nørskov
Phone: +45 4525 2952
E-mail: lin@kt.dtu.dk
Discipline: Reaction and Transport Engineering

Supervisors: Kim Dam-Johansen
Peter Glarborg
Peter Arendt Jensen
Morten Boberg Larsen, FLSmidth A/S

Industrial PhD Study
Started: January 2009
To be completed: December 2011

Fuel Flexible Burners for Cement and Mineral Industry

Abstract
In cement production there is an increasing environmental and financial motivation for substituting fossil fuels for alternative fuels; waste and biomass. The alternative fuels introduce new challenges in the combustion processes. The present Industrial PhD project focuses on combustion of alternative fuels in the cement rotary kiln burner. An experimental setup for simulating diffusion-controlled combustion of large suspended particles in a flame is being built for studies of combustion characteristics and conversion paths of the new fuels. Simplified one-dimensional models for predicting the resulting rotary kiln flame formation and properties are being developed.

Introduction
Alternative fuels are combustible waste-derived products or biomass that can replace traditionally fossil fuels for heat and energy generation. Cement production requires a high energy input for raw material calcination and clinker formation. During the last 20-30years an increasingly amount of fossil fuels have been replaced by alternative fuels, motivated by the following reasons:

- Low fuel cost.
- Waste disposal problems can be solved as waste is utilised as energy and the ash residue is incorporated into the product.
- The fossil fuel resources are saved.
- The alternative fuels may be partly or fully CO_2-neutral.

In cement production a suspension fired burner positioned in a rotary kiln provides the thermal energy for cement clinker reactions. The limiting parameter for maximising the substitution of fossil fuels with alternative fuels in the rotary kiln burner is not known to a sufficient degree. The limiting parameter may differ from one type of alternative fuel to another and from one cement production plant to another. At present, little systematic knowledge about the alternative fuels combustion properties and their influence on the flame formation is available, and industrial introduction of new fuels is often based on trial-and-error and prior experiences.

Specific Objectives
The objective of this project is to develop a novel scientific framework for effective utilisation of alternative fuels in the main burner of cement and mineral rotary kilns. Success criteria:

1. Develop simplified mathematical modelling tools for evaluating alternative fuels based on knowledge of their physical and chemical properties. The modelling tools could be able to describe and predict combustion behaviour and flame properties in the rotary kiln burner.
2. Verify model predictions from experimental data on pilot and/or full-scale.
3. Evaluate the influence of alternative fuel properties on flame formation, fuel burn-out, and heat transfer in the rotary kiln burner.
4. Evaluate the effect of fuel properties on clinker product quality, and production stability.
5. Provide recommendations for optimised use of alternative fuels in the kiln burner.

Results and Discussion
An experimental laboratory setup is being developed in this project for simulating diffusion-controlled combustion of suspended particles in a rotary kiln flame. The experimental combustion studies of single, large fuel particles can provide new fundamental knowledge of the combustion characteristics and combustion conversion paths.

A sketch of the experimental setup is shown in Figure 1. A fuel particle is held by a platinum wire and inserted into a flow of hot gases provided by a propane flame. The fuel particle will undergo heating,

devolatilisation, and char oxidation. The reactions and conversion are recorded by means of a high speed camera.

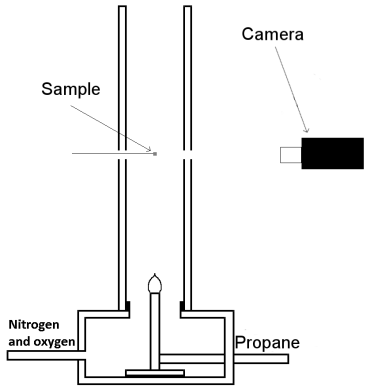

Figure 1: A sketch of the experimental reactor.

Figure 2 shows an example of a wood particle conversion in the experimental setup. From the experiments the time for ignition, devolatilisation and char oxidation may be found as function of oxygen concentration, temperature of the combustion gas, and gas flow velocity.

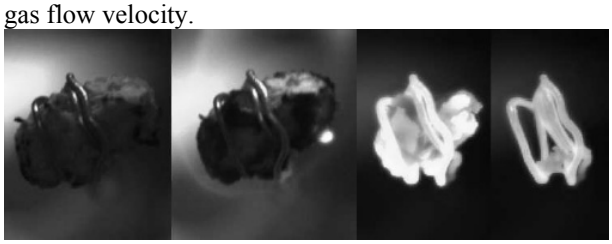

Figure 2: The combustion of a large fuel particle in the laboratory setup. From left; initial particle, volatile combustion, char oxidation, and ash residue.

The results from the experimental combustion studies will be modelled by simplified single particle conversion models. These fuel specific conversion models will be used as input for an overall model of the industrial scale flame.

Figure 3 shows a sketch of the simplified model system for the combustion calculations simulating a rotary kiln flame. Fuel particles and cold primary air is injected through a burner placed in a rotary kiln. Along the kiln length hot secondary air from cement clinker cooling is mixed into the reaction zone. The kiln length at which all secondary air is mixed into the flame is defined as l_{mix}. The fuel particles are initially heated by thermal radiation from the hot kiln walls and exchange heat with the combustion gases by convection. The combustion gas is heated by the energy released by combustion. In return, the hot combustion gas transfers heat to the surrounding kiln walls and the cement clinker bed mainly by thermal radiation. The model consists of coupled ordinary differential equations of gas temperature, particle temperature, and combustion rate.

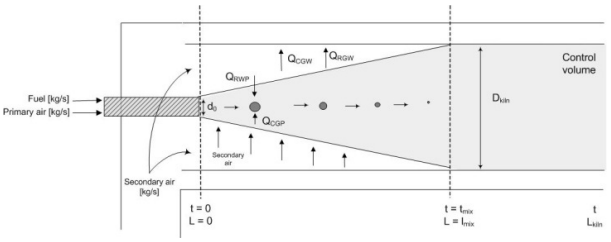

Figure 3: The model system of a rotary kiln flame.

An example of a calculated flame temperature profile in a rotary kiln is shown in Figure 4. The solid line is the gas phase temperature and the dotted line is the fuel particle temperature. Complete combustion is reached where the dotted line ends. The fuel particles and air are initially inserted at 100°C, and a rapid temperature increase is seen as the volatiles combust. Heat transfer to the surroundings causes the temperatures to decrease along the kiln length.

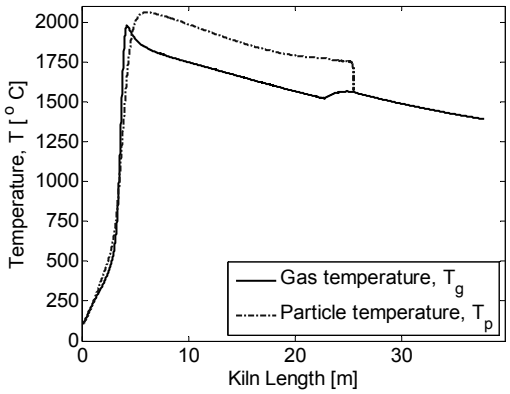

Figure 4: A calculated flame temperature profile.

Conclusions

The combustion process of alternative fuel differs from combustion of fossil fuel due to different physical and chemical characteristics. A laboratory setup is being built for studies of combustion of large particles in suspension. Simplified mathematical models of the combustion process are being developed.

Acknowledgements

This project is an Industrial PhD project performed in corporation between FLSmidth A/S and the CHEC Research Centre with co-funding from The Danish Agency for Science, Technology and Innovation. The project is a part of the research platform 'New Cement Production Technology', funded by the Danish National Advanced Technology Foundation, the Technical University of Denmark, and FLSmidth A/S.

List of publications

1. L. Nørskov, M.B. Larsen, K. Dam-Johansen, P. Glarborg, P.A. Jensen, Dansk Kemi. Oct. 2010
2. L. Nørskov, M.B. Larsen, K. Dam-Johansen, P. Glarborg, P.A. Jensen, Alternative fuel combustion in cement rotary kilns, Poster at Danish Chemical Engineering Conference (DK2), 16-17th July 2010

Sharat Kumar Pathi

Phone: +45 4525 2839
E-mail: skp@kt.dtu.dk
Discipline: Reaction and Transport Engineering

Supervisors: Kim Dam-Johansen
Jytte Boll Illerup
Weigang Lin
Klaus Hjuler, FLSmidth A/S

PhD Study
Started: January 2010
To be completed: December 2012

Processes for Low CO_2 Emissions

Abstract

Cement industry is one of the largest emitter of CO_2 other than power generation plants. In order to reduce CO_2 emissions from the cement plants, effective and economically feasible new technologies are to be developed. The carbonate looping process is a promising technology, which is particularly suitable for the cement industry as limestone in the raw meal could be used to capture CO_2. Integration of carbonate looping process into cement pyro-process has two advantages: 1) to capture emitted CO_2 and 2) to generate power for internal use, because high quality energy can be recovered from carbonate looping which is operated at high temperature unlike amine process. However, there are many challenges to this process like continuous and steady operation of dual fluidized bed reactors for calcination and re-carbonation, influence of different types of limestone, process integration and energy extraction which have to be overcome before realizing this process at industrial scale.

Introduction

According to Intergovernmental Panel on Climate Change, carbon capture from large stationary sources is considered as the mid-term mitigation option for climate change [1]. The major sources of CO_2 emitters are fossil fuel based power plants. The other major industry is the cement plants which emit CO_2 both from combustion and calcination process. One of the promising technologies for carbon capture applicable to any process is carbonate looping process, which is being investigated and developed aggressively in the recent years across the world. Carbonate looping process involves calcination and re-carbonation of sorbent material i.e. limestone, which is abundantly available and distributed across the globe. The main reaction of this process is calcination and carbonation of limestone,

$$CaO + CO_2 \rightarrow CaCO_3 \quad \Delta H_{298^oK} = -178 kJ/mol \qquad (1)$$

which is governed by equilibrium expression [2]

$$P_{CO_2,eq} = 4.137e^{12} \exp(-20474/T) \qquad (2)$$

By controlling temperatures and partial pressure of CO_2 in two inter-connected reactors, carbonation and calcination reactions are carried out for continuous capture of CO_2 from flue gas and release pure CO_2 for further storage [3]. The energy required for calcination can be supplied by oxy-fuel combustion or alternative energy sources [4] and high quality energy can be recovered from carbon capture reaction in the carbonator. Schematic representation of the carbonate looping process integrated to the cement plant is shown in Figure 1. In this process CO_2 is captured from flue gas emitted from a cement plant in the carbonator and carbonated particles are recycled back to the calciner. Oxy-fuel calciner is used for calcination of fresh and re-carbonated limestone. Part of calcined limestone is sent to the carbonator and the rest to the cement plant for clinker production. Thus, CO_2 emissions from cement production processes can be minimized.

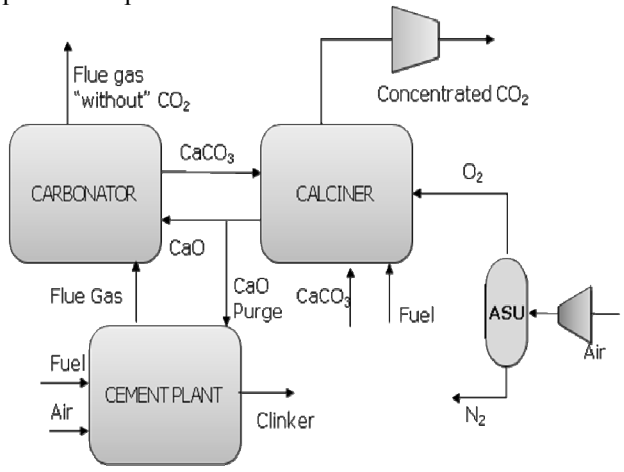

Figure 1: Schematic representation of de-carbonization of cement plant

However, before realizing the potential of this process, there are still many challenges to the process

like: continuous and stable operation of looping process in two fluidized bed reactors, oxy-fuel calcination process, and integration of the carbonate looping process in to existing or new cement plants. In order to overcome these challenges systematic study has to be conducted theoretically and experimentally.

Specific objectives

The objective of this project is to investigate the looping process at different operating condition and develop the carbonate looping process in a dual fluidized bed reactor which could be used for capturing CO_2 emitted from cement industries and power plants. In order to develop this process there are many unknown factors in understanding and implementing the process in industrial scale which has to be investigated. The specific objectives of the project are:

- Study the influence of different factors like particle size, type of limestone, operating conditions on the carbonate looping process
- Continuous and stable operation of the carbonate looping process in a dual fluidized bed reactor
- Modeling of the carbonate looping process integrated to cement pyro-process. This model could be used for optimization of the carbonate looping process and also for investigating the influence the different parameters.

Experimental setup

In order to perform looping experiments in dual fluidized bed reactors, an experimental setup has been designed and constructed. The schematic representation of the experimental setup is shown in Figure 2. A fluidized bed reactor shown in Figure 2 is a part of the looping setup. The strategy to achieve objectives is to perform experiments in single fluidized bed reactor determining adequate operational parameters and revealing potentially operational problems that may encounter in the looping setup.

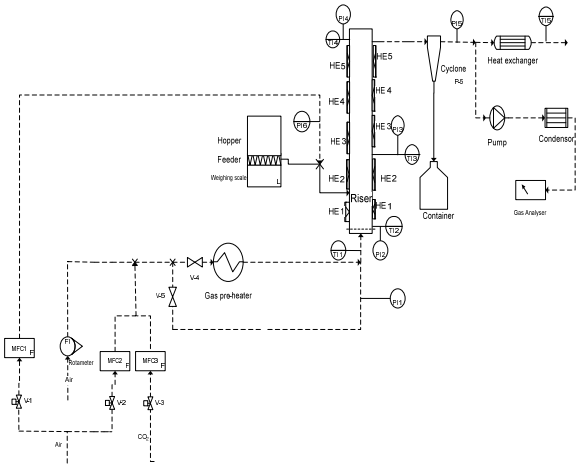

Figure 2: Schematic representation of experimental setup

Preliminary results

Preliminary experiments were performed in the single fluidized bed reactor to study the looping process operated in bubbling fluidized bed mode and fast fluidized mode for continuous re-carbonation of calcined limestone. Looping experimental results were compared with results from TGA under similar operating conditions to verify the deviation in degree of re-carbonation. Continuous re-carbonation experiments were performed at low particle circulation rate where carbon capture efficiencies were modest. Further there were no operational problems observed during the looping experiments conducted at low temperature.

Future work

Before installing the second fluidized bed reactors following studies will be carried out:

- Looping experiments in the bubbling fluidized bed reactor to investigate the influence of operating parameters
- Particle circulation rates with respect to gas velocity for different particle size ranges will be determined
- Calcination of limestone and re-carbonation of calcined limestone in a fast fluidization regime
- Based on above experimental data calciner will be designed and installed for continuous looping experiments

Conclusions

Carbonate looping process is a potential technology for reducing CO_2 emission from Cement industries. Objectives of this project are designed for systematic understanding of looping process. Achieving objectives of this project will be useful for successful implementation of looping process at the industrial scale.

Acknowledgement

This project is a part of Research Platform on New Cement Production Technology financed by Danish National Advanced Technology Foundation, FLSmidth A/S and DTU.

References

1. B. Metz, O. Davidson, H. de Coninck, M. Loos, L. Meyer, Special report on Carbon Dioxide Capture and Storage Intergovernmental Panel on Climate Change, Cambridge University Press, 2005.
2. E.H. Baker, J. Chem. Soc., 70 (1962) 464-470.
3. T. Shimizu, T. Hirama, H. Hosoda, K. Kitano, M. Inagaki, K. Tejima, Trans. IChemE. (1999) 62-68.
4. J.C. Abanades, J.C. Anthony, J. Wang, J.E. Oakey, Environ. Sci. Technol. 39 (2005) 2861-2866.

Ke Qin
Phone: +45 4525 2890
E-mail: ke@kt.dtu.dk
Discipline: Reaction and Transport Engineering

Supervisors: Anker Degn Jensen
Peter Arendt Jensen
Weigang Lin

PhD Study
Started: January 2009
To be completed: December 2011

High-Temperature Entrained Flow Gasification of Biomass

Abstract
Wood and straw gasification have been performed in a laboratory scale atmospheric pressure entrained flow reactor. Effects of reaction temperature, steam/carbon molar ratio, excess air ratio, and biomass type on the solid, liquid and gas products were investigated. With a rise of reaction temperature from 1000°C to 1350°C, the yield of producer gas (defined as the sum of H_2, CO, CO_2 and hydrocarbons up to C_3 species) increased dramatically. Higher temperature was beneficial to lower the tar yield while the soot yield showed a peak at 1200°C. With steam addition, the producer gas yield and in particular the H_2 yield increased gradually, while the CO yield decreased slowly. Steam addition gave an obvious reduction in the soot yield. Increasing excess air ratio from 0.25 to 0.50, there was no significant change in the producer gas yield, however the yields of H_2 and CO decreased and the soot yield also had a clearly decline. Moreover, wood and straw gasification provided similar product compositions. At 1350°C with steam addition, the experiment results are close to the equilibrium calculation results.

Introduction
Biofuels play an important role in helping to address some global challenges, such as energy supply security, and environment and climate protection. The biofuels are provided by both direct and indirect utilization of biomass. Gasification is a thermochemical process currently available for biomass utilization, and converts solid carbonaceous materials to a synthesis gas, a mixture rich in H_2, CO, CO_2, CH_4, by partial oxidation at elevated temperature. The syngas produced by gasification can be used to synthesize liquid fuels and chemicals or to produce power in a combined cycle plant.

Entrained flow gasification operates at higher temperature with smaller particles, often achieves a high carbon conversion, and produces a high quality syngas with low methane and tar content. Systematic studies on gasification of biomass in entrained flow gasifiers are scarce, and these studies mainly focus on the gas compositions and are performed at relatively low temperatures. Steam addition has a significant influence on the coal gasification, but there are no studies to reveal the effect of steam addition on biomass gasification in an entrained flow reactor. Although the entrained flow gasifier usually operates at high temperature (>1200°C) to produce a syngas with low or no tar content, soot produced at higher temperature is another serious issue, especially for biomass because of its high volatile content. Nevertheless, according to the authors' best knowledge, there is no literature considering soot formation in biomass entrained flow gasification. Therefore, a systematic study of biomass gasification in an entrained flow reactor is still of great interest.

Specific Objectives
In the present project, a gasification system including a bench-scale entrained flow reactor and other auxiliary facilities were developed, which is shown in Figure 1. The atmospheric pressure entrained flow reactor is externally heated by seven independent electric heating elements, which can be heated up to 1500°C. The SiC reaction tube inside the reactor has a length of 2 m and an inner diameter of 0.08 m. Besides the reactor, the complete facility includes equipments for fuel feeding, gas supply, solid particle sampling, tar sampling, and gas sampling and analysis.

Wood (beech saw dust) and straw (pulverized wheat straw pellet) were used in the present experiments. The wood and straw particles are smaller than 700 μm and 500 μm respectively. The medium diameter of wood particle (280μm) is bigger than that of straw particle (170μm).

Biomass gasification was investigated concentrating on the effects of reaction temperature (T), steam/carbon molar ratio (H_2O/C), excess air ratio (λ), and biomass

type (wood and straw) on the product yield. The fuel particle residence time (t) in the reactor was approximate 2-3 s. It was not possible to measure the total flow of gas products directly, so the total flow is calculated by using N_2 as a tracer. The yield of gas product from one kilogram fuel (Nm^3/kg fuel, dry and ash-free basis) can be calculated. Also, the yield of solid product can be expressed by the similar unit (g/kg fuel, dry and ash-free basis). The objective is to provide valuable insights into the biomass gasification in an entrained flow reactor.

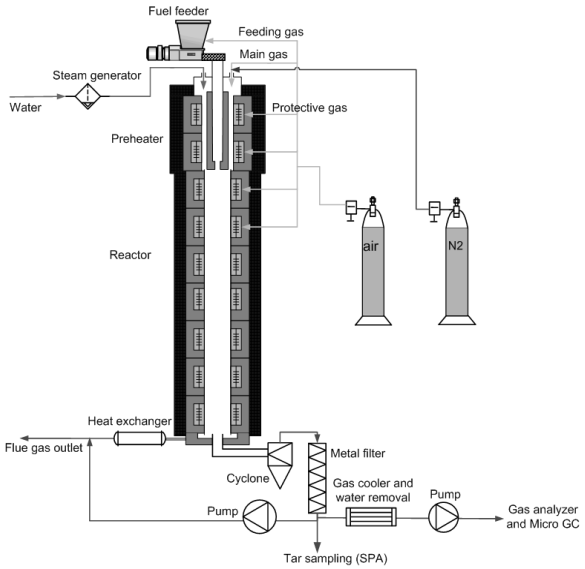

Figure 1: Sketch of entrain flow gasification system

Results and Discussion

Carbon mass balance

Based on the measured data of soot, gas, and hydrocarbons, carbon mass balances were calculated for all conducted experiments and the results are shown in Figure 2. The tar and larger hydrocarbons contents were estimated by the gap of carbon mass balance. A reasonable mass balance closure was achieved except for one experiment performed at 1000°C. Typically the mass balance closure was around ±9%. The largest deviation of the carbon mass balance (22%) at 1000°C may be caused by high tar levels and unmeasured larger hydrocarbon yields at this temperature.

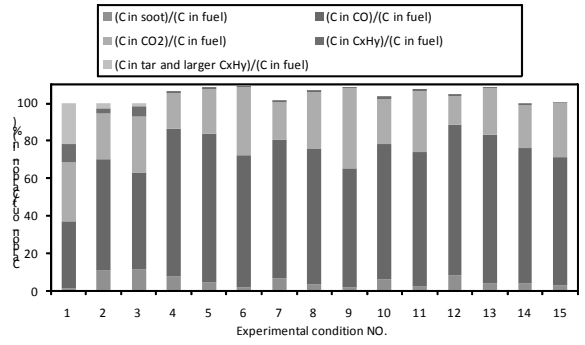

Figure 2: Carbon balances for all experiments

Effect of reaction temperature

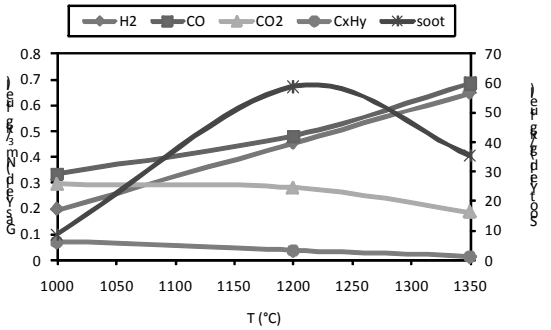

Figure 3: Effect of reaction temperature on the product yield in wood gasification at H_2O/C=0.5 and λ=0.25

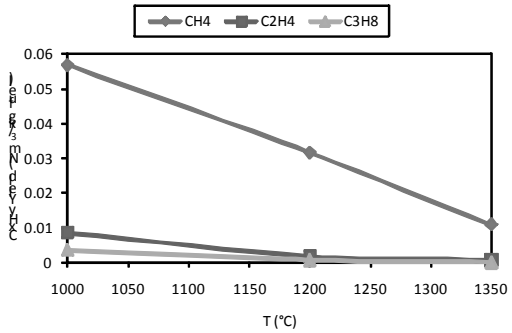

Figure 4: Effect of reaction temperature on the C_xH_y yield in wood gasification at H_2O/C=0.5 and λ=0.25

The effect of reaction temperature on the product yield for wood gasification at H_2O/C=0.5 and λ=0.25 is shown in Figure 3. The yields of H_2 and CO increased when the reaction temperature increased from 1000°C to 1350°C, while the yields of CO_2 and C_xH_y decreased. The yields of measured hydrocarbons at different temperatures are shown in Figure 4. CH_4 is the major product in hydrocarbons, which decreased quickly with a rise of temperature. The yields of C_2H_4 and C_3H_8 are very low in the whole temperature range, and especially at higher temperature, there is almost no formation of C_2H_4 and C_3H_8. As thermodynamically predicted, the declining yield of CO_2 may be explained as being due to the consumption of CO_2 by dry reforming reactions of hydrocarbons. These reactions increase with temperature and cause the yield of C_xH_y decreases and the yields of H_2 and CO increase [1,2]. The steam reforming reactions of hydrocarbons increase with temperature as well. These reactions also lead to the decreasing yield of C_xH_y and the increasing yields of H_2 and CO. Meanwhile, higher temperature (>1200°C) reverses the exothermic water gas shift reaction, which also reduces the yield of CO_2. Besides, the soot produced at higher temperature probably could be partly gasified by CO_2, which causes the reduction of the CO_2 yield too. The producer gas yield, which is defined as the sum of H_2, CO, CO_2 and C_xH_y, increased obviously with an increase of the reaction temperature from 1000°C to 1350°C. The molar ratio of H_2/CO increased when the reaction temperature was increased from

1000°C to 1200°C, and was then nearly constant even the temperature is increased to 1350°C. The gas product distribution displayed similar trends even though no steam was introduced ($H_2O/C=0$) at $\lambda=0.25$.

A sharp increase in the soot yield was observed when the reaction temperature was increased from 1000°C to 1200°C. Then it quickly declined as the reaction temperature further increased to 1350°C. It is widely observed that soot is produced in high temperature processes (1000°C-2500°C), such as pyrolysis and gasification. Thus increasing the reaction temperature favours soot formation. However, at higher temperature, soot or its precursors probably have higher gasification reactivity. As a result of the competition between soot formation and destruction, its yield starts to drop down after achieving a peak value at 1200°C. The same trend was found for the experiments at the same excess air ratio without steam addition ($H_2O/C=0$) and from 1200°C to 1350°C soot yield decreased.

Tar is formed during solid fuel pyrolysis and primarily consists of heavy hydrocarbons. It is often a product of gasification, especially at relatively low temperature. At 1000°C a significant amount of tar was produced, however at 1350°C the tar yields were lower nearly by two orders of magnitude. The lower tar yield at higher temperature could be attributed to the heavy hydrocarbon chains being cracked and reacting with steam to form H_2, CO and CO_2 [1]. The measured tar yield was highest at 1000°C, whereas the soot yield was lowest. At 1350°C, the amount of tar in the syngas was very low, but significant soot was produced. This shows that there is a tradeoff between tar and soot formation, which may result from soot formation by tar and hydrocarbon polymerization competing with soot gasification by CO_2 and H_2O at high temperature.

Effect of steam/carbon molar ratio

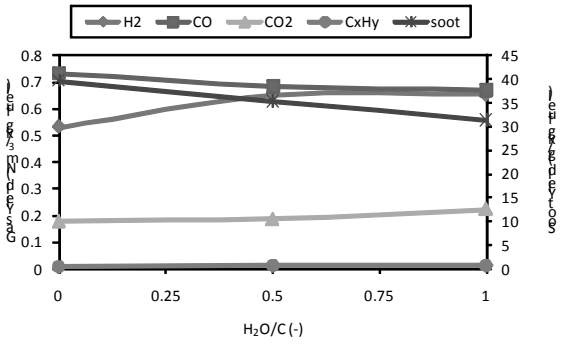

Figure 5: Effect of steam/carbon ratio on the product yield in wood gasification at 1350°C and $\lambda=0.25$

The effect of steam/carbon molar ratio on the product yield for wood gasification at 1350°C and $\lambda=0.25$ is shown in Figure 5. When the steam/carbon molar ratio increased from 0 to 1, the yields of H_2 and CO_2 increased gradually, accompanied with a little decrease of the CO yield. The probable reason is that the steam addition promotes the soot-steam gasification reaction and the water gas shift reaction [3,4]. The C_xH_y yield only had a small rise when the steam/carbon molar ratio was increased from 0 to 1, which might be caused by the cracking and reformation of larger hydrocarbons and tar. With addition of steam, the producer gas yield increased, but even a high amount of steam injection ($H_2O/C=1$) only makes small changes of the gas yield and composition. The molar ratio of H_2/CO increased with the increased steam/carbon molar ratio from 0 to 0.5 and was then nearly constant at steam/carbon molar ratio larger than 0.5. Similar trends were found at 1350°C and $\lambda=0.35$.

As the steam/carbon molar ratio was increased from 0 to 1, the soot yield decreased. Clearly, the steam addition is helpful to reduce the soot yield. However, even at large steam addition ratio of $H_2O/C=1$, there is still a certain amount of soot present in the syngas.

Effect of excess air ratio

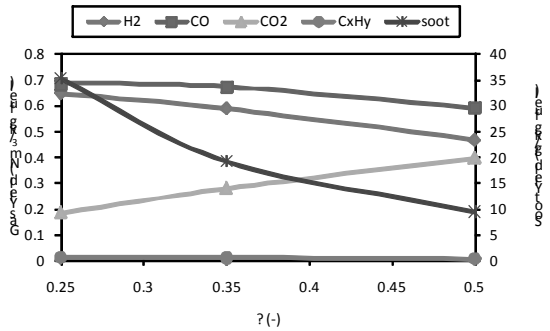

Figure 6: Effect of excess air ratio on the product yield in wood gasification at 1350°C and $H_2O/C=0.5$

The effect of excess air ratio on the product yield for wood gasification at 1350°C and $H_2O/C=0.5$ is shown in Figure 6. When the excess air ratio was increased from 0.25 to 0.5, the yields of H_2 and CO decreased, and the C_xH_y yield also reduced, whereas the CO_2 yield increased. This is due to the oxidation of soot, H_2, CO and other gaseous species. Moreover, the yields of H_2 and CO diminished more noticeably than that of C_xH_y when the excess air ratio was increased. Probably it indicates that the oxidation reaction between C_xH_y and oxygen is less important [5]. There was no obvious drop in the CO yield when the excess air ratio was between 0.25 and 0.35, probably because the partial combustion of hydrocarbons and soot could produce a certain amount of CO and then a part of them might be further oxidized to CO_2, which nearly keeps the CO yield constant. When the excess air ratio was increased to 0.5, the CO yield decreased. The amount of producer gas nearly kept constant with an increase of excess air ratio especially between 0.25 and 0.35. The molar ratio H_2/CO was decreased with the excess air ratio increased from 0.25 to 0.5. With and without steam addition, the gas yield had the same variation tendency as the excess air ratio increased.

The amount of soot decreased significantly with increasing excess air ratio from 0.25 to 0.5. This is because a larger part of the soot or soot precursors are combusted with increasing excess air ratio.

Effect of biomass type

Figure 7 compare the product yields in wood and straw gasification at 1350°C, $H_2O/C=0$, and $\lambda=0.25$. The results indicate that the wood and straw have similar gasification behavior in agreement with the literature [6,7]. That is to say, the biomass type has little influence on the product compositions and yields. An important difference between wood and straw is the high alkali content in straw. It is generally believed that the alkali has a catalytic role and thereby increases the char gasification rate. However, all the char was fully converted in the present study, so the influence of alkali catalysis on the char conversion cannot be observed in the product distribution. In other operating conditions, the product yields in wood and straw gasification have the similar tendency.

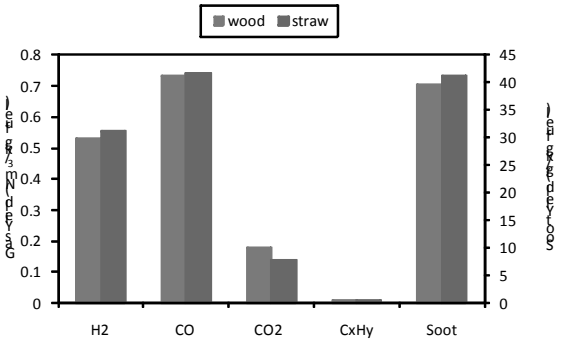

Figure 7: Effect of biomass type on the product yield gasification at 1350°C, $H_2O/C=0$, and $\lambda=0.25$

Comparison the results between experiment and equilibrium calculation

The equilibrium calculation is performed by Factsage. The reaction products were calculated at the chemical equilibrium conditions, which is according to the Gibbs free energy minimum. The calculation conditions are the same as the experimental conditions. There was not observed any carbon and hydrocarbons formation in equilibrium calculation, so the products are H_2, CO and CO_2. At 1350°C and with steam addition, the experiment results are similar to the calculation results. In other words, when highest temperature and steam addition are employed, the chemical reactions in the experiments are very close to equilibrium condition. Due to the highest temperature, faster reaction rates are obtained and chemical reactions easier achieve equilibrium conditions. With steam addition, the soot and hydrocarbons can react with steam, which is much easier to proceed than those react with CO_2, because the rate constant is larger in steam reaction than it in CO_2 reaction [8]. Steam addition helps reactions to approach to equilibrium condition quickly in limited residence time. As a result, highest temperature and steam addition are benefit to get closer to ideal equilibrium condition.

Conclusions

Gasification of two types of biomass, wood and straw, has been investigated in a laboratory scale atmospheric pressure entrained flow reactor. In all experiments, the char was completely converted and the calculated carbon mass balance closure was reasonable. The yields of producer gas (defined as the sum of H_2, CO, CO_2 and hydrocarbon up to C_3 species), H_2, and CO increased significantly when the reaction temperature was increased from 1000°C to 1350°C. The molar ratio of H_2/CO was close to 1 at higher temperatures (>1200°C) with steam addition. It was found that the tar content in the syngas was very low at 1350°C, while a significant level of soot was produced. However, the amount of tar was highest at 1000°C, whereas the soot yield was lowest. Thus, there is a tradeoff between tar and soot production. When steam was introduced, the yields of producer gas and H_2 increased slightly while the CO yield decreased a little. Steam addition tends to increase the molar ratio of H_2/CO, and a steam/carbon molar ratio equal to 1 is enough to achieve the requirement of $H_2/CO=1$. The soot yield can be reduced by the addition of steam. The amount of producer gas nearly kept constant with an increase of excess air ratio from 0.25 to 0.5 especially in the range of 0.25-0.35. Increasing excess air ratio decreased the yields of H_2 and CO, and affected the H_2 yield more than the CO yield. The molar ratio of H_2/CO also decreased with a rise of excess air ratio. However, increasing excess air ratio led to a sharp drop of the soot yield but an increasing of the CO_2 yield. The applied biomass type has little influence on the product compositions. At 1350°C and with steam addition, the experiment results are close to the gas composition in equilibrium calculation.

From the viewpoint of utilizing the syngas as a fuel, the highest temperature (T=1350°C), the largest amount of steam addition ($H_2O/C=1$), and a suitable excess air ratio ($\lambda=0.35$) are desirable because of the higher yields of H_2 and CO with lower yield of soot and almost without tar, the highest producer gas yield, and the expected molar ratio of H_2/CO (close to 1).

Acknowledgements

Danish Research Council for Technology and Production and the Danish Energy Agency are acknowledged.

References

1. S.N. Kriengsak, R. Buczynski, J. Gmurczyk, A.K. Gupta, Environ. Eng. Sci. 26 (2009) 739-744.
2. F. Pinto, C. Franco, R.N. Andre, C. Tavares, M. Dias, I. Gulyurtlu, Fuel 82 (2003) 1967-1976.
3. J. Gil, J. Corella, M.P. Aznar, M.A. Caballero, Biomass Bioenerg. 17 (1999) 389-403.
4. J.G. Lee, J.H. Kim, H.J. Lee, T.J. Park, S.D. Kim, Fuel 75 (1996) 1035-1042.
5. Y. Zhao, S. Sun, H. Tian, J. Qian, F. Su, F. Ling, Bioresour. Technol. (2009) 6040-6044.
6. M. Lapuerta, J.J. Hernández, A. Pazo, J. López, Fuel Process Technol. 89 (2008) 828-837.
7. Y. Lv, C. Ji, L. Guo, Journal of Xi'an Jiaotong University. 3 (2005) 238-242.
8. W. Klose, M. Wölki, Fuel 84 (2005) 885-892.

Alberto Quaglia
Phone: +45 4525 2812
E-mail: aq@kt.dtu.dk
Discipline: Systems Engineering

Supervisors: Rafiqul Gani
Gürkan Sin
Bent Sarup, Alfa Laval

PhD Study
Started: June 2010
To be completed: May 2013

Incremental Refinement of Process Design

Abstract
The use of process simulation tools is not common in the food and biofuels industries, much due to the complexity of fundamental modeling of thermodynamics and transport properties of the involved chemical species and their interactions. This project aims to introduce a paradigm shift in product-process design through application of Process Systems Engineering (PSE) tools.

Introduction
The design, development and reliability of a chemical product and the process to manufacture it, need to be consistent with the end-use characteristics of the desired product.

One of the common ways to match the desired product-process characteristics is through trial and error based experiments which can be expensive and time consuming. An alternative approach is the use of a systematic model-based framework in product-process design, replacing some of the time consuming and/or repetitive experimental steps.

In this approach, the development of a computer-aided tools for product-process design is very important for analysis, design, and/or identification of feasible chemical product candidates because it allows one to consider processing issues during the development of the product.

In general the use of process simulation tools is not common in the food and biofuels industries, much due to the complexity of fundamental modeling of thermodynamics and transport properties of the involved chemical species and their interactions. This project aims at introducing a paradigm shift in product-process design through application of Process Systems Engineering (PSE) tools.

Project Plan
The research will focus on the use of validated models in the early stages of product-process synthesis in order to eliminate redundant alternative process routes. The objective will be to identify the most promising process design routes so that the more time consuming and costly steps (computational as well as experimental) can be reduced.

To achieve this objective, a systematic framework for Computer-Aided Flowsheet Design (CAFD) will be developed and evaluated in collaboration with Alfa Laval. A particular emphasize will be given to deal with uncertainties in data and models that make part of the methodology (e.g. poor quality or limited amount of data, process model uncertainty). The task and training elements will include:

- Computer-aided design of candidate process flowsheets (CAFD).
- Integrated study of different time/length scales of the product-process chain.
- Development of models for the assessment of product performance.
- Feasibility assessment of the candidate flowsheets, comparison of the alternative flowsheets at their optimal operating points.
- Optimization of the most promising flowsheet via mixed-integer algorithms.
- Case studies from edible oil, biofuels and pharmaceutical industries would be selected to highlight the model-based methods and tools developed here.

Methodology for CAFD
A systematic framework for Computer-Aided Flowsheet Synthesis and Design has been developed and applied to the vegetable oil resources allocation problem. A graphical representation of the framework is given in Figure 1.

In the workflow the CAFD problem is first defined and identified (step 1, 2, 3), and then solved sequentially

by using simple and easy calculations to screen out infeasible alternatives and reduce the search space for the more complex part of the calculation [1].

The objective of step 1 is to define the synthesis/design problem. Also, project purpose (new product/process, process improvement, retrofit), performance metrics and objective function structure are defined at this stage.

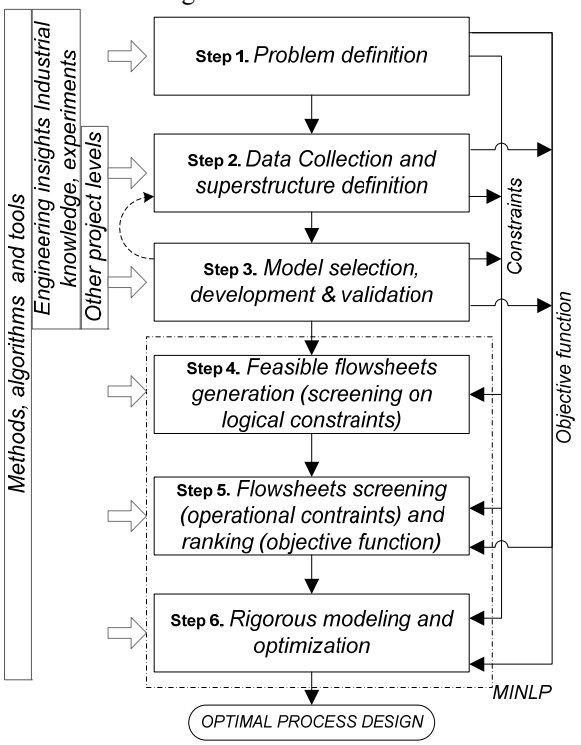

Figure 1: Systematic framework for CAFD

In Step 2 all the existing knowledge (industrial know-how, engineering insights, commercial knowledge...) relevant to the problem is collected. Being this knowledge multidisciplinary and multisource, particular emphasis is given to reconciliation and systematization, as well as to the development of an appropriate infrastructure for efficient data management, composed by a superstructure representing different flowsheet alternatives, structural constraints list, compounds and unit operations inventory and databases of reconciled data, structured in such a way to be accessible from all project levels [2]. Furthermore, performances metrics of similar and competing processes/products are collected for benchmark purposes.

All submodels needed for the multiscale model formulation are generated in step 3 (in collaboration with the Integrated Product-Process Design project). These include physical properties, unit operations, operational and investment cost and sustainability models; a systematic model generation framework is used to ensure consistency among the different models and scales. In order to cope with the lack of consolidated models and of public available data typical of this industry segment, an iterative procedure is followed for incremental model refinement and validation, based on uncertainty and sensitivity analysis to identify the model parameters which have the biggest impact on the model output and to estimate the uncertainty on model output due to parameter errors. Design of experiments techniques are then used to plan experiments in order to maximize the information gain with limited number of trials. Experimental results are added to the databases compiled in step 2 and used for model identification in step 3. The procedure is iterated until model output uncertainty is considered acceptable.

The objective of step 4 is to generate all feasible flowsheet alternatives by fixing sets of binary variables in the superstructure. A fast screening to eliminate unfeasible alternatives (violating structural constraints) as well as redundant options is performed at this stage to reduce the search space and the computational load for the further steps. In step 5 the search space is further reduced by screening out options that violate operational constraints (both shortcut and rigorous models can be used for this purpose). The remaining options are ranked with respect to the value of the minimized (or maximized) objective function, and the most promising alternative is selected.

If shortcuts models have been used in previous steps and one or more design variables is left for optimization, in step 6 the most promising alternative is further optimized with respect to the objective function using rigorous modeling. Performances metrics are calculated for the selected optimal options and are compared against the benchmark. Depending on the project purpose defined at level 1, project financial indicators (such as IRR, NPV etc) can be calculated for the selected option and used as inputs for project management decision.

Depending on the complexity of the model, step 4, 5 and 6 may be approached simultaneously via the solution of a MINLP problem [3].

The framework is applied to the flowsheet synthesis and design problem for soybean oil extraction and refining. According to the above described approach, the problem is formulated and solved to determine the optimal processing network for the vegetable oil extraction and refining (including biodiesel production and various options for byproducts valorization), as well as the optimal material flows to each processing step.

References

1. P. Lutze, R. Gani, J.M. Woodley, Chem. Eng. Process. 49 (2010) 547–558.
2. R. Singh, K. Gernaey, R. Gani, Comput. Chem. Eng. 33 (2009) 22–42.
3. H. Yeomans, I.E. Grossmann, Comput. Chem. Eng. 23 (1999) 709–731

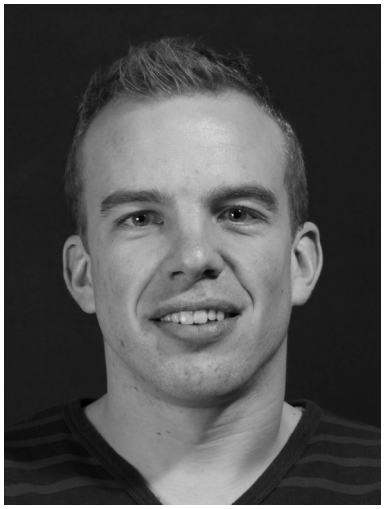

Claus Maarup Rasmussen
Phone: +45 4525 2829
E-mail: cma@kt.dtu.dk
Discipline: Reaction and Transport Engineering

Supervisors: Kim Dam-Johansen
Karsten H. Clement
Klaus Hjuler, FLSmidth

PhD Study
Started: January 2010
To be completed: January 2013

Preheater Design for High Energy Efficiency and Low Emissions

Abstract
The preheating facility in the cement industry facilitates the heat exchange between the hot flue gasses and the cold raw materials. The aim of this PhD project is to develop and test new a pre-kiln concept, which is more economic beneficial than the existing in terms of either capital or operational costs. This pre-kiln process can either be a new design for the preheating process or an alternative plant design with an integrated power production system, which obviates the need for a preheating process as we know it today.

Introduction
The chemical active component in cement is produced by burning mainly calcium carbonate and clay at temperatures above 1400 °C followed by a rapid cooling in order to freeze the high temperature crystalline structure of the clinker.

In a modern cement plant, this process is typically facilitated in a dry kiln system containing; a rotary kiln, a cyclone based preheater tower, a calciner and a clinker cooler.

The preheating process is carried out in a series of cyclones arranged in a counter current pattern where the cold raw meal is fed to the top cyclone, and the hot process flue gases is introduced to the bottom cyclone. The counter current pattern ensures high particle temperatures after preheating.

Figure 1 provides a schematic drawing of a typical pyroprocessing unit found in cement plants.

The basic layout for the preheating process is more than fifty years old [1], and parameters such as pressure drop, power consumption, heat loss, maintenance requirements and environmental impact have been optimized within the limitations of the overall design. However, the existing preheating process has some inherent disadvantages properties, such as:

- High capital costs, due to the necessary height of the preheating tower.
- High heat loss from unit surfaces and through hot dust and gases leaving the system.
- Not capable of operating with gas/solid ratios different from 1 (Process not adaptable to different operation conditions).

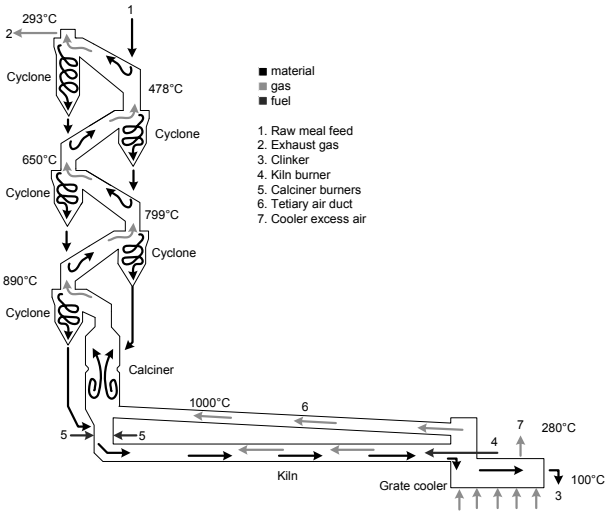

Figure 1: Schematic drawing of a typical pyroprocessing unit in a cement plant.

A new preheating process
Other process designs may be more suitable than the existing as cement manufactures faces a more and more restrictive legislation with respect to emissions of NO_x, SO_2, Hg and possible also CO_2 in the future, increasing energy prices and the wish for using alternative fuel sources, etc.

This new design must be cheaper to either operate or construct. There are several principal ways to achieve this. Some of these are:

- Compact, modular and scalable unit design (lower design and capital costs)

- Higher energy efficiency than existing design (lower heat losses or better utilization of the thermal energy)
- Acceptable operation over a range of G/S ratios
- Better emission control.

Specific Objectives

The main objective of this project is to investigate and develop a new pre-kiln concept for application in the cement industry, which can compete with the existing process design in terms of overall economy and environmental impact.

The first part of this project was a study of general heat exchange processes between particles and solids. This study, as well as a close cooperation with FLSmidth A/S has lead to several ideas for new pre-kiln concepts.

In the ongoing phase of this project, crucial elements in some of the most promising ideas are tested in order to clarify the potential of this concept for application in the cement industry. If the concepts show promising results, lab or pilot scale experimental setups will be constructed to analyze the processes further.

The third part of the project will concern developing a model which can describe the process and possible addressing scaling issues.

Raw Meal Fluidization Properties

The study of heat exchange processes between gas and particles clearly shows that only direct type heat exchange units are feasible for large scale cement plants, due to the limited heat transfer properties of the indirect type heat exchange units. The fluidization and transport properties of raw meal are therefore crucial for the any new design.

Raw meal is calcium carbonate and clay which is milled to sizes below d_{95}= 200 µm. An example of a cumulative size distribution is provided in Figure 2.

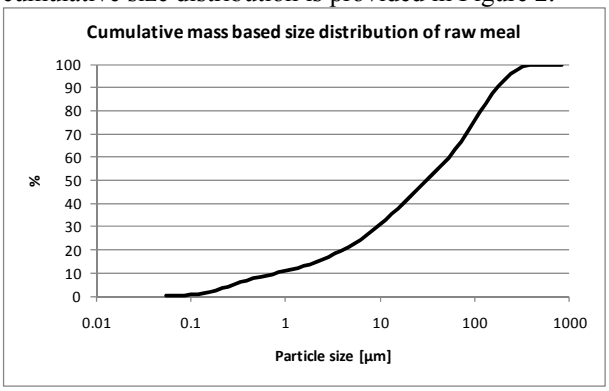

Figure 2: Typical cumulative mass based size distribution of raw meal [2].

From the data in Figure 2, it is evident that raw meal has a broad size distribution, which for fluidization purposes complicates matters, as the particles fluidize at different gas velocities.

Furthermore, raw meal is cohesive in nature, and will typically not fluidize at all. Particles with this behavior are categorized as group C particles by Geldart [3]. Typical fluidization behavior for this category is plug lift and/or generation channels upon attempt to fluidize.

This implies that normal fluidized processes like circulating fluidized or spouted bed cannot be utilized successfully for handling raw meal.

Alternative preheater designs

There are however some unit operations and designs that can handle cohesive group C particles, such as raw meal.

A cold lab-scale setup of a new gas/solid heat exchanger design has been constructed in order to study the particle and gas flows in this design. The operation principle is analogous to the existing preheating process, consisting of a series of alternating mixing and separation processes of particles and gas. The overall contacting pattern is counter current. This new design is modular and more compact than the existing design.

Experiments on a single stage setup indicate that it is possible to obtain an overall stage efficiency of up to 0.72 with raw meal. The gas/solid ratio was varied in the range from 0.2 to above 1.

Another possibility that has been investigated is the use of draft tube spouted beds. Initial experiments with a lab-scale draft tube spouted bed showed that stable operation with raw meal can be achieved. This phenomenon is not well documented in the published literature.

Other Process Designs

Other processes and process designs will also be investigated with focus on enabling production of electricity. This could imply that the future cement plant does not have a preheater, but instead a boiler configuration where the thermal energy of the hot gasses from the clinker production can be utilized for generating high pressure steam for power production and the raw meal is fed cold to a calciner.

Acknowledgements

This project is a part of a Research Platform on Future Cement Technology financed by Danish National Advanced Technology Foundation, FLSmidth A/S and DTU.

References

1 J.I. Bhatty, Innovation in Portland Cement Manufacturing, Portland Cement Association (2004), p. 224

2 Typical raw meal sample.

3 D. Geldart, Powder Technol. 7 (1973) 285-292.

Louise E. Rasmussen
Phone: +45 4525 2935
E-mail: ler@kt.dtu.dk
Discipline: Enzyme Technology

Supervisors: Anne S. Meyer
Jens F. Sørensen, Danisco A/S

PhD Study
Started: February 2007
To be completed: January 2011

Size Exclusion Chromatography for the Quantitative Profiling of the Enzyme Catalyzed Hydrolysis of Xylo-oligosaccharides

Abstract
High-performance size exclusion chromatography (HPSEC) is a widely used method for the *qualitative* profiling of oligosaccharide mixtures, including enzymatic hydrolysates of plant biomass materials. A novel method employing high-performance size exclusion chromatography for the *quantitative* analytical profiling of the progress of enzymatic hydrolysis of different xylan substrates was developed. The method relies on dividing the high-performance size exclusion chromatography elution profiles into fixed time intervals and utilizing the linear refractive index response (area under the curve) of defined standard compounds. A time study of the enzyme catalyzed hydrolysis of birchwood xylan and wheat bran by a *Bacillus subtilis* XynA xylanase (GH 11) was used as an example to demonstrate the workability of the high-performance size exclusion chromatography method for obtaining progress curves describing the evolution in the product profile during enzyme catalysis.

Introduction
Various xylans are currently under intensive study as carbohydrate sources for fermentation to biofuels or as sources of novel health-promoting food ingredients. Xylan basically consists of a backbone of β-1,4 linked D-xylopyranosyl residues that may be substituted to various degrees with arabinofuranosyl, glucuronate, or acetyl groups. The hydrolysis of the xylan backbone to a mixture of xylo-oligosaccharides can be catalyzed by endo-1,4-β-xylanases (xylanases, EC 3.2.1.8) [1]. With respect to investigation of the action pattern of endo-1,4-β-xylanases and in relation to the production and evaluation of potentially bioactive, prebiotic xylo-oligosaccharides, it is crucial to quantitatively asses the molecular size profile of the oligosaccharides. High-performance size exclusion chromatography (HPSEC) has been employed by several authors for analyzing the molecular weight distribution of different plant oligo- and polysaccharides in solution and to separate polydisperse materials into discrete molecular weight distributions [2]. HPSEC is based on permeation of a solute through a column packed with inert porous particles. The separation principle relies on the differentiation in the time of permeation of the polysaccharides into and out of the pores of the column packing which is related to their molecular size. The elution of the polysaccharide is then determined by the time it takes for the polysaccharides to travel through the pores [3]. In order to calculate the molecular weight of the polysaccharides, calibration curves can be constructed by measuring the retention volumes (or retention times) of synthetic polymer standards like pullulan or poly ethylene glycol molecules having a known narrow molar mass distribution.

Different detectors have been employed for HPSEC analysis of xylo-oligo profiles, but differential refractometry detectors are the most widely used [4]. Their operation is based on the continuous measurement of the difference in the refractive indices (RI) of the pure mobile phase and the mobile phase containing the substance. Generally, the area obtained underneath a RI curve represents the amount of sugars present [5].

When evaluating in detail the methods employed, it appears that no quantification has been used for xylo-oligosaccharide profiling by HPSEC. This makes it difficult to compare the results obtained by different groups. The question is therefore whether it is possible to use the HPSEC profiles for quantitative purpose. The objective of the work reported in the present paper was therefore to evaluate the possibilities for using HPSEC as a quantitative method to assess xylo-oligosaccharide profiles. As an example, we focused on analyzing the enzyme catalyzed hydrolysis of different xylan substrates by a wildtype *Bacillus subtilis* XynA xylanase. This particular enzyme has been widely used to study the hydrolysis of arabinoxylan and as a

template for evaluating the influence of wheat xylanase inhibitors on xylanase actitivy [6]. The hypothesis was that it was possible to exploit the HPSEC chromatographic profiles to obtain a quantitative, or at least semi-quantitative, insight into the evolution of the xylo-oligosaccharides during endo-xylanase treatment of xylan, and in this way use HPSEC to quantitatively assess different xylo-oligosaccharide product profiles.

Materials and Methods

Please see the original article

Results

Quantification

In order to verify that the area beneath a refractive index curve profile could be correlated to the concentration, a standard curve was measured for pullulan (1.0×10^4 g mol^{-1}) and xylohexaose (0.081×10^4 g mol^{-1}) – both at concentrations 0.2-2 mg ml^{-1}. R^2 values of 0.998 for pullulan and 0.994 for xylohexaose were obtained, indicating a linear correlation between the area and the concentration (Figure 1).

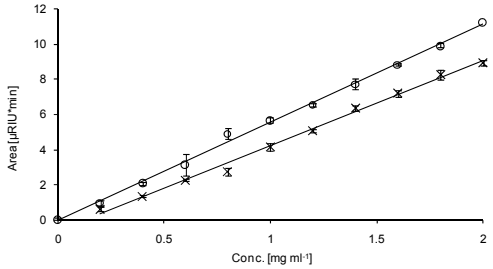

Figure 1: Standard curve (0.1-1 mg ml^{-1}) for Pullulan (1.0×10^4 g mol^{-1}) (○) and xylohexaose (0.081×10^4 g mol^{-1}) (x). Values represent the mean of three independent measurements and are shown ± 1 standard deviation.

The slopes of both standard curves appeared to be similar: 5.5 µRIU min ml mg^{-1} for pullulan and 4.8 µRIU min ml mg^{-1} for xylohexaose. However, a comparison of the 95% confidence intervals showed that there was a significant difference between the two slopes. Hence, for further quantification, pullulan was used, since the molecular weight was more equivalent to the assessed hydrolysis of birchwood xylan and wheat bran.

In principle, two different strategies may be applied when calculating the area of the chromatographic profiles in order to quantify molecules with a specific molecular weight distribution. First, the profile could be divided into fixed time intervals which are not directly correlated to the retention time of specific standards (Figure 2A). The area of the profile could then be calculated for each time interval. A second strategy could be to use time intervals based on the retention time of specific standards (Figure 2B). However, most likely the time intervals would then have different length and therefore have to be standardized by dividing the calculated area by the time interval. This would imply that much information would be lost. We therefore continued with fixed time intervals in order to make a quantification of the different molecular weight distributions.

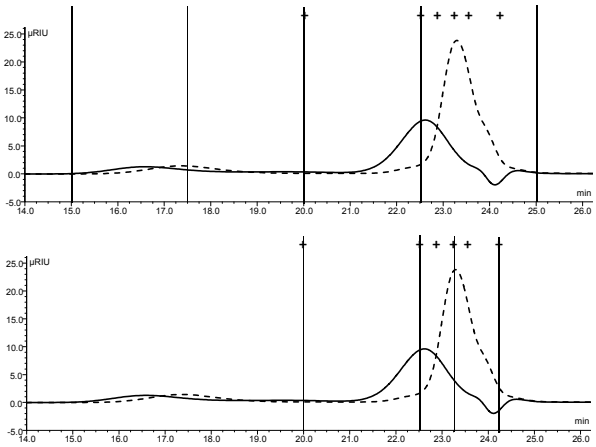

Figure 2: Two strategies for calculating the area of chromatographic peaks. A. Calculation of area based on fixed time intervals. B. Calculation of area was based on time intervals made from the retention time of specific standards. Molecular weight markers (+) from left to right are 40×10^4, 1×10^4, 0.6×10^4, and 0.13×10^4, xylohexaose, and xylose. The vertical lines in both figures represent the time intervals.

Enzymatic hydrolysis

The strategy with fixed time intervals was applied on a time study of the catalyzed hydrolysis of birchwood xylan by BsX. Since this substrate was water soluble, the initial profile of birchwood xylan after 0 h of incubation showed its molecular weight distribution (black line, Figure 3A).

The initial chromatographic profile was composed of three peaks, where the first peak appeared after 16.8 min. Since this was earlier than the elution of the 40×10^4 g mol^{-1} molecular weight standard, these fragments had a molecular weight larger than 40×10^4 g mol^{-1}. The birchwood xylan also contained smaller fragments, eluting at 22.5 min, and the molecular weight of these fragments was estimated to be 1.1×10^4 g mol^{-1} using the calibration curve (Data not shown). Since a third peak appeared at the same time as the standard xylose (24.2 min), some xylose was also present in the substrate solution. During the incubation period, the molecular weight of the large and small fragments decreased as a result of the xylanase activity, where the molecular weight of the small fragments reached approximately 0.09×10^4 g mol^{-1} after 4 h. The apparent molecular weight of the large fragments only decreased relative little during the incubation period and was still larger than 40×10^4 g mol^{-1}. This relatively small change might be explained by the HPSEC setup where only one HPSEC column, being able to separate low molecular weight fragments and not molecules larger than 40×10^4 g mol^{-1}, was used.

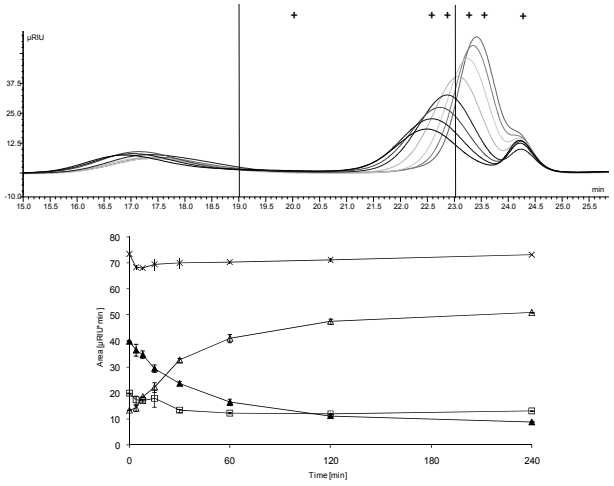

Figure 3: Catalyzed hydrolysis of birchwood xylan by BsX. **A**. HPSEC chromatographic profile after 0 min (black), 4 min (dark blue), 8 min (pink), 15 min (brown), 30 min (green), 60 min (light blue), 120 min (gray), and 240 min (gray blue). Molecular weight markers (+) from left to right are 40×10^4, 11×10^4, 1×10^4, 0.6×10^4, and 0.13×10^4, xylohexaose, and xylose. **B**. Progression curve of the area in the following time intervals: 15-19 min (□), 19-23 min (▲), 23-27 min (Δ), Total area 15-27 min (x). Values represent the mean of three independent measurements and are shown ± 1 standard deviation. The vertical lines represent the time intervals.

The HPSEC profiles were divided into three time intervals that resulted in an equal time division of 4 min, and the area underneath the curve in each interval was calculated (Figure 3B). The selection of the number of intervals was made as a compromise between obtaining detailed information and having a manageable overview.

For the time interval 15-19 min, which represented molecules larger than 40×10^4 g mol^{-1}, the area decreased only a little and mainly during the first 30 min of enzymatic treatment. Based on the areas in this time interval, the concentration of these relatively large fragments was 3.59 at 0 min and 2.37 mg ml^{-1} after 240 min. For the time interval 19-23 min representing fragments with a molecular weight between 0.29×10^4 g mol^{-1} and 40×10^4 g mol^{-1}, the area decreased mainly during the first 120 min. The concentration of these relatively smaller fragments prior to the enzymatic hydrolysis was 7.15 mg ml^{-1} and after 240 min 1.62 mg ml^{-1}. In contrast to the other two intervals, the area in the period 23-27 min representing fragments smaller than 0.29×10^4 g mol^{-1} increased during the whole incubation period, however leveling off after 120 min. At the beginning of the incubation period, the concentration was 2.41 mg ml^{-1}, and it increased to 9.13 mg ml^{-1} after 240 min.

The rate of attack of the xylanase could tentatively be evaluated by calculating the initial rate of decrease or increase in each time interval of the area curves for the first 15 min (Figure 3B). When the slopes were compared, the slope of the 15-19 min curve (0.14 µRIU) was smaller than the one of the time interval 19-23 min (0.70 µRIU). The rate of decrease for the 19-23 min time interval was similar to the rate of increase in the time interval 23-27 min (0.59 µRIU). This indicated that the concentration of the smaller fragments (0.29×10^4-40×10^4 g mol^{-1}) decreased faster than that of the large fragments (4×10^5 g mol^{-1}). It could therefore be inferred that the xylanase appeared to have a higher affinity for the smaller fragments, but the rate difference might also be a result of the differences in the concentration of the two different molecular size (substrate) profile groups.

When wheat bran was hydrolyzed by BsX, no molecules above 40×10^4 g mol^{-1} were measured (Figure 4A). Since wheat bran was insoluble and therefore was removed by centrifugation after the enzymatic hydrolysis, the HPSEC profiles only represent the soluble fragments released from wheat bran by the BsX action. Based on Figure 4A**,** the molecular weight of the released fragments was smaller than 0.55×10^4 g mol^{-1}. During the incubation period the molecular weight of the fragments decreased to an approximate molecular weight of 470 g mol^{-1} after 24 h of hydrolysis. This indicated that the released fragments apparently were the preferred substrate for the xylanase.

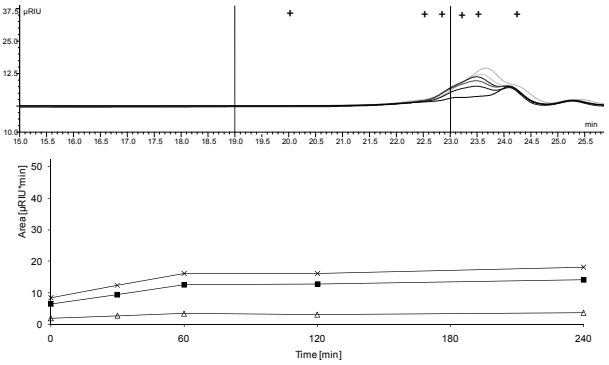

Figure 4: Catalyzed hydrolysis of wheat bran by BsX. **A**. HPSEC chromatographic profile after 0 min (black), 30 min (dark blue), 60 min (pink), 120 min (brown), 240 min (light blue), ánd 24 h (green). Molecular weight markers (+) from left to right are 40×10^4, 11×10^4, 1×10^4, 0.6×10^4, and 0.13×10^4, xylohexaose and xylose. **B**. Progression curve of the area in the following time intervals: 19-23 min (Δ), 23-27 min (■), Total area 15-27 min (x). Values represent the mean of three independent measurements and are shown ± 1 standard deviation. The vertical lines represent the time intervals.

As in Figure 3A**,** the profile in Figure 4A was divided into the same fixed time intervals in order to be able to compare results from both reactions. However, only the intervals 19-23 min and 23-27 min were used, since no fragments eluted earlier. As seen in Figure 4B**,** the area increased in both intervals mainly for the first hour and then only increased slightly. The initial concentration of the fragments with a molecular weight between 0.29×10^4 and 40×10^4 g mol^{-1} (eluting in the interval 19-23 min) was 0.36 mg ml^{-1} and increased to 0.66 mg ml^{-1} after 240 min of incubation. For fragments

smaller than 0.29×10^4 g mol^{-1}, the concentration increased from 1.17 mg ml^{-1} after 0 min to 2.55 mg ml^{-1} after 240 min of incubation. The initial rate of increase in the area in the time interval 23-27 was relatively larger (0.101 μRIU) than that in the 19-23 min period (0.028 μRIU). This, together with the larger area, again reflected the apparent preference of the xylanase for the smaller – or at least the soluble - fragments.

Discussion

The area of a chromatographic profile could in principle be used for quantification, since there was a linear correlation between the area and the concentration of specific standards (Figure 1). This linear correlation has been widely used in high-performance anion-exchange chromatography (HPAEC) for quantification, since most samples can be separated into distinct peaks where concentrations of specific molecules are estimated based on a standard curve of known standards [7]. However, HPSEC has mostly been used for measuring the molecular weight distribution, and therefore one peak could represent molecules with different molecular weights [5]. HPSEC has therefore until now mainly been used as a qualitative method, for monitoring the molecular weight distribution.

With this new method, it has now been possible to quantify how much a molecular weight distribution has changed and also to calculate parameters like standard deviation in order to tentatively estimate the reproducibility of the experiment and the method. Furthermore, the contribution from the substrate itself to the molecular weight distribution can now be subtracted, so only the enzyme activity can be estimated. This feature is particularly relevant when dealing with substrates like wheat bran which tend to auto-hydrolyze, at least wheat bran auto-hydrolyzes to a higher degree than for example birchwood xylan.

Despite our literature search on HPSEC, we found that only Kabel et al. [5] used a similar semi-quantitative method based on division of the HPSEC profiles into retention time intervals.

In the present study, birchwood xylan and wheat bran were enzymatically catalyzed by treatment with the xylanase BsX (Figure 3 and 4). Based on the HPSEC profiles, fragments with a molecular weight below 6×10^3 g mol^{-1} were produced from both substrates mainly during the first 4 h of incubation. When fragments after 4 h were compared, higher concentrations were released from birchwood xylan than from wheat bran. This corresponds to earlier results where the same enzymatic hydrolysis was analyzed by HPAEC yielding a total amount of xylo-oligosaccharides (DP 2-6) of 6.5 mM released from birchwood xylan and 3 mM from wheat bran. The observed differences in HPAEC and HPSEC of the two substrates may be related to differences in the complexity of the substrates. Since birchwood xylan was composed of approximately 97% xylose and therefore only had relatively few arabinose substituents, this substrate was more accessible than wheat bran where lower levels of fragments were produced. This was probably due to the more complex composition where physical access to the β-1,4 linkages in xylan was restricted by the various substituents on the xylan backbone [8].

Conclusion

A new method suitable for quantifying the molecular weights distribution of enzymatic hydrolysis allowed a more precise and detailed quantification of the product. The HPSEC cannot only be used as a qualitative method but also as a quantitative method where more information can be gained from HPSEC chromatograms. It is our belief that the quantitative approach reported here may be applied to other types of carbohydrate substrates and hydrolysates.

Acknowledgements

This study was partly supported by the Innovative Bioprocess Technology Research Consortium financed by the Danish Research Council for Technology and Production Sciences, Chr. Hansen A/S, Danisco A/S, Novozymes A/S. Financial support from the FOOD Denmark Graduate School, Center for Advanced Food Studies, Denmark, is also acknowledged.

References

1. P. Biely, Trends Biotechol. 3 (1985) 286-290.
2. M.J. Deery, E. Stimson, C.G. Chappell, Rapid Commun. Mass Spectrom. 15 (2001) 2273-2283.
3. S.S. Cutié, S.J. Martin, J. Appl. Polym. Sci. 55 (1995) 605-609.
4. S.C. Churms, J. Chromatogr. 720 (1996) 151-166.
5. M.A. Kabel, B. Bos, J. Zeevalking, A.G.J. Voragen, H.A. Schols, Bioresour. Technol. 98 (2007) 2034-2042.
6. J.F. Sørensen, O. Sibbesen, Protein Eng. Des. Sel. 19 (2006) 205-210.
7. A. Arnous, A.S. Meyer, Food Bioprod. Process. 86 (2008) 79-86.
8. C. Yang, S. Yang, W. Liu, J. Agric. Food Chem. 55 (2007) 3955-3959.

List of publications

1. L.E. Rasmussen, J.F. Sørensen, A.S. Meyer, J Biotechnol. 146 (2010) 146: 207-214.
2. L.E. Rasmussen, A.S. Meyer, J. Sci. Food Agric. 58 (2010) 762-769.
3. L.E. Rasmussen, A.S. Meyer, Biotechnol Lett. 32 (2010) 1883-1891.

Martin Hagsted Rasmussen

Phone: +45 4525 2923
E-mail: mhr@.dtu.dk
Discipline: Reaction and Transport Engineering

Supervisors: Kim Dam-Johansen
Stig Wedel
Jytte Boll Illerup
Kim Hougaard Pedersen, FLSmidth A/S

PhD Study
Started: September 2007
To be completed: March 2011

Reduction of SO_2 Emission from Modern Cement Plants

Abstract
The project concerns the emission of SO_2 from the preheater section of a modern cement plant, with primary attention on the reaction between CaO and SO_2. In this paper focus is on how CaO that recirculate from the calciner might contribute to the absorption of SO_2 in the top stages of the preheater tower. From the experiments it was found that high contents of CO_2 in the reaction atmosphere cause all CaO available for reaction with SO_2 to be consumed by CO_2 within the first 0.35 s. Our conclusion is that CaO from the calciner in it is present form does not contribute significantly to SO_2 absorption in the top stages of the preheater tower.

Introduction
Legislation concerning emission of SO_2 from cement plants has been tightened during the last decade, especially in the US and EU. The latest emission limit set by the US Environmental Protection Agency is 0.2 kg SO_2/ton of clinker. Tighter legislation calls for cheap solutions for reducing the SO_2 emission. To find such requires an understanding of the mechanisms that influence the emission of SO_2. In this paper we will look into how recirculation of CaO in a modern cement plant possibly can affect the emission of SO_2.

Today, most cement is produced by the dry process, illustrated in Figure 1. Raw meal, which mainly consists of limestone and clay, is fed to the preheater tower. It usually consists of 4-6 cyclone stages and a calciner. Through the cyclone stages the raw meal is, step by step and counter-currently, heat exchanged with the hot flue gas from the calciner/kiln.

The raw meal contains small amounts of sulfide, which is mostly found as pyrite (FeS_2). When pyrite is heated in an oxygen containing atmosphere, it will be oxidized to iron oxides and SO_2. This reaction is initiated between 400 and 600 ºC [1].

From full scale plants it is known that only about 50 w/w % of the incoming sulfide is emitted as SO_2 from the preheater tower, why some of the SO_2 formed must be absorbed by the raw materials inside the preheater tower. Literature [2-3] reports that CaO is a very reactive species towards SO_2. Internally recirculating calcined raw meal, which contains about 60 w/w % of CaO, might contribute to the absorption of SO_2 in the top stages, where SO_2 is formed. However, the CO_2 content in the preheater tower is about 30 vol %, why carbonization of CaO will take place at temperatures below 825 °C. Such conditions are present in most of the cyclone stages (see Fig. 1). Carbonization must therefore be considered a competing reaction for any available CaO in the calcined raw meal.

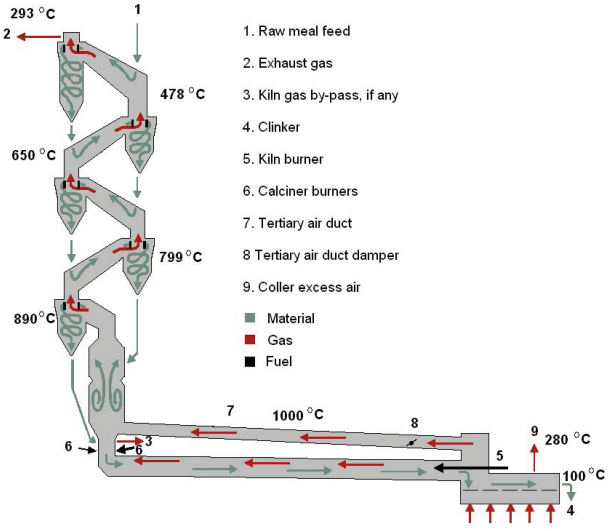

Figure 1: Illustration of the dry process for cement manufacturing.

Objectives
The goal of the Ph.d. project is to provide knowledge of the formation and absorption of SO_2 in the preheater, and to use that knowledge to diminish the SO_2 emission from present and future kiln system.

Experimental Procedure

The CaO used for reaction with SO_2/CO_2 was prepared from Faxe Bryozo limestone by flash calcination which was repeated twice. The method resulted in a partly calcined lime product which still contained about 40 w/w % $CaCO_3$. Next the CaO was reacted with SO_2/CO_2 in an entrained flow reactor, where it is possible to inject SO_2/CO_2 at four different locations in order to vary the contact time between particles and gas. All gases were preheated in order to ensure isothermal reaction conditions. The experiments were carried out with an SO_2 concentration of 1000 ppm and a CO_2 concentration of 25 vol%. The temperature setpoints were 500 and 550 ºC (in practice the temperature was about 15 ºC lower) and the feed rate into the reactor was 200 g/hr of partly calcined limestone particles.

Results

The full line graphs in Figure 2 show the conversion of CaO into sulfur species (left axis) while the dotted graph shows the unconverted fraction of the initial CaO (right axis), both plotted as function of reaction time.

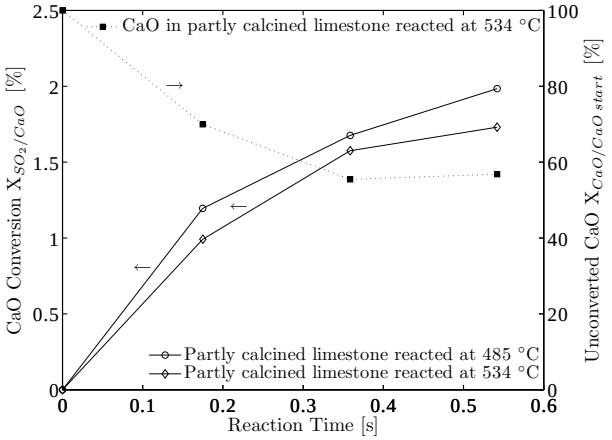

Figure 2: *Left axis*: CaO conversion with respect to SO_2. *Right axis*: Unconverted CaO.

It is seen that a higher conversion to sulfur species is observed at the lower temperature, showing a negative effect of temperature on SO_2 absorption. If the slopes of the CaO conversion measurements are interpreted as representing an apparent reaction rate it is seen that the reaction rate at both 485 °C and 534 °C continuously decrease as the reaction time increases. In fact the reaction is almost completed after 0.35 s at 534 °C. Considering the fraction of unconverted CaO in the partly calcined limestone, we see that it decreases very fast, reaching a constant level of about 55 % after 0.35 s. TGA measurements have shown that the decrease is due to an uptake of CO_2 which is about 25 times larger than the SO_2 uptake. BET measurements have furthermore shown that after 0.35 s only 10 % of the internal surface area found in the starting material is left.

Discussion and Conclusion

From the results presented here it is obvious that free CaO will react very fast with CO_2 if it is exposed to a CO_2 concentration higher than the equilibrium concentration. At temperatures used in our experiments it seems like the CaO/CO_2 reaction is completed within 0.35 s. The negative effect of higher temperatures as observed here is a consequence of the very fast uptake of CO_2. The partly calcined limestone used in our work will have a bipartite pore system with a main pore diameter of about 500 nm and a secondary pore diameter about 10-20 nm. In such a bipartite pore system the majority of the surface area will be situated in the secondary pore system. Both the CaO/CO_2 and the CaO/SO_2 reaction rates will increase with temperature. However, since the molar volume of $CaCO_3$ is about 2.5 times that of CaO. At higher temperature levels the secondary pore system blocks up faster so that the surface area available for reaction with SO_2 will decrease faster. This is observed as a negative effect of increasing the temperature level.

The reduction of surface area with decreasing fraction of unconverted CaO is also evidenced by that only 10 % of the initial BET area is left after 0.35 s.

The large uptake of CO_2 brings on the question whether SO_2 reacts with CaO or $CaCO_3$. This is important since the $SO_2/CaCO_3$ reaction is considerably slower than the SO_2/CaO reaction at low conversions [4]. The experimental results show that the CaO/SO_2 reaction only contributes to the observed conversion to sulfur species until the particles are saturated with CO_2. At a temperature of 534 °C, the CaO/SO_2 reaction only takes place within the first 0.35 s. At longer reaction times, the dominating mechanism for SO_2 absorption is the $SO_2/CaCO_3$ reaction. This is reflected in the leveling off of the reaction rate after 0.35 s at 534 °C.

These results, when interpreted in a preheater tower context, leads to the conclusion that recirculation of CaO from the calciner does not contribute to the absorption of SO_2 in the top stages of the preheater tower. The CaO that should be available for SO_2 absorption will have reacted with CO_2, forming $CaCO_3$, before reaching the cyclone stages where SO_2 is formed by pyrite oxidation.

Acknowledgements

This project is a part of a Research Platform on Future Cement Technology financed by Danish National Advanced Technology Foundation, FLSmidth A/S and DTU.

References

1. J.P. Hansen, SO_2 Emissions from Cement Production, Nørhaven Digital, Cph, Denmark, 2003.
2. R.H. Borgwardt, Environ. Sci. Technol. 4 (1) (1970) 59-63
3. S.K. Bhatia, D.D. Perlmutter, AIChE. J. 27 (2) (1981) 226-234
4. H. Liu, S. Katagiri, U. Kaneko, K. Okazaki, Fuel 79 (8) (2000) 945-953

Muhammad Riaz

Phone: +45 4525 2877
E-mail: ria@kt.dtu.dk
Discipline: Engineering Thermodynamics

Supervisors: Georgios M. Kontogeorgis
Erling H. Stenby
Wei Yan

PhD Study
Started: April 2008
To be completed: July 2011

Distribution of Complex Chemicals in Oil-Water Systems

Abstract
As the exploitable oil resources decrease, more sophisticated recovery methods are employed in the oil industry to produce the remaining resources. One result of using more sophisticated recovery methods is that oil field chemicals are more widely used, especially in the offshore oil production. These chemicals belong to different families and they have various functions. A fraction of added chemical goes into oil and the remaining is discharged to the sea via produced water. It is important to know accurately, how much of an added chemical will go to the water in order to report to the environmental authorities and how much of the chemical will go to the oil. This is becoming increasingly important for downstream processing. The objective of this project is to develop a predictive model for oil-water partition coefficients of complex chemicals, over a wide range of conditions and with minimum input of experimental information.

Introduction
Chemicals are added in almost all the stages in oil and gas production. It is generally accepted that efficient and cost effective oil and gas production is not possible without the use of chemicals [1,2]. Monoethylene glycol (MEG) is one of the most widely used production chemicals. It is used as a gas hydrate inhibitor to ensure safe production and transportation. The chemicals added to the oil and gas value chain at different stages reach to well stream and then to a series of separators and processing facilities. It is important to know the distribution of these chemicals in oil, water and gas streams because it is a key to the calculation of the amounts of chemicals required for a specific facility. It is also important information to fulfill the demand from environmental authorities in order to know the amount of chemicals and hydrocarbons (HC) in a processed water stream for ensuring the safety of marine life. Furthermore it is important for design and operation of separation equipments as well as to report the chemicals and water contents of fuel oil which may be crucial for downstream processing.

Over the last years, the use of these chemicals has increased considerably [1, 2] as shown in Figure 1. Here the production chemicals used at Statoil operated fields is shown on annual basis.

The partitioning of the chemicals can either be measured experimentally or predicted using a suitable thermodynamic model. The experimental method is expensive and challenging, partly due to the difficulties involved in measurements of such low solubilities. An evidence for this is the scarcity of such experimental data (with natural gas condensate and oil) in the literature.

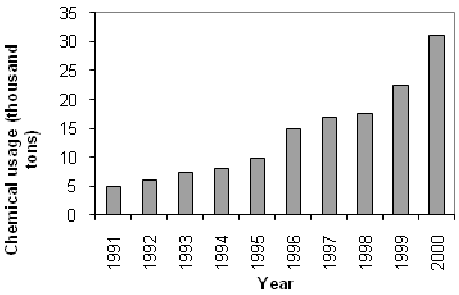

Figure 1: Trend in the use of production chemicals on Statoil operated fields [1].

The data are available for only few binaries and ternaries dealing with well defined hydrocarbon, MEG and water systems [3]. However for the development and validation of thermodynamic models experimental data are required. Therefore experimental work was carried out at Statoil Research Center, in Norway.

Specific Objectives
The general research issues to be addressed are the following:

- To identify the most important chemicals of interest

to Statoil applications, group them into families, collect experimental data of octanol-water partition coefficient (K_{ow}) and oil-water partition coefficient (K_{oil}) and investigate if correlations exist between them.

- To check different thermodynamic models and correlations against experimental values of Kow and Koil and select one to be used in the study, the model selected is the Cubic Plus Association (CPA) equation of state.
- To perform experiments for obtaining required phase equilibrium data and will then be used in model development.
- Extension of CPA to reservoir and refinery fluids and to develop a characterization method for CPA, to account for paraffinic (P), naphthenic (N) and aromatics (A) contents of a reservoir fluid.
- To calculate K_{ow} and K_{oil} of complex chemicals and evaluation of selected model.

Experimental Work

New experimental phase equilibrium data for "MEG + reservoir fluids" and "MEG + water + reservoir fluid" systems at temperatures 275-326 K and at atmospheric pressure are measured. The reservoir fluids used consist of two gas-condensates and light oil from the North Sea. The condensates are named as condensate-1(COND-1) and condensate-2 (COND-2). The properties of reservoir fluids such as mean molecular weight (MMW), density and PNA distribution is given in Table 1. Mutual solubility data and thermodynamic modeling are presented here for COND-1. The composition of COND-1 is given in Table 2.

Table 1: Properties of reservoir fluids used in this work.

Properties	COND-1	COND-2	Light Oil
MMW (g/mole)	112.7	106.9	266.00
Density (g/cm^3)	0.7562	0.7385	0.9055
C_{10+} (mass%)	40.766	28	91.45
P (mass%)	61	60	23
N (mass%)	27	28	57
A (mass%)	12	12	20

Apparatus and Procedure

The sketch for the experimental setup used in this work is shown in Figure 2.

Mixing and Equilibrium

MEG, condensate and water were mixed at a fixed temperature for 24 hours using a mixing machine in an air heated oven. For binary systems, approximately equal mass of MEG and condensate were added for mixing. The ternary system consists of MEG, condensate and water where the hydrocarbon phase was 50% (mass) and the polar phase was also 50% on mass basis. The polar phase consists of MEG and water where the composition of MEG ranges from 40% to 90% which is of interest to the industrial applications in the North Sea.

Table 2: Composition of condensate-1.

Component	Weight %	MW g/mole	Density g/cm^3
Ethane	0.001	30.07	0.3567
Propane	0.351	44.09	0.5067
iso-Butane	1.229	58.12	0.5621
n-Butane	4.031	58.12	0.5831
Neopentane	0.030	72.15	0.5970
iso-Pentane	3.494	72.15	0.6233
n-Pentane	4.659	72.15	0.6299
C_6 total	**7.770**	**85.0**	**0.6662**
n-Hexane	3.599	86.2	0.6627
iso-Paraffins (C_6)	3.722	86.2	0.6608
Naphtenes (C_6)	0.448	70.1	0.7481
C_7 total	**13.016**	**91.4**	**0.7362**
n-Heptane	2.911	100.2	0.6869
iso-Paraffins (C_7)	3.213	100.2	0.6905
Naphtenes (C_7)	5.811	86.1	0.7681
Aromatics (C_7)	1.081	78.1	0.8831
C_8 total	15.293	103.6	0.7686
n-Octane	2.197	114.2	0.7070
iso-Paraffins (C_8)	2.146	114.9	0.7068
Naphtenes (C_8)	7.968	103.0	0.7711
Aromatics (C_8)	2.982	92.1	0.8720
C_9 total	**9.363**	**118.5**	**0.7806**
n-Nonane	1.894	128.3	0.7230
iso-Paraffins (C_9)	2.479	128.3	0.7229
Naphtenes (C_9)	1.999	119.2	0.7944
Aromatics (C_9)	2.991	106.2	0.8721
C_{10+}	**40.766**	**189.4**	**0.8464**

After mixing the mixture was transferred to two identical glass equilibrium cylinders and was kept for at least 18 hours to attain equilibrium. The equilibrium cylinders contain holes and caps fitted with septa for sampling.

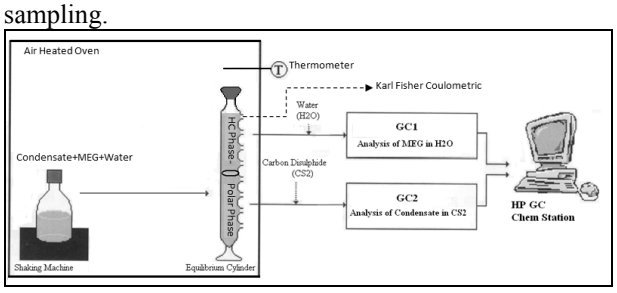

Figure 2: Sketch of experimental setup.

Both mixing and separation were carried out in an air heated oven which was used at the temperature range from 275 K to 326 K in this work. A DOSTMANN P500 thermometer (±0.1 ºC) was used for the temperature measurement.

Sampling and Analysis

At equilibrium, samples from two phases were drawn manually using a preheated syringe and needle. Preheated needle was used to avoid phase separation

due to temperature gradient. Two Agilent gas chromatographs (GCs) with different column specifications were used for composition analysis: one for the polar phase (glycol GC) while another for the condensate phase (condensate GC). The gas chromatographs are connected to a computer which has Chem Station package for data acquisition and quantification.

Polar Phase Analysis

For the polar phase analysis, hydrocarbons were extracted using the solvent extraction method. The solvent used in this work for the extraction of hydrocarbons from the polar phase is carbon disulphide (CS_2) which has negligible solubility in MEG but it is soluble in hydrocarbons. The extract phase is then analyzed on condensate GC using the standard temperature program from ASTM standard D5134-98 with an internal standard 1-heptene diluted in 1-dodecane (C_{12}).

Condensate Phase Analysis

MEG dissolved in condensate was extracted using water and analyzed at glycol GC. The water contents of condensate phase were analyzed using Karl Fisher Coulometer which provides very fast and reliable results, especially for systems with very low solubilities.

Thermodynamic Modeling

Thermodynamic modeling was carried out using the CPA EoS with the Yan et al.[4] correlation for characterization method. Using the association scheme based on terminology of Huang and Radosz [3], both water and MEG have been modeled using the 4C scheme. CPA has five pure component parameters including three for non-associating compounds and two for associating compounds. The pure component parameters for MEG and water are taken from previous works [3]. For mixtures containing more than one associating compounds such as the mixtures of glycols and water, combining rules are also needed for the association parameters. Different combining rules have been suggested, but in this work only the Elliott Combining Rule (ECR) has been used. ECR can satisfactorily describe the water + MEG system of relevance to this work.

In addition to mixing and combining rules for modeling of a mixture, a binary interaction parameter (k_{ij}) is also required for each binary pair. In MEG + condensate system, average k_{ij} have been used between MEG and all hydrocarbon fractions. This is done due to unavailability of k_{ij} values for several MEG-hydrocarbon mixtures. In MEG + condensate + water system, average k_{ij} similar to MEG + condensate system was used between MEG and hydrocarbon fractions. The binary interaction parameters between water and hydrocarbons are obtained from a generalized expression using a correlation in terms of carbon number as given by the following expression.

$$k_{ij} = -0.026 \times N_C + 0.1915$$

where N_C is carbon number of an alkane.

The k_{ij} = -0.115 was used between MEG and water using ECR.

Results and Discussions

For MEG + condensate system mutual solubilities were measured for the temperature range 275.15-323.15 K as given in Figure 3. About 75 components were detected in MEG from GC analysis up to C_9. The reported solubility of condensate in MEG is the sum of solubilities of all condensate's components. The solubility of aromatic HC is much higher than paraffinic and naphthenic. Therefore aromatic components contribute half of the total solubility of condensate in MEG. Mutual solubility of MEG and condensate increases with increasing temperature.

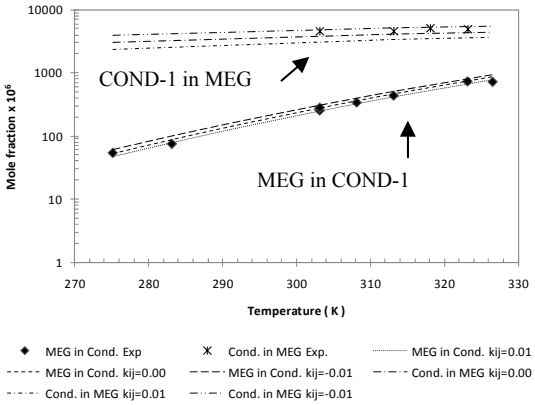

Figure 3: Prediction and correlation for mutual solubility of MEG and COND-1 using the CPA EoS and effect of using average binary interaction parameter (k_{ij}) between all MEG and HC pairs [5].

In the MEG + condensate system, MEG is a polar compound which self associates. Condensate consists of several hydrocarbon fractions which are modeled as non-associating or inert compounds. The modeling results for this system are shown in Figure 3 together with the experimental data. By using all k_{ij} = 0 for MEG-HC pairs (pure prediction), CPA can satisfactorily describe the phase behavior especially the solubility of MEG in condensate, while under predicting somewhat the solubility of condensate in the MEG phase. The MEG phase description can be improved considerably using non-zero k_{ij} between the MEG-HC pairs. As a result we get slight over estimation of the solubility of MEG in condensate while a better description of the solubility of condensate in MEG phase is obtained.

For MEG + water + condensate system the solubility of condensate in polar phase (MEG + water) at 323.15K is given in Figure 4. This shows that solubility of condensate and MEG decreases with increasing water content in polar phase. The modeling results are satisfactory considering that a single and same temperature independent binary interaction parameter is used for all MEG-hydrocarbon mixtures.

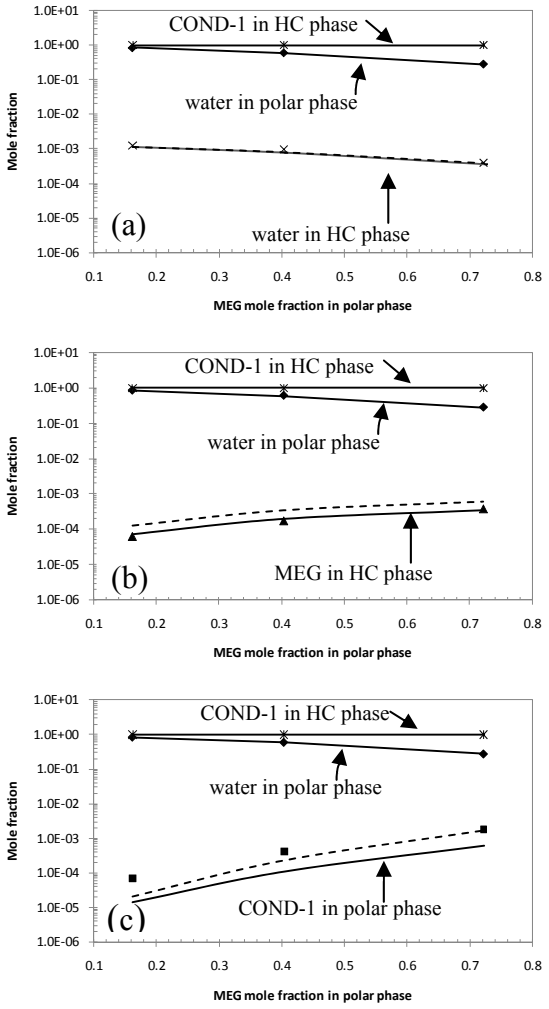

Figure 4: Mutual solubility of MEG-water and COND-1 at temperature 323.15 K and pressure of 1 atm. [5] (a) water in condensate (b) MEG in condensate (c) condensate in polar phase. The points are experimental data and the lines are modeling results using CPA. The continuous lines are by using average k_{ij}=0.05 for MEG-HC and the dotted lines by using k_{ij}=-0.01 for MEG-HC. The k_{ij}=-0.115 for MEG-water and HC-water are from correlation.

Conclusions

In this work new experimental data for the mutual solubility of the binary (MEG + reservoir fluid) and the ternary (MEG + water + reservoir fluid) systems are reported over a range of temperatures and at atmospheric pressure. The mutual solubility of MEG and condensate increases with increasing temperature. In MEG + condensate + water system, solubility of MEG and condensate decreases with increasing water contents in polar phase. The solubility of aromatic hydrocarbon in MEG and water is higher than for naphthenic and paraffinic hydrocarbons. It is therefore necessary to take PNA distribution into account in modeling.

The CPA EoS has been applied to the modeling of the mixture containing condensate + MEG + water systems and satisfactory modeling results are obtained.

Future Work

- Modeling of MEG + water + light-oil systems using CPA EoS and accounting for PNA distribution in characterization of oil.
- Experiments with aromatic oils at Statoil Research Centre, Trondheim.
- Comparison of CPA with commercial thermodynamic packages.
- Oil-water partition coefficient of polar chemicals.

Acknowledgements

The authors wish to thank the industrial partners in the CHIGP (Chemicals in Gas Processing) consortium (Statoil, BP International Limited, GASSCO, Mærsk Oil, DONG Energy) for financial support.

References

1. N. Ass, B. Knudsen, J.O. Sæten, E. Nordstad., SPE International 2002 (SPE No. 74083)
2. J. Fink, GP Press, 2003, p. ix
3. G.M. Kontogeorgis, G.K. Folas, Thermodynamic Models for Industrial Applications, from Classical and Advanced Mixing Rules to Association Theories, John Wiley & Sons, 2010.
4. W. Yan, G.M. Kontogeorgis, E.H. Stenby, SPE International, 2007 (SPE No. 110009-PP)
5. M. Riaz, G.M. Kontogeorgis, E.H. Stenby, W. Yan, T. Haugum, K.O. Christensen, E. Solbraa, T.V. Løkken. Fluid Phase Equilibr. 300 (2011) 172-181.

List of Publications

1. M. Riaz, G.M. Kontogeorgis, E.H. Stenby, W. Yan, T. Haugum, K.O. Christensen, E. Solbraa, T.V. Løkken. Fluid Phase Equilibr. 300 (2011) 172-181.
2. M. Riaz, G.M. Kontogeorgis, E.H. Stenby, W. Yan, T. Haugum, K.O. Christensen, E. Solbraa, T.V. Løkken. Poster Presentation, Presented at Special Symposium on SAFT, 2010, Barcelona, Spain.
3. M. Riaz, G.M. Kontogeorgis, E.H. Stenby, W. Yan, T. Haugum, K.O. Christensen, E. Solbraa, T.V. Løkken. Oral Presentation Presented at CHISA/ECCE7, 2010, Prague, Czech Republic.
4. M. Riaz, G.M. Kontogeorgis, E.H. Stenby, W. Yan, T. Haugum, K.O. Christensen, E. Solbraa, T.V. Løkken. Poster Presentation Presented at Danske Kemiinngeniør Konference (DK2), 2010, Lyngby, Denmark.

Alicia Román-Martínez
Phone: +45 4525 2910
E-mail: arm@kt.dtu.dk
Discipline: Process Technology and Unit Operations

Supervisors: Rafiqul Gani
John M. Woodley

PhD Study
Started: August 2008
To be completed: July 2011

A Model-Based Generic Framework for Design and Development of Integrated Enzymatic Processes

Abstract
This project consists in the development of a model-based generic framework for design of integrated enzymatic processes. In this framework, first, all the potential options are considered via a superstructure to search the domain of potential process design; and second, it uses a decomposition approach to manage the complexity of the mathematical formulations representing complex optimization problems and therefore, the search space is reduced stepwise in order to locate candidate process options, giving an optimal design. The framework is highlighted here to obtain an improved process for the Neu5Ac synthesis. The results show the relevance of one-pot reactions and *in-situ* product removal techniques to achieve an improvement in the process performance.

Introduction
Bioprocesses that use enzymes as biocatalysts are characterized by low productivity because of inhibition of the enzymes at low substrate and product concentrations. Besides, the product stream is dilute, which leads to high costs and difficulty in the subsequent purification steps of the products. The performance of this kind of processes can be enhanced by process engineering solutions, like process integration. Integration of enzymatic and chemo-enzymatic processes involves combinations of at least two unit operations, like reactive extraction, featuring simultaneous reaction and continuous product recovery. The most common approaches of integration are the removal of the products from the reaction medium *in-situ* (ISPR for *in-situ* product removal) and the integration of two or more chemical and/or enzymatic reactions in one pot.

However such processes have been hardly investigated comprehensively. Furthermore, use of integrated chemo-enzymatic processes at a commercial scale is still limited. Generally, design of this kind of process, involves an iterative, trial and error experiment-based procedure where the experience of the process engineer plays an important role. Since experiments are usually time consuming and expensive the search space of the potential designs needs to be significantly reduced, lacking also a systematic approach to the process as a whole. Because of time and financial constraints, it is inevitable that complete evaluation of all aspects is rarely achieved and sub-optimal processes may be introduced. In order to address these problems, it would be useful to develop systematic model-based methods assisted with computational tools, which enable the generation of all options and enhance the ability of the process to adapt to future needs. In this case, through a qualitative and quantitative analyses of models describing the design criteria, the different options, the process model, the process constraints as well as each of the constituent unit operations (e.g. bioreactor, adsorption, extraction, crystallization) at different modeling depths can lead to the efficient identification of the optimal integrated bioprocess design. Through a model-based computer aided methodology it is therefore possible to identify reliable and feasible integrated options, saving thereby development time and experimental resources, which could then be used only for implementation and verification of the design.

Objective
The objective of this project is to develop a model-based computer aided methodology for identifying feasible integrated options for processes including enzymatic and chemo-enzymatic synthesis. In this methodology, several features have been introduced. All potential options are considered via a superstructure to search the domain of potential synthesis routes. It uses also a decomposition approach to manage the complexity of the mathematical formulations

representing complex optimization problems so that the search space is reduced stepwise in order to locate candidate process options, giving an optimal design where further experimental efforts can be focused. The application of the methodology is illustrated through the Neu5Ac synthesis which represents two reaction steps (chemical and/or enzymatic) and several downstream processing methods to generate all possible operations.

General problem definition

The task achieved through the methodology can generally be described as the following synthesis problem definition: given the details of the feed mixtures (substrates), and the product(s) specifications (in terms of product purity or recovery), determine the optimal enzymatic process route specifying the reactions, separations, and their integration in the process, matching the given specifications and constraints. All the possible options are considered and analyzed, in order to avoid doubt that the best option will be selected. The goal takes into account different process routes including in a superstructure represented in Figure 1, where *NIU* is the number if identified operations in each processing unit *u*, optimize a defined performance criterion (or several performance criteria) defined by an objective function (*OF*) subject to a set of optimization variables (set of design variables $\underline{X}$, decision variables $\underline{Y}$ for describing existence of processing units, streams and operations in a processing unit *U*, known parameters $\underline{d}$ (e.g. equipment parameters and kinetic constants) and product parameters $\underline{\theta}$ and a set of constraint functions, which include logical, structural, operational (equally or unequally) bounded to lower boundaries (LB) and/or upper boundaries (UB), and the process model.

Therefore, the mathematical formulation of the problem is given as an overall optimization model:

$$OF = \min/\max \sum f_j\left(\underline{Y},\underline{X},\underline{d},\underline{\theta}\right) \quad (1)$$

s.t. $\underline{Y},\underline{X},\underline{d},\underline{\theta}$,

number of options:

$$NPO = \sum_{u=1}^{u}\left(\prod_{u=1}^{u} NIU_u\right)\left(\frac{(r\cdot u)!}{u!(r\cdot u-u)!}\right) \quad (2)$$

logical constraints :

$$g_{Logical,LB} \le g_{Logical}\left(\underline{Y}\right) \le g_{Logical,UB} \quad (3)$$

structural constraints:

$$g_{Structural,LB} \le g_{Structural}\left(\underline{Y}\right) \le g_{Structural,UB} \quad (4)$$

operational constraints :

$$g_{Operational,LB} \le g_{Operational}\left(\underline{Y},\underline{X},\underline{d},\underline{\theta}\right) \le g_{Operational,UB} \quad (5)$$

and the process model:

$$h_p\left(\underline{Y},\underline{X},\frac{\partial \underline{X}}{\partial \underline{X}},\underline{d},\underline{\theta}\right) = \frac{\partial \underline{X}}{\partial t} \quad (6)$$

The solution methodology to the problem is to find the values of the optimization variables that satisfy all the constraints and minimize (or maximize) the objective function. So, the general optimization objective is to choose a set of values of the variables subject to the various constraints that produce the desired optimum response for the chosen objective function.

Methodology

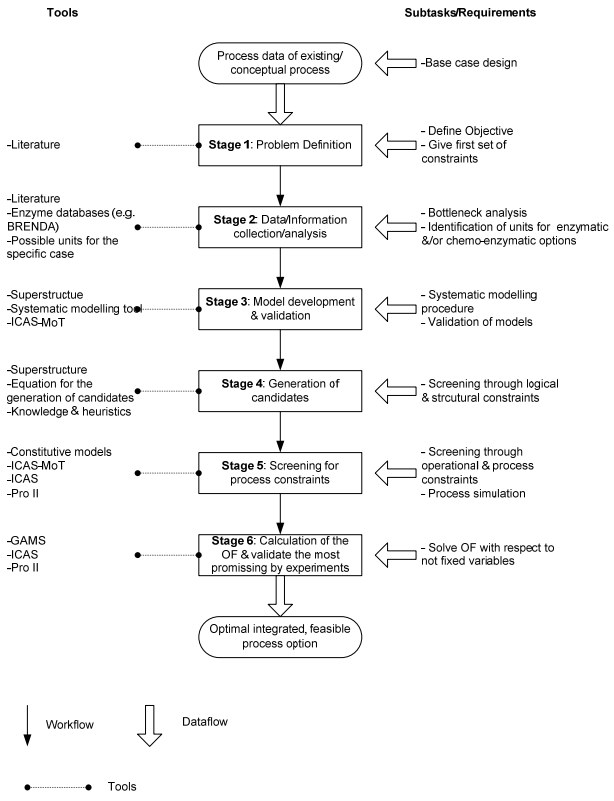

Figure 1: Flow diagram of the model-based methodology

The proposed methodology for design and development of integrated enzymatic and chemo-enzymatic processes consists of six stages. Its workflow is outlined in Figure 1. In Stage 1 the synthesis/design problem is defined, including the definition of the objective function, the process/operation scenario and the constraints that the options need to match. In Stage 2, the objective is to collect all data about the process, necessary to gain full understanding of the process which is needed to identify bottlenecks/limitations for improvement in order to search for integration strategies in a knowledge base. The objective of Stage 3 is to develop a simple generic model for any integrated chemo-enzymatic process represented by the superstructure that has been developed (Figure 1). The model consists on mass and energy balance and connection equations. Depending on

batch or continuous operation modes, dynamic or steady state models are generated for each process operation scenarios. In Stage 4 the objective is to generate all feasible intensified flow sheet options through synthesis rules (logical constraints) and structural constraints, by fixing sets of binary variables in the superstructure (Equations 2 - 4). Consecutively, in the same Stage 4, all options are screened for feasibility by additional structural and operational constraints, to match the target defined in Stage 1. Identified redundant options are removed. Subsequently, all remained options are screened using specific process models (Equation 5) derived from the generic model of Step 3 and further screened for process constraints (Equations 6 and 7). In Stage 5, trough the screening achieved in the previous Stage, only a small number of options are subjected to the calculation of the objective function (Eq. (1)) defined in Step 1. In Stage 6, the remained options are benchmarked with respect to the objective function, and then, the best single option based on the performance objective function has to be confirmed through experiments.

Superstructure

The superstructure features a number of different process units and their interconnections, for the problem formulated here, as shown in Figure 2, it consists of maximum four processing steps that can be reactors, separators or reactive separators. Also, it is considered that, in two reaction systems, we can run both reactions in a single reactor (one-pot synthesis), in the systems the option of remove/fed continuously reactant or product while the reaction is happening is also considered (in situ substrate supply/product removal). The reactors, separators and reactive separators may have at the most two phases (α and β). In each processing unit, there are inlet streams, and outlet streams in the β phase, outlet streams in the α phase, by-pass streams to all processing units and recycle streams. The reaction(s) can happen in aqueous and organic phases (no gaseous or solid phases). The catalyst (chemical or enzymatic) can be in solution, immobilized or supported. In Figure 2, T^k, P^k, pH^k, n_i^k and σ_i^k are the temperature, pressure, pH, moles of compound i and separation factor of the compound i in the unit k respectively. F_i^k, $F_i^{k\alpha}$, $F_i^{k\beta}$, $F_i^{k\alpha P}$, $F_i^{k\beta P}$, $F_i^{k\alpha R}$, $F_i^{k\beta R}$, $F_i^{k\alpha R1}$, $F_i^{k\alpha R2}$, $F_i^{k\beta R1}$, $F_i^{k\beta R2}$, $F_i^{k\beta P1}$, and $F_i^{k\alpha P1}$ are the inlet, outlet, product and recycle streams; $Y^{k\alpha}$, $Y^{k\beta}$, $Y^{k\alpha m}$, $Y^{k\beta m}$, $Y^{k\alpha R}$, and $Y^{k\beta R}$ are decision variables (values between 0 and 1) that connect the streams to a second unit directly, by bypass or by recycling.

Decomposition strategy

Due to the big complexity of the problem, it is time consuming and in many cases, not solvable only with conventional optimization techniques; a decomposition approach is proposed here which can reduce the computational time and effort; it mainly consists in dividing the whole mathematical problem into smaller solvable problems. The decomposition approach is divided into five stages:

- *Stage I*: Generation of options and screening by taking equations (2).
- *Stage II*: Screening by logical and structural constraints. Solving of equations (3) and (4).
- *Stage III and IV:* Screening by other constraints and the process model (equations (5) and (6)).
- *Stage V:* Evaluation of the feasible options. The objective function in equation (1) is calculated for all feasible solutions.

After obtaining the optimal solution(s), they are selected (Stage 6 of the methodology) as the best one(s) for experimental validation and rigorous simulation.

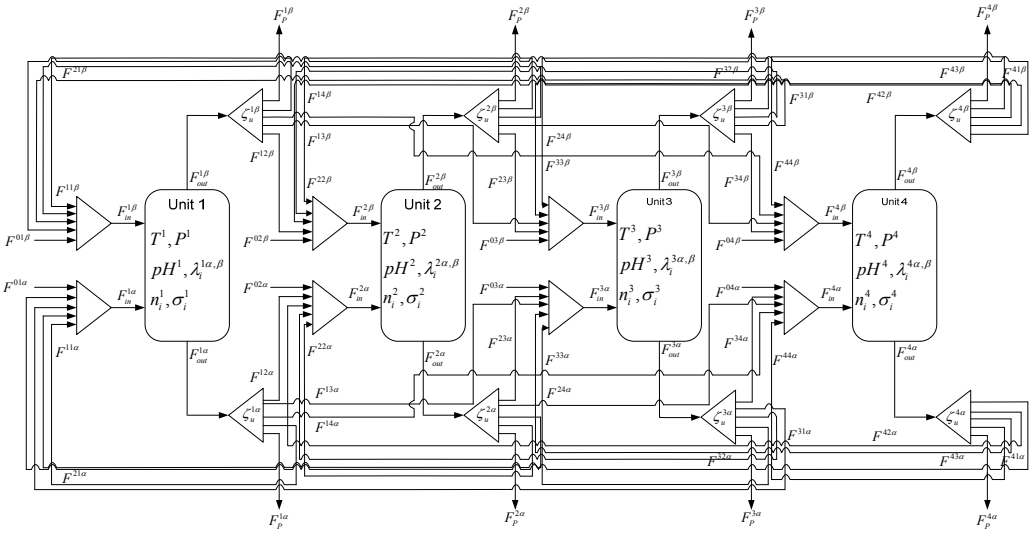

Figure 2: Superstructure for reaction-separation configuration of enzymatic processes (symbols: streams F [mol], temperature T [K], pressure P [bar], molar hold up's n [mol], separation factors σ [-], binary existence variable Y[0,1]; Subscripts: Bottom flow α, top flow β, product P)

Application of the methodology through the production of Neu5Ac

The methodology is highlighted through the production of N-acetylneuraminic acid (Neu5Ac) which is an important intermediate pharmaceutical due to its ant-viral, anti-cancer and anti-inflammatory effect [2]. The reactions taking place during the synthesis are outlined in Fig. 3, where, **A**: N-acetyl-D-glucosamine (GlcNAc); **B**: N-acetyl-D-manosamine (ManNAc); **C**: pyruvic acid (Pyr); **D**: N-acetylneuraminic acid (NeuAc); **epimerase**: N-acylglucosamine-2-epimerase (E.C. 5.1.3.8) and **aldolase**: N-acetylneuraminic acid aldolase (E.C. 4.1.3.3).

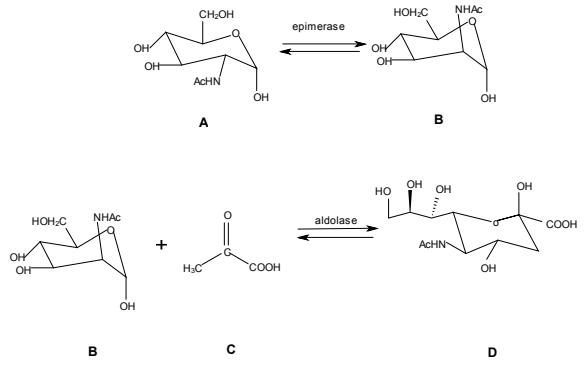

Figure 3: Synthesis of N-Acetyl-neuraminic acid from GlcNAc in two steps

Starting from the methodology, in the first step the problem is defined. The criteria for optimal selection that is given by the objective function is defined in this case as maximizing the yield which is given by the following equation:

$$OF = \max \frac{n_{product,end} - n_{product,0}}{n_{substrate,0}} \quad (7)$$

In the second stage, all data with respect to the process scenario, such as, enzyme properties, kinetic constants, properties with respect to inhibition of the enzyme, are collected. In stage 3, the generic model is developed, represented by the superstructure in Figure 2, and validated based on experimental data for the one-pot synthesis with a deviation in the product yield of less than 5%. In stage 4, the options for the synthesis routes are generated by means of Equation (2), the superstructure and all reported process equipment/task collected in stage 2. In total 191,917,488 options are generated. The generated options are stepwise screened with respect to structural and operational constraints. In this way the number of feasible process options has been reduced to 27 options before Stage 5, which in this Stage are screening for process constraints through simulation with the generated models derived from the generic model. In Stage 6, the most promising options are further optimized with respect to the objective function, the maximization of the product yield, results are shown in Table 1, being the best option the one characterized by one-pot reactive extraction plus ISPR by chromatography (Figure 4).

Conclusions

Integration of enzymatic processes can help to improve existing processes to overcome limitations like the low yield and high amount of wastes. Two of the most important methods of integration of this kind of processes are the one-pot synthesis and the ISPR. However, the number of options derived for all the possibilities of reaction and separation methods and configurations, is enormous and a systematic methodology to localize and determine the optimal solution is needed to systematically determine optimal options by stepwise reduction of the search space through constraints, performance evaluation and objective function.

Table 1: Calculation of the objective function for the feasible alternatives (OPRS: One-pot reactive extraction, OPR: One-pot reaction, R: Reaction, CRYST: Crystallization, CHRO: Chromatography, EVAP: Evaporation).

Option No.	Process	Product yield (%)
1	OPRS-CRYST	50.00
2	OPRS-CHRO	53.85
3	OPR-CRYST	40.00
4	OPRS-CRYST-EVAP	46.15
5	OPRS-CRYST-CRYST	37.70
6	OPRS-CHRO-CRYST	40.00
7	OPRS-CHRO-CHRO	43.08
8	OPR-EVAP-CHRO	39.23
9	R-EVAP-R-CRYST	40.77
10	R-EVAP-R-CHRO	43.20

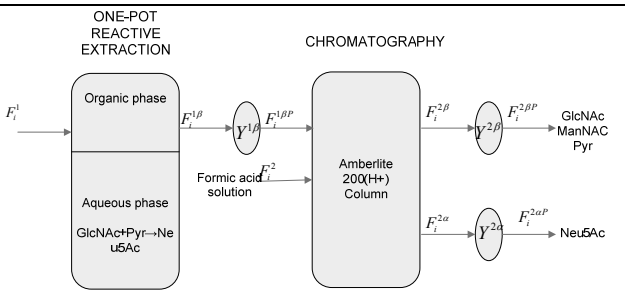

Figure 4: One-pot reactive extraction + ISPR by chromatography configuration

Acknowledgments

The author wishes to thank PROMEP (Mexico) for founding this PhD project.

References

1. V. Zimmermann, H. Hennemann, T. Dauβmann, U. Kragl, Appl. Microb. Biotechnol. 76 (2007) 597-605.
2. F. Tao, Y. Zhang, C. Ma, P. Xu, App. Microb. Biotechnol. 87 (2010) 1281-1289.

List of publications

1. A. Román-Martínez, R. Gani, J.M. Woodley, (2010). Implementation of Novel Integrated Pharmaceutical Processes: a Mode Based Approach. Oral Presentation Conference Contribution. AIChE Annual Meeting. Salt Lake City, USA. November 2010.

Negar Sadegh

Phone: +45 4525 2821
E-mail: nes@kt.dtu.dk
Discipline: Engineering Thermodynamics

Supervisors: Kaj Thomsen
Erling H.Stenby
Georgios Kontogeorgis

PhD Study
Started: April 2009
To be completed: March 2012

Thermodynamic Modeling of Water-Acid gases-Alkanolamine Systems

Abstract
This project is about thermodynamic modeling of natural gas cleaning process with alkanolamines as solvent. The research combines both experimental and thermodynamic modeling studies. Measuring high pressure VLE data for methane-water- acidic gases (CO_2 and H_2S) - MEA and MDEA as a solvent is planned for the experimental part. For the modeling part the Extended UNIQUAC model will be used for representation of the behavior of acid gas-alkanolamine mixtures over an extensive pressure range, with emphasis on mixed acid gases.

Introduction
The problem with thermodynamic modeling of acid gas treating plants is that the vapor–liquid equilibrium (VLE) data reported for these systems are not generally very consistent. Moreover, there are a few sources of consistent heat capacity and heat of absorption data for acidic gases/alkanolamines/water systems.

Thermodynamic modeling of these systems has been done through 3 different ways: empirical correlations, such as: Kent and Eisenberg (1976) for CO_2+MEA/DEA+H_2O systems and Gabrielsen et al. (2005) for CO_2+MEA/DEA/MDEA+H_2O systems; equations of State, such as: Chunxi and Fürst (2000), Huttenhuis (2008), Vrachnos et al. (2004) , Solbraa (2002) and activity coefficient models, such as: E-NRTL (Austgen et al. (1989)), Extended UNIQUAC (Faramarzi et al. (2009)), UNIQAC-NRF (Haghtalab and Dehghni (2007)), Modified Clegg-Pitzer (Kundu at al. (2003)).

Empirical correlations fail when being extrapolated to conditions other than what they are based on. Equations of state mostly are limited to certain conditions. For instance Solbraa EoS can only show good results at ambient temperature. Currently, the best approach for modeling the behavior of these systems is by activity coefficient models for electrolyte solutions.
In this work extended UNIQUAC model [1] is used to estimate various thermodynamic properties of the alkanolamine systems required for the design of natural gas treating units.

Specific Objectives
The purpose of this study is to get an accurate estimation of both gas solubility and thermal properties of the acidic gases/water/alkanolamine systems. This will be done by gathering experimental VLE data on water-acid gases- alkanolamine systems and thermodynamic modeling of the system with the Extended UNIQUAC model.

Results and Discussion
The extended UNIQUAC model as presented by Thomsen and Rasmussen [1] is used for the thermodynamic calculations of this work. Extended UNIQUAC is the original UNIQUAC equation (Abrams and Prausnitz [2] and Maurer and Prausnitz [3]) combined with the Debye–Hückel term. The latter term is added to account for the electrostatic interactions caused by the presence of the ionic species in the solution. Therefore, the excess Gibbs energy is expressed as the combination of three terms: the entropic and enthalpic terms of the original UNIQUAC equation to consider the non-electrostatic interactions and, the electrostatic term (Debye–Hückel):

$$\frac{G^E}{RT} = \left(\frac{G^E}{RT}\right)_{UNIQUACEntropic} + \left(\frac{G^E}{RT}\right)_{UNIQUACEnthalpic} + \left(\frac{G^E}{RT}\right)_{Debye-Huckel}$$

Parameter Regression Database:
Parameters are optimized from the available experimental solubility and thermal data, covering high pressure, high temperature and high amine content. Some of the modeling results are shown in the following figures.

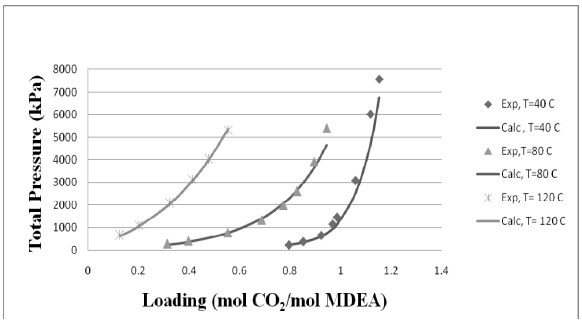

Figure 1: P-x diagram for MDEA-H_2O-CO_2 system for solvent molality of 8, at 40, 80, 120 °C and 0-80 bar

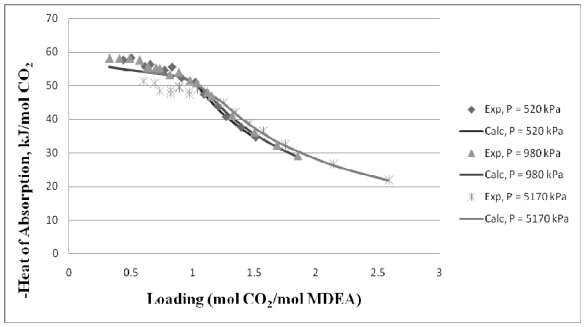

Figure 2: -Heat of absorption diagram for MDEA- H_2O -CO_2 system for solvent molality of 1.48 , at 50 °C and 5, 10, 50 bar

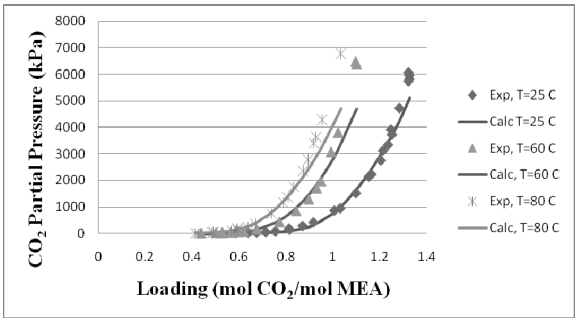

Figure 3: P-x diagram for MEA- H_2O -CO_2 system for solvent molality of 3, at 25, 60, 80 °C and 0-80 bar

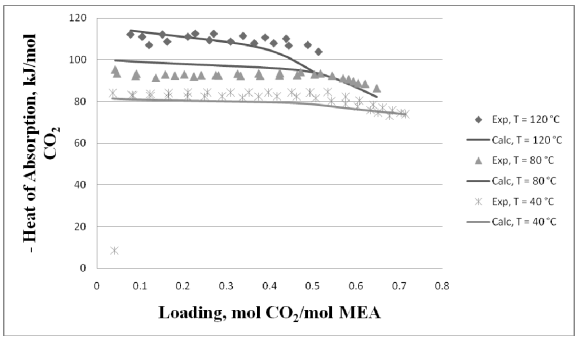

Figure 4: -Heat of absorption diagram for MEA- H_2O -CO_2 system for solvent molality of 7, at 40, 80, 120 °C and 0-1.2 bar

The obtained results revealed that the Extended UNIQUAC model can effectively predict both the gas solubility and heat of absorption over an extensive range of conditions with only a unique set of parameter.

Conclusion:

In this work Extended UNIQUAC is used for thermodynamic representation of water-acidic gases-alkanolamine systems**.**

It has been shown that Extended-UNIQUAC can accurately represent the behavior of these systems.

Acknowledgment:

We would like to thank Statoil for funding this PhD project.

References

1. K. Thomsen, P. Rasmussen, Chem. Eng. Sci. 54 (1999) 1787–1802.
2. D.S. Abrams, J.M. Prausnitz, AIChE. J. 21 (1975) 116–128.
3. G. Maurer, J.M. Prausnitz, Fluid Phase Equilibr. 2 (1978) 91–99.

List of Publications

1. N. Sadegh, K. Thomsen, E.H. Stenby, G. Kontogeorgis, Thermodynamic modeling of water-acid gases-alkanolamine systems, Proceedings of the 9th AIChE annual meeting , USA, 2009
2. N. Sadegh, E.H. Stenby, G. Kontogeorgis, K. Thomsen, Thermodynamic modeling of sour gas cleaning process with alkanolamines, Oral Presentation at ICCT-2010 conference, Japan
3. N. Sadegh, E.H. Stenby, G. Kontogeorgis, K. Thomsen, Thermodynamic modeling of sour gas cleaning process with alkanolamines, Invited speaker at SPE (STC-2010) conference, Germany

Suriyati binti Saleh
Phone: +45 4525 2927
E-mail: ss@kt.dtu.dk
Discipline: Reaction and Transport Engineering

Supervisors: Kim Dam-Johansen
Peter Arendt Jensen

PhD Study
Started: January 2010
To be completed: December 2012

Pretreatment of Biomass for the Use of 100% Renewable Fuels on Suspension Fired Boiler

Abstract
Biomass can be used as a renewable fuel but experience several shortcomings if it is directly combusted in a boiler. Biomass typically has high moisture content and a low energy density, leading to high transport cost and poor biomass grindability. This study investigates the possibility of using torrefaction process to pretreat biomass in order to produce fine char particles that is suitable to be used as a fuel for suspension fired boilers. Biomass was torrified at different temperatures and durations. After torrefaction, particle size analysis was carried out on each solid product. The grindability of biomass was improved by the torrefaction process.

Introduction
Renewable energy is a topic of great interest, as it represents a diversification of the energy sources and contributes to preserving the equilibrium of ecosystems. Among the different energy sources, biomass holds a large promise for increasing use in the next few years. Moreover, biomass is considered as a neutral carbon fuel because the carbon dioxide released during its utilization is an integral part of the carbon cycle [1]. Biomass can be processed to produce energy by different technologies such as thermochemical (combustion, pyrolysis and gasification), biological (anaerobic digestion and fermentation), and chemical processes (esterification) [2].

On the other hand, there are several major shortcomings in the direct utilization of biomass in energy supply owing to the characteristics of the biomass. The lignocellulosic materials with fibrous structure are difficult to grind where fine particles are needed during combustion of biomass in suspension fired boilers [2]. The other problem when dealing with biomass is the presence of inorganic elements such as chlorine, potassium and other alkali metals.

Pretreatment technology can improve the efficiency of biomass utilization or lead to a reduction of the cost of the transport and storage of biomass. Researchers have recently paid more attention to pretreatment technologies, especially those of thermal chemical conversion methods in order to upgrade the biomass properties. A well-known pretreatment technology is flash pyrolysis carried out at high heating rate and relatively higher temperatures with a short residence time of several seconds. However, another technology is a mild pyrolysis process called torrefaction. Torrefaction is a process of thermal degradation of biomass at relatively low temperatures (200-350°C) and low heating rate of less than 50 °C min^{-1} under anoxic conditions [3]. During torrefaction process, the density and the specific heating value of the product increase, and there is a reduction in moisture content.

Specific Objectives
An ideal biomass pretreatment method would provide the heating value of the biomass for the boiler, but in a way such that the fuel is easily pulverized. In order to achieve this goal, a simultaneous torrefaction and grinding process will be used as a pretreatment method. The main objective for the current study is to investigate the influence of temperature and residence time on the grindability of biomass. The focus will be on how to produce fine particles that is suitable for suspension firing. Furthermore, the heating value of the products from torrefaction process will be investigated.

Torrefaction process
Torrefaction is a thermal degradation of biomass that occurs under anoxic condition, which improves the thermo-chemical properties of biomass, making it more suitable for energy generation. The moisture and low weight organic volatile components will be removed and the long polysaccharide chains depolymerize, producing a hydrophobic solid product with an

increased energy density (on a mass basis) and a greatly improved grindability [4]. As a result, significantly lower energy is require to pulverize the torrefied fuel and it is no longer requires separate handling facilities when co-fired with coal in existing power stations.

Experimental work

The experiments were conducted by using a simultaneous torrefaction and grinding reactor. Straw has been torrified at temperatures range from 260 °C – 350 ° C with different residence time (30 minutes, 90 minutes and ball sizes (diameter: 10 mm, 15 mm, 20 mm). A continuous flow of nitrogen is used to keep the system inert. The weight of the char was measured in order to determine the mass loss of the samples. In order to study the grindability of the torrified biomass, the samples were sieved into different size fractions to evaluate the particle size distribution.

Results and Discussion

1. Yield of torrified product

The variation in the mass yield of torrified char product with the final reactor temperature is shown in Figure 1. More than 50% of weight loss of the torrified char product is observed for the torrefaction at a temperature higher than 330 °C. The weight loss can be attributed to the decomposition of hemicellulose, which starts at temperatures above 200 °C, as reported by Bridgeman *et. al.* (2008) [5].

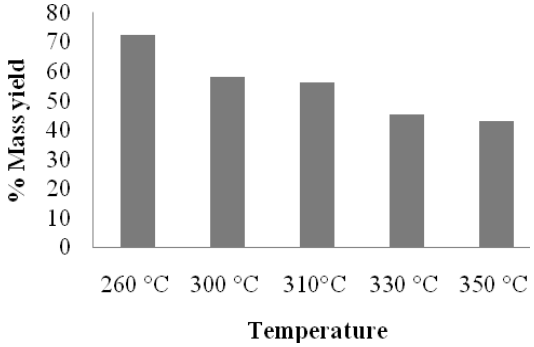

Figure 1: Variation in the solid mass yield of torrified straw

2. Grindability of torrified product

The torrified product is more brittle with much better milling properties compared to the raw biomass. Particle size analysis at various temperatures for untreated and torrified biomass is presented in Figure 2.

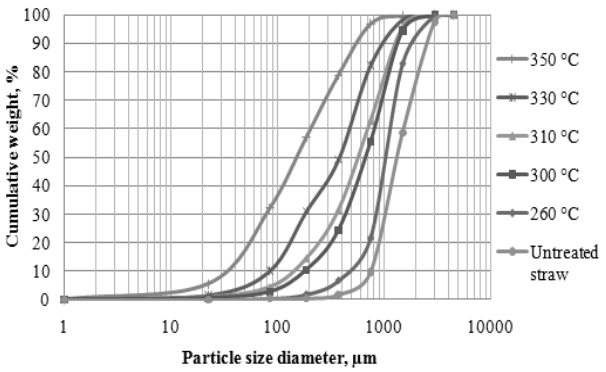

Figure 2: Effect of temperature on particle size distribution of untreated and torrified biomass

The percentage of fine particles increases with the increase of torrefaction temperature. For torrefaction at 260 °C, only 21.5% of sample passes through the 1 mm sieve, but the percentage is increase to 82.2% and 96.8% for the case of 330 °C and 350 °C, respectively. Extra moisture content in biomass is a factor affecting further grinding of the biomass. The decomposition reactions at higher temperature level cause the biomass to become completely dried and lose it tenacious and fibrous structure. Therefore the grindability of the biomass is significantly improved and the solid products with fine particles were produced.

Acknowledgement

The author acknowledges the financial support by the Ministry of Higher Education (MoHE) of Malaysia, Universiti Malaysia Pahang (UMP) and by the company Energinet.dk.

References

1. B. Arias, C. Pevida, J. Fermoso, M.G. Plaza, F. Rubiera, Fuel Process. Technol. 89 (2008) 169–175.
2. A. Demirbas, Prog. Energ. Combust. 31 (2005) 171–192.
3. J. Deng, G.J. Wang, J.H. Kuang, Y.L. Zhang, Y.L. Luo, J. Anal. Appl. Pyrol. 86 (2009) 169-175.
4. A. Dutta, A. Pimchuai, P. Basu, Energ. Fuel. 24 (9) (2010) 4638-4645.
5. T.G. Bridgeman, J.M. Jones, I. Shield, P.T. Williams, Fuel 87 (2008) 844-856.

Sara Bülow Sandersen

Phone: +45 4525 2983
E-mail: sbs@kt.dtu.dk
Discipline: Engineering Thermodynamics

Supervisors: Nicolas Smit von Solms
Erling H. Stenby

PhD Study
Started: May 2008
To be completed: January 2012

Enhanced Oil Recovery with Single Component Surfactant Flooding

Abstract
The phase behavior of single or simple component surfactant systems for enhanced oil recovery (EOR) is studied. Experimental work has been carried out on a DBR JEFRI PVT cell, which is high pressure equipment appropriate for phase behavior studies at pressures and temperatures in a wide range. A thorough study of a surfactant model system, (sodium chloride/water/sodium dodecyl sulphate/1-butanol/heptane), has been examined with a focus on the present pressure effect. Also this work encompasses an oil/brine study, to provide better understanding of which effects (salinity, sulphate content in brine, pressure, temperature, etc.) may alter the oil recovery.

Introduction
Around 50 % crude oil remains trapped in many mature oil reservoirs and as the demand for oil is increasing Enhanced Oil Recovery (EOR) is widely applied.

The scope for this project is to study surfactant flooding, which is one of several EOR techniques to attain higher and more optimal oil recovery. Surfactant flooding is where surfactants are injected into the reservoir to reduce the interfacial tension (IFT) to an ultra low IFT between oil and water, which should mobilize the oil. However, along with this EOR method, several complex issues are related, where the design of the added chemicals must be tailored to the specific rock and fluids. The principle of flooding is illustrated in Figure 1.

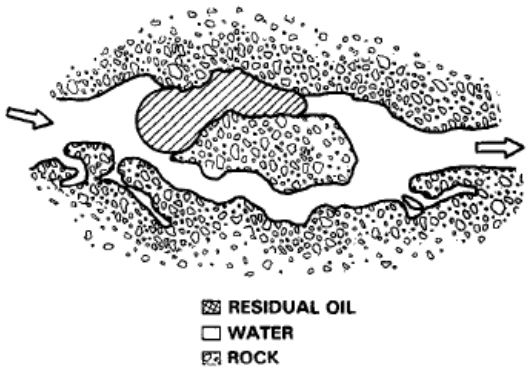

Figure 1: Principles of flooding, where residual oil is trapped in the reservoir, [1]. The residual oil trapped in narrow capillary pores is held back thanks to capillary forces and it is required to reduce the IFT between oil and water to 0.001 dynes/cm to mobilize the oil.

The aim for EOR operations are to alter the mobility of the remaining oil, still present after conventional primary and secondary reservoir techniques has been applied. Usually the remaining oil is distributed in the pores in the reservoir, where the oil is trapped due to capillary and viscous forces. The mobilization of the residual oil is achieved through surfactants generating a sufficiently low oil/water IFT. Low IFT further gives capillary numbers large enough to overcome the capillary forces. The recovery efficiency is highly dependent on the capillary number which is defined as equation 1.

$$N_c = \frac{\mu_w v_w}{\varphi \gamma_{wo}} \quad (1)$$

Where N_c is capillary number, μ_w is viscosity of the aqueous or displacing phase in [Pa Sec], v_w is flow rate of the displacing fluid in [cm/sec], φ is effective porosity of formation and γ_{wo} is interfacial tension between water and oil in [N/m].

It is not unusual that co-surfactants are blended into the liquid aqueous solution to improve the properties of the surfactant solution. Co-surfactants serve as a promoter or help the blend to meet optimal conditions with respect to reservoir temperature, pressure and salinity. It is experienced that due to chromatographic separation during flooding it is very complicated to design a surfactant/co-surfactant solution that can perform optimal throughout the reservoir. During surfactant flooding there will be losses due to adsorption

and trapping to the rock. It is essential to assure stability of the surfactant solution, which must resist physical conditions such as high temperatures, high pressures and high salinities. [2]

Recent experimental results have shown that an increase in oil recovery is observed with sulphate enriched brine. Could this be understood better from phase behavior studies? An oil/brine study has been carried out concurrently with the phase behavior study of surfactants, as IFT measurements at room temperature has shown that sulphate concentration did not induce any significant changes, [3]. One Latin America crude oil is exposed to reservoir conditions (pressure and temperature) while mixed with brine with different sulphate concentrations.

Specific Objective

This Ph.D.-project handles the study of the potential of single component surfactant systems in contrast to the more ordinary systems with surfactants and co-surfactants. Furthermore an oil/brine study is carried out to achieve better understanding for such systems, which is exposed to different sulphate concentration at reservoir conditions.

Surfactant Flooding and Emulsions

EOR with surfactant flooding has been investigated for many years. Unfortunately, the economic reality of the process is that the technique is very expensive and therefore it has not yet been commercial employed, as it has not been tested successfully in full scale yet. [4]

Chemical EOR is the injection of one or more specific liquid chemicals, the so-called surfactants, that controls the phase behavior properties in the reservoir. Injecting surfactants should reduce the IFT between the injected liquid and oil to 0.001dynes/cm, which will then overcome the existing capillary forces and thus mobilize the oil towards the production well.

There is a great potential of chemical EOR with surfactant flooding, as this technique encompasses the possibility of designing a process where the overall displacement efficiency can be increased. It is also expected that surfactant flooding could be designed to increase the economic productivity, as the economic productivity for some mature reservoirs nowadays are low despite having 50-70% of the original oil still in place. [5]

Surfactant flooding EOR involves microemulsions, where oil/water and water/oil micelles are formed. In the beginning of a surfactant flood the surfactant concentration is low and then the concentration increases as the amount of injected surfactant solution rises. At low surfactant concentrations the surfactant molecules are dispersed as monomers. As surfactant concentration is increased the surfactants molecules starts to aggregate and at some point the concentration will reach the critical micelle concentration (CMC). Any further addition of surfactants will form into micelles.

Surfactants are frequently classified by their ionic nature of the head group as anionic, cationic, nonionic or zwitterionic. Anionic surfactants are the most widely used surfactants for surfactant flooding and according to Austad *et al.* (1996) [6] promising surfactants, for single component surfactant flooding, are branched ethoxylated sulfonates.

The formation of microemulsions is very important to attain a successful surfactant flood, as the ultra low IFT is obtained when these are present. Also the formation of emulsions for general oil/brine systems can contribute to alter the oil recovery. A large amount of experimental work has already been carried out. However, there are still many remained questions and therefore an experimental work to achieve better physical understanding is carried out in this project as well.

Phase Behavior Experiments

It is reported in literature that an increase in temperature increases the optimal salinity for the surfactant system. Aside from the influence of temperature the effect of pressure on the phase behavior of the microemulsion is widely discussed as results from different researchers disagree. Reservoir conditions are typically at elevated pressures, why this is of importance.

Observing surfactant systems there are three types of systems to be considered.

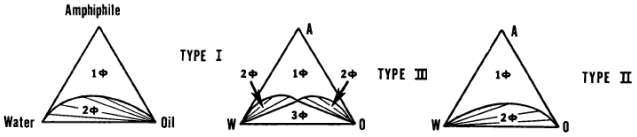

Figure 2: From left to right: multiphase region with lower-phase microemulsion with excess of oil, middle-phase microemulsion and upper-phase microemulsion with excess of water/brine.

Figure 2 represents the phase environment where surfactant/water/oil systems can equilibrate as either a single phase or as multiple phases. These generalized systems are often referred to as the so-called Winsor Type systems.

The experimental activities have initially been focused on the phase behavior of a model system; SDS/brine/1-butanol/heptanes, at elevated temperatures and pressures. The model system is investigated in a DBR JEFRI PVT cell, a high pressure and high temperature cell which allow visual observation of phase change and measurement of phase volume through its window. The set up is pictured in Figure 3. The purpose for the model system is to study if effects from mainly pressure would create any changes in the phase behavior, such as in the phase volumes and the number of present phases. Furthermore the same setup was used for an oil/brine study to examine oil/brine interaction at reservoir conditions, which where afterwards analyzed for any effects on the crude oil dependent on the operation or the different brine solutions with different sulphate content that the oil/brine system was exposed to.

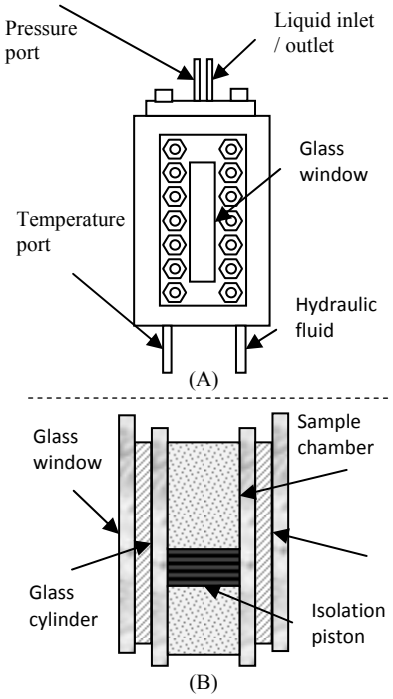

Figure 3: Drawing of the DBR JEFRI PVT cell used for high pressure phase equilibrium experiments. (A) shows the outside of the cell and (B) shows the inside construction of the cell.

As introduced there are two different experimental work carried out. One with a surfactant model system, where the dependency between, present phases, pressure and temperature is examined. Table 1 show examples of compositions of this system, which has been studied.

Table 1: Model surfactant system with two different examples of composition in wt%.

Comp.	water	NaCl	SDS	1-butanol	heptane
#1	0.616	0.043	0.025	0.051	0.265
#2	0.532	0.037	0.022	0.044	0.365

The other experimental part of this project is an oil/brine system, which is studied to clarify what effect both reservoir conditions and different brine solutions has on the crude oil in order to understand what mechanisms that occur during oil recovery. Table 2 shows the properties of the studied crude oil.

Table 2: Properties of Latin America crude oil.

Density [g/cm^3]	Acid No. [mhKOH/g]	Base No. [mgKOH/g]	Asphaltene [%]	Visc. [cp]
0.846	0.163	0.563	3.42	24.4

The oil/brine studied is carried out in collaboration with another Ph.D. from this group (CERE).

Results from Work with Surfactant System

The model surfactant system has earlier been studied at room temperature and at atmospheric pressure [7], where the present phase diagram in Figure 4 shows the results.

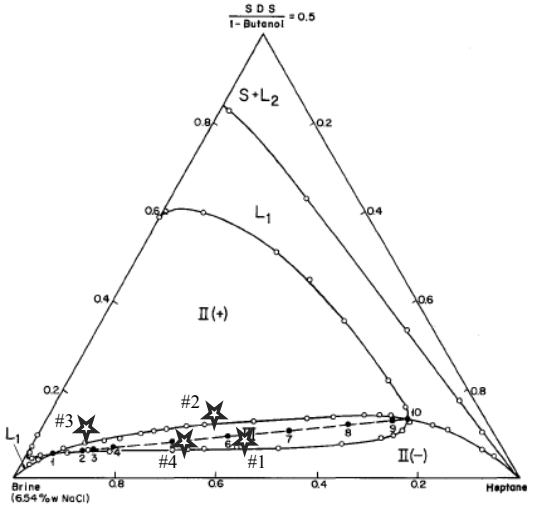

Figure 4: Phase diagram for brine/SDS/1-butanol/heptane at atmospheric pressure and room temperature. Stars indicate at which compositions this system has been studied at elevated pressure and temperature, where phase behavior depends on these parameters.

A number of experiments have been carried out at different compositions for the model surfactant system, where it has been exposed to different pressures and temperatures in the range of 1-400 bars and 35-50˚C, respectively. At several compositions it was observed that e.g. a two phase system could be changed to a three phase system only dependent on an increase in pressure, which is located by the stars in Figure 4. The physical conditions, pressure and temperature, are tabulated in Table 3.

Table 3: Overview of the physical conditions when phase shifts are observed and the changes in the number of phases.

Experiment No.	Phase shift	Temp. [˚C]	Pressure [Bar]
#1	3 to 2	35	156
#2	2 to 3	35	302
#3	2 to 3	40	100-200
#4	3 to 2	40	160

All observations for the experimental work are reversible. They include shift from a lower-phase microemulsion with excess of oil to the middle-phase microemulsion region and further shift from the middle-phase microemulison region to the upper-phase microemulsion with excess of water/brine all due to an increase in pressure.

Results from Work with Oil/Brine System

The oil/brine study is carried out experimentally similar to the surfactant study approach. The purpose is to study if different brine solutions, (with varying sulphate concentrations), has an effect on the crude oil. After operation on the DBR JEFRI PVT cell the crude oil is analyzed, where the viscosity is measured. The viscosity results are graphically shown in Figure 5.

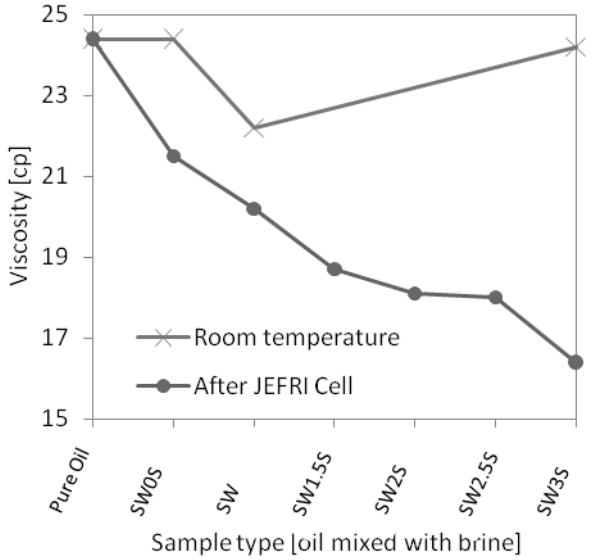

Figure 5: Graphical illustration of the viscosity results of the crude oil before and after the oil/brine system was processed in the DBR JEFRI PVT cell. Measurments are at different brine solutions, where SW0S is with no sulphate and then the sulphate concentration is increased from 1 to 1.5to 2 to etc. thereafter.

With respect to the viscosity of the crude oil, it is found that there is a significant decrease in the crude oil viscosity when the measurements are done before and after operation. Another observation is that before operation the crude oil viscosity seems independent on the sulphate concentration, where the increase in sulphate concentration alters the viscosity after operation.

Formation of emulsions at the oil/water interface was also studied, where increase in temperature and pressure had an effect, where almost all cases was de-emulsified during operation.

Discussion

The surfactant model system tested is only a model system. Therefore further studies will be required and the work must continue to establish a more general understanding of the observations. However, the results do agree that the phase behavior is dependent on the pressure.

Regarding the oil/brine study the work is so far limited to only one crude oil. To establish any kind of trend further work must be carried out to understand what mechanism that is the reason for the observations and to know if this is a general observation or not.

Conclusion

Experimental activities regarding phase behavior has been conducted.

Phase behavior of oil/ surfactant/ alcohol/ brine systems at elevated temperatures and pressures has been examined. The model system studied, heptane/ SDS/ 1-butanol/ brine, shows that both temperature and pressure has an effect on the equilibrium system. As this is observed at common reservoir pressure this is very relevant for further EOR studies.

The oil/brine study showed that increase in temperature and pressure has an effect on the system. The oil/water interface was in almost all cases de-emulsified. Furthermore the crude oil viscosity is decreased after operation in the DBR JEFRI PVT cell. This viscosity decrease is further enhanced when considering different brine solutions, where viscosity decreases as the sulphate concentration is increased.

References

1. B.M. O'Brian, J. Am. Chem. Soc. 59 (1982) 839a-852s
2. D.W. Green, G.P. Willhite, Enhanced Oil Recovery, SPE Textbook Series, 6(1998) 7
3. P. Zhang, Austad, SPE 94209, SPE/Europe/EAGE Annual Conference, Spain July 13th-16th, (2005)
4. Y. Wu, P. Shuler, Y. Tang, W.A. Goddard, SPE 95404 presented at SPE Annual Technical Conference and Exhibition, Dallas, Texas, (2005)
5. A.K. Flaaten, Q.P. Nguyen, G.A. Pope, J. Zhang, SPE 113469 presented Improved Oil Recovery Symposium, Tulsa, Oklahoma, (2008)
6. T. Austad, H. Hodne, S. Starnd, K. Veggeland, Colloid. Surface. 108 (1996) (253-262)
7. J. van Nieuwkoop, G. Snoei, J. Colloid Interf. Sci. 103 (1984) 400-416

Samira Telschow

Phone: +45 4525 2952
E-mail: ste@kt.dtu.dk
Discipline: Reaction and Transport Engineering

Supervisors: Kim Dam-Johansen
Stig Wedel
Flemming Frandsen
Kirsten Theisen, FLSmidth A/S

PhD Study
Started: March 2008
To be completed: August 2011

Investigation of the Reaction Mechanism and Kinetics During the Clinkerization of Cement Raw Meal at High Temperatures and Improvement of the Burning Technology

Abstract
In the cement manufacturing industry, reduction of the energy consumption and the CO_2 and NO_x emission levels while simultaneously increasing of the cement quality, is of great interest. The aim of this project is to investigate the development of the cement properties, depending on process conditions. Special focus is on the clinker properties: product composition, porosity and crystal/particle size distribution.

Introduction
Concrete is one of the most important materials in the construction industry worldwide. The main component of concrete is cement, a hydraulic binder (characterized by its ability of hardening under water). The world production capacity of hydraulic cement was in 2006 3-5 Gt [1, 2]. One of the most common cement types is Portland cement, which consists of Portland cement clinker ground with ~5wt.% gypsum. By addition of granulated slag, pozzolan, sulfate or lime to Portland cement clinker, cement with special properties e.g. higher concrete strength or special resistance against aggressive agents is obtained. Examples are e.g. Blast-furnace cement, Pozzolan-lime cement or Supersulfated cement.

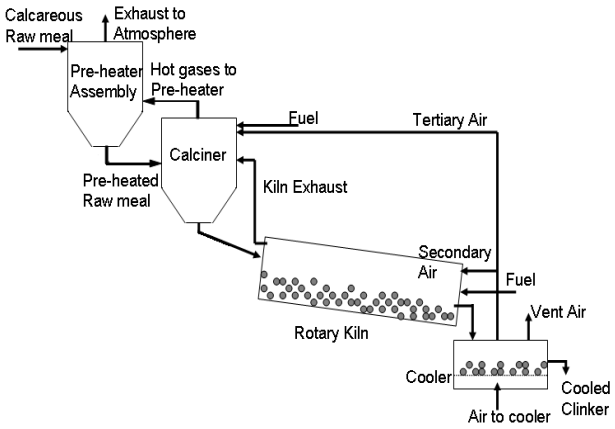

Fig. 1: A flow diagram of a cement kiln system [3].

A typical raw meal is composed of a mixture of calcareous material, such as limestone or marble, and SiO_2/Al_2O_3-rich clays (kaolinite, illite) or shale, as well as iron ore. Additionally, minor compounds e.g. Mg, Na, K as well as sulphates, phosphates, halogens etc. may also be present in the raw materials [4-6]. The crushed raw materials are blended and ground, before the raw meal is fed into the preheater section (a series of cyclones, see Fig. 1). There the materials are heated up to 800°C by hot gases from the calciner and kiln. Water, which is contained in the raw materials, is released. In the calciner most of the limestone is decomposed at ~900°C, i.e. CO_2 is removed and CaO is formed [7]. The degree of calcination is approximately 90-95%. In order to achieve the necessary temperatures in the calciner, fuel is burned there. Thereafter the material enters the rotary kiln. The material moves along the kiln to the lower end and is heated by hot gases from combustion of fuel at the outlet from the kiln. In the hot zone at the lower end of the kiln (gas temperatures of ~1800°C) the mixture reaches a temperature of ~1500°C, and melts partly [1, 7, 8]. In the kiln at temperatures of 1100-1500°C a series of reactions is occurring, resulting in the formation of the major crystal phases in the clinker product: Ca_2SiO_4 (belite), Ca_3SiO_5 (alite) and the so-called liquid phase (melt) $Ca_3Al_2O_6$ (aluminate) and $Ca_4Al_2Fe_2O_{10}$ (ferrite) [4, 7].

In the cooler, the hot clinker is rapidly cooled by heat exchange between the clinker solids and air, in order to recover the heat. The clinker product is ground

with gypsum and possibly other additives, stored, packed and sold.

The processes from drying of raw material to the clinkerization consumes an average thermal energy of 3.1-3.5 MJ/kg of produced clinker [2]. Additionally, ~100 kWh/t of electrical power is necessary e.g. for grinding of the raw material and the cement product [9]. The highest proportion of the electrical energy is attributed to cement grinding due to the clinker properties (the different clinker phases and other clinker characteristics).

Specific Objective

A critical product property is the clinker hardness, which is mainly influenced by the kind of crystal phases in clinker, the crystal/particle size distribution, and, the clinker porosity. Decreasing the clinker hardness facilitates the cement grinding and reduces the energy consumption of this process, as well as the material attrition of the mills. In general, the smaller the crystal sizes in clinker, the better the grindability of clinker. The preferred crystal phase in clinker is alite, since it controls the strength development of concrete. Also, it forms more brittle crystals, containing micro-cracks, than belite, which eases the clinker grinding. Therefore, high alite and low belite concentrations in the clinker are desired. The distribution of the clinker phases influences greatly the grindability. Often, belite crystals are arranged in clusters (Fig. 2), which are harder to grind than belite crystals distributed between alite crystals.

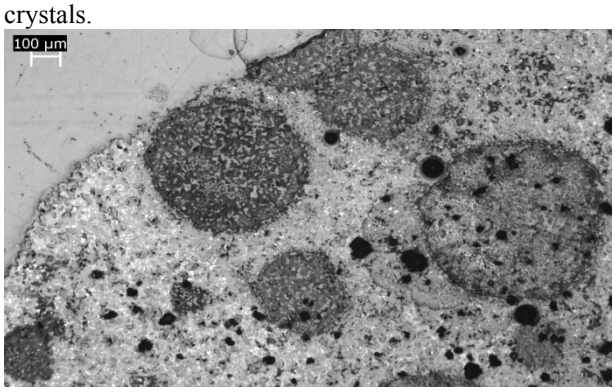

Fig. 2: Belite crystal cluster (blue areas) surrounded by alite crystals (brownish areas).

The focus in this project is on how the three properties (crystal phases, the crystal size distribution and the porosity) are developed as a function of different process conditions,

- Maximum burning temperature
- Temperature profiles
- Heating rates
- Burning time
- Rotation velocity

Mode of action of the setup

The clinker formation experiments need to be automated as much as possible in order to study the influence of only one parameter at a time on the clinker property development. Therefore, a new setup has been built. The setup (Fig. 3) simulates an industrial rotary kiln of a cement plant. It consists of two main parts: an ordinary horizontal heating furnace with an alumina tube and a sample motion system. The horizontal heating furnace contains five individually adjustable heating zones (Fig. 4, HZ1-HZ5). They are heated by $MoSi_2$ type heating elements. The heating elements are protected by an alumina tube through the center of the furnace (Fig. 3). All five zones together are set to simulate temperature profiles, which could occur in an industrial reactor. The furnace can be operated at temperatures between 900 and 1500 °C, which are the typical temperatures of the solid materials in the rotary kiln in the industrial process.

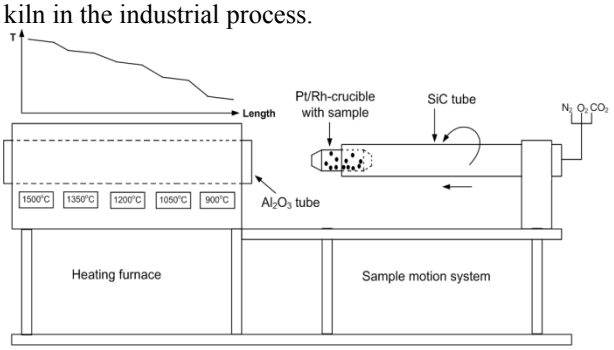

Fig. 3: A Sketch of the setup: the heating furnace on the left side and the motion part on the right side.

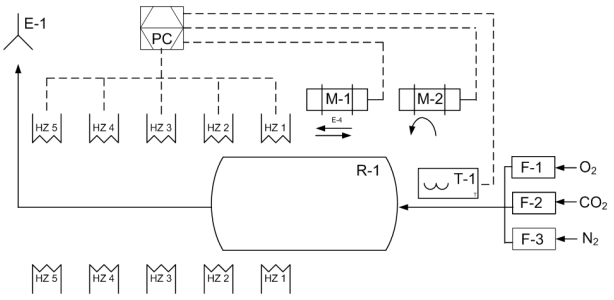

Fig. 4: The PI diagram of the setup: 5 individual heating zones (HZ1-HZ5); two step motors (M-1 and M-2) for the horizontal motion as well as for the rotation of the SiC tube; gas flow meters (F-1 – F3) for oxygen (O_2), carbon dioxide (CO_2) and nitrogen (N_2); a S-type thermocouple (T-1) behind the platinum crucible (R-1). Temperature and velocities are controlled from a PC.

The movement of the solid material through the industrial rotary kiln occurs due to a tilted positioning and the rotation of the reactor. This is simulated with the sample motion system of the setup. It consists mainly of a ceramic SiC tube, which is connected to two step motors. One of the motors is moving the ceramic tube along the horizontal into the alumina tube of the heating furnace. The second step motor rotates the tube around its horizontal axis. Both motions are adjustable in the velocity.

The raw meal for clinker formation is placed into a special designed Pt/Rh-crucible. The crucible consists of a cylindrical main body and a conical shaped lid (Fig. 5 and 6). About 80% of the main body is placed into the

SiC rube of the pushing system. The lid part remains outside of the tube. Both ends of the whole crucible have openings to ensure a sufficient gas flow through the reactor. The entrance opening is special design to ensure a well distributed gas flow through the furnace. An inner cone is attached to the opening, which channels the gas flow along the platinum wall and through the center of the crucible (Fig. 5 and Fig. 6, right). Nitrogen, oxygen and CO_2 are utilized to simulate different atmospheres inside the crucible. The gas temperature inside the Pt/Rh-crucible cannot be measured directly. The gas openings are too small to insert a thermocouple. Therefore, a S-type thermocouple is placed inside the SiC tube right behind the platinum reactor. The crucible holds ca. 25 g raw meal at maximum which relates to a fill height of 28 %.

The heating furnace temperature, the motion velocity through the furnace and the rotation velocity are controlled from LabView. The measured temperature inside the SiC tube is logged on a PC.

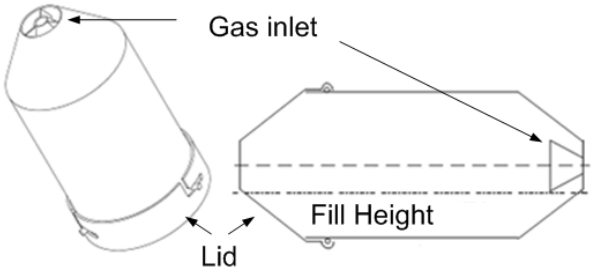

Fig. 5: A sketch of the platinum crucible. It consists of a main body and a lid. To ensure sufficient gas flow, the gas inlet contains an inner cone to distribute gas along the crucible wall and the center.

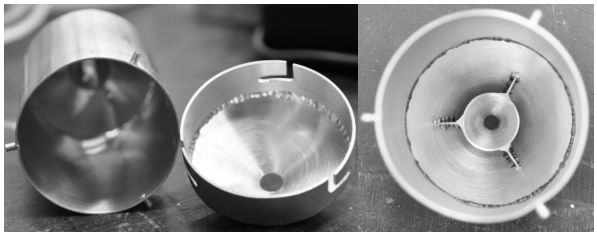

Fig. 6: The platinum crucible main body and lid (left); the inner cone of the gas inlet (right).

Test burns of clinker samples

Typical clinker obtained from test burnings in the new setup is shown in Fig. 7. Generally, it consist of agglomerates of two different types: a) nearly spherical shaped clinker nodules (Fig. 7) and b) unshaped agglomerates characterizes by small clinker nodules molten together (defined here as "melt agglomerates") (Fig. 8). The clinker nodules have been formed due to particles rolling on top of the solid core material due to the rotation motion, whereas the melt agglomerates have been formed as lining on the hot platinum walls. The same is observed in the industrial clinker burning process.

For all tests carried out so far, the main size fractions of the spherical clinker agglomerates are <0.5 mm (ca. 20 wt.%), 1-2 mm (ca. 32 wt.%) and 2-4 mm (ca. 23 wt.%). The concentration of other size fractions is below 10 wt.-%.

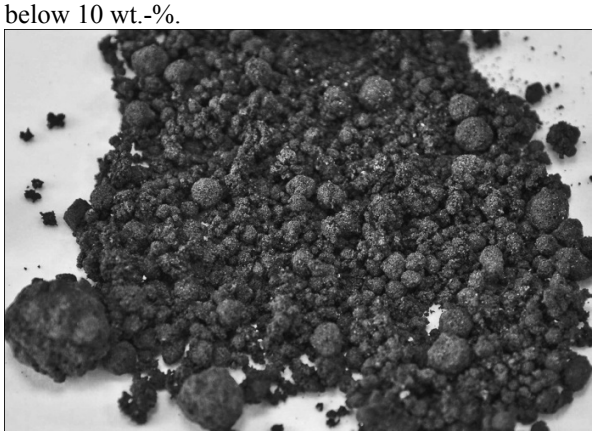

Fig. 7: Clinker nodules, which have been rolling on top of the lining in the crucible.

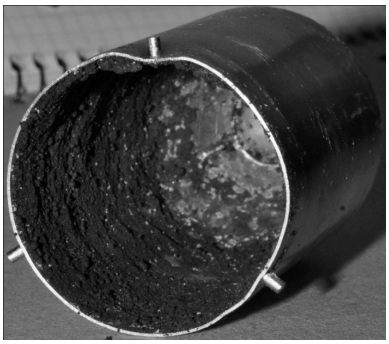

Fig. 8: The inside of the platinum crucible after test burning. Lining of the solid and partly molten material on the walls occurred.

The clinker burning in the setup features repeatability not only in the size distribution of the obtained clinker agglomerates but also in the clinker phase composition. The clinker phase composition of three clinker samples burned in the setup is shown in Fig. 7. All three samples have been obtained from a raw meal prepared from purchased chemicals: $CaCO_3$, SiO_2, Al_2O_3 and Fe_2O_3. The raw meal was pre-calcined at 950 ˚C for 30 min at once. Thereafter three samples were heat treated isothermally at 1450 °C for 35 min with a rotation velocity of 3 rpm in the new setup.

All three samples contain nearly the same high concentrations of alite (C_3S) and lower concentrations of belite (C_2S), aluminate (C_3A), ferrite (C_4AF) and non-reacted CaO. Additionally an amorphous phase is shown, which is related to the analysis method (XRD) and represents more the uncertainty of the analysis than a true amorphous phase. The slight difference of the belite and amorphous phase concentration of the last sample are - similarly - due to the uncertainty of the analysis method.

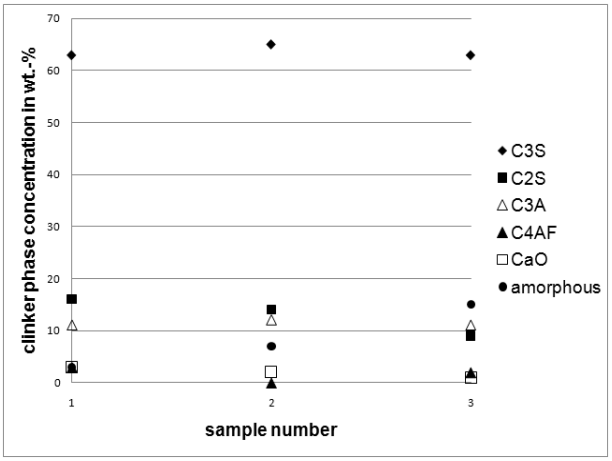

Fig. 9: Clinker phase composition of 3 samples of the repeatability test.

One goal in the utilization of the setup is to obtain clinker, comparable with industrial produced clinker. Therefore, a raw meal from a cement plant was used for test burns and the obtained clinker compared with the industrial clinker. This industrial raw meal was pre-calcined at 950 ˚C for 30 min. Thereafter, different samples were heat treated a) isothermally at 1400, 1450 and 1500 ˚C (classical clinker test burning) and b) non-isothermally at a linear temperature gradient from 900-1500 ˚C. The chosen treatment time of 35 min was orientated on random retention times of solid materials in the industrial rotary kiln, since no exact information was available from the cement plant. The rotation velocity was for all samples 5 rpm.

The clinker phase compositions of the samples burned in the new setup (Table 1) show significant differences in the alite and belite concentration compared to the industrial clinker (Table 2). The alite (C_3S) concentration is ca. 25-50 % lower than in the industrial clinker. In contrary, the belite (C_2S) concentration is higher as well as the free CaO concentration. Obviously, the formation of alite from belite and free CaO was not completed. It might be a result of too short chosen burning time (35 min) or a too low heating rate.

The aluminate and the ferrite phase of the setup clinker samples and the industrial clinker are similar. Those clinker phases are mainly formed at lower temperatures (900 -1200 ˚C) at the beginning of the burning process. Therefore the reactions were completed within the heat treatment time. It indicates that the clinker formation processes in the setup are similar with the processes in the industrial reactor. Increasing either the heat treatment time or the heating rate will most likely result in similar alite, belite and CaO concentrations of both clinker types.

A comprehensive conclusion of the comparability of the clinker burning cannot be drawn yet, since physical clinker properties, e.g. clinker phase distribution, agglomerate size distributions or porosity, of both clinker types have not been evaluated yet.

Table 1: The clinker phase composition of the self burned samples: isothermally at 1400, 1450 or 1500 ˚C burned clinker (I); and non-isothermally burned clinker (NI)

Sample	C_3S	C_2S	C_3A	C_4AF	CaO	Amorphous
I-1400	34	37	6	12	10	1
I-1450	45	29	6	13	6	1
I-1500	47	27	6	12	5	3
NI-900-1500	30	37	7	12	9	5

Table 2: The clinker phase composition of three industrial clinker (IC) portions obtained from a cement plant.

Sample	C_3S	C_2S	C_3A	C_4AF	CaO	Amorphous
IC-1	60	20	4	13	1	1
IC-2	56	25	6	12	1	0
IC-3	61	20	7	12	1	0

Conclusions

A new setup has been built, which simulates the industrial rotary kiln of a cement plant. It allows the step wise and controlled study of clinker formation processes at high temperatures. The advantage over the classical clinker burning methods is the possibility of a combined study of chemical, mineralogical and physical process at one.

Acknowledgement

The Danish National Advanced Technology Foundation and FLSmidth A/S are acknowledged for financial support of this project.

References

1. U.S. Environmental Protection Agency, Inventory of U.S. Greenhouse Gas emissions and Sinks: 1990-2006, 2008.
2. Verein Deutscher Zementwerke e.V., Forschungsinstitute der Zementindustrie, VDZ Activity report 2005-2007, Verlag Bau + Technik GmBH, Duesseldorf, 2008, p. 26, 74.
3. A. Z. Jensen, Master thesis, Institute of chemical and biochemical engineering at DTU; 2008.
4. G.C. Bye, Portland Cement-Composition, Production and Properties, Pergamon Press, Oxford, 1983, 8pp.
5. F.P. Glasser, J.I. Bhatty, F. McGregor, S.H. Kosmatka, Innovations in Portland Cement Manufacturing, Portland Cement Association, Skokie, Illinois, 2004, p. 332.
6. F. Nishi, Y. Takéuchi, I. Maki, Zeit. Krist. 172 (1985) 297.
7. H.F.W. Taylor, Cement Chemistry, Academic Press Thomas Telford, London; 1997, 55pp.
8. J. Klauss, ZKG International 53 (3) (2000) 132-144.
9. V. Johansen, T.V. Kouznetsova; 9th ICCC; New Delhi, 1992.

Lise Vestergaard Thomassen
Phone: +45 4525 2979
E-mail: lvt@kt.dtu.dk
Discipline: Enzyme Technology

Supervisors: Anne S. Meyer

PhD Study
Started: April 2008
To be completed: March 2011

Maximal Release of Highly Bifidogenic Soluble Dietary Fibers from Industrial Potato Pulp by Minimal Enzymatic Treatment

Abstract
Potato pulp is a co-processing product from industrial potato starch manufacturing and consists mainly of the tuber plant cell wall material. It is particularly rich in pectin, notably galactan branched rhamnogalacturonan I which has previously been shown to exhibit promising properties as dietary fiber. The objective of this study was to solubilize dietary fibers from potato pulp by a one-step minimal treatment procedure and evaluate the prebiotic potential of the fibers. The result was a method that within one minute released 75% (w/w) dry matter from 1% (w/w) potato pulp treated with 1.0% (w/w) (enzyme/substrate, E/S) pectin lyase from *Aspergillus nidulans* and 1.0% (w/w) E/S polygalacturonase from *Aspergillus aculeatus* at pH 6.0 and 60°C. Molecular size fractionation of the solubilized fibers revealed two major fractions. When fermented *in vitro* by microbial communities derived from faecal samples from three healthy human volunteers, both of the solubilized fiber fractions were more bifidogenic than fructo-oligosaccharides (FOS).

Introduction
The fermentability of enzymatically solubilized fibers from potato pulp has previously been studied [1,2]. In these studies the solubilized potato fibers were mixtures of different molecular structures having different molecular masses. A first step in obtaining at least a provisional understanding, and a direction for designing the enzymatic solubilization to produce fibers exerting maximal biological benefits, would be to map the possible relationship between the solubilized polysaccharide structures and their putative biological effects by assessing the influence of the molecular size and composition on the growth of human intestinal bacteria.

Pectin can be solubilized from plant material by different enzymes which have been shown by e.g. Ishii [3,4]. Previously in our lab, multicomponent plant cell wall degrading enzyme preparations were used to solubilize pectinaceous fibers from potato pulp [5]. However, the use of monocomponent enzymes for solubilization entails the possibility of targeting the enzymatic attack of the substrate, avoiding undesirable enzyme catalyzed degradation of the released fibers, and may furthermore provide knowledge about the accessibility of the pectin in the plant cell wall material. Based on the available compositional data the soluble potato fibers may be hypothesized to be mainly made up of rhamnogalacturonan I fragments having extensive galactan side chains [5]. Pectin lyase, polygalacturonase and presumably pectin methyl esterase would therefore be relevant enzyme candidates for solubilization of such dietary fibers from potato pulp.

Specific objectives
The hypothesis behind this study was that it should be possible to solubilize the potential galactan-rhamnogalacturonan I dietary fiber fraction from potato pulp by use of a few selected enzyme activities attacking the pectin homogalacturonan backbone.

Experiments
The action of selected pectinolytic enzymes on potato pulp was examined in statistically designed experiments in which the separate and interactive effects of different reaction factors were also evaluated in order to design a minimal procedure by which the maximal amount of fiber could be released. The solubilized fibers were subsequently fractionated into two large fractions according to molecular mass and the effect of the potential dietary fibers on the composition of human intestinal bacterial ecosystems was evaluated by small scale *in vitro* fermentation.

Results

Statistically designed experiments indicated that it was possible to release at least 70% of the dry matter by employing only a pectin lyase and a polygalacturonase. Further optimization of the experimental conditions entailed achievement of the best minimal procedure for releasing 75% of the dry matter: 1.0% (w/w) E/S pectin lyase from *A. nidulans* and 1.0% (w/w) E/S polygalacturonase from *A. aculeatus* incubated with 1% (w/w) destarched potato pulp for 1 min at pH 6, 60 °C.

The released fibers were fractionated into three fractions: >10, 10-100 and >100 kDa. The monosaccharide composition in the sample CPP>100 contained approximately 66% galactose, 9% arabinose and 1.7% rhamnose. In contrast, the main component in CPP10-100 was galacturonic acid (48%) and rhamnose level was approximately 1.4%.

After fermentation in fecal slurries obtained from three different subjects, quantitative real-time PCR was applied to measure the density of gene targets encoding 16S rRNA of selected bacterial taxonomic units. The ability of the released fibers to selectively stimulate the growth of the given bacterial taxa was compared to that of FOS. The fecal communities fermented on CPP>100 had a significantly higher content of *Bifidobacterium* than the same fecal communities fermented on FOS ($P<0.05$) (Figure 1). A similar trend was found for the samples fermented on CPP10-100, but the difference to FOS did not reach statistical significance ($P<0.10$). There were no differences in the Lactobacillus and Firmicutes content between the fermentation samples containing the applied fibers and FOS (data not shown).

In any case, the results obtained in this study indicate that the enzymatically produced β-1,4-galactan rich potato fibers, especially those with high molecular weights, may have potential as functional food ingredients with bifidogenic properties.

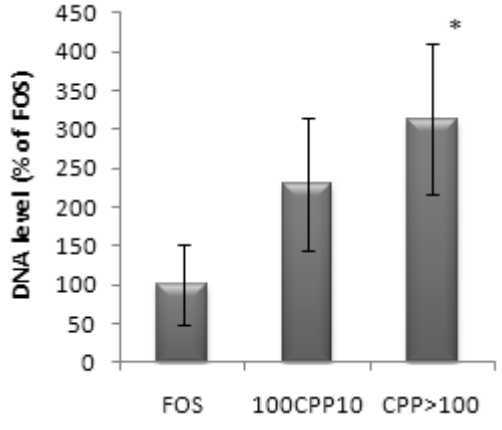

Figure 1: The biological activity of the enzymatically solubilized fibers on Bifidobacterium. The bars represent the average±SEM of triplicate fermentations. DNA amount in the fermentation samples of FOS was set to 100%. Asterisks indicate a significant difference from the fermentation samples containing FOS; *P < 0.05.

Acknowledgements

This study was supported by the Danish Strategic Research Council´s Committee on Food and Health (FoSu, Center for Biological Production of Dietary Fibres and Prebiotics, no. 2101-06-0067). Financial support from the FOOD Denmark Graduate School, Center for Advanced Food Studies, Denmark, is also acknowledged. Lyckeby Stärkelsen (Kristianstad, Sweden) is acknowledged for supplying the potato pulp.

References

1. M. Olesen, E. Gudmand-Hoyer, M. Norsker, L. Kofod, J. Adler-Nissen, Eur. J. Clin. Nutr. 52 (1998) 110-114
2. H.N. Larke, A.S. Meyer, K.V. Kaack, T. Larsen, Nutr. Res. 27 (2007) 152-160
3. S. Ishii, Phytochemistry 20 (1981) 2329-2333
4. S. Ishii, Phytochemistry 21 (1982) 778-780
5. A.S. Meyer, B.R. Dam, H.N. Laerke, Biochem. Eng. J. 43 (2009) 106-112

List of publications

1. L.V. Thomassen, A.S. Meyer, Enzyme Microb. Tech. 46 (2010) 297-303.
2. L.V. Thomassen, L.K. Vigsnæs, T.R. Licht, J.D. Mikkelsen, A.S. Meyer (2011) DOI: 10.1007/s00253-011-3092-y

Maja Bøg Toftegaard
Phone: +45 4525 2830
E-mail: mbt@kt.dtu.dk
Discipline: Reaction and Transport Engineering

Supervisors: Anker Degn Jensen
Peter Glarborg
Peter Arendt Jensen
Bo Sander, DONG Energy

Industrial PhD Study
Started: April 2007
To be completed: March 2011

Oxy-Fuel Combustion of Coal and Biomass

Abstract
A drastic decrease of the CO_2 emission from power production is necessary to limit global warming. One of the promising technologies which will enable almost complete capture of CO_2 from power plants burning fossil fuels is oxy-fuel combustion. There is a need for a more in-depth insight into the fundamental aspects of the effects of oxy-fuel combustion regarding combustion chemistry and the effects on especially ash quality in relation to cement and concrete production. The PhD study includes an experimental and theoretical investigation of these aspects.

Introduction
Several technologies have been proposed and are investigated for carbon capture and storage (CCS), i.e. the removal of CO_2 from exhaust gases from e.g. power plants or other fossil fuel fired processes. Oxy-fuel combustion is one of the more promising of these technologies [1]. Figure 1 shows the principle in an oxy-fuel power plant. The fuel, e.g. coal, biomass, or others, is burned in an atmosphere consisting of oxygen and recirculated flue gas (consisting primarily of CO_2 and water). The resulting flue gas has a CO_2 content of up to 95 % on a dry basis compared to about 14 % from a conventional plant. The CO_2 can be stored after cleanup and compression.

Generally, there is insufficient knowledge on many fundamental and practical aspects related to the change from the conventional to the oxyfuel combustion process. From a chemical engineering point of view this concerns amongst others the emission levels of CO, NO_x, and SO_2, the quality of the ash fractions, the risk of increased corrosion due to a change in the chemical composition of the combustion atmosphere and deposits, and the temperature and radiation in the boiler which are affected by the changed gas phase composition, i.e. the increased levels of CO_2 and water. Especially aspects regarding the effect of the flue gas cleaning strategy on fly ash quality and corrosion still need significant further investigations. Furthermore, the effect of using biomass as fuel in CCS has only been investigated experimentally by very few research groups [1]. This approach involves the possibility of operating power plants with negative CO_2 emissions.

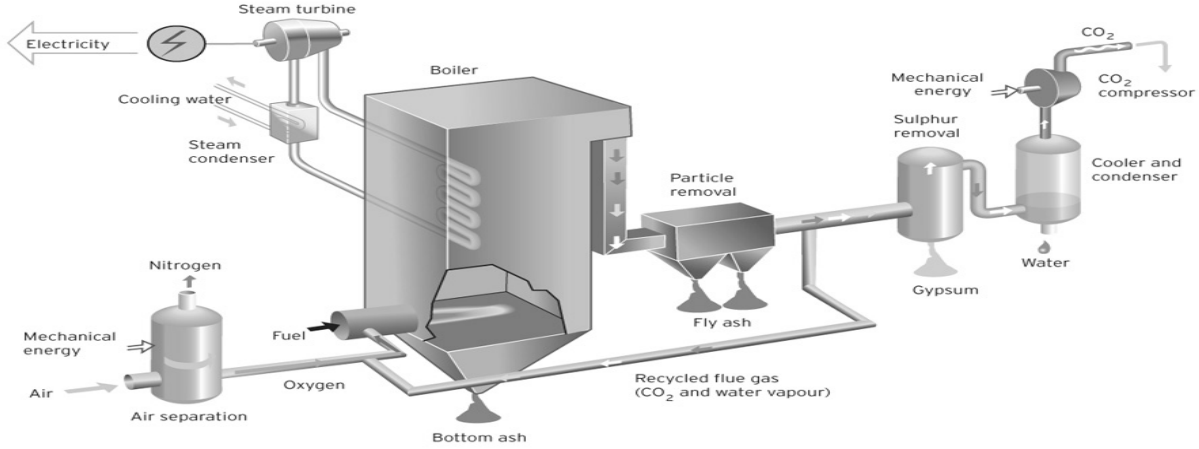

Figure 1: Possible layout of an oxy-fuel power plant showing the air separation, flue gas recirculation, and flue gas treatment new to the plant compared to a conventional air-fired power plant. Graphics: www.kjell-design.com

Specific Objectives

The aim of the PhD study is to strengthen the scientific basis for the development and application of the oxyfuel combustion technology to thermal power plants. Experimental investigations of the fundamental aspects of the combustion chemistry obtained when burning coal and biomass are performed. Specific topics addressed are:

- Ash composition and quality, especially related to sulphur retention – because of the application of fly ash in cement and concrete production this is a very important area of investigation.
- Deposits composition – the chemical composition is indicative of the risk of corrosion on heat transfer surfaces.
- Emissions of CO, NO_x, and SO_2 from the boiler – the recirculation of flue gas will play a role in the obtained levels of the emission of harmful gas phase pollutants together with the chosen strategy for flue gas cleaning.
- Necessary excess oxygen level – Oxygen is produced in a cryogenic air separation unit. Excess oxygen for combustion is thus associated with a significant economic penalty compared to air-firing.
- The effect of co-firing coal with straw.

Experimental setup

An existing experimental setup is applied in the investigations, see Figure 2. The setup consists of a cylindrical reactor (inner diameter 31.5 cm, height 1.9 m) with a top-mounted swirl burner. The setup is equipped with a solid fuel feeder, a fly ash sample system, and 8 measuring ports for temperature and gas phase composition measurements and deposit collection. The setup is run at a thermal input of approximately 30 kW.

As part of the project the setup has been rebuilt to be able to run at oxyfuel conditions. In full scale, flue gas will be recirculated to adjust the flame temperature. However, the pilot plant is a once-through reactor and flue gas recirculation is not applied. Instead, synthetic flue gas consisting of pure CO_2 from gas cylinders is used. Pure oxygen is likewise delivered to the setup from gas cylinders and mixed with CO_2 in a special mixing panel. A system to enable addition of both N_2, NO and SO_2 to the CO_2 stream is likewise included in the setup.

Online gas analysers measure the flue gas composition during experiments (O_2, CO_2, CO, NO, and SO_2). For oxyfuel experiments a GC is used simultaneously to measure CO_2, O_2, and N_2.

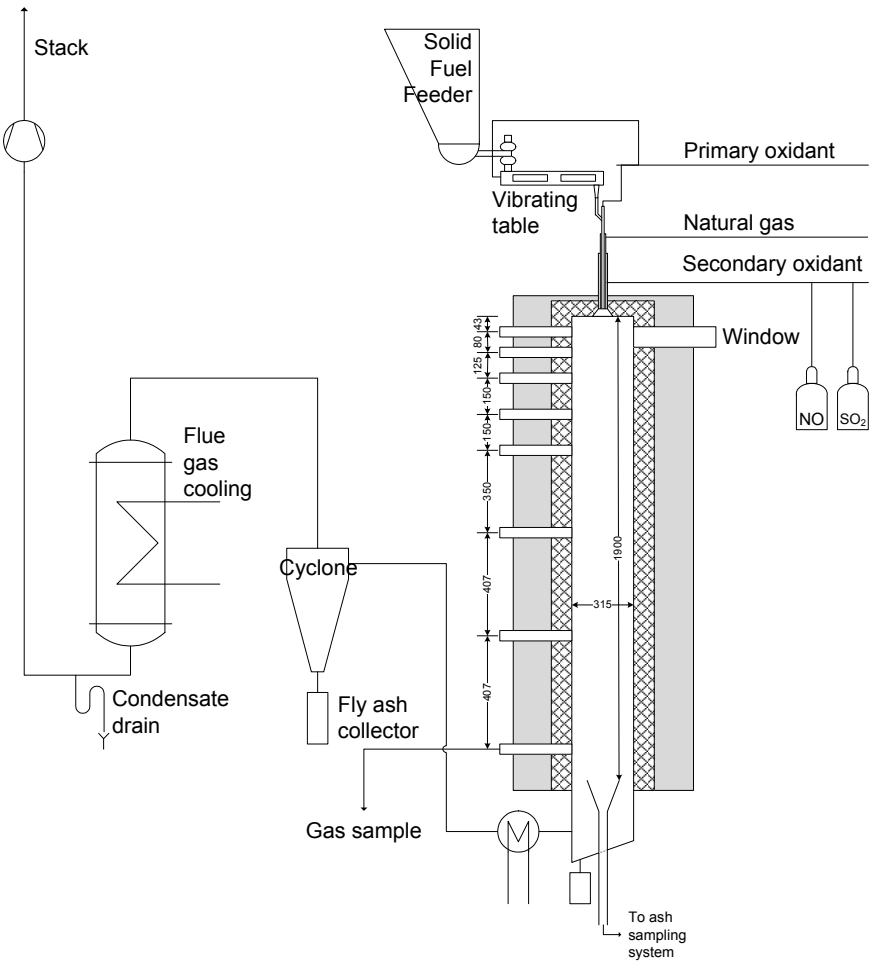

Figure 2: Sketch of the experimental setup – a 30 kW down-fired swirl burner.

Results and Discussion

A series of experiments have been performed from which 52 have been selected for further data treatment. The experiments have been run with four different fuels; pure coal, pure straw, and two coal/straw blends with 20 and 50 wt% straw, respectively. For all fuels, combustion has been performed in both air and an O_2/CO_2 mixture with 30 % O_2. For the pure fuels experiments with varying stoichiometry and oxidant composition have likewise been performed in order to determine reference conditions and investigate other specific subjects within the project.

The results discussed here will be concerned with the investigations of the effect of co-firing coal with straw on emissions and ash chemistry at the reference conditions for both air and oxyfuel as oxidant.

Reference conditions

In order to compare air and oxyfuel combustion a set of reference conditions were chosen based on a series of experiments with coal as fuel. The parameters to define were the combustion stoichiometry and the oxyfuel oxidant composition.

The combustion stoichiometry for the air reference was determined based on the requirement of a satisfying burnout, i.e. the fly ash being comparable to fly ash from full-scale plants (less than 5 % C in fly ash). An oxygen excess ratio of $\lambda = 1.3$ was selected, corresponding to 5 % O_2 in the dry flue gas.

For oxyfuel combustion, a match of the flue gas O_2 concentration rather than λ was decided on as this most likely would be the case in full-scale plants. Based on measured temperature profiles for oxyfuel combustion with three different inlet O_2 concentrations (25, 30, and 35%) and the air reference 30 % O_2 in the oxidant was selected as reference value for oxyfuel. Figure 3 shows the measured temperature profiles.

The selected reference operating conditions were applied to all investigated fuels.

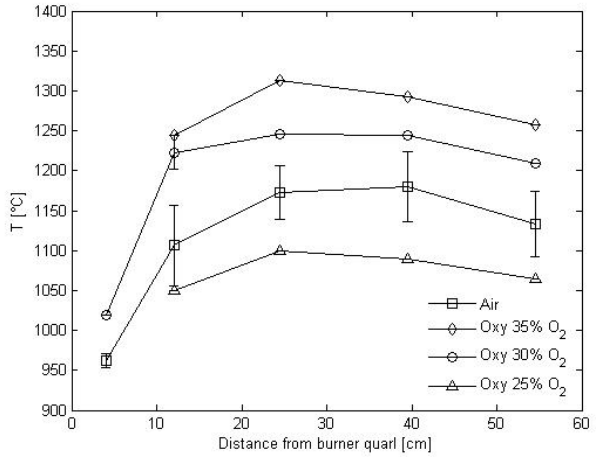

Figure 3: Temperature profiles measured along the reactor centreline for pure coal combustion in air and oxyfuel atmospheres with different inlet oxygen concentrations. Error bars correspond to two times the standard deviation for repeated measurements.

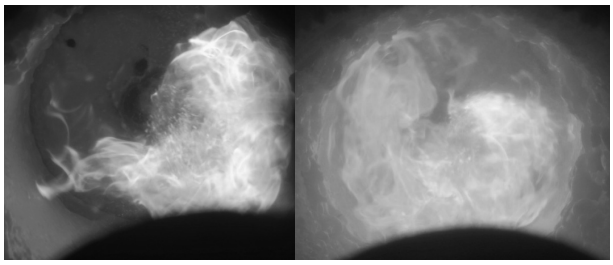

Figure 4: Picture of left: pure straw and right: the 50/50 wt% coal/straw blend, both burned in the reference 30% O_2/70% CO_2 oxyfuel atmosphere. The pictures are taken from the bottom of the reactor.

Figure 4 shows typical appearances of the swirling solid fuel flames. No visual difference could be determined between air and oxyfuel flames. However, increasing straw share in the fuel yielded longer and less attached flames due to delayed ignition of the larger straw particles.

Emissions

The specific emissions of CO, NO, and SO_2 are determined from Eq. 1:

$$E_i = \frac{y_i \cdot M_i \cdot F_{FG,dry}}{\dot{m}_{fuel} \cdot LHV} \quad (1)$$

where y_i is the measured concentration of component i in the dry flue gas sample, M_i is the molar mass of component i, $F_{FG,dry}$ is the molar flow rate of flue gas, m_{fuel} is the feeding rate of solid fuel, and LHV is the lower heating value of the fuel.

Figure 5 shows the emission rate for NO as a function of the straw share of the fuel for air and oxyfuel conditions. The figure illustrates an important advantage of the oxyfuel combustion technology compared to conventional air-firing when considering pollutants emissions. The near elimination of N_2 from the flue gas reduces NO emission with 20-45 %. This would have a positive impact on the operating expenses concerned with flue gas cleaning.

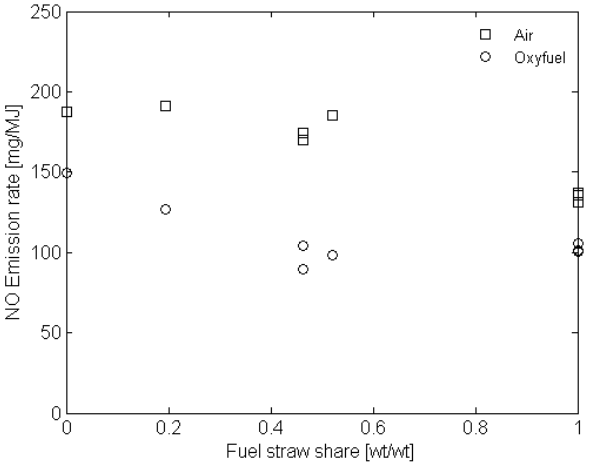

Figure 5: Specific NO emissions as function of the straw share in the fuel for air and oxyfuel reference experiments.

Several mechanisms, both chemical and transport phenomena related, are influencing the formation and reduction of NO during combustion of solid fuels. For the presented results, the difference between the air and oxyfuel data could be caused by e.g.:

- Less thermal NO formation – The near elimination of N_2 from the reaction mixture could drive the equilibrium reactions in the thermal NO formation mechanism toward NO reduction at high temperatures.
- Change of flow pattern in flame – NO formation is highly sensitive to the mixing of fuel and oxidant in the flame. During oxyfuel combustion the total oxidant flow is lower than for air as oxidant due to the necessary increase of the inlet O_2 concentration (from 21 to about 30 %). The change in flow rates may change the fluid dynamics in the flame zone.

From the data a trend of decreasing NO emission with increasing straw share is observed. This is assumed to be a direct consequence of the decreasing Fuel-N content of straw compared to coal.

Emission rates of CO and SO_2 have likewise been determined. No significant difference between the combustion atmospheres could be detected. However, the SO_2 emission decreases drastically with increasing fuel straw share and is close to zero for pure straw combustion (coal ~ 350 mg/MJ).

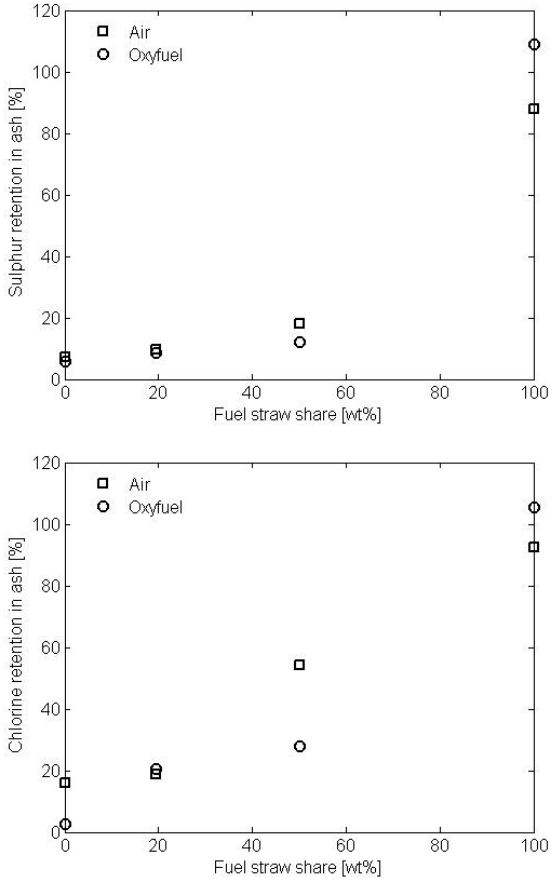

Figure 6: Sulphur and chlorine retention in fly ash as function of the straw share in the fuel for air and oxyfuel reference experiments.

Ash Chemistry

Fly ash samples were collected during selected experiments and analysed with respect to their composition. Figure 6 shows the retention of S and Cl as function of the fuel straw share for the air and oxyfuel reference operating conditions.

No significant difference between air and oxyfuel atmospheres is seen. However, the impact of the change in fuel ash chemistry when increasing the fuel straw share is clear from the figure. For both ash species an increasing retention with increasing straw share is observed. Most marked is the sharp increase in the S retention from about 20 % at 50% straw in the fuel blend to full retention (within the experimental uncertainty) for pure straw as fuel. For Cl a more linear relationship between fuel composition and retention can be determined. Full retention is likewise seen for pure straw combustion.

Sulphur is typically included in the ash as sulphates, e.g. K_2SO_4 and chlorine is bound as the equivalent chlorides, e.g. KCl. The retention of S and Cl in the ash is thus dependent on the available alkali and alkali-earth species. For fuels with high coal content the ash is rich in alumina and silica. K, etc., can thus be bound in Al-Si compounds and the retention of S and Cl is low. For pure straw the surplus of K and other alkali species is large enough for the ash to capture all S and Cl.

Conclusions

A series of air and oxyfuel experiments have been performed on four different fuel blends. The investigations have shown that for a given fuel the combustion process differs primarily regarding NO emissions when changing oxidant. No significant differences between air and oxyfuel combustion have been observed when comparing emission of other pollutants such as CO and SO_2 or for fly ash and deposits compositions.

Acknowledgements

The PhD study is part of PSO project 7171 (Oxy-fuel Combustion for below zero CO_2 emissions) which is carried out in collaboration between DONG Energy, Vattenfall A/S, the Combustion and Harmful Emission Control (CHEC) group at the Chemical Engineering department (KT), and department of Manufacturing Engineering and Management, DTU.

The PhD study is financially supported by PSO, DONG Energy, and the Ministry of Science Technology and Innovation (VTU).

Thanks to Bjørn Maribo-Mogensen who was the key figure in performing the experiments on coal as part of his Master's thesis.

References

1. M.B. Toftegaard, J. Brix, P. Glarborg, P.A. Jensen, A.D. Jensen, Prog. Energ. Combust. Sci. 36 (5) (2010) 581-625.

Rasmus Trane
Phone: +45 4525 2809
E-mail: rt@kt.dtu.dk
Discipline: Reaction and Transport Engineering

Supervisors: Anker Degn Jensen
Søren Dahl, DTU Physics

PhD Study
Started: August 2010
To be completed: August 2013

Catalytic Steam Reforming of Bio-Oil to a Hydrogen Rich Gas

Abstract
The catalytic steam reforming (SR) of bio-oil is a sustainable and renewable route to H_2 and synthesis gas, which makes it an interesting process to investigate. High degrees of conversion and high selectivities towards the desired products are possible with the current catalysts, but a major concern is coke deposition, which causes fast deactivation of the catalysts. This PhD. project aims to investigate different catalysts in the SR of model compounds of bio-oil and elucidate reaction mechanisms and kinetics for the process.

Introduction
In the recent decades it has become evident that the fossil fuels are a limited resource and that the emission of CO_2 could cause global warning with severe changes to the climate. To diminish the dependency on the fossil fuels and to reduce CO_2 emissions much research is focused on new or alternative and sustainable fuels and energy sources. One of the possible alternative energy sources is biomass, which is a renewable and CO_2-neutral fuel and carbon source.

An interesting possibility for utilization of biomass is to flash pyrolyze it, which produces gases, liquids, and solids. Liquid yields up to 75 *wt%* can be achieved by a proper choice of operating conditions. The gas and char yields typically range between 10-20 *wt%* and 10-15 *wt%,* respectively [1; 2]. The gases can be used to provide energy for pyrolysis and the solids can be returned to the fields as a fertilizer.

The liquid from the pyrolysis is called bio-oil and can have an energy density ten times larger than biomass and is therefore more suitable for transport as the cost associated with this will be much lower compared with biomass [3]. The pyrolysis can be performed at regional plants and the bio-oil can be transported to a central plant, which can upgrade or convert the bio-oil into the desired products. This can decrease the transport cost associated with utilizing biomass in the energy production by a factor of 5 hereby making the overall process more feasible [3]. One of the problems with utilizing biomass in the energy sector can therefore be solved by the flash pyrolysis.

The bio-oil consists of many different oxygenated compounds of various molecular weights and has a high oxygen content, which induces a low heating value, acidity of the oil, and instability. The oxygenates can polymerize under storage, which causes an increase in viscosity and average molar weight with time. The bio-oil should be converted to other products as it is not suitable for direct use neither in engines nor boilers.

One of the possible routes for utilization is to hydrodeoxygenate the bio-oil to a gasoline like product. For this process H_2 is needed which can be provided by SR of some of the bio-oil. The SR of bio-oil can also be used to produce H_2 or synthesis gas for chemical processes in a sustainable and renewable manner. A simple flow diagram for the process from biomass to synthesis gas via SR of bio-oil is shown in Figure 1.

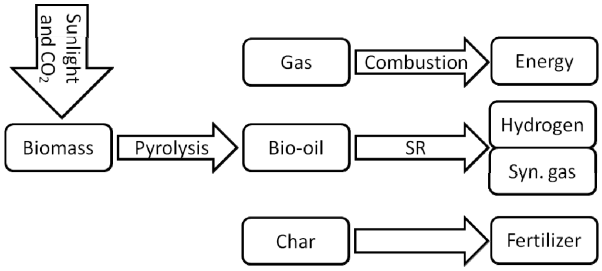

Figure 1: Simple flow diagram for the complete path from biomass to synthesis via bio-oil SR.

SR of oxygenates
Steam reforming is a process where hydrocarbons are reacted with steam at elevated temperatures to produce carbon oxides and hydrogen. For oxygenates the reaction scheme is:

$$C_nH_mO_p + (n-p)\,H_2O \rightarrow n\,CO + (n + m/2 - p)\,H_2 \quad (1)$$

The product distribution is influenced by the water gas shift (WGS) and methanation reactions. The extents of both these reactions are determined by the operating conditions. The SR reaction is endothermic and favored by high temperatures and low pressures. The ratio between steam and carbon (S/C) is an important parameter as well as high ratios will increase the conversion, shift the WGS towards H_2 and CO_2, and decrease the coke formation [4; 5]. The equilibrium offgas composition from the SR of ethanol as a function of the temperature is shown in Figure 2. Here it can be seen that the conversion is to CO_2 and CH_4 at low temperatures and as the temperature increases the products shifts towards H_2 and CO.

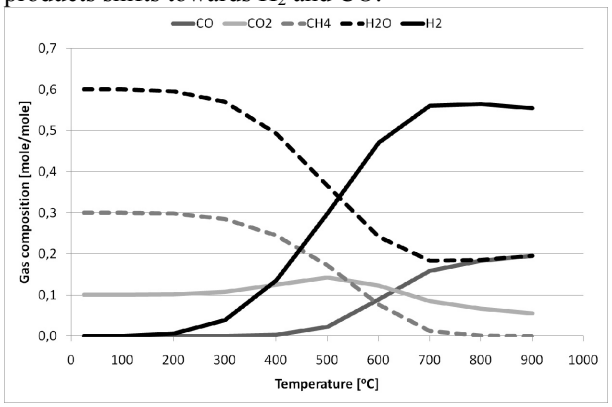

Figure 2: The equilibrium offgas composition as function of the temperature in the SR of ethanol at 1 *bar* and S/C-ratio of 1.5.

The catalysts used in the SR of oxygenates are supported metal catalysts. The metals are often Ni or noble metals, like Pt, Rh, or Ru. Ni is the most interesting from an industrial point-of-view as it is cheap and abundant. The activity of Ni is comparable to the noble metals, but Ni is more prone to coke formation [5; 6]. Spinel type supports, like $MgAl_2O_4$, has shown good performance in SR due to a low acidity, which decreases the cracking and coke formation. Mixtures of basic oxides like MgO, La_2O_3 or CeO_2 with Al_2O_3 are also suitable because these supports have a low acidity as well [6]. The catalyst performance can be enhanced be adding K to the catalyst, which can increase conversion, H_2-yield, and the long term stability [7]. The catalysts investigated in the literature can initially achieve high degrees of conversion and high selectivities. Nevertheless, one of the main concerns is the low stability with typical operating hours for acceptable rates being less than 100 *h*. The main source of the deactivation is coke deposition.

The mechanism and kinetics of SR of oxygenates such as those present in bio-oil is not yet well understood and the attempts to elucidate these have mainly been done for SR of ethanol and acetic acid.

Specific objectives

The main objective in this thesis is to investigate SR of model compounds of bio-oil to elucidate the reactions that occur and find suitable catalysts. Tests of different catalysts under various conditions will be conducted in order elucidate reaction mechanism and kinetics and identify new promising catalyst. Different feeds and contaminants will also be tested to investigate the versatility and stability of the catalysts.

Experimental

The experiments for this PhD.-study will at first by conducted in an atmospheric pressure gas flow reactor, where the SR of ethanol will be investigated. The first experiments will be a screening of different catalysts, selected based on the literature. The catalyst will mainly be based on Ni and the variations will be in support and promoters.

A high temperature and high pressure setup, shown in Figure 3, is in the design phase and will be finished in the end of the summer. This setup allows for the use of other model compounds and high pressure operations and will be used to investigate SR of larger model compounds like furan, furfural, or phenol.

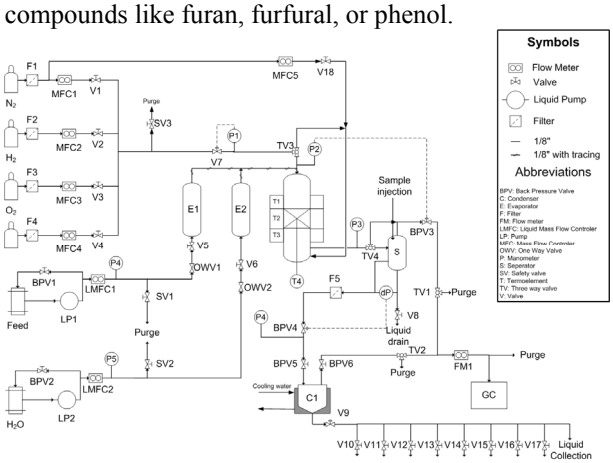

Figure 3: Flow sheet for the high pressure and high temperature setup.

Conclusion

The SR of bio-oil can produce H_2 or synthesis gas in a renewable and sustainable manner. This process is still in an early stage of development and many issues needs clarification and resolution before it can be used industrially. One of the major concerns with this process is the coke formation, which cause deactivation.

References

1. G.W. Huber, S. Iborra, A. Corma, Chem. Rev. 106 (2006) 4044-4098
2. R.H. Venderbosch, W. Prins, Biofuel Bioprod. Bioref. 4 (2010) 178-208
3. K. Raffeldt, E. Henrich, A. Koegel, R. Stahl, J. Steinhardt, F. Weirich, Appl. Biochem. Biotechnol. 129 (2006) 153-164
4. E.C. Vagia, A.A. Lemonidou, Int. J. Hydrogen Energ. 2008 (33) 2489-2500
5. B. Zhang, X. Tang, Y. Li, W. Cai, Y. Xu, W. Shen, Catal. Commun. 7 (2006) 367-372
6. A.C. Basagiannis, X.E. Verykios, Appl. Catal. A Gen. 308 (2006) 182-193
7. X. Hu, G. Lu, Green Chem. 11 (2008) 724-732

Anna Katrine Vangsgaard
Phone: +45 4525 2910
E-mail: akv@kt.dtu.dk
Discipline: Systems Engineering

Supervisors: Gürkan Sin
Krist V. Gernaey
Barth F. Smets, DTU Environment

PhD Study
Started: September 2010
To be completed: August 2013

Validation of Structured Model for Autotrophic Nitrogen Removal in High Strength Wastewater

Abstract
Autotrophic nitrogen removal is a relatively new and emerging technology for treatment of sidestream wastewaters with high nitrogen concentrations, such as sludge digestion liquor or landfill leachate. It is therefore of great importance that a better understanding of the process dynamics is established. In this project, a model to be used for design of experiments will be developed according to a structured modeling framework. The aim is to obtain a validated model, which can be used for process prediction, design, and optimization.

Introduction
For wastewaters containing high concentrations of nitrogen and low organic carbon to nitrogen ratios, such as sludge digestion liquor, landfill leachate, or special industrial wastewaters, the conventional nitrification-denitrification treatment method is either not very efficient or a rather costly method. Complete autotrophic nitrogen removal (CANR) combining partial nitritation (eq. 1) with anaerobic ammonium oxidation (anammox) (eq. 2) can overcome these difficulties, because the requirement for aeration is lowered and the need for addition of organic carbon is eliminated [1]. Meanwhile, the sludge production and the need for treatment of excess sludge are significantly lowered.

$$NH_4^+ + 1.5O_2 \rightarrow NO_2^- + H_2O + 2\ H^+ \quad (1)$$

$$NH_4^+ + 1.32\ NO_2^- + 0.066\ HCO_3^- + 0.13\ H^+ \rightarrow 0.26\ NO_3^- + 1.02\ N_2 + 0.066\ CH_2O_{0.5}N_{0.15} + 2.03\ H_2O \quad (2)$$

The processes are performed by ammonium oxidizing bacteria (AOB) and anaerobic ammonium oxidizing bacteria (AnAOB), which require aerobic and anoxic conditions, respectively. An environment where both groups of bacteria can co-exist can be created in biofilms or granular biomass, where both anoxic and aerobic conditions are created. In the outer layers AOB will grow, consume oxygen, and prevent oxygen from penetrating further than a certain depth. In the anoxic inner biofilm layers the AnAOB will exist. In a mixed culture system, such as a wastewater treatment plant (WWTP) a range of other microorganisms, affecting the nitrogen conversion, will also be present. Especially nitrite oxidizing bacteria (NOB) will have a great effect because they compete with both AOB and AnAOB for substrate. A model capturing the microbial interactions and community dynamics could therefore be an important tool for better understanding, optimizing, and controlling CANR.

Models have previously been utilized in wastewater treatment technology for multiple purposes; designing and supporting process operation and control in WWTPs, evaluating specific process performances, and for designing experiments when testing new technologies. A structured framework for construction of models for emerging processes is therefore of great importance in order to ensure fast and efficient model construction.

Specific Objectives
The aim of this project is to develop a detailed metabolic model for the selected bacterial groups, performing autotrophic nitrogen conversion, and integrate that into complete ecosystem models, which describe how the major microbial groups interact. This insight will be used to design experiments in which relevant operational conditions will be identified and tested. The relevant conditions are those under which the nitrogen removal process is optimized through the development of selection pressure, resulting in a targeted removal or enhancement of specific microbial groups.

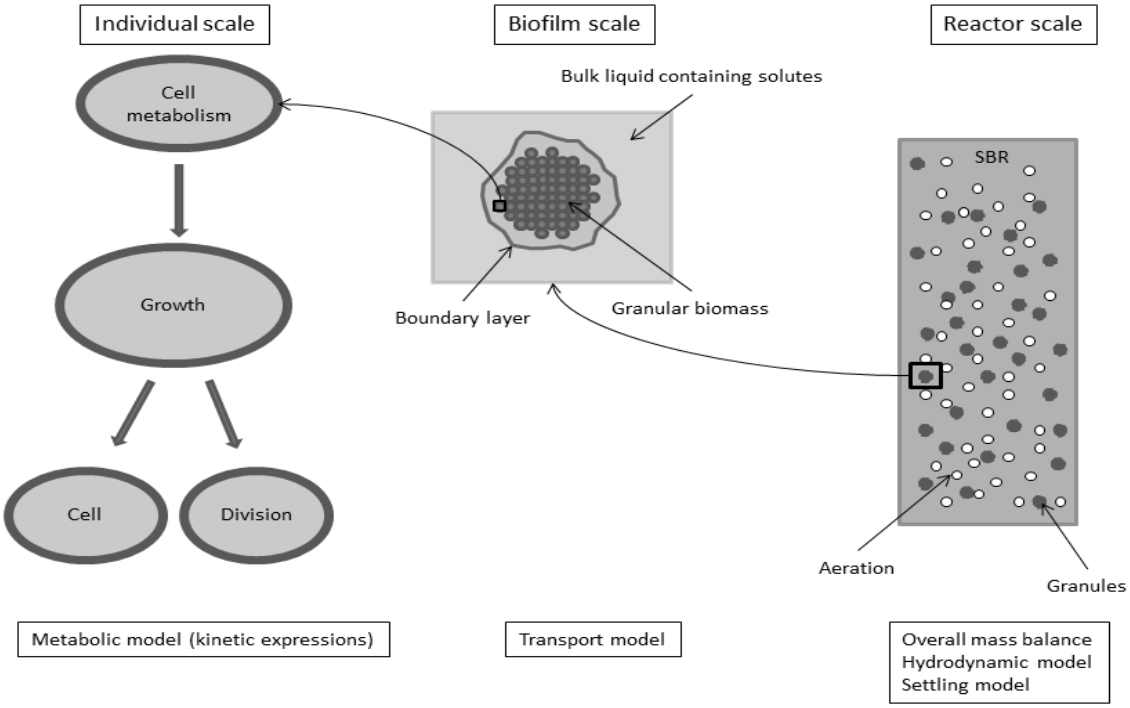

Figure 1: Conceptual model of a sequencing batch reactor (SBR) with granular biomass. Three spatial scales are considered; the individual or cellular, biofilm, and reactor scale (adapted from [2]).

The final objective is to obtain a validated model which can be used for process prediction and thus determination of optimal operational conditions.

Methods

In biofilm systems, processes happen at very different spatial and temporal scales. Modeling biofilm systems typically involves three spatial scales [2]; individual cells, biofilm, and reactor scale, as shown in Figure 1. On the individual or cellular scale the growth and metabolism of the microorganisms are captured. On the biofilm scale the spatial location of the bacteria is described, and also the transport of soluble and particulate compounds is included here. At the reactor scale the overall mass balances are considered along with the hydrodynamic conditions and biomass settling properties in the reactor.

A structured framework for construction of multi-scale models makes the development of a model tailored to the specific purpose − in terms of level of detail (spatial scale), system information, and assumptions − fast and efficient. Such a model will be used to design lab experiments with granular biomass in SBRs conducting CANR. From these experiments, detailed information about the actual effect of operational conditions on the process dynamics will be obtained. The model will subsequently be calibrated and validated against data obtained from experiments in the lab scale reactors.

The multi-scale model constructed according to the principles embedded in the model framework will be implemented in the ICAS-MoT software. Multi-scale models have previously been successfully implemented in the MoT software [3]. The model consists of a system of partial differential equations, and MoT is a very good tool for solving such systems. The model solution will be exported to Matlab-Simulink, in which different operational conditions can easily be tested.

Conclusions

The project will optimize the removal of nitrogen from wastewater sidestreams with high nitrogen concentrations through development of a novel and feasible technology, supported by modeling and experimentation.

Acknowledgements

The author would like to thank the Technical University of Denmark for financial support and the Danish Agency for Science, Technology and Innovation for funding though the Research Centre for Design of Microbial Communities in Membrane Bioreactors (EcoDesign MBR).

References

1. M. Strous et al. Water Res. 31 (1997), 1955-1962.
2. J.B. Xavier et al. Environ. Microbiol. 7 (2005), 1085-1103.
3. M. Heitzig et al. A computer-aided framework for regression and multi-scale modeling needs in innovative product-process engineering. Conference paper. 20th European Symposium on Computer Aided Process Engineering – ESCAPE20 (2010).

Bodil Voss
Phone: +45 4525 2826
E-mail: bov@kt.dtu.dk
Discipline: Process Technology and Unit Operations

Supervisors: John M. Woodley
Niels Christian Schjødt, Haldor Topsøe
Jan-Dierk Grunwaldt, KIT

Industrial PhD Study
Started: May 2008
To be completed: May 2011

Sustainability and Catalytic Conversion of Bio-Ethanol on a Cu Catalyst

Abstract
Bio-ethanol has attracted great interest mainly due to its use as a gasoline supplement. However, the production cost optimization done in the field of ethanol fermentation for fuel production may furthermore lever the sustainable use of biomass as a feedstock for chemical production. The conversion of ethanol on a selective catalyst to value added products could form a prosperous process route as an alternative to existing fossil based technology, or bridging via ethanol reforming may be done. Catalyst development through characterization and testing is the key to establish such new processes. The conversion of ethanol to acetic acid, $CH_3CH_2OH + H_2O \doteq CH_3COOH + 2\ H_2$, as an alternative to methanol carbonylation was specifically investigated in this project.

Introduction
In view of the on-going climate debate the research in resource utilization becomes ever more important. The sustainability issue pinpoints the utilization of biomass as a sustainable carbon resource which has recently been extensively discussed [1]. By choosing biomass as a feedstock to chemical processes it is possible to reduce the net emission of CO_2 to the atmosphere. Biomass based processes require completely different process routes to be developed.

But biomass feedstock may also be used in combination with fossil feedstocks, or after a pre-conversion it may be used for the existing conversion technologies in order to reduce the CO_2 emission.

Here, steam reforming of ethanol is highlighted as an example of a bridging pre-conversion technology [2], constituting an alternative route to the production of synthesis gas (syngas) as make-up gas for the synthesis of chemicals which is presently produced by means of steam reforming of e.g. desulfurized natural gas and naphtha feedstocks both originating from fossil sources. Figure 1 shows how the steam reforming of ethanol eases the shift from a fossil feed based platform to a renewable platform for the production of chemicals as an alternative to establishing an entirely new technology.

Amongst other Cu based catalysts have been found useful for numerous applications in biomass conversion. Typically the Cu catalysts are reduced prior to their use as catalyst, or the catalysts are subjected to reducing conditions in the reaction medium. Examples of such Cu catalyzed reactions are the conversion of biomass platform molecules, such as ethanol, the reduction of NO and the common water gas-shift reaction (CO reforming) [2-4].

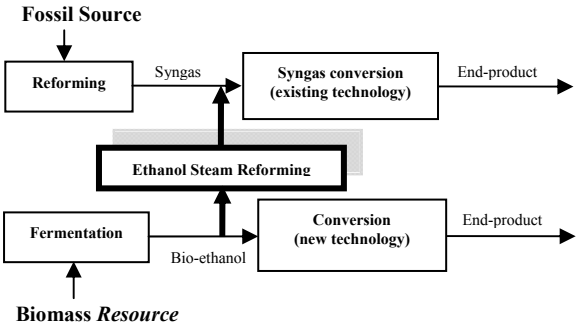

Figure 1: Bio-ethanol may be steam reformed into synthesis gas (syngas) bridging renewable biomass as a feedstock to existing syngas conversion technology.

Specific Objectives
The aim of this project is to find a catalyst capable of converting a biomass-based feed stream such as bio-ethanol to a value added product over a catalyst. Requirements must furthermore be set as to selectivity to obtain a viable process alternative to the conventional. In the present study bio-ethanol conversion has been selected as the biomass based feedstock. A Cu based catalyst ($CuAl_2O_4$) has been characterized and investigated with respect to its catalytic performance in the synthesis of acetic acid.

The economic and the environmental sustainability of the proposed process were analyzed through economic studies.

Evaluation by means of a green metric, the C-factor [1], expressing the amount of CO_2 emitted per kg of product throughout its production route.

The experimental work done for developing a catalyst for the process has been carried out in a single-pellet-string reactor. A diagram of the experimental set-up is shown in Figure 2.

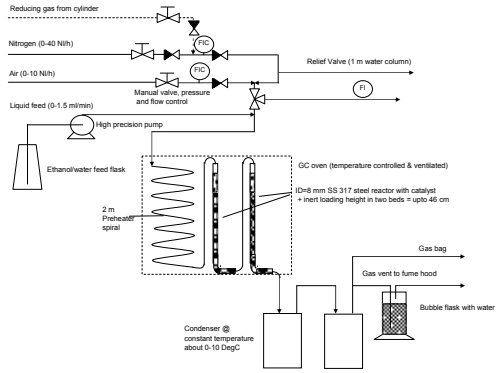

Figure 2: The experimental set-up.

The catalyst bed is contained in an ID=8 mm SS 316L temperature controlled steel reactor in a ventilated oven and with a thermocouple installed for the measurement of bed temperature. The individual catalyst pellets are separated by inert beads. The bio-ethanol is pumped and evaporated in a coil in the oven and nitrogen is added to the feed stream in order to improve the fluid dynamic properties. After conversion, the product is collected in a condenser being cooled to about -5°C. The liquid and the gaseous products are individually analyzed by GC and the results are recorded. Characterizations of the catalysts have been made according to well-known techniques such as HBET, XRD, HGA, TPR and EXAFS.

Results and Discussion

The conversion of ethanol to acetic acid represents an alternative route to the conventional carbonylation of methanol. While the ethanol prices increased 2008-2010, to >900USD/MT, on the back of legislation the unit prices of bulk chemicals have dived as a response to the lower demand situation during the recent financial crisis. The Q4 2010 acetic acid spot prices moved up a little, to about 500USD/MT, but the market is soft.

The C-factor calculated for the ethanol to acetic acid route is in the range ÷0.6-0.1kg CO_2/kg acetic acid depending on the origin of the biomass fermented, whereas the conventional acetic acid technology burdens the environment with 0.3-0.9 kg CO_2/kg acetic acid produced.

The combination of characterization techniques elucidated the nature and behavior of the catalyst. Via calcination and reduction a surface of highly dispersed ~50Å Cu crystals emerges on the catalyst support. The reduction temperature is decisive for the resulting Cu surface area. Figure 3 shows the CO adsorption, representing the arbitrary Cu surface area, versus the reduction temperature in a chemisorption experiment. Clearly, the Cu surface area goes through a maximum. These findings are consistent with experimental activity measurements.

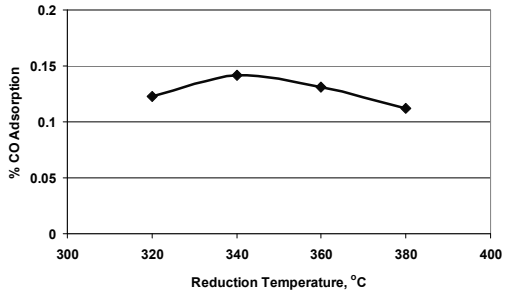

Figure 3: The CO adsorption vs. the reduction temperature for a $CuAl_2O_4$ catalyst.

Observed catalyst deactivation may be explained by the wax formation seen in the inner part of the spent catalyst pellet on recorded TEM images.

Conclusions

The synthesis of acetic acid from bio-ethanol may become viable on the long term if adequate stability and activity of the involved catalyst is obtained. The C-factor found for the process is as low as ÷0.6 kg CO_2/kg acetic acid, i.e. carbon capturing. The conversion of bio-ethanol to acetic acid over a $CuAl_2O_4$ catalyst was investigated and important information on its stability and activity as a function of reduction temperature (optimum at 340°C) has been found via fundamental characterization methods.

Acknowledgements

This work is part of an industrial PhD study in collaboration with Haldor Topsøe A/S. The work is financed by Haldor Topsøe A/S and the Danish Council for Technology and Innovation. Beam time at MAXLAB (Lund) amd HASYLAB (Hamburg) are gratefully acknowledged.

References

1. B. Voss, S.I. Andersen, E. Taarning, C.H. Christensen, ChemSusChem. 2 (2009) 1152–1162.
2. M.N. Barroso, M.F. Gomez, L.A. Arrúa, M.C. Abello, Catal. Lett. 109 (2006) 13-19.
3. T.-W. Kim, M.-W. Song, H.-L. Koh, K.L. Kim, Appl. Catal. A 210 (2001) 35-44.
4. H. Yahiro, K. Nakaya, T. Yamamoto, K. Saiki, H. Yamaura, Catal. Comm. 7 (2006) 228-231.

List of Publications

1. B. Voss, J.D. Grunwaldt, J. Woodley, S.I. Andersen, Dansk KemiingeniørKonference 2010, Institut for Kemiteknik, Kgs. Lyngby, 2010, p.112-113
2. E. Taarning, C.M. Osmundsen, X. Yang, B.Voss, S.I. Andersen, C.H. Christensen, Energ. Environ. Sci. 2011 (2010), DOI: 10.1039/C004518G, Advance Article.

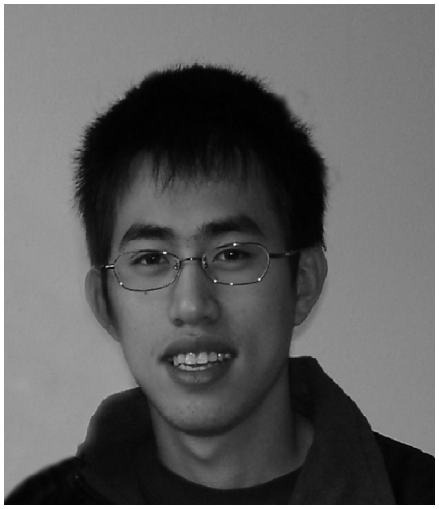

Hao Wu
Phone: +45 4525 2927
E-mail: haw@kt.dtu.dk
Discipline: Reaction and Transport Engineering

Supervisors: Peter Glarborg
Kim Dam-Johansen
Flemming J. Frandsen

PhD Study
Started: November 2007
To be completed: May 2011

Co-combustion of Fossil Fuels and Waste

Abstract
Co-combustion of fossil fuels and waste offers an opportunity to reduce the CO_2 emission of traditional fossil fuel-fired power plant and at the same time increase the efficiency of utilizing waste energy. In the present work, co-combustion of solid recovered fuel (SRF) and coal was studied through laboratory-scale experiments in an entrained flow reactor, full-scale measurements in a pulverized coal-fired power plant, and thermodynamic modeling. The work was concerned with carbon burnout, gaseous emissions, ash chemistry, fine particle formation, ash deposition, and trace element partitioning in co-combustion of coal and SRF. The influence of SRF properties and fraction on co-combustion was investigated systematically, and the underlying mechanisms were identified via experiments and modeling.

Introduction
With the target of reducing the CO_2 emission, replacing part of the fossil fuel consumption by biomass or waste which is usually considered to be CO_2 neutral fuel has become an attractive option. Among the various technologies that utilize biomass or waste as an energy source, one of the most simple and promising methods is co-firing biomass or waste together with coal in existing coal-fired power stations.

Solid recovered fuel (SRF) derived from nonhazardous waste streams such as industrial waste and bulky waste is considered as an advantageous secondary fuel to be co-fired in pulverized coal-fired power stations. Although waste is normally regarded as a highly heterogeneous fuel with low thermal value, the production technologies of SRF can significantly improve the combustion properties of waste. After processing steps such as screening, mechanical sorting and size reduction, the lower heating value of SRF could become approximately 20 MJ/kg (dry basis), which is comparable to biomass such as straw and wood. Besides, SRF can be produced as a fluffy form, which allows it to be injected into a pulverized coal-fired boiler directly. Moreover, since SRF normally contains 40-80 wt% of biogenic components, co-combustion of coal and SRF will reduce the net CO_2 emission from a pulverized coal-fired power plant. This technique also has the potential to increase the efficiency of utilizing waste fuels, as the electrical efficiency of a pulverized coal-fired plant is usually 10-20% higher than that of a waste incineration plant. Furthermore, if the SRF contains lower nitrogen and sulphur contents than the coal, the emission of NO_x and SO_x from the coal-fired boiler may be decreased by co-firing coal with the SRF.

Besides the advantages aforementioned, several problems may be associated with co-combustion of coal and SRF. In comparison with coal, SRF is often characterized of higher chlorine content (0.3-0.8 wt%, dry basis). When coal is co-fired with SRF, the high chlorine content in SRF may aggravate the ash deposition and corrosion problems in boiler, since the organically associated alkalis in coal and SRF may react with gaseous chlorine and generate alkali chlorides which could increase the deposit formation and corrosion of superheaters. Besides, the trace element content in SRF may be considerably higher than that of coal. This is likely due to that SRF may contain waste fractions with high trace element concentration, such as CCA impregnated wood and plastics with stabilizers. Therefore, co-combustion of coal and SRF may significantly increase the trace element emission from a pulverized coal-fired power plant, and generate fine particles which are potentially more harmful than those from coal combustion. In addition, since SRF is a more heterogeneous fuel than coal, the variation of SRF properties may be significant in practical operations and may greatly influence co-combustion of coal and SRF. Furthermore, co-firing of coal and SRF may affect the fly ash quality, fine particle formation, and the

performance of the SCR system in a pulverized coal-fired power plant. As a consequence, a systematic evaluation of co-combustion of coal and SRF is necessary in order apply this technique in a full-scale plant.

Specific objective

The objective of the project is to identify suitable waste types, fraction and particle size that can be co-combusted in pulverized coal-fired power stations, and to optimize the co-combustion of coal and waste through laboratory, pilot- and full-scale experiments, supplemented by modeling work. The impact of co-firing on deposit formation, fly ash quality, and trace element partitioning will be the main focus. The mechanisms governing the transformation and the partition of major- and trace elements during co-combustion of coal and waste will be studied through experiments and modeling

Co-firing of coal and SRF in EFR

In order to study co-combustion of coal and SRF at conditions similar to a pulverized coal-fired power plant, experiments were carried out in an entrained flow reactor (EFR) which was designed to simulate the conditions of a suspension-fired boiler. During the experiments, a bituminous coal was co-fired with different share of SRF (7.9 wt%, 14.8 wt% and 25 wt%). Besides, in order to evaluate the influence of SRF properties on co-combustion, additives such as NaCl, PVC, $(NH_4)_2SO_4$ (AmSulf), and kaolinite were blended with the mixture of coal and SRF, and combusted in the reactor. Based on the experimental results, the impact of co-firing on fuel burnout, NO and SO_2 emissions, fly ash properties, and deposit formation was investigated.

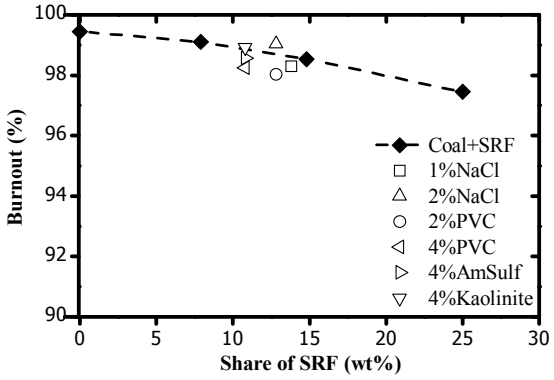

Figure 1: Carbon burnout in different experiments (open symbols denote the experiments with additives).

Figure 1 shows the carbon burnout obtained from different experiments. It can be seen that when coal is co-fired with SRF, the burnout is decreased with increasing share of SRF. This is primarily due to that the SRF particles are larger than the coal particles and can form agglomerate easily. The injection of different additives generally reduces the burnout. However, the addition of 2 wt% NaCl shows a slight enhancing effect, which is probably linked to the catalytic effect of NaCl on char reactivity.

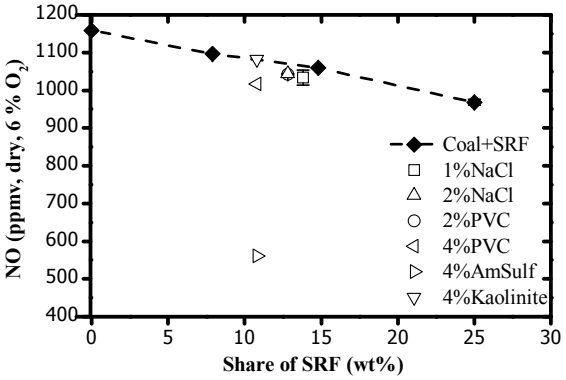

Figure 2: NO emission in different experiments.

The NO emission in different experiments is depicted in Figure 2. It can be seen that the NO concentration in flue gas is lowered with increasing share of SRF. This suggests both the relatively low nitrogen content and high volatile content in SRF are favorable conditions for reducing the NO emission. The additives generally have insignificant effect on NO emission, whereas the addition of 4 wt% ammonium sulphate greatly inhibits the NO formation, which is due to the release of NH_3 via the thermal decomposition of ammonium sulphate.

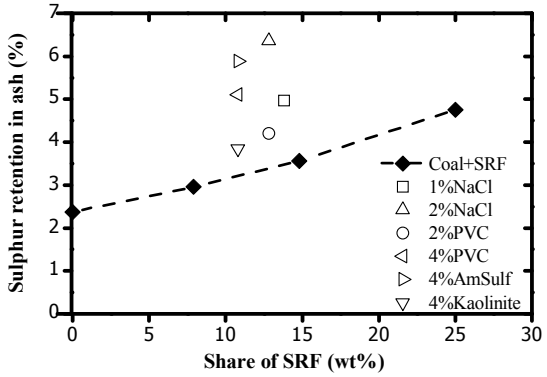

Figure 3: Sulphur retention in ash during different experiments.

Figure 3 illustrates the effect of co-combustion and additives on the sulphur retention in ash. It reveals that the sulphur retention in ash is increased with increasing share of SRF, which is likely related to the higher Ca content in the SRF as compared to coal. All of the additives appear to have a promoting effect on the sulphur retention, either because of chemical reactions or physical absorptions. The results imply that co-combustion of coal and SRF would reduce the SO_2 emission in flue gas, both due to the low sulphur content in SRF and the sulphur retention effect of the ash from SRF.

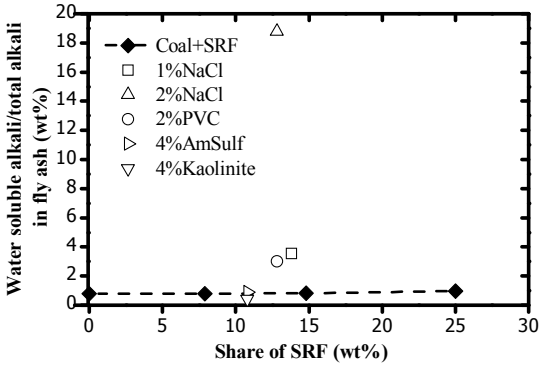

Figure 4: Percentage of water soluble alkali in the fly ash from different experiments.

The influence of co-combustion on the alkali species distribution is illustrated in Figure 4. It can be seen that when co-firing coal and SRF, the majority (~99 wt%) of the K and Na in fly ash is present as water insoluble form such as aluminosilicates or silicates. The addition of NaCl or PVC significantly enhanced the formation of water soluble alkalis. The results indicate that the fly ash from co-firing of coal and SRF would not introduce severe corrosion problems in the boiler, whereas the addition of NaCl or PVC may greatly increase the corrosion potential.

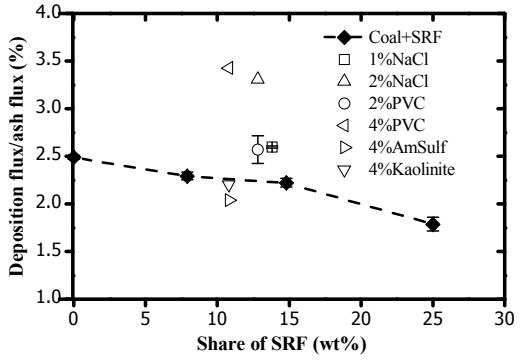

Figure 5: Deposition flux/ash flux (%) in different co-combustion experiments.

Figure 5 shows the deposition flux/ash flux obtained in different experiments. The parameter is used to estimate the deposition propensity of fly ash. When co-firing coal and SRF, the deposition propensity of fly ash is decreased with increasing share of SRF. However, with the injection of Cl-based additives, the ash deposition propensity is increased significantly, which is likely because of an increased formation of gaseous alkali chlorides. The results imply that co-combustion of coal and SRF may not influence the ash deposition behavior greatly, if the chlorine content in the SRF is well-controlled.

Trace elements in co-firing of coal and SRF

The partitioning of trace elements during co-combustion of coal and SRF was studied by analyzing the trace element content in different ash fractions collected in the entrained flow reactor. In addition, the volatility of trace element was investigated by introducing a relative enrichment (RE) factor, which compared the trace element content in filter ash with that of cyclone ash.

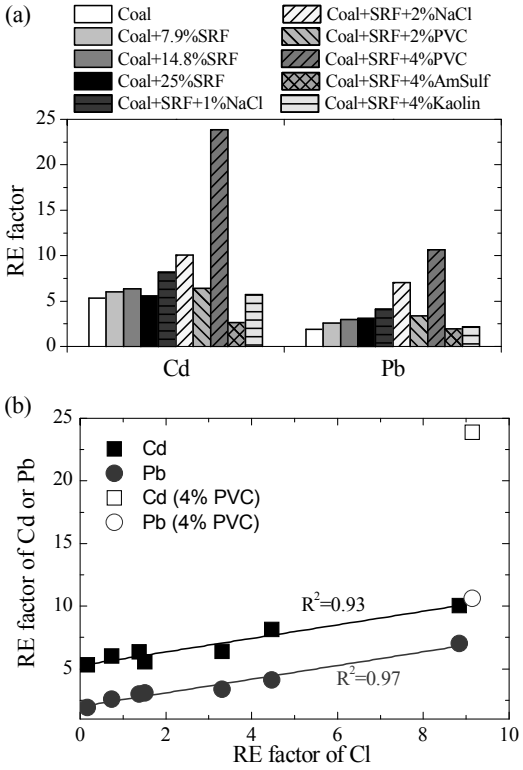

Figure 6: (a) The RE factor of Cd and Pb in different experiments; (b) Comparison of the RE factors of Cd and Pb versus the RE factor of Cl (the open symbols denote the results from 4 wt% PVC addition).

Typical results of the trace element volatility in co-combustion of coal and SRF are given in Figure 6a. It is seen that the volatility of Cd and Pb is slightly increased when coal is co-fired with SRF. In addition, the volatility of Cd and Pb is further increased with the addition of Cl-based additives, particularly for the experiment with 4 wt% PVC addition. Thermodynamic calculations reveal that the addition of Cl-based additives would promote the formation of Cd and Pb chlorides, which leads to an increased vaporization of Cd and Pb in combustion. The effect is supported by the positive correlation between the RE factor of Cd/Pb and the RE factor of Cl, as demonstrated in Figure 6b. The addition of ammonium sulphate and kaolinite both show a reducing effect on the volatility of Cd and Pb, which is probably due to the chemical reactions between the two additives and the trace elements.

The results from the trace element study indicate that trace element emission may become a significant concern in co-combustion of coal and SRF, not only due to the high trace element content in SRF, but also related to the increased volatility in co-combustion. In order to minimize the trace element emission, utilizing SRF with relatively low Cl content and coal with relatively high sulphur and aluminosilicates content is desirable.

Fine particle formation in co-firing of coal and SRF

Full-scale tests on co-combustion of coal and SRF were carried out by DONG Energy A/S at the 400MW Esbjerg Power Station in December 2008 and January 2009. During the campaign, the SRF type, share and injection position were varied, and a comprehensive measuring program was carried out. As a part of the measuring program, a low-pressure cascade impactor was applied to sample the fine particles in flue gas, and the composition and morphology of the collected particles were analyzed by SEM-EDS.

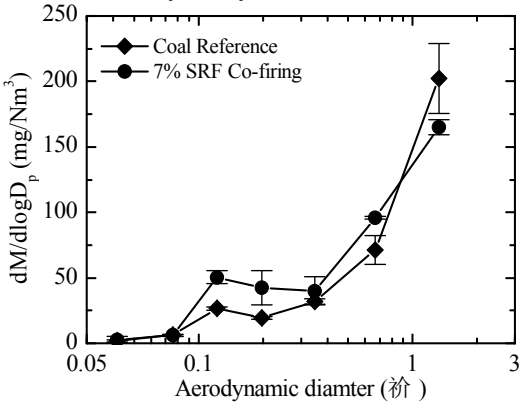

Figure 7: Mass-based particle size distribution of the fine particles from coal combustion and co-firing of coal and 7 th% SRF.

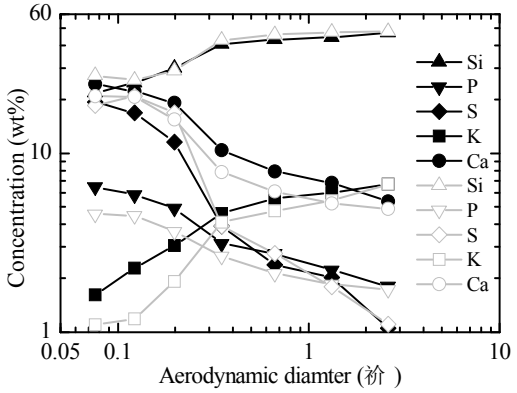

Figure 8: Comparison of the particle elemental composition from co-combustion of coal with 7th% SRF (solid symbol) and coal combustion (open symbol).

Figure 7 presents the typical mass-based particle size distribution obtained from the full-scale measurement. It can be seen that when coal is co-fired with 7 th% SRF, the formation of submicron particles with diameter below 0.2 μm is promoted. These particles are mainly formed through the nucleation and condensation of the vaporized inorganic species. The increased formation of submicron particles may result in a greater dust emission from the coal-fired power plant, as these particles are more difficult to be removed by the flue gas cleaning system, compared to the supermicron particles.

The influence of co-combustion on the composition of fine particles is shown in Figure 8. It is seen that the fine particles from co-firing is of higher Ca, P and K content compared to that of coal combustion. Since both Ca and P have been proven to be important for the formation of fine particles with aerodynamic diameter around 0.2 μm, it suggests that the increased formation of fine particles in co-combustion of coal and SRF is probably caused by the relatively high Ca and P in SRF.

Conclusion

The results from this work indicate that co-combustion of coal and SRF could reduce the NO and SO_2 emissions from a pulverized coal-fired power plant, not only due to the relatively low nitrogen and sulphur content in SRF, but also because of the synergy effect between the fuels. The carbon burnout in the plant may be adversely affected by co-combustion, but it would to a large extent depend on the physical properties of SRF and its injection method. By using the coal and SRF used in the present work, co-combustion of coal and up to 25 wt% SRF would not aggregate the ash deposition and corrosion problems in the boiler. However, the problems may appear if a SRF with significant high chlorine content is used. This suggests the importance of controlling SRF properties during co-combustion.

Both the trace element emission and fine particle formation would be increased when coal is co-fired with SRF. The increased fine particle formation is probably linked to the relatively high Ca content in the SRF. For the trace elements, the significant higher trace element content in SRF compared to coal is the primary reason for the increased emission. In addition, the volatility of some trace elements is higher in co-firing as compared to coal combustion, particularly when the SRF is of high Cl content. The volatility of trace elements is generally reduced when sulphur and aluminosilicates additives were used in co-combustion. Therefore, in order to minimize the trace element emission, it would be an advantage to use SRF with relatively low Cl content and coal with high sulphur and aluminosilicates content.

Acknowledgements

The work is part of the CHEC (Combustion and Harmful Emission Control) Research Center. The present work is sponsored by The Technical University of Denmark (DTU), ENERGINET.DK, and BiofuelsGS-2 (Nordic Graduate School in Biofuel Science and Technolog-2). DONG Energy Power A/S is gratefully acknowledged for the assistance in performing the experiments and chemical analysis.

List of Publications

1. H. Wu, A.J. Pedersen, P. Glarborg, F.J. Frandsen, K. Dam-Johansen, B. Sander, Proc. Combust. Inst. 33 (2011) 2845-2852
2. H. Wu, P. Glarborg, F.J. Frandsen, K. Dam-Johansen, P.A. Jensen, B. Sander, Fuel (2011), submitted.
3. H. Wu, P. Glarborg, F.J. Frandsen, K. Dam-Johansen, P.A. Jensen, B. Sander, Fuel Procss. Technol. (2011), submitted.

Qiongxiao Wu
Phone: +45 4525 2837
E-mail: qw@kt.dtu.dk
Discipline: Reaction and Transport Engineering

Supervisors: Anker Degn Jensen
Jan-Dierk Grunwaldt, KIT
Burcin Temel, Haldor Topsøe A/S

PhD Study
Started: January 2010
To be completed: December 2012

Supported Cu-Ni Catalysts for CO Hydrogenation

Abstract
This work provides a systematic study of higher alcohols synthesis from syngas over Cu-Ni based catalysts, which are supported on conventional supports like Al_2O_3 and ZrO_2. Different metal ratios and operating conditions such as temperatures and pressures were tested. Catalysts were characterized by X-ray diffraction (XRD), temperature programmed reduction (TPR), in-situ transmission electron microscopy (TEM), and X-ray adsorption spectroscopy (XAS).

Introduction
Currently, the world is experiencing rising oil prices and dwindling of resources, ethanol and other alternative energy sources have moved into the spotlight as clean, sustainable and transportable fuel alternatives or fuel additives [1,2]. Alcohols as fuels, especially higher alcohols (C_{2+} alcohols) such as ethanol and butanol are being considered as potential alternative synthetic fuels, as they can be catalytically produced by syngas that is derived from biomass [3,4]. Several different types of catalysts have been developed for higher alcohols synthesis (HAS), but until now they all suffer from low activity and selectivity for higher alcohols, with main by-products either methanol or hydrocarbons [4]. Therefore R&D work for improvement of selectivity and yield of higher alcohols is necessary.

Catalysts containing copper and group VIIIB metals such as Co [5] and Ni [6] have shown promising results for higher alcohols synthesis regarding selectivity and activity. However, the limited information on Cu/Ni catalysts in the literature directed us towards a more systematic study of Cu/Ni catalyst system for higher alcohols synthesis from syngas. Different Cu/Ni molar ratios, supports and operating conditions such as pressure and temperature have been investigated. The work includes different characterization techniques such as XRD, TEM, TPR and spectroscopic investigations.

Specific Objectives
This work aims at providing a systematic study of Cu/Ni catalysts for higher alcohols synthesis from biomass-derived syngas.

Experimental
Cu/Group VIII metal based catalysts were prepared by impregnation method. Cu and Ni nitrate precursors as well as ZrO_2 and Al_2O_3 were used for preparation of catalysts. All catalyst precursors were dried at 120 °C overnight and calcined in air at 400 °C for 4 h. Performance of catalysts for HAS from syngas has been evaluated in a fixed-bed continuous-flow reactor with GC-FID/TCD detectors. Prior to the reaction, samples of the oxide precursors were reduced in situ by a 10% H_2 in N_2 gaseous mixture for 12 h in the range of 200-300 °C with a heating rate of 1 °C/min. Typical operating conditions are: P = 60-100 bar; T = 250-300 °C; GHSV = 2000-4000 h^{-1}; Feed: H_2/CO=1 (v/v). TPR was carried out on a Micromeritics Autochem-II instrument for identifying the reduction temperatures of catalysts. Particle sizes and phase composition were investigated using XRD. The specific surface areas of both fresh and used catalysts were determined by N_2 adsorption on an Autosorb-iQ_2 (Quantachrome Instruments) at 77 K. In-situ TEM was used to study the catalyst morphology in H_2 gas flow from 25 to 600 °C. X-ray adsorption spectroscopy studies were performed at ANKA-XAS (KIT, Karlsruhe).

Results and Discussion
Figure 1 shows that CO conversion and CO_2-free selectivity of alcohols, hydrocarbons (HC) and dimethyl ether (DME) on Cu/Ni/Al_2O_3 catalyst. The CO conversion and productivity of DME, HC and alcohols were enhanced by increasing temperature. The selectivity to DME was decreased by increasing temperature, while the selectivity to hydrocarbons was

increased. The selectivity of alcohols (methanol) was kept constant with increasing temperature. The CO conversion and selectivity to hydrocarbons at a constant temperature such as at 250 and 300 **°C** were increased with time on stream, while the selectivity to DME was slightly decreased. This may be due to the instability of Cu/Ni alloys, so that more nickel moved to the surface of catalyst upon time on stream.

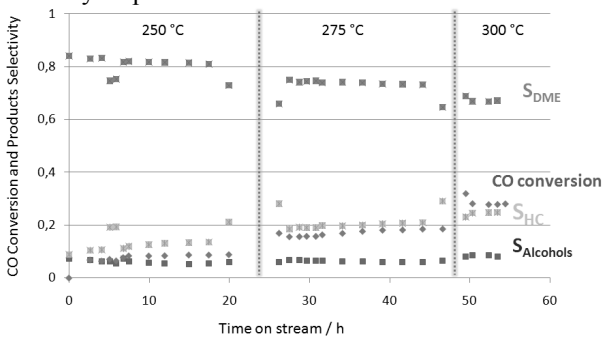

Figure 1: CO conversion, CO_2 free selectivity of alcohols, hydrocarbons (HC) and dimethyl ether (DME) at 100 bar, 250-300 °C, GHSV 2000 h^{-1} and $V(H_2)/V(CO)=1$ over Cu_1Ni_1 / Al_2O_3.

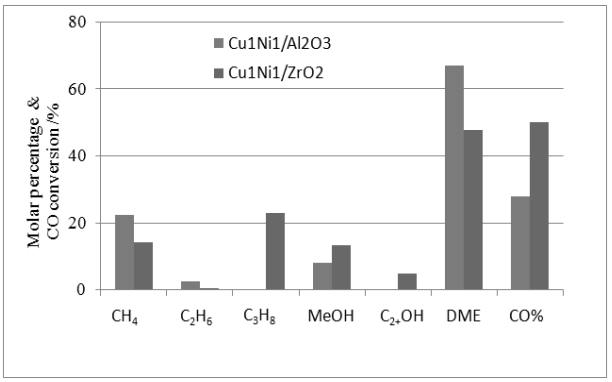

Figure 2: The steady state distribution of the products obtained from the Cu_1Ni_1/Al_2O_3 and Cu_1Ni_1/ZrO_2 catalysts operated at 300 °C, 100 bar, $V(H_2)/V(CO)=1$, 53 h on stream.

Figure 2 shows that Cu/Ni catalysts supported on Al_2O_3 and ZrO_2 exhibited different catalytic behaviors for CO hydrogenation. The ZrO_2 supported catalysts showed much higher activity than the Al_2O_3 supported one. Both catalysts mainly produced DME, which is due to the Lewis acidic sites of γ-Al_2O_3 and ZrO_2 that can dehydrate methanol to DME. Alumina supported catalysts showed no higher alcohols selectivity, while ZrO_2 supported one showed 5% higher alcohols selectivity. ZrO_2 supported catalysts exhibited much higher selectivity to hydrocarbons. The current work is focused on changing the catalytic selectivity of the catalysts towards ethanol and higher alcohols by modifying the basicity of the catalysts with alkali and other promoters.

TPR and XAS studies showed a variation in the reduction behavior depending on Ni/Cu loading and the support.

Future work

Different support materials such as active carbon, carbon nanotubes, TiO_2, and MnO will be studied for the optimal Cu/Ni ratio. For better understanding of Cu/Ni catalyst system, some further characterization is necessary. Firstly, the active surface area or active sites are important for the activity of the catalyst. Thus, BET surface area and chemisorption with a probe molecule will be evaluated for samples after preparation, calcination, reduction, and testing. Secondly, XRD measurements will be used to study metallic phases and particle sizes. Thirdly, X-ray photoelectron spectroscopy (XPS) studies will be used to understand surface elemental composition and oxidation states of metals. Fourthly, TEM can be used for surface morphology and in-situ studies. Finally, extended X-ray absorption fine structure (EXAFS) will be used for studies of the local structure in-situ, and in-situ X-ray absorption near edge structure (XANES) for studying the reduction behavior of Cu and Ni.

Acknowledgements

Thank you for Jakob Munkholt Christensen's help with experimental work and discussion. This specific work was financially supported by CASE, Catalysis for Sustainable Energy. The work was carried out in collaboration between the Combustion and Harmful Emission Control Research Centre (CHEC), Haldor Topsøe, and Center for Electron Nanoscopy (CEN) of DTU. Thank you for all the supports. Finally, ANKA (Karlsruhe) is gratefully acknowledged for beam time and the EU and DANSCAT for experiment financial support for the synchrotron.

References

1. V. Subramani, S.K. Gangwal, Energ. Fuel. 22 (2) (2008) 814-839.
2. J.J. Spivey, A. Egbebi, Chem. Soc. Rev. 36 (9) (2007) 1514-1528.
3. J.M. Christensen, P.M. Mortensen, R. Trane, P.A. Jensen, A.D. Jensen, Appl. Catal. A Gen. 366 (2009) 29-43.
4. P. Courty, D. Durand, E. Freund, A. Sugier, J. Mol. Catal. 17(1982) 241-254.
5. M.A. Fraga, E. Jordão, React. Kinet. Catal. Lett. 64 (1998) 331-336.
6. P. Serp, E. Castillejos, ChemCatChem. 2 (2010) 41-47.

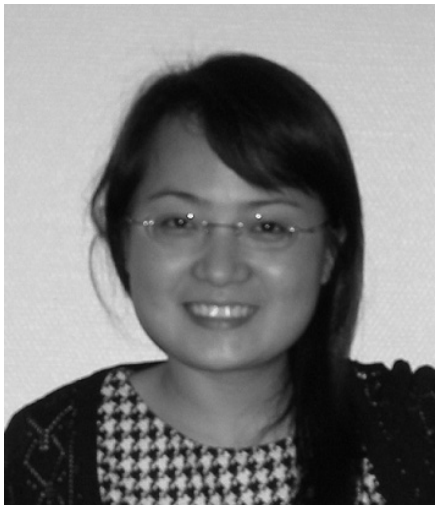

Yuan Xu
Phone: +45 4525 2960
E-mail: xuy@kt.dtu.dk
Discipline: Process Technology and Unit Operations
Enzyme Technology
Supervisors: John M. Woodley
Mathias Nordblad
Lars Georg Kiørboe

PhD Study
Started: March 2009
To be completed: February 2012

Process Technology for Lipase-catalyzed Reactions

Abstract
The enzymatic production of biodiesel, specifically using immobilized lipase as the transesterification catalyst, could avoid many disadvantages of the conventional base-catalyzed reactions. However, glycerol, the byproduct of the biodiesel production, imposes potential problems for the biocatalytic process because it is known to inhibit immobilized lipases most likely by clogging of the catalyst particles, limiting mass transfer of substrates as previously suggested [1]. Here we present a systematic study on this negative effect and also a developed dyeing method for *in-situ* indication of glycerol partitioning and accumulation during the ethanolysis reaction catalyzed by different immobilized lipases. The method was used to illustrate the interaction of glycerol with immobilized lipases and thus provided an aid for screening supports for lipase immobilization according to their affinity for glycerol.

Introduction
Biodiesel is one of the lower-value products from lipase-catalyzed reactions. However, lipases themselves are costly, especially when they are immobilized. An effective process should improve the catalytic activity and stability of the enzyme and thus offer the possibility for a cost-efficient application of lipase in biodiesel, which is produced via transesterifications of fats and oils (Figure 1).

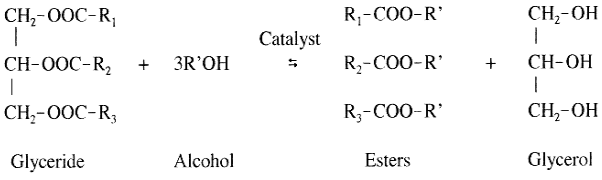

Figure 1: Transesterification of triglycerides with alcohol [2]

Compared to the conventional base-catalyzed biodiesel process, the enzymatic process requires less energy and is also highly selective producing less byproducts or waste. Using immobilized lipases also makes it easy to remove and reuse the catalysts [3]. The biodiesel production catalyzed by lipases is considered as a "green reaction". Involving ethanol turns the biodiesel even "greener", because ethanol can be obtained from agricultural products and hence is more environmentally friendly and renewable than methanol, which is commonly used in chemical biodiesel production. Additionally, the extra carbon brought by the ethanol molecule slightly increases the mass yield as well as the heat content and the cetane number [4].

Glycerol is the byproduct of biodiesel, taking up 10 wt% of the final product. It is well known that glycerol has a negative effect on lipase activity and stability. The inhibition could likely be caused by the glycerol being adsorbed onto the support of the immobilized lipases, thereby forming a layer surrounding the enzyme, which could reduce the diffusion of the hydrophobic substrate to the active site of the lipase [1]. This undesirable effect of glycerol will greatly shorten the life time of the expensive catalyst and consequently influence the economic viability of a process. The affinity of glycerol for immobilized lipases also hinders the separation of glycerol as a byproduct from the biodiesel product. Since the glycerol issue could increase the production cost and affect the process design, it needs to be taken into account when the immobilized lipases are applied for large scale biodiesel production.

Although glycerol is immiscible with oil and biodiesel and has a higher density than any other component in the liquid phase of the reaction system, it is difficult in a small laboratory-scale apparatus to observe the separate glycerol phase because the glycerol-rich phase is relatively small and colorless [5]. The dyeing method is introduced to indicate the glycerol partitioning.

Results and Discussion

1. Effect of glycerol on the activity of immobilized lipase

The effect of glycerol on the activity of immobilized lipase in the ethanolysis of rapeseed oil was studied by addition of external glycerol to the reaction mixture, with the results shown in Figure 2. In this case the catalyst (Lipozyme TL HC) lost most of its activity with glycerol addition increasing from 2 wt% to 10 wt% compared to the control reaction. Hence, the glycerol greatly inhibited the immobilized lipase. Even a little glycerol (2%) reduced the final conversion by 21% in the absence of agitation. It was observed that the immobilized catalyst was aggregated by the viscous glycerol and the liquid phase was opaque throughout the 24-hour reaction. The inactivation is commonly recognized as the glycerol clogs the pores of the support so that the substrate cannot access the lipase. This phenomenon is visualized by a dyeing method described in the next section.

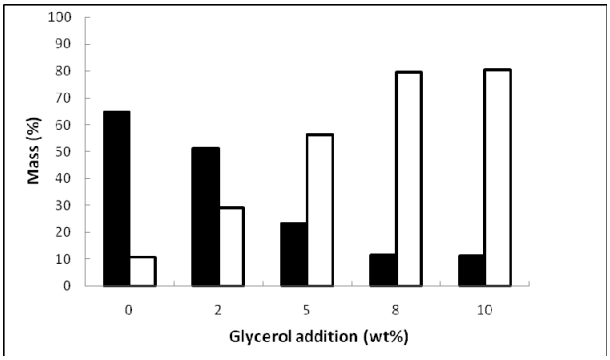

Figure 2: Effect of glycerol coexistence on the activity of Lipozyme TL HC in reactions without agitation. Amount of glycerol is calculated as percent to the oil (w/w). (■) FAEE content after 24h, (□) TAG content after 24h.

2. Affinity of glycerol byproduct for immobilized lipases in ethanolysis

The glycerol affinity for immobilized lipase was investigated in enzyme-catalyzed ethanolysis reactions. Reactions took place at 35 ^{o}C with 5% catalyst loading, 1.0 molar equivalent of anhydrous ethanol for 24 h without any agitation. The photos in Figure 3 show the partitioning of glycerol during the ethanolysis in this multiphasic system. As can be seen in Figure 3-1, glycerol formed a layer on the surface of Lipozyme TL IM particles. The liquid phase was clear with no free glycerol being released from the catalyst to the bulk solution. Since the conversion of 10 g rapeseed oil can only generate about 1 g glycerol at the most, the 0.5 g Lipozyme TL IM used in this experiment adsorbed all the glycerol produced.

The affinities of Novozym 435 (N435) and Lipozyme TL HC for glycerol are less than that of Lipozyme TL IM, as can be seen in Figures 3-2 and 3-3. Part of the produced glycerol stayed on the surfaces of both catalysts and some free glycerol droplets are noticeable in the oil phase of each reaction. It was also observed that the aggregation of Lipozyme TL HC was more severe than that of N435 (photo not shown), which can probably be explained by more glycerol being produced by the former catalyst.

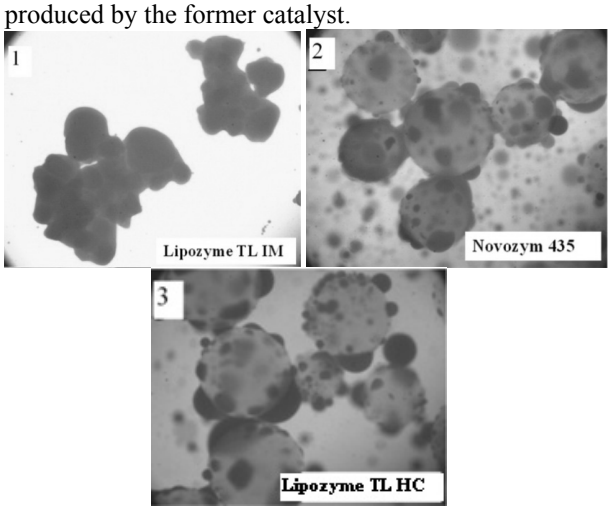

Figure 3: Glycerol partitioning in ethanolysis of rapeseed oil, catalyzed by different immobilized catalysts. Photo 1 is Lipozyme TL IM, photo 2 is N435 and photo 3 is Lipozyme TL HC.

Conclusions

Glycerol exhibits an inhibitory effect on the tested immobilized lipases by blocking the pores of the supports so that the diffusion of the substrate to the lipase becomes limiting to the reaction.

The dyeing method makes it possible to visualize the partitioning of glycerol and its accumulation on the catalysts *in situ* during ethanolysis catalyzed by the immobilized lipases. The entire amount of glycerol produced by 5 wt% Lipozyme TL IM remained on the catalyst, while some of the glycerol produced by the same amount of N435 and Lipozyme TL HC was released to the bulk solutions. This could help to explain the performance of immobilized lipases in this type of reaction.

Acknowledgements

The project is funded by Danish National Advanced Technology Foundation, Novozymes A/S, Emmelev A/S and DTU.

References

1. V. Dossat, D. Combes, A. Marty. Enzyme Microb. Technol. 25 (1999) 194-200.
2. F. Ma, M.A. Hanna, Bioresour. Technol. 70 (1999) 1-15.
3. P.M. Nielsen, J. Brask, L. Fjerbæk, Eur. J. Lipid Sci. Tech. 110(2008) 692.
4. C.C. Akoh, S. Chang, G. Lee, J. Shaw, J. Agr. Food Chem. 55 (2007) 8995-9005.
5. W. Zhou, D.G.B. Boocock, J. Am. Oil. Chem. Soc. 83 (2006) 1041-1045.

Hao Yuan
Phone: +45 4525 2864
E-mail: hy@kt.dtu.dk
Discipline: Reaction and Transport Engineering

Supervisors: Alexander A. Shapiro
Erling H. Stenby

PhD Study
Started: Oct.2009
To be completed: Oct 2012

Modeling Reservoir Formation Damage due to Water Injection for Oil Recovery

Abstract
The elliptic equation for non-Fickian transport of suspension in porous media is applied to simulate the reservoir formation damage due to water injection for oil recovery. The deposition release (erosion of reservoir formation) and the suspension deposition (pore plugging) are both taken into account. 1-D numerical simulations are carried out to reveal the erosion of reservoir formation due to water injection. 2-D numerical simulations are carried out to obtain the suspension and deposition profiles around the injection wells. These preliminary results indicate the non-Fickian behaviors of suspended reservoir fines and the corresponding formation damage due to erosion and relocation of reservoir fines.

Introduction
The migration of reservoir fines may give rise to severe permeability damage and oil productivity decline. This phenomenon has been widely observed in petroleum industry [1-7]. There is a considerable and ongoing effort aimed at understanding release of reservoir fines, particle transport, and caused formation damage.

The release of reservoir fines may be caused by change of water chemistry, hydraulic drag, and reaction between the acid in water and the reactive mineral of porous media [8-17].

A porous medium is "water-sensitive" if its permeability is dependent on the chemistry of the flowing fluid. The causes are believed to be in situ swelling of clay and migration of reservoir fines due to the change of water chemistry. It has been observed that injecting water of low salinity into a saturated sand core of high salinity leads to the reduction of permeability owing to the migration and the redeposition of clay [12, 18]. There exists a critical salt concentration (CSC) below which the clay starts to release. The clay detachment due to this mechanism is usually fast, while the available amount of clay for release at the specific salinity is limited. Multiple CSCs have been observed for different types of clay in the same porous medium [18].

Another mechanism for particle release is the hydraulic drag from the flowing fluid [8, 19-22]. When the viscous torque from the flowing fluid is larger than the adhesive torque along the pore walls, the attached particles start to depart. The process is strongly affected by pore structure, the local flow rate, the particle size and the adhesion mechanism. Induced detachment can be significant at high flow rate and recover the permeability to some extent [16, 23]. Numerous works focus on the corresponding permeability damage [7, 12, 14-17] whilst only a few studies on the transport of the reservoir fines [9, 18].

The transport of reservoir fines in porous media is usually described by a parabolic advection dispersion equation (ADE) with a sink term representing the deposition and a source term representing the release of particles [8, 22, 24-27]. For the cases without particle release, the classical methodology can merely catch stepwise symmetric breakthrough curves and predict exponential deposition profiles. On the other hand, a growing body of experiments shows that the deposition profiles may be hyperexponential or even nonmonotonic [28-36]. In artificially heterogeneous porous media and natural porous media the experiments may result in dispersed breakthrough curves of the non-Fickian type (asymmetric with early arrivals or large tails) [32, 37-41].

It is believed that the heterogeneity of the particle population is the main reason for hyperexponential deposition profiles in homogeneous porous media [40-45]. The heterogeneity of the particle population encompasses the physical heterogeneity (size and shape) and the physiochemical heterogeneity (surface charge and multiple energy minima). Even flow of a

monodisperse suspension (uniform shape and size) in a homogeneous porous medium under unfavorable attachment conditions is observed to result sometimes in a hyperexponential deposition profile, due to the heterogeneity of particle surface charge and second energy minimum [28, 29]. Mathematically, the heterogeneity of the particle population is described by the distribution of the filtration coefficients. The deposition patterns may be interpreted by application of various distribution types: the log-normal distribution, the power law distribution, the bimodal distribution and others [28, 30, 34, 44]

Besides the heterogeneity of the particle population, the media heterogeneity in connection with the non-Fickian transport may also lead to hyperexponential deposition [44, 46]. Recent works indicate that non-Fickian transport of a solute or a suspension may be modeled more accurately by approaches based on the continuous time random walk (CTRW) theory compared to the classical advection dispersion equation (ADE) [44, 46]. In the framework of the CTRW approach A. Shapiro and P. Bedrikovetsky proposed a macroscopic elliptic equation for non-Fickian transport in porous media [47, 48]. Recently, this approach has been extended in order to incorporate the distributed particles, as well as plugging of the porous medium [27, 44, 46].

Compared to the conventional ADE the elliptic equation has two additional terms reflecting the distributed residence time or flight time of the particles: the temporal dispersion term and the mixed dispersion term. In cases where the particles of n different types are filtered in a porous medium, n elliptic equations (plus deposition-plugging equations) are required for description of the filtration.

Neither the particle population heterogeneity in connection with the distributed deposition and release rates, nor the median heterogeneity in connection with the non-Fickian transport has been considered in the convection models for the release of reservoir fines. The elliptic methodology has been proved to excel the conventional ADE in both modeling the dispersed breakthrough curve and the hyperexponential deposition [44]. It has not been applied in the system with both particle release and particle deposition, either.

Elliptic Model

The elliptic equation for particle transport, release and deposition in porous media is adopted for modeling the formation damage around the injection wells in oil reservoirs. Details can be found in previous works [44, 45].

Implementation

The basic calculations are carried out in FORTRAN. Some of the results are illustrated in MATLAB and COMSOL Multiphysics. Finite element methods (2nd order) and finite difference methods (central difference scheme) are applied to transform the elliptic partial differential equation into an algebraic equation. Gaussian elimination with partial pivoting for sparse matrices is performed to solve the algebraic equations numerically.

Results

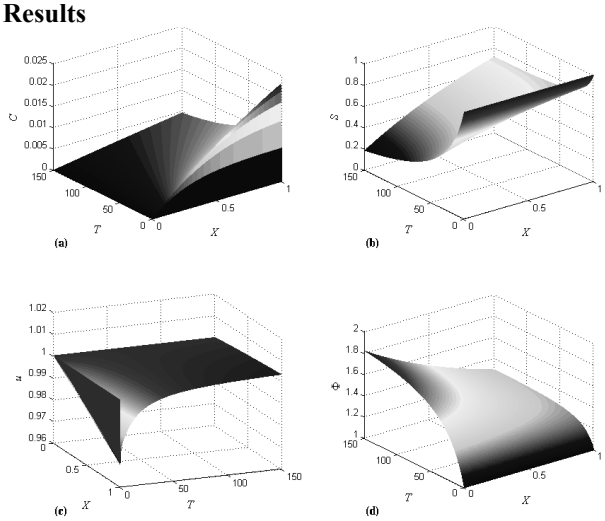

Figure 1: Modeling results for 1-D erosion of porous media due to water injection, (a) suspension concentration, (b) deposition, (c) velocity, (d) porosity

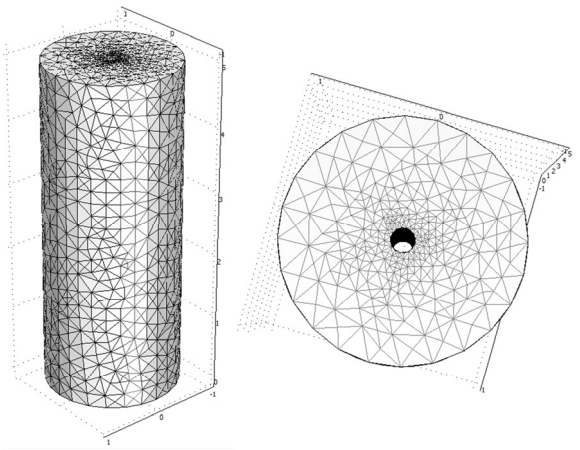

Figure 2: Illustration of the mesh for an injection well in oil reservoir

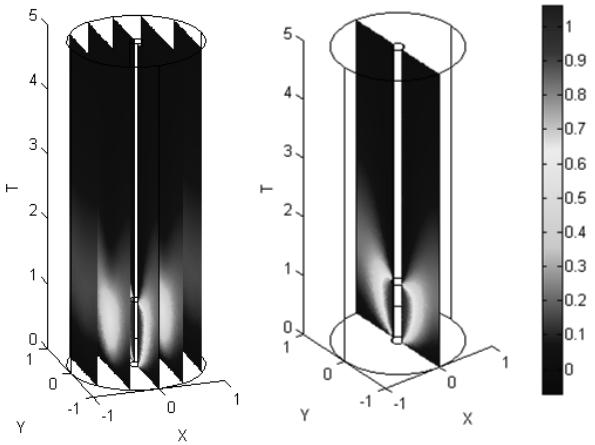

Figure 3: Suspension injection in oil reservoirs

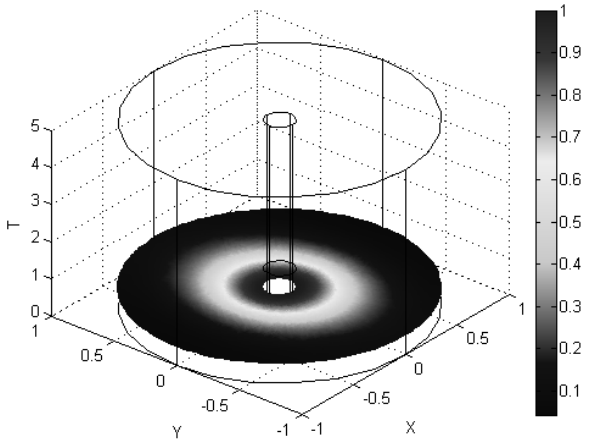

Figure 4: Horizontal cross-section around the injection well

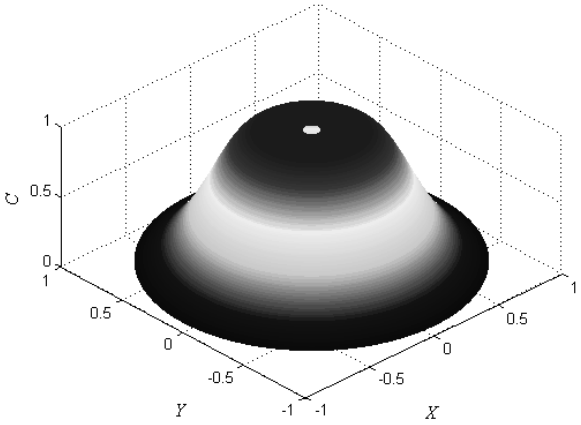

Figure 5: Suspended concentration profile at T=0.5

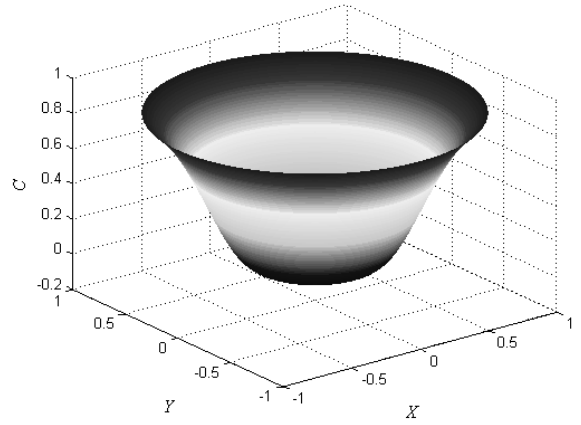

Figure 6: Suspended concentration profile at after injection T=2.5

Modeling results for 1-D erosion of reservoir formation are obtained, as seen in Fig. 1. The release of deposited particles are flushed out of the system, and recaptured by the porous media. Complete pore plugging mechanism is also taken into account. It can be seen that the erosion is stronger close to the inlet of injection since the porosity is lower.

2-D modeling for the formation damage around the injection wells is carried out, as seen in Fig. 2. The injection well lies in the center of a pie of reservoir. It is worth mentioning that the 3rd dimension is time. The injection follows a pulse injection procedure, i.e. suspension injection till T=1 and water injection till T=5. The concentration profiles are revealed in Fig. 3 to Fig. 6.

Acknowledgement
This work is funded by the Danish Council for Independent Research, Technology and Production Sciences (FTP), which is kindly acknowledged for financial support.

References

1. C.N. Fredd, H.S. Fogler, J. Coll. Interf. Sci. 204 (1998) 187-197.
2. F. Civan, Evaluation and Comparison of the Formation Damage Models, in: SPE Formation Damage Control Symposium, Society of Petroleum Engineers. Inc., Lafayette, Louisiana, 1992.
3. P. Bedrikovetsky, D. Marchesin, F. Shecaira, A.L. Souza, P.V. Milanez, E. Rezende, J. Petrol. Sci. Eng. 32 (2001) 167-177.
4. P. Bedrikovetsky, R.M.P. Silva, J.S. Daher, J.A.T. Gomes, V.C. Amorim, J. Petrol. Sci. Eng. 68 (2009) 60-70.
5. P. Bedrikovetsky, F. Siqueira, C. Furtado, A. Souza, Transport Porous Med. (2010) 1-31.
6. P.G. Bedrikovetsky, E.J. Mackay, R.M.P. Silva, F.M.R. Patricio, F.F. Rosio, J. Petrol. Sci. Eng. 68 (2009) 19-28.
7. F. Civan, Reservoir Formation Damage, in, Gulf Professional Publishing, U.S.A., 2000.
8. J. Bergendahl, D. Grasso, Chem. Eng. Sci. 55 (2000) 1523-1532.
9. T. Blume, N. Weisbrod, J.S. Selker, Geoderma 124 (2005) 121-132.
10. R.G. Guedes, F. Al-Abduwani, P. Bedrikovetsky, P. Currie, Injectivity Decline Under Multiple Particle Capture Mechanisms in: International Symposium and Exhibition on Formation Damage Control, SPE, Lafayette, Louisiana U.S.A., 2006.
11. T. Huang, L. Ostensen, A. D. Hill, Carbonate Matrix Acidizing with Acetic Acid, in: SPE International Symposium on Formation Damage Control, SPE, Lafayette, Louisiana, 2000.
12. A. Lever, R.A. Dawe, Mar. Petrol. Geol. 4 (1987) 112-118.
13. K.K. Mohan, R.N. Vaidya, M.G. Reed, H.S. Fogler, Colloid. Surf. A 73 (1993) 237-254.
14. R.N. Valdya, H.S. Fogler, SPE Production Engineering 7 (1992) 325-330.
15. J.P. Veerapen, B. Nicot, G.A. Chauveteau, SPE European Formation Damage Conference, Society of Petroleum Engineers Inc., The Hague, Netherlands, 2001.
16. A.K. Wojtanowicz, Z. Krilov, J.P. Langlinais, Study on the Effect of Pore Blocking Mechanisms on

Formation Damage in: SPE Production Operations Symposium, Oklahoma City, Oklahoma, 1987.
17. A.K. Wojtanowicz, Z. Krilov, J.P. Langlinais, J. Energ. Res. Tech. 110 (1988) 34-42.
18. M.-H. Fauré, M. Sardin, P. Vitorge, J. Contam. Hydrol. 26 (1997) 169-178.
19. W.P. Johnson, X. Li, S. Assemi, Adv. Water Res. 30 (2007) 1432-1454.
20. X. Li, P. Zhang, C.L. Lin, W.P. Johnson, Environ. Sci. & Technol. 39 (2005) 4012-4020.
21. J.E. Tobiason, B. Vigneswaran, Water Res. 28 (1994) 335-342.
22. R. Bai, C. Tien, J. Coll. Interf. Sci. 186 (1997) 307-317.
23. F. Civan, Reservoir Formation Damage - Fundamentals, Modeling, Assessment, and Mitigation, Gulf Professional Publishing, 2000.
24. M. Elimelech, J. Gregory, R. Williams, X. Jia, Particle Deposition & Aggregation: Measurement, Modelling and Simulation (Colloid & surface engineering), Butterworth-Heinemann, 1998.
25. J.P. Herzig, D.M. Leclerc, P.L. Goff, Ind. Eng. Chem. 62 (1970) 8-35.
26. S.A. Bradford, J. Simunek, M. Bettahar, M.T. Van Genuchten, S.R. Yates, Environ. Sci. Technol. 37 (2003) 2242-2250.
27. A.A. Shapiro, P. Bedrikovetsky, A. Santos, O. Medvedev, Transport Porous Med. 67 (2007) 135-164.
28. N. Tufenkji, M. Elimelech, Langmuir, 21 (2005) 841-852.
29. N. Tufenkji, M. Elimelech, Langmuir, 20 (2004) 10818-10828.
30. N. Tufenkji, J.A. Redman, M. Elimelech, Environ. Sci. Technol. 37 (2003) 616-623.
31. J.A. Redman, S.L. Walker, M. Elimelech, Environ. Sci. Technol. 38 (2004) 1777-1785.
32. S.A. Bradford, M. Bettahar, J. Simunek, M.T.v. Genuchten, Vadose Zone J. 3(2004) 384-394.
33. S.A. Bradford, S. Torkzaban, S.L. Walker, Water Res. 41 (2007) 3012-3024.
34. S.A. Bradford, N. Toride, J. Environ. Qual. 36 (2007) 1346-1356.
35. X. Li, W.P. Johnson, Environ. Sci. Technol. 39 (2005) 1658-1665.
36. X. Li, C.L. Lin, J.D. Miller, W.P. Johnson, Environ. Sci. Technol. 40 (2006) 3769-3774.
37. J.M. Boggs, S.C. Young, W.R. Waldrop, L.W. Gelhar, E.E. Adams, K.R. Rehfeldt, Field study of macrodispersion in a heterogeneous aquifer. 1. Overview of tracer experiment in: AECL Report Series, 1990, pp. 34-56.
38. S.E. Silliman, E.S. Simpson, Water Resour. Res. 23 (1987) 1667-1673.
39. B. Berkowitz, H. Scher, Transport Porous Med. 42 (2001) 241-263.
40. A. Cortis, B. Berkowitz, Soil Sci. Soc. Am. J. 68 (2004) 1539-1548.
41. M. Levy, B. Berkowitz, J. Contam. Hydrol. 64 (2003) 203-226.
42. B. Berkowitz, A. Cortis, M. Dentz, H. Scher, Rev. Geophys. 44 (2006) RG2003.
43. M. Fourar, G. Radilla, Transport Porous Med. 80 (2009) 561-579.
44. H. Yuan, A.A. Shapiro, Chem. Eng. J. 162 (2010) 974-988.
45. H. Yuan, G. Sin, Chem. Eng. J. In Press, Corrected Proof (2011).
46. A.A. Shapiro, P.G. Bedrikovetsky, Physica A 389 (2010) 2473-2494.
47. A.A. Shapiro, Physica A 375 (2007) 81-96.
48. A.A. Shapiro, P.G. Bedrikovetsky, Physica A 387 (2008) 5963-5978.

List of Publications

1. C. Wang, H. Yuan, Y. Lv, J. Li, W. Qu, Journal of Daqing Petroleum Institute 32 (2008) 13-15.
2. Y. Gong, H. Yuan, Y. Feng, W. Liu, B. Huang, International Conference on Information and Management Sciences, California Polytechnic State University, Urumqi China, 2008, pp. 696-699.
3. H. Yuan, A.A. Shapiro, E. Stenby, Poster: A New Approach to Modeling Immiscible Two-phase Flow in Porous Media in: IVC-SEP Discussion Meeting, Holte, Denmark, 2009.
4. Z. He, H. Yuan, J.A. Glasscock, C. Chatzichristodoulou, J.W. Phair, A. Kaiser, S. Ramousse, Acta Materialia. 58 (2010) 3860-3866.
5. H. Yuan, A.A. Shapiro, Chem. Eng. J. 162 (2010) 974-988.
6. H. Yuan, A.A. Shapiro, E. Stenby, Poster: Transport of reservoir fines: a novel model for formation heterogeneity and particle heterogeneity in: CERE Discussion Meeting, LO-skolens konferencecenter, Gl. Hellebækvej 70, DK-3000 Helsingør Denmark, 2010.
7. H. Yuan, G. Sin, Chem. Eng. J. In Press, Corrected Proof (2011). DOI: 10.1016/j.cej.2011.01.051
8. H. Yuan, A.A. Shapiro, Chem. Eng. J. 166 (2011) 105-115.

Linfeng Yuan
Phone: +45 4525 2955
E-mail: lfy@kt.dtu.dk
Discipline: Process Technology and Unit Operations

Supervisors: Gunnar Jonsson
John M Woodley
Lars Korsholm, Novozymes A/S
Sune Jakobsen, Novozymes A/S

PhD Study
Started: March 2008
To be completed: March 2011

Membrane Assisted Enzyme Fractionation-using amino acids as a model

Abstract
An enzyme concentrate produced by fermentation will often contain two or more enzyme activities. For application it is often necessary therefore to separate the enzymes so as to remove any side activity. The aim of this project is to develop a suitable membrane fractionation process and to assess the economics of such a process for industrial scale production. Like enzymes, amino acids have an amphoteric character and therefore the separation of amino acids in solution is an interesting model for the separation of charged compounds with similar properties. In this work we report studies concerning the separation of L-leucine (Leu) from L-glutamic acid (Glu) by electro-membrane filtration (EMF) with an ultrafiltration (UF) membrane. The highest Leu fraction in the permeate and highest separation factor were 96.4% and 28.5 respectively.

Introduction
Large-scale economic purification of proteins is an increasingly important problem for the biotechnology industry. Separation of the desired protein from other proteins produced by the cell is usually attempted using a combination of different chromatography techniques. Adequate purity is often not achieved unless several purification steps are combined, thereby increasing cost and reducing product yield. Consequently there is a need for processes that purify protein mixtures using fewer steps and without the need for a costly affinity step.

Membrane processes are widely used in the biochemical industry for separation and concentration of protein. Traditionally fractionation of enzymes using membranes due to the variation in size of the proteins is rather limited, which is partly caused by concentration polarization and membrane fouling.

Motivation
Recent publications have shown that by careful control of the concentration polarization, and use of charged membranes, a dramatic effect can be seen on the separation efficiency of such membranes.

Enevoldsen *et. al*. has shown that by using an electrical field during crossflow ultrafiltration (EUF), a 3-7 times improvement in flux has been obtained. This indicates that using an overlaid electric field is an effective way to depolarize the membrane surface when operating with enzyme solutions [1,2]. It is possible that EUF can be used for the separation of two enzymes with opposite charge sign since enzymes can carry different charges by adjusting the pH of the solution. Another possibility is to separate the enzyme product from impurities in the solution by dragging the charged enzyme through the membrane. This could also improve the purity of the enzyme product.

In addition, Jonsson et. al. has shown that using high frequency backflushing of the membrane surface is very effective at reducing the concentration polarization and can further be used to tune the membrane selectivity and therefore in principle be used to make a fractionation of enzymes [3, 4].

Combining these techniques with the use of a charged membrane is expected to give the desired separation properties which can further be scaled-up to a feasible ultrafiltration membrane system.

Specific Obejctives
The project aims at developing and economically assessing a pilot scale membrane fractionation process as this might be more economical for bulk enzyme purification compared to current technologies.

The feasible membrane fractionation process to be considered or investigated will potentially include:

- EUF
- Charged membranes
- Membrane systems using high frequency pulsation and / or vibration

Feed solution properties such as pH, ionic strength, additives can be chosen as appropriate.

If an efficient process is developed then pilot up-scaling of the membrane fractionation process will be considered.

Experimental

Materials

The main physical-chemical properties of each amino acid under study are presented in Table 1. L-Leucine (≥99.5%(NT)), L-Lysine(≥97%) and L-Glutamic acid(≥99.5%(NT)) were obtained from Sigma-Aldrich. The feed solution of the amino acids for the experiments was prepared by dissolving the amino acids in RO water. Before all the EMF experiments the pH was adjusted to a certain value by adding 0.1M NaOH or 0.1M HCl.

Table 1: Physical-chemical properties of amino acids used in the study [5]

Amino acid	MW	pI	pKa Values		
			α-COOH	α-$^{+}$NH3	Side chain
Leucine (Leu)	131.18	6.01	2.33	9.74	/
Lysine (Lys)	146.19	9.60	2.16	9.06	10.54
Glutamic acid (Glu)	147.13	3.15	2.10	9.47	4.07

EMF module and set-up

To prevent direct contact between the solutes (enzymes or amino acids in this case) and the electrodes, the EMF cell is configured according to Figure 1.

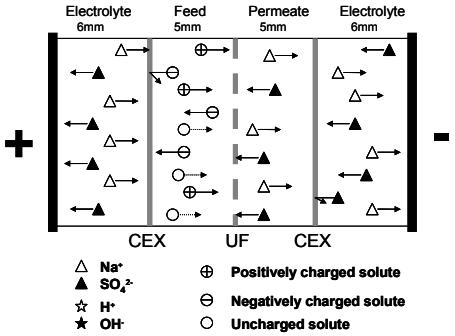

Figure 1: EMF module with an UF membrane (10KDa) placed between two cation exchange membranes [1].

A schematic representation of the EMF set-up used in this study is presented in Figure 2. The EMF cell consisted of four chambers. A UF membrane was placed between two cation exchange membranes (CEX), depending on the pore size of the UF membrane compared to the size of the solutes; it either retained solutes or let them pass through it. Flow spacers were used to enable adequate flow of the different streams. By using CEX membranes in front of both the anode and cathode it was possible to prevent an accumulation of salt ions in the feed stream.

The volume of the feed compartment (F), permeate compartment (P) and two electrolyte compartments (E) (including supply tank and piping volume) were 2.5L, 0.3L and 1L, respectively. The set-up was operated in a batch-wise manner. Both retentate and electrolyte were recirculated back to the feed and electrolyte tank, apart from that removed for sampling. The permeate stream was kept at a constant volume by an overflow pipe in the permeate tank, in which the excess amount of permeate was taken during a certain time for flux measurement and sampled for analysis. The recirculation flow rate of permeate and electrolyte solution were at a rate of 22L/h and 80L/h, respectively. In order to equalize the pH change in the anolyte and catholyte, the two streams were mixed. The two electrodes were made of platinized titanium. The electric field was generated by a power supply from xantrex (XHR 150-7). The TMP can be set by adjusting a valve placed on the retentate side. The electrolyte consisted of 0.1M Na_2SO_4. The initial permeate was 0.05M Na_2SO_4.The UF membrane was a 10kDa surface-modified PVDF ETNA 10PP membrane from Alfa Laval and the CEX membrane was a RELAX-CMH membrane from Mega. The membrane area was 10×10 cm^2. More details about the set-up have been described elsewhere [1,2].

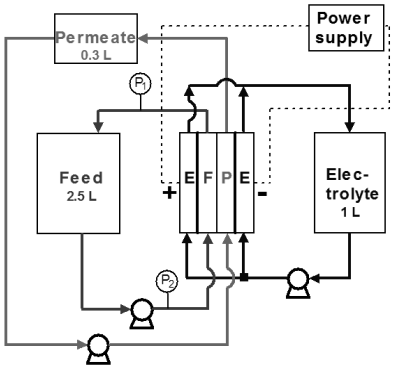

Figure 2: The experimental set-up, in which the EMF cell consists of 4 chambers separated by a 10KDa ultrafiltration (UF) membrane flanked by two cation exchange membrane (CEX)

Analytical methods

The concentration determination of Lys, Glu and Leu was done by HPLC (DIONEX, UltiMate 3000).
Column: Acclaim OA, 5 µm
Dimensions: 4 × 150 mm
Mobile Phase: 40 mM Na_2SO_4, pH 2.60 (adjusted with methanesulfonic acid)
Temperature: 30 °C; Flow Rate: 0.6 mL/min
Injection Volume: 20 µL; Detection: UV, 210 nm

Results and Discussion

Calculation of the net charge percentage of amino acid at a given pH

We can calculate the relative fraction of the various forms of amino acid as a function of pH by using the Henderson-Hasselbalch equation described below:

$$\text{pH}=\text{pKa}+\log\frac{[A-]}{[HA]}$$

$$\text{and pH}=\text{pKa}+\log\frac{[base]}{[acid]}$$

pKa is –log(Ka), where Ka is the acid dissociation constant.

The relative fraction for various forms of Glu, Leu and Lys as a function of pH is shown in Figure 3a, Figure 3b and Figure 3c respectively.

These plots help to identify what forms of amino acid exist at a given pH value and eventually predict the migration direction through the membranes. In addition, one can obtain the specific form by adjusting the pH using these plots.

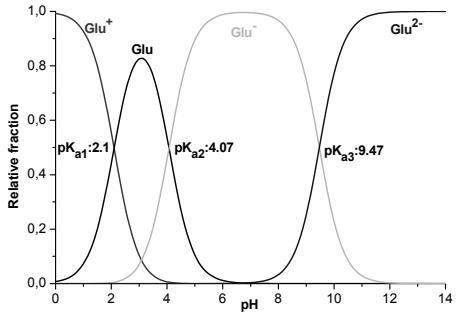

Figure 3a: Relative fraction for various forms of Glu as function of pH

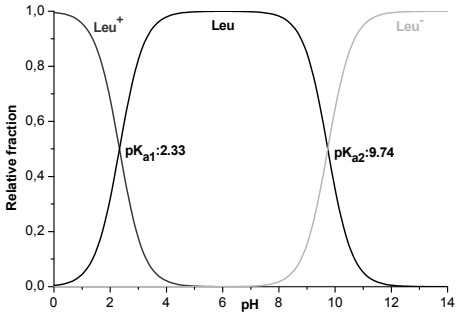

Figure 3b: Relative fraction for various forms of Leu as function of pH

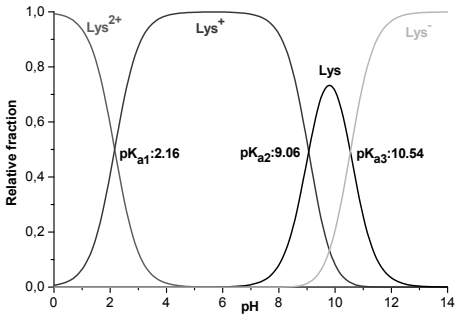

Figure 3c: Relative fraction for various forms of Lys as function of pH

Single amino acid

The transport of a single amino acid (Glu or Lys in this study) at different polarity was conducted in order to investigate the effect of electrophoresis due to the electric field.

Figure 4 shows the Glu concentration change in permeate both with and without applying electric field at 2 different polarities. The feed pH stayed at 6.5-8, hence Glu was negatively charged according to Figure 3a. The initial feed concentration of Glu was around 9mM. In the first 45min, there was no electric field applied, therefore the negatively charged Glu migrated into the permeate compartment because of convective transport due to trans membrane pressure (TMP). After 45min when applying the electric field in the direction of –UF+, it can be seen in Figure 4 the permeate concentration change of Glu was much enhanced due to the electrophoretic effect in addition to convective transport. While in the case of alternating the polarity into +UF-, the permeate concentration of Glu started slowing down after 45 min, again due to the electrophoretic effect which dragged the Glu away from UF membrane in direct competition with convective transport.

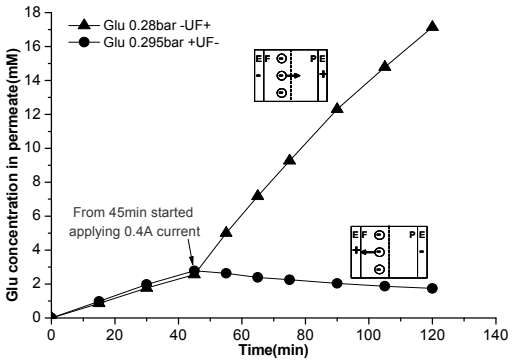

Figure 4: The change of Glu concentration in permeate with and without the application of electric field at different polarity when Glu was negatively charged in the feed.

Figure 5 shows the Lys concentration in permeate both with and without applying electric field at polarity +UF-. The feed pH stayed at 7-7.6, hence Lys was positively charged according to Figure 3c. The initial feed concentration of Lys was 8mM. As can be seen in Figure 5, the permeate concentration of Lys increased when the electric field was applied in comparison with the first 45min where there was only convective transport taking place. However, after 80min the permeate concentration of Lys started decreasing dramatically to 0 mM at 160min. By checking the Lys concentration in the electrolyte compartment, we found that Lys started being transported into the electrolyte compartment from 80min. The phenomena that the permeate concentration of Lys decreased from 80min could be explained a follows: first, positively charged Lys can pass through the cation exchange membrane;

secondly, after 80min the conductivity of permeate was quite low hence the Lys was transported instead of Na^+.

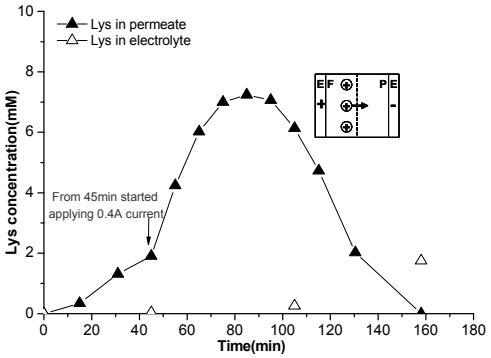

Figure 5: The change of Lys concentration in permeate without and with the application of electric field at polarity +UF- at constant TMP 0.28bar when Lys was positively charged in the feed

Binary mixture

Glu and Leu cannot be separated by a normal UF membrane based on the molecular size difference (data not show), therefore we have examined if separation could take place by applying an electric field.

The binary mixture of Glu and Leu with initial feed concentration around 10.5mM was used. The feed pH during the experiments stayed 6.3-6.7. According to Figure 3a and 3b, Leu is neutral and Glu is negatively charged.

As can be seen from Figure 6, separation of Leu and Glu proved possible by applying an electric field through the UF membrane. Leu was transported to the permeate only due to convective transport. However, the transport of charged Glu was controlled both by the electrophoretic effect and the convective effect, in which the electrophoretic effect dragged Glu away from UF membrane. Therefore the transport of Glu to permeate was a cause of the competition between convective transport and the electrophoretic transport due to TMP and current, respectively.

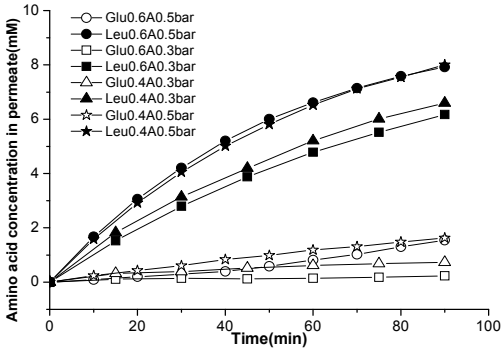

Figure 6: Leu and Glu concentration change in permeate at different current and TMP at polarity +UF-

In addition, as Table 2 shows, the selectivity and purity were very much dependent on the operational parameters (current and TMP). When having a combination of the highest current 0.6A and lowest TMP 0.3bar, the highest selectivity 28.5 and highest purity 96.4% can be obtained.

Table 2: Selectivity and purity comparison of each experiment at 90min

Current, TMP	Selectivity($\alpha_{Leu/Glu}$)	Purity (Leu% in permeate)
0.6A,0.3bar	28,5	96,4
0.6A,0.5bar	6,5	83,7
0.4A,0.3bar	9,8	90
0.4A,0.5bar	5,4	83,1

Conclusions

In this study, we have used amino acids as model to investigate the possibility of using EMF to separate charged components. The experimental study was carried out with solutions of increasing complexity, i.e. single amino acid solution and subsequently, binary mixtures. This work clearly indicates that the:

- electric field has a big effect on the transport of a charged amino acid
- EMF shows great potential to separate two amino acids with high separation factor and purity, which normal UF cannot achieve
- selectivity and purity can be tuned by using different combinations of current and TMP
- permeate conductivity is crucial to control the pH in the permeate (data not show)
- water splitting could take place when the permeate conductivity is low.

Acknwdegements

The Novozymes Bioprocess Academy is acknowledged for the financial support of this project.

References

1. A.D. Enevoldsen Electrically enhanced ultrafiltration of industrial enzyme solutions, Technical University of Denmark, Ph.D. thesis, 2007
2. A.D. Enevoldsen, E.B. Hansen, G. Jonsson, J. Membrane Sci. 299 (2007) 28-37
3. S.P. Beier, G. Jonsson, Sep. Purif. Technol. 53 (2007) 111–118.
4. G. Jonsson, Fractionation of macromolecules by dynamic ultrafiltration, 7th World Conference on Chemical Engineering in CD, Glasgow, 2005
5. http://www.unc.edu/~bzafer/aminoacids/

Nor Alafiza Yunus
Phone: +45 4525 2812
E-mail: noy@kt.dtu.dk
Discipline: Systems Engineering

Supervisors: Rafiqul Gani
John M. Woodley
Krist V. Gernaey

PhD Study
Started: July 2010
To be completed: July 2013

Tailor-made Design of Chemical Products: Bio-fuels and Other Blended Products

Abstract
In chemical blending, one tries to find the best candidate that satisfies the product targets. Traditionally, an experimental-based trial and error method is used in searching and identifying the best blending formulation. This project proposes a systematic computer-aided approach for reducing the searching space in order to find the optimal blend formulation. This technique first establishes the search space, and then narrows it down in subsequent steps until a small number of feasible and promising candidates remain. At this point, experimental work may be conducted to verify if any or all the candidates satisfy the desired product attributes.

Introduction
The application of computer-aided design techniques, in molecular and mixture design problems, has been practiced since the 1980s. Computer-Aided Molecular/mixture Design (CAMD) has been used extensively for the design of solvents, polymers, polymeric composites, paints, pesticides, drugs, and also blends [1, 2]. Computer-aided mixture design, with specified property constraints, was applied to solvent selection, by integrating an optimisation with computer-aided mixture design (CAMD) [3]. Later on, the methodology for computer-aided molecular and mixture design, with specified property constraints, was developed with the aim to predict the nature and properties of molecules, and/or mixtures [4]. In many cases, these methods proved the effectiveness of the computer-aided approach, in the design of molecules and mixtures. However, design of tailor-made chemical blends, dealing with special or new compounds, has not yet been reported.

A tailor-made chemical blend is defined as a mixture of chemicals with specific (derived/target) properties. The mixture is specifically designed for a purpose. Many liquid chemical blends (also known as liquid formulations) are used in daily life, such as detergents, paints, and drugs, were designed for a specific purpose. The traditional method of design, involves difficult and expensive trial-and-error processes. For instance, new drugs often cost millions of dollars and consume several years of development time. If the drug does not obtain a marketing license, then all that effort and money is wasted. Chemical selection is an important step in product design, which could enhance the likelihood of developing successful products. Therefore, the role of computer-aided methods and tools is crucial during the early stages of blend design to quickly identify the most suitable candidates and to avoid efforts for infeasible regions of the search space [5].

Specific objectives
The aims of this project are to:
i. Develop a systematic methodology for blend/mixture chemical product emphasis on bio-derivative chemicals (chemicals produce from biomass and/or renewable sources)
ii. Develop a model-based approach for chemical blend/mixture product design
iii. Validate the blend design algorithm through case studies which are fuel, lubricant and refrigerant blend

A Systematic Computer-Aided Approach
Moggridge and Cussler [7] propose a four steps design scheme for product design: define the consumer needs, generate the ideas to meet the needs, select the best ideas and finally, design the process to manufacture the selected ideas.

Based on this basic product design, a systematic computer-aided approach was constructed for designing of tailor-made chemical liquid-liquid blends. The main tasks in the proposed methodology comprising:

1. Define the target properties and target values of blend products.
2. Collect and/or develop the property models
3. Check the blends stability
4. Generate the potential blend candidates
5. List the potential candidates and order according to the prescribed performance index

Case study

The first case study involves the design of a gasoline blend with bio- derivative chemicals from biomass or other renewable sources. Adding bio-derived chemicals to conventional hydrocarbon fuels for use in a spark-ignition engine could enhance the engine efficiency as well as reducing fossil-fuel consumption and CO emissions. Therefore, the goal of this study is to design a green gasoline blend, which should contain at least one chemical from biomass or renewable resources. The preselected chemicals from biomass are bio-ethanol, bio-butanol, methyl tetrahydrofuran (MTHF) and 5-(hydroxymethyl) furfural (5-HMF).

As the results of Task 1 and Task 2, the target properties, target values and property models are summarized in Table 1.

Table 1: Target properties of fuel blend

Property	Model	Lower bound	Upper bound
Heating value, MJ/kg	$HHV_B = \sum_i x_i HHV_i$	35	-
Octane number	$ON_B = \sum_i v_i ON_i$	92	
Oxygen content, %	$Wo_B = \sum_i x_i Wo_i$	2	20
Density, kg/m^3	$\rho_B = \sum_i v_i \rho_i(T)$	710	770
Dynamic viscosity, g/m.s	$\mu_B = \exp \sum_i x_i \ln \mu_i$	5.7×10^{-4}	6.4×10^{-4}
Reid vapor pressure, kPa	$P_B = \sum x_i \gamma_i P_i^{sat}(T)$	-	62

In Task 3, the blend stability test is establishes the miscibility of liquid mixtures. A stable mixture has to satisfy the following equation:

$$\frac{d \ln \gamma_i}{dx_i} + \frac{1}{x_i} > 0 \qquad (1)$$

Blends of gasoline and MTHF or 5-HMF do not satisfy Eq. 1 because they formed a partially miscible mixture at certain compositions. Therefore, only mixture of gasoline, ethanol and butanol are considered in the next task.

Then, the potential blend candidates are generated in Task 4. In this step, the numbers of possible candidates are reduced gradually according to the target property constraints in Table 1. The results of Task 3 and 4 are clearly illustrated in Figure 1.

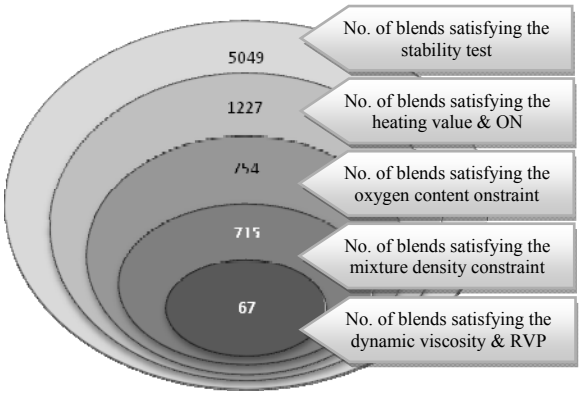

Figure 1: Number of feasible candidates generated through each property constraints

Among the 67 of feasible candidates, only the promising candidates are selected for final verification by ordered them according to the prescribed performance index. Product cost is an example of the performance index used for products comparison. The final selections will be validated by experimental works and/or rigorous models.

Conclusions

Tailor-made chemical blends can be designed using computer-aided approach. The developed methods and computer-aided tools are able to quickly generate and screen the alternative very efficiently and reliably. This technique requires the use of multiple mixture property models, which need carefully selected and when necessary, validated. Each case study needs different set of the product property constraints. Current and future work is developing a library of validated property models needed for different blend design problems (such as fuels, lubricants, process fluids).

References

1. R. Gani, E.A. Brignole, Fluid Phase Equilibr. 13 (1983) 331 – 340.
2. L.E.K. Achenie, A.T. Karunanithi, R. Gani, Ind. Eng. Chem. Res 44 (2005) 4785 – 4797.
3. J.A. Klein, D.T. Wu, R. Gani, European Symposium on Computer Aided Process Engineering-1 16 (1992) S229 – S236.
4. R. Gani, A. Fredenslund, Fluid Phase Equilibr. 82 (1993) 39 – 46.
5. E. Conte, R. Gani, K.M. Ng, AIChE. J. (2010) DOI: 10.1002/aic.12458
6. A. Fredenslund, P. Rasmussen, T. Magnussen, Ind. Eng. Chem. Process Des. Dev., 20 (2) (1981) 331 – 339.
7. G.D. Moggridge, E.L. Cussler, Trans IChemE, 78 (2000).

Adeel Zahid
Phone: +45 4525 2876
E-mail: adz@kt.dtu.dk
Discipline: Engineering Thermodynamics

Supervisors: Alexander Shapiro
Erling H Stenby
Wei Yan

PhD Study
Started: January 2009
To be completed: December 2011

Advanced Waterflooding in Low Permeable Carbonate Reservoirs

Abstract
Improved oil recovery from low permeable chalk reservoirs is regarded as a great challenge because of their complexity and heterogeneity. Over the last decade, a number of laboratory studies reported SO_4^{2-}, Ca^{2+} and Mg^{2+} as a potential determining ions for improving the oil recovery. We have conducted flooding experiments with outcrop chalk and reservoir chalk core plugs at different conditions to understand the mechanism of this waterflooding process. In addition to this, crude oil-brine phase behavior experiments were also carried out both at room and reservoir temperature to understand the crude oil-brine interaction.

Introduction
More than half of the world's remaining oil exists in carbonate (chalk and limestone) reservoirs [1]. They are characterized by rather low primary oil recovery; therefore, the improved oil recovery potential of these reservoirs is high. Many carbonate reservoirs are intermediate oil wet and very low permeable, so the improved oil recovery from such reservoirs is regarded as a great challenge.

Historically seawater salinity has not been considered as an important factor in determining the amount of oil recovered. Over the last decade, a number of studies have shown that waterflooding performance is dependent on the composition of injecting brine solution. Optimizing this composition has been developed into an emerging IOR technology for both sandstone and carbonate reservoirs. Extensive laboratory research has been carried out in order to understand improved oil recovery from chalk using surfactant solutions and later on using the modified sea water [2,3]. The researchers suggested wettability alteration towards more water wetting conditions to be the reason for improvement in oil recovery

In spite of a large body of experimental work, many questions still remain unclear. A conclusion about wettability alteration as a main mechanism for improving the oil recovery was achieved by exclusion of other reasons: miscibility, mobility control or significant reduction of the interfacial tension. This is by no means the proof. Without understanding why and how the recovery method works, its application on the industrial scale is doubtful, since it is not clear under what conditions it will lead to additional recovery.

Fundamental Concept of Wettability
In a rock/brine/oil system, wettability is a measure of the preference that the rock has either for oil or water [4].

Wettability of formation is of utmost importance which controls the location, flow and spatial distribution of fluid in the rock. Wettability also has been shown to affect the waterflood behavior, relative permeability, capillary pressure, irreducible water saturation and electrical properties in the open literature. Fundamental understanding of wettability and the reliable data of the wettability of rock is extremely important for the development of a production scheme. Below is the illustration of different wetting states of reservoir rocks.

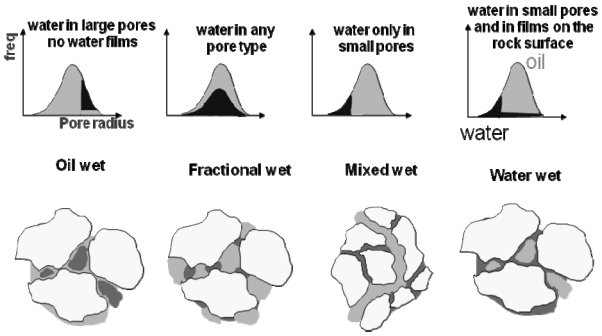

Figure 1: Illustration of different wetting conditions of rock

Specific Objectives

The Objectives of this PhD project are

- Understanding the effect of injecting brine composition, temperature and crude oil properties on waterflood oil recovery.
- What is the exact mechanism of increment in oil recovery with seawater ions (SO_4^{2-}, Ca^{2+} and Mg^{2+})?
- Exploring the possible benefit of these ions for limestone, dolomite and reservoir chalk cores.

Experiments

Experimental section can be divided into three parts. As a first part of the experimental work, we investigated the reasons of observed improvement in oil recovery with sulfate ions. Is it really wettability alteration or something else also? Most of the previous work has been made on the basis of spontaneous imbibition using core plugs aged in crude oil. Our study is based on flooding and utilizes completely water wet Stevens Klint cores without being aged in crude oil, just saturated with crude oil under vacuum. This would exclude alteration of wettability as a positive factor. Brine without sulfate (SW0S) is considered as the base injected fluid. Waterflooding experiments were carried out with SW0S, seawater (SW) and seawater with three times sulfate (SW3S). The effect of temperature, injection rate, crude oils and different sulfate concentration on the total oil recovery and the recovery rate was investigated.

What could be the reasons beside wettability alteration for the observed improvement in oil recovery? As a second part, we carried out phase behavior study of crude oil and brine with different sulfate concentration at room temperature in normal glasses and also at high temperature and pressure in a JEFRI PVT cell. Different measurements like crude oil viscosity, water content in the crude oil and pH of brine solutions were carried out before and after the phase behavior experiments.

As a third part of the experiments, flooding tests with North Sea chalk core plug were carried out. Two flooding schemes were used, flooding sequence 1 with core plug without being aged in crude oil and flooding sequence 2 is with core plug being aged for 3 days in the crude oil. Different injection brine solutions were used and effluent is collected using fractional collector at different time intervals and analyzed for potential determining ions (SO_4^{2-}, Ca^{2+} and Mg^{2+}) in most of the flooding tests.

Results and Discussion

Flooding tests were conducted at high temperature, 110 ºC. The three different core plugs from the same block were saturated with the Latin American crude oil. The first plug was flooded with the brine SW0S, the second with SW, and the last with SW3S, correspondingly. The total oil recovery and the recovery rates for the three tests are shown in Figure 2.

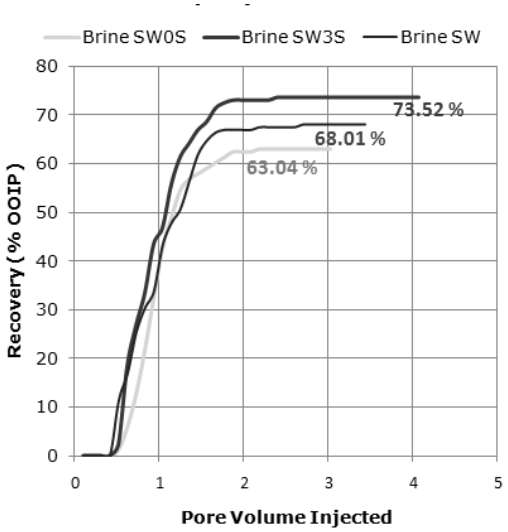

Figure 2: Oil Production curves for different brines for Stevens Klint chalk core plugs

There is a clear difference in the total oil recovery and also in the recovery rates for the different sulfate concentrations. For brine SW3S injection, the highest oil recovery is 73.52 %, while for SW and SW0S it is 68.01% and 63.04%, respectively. Thus, at such water wetting conditions there is a 10% higher oil recovery for the sulfate rich brine as compared to the brine solution with no sulfate. These results indicate presence of other physical mechanisms in increasing the oil recovery than just wettability alteration.

In first phase of second part of experiments, the crude oil was mixed with various synthetic brine solutions. 20 % (2ml) of crude oil and 80% (8ml) of brine was placed in a small glass for every test. The mixtures were thoroughly stirred together at 1000 rpm for 15 minutes. Afterwards the samples were left for some time, until the crude oil and the brine solution were separated. Viscosity of the crude oil was measured before and after mixing with brine solutions and given in Table 1 below

Table 1: Experimental data from crude oil/brine study at room temperature

	Latin American	
	Viscosity (cp)	**Density (g/cm^3)**
Only Oil	24.4	0.877
SW0S	24.4	0.897
SW	22.2	0.901
SW3S	24.2	0.894
0.1 M $MgCl_2$	24.7	0.890

We did not observe any significant change in density and viscosity of the crude oil as shown in the Table 2.

In second phase of second part of experiments, each test consists of a system containing 30 % crude oil (15 ml) and 70 % brine solution (35 ml). During the operation, the system is exposed to the following conditions; temperatures are chosen to be 37˚C and 110˚C and pressures are 15 Bars and 300 Bars. When the PVT cell is loaded with the desired system, the rocking mechanism is activated for 30 minutes and thereafter the system is left to equilibrate for 30 minutes to 2 hours depending on the conditions, which is decided from experiment to experiment. After finishing the experiment in the JEFRI cell, we removed the sample from the cell into a glass and waited overnight. Then the viscosity measurements of the crude oil phase of every test were carried out. Results are shown in Table 2

Table 2: Experimental data from crude oil/brine study in Jefri cell

Latin American Crude Oil	
Samples	**Viscosity (cp)**
Only Oil	24.4
SW0S	21.5
SW	20.2
SW1.5S	18.7
SW2S	18.1
SW2.5S	18
SW3S	16.4

We can see that the viscosity of the crude oil is decreased with the increase in sulfate concentration. This clear trend shows that sulfate ions help in some way to decrease the viscosity of the crude oil. This observed decrease in viscosity of crude oil with sulfate ions can explain the high oil recovery in Stevens Klint chalk core plugs at high temperature. However, how sulfate ions interact with the crude oil to decrease the viscosity is still not clear.

As a third part of the experiments, flooding tests with North Sea chalk core plug were carried out. For every injectant brine solution for all the experiments, first flooding was carried out at 40 °C and when there was no more oil coming out then temperature was increased to 70 °C and in the same way temperature was increased to 120 °C. Total oil recovery curves for different brine solutions for flooding sequence 1are shown in Figure 3.

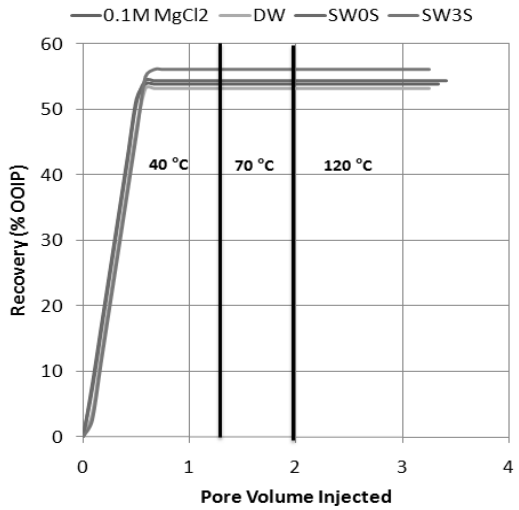

Figure 3: Oil Production curves for different brines for North Sea reservoir chalk core plug without aging

So even for reservoir chalk, brine containing SO_4^{2-} ions helped to improve oil recovery as compared to the brine without SO_4^{2-} but the magnitude is less as compared to we observed for Stevens Klint case in our previous study. But in this case, increasing temperature to 70 and 120 °C did not help to improve the oil recovery. Effluent ions analysis is plotted below in Figure 4 for flooding sequence 1.

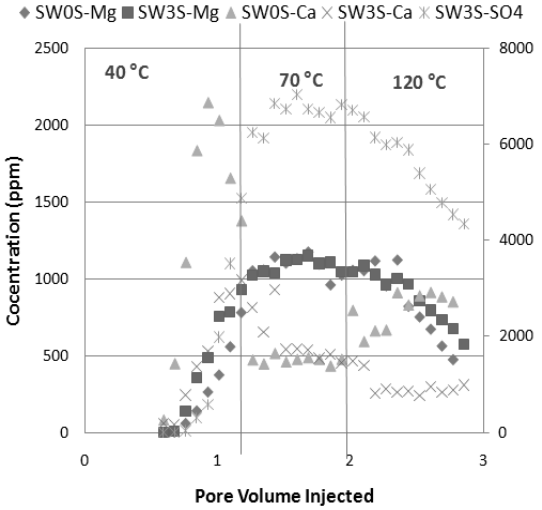

Figure 4: Effluent ion analysis for different brines for North Sea reservoir chalk core plug without aging

Interaction of different potential determining ions is same till 70 °C but at 120 °C, concentration of all the ions decreased in the effluent. We can see that oil recovery did not depend upon temperature but ion interaction with reservoir chalk is dependent upon temperature. This means that it is not ion interaction which is controlling the oil recovery process in reservoir chalk. At 120 °C, we observed more adsorption of SO_4^{2-} at high temperature but this adsorption did not help to increase the oil recovery.

In flooding sequence 2, flooding tests were carried out with brine SW0S and SW3S only. Most of the oil produced before the water breakthrough but some oil was also produced after the breakthrough. This made clear that three days aging affects the wettability of the core plug. Total oil recovery curves for flooding sequence 2 are shown in Figure 5

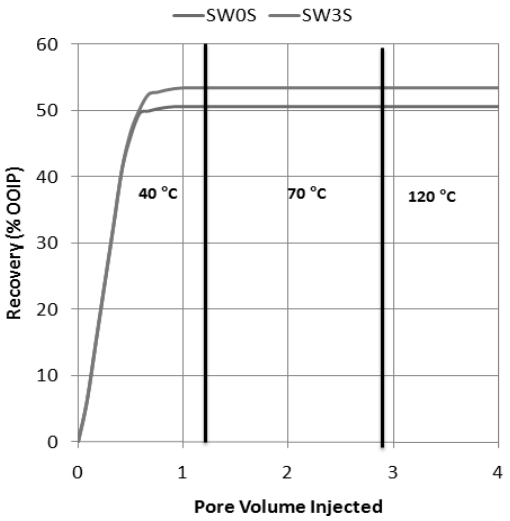

Figure 5: Oil Production curves for different brines for North Sea reservoir chalk core plug with aging

No more oil was produced with the increase in temperature even in this case. Effluent ions analysis for flooding sequence 2 is plotted below in Figure 6

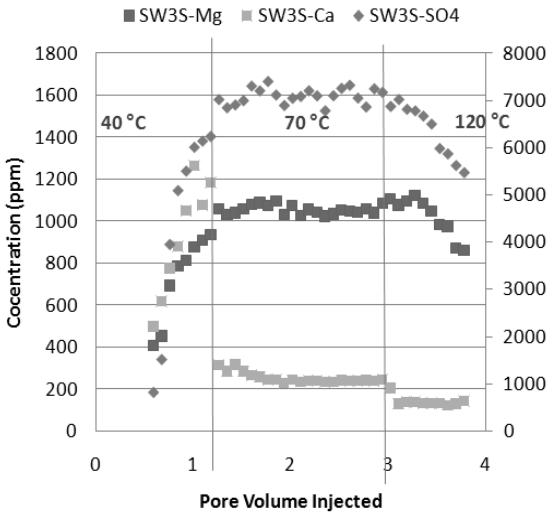

Figure 6: Effluent ion analysis for North Sea reservoir chalk core plug with aging

Ion interaction behavior for SW3S brine is same in both cases but relatively less loss of ions was observed in case of aging

Conclusions

- Increment in oil recovery with sulfate ions cannot be explained just by the rock wettability alteration.
- Viscosity of the crude oil was significantly reduced after interacting with sulfate ions at high temperature and high pressure conditions in the JEFRI cell.
- This decrease in oil viscosity with sulfate ions could be the possible reason for increment in oil recovery with sulfate ions.
- Temperature did not affect the oil recovery for North Sea reservoir chalk case at both wettability conditions.
- Interaction of different ions with rock depends upon temperature. This makes clear that it is not the interaction of the ions with rock which controls the oil recovery process.

Future Work

We will study the effect of initial water composition on waterflooding at both wettability conditions. Further, we will also focus on investigating the reasons of decrease in viscosity of crude oil with sulfate ions? In addition to these, we will use other crude oils for crude oil brine phase behavior study.

Acknowledgements

We are grateful to DONG Energy and The Danish Council for Independent Research |Technology and Production Sciences (FTP) for funding this study as a part of the ADORE project (09-062077/FTP).

References

1. M. Akbar, et al. Oilfield Review, 12(2001), 20-21.
2. T. Austad, D.C. Standnes, J. Petrol. Sci. Eng. 28 (2002) 123-143.
3. T. Austad, P. Zhang, Colloid. Surface. A. 301 (2007) 199-208.
4. W.G. Anderson, Journal of Petroleum Technology, SPE 13932, 1986.

List of Publications

1. A. Zahid, E.H. Stenby, A. Shapiro, SPE 131300 presented at SPE EUROPEC/EAGE Annual Conference and Exhibition, Barcelona, Spain, 2010.
2. A. Zahid, E.H. Stenby, A. Shapiro, P3 presented at 11th International Symposium on Evaluation of Wettability and Its Effect on Oil Recovery, University of Calgary, Alberta, Canada, 2010.

Birgitte Zeuner
Phone: +45 4525 2610
E-mail: biz@kt.dtu.dk
Discipline: Enzyme Technology

Supervisors: Anne S. Meyer
Anders Riisager, DTU Kemi

PhD Study
Started: December 2009
To be completed: December 2012

Activity and Stability of Feruloyl Esterase A from *Aspergillus niger* in Ionic Liquid Systems

Abstract
Interest in performing enzyme-catalyzed reactions in ionic liquids (ILs) has increased rapidly over the last decade. In the present work, activity and stability of feruloyl esterase A from *Aspergillus niger* (AnFaeA) was investigated in four different IL-buffer systems. Thermal stability was generally higher in buffer, but at 40ºC and below there was no significant difference in AnFaeA stability between buffer and the $[PF_6]^-$-based systems. The IL anion had a major effect on stability: $[BF_4]^-$ caused rapid inactivation of AnFaeA, while $[PF_6]^-$ did not. Hence, no appreciable activity was observed in the $[BF_4]^-$-based systems. The cation did not have a similar effect. These observations could be explained in terms of hydrogen bonding capacity of IL cations and anions by COSMO-RS simulations.

Introduction
During the last decade, the interest in performing enzyme-catalyzed (trans)esterification reactions in ionic liquids (ILs) has increased rapidly. This interest has mainly been fuelled by a desire to replace volatile organic solvents with non-volatile ILs, which also have the advantages of increased enzyme (enantio)selectivity and possibility for solvent tailoring [1]. Most of these reactions have been carried out with lipases, especially lipase B from *Candida antarctica*, which is an unusually stable enzyme. The present work [2] aims at taking the field of enzymatic synthesis reactions beyond lipases by studying a class of enzymes which is related to lipases, but probably more typical in terms of stability in non-conventional media, namely the feruloyl esterases (FAEs; EC 3.1.1.73). It is an obvious premise for successful catalysis that the enzyme is active in the IL system. However, enzyme stability has been found to be a major issue in non-conventional media and must therefore be assessed before designing a new reaction.

Specific objectives
It is hypothesized that the activity and stability of FAE A from *Aspergillus niger* (AnFaeA) in ILs will be affected by the reaction temperature and that different ILs may affect the stability differently. The present work also aims to explore the use of the quantum chemistry-based COSMO-RS method for explaining and predicting the effect of given ILs on enzyme stability.

Results and Discussion
The synthetic activity (esterification of sinapic acid with glycerol) and thermal stability of AnFaeA was assessed in IL systems containing 15% (v/v) buffer (pH 6) using a carefully selected series of four ILs with cations and anions of varying hydrophobicity and polarity: [BMIm][PF_6], [C_2OHMIm][PF_6], [BMIm][BF_4], and [C_2OHMIm][BF_4].

Table 1 shows that AnFaeA had appreciable activity in the $[PF_6]^-$-based systems only. The higher conversion observed in [C_2OHMIm][PF_6] (21%) compared to that in [BMIm][PF_6] (13%) may be due to mass transfer limitations caused by the two-phase system.

Table 1: Number of phases in IL-buffer systems and synthetic activity of AnFaeA given as conversion (%) of sinapic acid to glycerol sinapate after 30 minutes of reaction at 40ºC.

Ionic liquid	No. of phases	Conversion
[BMIm][PF_6]	2	13±3
[C_2OHMIm][PF_6]	1	21±2
[BMIm][BF_4]	1	0.9±0.1
[C_2OHMIm][BF_4]	1	0

Table 2 shows that AnFaeA is generally more stable in buffer – its natural, aqueous solvent – than in the IL systems. However, at 40ºC and below there is no significant difference in AnFaeA stability between buffer and the $[PF_6]^-$-based systems: the enzyme is

completely stable for more than 1 hour at 30ºC and 40ºC, and 40ºC can thus safely be chosen as reaction temperature. At 50ºC, the residual activity of AnFaeA after 1 hour is only ~40% in the $[PF_6]^-$-based IL systems, but 87% in buffer. AnFaeA is unstable at 60ºC, regardless of the solvent. There is no significant difference in AnFaeA stability between [BMIm][PF_6] and [C_2OHMIm][PF_6].

Table 2: Residual activity (%) of AnFaeA after 60 minutes of incubation in IL-buffer systems at 30-60ºC. Residual activity (%) in buffer included for comparison.

Solvent	30ºC	40ºC	50ºC	60ºC
Buffer	96±0	95±2	87±2	0
[BMIm][PF_6]	96±0	93±6	38±3	0
[C_2OHMIm][PF_6]	97±5	92±3	44±4	0
[BMIm][BF_4]	19±3	16±3	0	0
[C_2OHMIm][BF_4]	0	0	0	0

Similar stability was however not observed in the $[BF_4]^-$-based IL systems (Table 2): after 1 hour, the residual activity is less than 20% in [BMIm][BF_4], and in [C_2OHMIm][BF_4] complete inactivation takes place within 10 minutes of incubation (data not shown). This explains why (almost) no activity is observed in the two $[BF_4]^-$-based IL systems (Table 1).

The effect of the cation is less pronounced. While the difference in water-miscibility did affect AnFaeA activity in the two $[PF_6]^-$-based IL systems (Table 1), the cation did not have any effect on AnFaeA stability in these (Table 2). In the $[BF_4]^-$-based IL systems, AnFaeA is slightly more active and stable in [BMIm][BF_4] compared to [C_2OHMIm][BF_4], but both stability and activity are clearly dominated by the IL anion nature (Tables 1 and 2).

The results thus show that activity and stability of AnFaeA in IL systems are strongly dependent on the IL anion, whereas the cation does not have a similarly important effect. This is in accordance with literature, and it has been found that anions with a strong hydrogen bonding capacity tend to dissolve enzymes, thus inactivating them [3]. The quantum chemistry-based COSMO-RS method has been introduced as a fast way of performing solvent screening, especially for complex solvents such as ILs, and its ability to explain the effects of the four ILs on AnFaeA stability was therefore tested in the present work. The σ-profiles (i.e. frequencies of screening charge density (SCD), σ, which can be seen as a local measure of polarity) for the cations and anions are shown in Figure 1. The hydrogen bonding threshold is $\sigma_{HB} = \pm 0.79$ e/nm^2, but as hydrogen bonding is weak below ±1 e/nm^2 only surface segments with a σ-value beyond ±1 e/nm^2 are considered strongly polar and potentially hydrogen bonding [4]. From the σ-profiles in Figure 1 it is thus seen that the peak SCD of $[BF_4]^-$ is found outside the hydrogen bonding limit, whereas the peak SCD of the more hydrophobic $[PF_6]^-$ is inside this limit. Thus, the destabilising effect of $[BF_4]^-$ on AnFaeA can be explained by the tendency of $[BF_4]^-$ to act as a hydrogen bond acceptor and thus interact with the enzyme and disturb its hydrogen bond-based structure. Although the difference in water-miscibility between the two cations is harder to account for from the σ-profiles (the contribution of the hydroxyl group in $[C_2OHMIm]^+$ can be seen in the range from 0.5 to 1 e/nm^2), the fact that no major difference in the effect on AnFaeA stability is seen between $[BMIm]^+$ and $[C_2OHMIm]^+$ is supported by the two cations having similar σ-profiles in the hydrogen bond donor range ($\sigma <$ -1 e/nm^2).

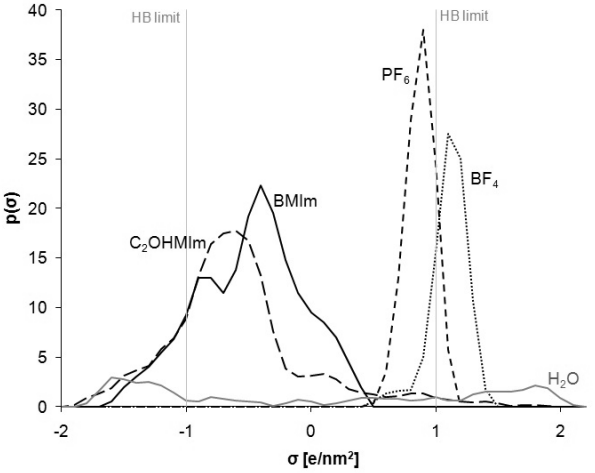

Figure 1: Sigma(σ)-profiles of $[BMIm]^+$, $[C_2OHMIm]^+$, $[PF_6]^-$, and $[BF_4]^-$. H_2O is included for comparison. The vertical lines show the hydrogen bonding (HB) limits: SCDs, σ, outside these lines indicate tendency to form hydrogen bonds.

Conclusions

Stability of AnFaeA is an issue when working in IL solvent systems. It was shown that AnFaeA stability and thus activity depend on the IL anion nature, and that the enzyme is stable in $[PF_6]^-$-based ILs, but not in $[BF_4]^-$-based ILs. This could be explained in terms of hydrogen bonding capacity by COSMO-RS simulations.

References

1. F. van Rantwijk, R.A. Sheldon, Chem. Rev. 107 (2007) 2757-2785.
2. B. Zeuner, O.N. van Buu, T. Ståhlberg, A.J. Kunov-Kruse, A. Riisager, A.S. Meyer (2011) [submitted].
3. R.M. Lau, M.J. Sorgedrager, G. Carrea, F. van Rantwijk, F. Secundo, R.A. Sheldon, Green. Chem. 6 (2004) 483-487.
4. A. Klamt, COSMO-RS. From quantum chemistry to fluid phase thermodynamics and drug design, Elsevier, Amsterdam, 2005.

Xuan Zhang

Phone: +45 4525 2892

E-mail: xz@kt.dtu.dk

Discipline: Engineering Thermodynamics

Supervisors: Alexander Shapiro

PhD Study

Started: September 2008

To be completed: August 2011

Multiphase Flow in Porous Media

Abstract

A new analytical upscaling method for waterflooding is described. This method is for stratified reservoirs with very good communication between layers, but negligible capillary forces. Asymptotic method is used for reduction of the multidimensional problem of displacement in a layer-cake reservoir to a pseudo single-dimensional problem. Both cases of discontinuous and continuous (log normal) distributing permeability are studied. COMSOL is used, as comparison, to solve the full 2D problems. The results of the pseudo 1D method are very close to the results by COMSOL.

Introduction

Waterflooding is the most widely used method in improved oil recovery. Since the reservoir rocks are heterogeneous, and it is not practical for people to get very detailed information of reservoir, upscaling techniques are needed to get the pseudo properties of the reservoirs: pseudo relative permeabilities and pseudo fractional flow functions. These functions are used in the framework of the classical Buckley-Leverett theory of waterflooding.

Upscaling is to transfer from specific parameters of small scale to average (pseudo-) functions for the whole reservoir. Upscaling techniques are often used to coarsen the geological models to manageable levels for flow calculation. It is important that these coarsened flow models replicate the fine scale characteristics in terms of key behaviors, such as overall flow rate and the appearance of injected fluid.

A model of flow upscaling in a layered reservoir with perfect vertical connection has been developed in this article. The model describes displacement of oil by water in a viscous dominant regime. By using this method, we can calculate pseudo relative permeabilities, pseudo fractional flow function and pseudo water saturation profile without rearranging the layers, as Hearn did [5]. And we can apply this method to cases of any layers, as well as continuously distributed layers. Numerical and analytical algorithms to obtain the pseudo-functions have been worked out. The results were compared with the model of disconnected layer-cake reservoir.

Model Description

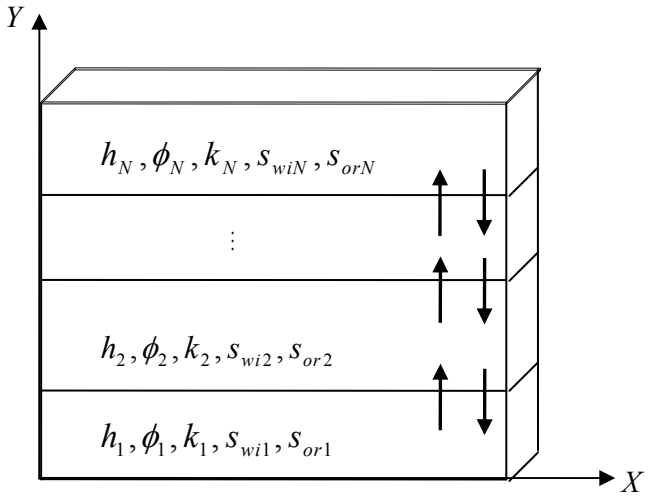

Figure 1: The layered reservoir model. The top and bottom of the reservoir are assumed to be impermeable. Each layer has individual height h_i, porosity ϕ_i, permeability k_i, irreducible water saturation $s_{wi,i}$, residual oil saturation $s_{or,i}$.

Theory

The dimensionless mass balance and continuity equations for incompressible flow with negligible gravity effect are:

$$\Phi \frac{\partial s_w}{\partial T} + \frac{\partial}{\partial X}\left(F\bar{U}_X\right) + \frac{\partial}{\partial Y}\left(F\bar{U}_Y\right) = 0 \quad (1)$$

$$\frac{\partial \bar{U}_X}{\partial X} + \frac{\partial \bar{U}_Y}{\partial Y} = 0 \quad (2)$$

where Φ is porosity, s_w water saturation, $\bar{U}_X$, $\bar{U}_Y$ total flow velocity, F fractional flow function. Darcy's law for porous media flow are:

$$\bar{U}_X = -\Lambda_X \frac{\partial P}{\partial X} \quad (3)$$

$$\bar{U}_Y = -E\Lambda_Y \frac{\partial P}{\partial Y} \quad (4)$$

where $E=(\lambda_{0y}x_0^2)/(\lambda_{0x}y_0^2)$ defined as the anisotropy ratio of the reservoir, which is dependent on length x_0, height y_0, mobility scales λ_{0x} and λ_{0y} of the reservoir. P is dimensionless pressure, Λ_X and Λ_Y are dimensionless mobility.

Substitution of Eqs. 3, 4 into 1, 2 and assumption of very good inter-layer communication result in very small pressure gradient across the layers. We can set $\partial P/\partial Y=0$ and then get the expression for velocities under the condition of constant injection rate Q (injection rate does not change with positions).

$$\bar{U}_X = \frac{\Lambda_X}{\int_0^1 \Lambda_X dY} Q \quad (5)$$

$$\frac{\partial \bar{U}_Y}{\partial Y} = -Q\frac{\partial}{\partial X}\frac{\Lambda_X}{\int_0^1 \Lambda_X dY} \rightarrow \bar{U}_Y = -Q\frac{\partial}{\partial X}\left[\frac{\int_0^Y \Lambda_X dY'}{\int_0^1 \Lambda_X dY}\right] \quad (6)$$

This is a closed equation for saturation $s_w(X,Y,T)$. Both pressure and velocity are excluded. It should be stressed that the only assumption made for derivation of this equation is the pressure independence on vertical coordinate. Other assumptions in the Hearn method (like exchangeability of the layers or a piston-like character of displacement) are not applied.

The interpretation of Eq. 5 is as follows: variation of s_w in layer Y is due to transfer along the layer plus exchange between layers. The "layer distribution function" $\Lambda_X / \int_0^1 \Lambda_X dY$ expresses redistribution of flows between layers due to pressure interaction.

In the layered reservoir model, as shown in Fig 1, summation can be used in terms of the height of each layer and certain quantity. Since no gravity is included in the equations, $\partial/\partial Y$ can be replaced by $1/\alpha_m$, where α_m is the height fraction of layer m. The mass balance equation for this layer is expressed as:

$$\Phi_m \frac{\partial s_{wm}}{\partial T} + \frac{\partial F_m \bar{U}_{Xm}}{\partial X} + \frac{(F\bar{U}_Y)_{m-1} - (F\bar{U}_Y)_m}{\alpha_m} = 0 \quad (7)$$

Consider addendum $(F\bar{U}_Y)_{m-1}$. If $\bar{U}_{Y,m-1} > 0$, then this term describes the inflow from layer m-1 to layer m. In this case it is logical to set $F=F_{m-1}$. However, if $\bar{U}_{Y,m-1} < 0$, this term describes the outflow from layer m to layer m-1. Then it should be set $F=F_m$. In a similar way, in the second addendum $(FU_Y)_m$, we should set $F=F_m$ if $\bar{U}_{Ym} > 0$ and $F=F_{m+1}$ otherwise. This is a common approach to hyperbolic equations with a sign changing velocity.

Results and Discussion

Two-Layer Model

For analysis of the peculiarities of displacement in a stratified reservoir we have performed a series of computations for waterflooding in a two-dimensional two-layer reservoir. The parameters of our calculation are listed in Table 1.

Table 1: Dimensionless parameters for the two-layer model. The values in brackets correspond to the mobility ratio (oil to water) M=1.33, other values correspond to M=0.33. ($M=(kr_{owi}M_w)/(kr_{wor}M_o)$)

Dimensionless parameters	**Layer 1**	**Layer 2**
Fraction of thickness α	1/3	2/3
Irreducible water saturation s_{wi}	0.05	0.2
Residual oil saturation s_{or}	0.25	0.2
Relative water permeability at residual oil saturation kr_{wor}	0.8(0.4)	0.8(0.4)
Relative oil permeability at irreducible water saturation kr_{owi}	0.8	0.8
Dimensionless permeability in x-direction K_x	1/3	2/3
Dimensionless porosity Φ	1	
Dimensionless dynamic viscosity of water and oil	M_w=1, M_o=3(1.5)	
Dimensionless injection rate Q	1	

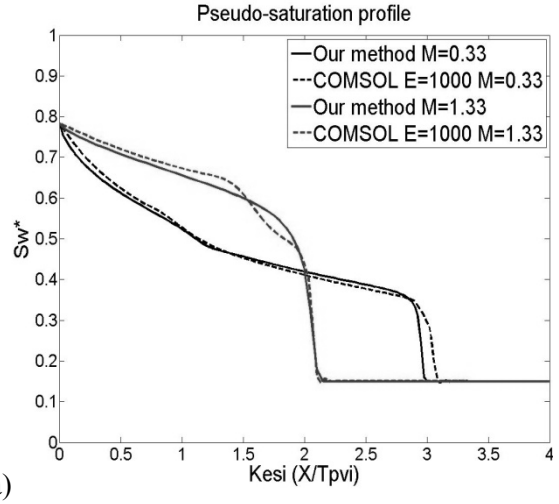

a)

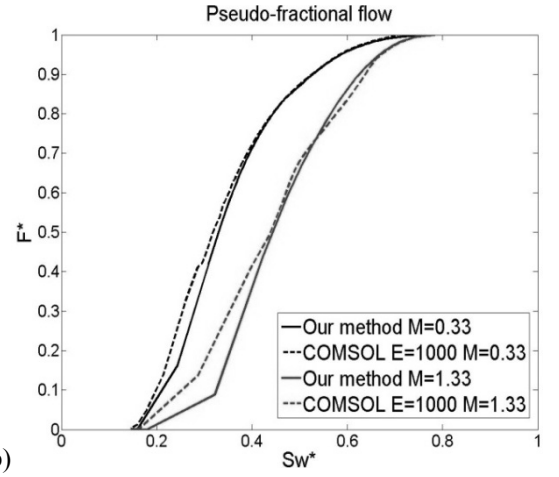

b)

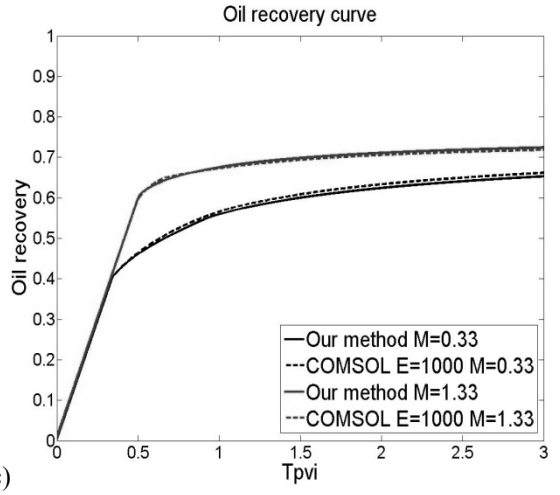

c)

Figure 2: Comparison of the results obtained by our method and by the 2D simulation for a reservoir consisting of two communicating layers. Solid lines represent the results of our method; dashed lines the results of the 2D simulation with E=1000. Black and red lines represent the results for an unfavorable and a favorable mobility ratio, respectively. (a) Water saturation profiles, (b) pseudofractional flow functions, (c) oil recovery curves.

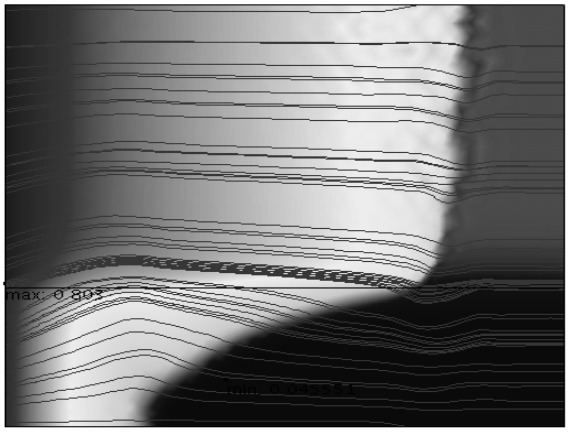

Figure 3: 2-dimentional water saturation profile, and stream line of total velocity U_i, simulation of communicating layers by Comsol.

Log-Normal Distributed Permeability

The log-normal probability distribution density of permeability is given by

$$\varphi(\ln k) = \frac{1}{\sqrt{2\pi}\sigma} \exp\left[-\frac{(\ln k - \beta)^2}{2\sigma^2} \right] \tag{8}$$

The relation between k and the height of the reservoir Y is

$$Y(k) = \int_{\ln k}^{+\infty} \varphi(\ln k') d \ln k' \tag{9}$$

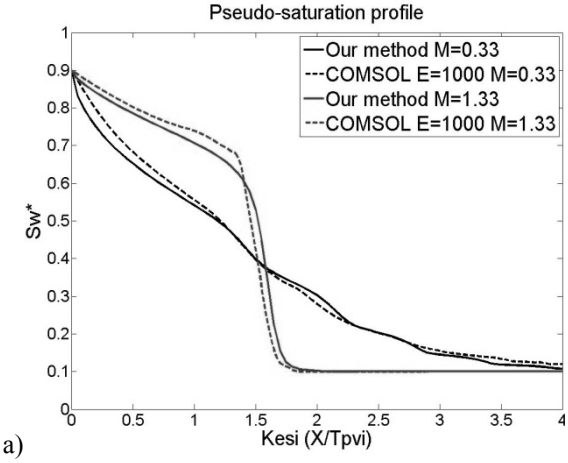

a)

b)

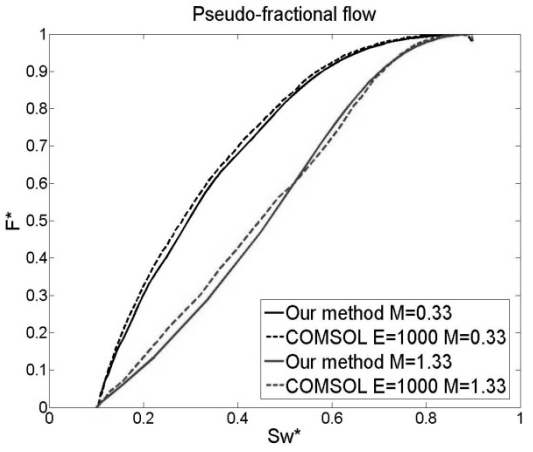

c)

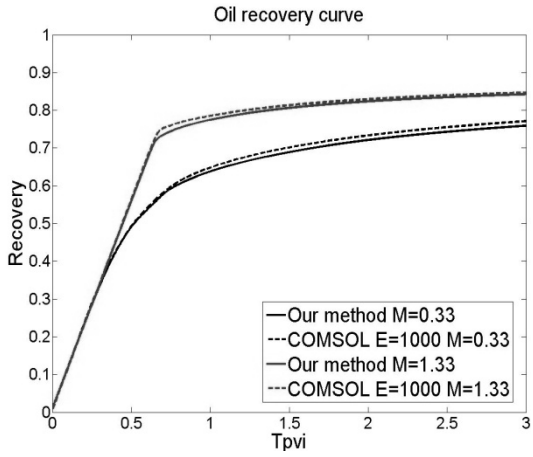

Figure 4: Comparison of the results obtained by our method and by the 2D simulation for the reservoir with log-normal permeability distribution. Solid lines represent our method; dashed lines the 2D simulation. Black lines correspond to an unfavorable mobility ratio, red lines to a favorable mobility ratio. (**a**) Water saturation profiles, (**b**) pseudo-fractional flow functions, (**c**) oil recovery curves.

Conclusions

We have developed an analytical method for pseudo-1D simulation of waterflooding in a layer-cake reservoir. It may be used for upscaling of waterflooding in a stratified reservoir of a viscous dominant regime, accounting also for gravity segregation. For the waterflooding problems in well defined multilayer reservoirs, as well as reservoirs with log-normal distributed permeabilities, the results obtained by our method are all very close to the results obtained from the complete 2D displacement simulation. The saturation profile calculated by our method is slightly different from the 2D simulation result. However, the difference is within the degree of approximation and the positions of the displacement fronts are almost the same.

Acknowledgements

The Danish Council of Technology and Production (FTP) is kindly acknowledged for financial support in the framework of the ADORE project. The authors are grateful to Kent Johansen, who has drawn their attention to apparent problems with the Hearn method.

References

1. Y. Chen, L.J. Durlofsky, M. Gerritsen, X.H. Wen, Adv. Water. Resour. 26 (2003) 1041-1060
2. Jon Kleppe, Handout note 6-Dykstra-Parsons method, TPG 4150 Reservoir recovery techniques, Norwegian University of Science and Technology, 2008
3. R.R. Gasimov, Modification of the Dykstra-Parsons method to incorporate Buckley-Leverett displacement theory for water floods, Petroleum engineering, Texas A&M University, August 2005, P3
4. C.L. Hearn, SPE-AIME Service Oil Co. Simulation of Stratified Water Flooding by Pseudo Relative Permeability Curves, SPE 2929, July 1971
5. N. El-Khatib, SPE, King Saud U, Waterflooding performance of communicating stratified reservoir with log-normal permeability distribution
6. P. Bedrikovetsky, Mathematical theory of oil and gas recovery-with applications to ex-ussr oil and gas fields, P3-7, P12, P22, ISBN 0-7923-2381-5, Kluwer academic publishers
7. T.I. Bjørnarå, E. Aker, NGI, Norway Comparing Equations for Two-Phase Fluid Flow in Porous Media, COMSOL Conference 2008 Hannover
8. M.A. Diaz-Viera, D.A. Lopez-Falcon, A. Moctezuma-Berthier, A. Ortiz-Tapia, Instituto Mexicano del Petroleo, COMSOL Implementation of a Multiphase Fluid Flow Model in Porous Media

List of Publications

1. X. Zhang, A. Shapiro, E.H. Stenby, Transport Porous. Med. (2010)
2. X. Zhang, A. Shapiro, E.H. Stenby, Upscaling of Two-Phase Immiscible Flows in Communicating Stratified Reservoirs, 12th European Conference on the Mathematics of Oil Recovery, Oxford, UK, 2010
3. X. Zhang, A. Shapiro, E.H. Stenby, COMSOL Implementation for Upscaling of Two-Phase Immiscible Flows in Communicating Layered Reservoirs, COMSOL Conference, Paris, France, 2010

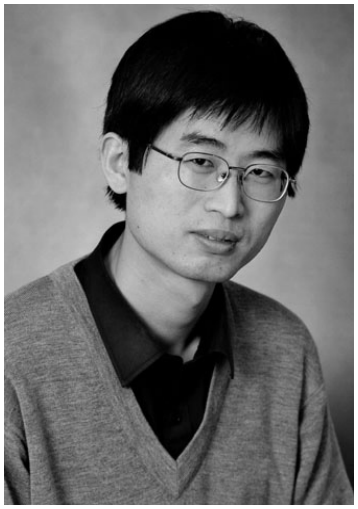

Yuanjing Zheng
Phone: +45 4525 2830
E-mail: yjz@kt.dtu.dk
Discipline: Reaction and Transport Engineering

Supervisors: Anker Degn Jensen
Christian Windelin, FLSmidth A/S
Flemming Jensen, FLSmidth A/S

Industrial PhD Study
Started: April 2008
To be completed: March 2011

Mercury Removal from Cement Plants by Sorbent Injection upstream of a Pulse Jet Fabric Filter

Abstract
In this work the removal of mercury from simulated cement plant flue gas by different sorbent materials has been studied. A new experimental setup was designed to perform the experimental studies including the development of sulfite-based converter for total gaseous mercury measurement. Screening tests of sorbents in the simulated cement kiln flue gas with elemental mercury source show that activated carbon has the best mercury adsorption performance among the tested sorbents. Parametric study of mercury adsorption by activated carbon is performed regarding flue gas composition, adsorption temperature, and carbon particle size etc. Models are developed to simulate mercury adsorption in a single carbon particle, by fixed carbon bed and by carbon injection upstream of a fabric filter.

Introduction
There has been an increased focus on mercury emission from industry during the latest years as a consequence of the environmental impact and potential risk for human health of mercury compounds. Some cement raw materials have high mercury contents and very high mercury emissions from cement plants have been observed. Mercury removal from cement plant flue gases has been required in both EU and the U.S.

The U.S. environment protection agency recently set the nation's first limits on mercury air emissions from existing cement kilns and strengthened the limits for new kilns [1]. The mercury emission limit for existing and new cement plants is 55 and 21 pound/million tons of clinker, respectively. These emission limits correspond to 13 and 5 $\mu g/Nm^3$. When fully implemented in 2013, EPA estimates the annual mercury emissions will be reduced about 92% [1]. It is estimated that only few cement kilns in U.S. can achieve this new mercury emission limit without some changes to the system, either through operational adjustment or use of add-on technology. To ensure that the mercury emission limit is met, FLSmidth has initiated research on mercury removal from cement plants.

Mercury can be removed from the flue gas by fuel cleaning and switching, raw material cleaning, sorbent injection, fixed sorbent bed, oxidation and removal by catalyst and wet scrubber. Activated carbon injection upstream of a particulate control device such as fabric filter has been shown to have the best potential to remove both elemental and oxidized mercury from the flue gas for plants not equipped with a wet flue gas desulphurization plant. However, mercury adsorption by activated carbon is not clearly understood yet, research and development efforts are still needed before carbon injection is considered as a commercial technology for wide use.

Extensive research has been carried out to reduce mercury emissions from coal combustion and waste incineration, but very little efforts have been concentrated on mercury removal in the cement plant. The application of sorbent injection to cement kilns appears to be more challenging and knowledge obtained from mercury removal in power plant and incinerator might not be applied to cement plant directly.

Specific Objectives
The overall goal of this project is to develop and advance improved mercury control technologies using sorbent injection upstream of a pulse jet fabric filter for cement plants. Specific objectives are as follows:

1. To develop an experimental fixed-bed unit for sorbent study and thermal catalytic converters for oxidized mercury reduction and total mercury measurement.
2. To screen sorbents for capturing mercury from cement kiln flue gas and develop an understanding of sorbent chemistry and provide mechanistic

understanding and kinetic rates for sorbents of interest.

3. To develop mathematic models that can describe mercury removal in the fixed-bed and predict mercury removal efficiency in cement plant by injecting sorbent upstream of a fabric filter.

Experimental Setup

A lab-scale fixed bed reactor for screening the sorbents has been built. Figure 1 illustrates the sketch of the reactor system. The system consists of a mercury vapor generator, gas addition system, a gas-solid glass reactor, an electrical heated oven, oxidized mercury to elemental mercury converter, a Lumex mercury analyzer, flue gas treatment units, and data sampling. The mercury analyzer can analyze gas of up to 30% water, and therefore no drying of the gas is needed. To avoid mercury condensation and accumulation in the system, all the gas lines before and in the analyzer are heated at 150°C. The mercury source, reactor and heated gas lines are located in a dedicated ventilation hood.

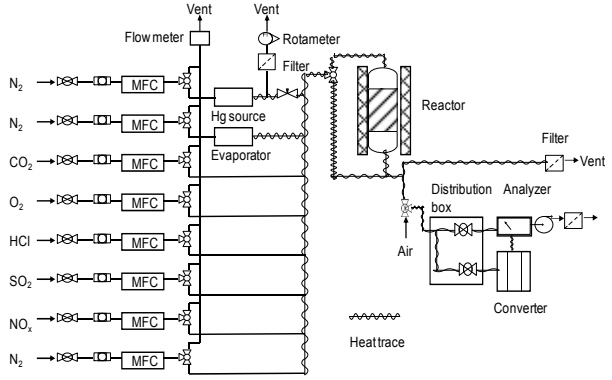

Figure 1: Sketch of the fixed-bed reactor system.

The total flow rate through the reactor is 2.75 Nl/min and of which about 2 Nl/min is passed through the analyzer. The typical composition of the simulated cement kiln flue gas applied in this work includes 21% CO_2, 6% O_2, 1% H_2O, 10 ppmv HCl, 1000 ppmv NO, 30 ppmv NO_2, and 1000 ppmv SO_2. The applied mercury concentration is about 160-180 µg/Nm^3 by keeping the elemental mercury and mercury chloride at 70ºC and 50ºC, respectively, and using 0.275 Nl/min nitrogen as carrier gas.

Red brass chips for the converter are obtained through the supplier of the gas analyzer, Lumex. Alternatively, sulfite converter material was prepared by dry impregnation of sodium sulfite and calcium sulfate powders on zeolite pellets using water glass as binder. To be able to quantify the oxidized mercury reduction efficiency, the oxidized mercury is produced by passing the flue gas with known concentration of elemental mercury to the reactor with 4 g catalyst.

More than 20 sorbent candidates are collected for screening tests. Particle size distributions are measured by Malvern laser diffraction equipment. Selected samples are analyzed by SEM-EDX. Mercury content in the exposed sorbent is analyzed by a DMA-80 analyzer from Milestone.

Results

Initially tests were made to check whether the commercial oxidized to elemental mercury converter works properly. Test of the red brass converter using only elemental mercury shows that when HCl is added together with either SO_2 or NO_x the mercury measurement through the converter is unstable and lower than the elemental mercury inlet level. The red brass chips cannot fully reduce oxidized mercury to elemental mercury when simulated cement kiln gas is applied.

Then the sulphite converter was developed and optimized. The dynamics of the converter was investigated by studying the cycle response time of mercury measurement to the change of mercury addition and switching between the reactor and bypass. Figure 2 shows the response of both Hg^0 measurement bypassing the converter and SCR catalyst and total mercury measurement through the SCR catalyst and converter with a Hg^0 inlet level of 112 µg/Nm^3. Close look at the response shows that the response of mercury measurement is very fast for both step up and step down tests. The cycle response time is typically within one minute. All further tests have been done with this converter.

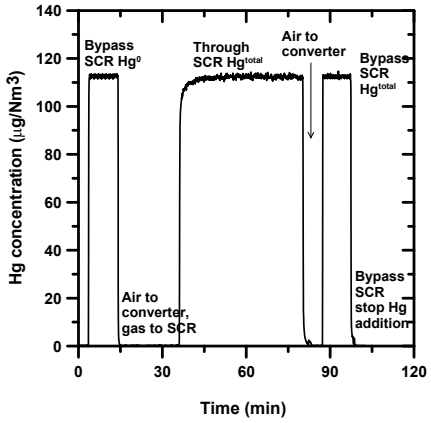

Figure 2: Dynamic test of 20 g sulfite compounds at 500ºC with 10 ppmv HCl in the flue gas.

Figure 3 illustrates the screening results of different sorbents using elemental mercury source. Generally non-treated activated carbon Darco Hg and HOK show similar mercury adsorption behavior. The bromine treated carbon Darco Hg-LH has larger adsorption capacity but smaller adsorption rate. Sorbalit, which is a mixture of lime and carbon, shows poorer performance than the carbons. Minsorb ME, which is aluminiumsilicates based sorbent shows the poorest performance among the tested commercial sorbents. Some mercury adsorption on the calcium bromide salt is also observed.

The extent of mercury oxidation is evaluated by measuring the elemental mercury when the complete mercury breakthrough using total mercury measurement is obtained. Figure 4 shows the extents of mercury oxidation by 30 mg sorbents in 2 g sand at 150°C using simulated kiln gas. Comparison with Figure 3 indicates

that the sorbents with larger mercury adsorption capacity are also good catalysts for mercury oxidation.

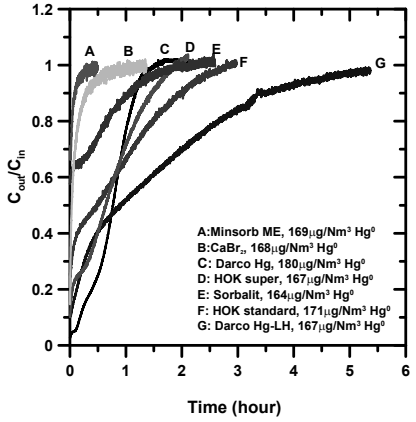

Figure 3: Screening tests of 30 mg sorbents in 2 g sand at 150°C using simulated kiln gas with elemental mercury source.

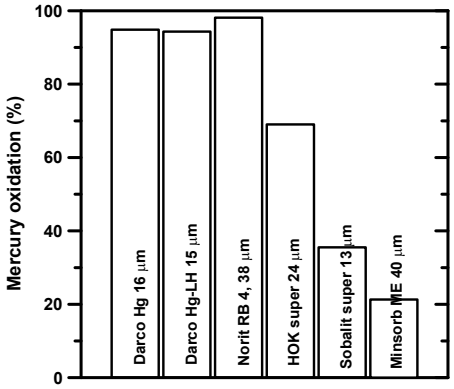

Figure 4: Extent of mercury adsorption by 30 mg sorbents in 2 g sand at 150°C using simulated kiln gas with elemental mercury source.

The effects of adsorption temperature and sorbent particle size on mercury adsorption are illustrated in Figure 5 and 6, respectively. As expected, faster mercury breakthrough is obtained at higher adsorption temperature. The final mercury adsorption capacity is the same for carbon particles with different sizes. Higher mercury oxidation and initial adsorption rate are also observed for smaller carbon particles. This indicates that the diffusion resistance in the carbon particle is an important factor.

Gases such as SO_2, H_2O and NO_2 have important influence on mercury adsorption by the activated carbon and the effects are shown in Figure 7, 8, and 9, respectively. Generally, faster mercury breakthrough is observed when higher levels of SO_2, H_2O and NO_2 are applied. In addition to removing mercury, activated carbon is also used as catalyst for oxidation SO_2 to SO_3 and sulphuric acid [2]. There is competitive adsorption between Hg and SO_3 since both mercury and SO_3 bind to the Lewis base sites on the activated carbon surface [3]. Oxidation of SO_2 on carbon particles is greatly enhanced by the presence of trace quantities of gaseous NO_2. Interaction between SO_2 and NO_2 causes the previously formed nonvolatile mercuric nitrate to transform into the volatile form leading to reduced mercury adsorption [4]. The negative effects of water presence in the gas on mercury adsorption on the carbon could be due to the competitive adsorption of water on the carbon.

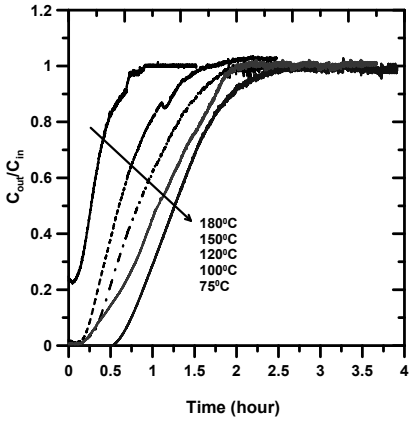

Figure 5: Effects of adsorption temperature on mercury breakthrough with 30 mg Darco Hg activated carbon in 2 g sand using simulated kiln gas with elemental mercury source.

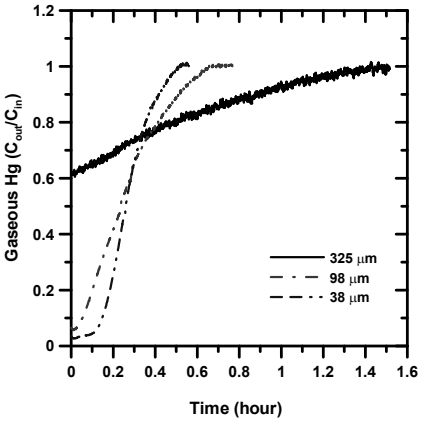

Figure 6: Effects of particle size on mercury breakthrough for 10 mg NORIT RB 4 crushed pellets in 2 g sand at 150°C using simulated kiln gas with elemental mercury source.

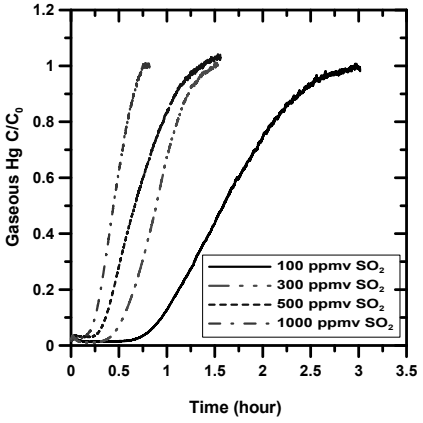

Figure 7: Effects of SO_2 level on mercury breakthrough for 10 mg Darco Hg carbon in 2 g sand at 150°C using simulated kiln gas with elemental mercury source.

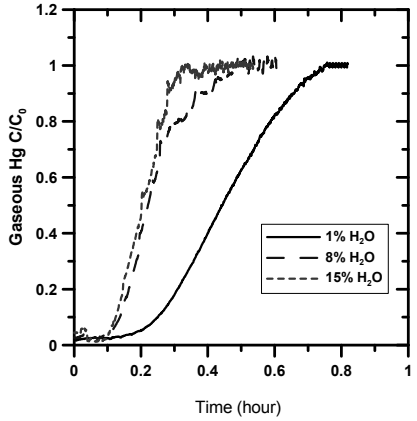

Figure 8: Effects of water vapor level on mercury breakthrough for 10 mg Darco Hg carbon in 2 g sand at 150°C using simulated kiln gas with elemental mercury source.

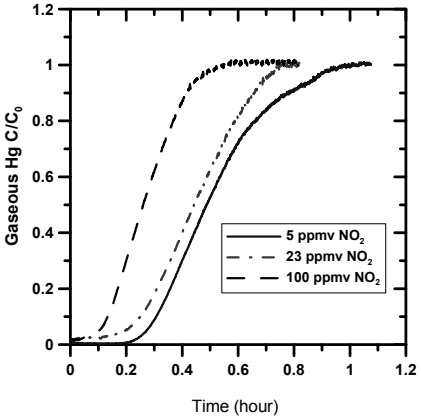

Figure 9: Effects of NO_2 level on mercury breakthrough for 10 mg Darco Hg carbon in 2 g sand at 150°C using simulated kiln gas with elemental mercury source.

Modeling Work

Mathematical models are developed assuming linear adsorption and local equilibrium within the sorbent particles. Orthogonal collocation method is used to solve mercury diffusion and adsorption inside a sorbent particle. For mercury adsorption in the duct another mass balance equation for bulk gaseous mercury is coupled and solved simultaneously using Matlab routine ode15s. The fixed-bed model is solved by tank-in-series method. Figure 10 shows the comparison between model simulation and experimental data.

The fixed-bed model is then extended to moving boundary problem assuming a new sorbent layer is accumulated on the bag and acts as a well-mixed tank. Finally the duct model and fabric filter model are coupled to a two-stage model. The model can simulate the mercury removal profile with features of sorbent cake accumulation on the filter bag, and periodical cleaning fractions of the bags.

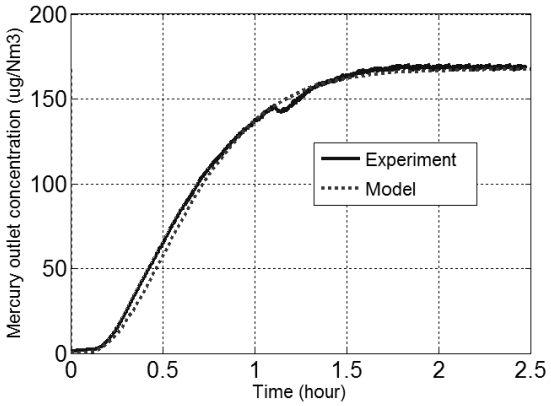

Figure 10: Simulation of mercury adsorption by 30 mg Darco Hg in 2 g sand at 150°C using simulated kiln flue gas with elemental mercury source.

Conclusions

The commercial red brass converter does not work properly in simulated cement kiln flue gas. HCl is a key factor for oxidized mercury reduction by the sulfite converter. With 10 ppmv HCl in the simulated flue gas the sulfite converter can work properly for several months. Among the tested sorbents activated carbons show the best performance. Investigation shows that significant amount of mercury is oxidized over the activated carbon. Gases such as SO_2, H_2O and NO_2 have important influence on mercury adsorption by the activated carbon. Mathematical models are developed to simulate mercury adsorption both in fixed bed and in continuous carbon injection upstream of a fabric filter. The models can be used to design and optimize the mercury adsorption process.

Acknowledgments

This project is a part of the Research Platform on New Cement Production Technology financed by Danish Advanced Technology Foundation, FLSmidth A/S, and DTU. Financial support of the industrial PhD study by the Ministry of Science Technology and Innovation is gratefully acknowledged.

References

1. U.S. EPA, Fact sheet, Final amendments to national air toxics emission standards and new source performance standards for Portland cement manufacturing, 2010.
2. E. Raymundo-Piñero, D. Cazorla-Amorós, C. Salinas-Martinez de Lecea, A. Linares-Solano, Carbon. 38 (2000) 335-344.
3. A.A. Presto, E.J. Granite, Environ. Sci. Technol. 41 (2007) 6579-6584.
4. S.J. Miller, G.E. Dunham, E.S. Olson, T.D. Brown, Fuel Process Technol. 65 (2000) 343-363.